

Wissenschaftlich-Technische Berichte
FZD-505
October 2008

M. Beyer, D. Lucas, J. Kussin, P. Schütz

Air-water experiments in a vertical DN200-pipe

Technical Report



**Forschungszentrum
Dresden** Rossendorf

Technischer Fachbericht

Luft-Wasser Experimente im vertikalen DN200-Rohr

Technical Report

Air-water experiments in a vertical DN200-pipe

Reaktorsicherheitsforschung-Vorhaben-Nr./
Reactor Safety Research-project No.:

150 1329

Vorhabentitel: **TOPFLOW-Experimente, Modellentwicklung und Validierung von CFD-Codes für Wasser-Dampf-Strömungen mit Phasenübergang**

Project Title: **TOPFLOW-Experiments, development and validation of CFD models for steam-water flows with phase transfer**

Autoren / Author(s): **M. Beyer, D. Lucas, J. Kussin, P. Schütz**

Dienststelle der Autoren /
Performing Organisation: **Forschungszentrum Dresden-Rossendorf e.V.
Institut für Sicherheitsforschung**

Berichtsdatum /
Publication Date: **October 2008**

Berichts-Nr. / Report-No.: **FZD-505**

Das diesem Bericht zugrundeliegende Vorhaben wurde mit Mitteln des Bundesministeriums für Wirtschaft und Technologie unter dem Förderkennzeichen 150 1329 gefördert. Die Verantwortung für den Inhalt dieser Veröffentlichung liegt bei den Autoren.

Berichtsblatt

1. ISBN oder ISSN	2. Berichtsart Technischer Fachbericht	
3a. Titel des Berichts Luft-Wasser Experimente im vertikalen DN200-Rohr		
3b. Titel der Publikation		
4a. Autoren des Berichts (Name, Vorname(n)) M. Beyer, D. Lucas, J. Kussin, P. Schütz		5. Abschlussdatum des Vorhabens 30.09.2010
4b. Autoren der Publikation (Name, Vorname(n))		6. Veröffentlichungsdatum October 2008
		7. Form der Publikation Broschüre
8. Durchführende Institution(en) (Name, Adresse) Forschungszentrum Dresden-Rossendorf e.V. Institut für Sicherheitsforschung Postfach 510119 01314 Dresden		9. Ber.Nr. Durchführende Institution
		10. Förderkennzeichen 150 1329
		11a. Seitenzahl Bericht 253
		11b. Seitenzahl Publikation
13. Fördernde Institution (Name, Adresse) Bundesministerium für Wirtschaft und Technologie (BMWi) 11019 Berlin		12. Literaturangaben 38
		14. Tabellen 5
		15. Abbildungen 51
16. Zusätzliche Angaben		
17. Vorgelegt bei (Titel, Ort, Datum)		
18. Kurzreferat <p>Die im Rahmen dieser Versuchsserie erzielten umfangreichen experimentellen Ergebnisse bilden eine hochwertige Datenbasis für Luft-Wasser-Strömungen in einem vertikalen DN200-Rohr, die für die Entwicklung und Validierung von CFD-Modellen, beispielweise bzgl. Blasenkoaleszenz und -fragmentierung, genutzt werden können. Besonderes interessant ist die Untersuchung der Entwicklung der Zweiphasenströmung über der Rohrhöhe. Aus diesem Grund wurden für jede der 92 betrachteten Kombinationen aus Gas- und Wasser-Volumenstromdichten bis zu 18 Messungen mit variablen Abständen zwischen Gaseinspeisung und Messebene durchgeführt. Dabei wurde der Druck an der Gaseinspeisestelle konstant auf 0,25 MPa(a) gehalten. Dies Randbedingung bietet den Vorteil, dass die so gemessenen Daten die Entwicklung der Strömung über der Rohrhöhe widerspiegeln, d.h. eine Konfiguration beschreiben, bei der das Gas an einer festen Höhenposition eingespeist wird und die Messungen in verschiedenen darüberliegenden Ebenen erfolgen. Wesentliche Ergebnisse dieser Messserie sind radiale zeitgemittelte Profile für den Gasgehalt und die Gasgeschwindigkeit sowie zeit- und querschnittsgemittelte Blasengrößenverteilungen. Außerdem liegen blasengrößen- und orts aufgelöste Gasgehaltsdaten vor. Wie bereits bei früheren Versuchsserien wurden auch in diesem Fall die Strömungsformen analysiert, wobei die Klassifizierung anhand der Blasengröße erfolgte.</p> <p>Ein wesentlicher Bestandteil dieser neuen Luft/Wasser-Versuche war die Qualitäts- und Plausibilitätsprüfung der Messdaten. Es konnte festgestellt werden, dass die Daten einen eindeutigen, widerspruchsfreien Trend bzgl. ihrer Entwicklung mit zunehmendem Abstand von der Gaseinspeisung aufweisen. Zur Plausibilitätsprüfung wurden Vergleiche des Gasgehaltsverlaufes über der Rohrhöhe mit theoretisch zu erwartenden Kurven durchgeführt.</p> <p>Zusätzlich zu diesen Ergebnissen enthält der Bericht eine Einschätzung des Einflusses des Bohrungsdurchmessers an der Gaseinspeisung auf die sich einstellende Strömung.</p>		
19. Schlagwörter Zweiphasenströmung, Gasblasen, Gasgehaltsverteilungen, Gasgeschwindigkeit		
20. Verlag		21. Preis

Document Control Sheet

1. ISBN or ISSN	2. Type of Report Technical Report	
3a. Report Title Air-water experiments in a vertical DN200-pipe		
3b. Title of Publication		
4a. Author(s) of the Report (Family Name, First Name(s)) M. Beyer, D. Lucas, J. Kussin, P. Schütz		5. End of Project 30.09.2010
4b. Author(s) of the Publication (Family Name, First Name(s))		6. Publication Date October 2008
8. Performing Organisation(s) (Name, Address) Forschungszentrum Dresden-Rossendorf e.V. Institut für Sicherheitsforschung Postfach 510119 01314 Dresden		7. Form of Publication Booklet
		9. Originator's Report No.
		10. Reference No. 150 1329
		11a. No. of Pages Report 253
13. Sponsoring Agency (Name, Address) Bundesministerium für Wirtschaft und Technologie (BMWi) 11019 Berlin		11b. No. of Pages Publication
		12. No. of References 38
		14. No. of Tables 5
16. Supplementary Notes		15. No. of Figures 51
		17. Presented at (Title, Place, Date)
18. Abstract <p>The extensive experimental results presented in this report provide a high-quality database for air/water flows in a vertical pipe with a nominal diameter of 200 mm. This database can be used for the development and validation of CFD-like models for two-phase flows, e.g. for bubble coalescence and fragmentation. In particular, the investigations aim on the evolution of the two-phase flow along the pipe height. Therefore, up to 18 single measurements with varying distances between the gas injection and measurement plane were realised for each of the 92 combinations of gas and water flow rates. The pressure at the position of the activated gas injection was kept constant at 0.25 MPa(a). This boundary condition has the advantage that the measured data represent exactly the evolution of the flow along the pipe, i.e. they reflect a configuration at which the gas injection is at a fixed height position, while the measurement plane varies.</p> <p>Important results of this test series are time averaged radial profiles of the gas fraction, and the gas velocity, as well as the time and cross-section averaged bubble size distributions. Furthermore, gas fraction data resolved regarding the bubble size and spatial distribution are presented. As in previous test series, flow patterns were analysed, whereby the classification results from the bubble size.</p> <p>A substantial part of these new air/water experiments were quality and plausibility checks of the measured data. In the result, a clear and consistent trend regarding their evolution with increasing distance from the position of the gas injection was found. Comparisons of the trend of time and cross section averaged gas volume fraction along the pipe height with the theoretically expected values were carried out.</p> <p>The influence of the orifice diameter of the gas injection on flow patterns is also discussed in the report.</p>		
19. Keywords Two-phase flow, Gas bubbles, Gas volume fraction distribution, Gas velocity		
20. Publisher		21. Price

Contents

1. Documentation of the experiments	11
1.1 Objective of the new experimental series	11
1.2 Design and realisation of the tests	12
1.2.1 Description of the test facility and construction of the test section	12
1.2.2 Estimation of the boundary conditions for pressure	16
1.2.3 Test procedure	19
1.3 Measurement matrix	20
1.4 Instrumentation	22
1.4.1 Special measurement technique	22
1.4.1.1 Operating mode of the wire-mesh sensor	22
1.4.1.2 Construction of the wire-mesh sensor	23
1.4.2 Operational measurement technique	25
1.4.2.1 Description of the measurement technique	25
1.4.2.2 Calibration	26
1.5 Data evaluation	28
1.5.1 Calibration of the measurement data	28
1.5.2 Void fraction profiles	31
1.5.3 Gas velocities	32
1.5.4 Bubble identification	33
1.5.5 Bubble size distribution and data decomposed according to the bubble size	37
1.6 Estimation of data accuracy	38
1.6.1 Void fraction	38
1.6.2 Bubble diameter	39
1.6.3 Azimuthally averaged gas velocities	40
1.6.4 Errors of the calculated pressures at the gas injection	43
1.7 Accuracy checks on the basis of the superficial gas velocity	46
2. Results	51
2.1 Flow patterns	51
2.1.1 Observed flow patterns	51
2.1.2 Criteria for the definition of flow pattern	51
2.1.3 Dependence of flow pattern on the relative test section height	52
2.1.4 Dependence of the pattern on the diameter of the injection orifices	58
2.1.5 Analysis of the flow pattern for the test series II – IV	59
2.1.6 Summary of the observed flow patterns	64
2.2 Plausibility of the integral void fraction values	66
2.2.1 Drift velocity for the validation of experimental results	66
2.2.2 Calculation of the weighted drift velocities	67
2.2.3 Interpretation of the evolution of the gas volume fraction with increasing L/D	70
2.3 Distribution of the bubble diameter	72
2.3.1 Orifice diameter of the gas injection	72

2.3.2	Average values of the bubble size distribution	74
3.	Conclusions	84
4.	References.....	86
5.	Nomenclature and indexes	90
5.1	Symbols	90
5.2	Indices and abbreviations	91
5.3	Abbreviations	92
5.4	Figures.....	93
5.5	Tables	97
6.	Appendix	98
I.	Characteristic data of the measurement points.....	99
II.	Median and Modal	191
III.	Additional results of the accuracy check (see chapter 1.7).....	195
IV.	Operating data	198
V.	Calibration protocols	216
VI.	Description of the data files available for the air/water test series L12	244

1. Documentation of the experiments

1.1 Objective of the new experimental series

The aim of the experiments presented in this report was to provide a high-quality database for upwards air/water flows in a vertical pipe with a nominal diameter of 200 mm. This database can be used for the development and validation of CFD-codes for two-phase flows. Based on the experiences gained from previous experimental series, continuous high quality and consistency of the data have been basic requirements for these tests. The measurements were now accomplished in such a way that they reflect the development of the two-phase flow along the pipe under constant conditions for the gas injection.

The previous experiments and their results are described in detail by Prasser et al. 2007a. The report also comprises of results for the development of the flow pattern, the behaviour of the boundary between the phases, as well as for the heat and momentum transfer between the phases. For the experiments with variable gas injection, the measurement plane is always at the upper tube end while gas is injected over orifices in the tube wall in different distances of this measurement plane. A disadvantage of the previous experiments was that the pressure at the individual positions of the gas injection varied due to the hydrostatic pressure, because the pressure was almost constant at the measurement plane.

CFD simulations for the evolution of polydisperse bubbly flows have particularly shown that the models of bubbly coalescence and fragmentation must be further optimised (Lucas & Krepper 2007). At relatively small void fractions, the pressure effect on the increase in bubble size can have a larger influence on the evolution of the bubble size distribution than coalescence and fragmentation. Prasser et al. 2007a describe which essential influence the bubble expansion may have on the bubble size distribution basing on experimental and numerical results.

Therefore, in the new series the pressure was kept constant at the respective gas injection. The measurement data represent the development of the flow along the pipe, as it would be observed for an injection at a constant height position with an associated shift of the measurement plane. A further disadvantage of the previous measurement was the non-constant water temperature, which varied between 20 °C and 37 °C during the measurement series. Unlike the previous series, all measurements were now performed at a nearly constant temperature of $T = 30$ °C. The deviations were smaller than 1 K. This is important because the coalescence rate and break-up frequency sensitively depend on the temperature caused by the effect of the surface tension. In addition, the number of the measured combinations of air and water volume flow rates was clearly increased in comparison to former measurements.

In addition to the documentation of the experiments, the report is extensively devoted to cross-check of the plausibility of the data against each other. This concerns the continuous development of time averaged profiles and the bubble size distribution with increasing height scale L/D as well as the comparison of the gas volume flow obtained from measurement data with the setting data. This enables a global error assessment and shows the dependence of the precision of the measurements on the

respective flow conditions. In the second chapter, an interpretation of the integral void fraction derived from the measurements, the bubble size distributions, and the middle bubble size is presented.

1.2 Design and realisation of the tests

1.2.1 Description of the test facility and construction of the test section

As the experiments conducted in the previous project “Construction and execution of experiments at the multi purpose thermal hydraulic test facility TOPFLOW for generic investigations of two-phase flows and the development and validation of CFD codes“, the measurements for this extensive test series were carried out at the **Transient two Phase FLOW** test facility (TOPFLOW) of the Institute of Safety Research at the Forschungszentrum Dresden-Rossendorf. The construction and function of this installation are described in detail by Schaffrath et al. 2001 and Beyer et al. 2004. For this reason, this report only considers systems and installation parts which are relevant to the execution of this test series.

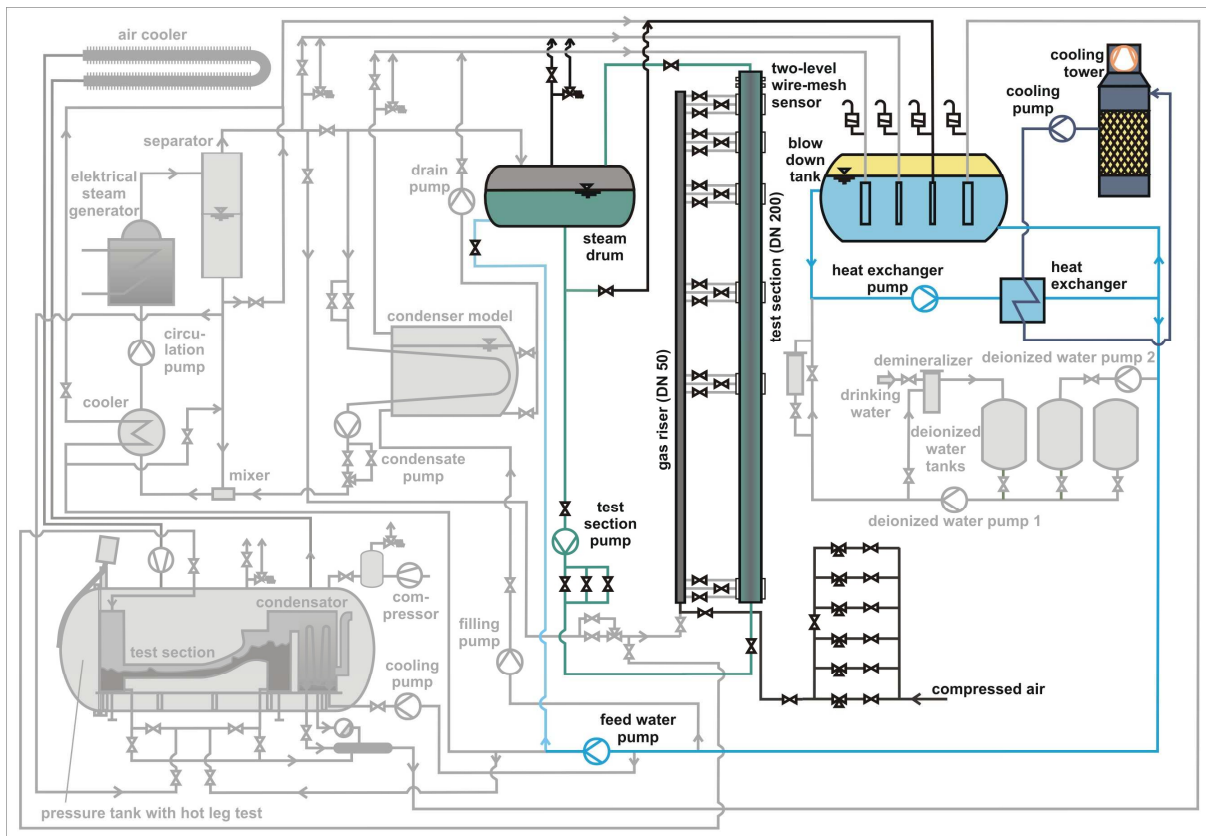


Fig. 1-1 General scheme of the thermal hydraulic test facility TOPFLOW; test section circuit and compressed air system are highlighted by colour

This particularly concerns the test section circuit and the compressed air system emphasised by colour in Fig. 1-1. In addition to these facility components, elements of the blow down and cooling system are marked, which were necessary for the control of the temperature in the test section.

To analyse the evolution of the flow and especially the bubble size distribution and gas fraction profiles, a particular design of the vertical test section DN 200 with an inner diameter of 195.3 mm was used. It is the so-called variable gas injection, which has been built and installed during the previous project.

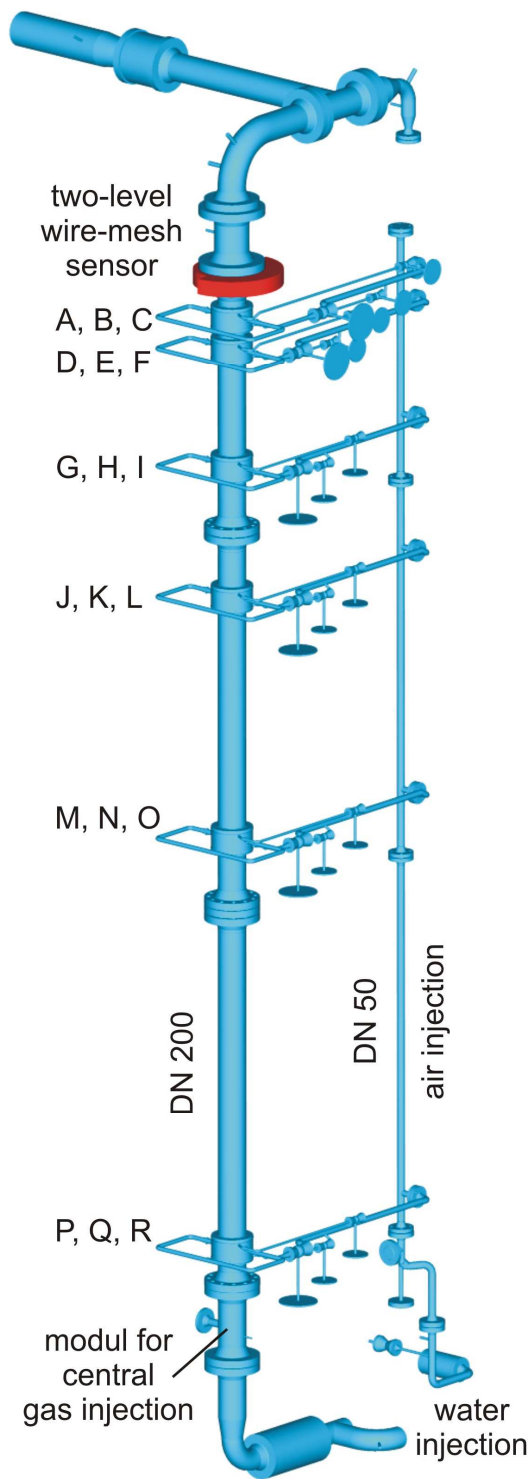


Fig. 1-2 Vertical test section of the TOPFLOW facility with variable gas injection system (DN 200)

Fig. 1-2 shows the geometrical construction of the variable gas injection with six almost logarithmic injection modules distributed over the total height. Each module (Fig. 1-3) consists of three chambers. Gas is injected through orifices into the pipe wall. This gas injection offers the advantage that the two-phase flow can rise smoothly to the measurement plane, without being influenced by the feeder within the tube in other height positions.

Two of the three chambers (the uppermost and the lowest) are provided with 72×1 mm orifices. The middle chambers have 32×4 mm orifices. For rotation-symmetric gas injection, all orifices per chambers are equally distributed over the circumference of the pipe. This construction offers the possibility to analyse the influence of different primarily bubble diameters on the development of the flow.

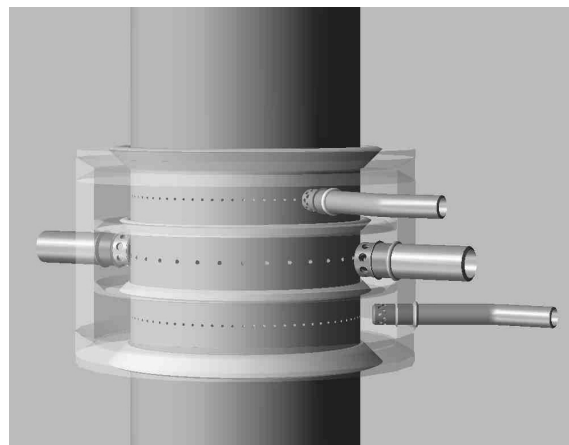


Fig. 1-3 Injection module of the variable gas injection

The chambers are connected with a gas injection pipe and the compressed air system (Fig. 1-1) can be operated separately. The supply of the liquid phase is done from the bottom of the test section by means of an isolating valve and a 90° bend. During the experiments, a module for central gas injection has been mounted at the lower end of the test section (Fig. 1-2). However, it was not employed in this test series. As a result of the large distance to the measurement plane, the influence of this component on the measured flow properties can be neglected. A description of the construction of this feeder is given by Prasser et al. 2007a.

For these experiments, the measurement plane was always situated at the upper end of the test section (Fig. 1-2). A two level low temperature wire-mesh sensor was used. It is described in detail in chapter 1.4.1. Table 1 lists the vertical distances between the individual gas injections and the first measurement plane of the wire-mesh sensor located in direction of flow.

Table 1: Absolute and relative heights at the test section variable gas injection

injection chamber	position of height	diameter of the inlet orifice [mm]	injection length [mm]	L/D ratio
1	A	1 mm	221	1.1
1	B	4 mm	278	1.4
1	C	1 mm	335	1.7
2	D	1 mm	494	2.5
2	E	4 mm	551	2.8
2	F	1 mm	608	3.1
3	G	1 mm	1438	7.4
3	H	4 mm	1495	7.7
3	I	1 mm	1552	7.9
4	J	1 mm	2481	12.7
4	K	4 mm	2538	13.0
4	L	1 mm	2595	13.3
5	M	1 mm	4417	22.6
5	N	4 mm	4474	22.9
5	O	1 mm	4531	23.2
6	P	1 mm	7688	39.4
6	Q	4 mm	7745	39.7
6	R	1 mm	7802	39.9

The two-phase mixture flows downstream of the wire-mesh sensors through a 500 mm long straight tube section, through a 90° bend, and finally via a T-fitting into the steam drum, in which the phase separation takes place (Fig. 1-1 and Fig. 1-2).

1.2.2 Estimation of the boundary conditions for pressure

As already mentioned, one aim of this test series was to investigate as exactly as possible the evolution of a two-phase flow along the tube height. That would be the case if the gas injection always occurs at the same position and the measurement would be carried out in different distances (= height positions). Due to the fact that the height of the injection is varied during the gas injection, while the position of the measurement plane remains constant, a pressure correction is required. Therefore, a constant pressure of 0.25 MPa (a) was defined as target pressure at the location of the gas injection respectively used. Fig. 1-4 shows a cut through the variable gas injection test section and the positions of the temperature (T14-08), as well as the pressure measurement point (PI4-07) located above the wire-mesh sensor. The distance between these measurement positions and the lowest of the wire-mesh sensor is equal to 0.87 m. There are no measurements of the pressure difference between the individual injection positions and the measurement plane available at this test section.

In order to guarantee constant boundary conditions at the gas injection position, the given two-phase pressure drop along the test section was determined for all measured combinations of superficial gas and liquid velocities. The individual injection heights were thereby considered. In the result, the adjustable pressure at the position of the measurement can be derived. The calculation of the two-phase pressure drop considers the hydrostatic pressure drop Δp_H , as well as the pressure drop of friction Δp_R . The acceleration pressure drop was neglected due to its minimal share (< 1 %) of the total pressure drop.

The hydrostatic pressure drop is calculated according to:

$$\Delta p_H = \rho_F \cdot g \cdot \Delta L \quad (1.1)$$

Here g is the acceleration due to gravity (9.81 m/s²), ΔL the distance between the gas injection and pressure measurement point. The density of two-phase mixture is calculated with equation (1.2):

$$\rho_F = \varepsilon \cdot \rho_G + (1 - \varepsilon) \cdot \rho_W \quad (1.2)$$

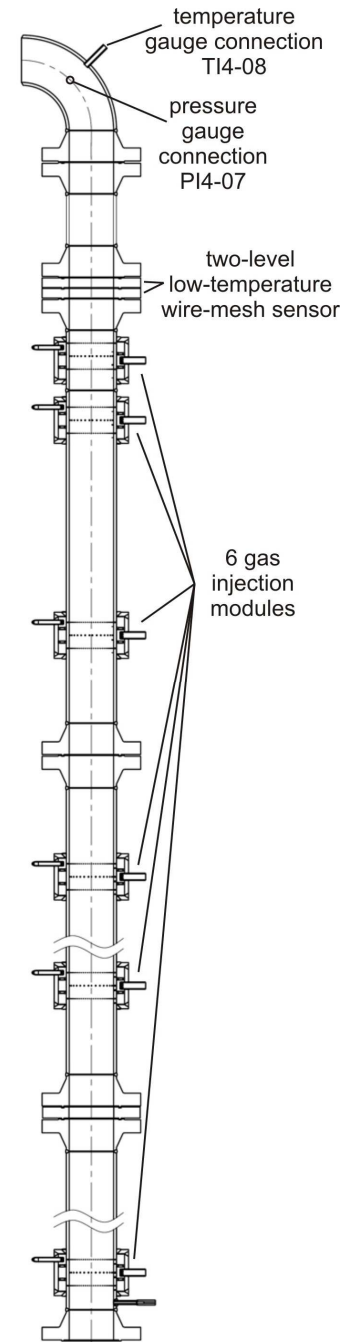


Fig. 1-4 Variable gas injection with positions of pressure and temperature measurement points

In this equation, ε stands for the volumetric gas fraction, ρ_G and ρ_W are the densities for air and water, respectively. The material properties were defined basing on the database IAPWS–IF97 (Wagner et al. 2000). The volumetric void fraction was determined by the equation (1.3).

$$\varepsilon = \frac{J_G}{J_G + J_W + \bar{U}_D} \quad (1.3)$$

Equation (1.3) uses the superficial velocities of the two-phases and the averaged drift velocity \bar{U}_D . \bar{U}_D is still unknown before the experiments. For this reason, a constant value of 0.25 m/s was used in the calculation. This value is a good approximation for the drift velocity of bubbles within a diameter range from 5 to 9 mm, in which the maximum of the bubble size distribution for most matrix points of this test series lies. The uncertainty, which results from this assumption, will be analysed in the chapter uncertainty analysis (chapter 1.6.4).

The method of Lockhart/Martinelli (see Huhn et al. 1975) was used to detect the two-phase friction pressure drop. It bases on a slip-model. First, the friction pressure drop of the individual phases involved in the flow is determined assuming that the phases flow separately in the pipe, i.e. the phases fill out the total tubing cross-section. With the help of the correcting function Φ – also referred to as “two-phase multiplier” – the two-phase friction pressure drop is calculated:

$$\left(\frac{\Delta p}{\Delta L}\right)_F = \Phi_W^2 \left(\frac{\Delta p}{\Delta L}\right)_W = \Phi_G^2 \left(\frac{\Delta p}{\Delta L}\right)_G \quad (1.4)$$

Equation (1.4) supplies the ratio of the function Φ_G to Φ_W , dependent on the quotient of the friction pressure drops of both phases, which is called LOCKHART/MARTINELLI - parameter:

$$X_{LM} = \left[\frac{(\Delta p/\Delta L)_W}{(\Delta p/\Delta L)_G} \right]^{0.5} = \frac{\Phi_G}{\Phi_W} \quad (1.5)$$

For the investigation of the friction pressure drop of the single-phase p, the Reynolds numbers are defined according to the following equation (1.6):

$$Re_p = \frac{J_p \cdot d_i}{\nu_p} \quad (1.6)$$

J is the superficial velocity, d_i the inner diameter of the pipe (0.195 m) and ν the kinematic viscosity of the single-phases. Considering the test matrix (Table 2), for the resulting values are for the water phase range $10^5 < Re_W < 4 \cdot 10^6$ and for the gaseous phase $75 < Re_A < 10^6$, respectively. For laminar flows ($Re < 2320$), the friction in pipes value is calculated by the equation (1.7) (Matek et al. 2000). For turbulent flows, the tubing roughness k (0.1 mm) must also be considered, so that λ_p was used independently from the Reynolds number according to the equation (1.8) (VDI 1988a):

$$\lambda_p = \frac{64}{\text{Re}_p} \quad (1.7)$$

$$\lambda_p = \frac{1}{[2 \cdot \lg(d_i/k) + 1,14]^2} \quad (1.8)$$

Using the friction in pipes value λ_p , the friction pressure drop of the individual phase p is calculated according to:

$$\Delta p_p = \lambda_p \cdot \frac{\rho_p}{2} \cdot J_p^2 \cdot \frac{\Delta L}{d_i} \quad (1.9)$$

With the pressure drop of the individual phases Δp_p , the pressure drop gradients $(\Delta p/\Delta L)_G$ and $(\Delta p/\Delta L)_W$ can be calculated, as well as with the help of the equation (1.5) X_{LM} . For the determination of the dependency of the functions Φ_W and Φ_G with the parameter X_{LM} , the WALLIS procedure was selected (Huhn et al. 1975). This procedure also bases on the slip-model and assumes that both phases flow in separate cylinders, whose sum of cross-section areas amounts the cross-section of the pipe. The pressure drop in each cylinder equals to the pressure drop of the total flow and is composed of the single-phase flow and averaged velocity values.

The general solution is:

$$(1/\Phi_G^2)^{1/n} + (1/\Phi_W^2)^{1/n} = 1 \quad (1.10)$$

From this follows with equation (1.5):

$$\Phi_G^2 = [1 + X_{LM}^{2/n}]^n \quad X_{LM} < 1 \quad (1.11)$$

$$\Phi_W^2 = [1 + 1/X_{LM}^{2/n}]^n \quad X_{LM} > 1 \quad (1.12)$$

Whereby, the parameter n depends on the flowing state:

$n = 3.5$	$\text{Re}_W > 10^3, \text{Re}_G < 10^3$	The Reynolds numbers of the individual phases were determined in accordance with equation (1.6).
$n = 4$	$\text{Re}_W > 10^3, \text{Re}_G > 10^3$	

Results of these calculations are the two-phase pressure drops in the test section for all measured combinations of the superficial velocity for air and water, which consist of the hydrostatic and the friction pressure drops. The fraction of the friction pressure drop on the total pressure drop varies from approx. 2 % for small superficial velocities (measurement point 041, see Table 2) up to 23 % at measurement point 184.

Due to the fact that the position of the pressure measurement (PI4-07) is located in a bend downflow the wire-mesh sensors, half of the pressure drop in the bend Δp_B was considered for the determination of the total pressure drop. For this reason, the

pressure drop for the individual phases is calculated by the equation (1.13) (VDI 1988b):

$$\Delta p_{B,p} = k_{B,p} \cdot \frac{\rho_p}{2} \cdot J_p^2 \quad (1.13)$$

The coefficient $k_{B,p}$ contains both the friction in pipes factor λ_p (by equations (1.7) and (1.8)) the drag coefficient $\zeta_{B,p}$. The drag coefficient considers the reverse figure, the Reynolds number of the bends and the roughness factor according to VDI 1988b. After this step, the estimation of the two-phase pressure drop can be performed over the bend, likewise after the methodology by LOCKHART/MARTINELLI and WALLIS.

The pressure values determined in this way are listed in the test logs, as gauge pressure in the column "pressure at the GS(g) PI4-07 [kPa]", which are found in the appendix IV. The results were used as set values for the experiments.

1.2.3 Test procedure

The variable gas injection is implemented into the test section circuit of TOPFLOW (Fig. 1-1) in the same way as during the previous project. During each experiment, water is fed from the steam drum via the test section pump through the vertical test section. The control of the water mass flow was done using three parallel switched regulating valves and the associated automatic control loops for the ranges 0 - 0.5 kg/s; 0.5 - 5 kg/s and 4.75 - 50 kg/s. For the experiments, water mass flow rates between 1.2 and 48 kg/s were applied. To guarantee the temperature boundary conditions ($30 \text{ }^\circ\text{C} \pm 1 \text{ K}$), before starting the measurements the temperature of the water contained in the test section circuit was increased by the energy entry of the test section pump up to $30 \text{ }^\circ\text{C}$. Since the temperature of the water in the section circuit further increases during pump operation, feed water with a temperature of approx. $20 \text{ }^\circ\text{C}$ was pumped from the blow down tank (see Fig. 1-1) into the steam drum via the feed water pump. Furthermore, water was returned from the steam drum into the blow down tank via the outlet.

After reaching the envisaged temperature range, the water mass flow was adjusted. Compressed air was injected into the test section circuit in order to approximately achieve the necessary pressure at PI4-07 downstream the wire-mesh sensor. Afterwards the volumetric airflow can be reduced to its set value. In the following, the pressure value can be adjusted to the set value by varying the blow down flow rate from the steam drum.

After setting all technical boundary conditions, the measurement can be accomplished. For this, the wire-mesh sensor electronics have to be prepared for the measurement and the flow structure has to be checked by means of on-line visualisation. After fulfilling these conditions, the measurement is done off-line. In order to be able to determine characteristic flow parameters, such as void fraction profile, velocity profile and bubble size distribution from the measured data, the time for each single measurement was fixed for all experiments of this test series at 10 s. The measurement frequency is kept at 2.5 kHz. Directly after the measurement, the quality of the data can be checked by visualisation on the measurement computer.

In parallel to the recording of the volumetric void fraction with the wire-mesh sensor, all available operational data of the test section circuit are stored. The following parameters belong to this measurement series: water mass flows, volumetric air flow rates, temperature and pressure above the wire-mesh sensor. For the synchronisation of the operational data with the wire-mesh sensor data, an impulse is produced by the process control system when the measurement is starting. It sets a signal for the time of the measurement in the data acquisition system and simultaneously starts the measurement procedure in the electronic unit of the wire-mesh sensor. This allows to select exactly the stored operational data, which correspond to the measurement interval. Afterwards, these values are averaged arithmetically and stored in the tables given in appendix IV - column operational data.

1.3 Measurement matrix

Experiments on two-phase flows are conducted by the department "Experimental Thermal Fluid Dynamics" of the FZD for many years. In order to simplify a comparison of the individual measurements with each other, a general test matrix was compiled. However, for this comparison of different measurement series, the differences of the pressure boundary conditions have to be considered. Contrary to the described measurement series where a constant pressure (0.25 MPa(a)) at the gas injection was kept, earlier experiments had been performed with an ambient pressure in the steam drum (see Fig. 1-1).

Table 2 shows the FZD-Matrix composed of 231 measurement points. Each matrix point characterises a combination of superficial velocities for the liquid and gaseous phase. The range of superficial velocities was divided logarithmically and is increased to approximately 4 m/s for the liquid phase and to 19 m/s for the gaseous phase. Therefore, all important flow patterns (bubbly, slug, churn-turbulent and annular flow) are realised. In Table 2 the measurement points selected for the **present test series (pressure at the gas injection: 0.25 MPa(a); Temperature of the two-phase mixture: 30 °C ± 1 K)** are highlighted. They can be grouped in four lines at which the superficial velocity of the liquid or gaseous phase remains constant in two rows, respectively. This selection has the advantage that the flow phenomena are only dependent on one variable parameter, which can be evaluated regarding its effect on the flow properties, e.g. two "water rows", can be compared with each other.

For investigations on the development of the two-phase flow over the height of the test section, all levels (A-R) shown in table 1 and Fig. 1-2, were measured for any point of series < 149 (table 2), respectively. The maximum possible gas flow rate, which can be injected through the injection chambers (see Fig. 1-3) with a diameter of 1 mm into the pipe, is limited by number and diameter of the orifices. The following restriction on the measurement points ≥ 149 result from this: At the points 149, 151, 160 and 162 all heights with 4 mm of injections were measured (B, E, H, K, N, Q) and both injection chambers with 1 mm orifices were operated parallel.

Table 2: General experimental matrix of the FZD for vertical pipe flows; test points of the current series are highlighted

		Superficial gas velocity J_G [m/s]																				
		0.0025	0.004	0.0062	0.0096	0.0151	0.0235	0.0368	0.0574	0.0898	0.14	0.219	0.342	0.534	0.835	1.305	2.038	3.185	4.975	7.772	12.14	18.97
Superficial water velocity J_L [m/s]	4.047	011	022	033	044	055	066	077	088	099	110	121	132	143	154	165	176	187	198	209	220	231
	2.554	010	021	032	043	054	065	076	087	098	109	120	131	142	153	164	175	186	197	208	219	230
	1.611	009	020	031	042	053	064	075	086	097	108	119	130	141	152	163	174	185	196	207	218	229
	1.017	008	019	030	041	052	063	074	085	096	107	118	129	140	151	162	173	184	195	206	217	228
	0.641	007	018	029	040	051	062	073	084	095	106	117	128	139	150	161	172	183	194	205	216	227
	0.405	006	017	028	039	050	061	072	083	094	105	116	127	138	149	160	171	182	193	204	215	226
	0.255	005	016	027	038	049	060	071	082	093	104	115	126	137	148	159	170	181	192	203	214	225
	0.161	004	015	026	037	048	059	070	081	092	103	114	125	136	147	158	169	180	191	202	213	224
	0.102	003	014	025	036	047	058	069	080	091	102	113	124	135	146	157	168	179	190	201	212	223
	0.0641	002	013	024	035	046	057	068	079	090	101	112	123	134	145	156	167	178	189	200	211	222
	0.0405	001	012	023	034	045	056	067	078	089	100	111	122	133	144	155	166	177	188	199	210	221

- test series I $J_W = 1.017$ m/s
- test series II $J_W = 0.405$ m/s
- test series III $J_G = 0.219$ m/s
- test series IV $J_G = 0.0096$ m/s

The data of these measurements were marked in the appropriate files by the corresponding combination of letters for both chambers of one module (AC, DF, GI, JL, MO, PR). For the measurement points **171**, **173**, **182**, **184**, the cross-section of both 1 mm injection chambers was not sufficient for the higher gas flow rate. For these points only data of the 4 mm injections are available.

The measurements described in this report were conducted between January 11th and June 29th, 2007. The tables in the appendix IV provide the operational data, water mass flow rate, volumetric airflow rate, pressure and temperature boundary conditions. Also the convention for the data files names can be found in appendix VI. The volumetric airflow rates (V_{GN} [nm³/h]), which were adjusted at the air controllers, were calculated from the superficial gas velocities given in table 2 according to:

$$V_{GN} = \frac{p_{in} \cdot T_N \cdot J_{G,in} \cdot \pi \cdot d_i^2}{4 \cdot T_{in} \cdot p_N} \quad (1.14)$$

p_{in} and T_{in} are the pressure (0.25 MPa(a)) and temperature (303.15 K) at the gas injection position, p_N and T_N , the normal pressure (0.1013 MPa(a)) and standard temperature (273.15 K) and $J_{G,in}$ is the superficial gas velocity at the injection position (according to test matrix - table 2).

1.4 Instrumentation

1.4.1 Special measurement technique

1.4.1.1 Operating mode of the wire-mesh sensor

Electrode-mesh sensors are based on the measurement of the electrical conductivity of a two-phase mixture. In the case of a gas/liquid two-phase flow, the liquid phase (deionised water) is slightly conducting, while the gas (air) phase is practically an ideal insulator. The sensor consists of two grids of parallel isolated wires, which span over the measurement cross-section. The wires of both planes cross under an angle of 90°. At the crossing point of the wires, the measurement of conductivity takes place. Fig. 1-5 shows schematically a wire-mesh sensor with 4 x 4 wire electrodes and the most important electronic components.

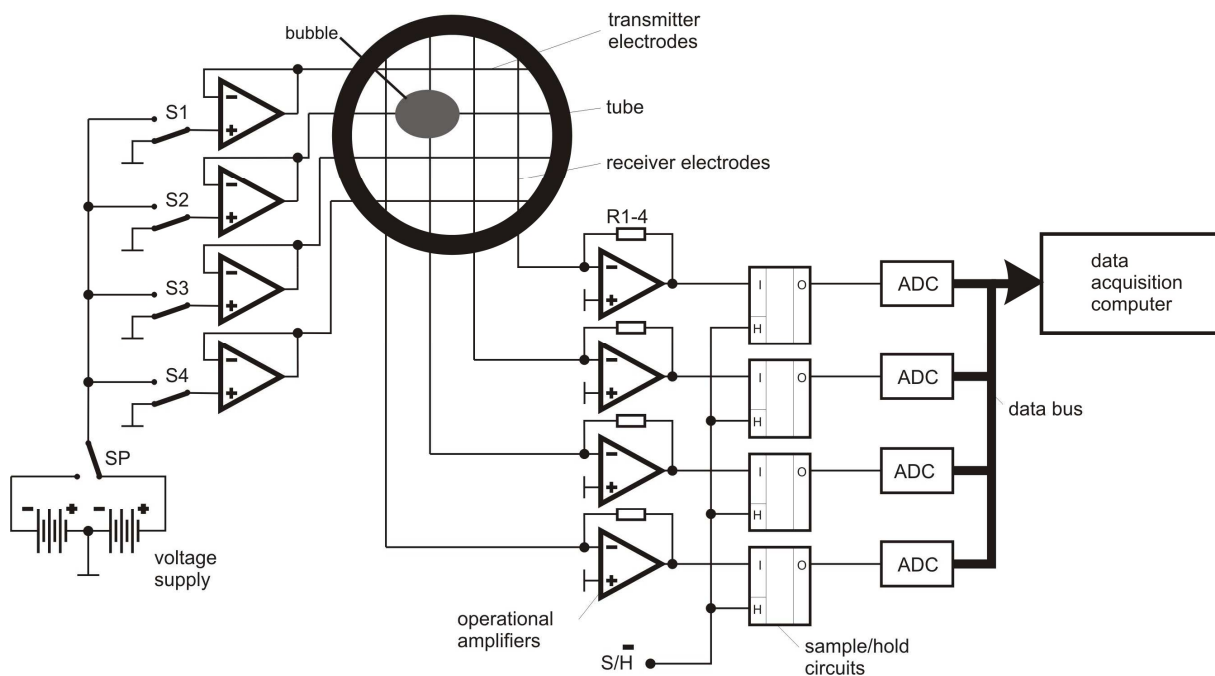


Fig. 1-5 Measurement principle of the wire-mesh sensor, simplified scheme of a wire-mesh sensor with 4 x 4 electrodes

During the signal acquisition, one plane of electrodes is used as transmitter, the other one as receiver. The transmitter electrodes are activated successively by supplying them with voltage pulses. For this reason, a current flows at a receiver wire, which is a measure of the conductivity of the fluid in the corresponding control volume around the crossing point of the two wires. The currents of all receiver wires are scanned simultaneously, converted into voltage levels for better signal processing and digitised into 12 bits values (resolution: 4,096 conditions). This process is repeated for all transmission electrodes. After activating the last transmitter wire, the voltage signals for a complete two-dimensional measurement cross-section are stored by the wire-mesh sensor electronics.

In order to avoid polarisation effects at the electrodes, the voltage pulse, with which the transmitter electrodes are subjected, divides into a positive and a negative half wave. Currents are measured for both voltage pulses and their difference is processed in the electronic unit.

The selected measurement principle offers the advantage that the measured data do not have to be reconstructed with complex tomography, but after a calibration, they can be directly used as locally and temporally high-resolution information on the volumetric gas content. In the case of a spatial resolution of 64 x 64 measurement points, the electronic unit enables measurement frequencies up to 2.5 kHz. A detailed description of structure and function of the wire-mesh sensor is contained in Prasser et al. 1998 and 2000a.

A disadvantage of the wire-mesh sensor is the influence on the flow due to the usage of an invasive measurement procedure. This disadvantage hardly plays any role in the measurement with one sensor, because the gas content is detected in the moment in which the sensor wire affects the structure of the phase boundary. The disadvantage, however, is when considering to use two sensors directly installed one behind the other, or using a two-level sensor, that are used for the determination of local gas velocities. More information on the measurement accuracy of this kind of sensors and comparisons with alternative measurement procedures are summarised in chapter 1.6.

Wire-mesh sensors have been employed successfully for more than 15 years both in the FZD and internationally. Their task is to measure gas contents in two-phase flows at pressures up to 7 MPa and temperatures to 290 °C. The current reachable maximum temporal resolution amounts 0.1 ms. The minimum wire distance currently realised is 0.5 x 0.5 mm.

1.4.1.2 Construction of the wire-mesh sensor

The described tests were accomplished with air/water flows according to table 2 at a water temperature of 30 °C and pressures at the sensor smaller than 0.25 MPa(a). The requirements on the construction of the wire-mesh sensor result from these boundary conditions and the operational principle.

In the present case, a two-level low temperature wire-mesh sensor was employed. Each measuring plane is composed of 64 x 64 wires. It consists of two printed circuit boards (material thickness: 2.5 mm). Both of them are equipped with pre-stressed wire electrodes being soldered at a 90° angle to each other on the upper and lower surface. The wires have a lateral distance of 3 mm. In order to make the mechanical sealing of the sensor possible, the wire electrodes with a diameter of 0.125 mm were mounted in approx. 0.3 mm deeply in-milled slots on the printed circuit board. As a result of this construction form, the distance between the two grid levels arises to approx. 2 mm.

The prepared printed circuit boards are installed between two flanges and the intermediate ring (see Fig. 1-6, detail z). The distance of 40.5 mm between both printed circuit boards, and thus between the measurement planes results from the thickness of the intermediate ring, as well as from the pressed silicone seals. In order

to reduce the weight of the sensor, the intermediate ring is partially made of aluminium. Four plastic spacer rings are used in the sensor, in order to limit the contact pressure on the silicone sealing rings and, in the case of a repeated assembling (Fig. 1-11), to ensure a reproducible distance of the planes of measurement.

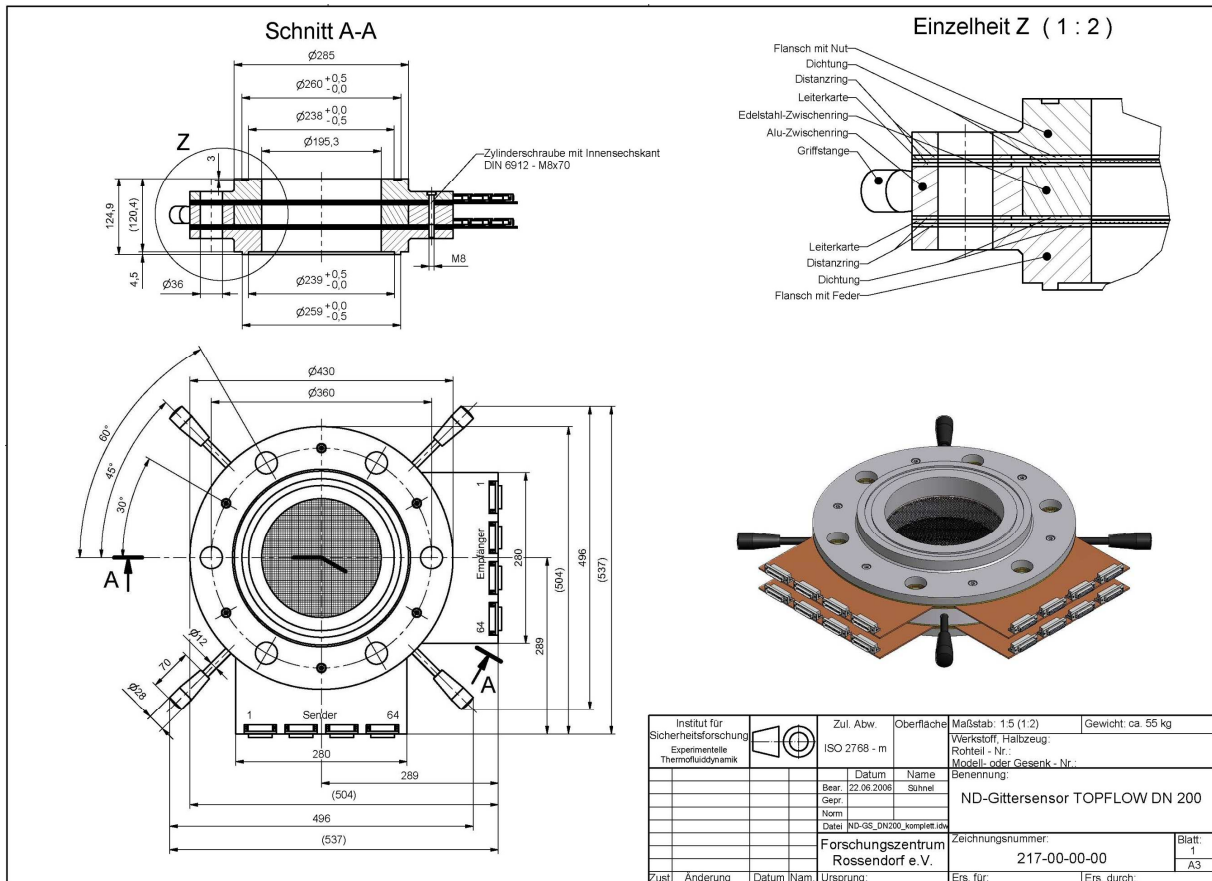


Fig. 1-6 Construction design of the double low temperature wire-mesh sensor

For the electrical connection of the wire electrodes, electrical conductors are connected from the soldered point of the wires to the sockets at the edge of the circuit board (Fig. 1-6), to those preamplifiers are joined. The preamplifiers are connected with the electronic unit via screened cable.

Pietruske 2007 contains further detailed information on the construction of wire-mesh sensors. Details about the construction of measurement electronics are described in Prasser et al. 2000a.

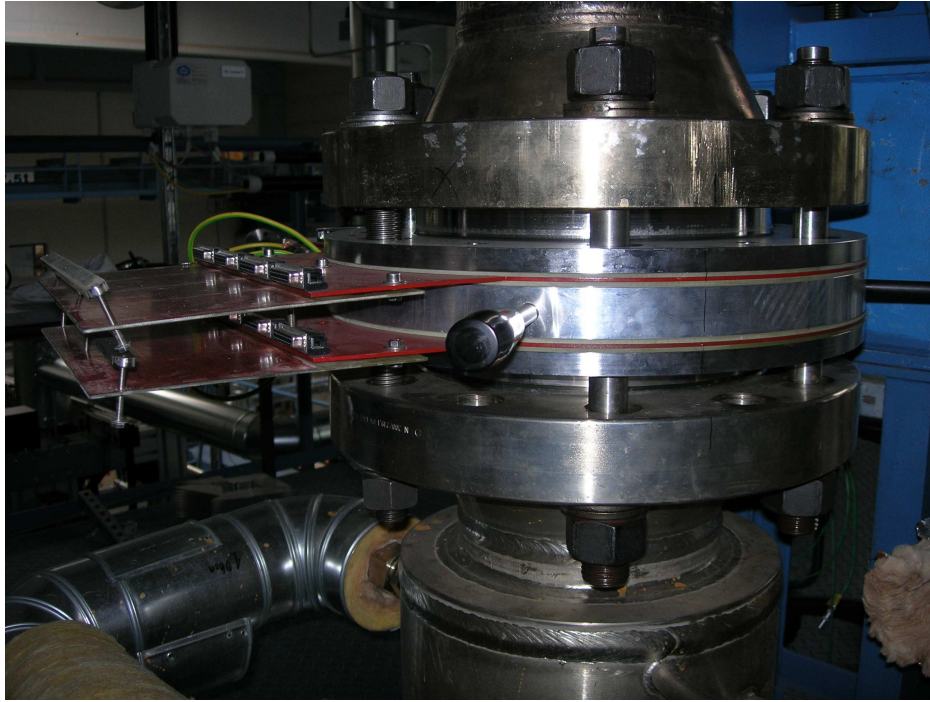


Fig. 1-7 Installation of the sensor in the upper range of the test section

1.4.2 Operational measurement technique

1.4.2.1 Description of the measurement technique

Apart from the appropriate special measurement technique, the exact knowledge of the boundary conditions is important for a high-quality execution and evaluation of the experiments.

From the extensive measurement technique at the test facility TOPFLOW, only the parts being relevant to this test series are regarded in this report.

Fig. 1-8 shows the positions of important measurement positions at the test section circuit of TOPFLOW. The used identification labels have the following meaning: The first letter describes the physical value (F - flow, T - temperature, P - pressure). The second and third letter classifies the type (I - indication, C - controller), respectively. The following number marks the measurement point, whereby the first number indicates the belonging to a system or circuit (4 - test section circuit). All relevant operational data for the accomplished experiments are registered in the tables in the appendix IV.

The two water mass flow controllers FIC4-01 and FIC4-02 are measurement chains prefabricated by the manufacturer. The relevant transmitters determine the density of the liquid from the absolute pressure and the temperature. After this, they calculate the mass flow by means of the density and the differential pressure (measured over a venturi nozzle) and the flow geometry. The regulation of the necessary water mass flow takes place with the test section pump controlled by a frequency inverter. The operating points for this are adjusted with the help of the regulating valves arranged directly after the measurement systems. The parallel controllers FIC4-10 -FIC4-13

are used for the supply of the volumetric airflow. These are thermal mass flow meters and controllers for gases of the type EL-FLOW (FIC4-12 and 13) and IN FLOW (FIC4-10 and 11) delivered by the company Bronkhorst.

For the measurement of the air mass flow, a defined partial flow is separated from the total airflow after a turbulence filter and is led through the measurement cell. In the measurement cell, a heater element is situated between two measurement resistors, which are arranged successively in direction of flow. The adjusted temperature difference is a function of the air mass flow flowing through the measurement cell. In order to determine the volumetric airflow from the air mass flow, the density is used again, which can be detected from the pressure and the temperature before the heating. The regulation of the volumetric air flow takes place with the FIC4-11 to 13 by means of measurement cells arranged directly after the magnet valves. A downstream pneumatic operated control valve observes very large airflows (FIC4-10).

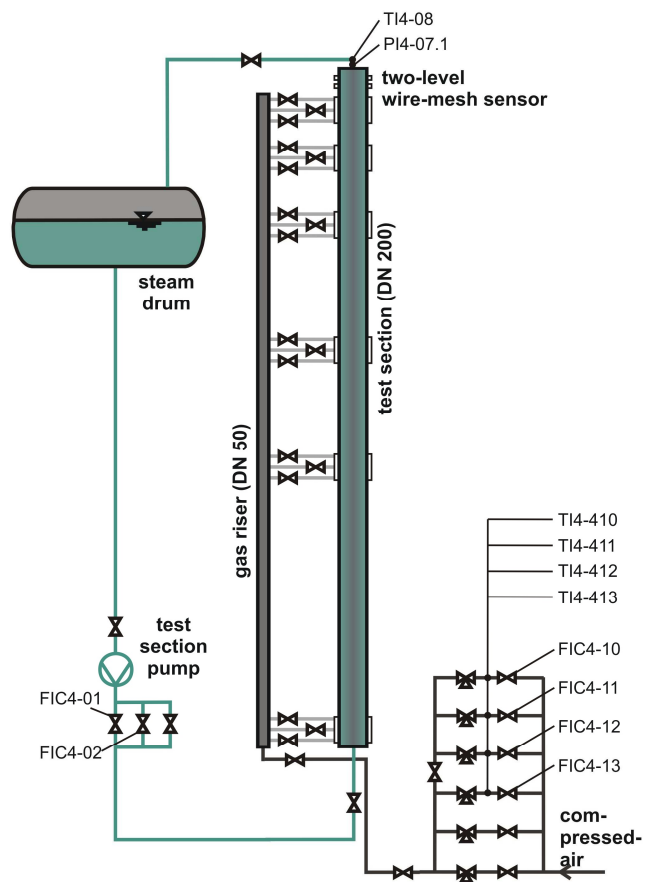


Fig. 1-8 Positions of the relevant measurement points at the test section circuit.

In order to avoid leakage rates from all of the six parallel switched air controllers into the test section circuit, each three-way valve blocks the inactive control loops from the test section circuit and drains possible leakage rates into the TOPFLOW building. The compressed air regulators of TOPFLOW, can stationary be vary the flow rates up to 750 nm³/h.

The measurement of the pressure downstream the wire-mesh sensor is done using a pressure transmitter of the type Smar LD 301, which is adjusted to a measurement range from 0 to 250 kPa. The temperatures after the air controllers and after the wire-mesh sensor are detected with thermocouples of the type K.

1.4.2.2 Calibration

For the maintenance of the accuracy of the measurement channels, it is necessary to calibrate the transducer and electronic components relevant to the test series as far as this is possible. An overview of the results of the calibration for the measurement technique represented in Fig. 1-8 is summarised in Table 3.

Table 3: Measurement devices in the test section circuit, which were used during the experiments and for the data evaluation of the air/water series of tests L12

transducer	range	range of calibration	date of calibration	max. error	comments
FIC4-01	4.75 - 50 kg/s		21.05.02	1 %	5 years guarantee from the date of fabrication
FIC4-02	0.5 - 5 kg/s		21.05.02	1 %	
FIC4-10	500 - 1000 nm ³ /h	400 - 950 nm ³ /h	02.10.06	0.83 %	Bronkhorst (of the measured value)
FIC4-11	50 - 500 nm ³ /h	50 - 450 nm ³ /h	04.10.06	6.66 %	Bronkhorst (of the measured value)
FIC4-12	5 - 50 nm ³ /h	5 - 50 nm ³ /h	15.09.06	1.58 %	Bronkhorst (of the measured value)
FIC4-13	0.5 - 5 nm ³ /h	0.5 - 5 nm ³ /h	10.10.06	1.9 %	Bronkhorst (of the measured value)
PI4-07.1	0 - 250 kPa(g)	0 - 250 kPa	07.02.07	1.5 %	Smar LD 301(of the measured value)
TI4-08	-270 - 1200 °C	50 – 300 °C	08.11.06	0.5 K	TE Typ K
TI4-410	-270 - 1200 °C	35 – 50 °C	16.11.06	0.0 K	TE Typ K
TI4-411	-270 - 1200 °C	35 – 50 °C	16.11.06	0.0 K	TE Typ K
TI4-412	-270 - 1200 °C	35 – 50 °C	16.11.06	0.1 K	TE Typ K
TI4-413	-270 - 1200 °C	35 – 50 °C	16.11.06	0.1 K	TE Typ K

For the mass flow, controllers FIC4-01 and FIC4-02 are guaranteed by the fabricator for 5 years after the delivery that the error does not exceed 1 % of the measured value. The manufacture date of the devices used at TOPFLOW was the 21st May 2002. A calibration of these devices directly at the TOPFLOW facility is not possible.

The polynomial calibration of the volumetric airflow controllers (FIC4-10 - FIC4-13) took place by using the data indicated in Table 3 at the manufacturer (FIC4-10 - FIC4-12) and at the company Wagner (FIC4-13), respectively.

The pressure transducer PI4-07.1 was calibrated with a UNOMAT MCX/1910 being calibrated annually (last inspection: 20.06.06) at the company Druck Lfd. The calibration is done by adjusting several pressure values within the calibration range, whereby, the points are checked both at the increment and decrement of the pressure. Afterwards the output signals are compared with the set values and, if necessary, the transducer is adjusted accordingly.

The thermocouples were examined with a metal block calibrator of the type Jupiter 650SN. For the comparison of the temperature indications, a platinum thermocouple comes into operation. Both reference devices were controlled on 10th October 2006 for the last time by the company Klasmeier Kalibrier- und Messtechnik GmbH. In case of the deviations from the set values it is possible to compensate the deviation at the digital/analogue converters. The maximum deviation within the calibration range after the compensation is indicated in Table 3.

Technical parameters of the measurement technique and the detailed results of the examinations, as well as the documents on the calibration devices are added in the calibration protocols in the appendix V.

1.5 Data evaluation

After completion of the experiments, the measurement data are available as compressed binary files. In such a file, 25,000 cross-section data fields, the so-called “frames”, are stored. Each of these frames contains 64 x 64 digitised voltage signals in special 12 bits dimensions. In the following chapters, the individual steps are described, which are necessary for the numerical evaluation of the raw data. The structure of all file types described in this chapter is specified in more detail in the appendix VI.

1.5.1 Calibration of the measurement data

The purpose of this procedure is the conversion of the voltage signals from the data files obtained from the measurements into volumetric gas fractions. For this, two procedures are used: On the one hand, the measured values of the two-phase flow can be weighted with calibration values of a pure water flow, since, as already mentioned in chapter 1.4.1.1, the electrical conductivity of air is negligibly small:

$$\varepsilon = \frac{U_W - U_{\text{meas}}}{U_W} = 1 - \frac{U_{\text{meas}}}{U_W} \quad (1.15)$$

ε - the volumetric void fraction, U_W the voltage signal of the calibration value (water) and U_{meas} is the voltage signal of the measured value.

For the determination of the calibration values for the individual mesh points of the sensor, the data in the calibration file are checked to be free of gas. Afterwards, the signals of the usable frames are averaged. This method offers the advantage that it can be applied to all measurement data independently from the superficial gas velocity. The disadvantage consists of the fact that calibration files must be obtained, which is usually done with some temporal shift to the actual measurements. Therefore, the operating conditions (pressure, temperature, conductivity of the water) can vary and increase the error for the determination of the volumetric void fraction.

On the other hand, there is the possibility to do a histogram calibration. With this method, for each mesh point of the sensor, histograms of the digitised voltage signals of all frames of a measurement file are numerically analysed. The histograms usually have two maxima. One maximum lying close to the zero value characterises gas value, a second maximum the water value. This second maximum is used as calibration value for the current mesh point. Fig. 1-9 represents exemplarily a histogram for the test point 140.

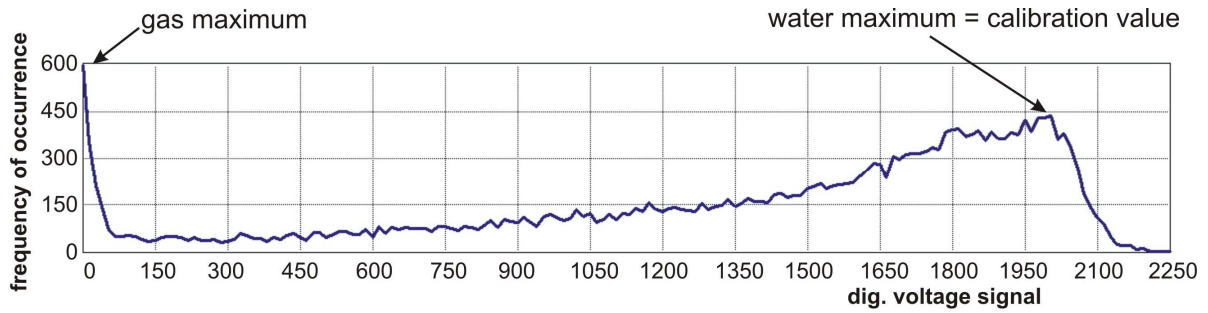


Fig. 1-9 Histogram of the mesh point 43 x 43 for the test point 140

The advantages and disadvantages of this method result from the principle used. The substantial advantage is the determination of the calibration values directly from the measurement data. Errors by changing the boundary conditions are minimised with this method. A disadvantage of the histogram calibration results from the limitation in the volumetric gas content, i.e. if at high gas volume fraction only few values for pure liquid are available, i.e. in which the measurement volume around the mesh point is totally filled with water. In this case, no clear water maximum can be determined in the histogram and the histogram calibration supplies an incorrect calibration value. In order to be able to use the advantages of this method, the calculated matrix composed of calibration values is azimuthally averaged for each test point and the radial profiles are checked.

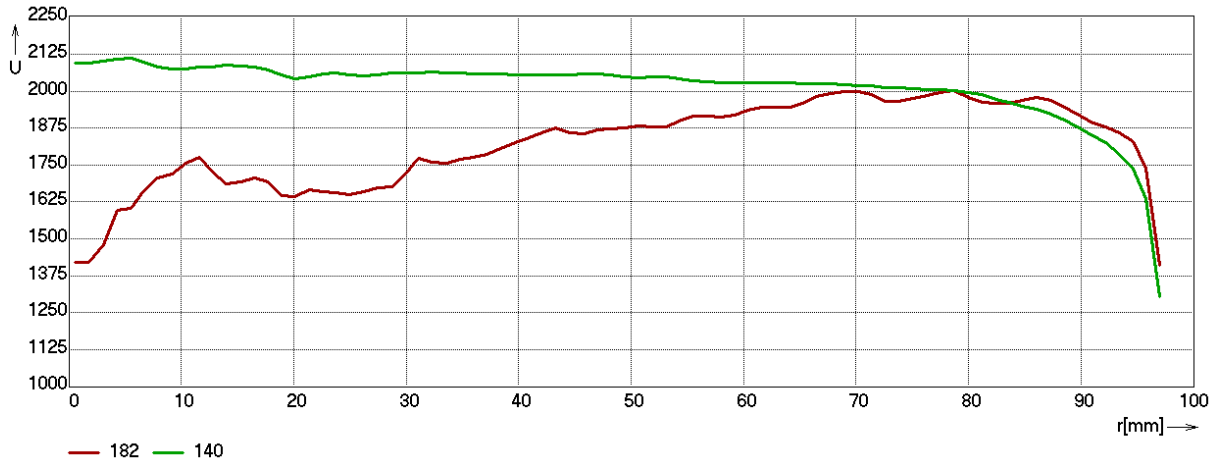


Fig. 1-10 Comparison of radially averaged calibration profiles for the test points 140 - green and 182 - red (histogram calibration)

Fig. 1-10 shows two radial profiles of calibration values for the measurement points 140 (green) and 182 (red), respectively. The curve of the point 140 describes an almost ideal calibration profile and confirms the applicability of the method for this point. This curve remains approximately constant for a long distance from the pipe centre ($r = 0$) and only drops steeply directly at the edge of the sensor. On the contrary, the calibration profile of point 182 breaks down in the centre. The red curve shows clearly that in the centre of the flow no satisfying calibration values can be determined. At the mesh points in the centre of the pipe, there are hardly any frames

with pure water in the measurement data according to this high superficial gas velocity which is associated with annular flow.

The decrease in the calibration profiles at the edge of the wire-mesh sensor results from the proximity of the mesh points to the electrically grounded pipe wall. Thus a part of the transmitter potential flows off not to the receiver wire but to the pipe wall. An additional reason for this effect is that many of the measurement volumes are smaller for the mesh points at the edge of the sensor than the standard volume on the inside (see Fig. 1-11).

Therefore, the calibration of the measurement data of this test series was accomplished in two steps: first, the determination of the radial calibration profiles for all available data was done by means of histogram calibration. Beginning at the test points with high superficial gas velocities, the radial calibration profiles were checked. Test points with unsatisfactory results were re-calculated using the file calibration. In the result for this measurement series, the volumetric gas contents for the test points 171, 173, 182 and 184 (see Table 2) were obtained using calibration files, while the histogram calibration was employed for all other points. The results of the calibration are stored in the form of a ASCII file (*.uw), which contains the calibration values for each mesh point as matrix. In addition, the radial calibration profiles (*.uwrاد_80) are available after successful histogram calibration.

With the help of the calculated calibration values, the values for the volumetric void fraction are determined from the measurement data by equation (1.15). Due to the presence of signal noise in the measurement data (wire oscillations, noise in analogue electronic components, electrical smog), the calculated volumetric void fraction is filtered before the further processing. No normal noise filter can be used because the measurement signals with small variations can also occur (see Prasser et al. 2001). For example, if a bubble penetrates the wire, the edge of the bubble can cut a measurement volume of the wire-mesh sensor, in which a small, however, realistic gas content is measured. In order to be able to distinguish these small but realistic signals from the signal noise, a special filter is used. This filter considers the void fraction values of the surrounding mesh points. That means before a value of the void fraction $\varepsilon_{i,j,k}$, which is smaller than the limit value of the filter (20 %), is set to zero, the filter analyses the environment of this void fraction value. Only if all 26 surrounding values are also below the limit value, the void fraction $\varepsilon_{i,j,k}$ is set to zero. If this condition does not apply, then it can be assumed that the measurement signal belongs to the edge region of a bubble. In this case, the measured value remains unchanged.

The limit value of 20 % theoretically restricts the sensitivity of the wire-mesh sensor used here to a minimum equivalent diameter of 3 mm related to the bubble size. This is the most unfavourable case, if the gas bubble goes through the measurement plane of the sensor in such a way that it begins to cut four measurement volumes equally. In the reality, the wire-mesh sensor, however, still registers most of these bubbles, since the probability that a bubble penetrates the sensor exactly symmetrically between four wire electrodes and thus producing a void fraction of > 20 % only in one of the four measurement volumes is very small. With a further decrease of the bubble size also the probability that the bubble is still recorded by the sensor decreases.

After the filtering, the void fraction is limited at 0 and 100 %, respectively. The data are saved in byte-format in a binary file with the extension *.v successively for each frame of the measurement. For numerical reasons, these files also contain values for points, which are outside of the circular measurement cross-section. These points are marked with the number 255.

1.5.2 Void fraction profiles

After calibration, the data present the local instantaneous volumetric void fraction $\varepsilon_{i,j,k}$ (i, j are the indices of the grid points in the measurement plane and k is the number of the frame) with a spatial resolution of 3 x 3 mm and a time resolution of 0.4 ms. In order to obtain quantitative information on the flow, a time and spatial averaging of the void fraction data can be used (Prasser et al. 2002). Contrary to the void fraction values stored in the v-files, the data used for averaging are not limited at 0 or 100 %.

The averaging is based on weight coefficients that define the contribution of each crossing point of wires (i,j) in the sensor matrix to the size of the domain, over which the averaging has to be performed. The definition of the weight coefficients necessary to obtain a cross-section averaged void fraction is shown in Fig. 1-11. The average can be calculated for each sampling period individually:

$$\bar{\varepsilon}_k = \varepsilon(t) = \sum_i \sum_j a_{i,j} \cdot \varepsilon_{i,j,k} \quad (1.16)$$

The result of the data evaluation with equation (1.16) is a sequence of instantaneous average volumetric gas fractions, which is available with the full measurement frequency of 2.5 kHz. If required, these values are stored in a separate file.

Another option is the averaging in time. Two-dimensional void fraction distributions are provided by the following equation:

$$\bar{\varepsilon}_{i,j} = \frac{1}{k_{\max}} \sum_{k=1}^{k_{\max}} \varepsilon_{i,j,k} \quad (1.17)$$

With equations (1.16) and (1.17) an average void fraction for the total measurement cross-section can be obtained as follows:

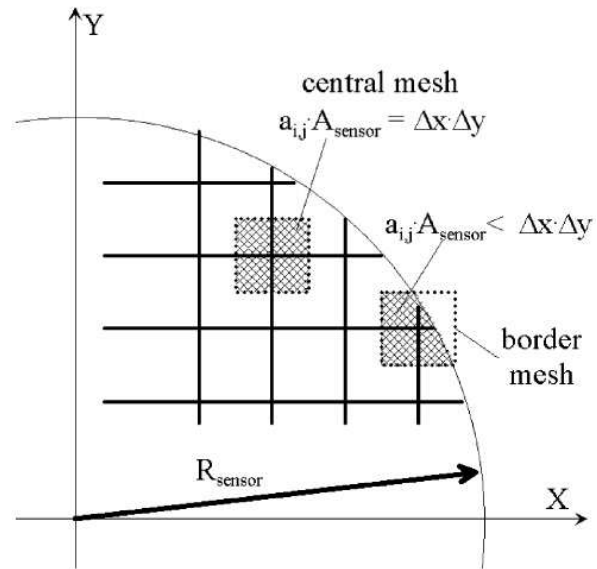


Fig. 1-11 Weight coefficients for the cross-section averaging of local gas fractions measured by the wire-mesh sensor

$$\bar{\varepsilon} = \sum_i \sum_j a_{i,j} \cdot \bar{\varepsilon}_{i,j} = \frac{1}{k_{\max}} \sum_{k=1}^{k_{\max}} \bar{\varepsilon}_k \quad (1.18)$$

Moreover, a radial gas fraction profile can be calculated by averaging the local instantaneous gas fractions over the measurement period of 10 s and over a number of ring-shaped domains. The latter is done by the following equation:

$$\bar{\varepsilon}_m = \frac{1}{k_{\max}} \sum_k \sum_i \sum_j a_{i,j,m} \cdot \varepsilon_{i,j,k} \quad (1.19)$$

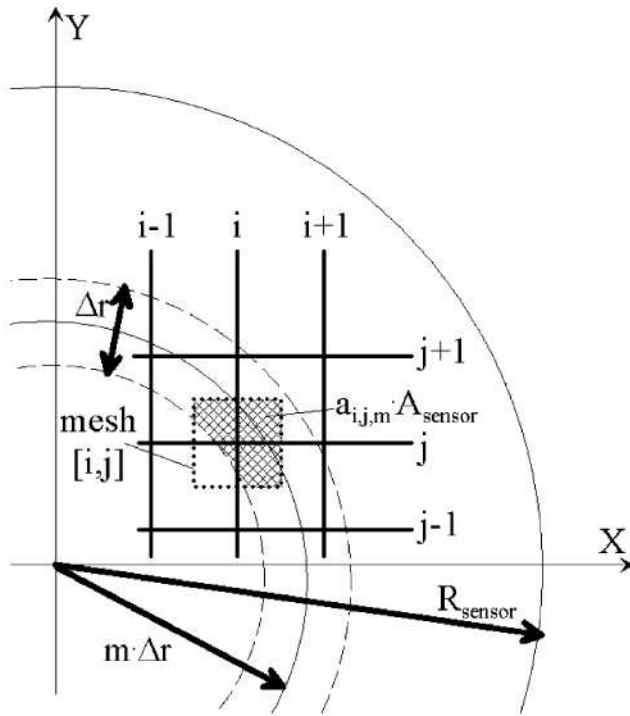


Fig. 1-12 Weight coefficients for the cross-section averaging of local gas fractions over a number of ring-shape domains

where $a_{i,j,m}$ are weight coefficients denoting the contribution of each measurement point with the indexes i,j to a ring with the number m (see Fig. 1-12). This ring-shaped averaging domain covers a given radial distance from the centre of the sensor:

$$(m-1) \cdot \frac{R_{\text{sensor}}}{m_{\max}} \leq r \leq m \cdot \frac{R_{\text{sensor}}}{m_{\max}} \quad (1.20)$$

where m_{\max} is the total number of radial steps ($m_{\max} = 80$ for DN200).

Additionally, gas fraction profiles can be obtained for a limited range of the bubble size (see also chapter 1.5.5). This requires a bubble identification and size measurement, which will be described in the following chapter (Prasser et al. 2002).

Thus, azimuthally and time averaged gas volume fraction profiles (*.epsrad_80), as well as the time averaged local gas fractions for each measurement point of the pipe cross-section (*.epsxy) are available. To allow cross-checks between the data for the latter ones the radial distances from the centre of the pipe are stored in ASCII files with extension *.epsr. Furthermore, the time and space averaged gas volume fractions according to equation (1.18) (eps_all.asc) can be used for the comparison of the individual experiments among themselves.

1.5.3 Gas velocities

The use of a sensor with two measurement planes (see also chapter 1.4.1.2) allows the determination of time and azimuthally averaged gas velocities. To do this, the signals from both measurement planes are cross-correlated separately for each pair of mesh points, which are located above each other. For time-discrete series of this

fluctuation components of the local instantaneous void fraction from the first measurement plane ($\varepsilon'_{1,i,j,k}$) and the second plane ($\varepsilon'_{2,i,j,k}$) of the sensor, the cross-correlation can be defined as follows:

$$F_{i,j,\Delta k} = \frac{\sum_k \varepsilon'_{1,i,j,k} \cdot \varepsilon'_{2,i,j,k+\Delta k}}{\sqrt{\sum_k \varepsilon'^2_{1,i,j,k}} \cdot \sqrt{\sum_k \varepsilon'^2_{2,i,j,k}}} \quad (1.21)$$

The index Δk corresponds to the time-shift of $\Delta t = \Delta k / f_{\text{meas}}$. Fluctuation components were calculated by subtracting the time-average from the instantaneous value: $\varepsilon'_{i,j,k} = \varepsilon_{i,j,k} - \bar{\varepsilon}_{i,j}$. The cross-correlation was carried out by means of Fast Fourier Transformation (FFT). The obtained cross-correlation functions were averaged in circumferential direction for different radii (m) using the same weight coefficients as for the calculation of radial gas fraction profiles:

$$F_{m,\Delta k} = \frac{1}{k_{\text{max}}} \sum_i \sum_j a_{i,j,m} \cdot F_{i,j,\Delta k} \quad (1.22)$$

In the next step, the location of the maximum in the cross-correlation functions averaged by equation (1.22) was found. The average gas-phase velocity for the given radius is calculated from the corresponding time-shift:

$$w_G(r) = w_G(m) = \frac{\Delta L}{\Delta k_{\text{max}}} \cdot f_{\text{meas}} \quad (1.23)$$

With Δk_{max} corresponding to $F_{m,\Delta k_{\text{max}}} = \max(F_{m,\Delta k})$

In equation (1.23) ΔL is the axial distance between the two planes of the sensor. The technique of averaging the cross-correlation functions before searching for the maximum has proven to supply more stable velocity values, than the velocities directly deduced from the result of a point-to-point cross-correlation according to equation (1.21), which suffers from a high scattering of the results.

For the documentation of the evaluation process, the results of the point-to-point cross-correlation are stored in a ASCII file (*.v00) in two columns. The first column contains the radial distance of the measurement point from the tube centre and the the second column the velocity value. The azimuthally averaged gas velocities and the centre radii of the 80 rings are stored in the ASCII files *.vel. Graphs showing the radial profiles of the gas velocities can be found in Appendix I.

1.5.4 Bubble identification

The bubble identification and the determination of important characteristics of the bubbles were done using special evaluation algorithms, which were described in detail by Prasser et al. 2001. Thereby, a bubble is defined as a region of connected gas-containing elements in void fraction data $\varepsilon_{i,j,k}$ which is completely surrounded by elements containing the liquid phase. To each element which belongs to one bubble, the same identification number is assigned. Different bubbles receive different identification numbers. These numbers are stored in the elements $b_{i,j,k}$ of a second

array. This array has the same dimension as the void fraction array. After the bubble recognition algorithm is completed, each element $b_{i,j,k}$ carries the number of the bubble to which the given element with the indexes i,j,k belongs.

Local instantaneous gas fractions can have values between 100 % (gas) and 0 % (liquid), if the corresponding measurement volume formed by two crossing wires contains both gas and liquid at the same time. Furthermore, signal noise may also lead to such intermediate values. Consequently, a sharp distinction between elements filled with gas and elements filled with water is not possible and the introduction of a threshold is necessary. The choice of the threshold influences the result of the bubble identification. A too small threshold leads to unrealistic coalescence of single bubbles, because the filling procedure merge bubbles across measurement volumes which are touched by neighbouring bubbles. On the other hand, a too high threshold may lead to a splitting of a bubble into unrealistic fragments, when the filling algorithm stops in elements where the gas fraction is decreased due to signal noise. It was found that a combination of a recursive filling algorithm with a subsequent agglomeration of peripheral elements insures the best results (Prasser et al. 2001).

The filling procedure starts at a local maximum of the gas fraction and stops at elements with a local gas fraction below the threshold. Best results were obtained by defining the threshold for the termination of the filling process for each bubble individually. This is done by subtracting a fixed value called "differential threshold" from the value of the maximum gas fraction of the respective bubble. Each start of the recursive filling procedure creates a new bubble. When no more start elements for the filling algorithm are found, the agglomeration procedure is started. This module does not search for more new bubbles, but completes the bubble surfaces. This is done by adding neighbouring elements with a gas fraction smaller than the threshold of the filling algorithm to the bubble. These elements get the same number that was already assigned to the bubble, to which they are being connected, i.e. the respective bubble number is added at the position in the matrix with the elements $b_{i,j,k}$.

This algorithm shows good results for two-phase flows with water superficial velocities larger than 0.1 m/s. Unrealistic fragmentations, however, arise below this value. This is caused by the fact that at such small flow velocities, the single bubbles are identified within essentially more cross-sections at constant measurement frequency. For this reason, the probability that due to signal noise the filling algorithm is terminated within the bubble is increasing. This effect is strengthened by the fact that at superficial water velocities < 0.1 m/s bubbles are decelerated, while penetrating the grid. Thereby, the staying time of the bubble in the measurement plane is increased (see also Prasser et al. 2001). In order to compensate the negative aspects of the agglomeration procedure, a defragmentation model was added. This program module scan the bubbly flow towards the time axis and examines on the basis of parameters of the single bubbles (gas fraction, centre of gravity, gas fraction gradient over the contact surface), whether unrealistic fragmentation exists. In this case, the smaller fragment is overwritten with the identification number of the larger one in the bubble identification matrix. The results of the bubble identification are stored as matrix of identification numbers in a binary file (*.b).

Together with the information about the gas fraction, now important parameters can be determined for each bubble. It has to be noted that in the code the index i refers to the serial number of the frames, while j and k , in this case, serve as indices in the measurement plane. This assignment of the indices is also used in the equations given in this section.

The **volume of a bubble** with the number n is obtained by integrating the local void fraction of all elements owning the given bubble number:

$$V_{b,n} = \Delta x \Delta y \Delta t \cdot w_b \sum_{i,j,k} \varepsilon_{i,j,k} \quad \forall [i, j, k]: b_{i,j,k} = n \quad (1.24)$$

The sum of void fractions is multiplied by the measurement volume, which is the product of the distance of the electrodes in x and y directions and the sampling period, as well as the bubble velocity. In this case, the pitch of the electrode wires is 3 mm and the sampling frequency amounts 2,500 Hz:

$$\Delta x = \Delta y = 3 \text{ mm and } \Delta t = \frac{1}{f_{\text{sample}}} \quad (1.25)$$

Due to the fact that the individual velocity of bubbles is unknown, the gas phase velocity obtained by cross-correlation is taken as an approximation at the location of the centre of mass of the given bubble:

$$w_b = w_G(r_n) \text{ with } r_n = \sqrt{(x_{\text{CM},n} - x_0)^2 + (y_{\text{CM},n} - y_0)^2} \quad (1.26)$$

The **coordinates of the centre of mass** can be obtained by averaging the measurement coordinates of all elements belonging to the selected bubble using the local void fraction values as a weight function:

$$x_{\text{CM},n} = \frac{\sum_{i,j,k} j \cdot \Delta x \cdot \varepsilon_{i,j,k}}{\sum_{i,j,k} \varepsilon_{i,j,k}}; \quad y_{\text{CM},n} = \frac{\sum_{i,j,k} k \cdot \Delta y \cdot \varepsilon_{i,j,k}}{\sum_{i,j,k} \varepsilon_{i,j,k}} \quad (1.27)$$

$$z_{\text{CM},n} = \frac{\sum_{i,j,k} i \cdot \Delta z \cdot \varepsilon_{i,j,k}}{\sum_{i,j,k} \varepsilon_{i,j,k}}; \quad \Delta z = w_b \cdot \Delta t \quad \forall [i, j, k]: b_{i,j,k} = n$$

After that, the equivalent diameter of the bubble can be determined, which is defined as the diameter of a sphere that has the volume according to equation (1.24):

$$D_{b,n} = \sqrt[3]{\frac{6V_{b,n}}{\pi}} \quad (1.28)$$

For the evaluation of asymmetries of the bubble, **moments** for each bubble are determined. Likewise, the void fraction served as weight function:

$$rm_{x,n} = \sqrt{\frac{5 \cdot \sum_{i,j,k} \varepsilon_{i,j,k} \cdot (j \cdot \Delta x - x_{CM,n})^2}{\sum_{i,j,k} \varepsilon_{i,j,k}}}; \quad rm_{y,n} = \sqrt{\frac{5 \cdot \sum_{i,j,k} \varepsilon_{i,j,k} \cdot (k \cdot \Delta y - y_{CM,n})^2}{\sum_{i,j,k} \varepsilon_{i,j,k}}} \quad (1.29)$$

$$rm_{z,n} = \sqrt{\frac{5 \cdot \sum_{i,j,k} \varepsilon_{i,j,k} \cdot (i \cdot \Delta z - z_{CM,n})^2}{\sum_{i,j,k} \varepsilon_{i,j,k}}}; \quad \Delta z = w_b \cdot \Delta t; \quad \forall [i, j, k]: b_{i,j,k} = n$$

From the moments for the coordinates x and y in the measurement plane of the wire-mesh sensor, the radial moment results:

$$rm_{r,n} = \sqrt{rm_{x,n}^2 + rm_{y,n}^2} \quad (1.30)$$

Further information on the distortion of the bubble can be obtained by calculating the maximum equivalent diameter in the x-y plane. For this matter, the area being occupied by the bubble in the x-y plane is added. Similar to equation (1.24), the sum of the local instantaneous void fractions of the measurement volumes belonging to the bubble is multiplied by the area of the measurement volume in the x-y plane. This procedure is done for each single sampling time characterised by index i:

$$A_{xy,n,i} = \Delta x \Delta y \sum_{j,k} \varepsilon_{i,j,k} \quad \forall [i, j, k]: b_{i,j,k} = n \quad (1.31)$$

Afterwards, the maximum area is found and converted into the **diameter of an area equivalent circle**:

$$D_{xy,n} = \sqrt{\frac{4A_{xy,n,\max}}{\pi}} \quad \text{mit} \quad A_{xy,n,\max} = \max(A_{xy,n,i}) \quad (1.32)$$

In addition to these bubble characteristics, **the minimum and maximum coordinates** of the bubbles are determined. For the calculation of these values, it is necessary to define a threshold value of the gas fraction which represents the bubble interface. As described by Prasser 2007b, for bubble sizes > 20 mm a threshold 50 % is a good approximation. If bubble diameters are smaller this value is reduced to approx. 20 %. The maximum of gas fraction in the bubble (starting at 100 % for large bubbles) also reduces with decreasing bubble diameter. This reduction is observed for bubbles with a diameter less than approx. 20 mm. This effect results from the limited spatial resolution of the wire-mesh sensor which is 3 x 3 mm. Small bubbles cannot completely fill the associated measurement volumes. For this reason maximum gas fractions lower than 100 % are observed. Taking these boundary conditions into consideration, as a compromise, the gas fraction threshold representing the bubble interface is taken as half of the maximum gas content of the bubble.

Another important parameter for the characterisation of gas bubbles is the **volume fraction of the bubble related to the total volume of the flow**:

$$\varepsilon_{b,n} = \frac{V_{b,n}}{V_{ges}}; \quad V_{ges} = t_{meas} \cdot f_{meas} \cdot \Delta x \cdot \Delta y \cdot \Delta t \cdot \bar{w}_A \cdot \sum_j \sum_k a_{j,k}; \quad \bar{w}_A = \frac{J_A}{\varepsilon} \quad (1.33)$$

Apart from the already mentioned parameters, the maximum gas fraction and the number of measurement volumes per bubble are determined. All values are stored in an ASCII file (*.a) as table for each identified bubble.

1.5.5 Bubble size distribution and data decomposed according to the bubble size

After evaluation of the data described in the previous chapters, three-dimensional information for gas fraction distribution and for bubble identification is available. Additionally, a list with characteristics of each bubble is generated for each measurement.

The combination of this data makes it possible to obtain bubble size distributions. To do this histograms are calculated in which the void fraction per bubble class is summed. This is done related to the volume equivalent diameter according to equation (1.28) as well as related to the area equivalent diameter of the gas bubbles according to equation (1.32). This information is available in a representation with a linear bubble class width of 0.25 mm and also for a logarithmically increasing width of the bubble classes. The smallest bubble size class for the logarithmic representation has a lower boundary of 0.1 mm. The bubble size distributions are stored in ASCII files with the extensions *.his_lin and *.his_log, respectively. The linear distributions are preferably used for the numerical investigations and the logarithmic information for visualisation (bubble size distributions in appendix I).

In both types of bubble size distributions, the void fraction that is related to the bubble class width is represented by $(\Delta\varepsilon/\Delta D_b)$, which gives:

$$\varepsilon_{ges} = \sum_0^{D_{b,max}} \frac{\Delta\varepsilon}{\Delta D_b} \cdot \Delta D_b \quad (1.34)$$

In addition these distributions related to the total gas content $(\Delta\varepsilon/\Delta D_b/\varepsilon_{ges})$ are listed in both files. Furthermore, the files contain the bubble number distributions with which the absolute number of bubbles per bubble class is referred to the bubble class width and the total measurement time.

The data also enable to present the azimuthally and time averaged gas fraction distributions (as defined by equation (1.19) decomposed according to bubble size). Such data are stored in the files *.epsrad_80_bub in dependence on the radius and a division into four bubble classes (0 - 4 mm, 4 mm - 5.8 mm, 5.8 mm - 7 mm and 7 mm - 200 mm). For the air/water flow, at the boundary conditions presented above the Tomiyama lift force changes its direction at an equivalent bubble diameter of about 5.8 mm. For this reason, two bubble classes with a smaller width were chosen above and below this value, as well as two classes containing the void fraction for the remaining bubbles. Additionally, these files contain the total void fraction per radial ring.

In addition, the previously described linear bubble size distributions (*.his_lin) were split up for the single radial rings. To do that, position (i,j) and diameter (D_b) of each reconstructed bubble is checked and the related void fraction is assigned to a two-dimensional array according to the associated bubble class and the respective radial ring $m(r)$. Again the weight coefficient $a_{i,j,m}$ (see also Fig. 1-12) is used for this procedure. These void fraction distributions are related to the bubble class width, as in the *.his_lin files. The cross section averaged bubble size distributions discussed above $\Delta\varepsilon(r)/\Delta D_b$ can be obtained from these data according to:

$$\frac{\Delta\varepsilon}{\Delta D_b} = \frac{1}{2 \cdot R_{\text{Sensor}}^2} \sum_{r=1}^{R_{\text{Sensor}}} \frac{\Delta\varepsilon(r)}{\Delta D_b} \cdot r \cdot \Delta r \quad (1.35)$$

Furthermore, these results were related to the total void fraction per radial ring: $\Delta\varepsilon(r)/\Delta D_b/\varepsilon_{\text{ges}}(r)$. For the determination of the bubble number distribution, the following conditions were considered: Each bubble is only once registered per radial ring. If a bubble penetrates several radius rings, then it is detected separately in each ring.

These data are available in the files *.his_lin_r as 80 individual bubble size distributions, each per radius ring (1.20). To enable some checks, these files contain at the end the bubble size distribution, an integration over the radius according to equation (1.35), which corresponds to the data in the *.his_lin file.

1.6 Estimation of data accuracy

Errors of the values obtained by the wire-mesh sensor for the gas fraction and bubble size are mainly caused by the lateral pitch of the wires which is 3 x 3 mm and the distance of the wire planes which is 2 mm. Comparative measurements between the wire-mesh sensor and other research methods supplied information on the accuracy of the measurement technique and the evaluation algorithms for the experimental determination of these flow parameters.

1.6.1 Void fraction

The measurement error of wire-mesh sensor for the determination of void fraction profiles was examined by comparative measurements by means of X-ray tomography and gamma radiography. Due to the limited functionality of the reference procedures, all these comparisons were done for tubes with a diameter of 50 mm.

The gamma radiography of an air/water flow for varying superficial velocities of both media resulting in a gas volume fraction between 0 and 100 % showed that the deviations between wire-mesh sensor and gamma measurement are limited to ± 5 % (Prasser 2000b). The radiography of a steam/water flow at atmospheric pressure confirmed this statement (Manera et al. 2001). It has to be considered that the reference procedure has measurement errors, too.

Comparative measurements between wire-mesh sensor and an X-ray tomography, which is a more exact reference procedure, were also done for air/water flow. A result of this investigation was the statement that the accuracy of the gas volume

fraction averaged over the flow cross-section depends on the two-phase flow regime. Differences in the absolute void fraction were determined (Prasser et al. 2005):

- at a bubbly flow of $\pm 1 \%$ and
- at a slug flow, a systematic underestimation of approx. - 4 %.

Prasser et al. 2005 also discuss that the integration of void fraction and velocity profiles measured in a DN200 pipe result in a good reproduction of the injected gas volume flow at superficial velocities up to approximately 1 m/s. This confirms the applicability of the sensor (see also chapter 1.7). Unfortunately, this method is not useful to derive a direct evaluation of the accuracy of the void fraction measurement with the wire-mesh sensor. For the estimation of the error, it is assumed that the measurement error in the pipe DN200 is analogous to the one, which is determined for a bubbly flow in a nominal diameter of DN50. The larger systematic underestimation, which was observed during a plug flow in pipes with a smaller cross-section, is not taken into account. It is well known that in pipes of larger diameter with present boundary conditions, the development of gas-slugs is less pronounced and if it does occur, it is only at very high superficial gas velocities (Ohnuki et al. 2000).

1.6.2 Bubble diameter

Comparative measurements with a high-speed camera are available to estimate the measurement error for the determination of the volume equivalent bubble diameter according to equation (1.28). The investigations were performed in a transparent flow channel DN100 where air/water flows with different bubble sizes and water velocities between 0 and 0.8 m/s were realised.

Scholz 2000 demonstrated that only bubbles with an diameter larger 1.6 mm can be recorded due to the limited spatial resolution in case of a wire-mesh sensor with a pitch of the wires of approx. 3 x 3 mm (distance of the planes: 1.5 mm, wire sizes: 0.12 mm). In addition, the comparisons between the data of the wire-mesh sensor and the high-speed camera showed that the volume equivalent diameter is measured at superficial water velocities of > 0.2 m/s with an accuracy of $\pm 20 \%$. At smaller water velocities, overestimations up to $+50 \%$ were observed. Note that the dispersion of the determined bubble sizes under constant flow conditions is significantly larger for the high-speed camera measurement than for the wire-mesh sensor. For this reason, it is assumed that the indicated deviations between both procedures mainly results from the inaccuracy of the optical method. At higher water velocities, the results are in a range of approx. ± 2 mm (Prasser et al. 2001).

In a presently running project, a comparison between measurement data of a wire-mesh sensor with a fast X-ray tomograph is planned. Since the X-ray tomography (measurement frequency up to 7 kHz) is a good reference procedure these investigations should enable an improved error estimation of the wire-mesh sensor data.

1.6.3 Azimuthally averaged gas velocities

In chapter 1.5.3, the methodology of the cross-correlation was described, which allows the determination of the azimuthally averaged gas velocities. They result from the pattern of the void fraction, which is measured with the help of the mesh sensors. Unfortunately, information on the error associated with this method do not currently exist, as no reference method is able to provide velocity data in two-phase flows with an appropriate spatial resolution. There is, however, the possibility of estimating the discretisation error on the basis of the distance between the two measurement planes (see chapter 1.4.1.2) with consideration of the average gas velocity and the measurement frequency. For this, the average gas velocity was calculated by means of the superficial gas velocity and the average void fraction. Dividing the distance between the measurement planes by this velocity, the travelling time of the gas phase between the meshes is calculated. Relating this time to the sampling period (1/frequency of measurement), the discretisation error of the gas velocity can be determined.

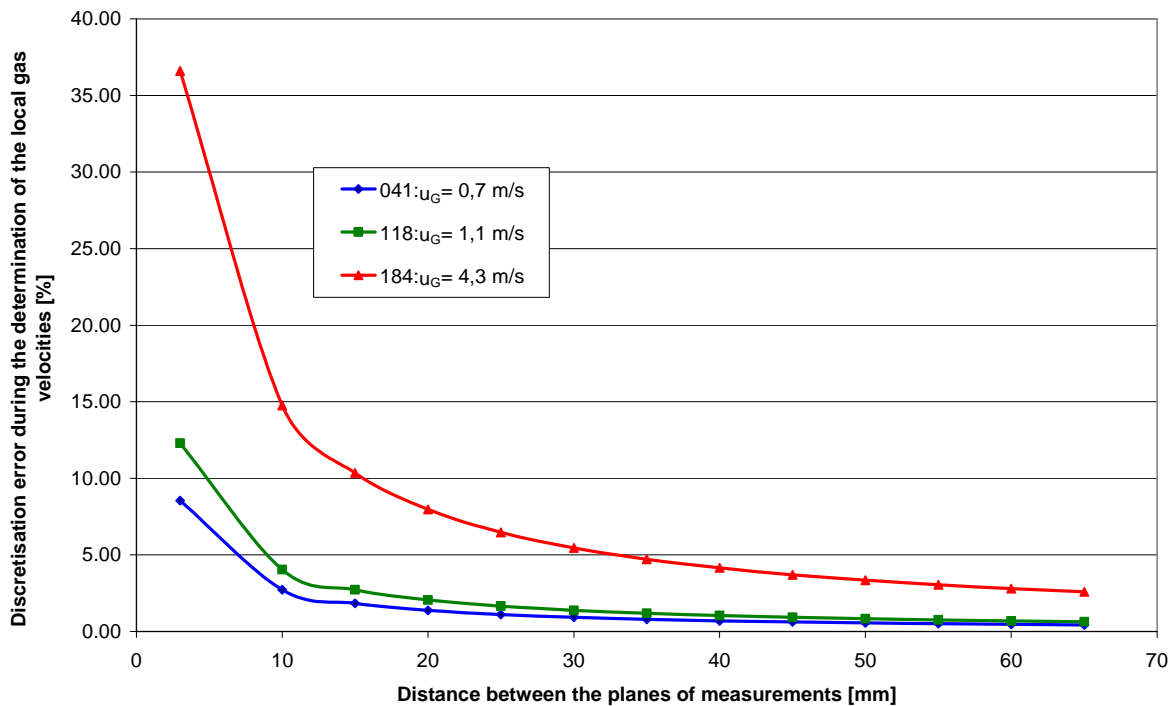


Fig. 1-13 Discretisation error of the determination of the local gas velocities in dependence of the distance between the planes of measurements

Fig. 1-13 shows the results for selected measurement points (041, 118, 184, see Table 2). It shows clearly that with decreasing distance between the measurement planes, the error strongly rises. This is because of the fact that the travelling time of the gaseous phase at small distances between the measurement planes approximates to the sampling period. On the other hand, the quality of the cross-correlation results improves with smaller distances between the planes of measurement, because the cross-correlation function forms more distinctive maxima. Keeping in mind these two opposite effects and the constructional conditions during

the sensor fabrication, a good compromise for geometry of the wire-mesh sensor must be found. The double sensor used for this measurement series has a distance between the measurement planes of 40 mm, so that the discretisation error of maximally 4 % emerges for matrix point 184 at the highest gas velocities. At this distance the test matrix point 118 displays decreased discretisation errors smaller than 1 %.

A critical evaluation of the azimuthally averaged velocities determined according to chapter 1.5.3 shows that at individual values outliers appear despite the averaging procedure. In order to be able to use the local gas velocities, particularly for the reconstruction of the superficial gas velocities and for the determination of the weighted drift velocities, all velocity data in the *.vel files were examined and values deviating more than approx. 80 - 100 % of the average velocities (m) are replaced by interpolations of the values for the m_{-1} and m_{+1} radius ring. The number of the corrected local gas velocities is listed in Table 4 for each matrix point (see. Table 2) and for each injection length (see Table 1 and Fig. 1-2). Empty fields mean that the data determined by cross-correlation and averaging were used for the evaluation without any change. This applies to approx. 85 % of the measurements. The indicated numbers have to be related in each case to the 80 radius rings.

In Table 4 two tendencies are clearly visible: on the one hand, the errors at small superficial liquid velocities (test matrix points: 34 - 37 and/or 111 - 114) increase. A reason for this effect could result from the cross-correlation method, whose results are based on the maximum of the cross-correlation function. At the investigation of two-phase flows with small superficial liquid velocities, i.e. also small local gas velocities, this maximum is small and lies within the range of the signal noise. Therefore, it is not always possible to filter this "correct" signal from the result matrix.

On the other hand, several outliers have been found for a gas injection close to the measurement plane A-F (see Table 1 and Fig. 1-2). If high radial velocity components occur between the two measurement planes of the wire-mesh sensor, the radial alignment of the gas bubbles becomes misaligned. This gas misalignment causes a degradation of the point-to-point cross-correlation results. The content of Table 4 also shows that the errors arise for these injection positions only at a superficial liquid velocity of 0.405 m/s (test series II), whereas the gas velocities of the test series I exhibit a good quality. Also in this case, the smaller gas velocity seems to have a negative affect on the results of the cross-correlation.

Table 4 Number of interpolated azimuthally averaged gas velocities per measurement point and injection length (out of 80 radius rings)

		Test section length →																	
		A	B	C	D	E	F	G	H	I	J	K	L	M	N	O	P	Q	R
Matrix point ↓	6									2									
	8				2														
	17											3							
	19																		
	28					2		4	2			5							
	30			1									2						
	34	19	2	1		3	4			4	1						2	1	5
	35	6	4			3					3							1	2
	36	4		15		14			1										
	37		1	17	2		1												
	38					3													
	39					2						2							
	40																		
	41																		
	42						1												
	50	8			2														
	52			2		3													
	61		3				5												
	63																		
	72	3				11	7												
	74																		
	83			7	9	10	1												
	85																		
	94	3		1	8		3											3	
	96						6												
	105		1	16	10	2	3												
	107					3	5												
	111	11	6	9	6	3		3	7	10	10	3		7	3	13	7	2	3
	112	5	15	5	5	6	5	5	2	7	3	8		9	7	6	1	7	11
	113		10		3	7	3			3	1	5					2		2
114		2	1	5	6	2	5	3	3		4	1		3		5	3		
115		16	8		4				2										
116		13	11																
117			1		2														
118																			
119																			
127	13	15	8																
129																			
138		7															3		
140		5				2													
149		6																	
151																			
160																			
162																			
171																			
173																			
182																			
184																			

1.6.4 Errors of the calculated pressures at the gas injection

To set a constant pressure at the gas injection (0.25 MPa), the two-phase pressure drop in the test section was calculated (see 1.2.2) to define the pressure boundary condition at the position of the pressure measurement. For this, the drift velocity is needed, which was still unknown before the beginning of the experiments. A constant velocity of 0.25 m/s was used for the calculation, which is a good approximation for bubbles with an equivalent diameter range 5 to 9 mm. After completion of the experiments, a weighted drift velocity (see chapter 2.2.2) can be calculated from the measured void fraction profiles, velocity profiles, and bubble size distributions. Basing on this information, the error which results from the assumption of a constant drift velocity can be estimated. Therefore, the pressure drop was recalculated with the weighted drift velocities and these results were compared with the initial values.

For the calculation of the gas fraction, the drift velocity is used and the gas fraction is needed again to calculate the material properties of the two-phase mixture. The influence of the drift velocity on the pressure drop is highest for experiments with the largest injection lengths (P, Q, R; see Fig. 1-2). Fig. 1-14 to Fig. 1-17 shows these errors arranged according to the test series I - IV, as defined in Table 2.

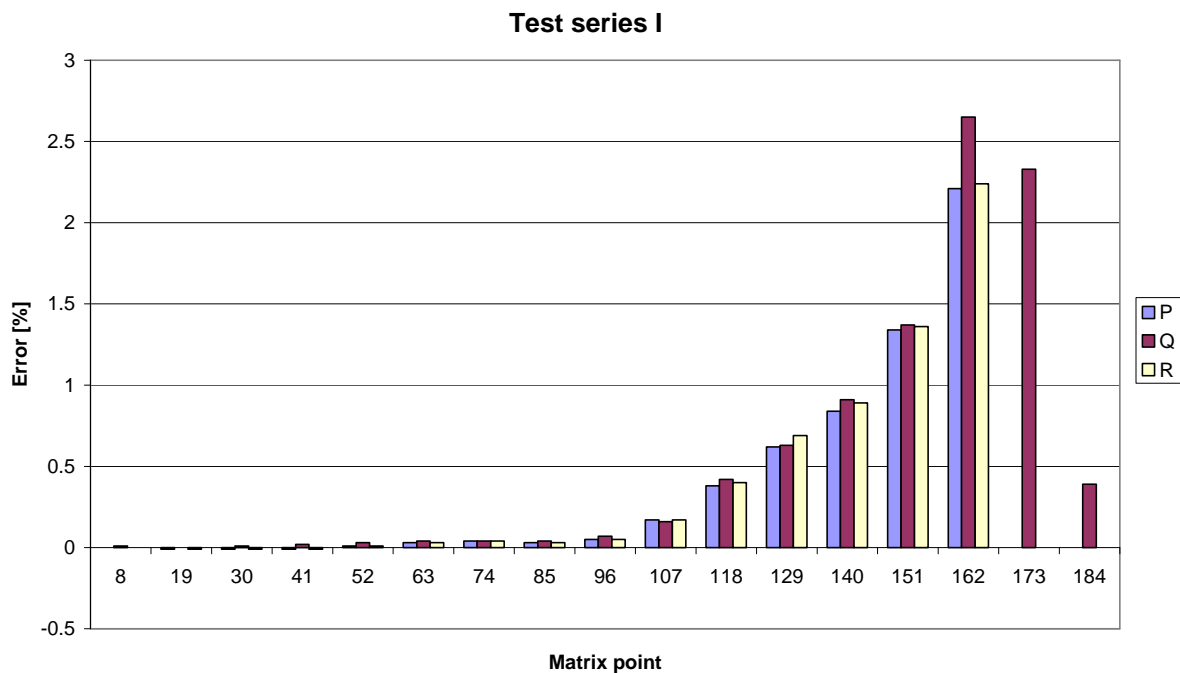


Fig. 1-14 Error for the pressure boundary condition above the wire-mesh sensor for the test series I

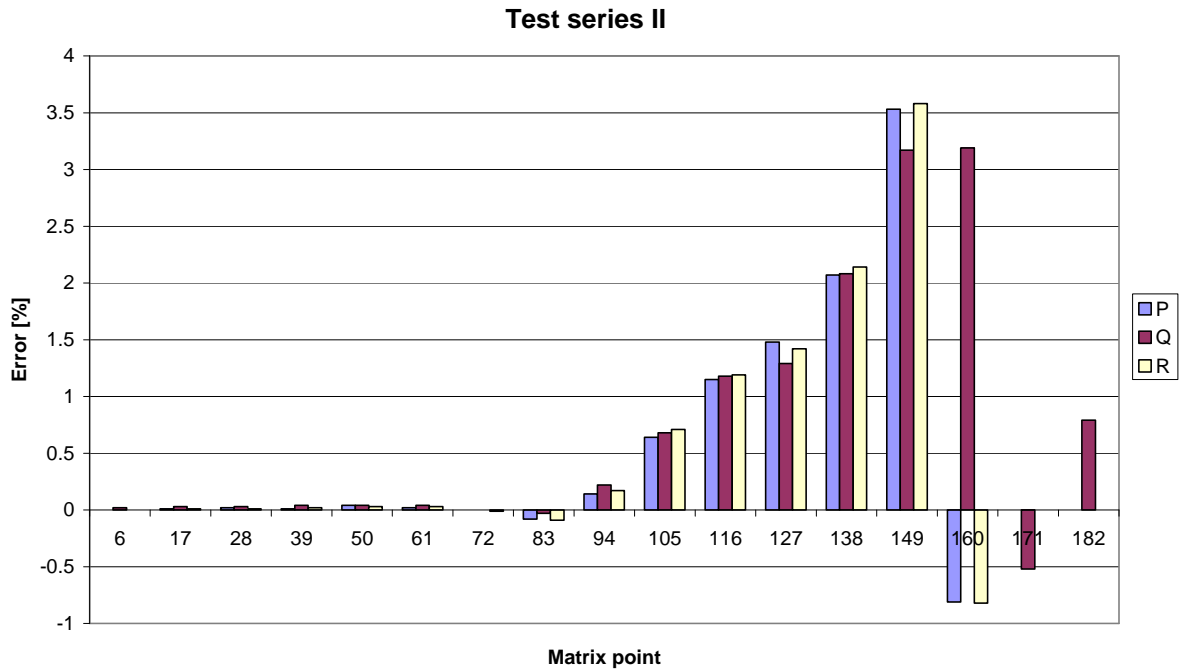


Fig. 1-15 Error for the pressure boundary condition above the wire-mesh sensor for the test series II

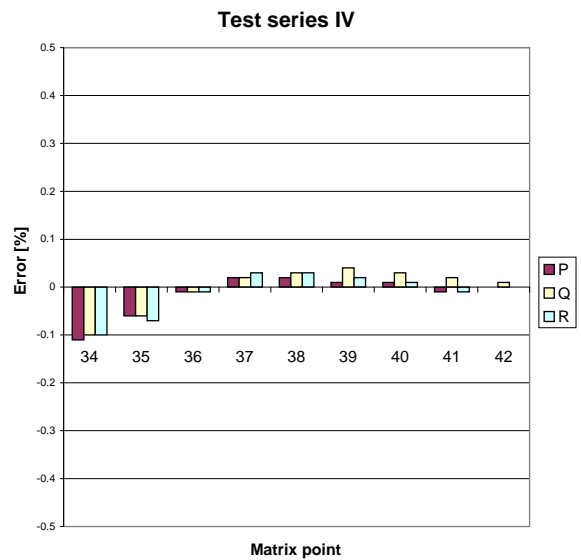
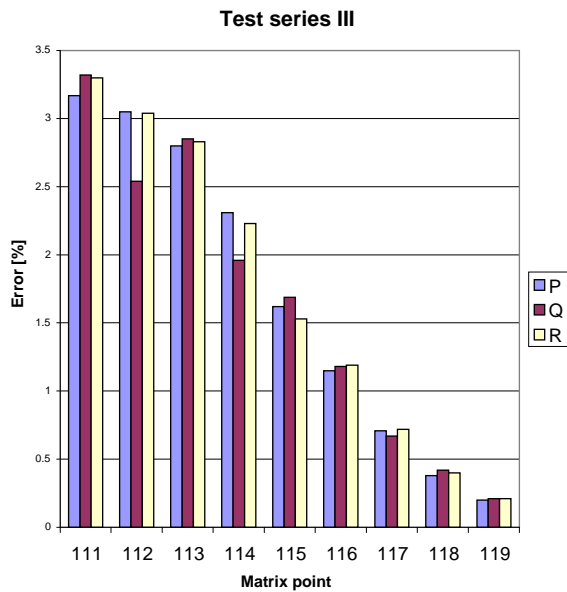


Fig. 1-16 & Fig. 1-17 Error for the pressure boundary condition above the wire-mesh sensor for the test series III and IV

For the test series I and II, a similar tendency of the errors was determined, which are, however, smaller for test series I in the absolute value. This effect results from the smaller void fraction caused by the approx. 2.5 times larger superficial liquid velocity compared to test series II. Smaller void fraction means that the drift velocity has less influence on the total pressure drop causing smaller errors. This effect also explains the increase of the error with increasing test matrix point (increasing superficial gas velocity). For the diagrams in Fig. 1-14 and Fig. 1-15 is to be noted that for test matrix points 171 – 184, the gas was only be injected into the test section through 4 mm orifices, i.e. for the injection lengths P and R no errors were determined. In test series IV, the error of all measurements is practically zero, because void fraction was very small in these experiments. The tendency to smaller errors at rising matrix points (smaller void fractions) is, however, already recognisable. This trend becomes more obviously in the test series III, because the superficial gas velocity is substantially higher (0.22 m/s) than in test series IV (0.01 m/s).

1.7 Accuracy checks on the basis of the superficial gas velocity

From the measured radial profiles of the void fraction $\varepsilon(r)$ and the velocity of the gas phase $u_G(r)$, the superficial gas velocity at the sensor integrated over the cross-section can be calculated according to:

$$J_{G,S} = \frac{\dot{V}_G}{A} = \frac{2}{R^2} \int_0^R u_G(r) \cdot \varepsilon(r) \cdot r \cdot dr = \langle \varepsilon \cdot U_G \rangle. \quad (1.36)$$

Dependent on the test section height, the superficial gas velocity at the injection follows by considering the Boyle-Mariotte's law:

$$J_{G,in} = J_{G,S} \cdot \frac{p_{\text{Sensor}}}{p_{\text{in}}}. \quad (1.37)$$

This can be compared with the set value J_G . In Fig. 1-18 such a comparison is given for the test series I for the maximum relative test section height. The associated relative deviation:

$$\Delta J_G = \frac{J_{G,in} - J_G}{J_G} \quad (1.38)$$

is shown in Fig. 1-19.

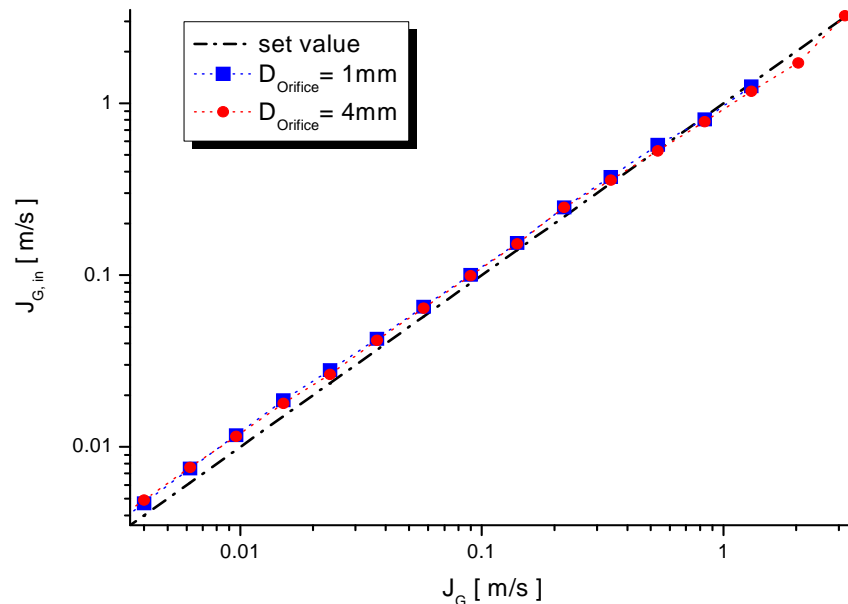


Fig. 1-18 Comparison of the superficial gas velocity $J_{G,in}$ calculated from experimental data with the set value J_G at maximum L/D for the test series I ($J_L = 1.017$ m/s) with different injection $D_{\text{Orifice}} = 1$ and 4 mm

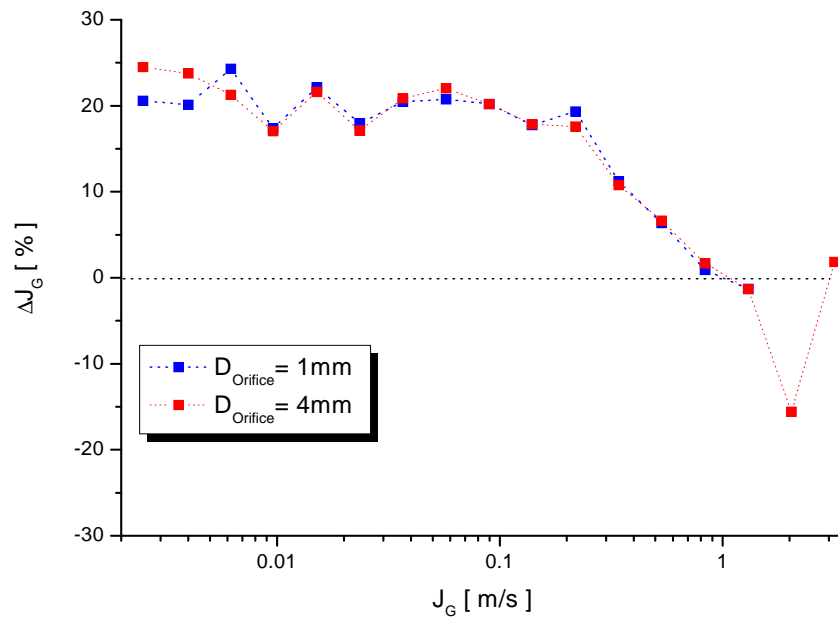


Fig. 1-19 Relative deviation of J_G obtained from the measurement compared to the set value of the superficial gas velocity for different diameters of the gas injection at maximum L/D

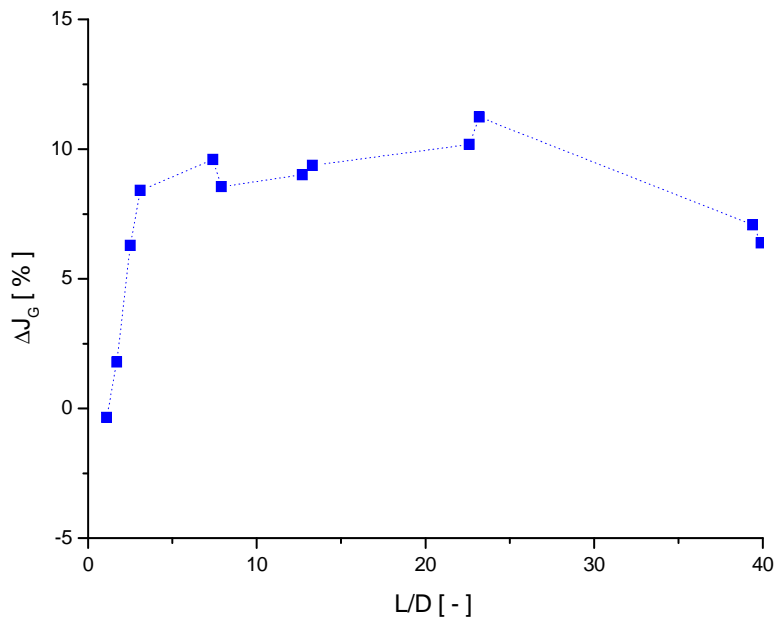


Fig. 1-20 Variation of the relative deviation of J_G obtained from the measurement compared to set value along the relative test section height L/D by the example of the measurement point 140 of the test series I with $D_{\text{orifice}} = 1$ mm

While within the range of the bubbly flow, the superficial gas velocity determined from the measurements is overestimated by about 20 %, the error for medium and high superficial gas velocities drops down below approx. 15 %, starting from $J_G > 0.2$ m/s. No significant differences of ΔJ_G were observed with the diameter of the gas injection orifices used.

Note that the deviations from the set value result from both the gas fraction and the velocity measurement. To calculate $J_{G,S}$ according to equation (1.36), the measured and azimuthally averaged (over ring-shaped domains) bubble rise velocity $u_G(r)$ is used. For the more detailed investigation of these effects, chapter 2.2 describes the calculation of weighted drift velocities.

At the individual measurement points of the matrix, the deviation from the set value J_G changes and thus the accuracy of the measurement along the test section height (Fig. 1-20) is also varying. Differences of ΔJ_G , between small L/D (injection at level A) and the maximum relative height L/D occur particularly in the range of the superficial gas velocities of $0.05 \text{ m/s} \leq J_G \leq 0.4 \text{ m/s}$ as shown for test series I in Fig. 1-21.

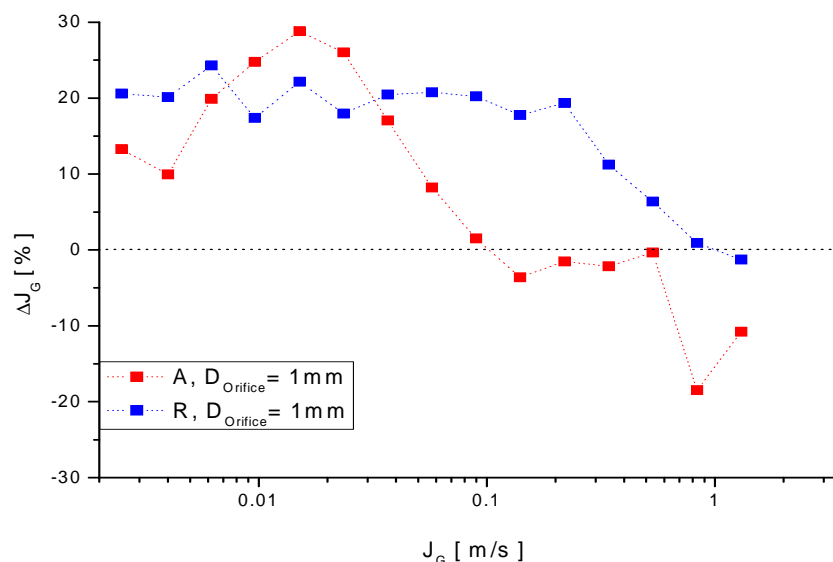


Fig. 1-21 Variation of the difference ΔJ_G with the superficial gas velocity for the smallest (A) and at maximum (R) relative height L/D (test series I $D_{Orifice} = 1$ mm)

The results for the accuracy test on the test series II are specified in the appendix III, starting from page 195 and show tendentially similar results to the test series I.

The test series III (constant $J_G = 0.219$ m/s) demonstrates the limits of the measurement method in the case of small liquid velocities. In the range of approx. $J_L < 0.2$ m/s, the superficial gas velocity of $J_{G,in}$ calculated from the measurements of the gas fraction and the velocity becomes up to 50 – 100 % larger than the set value (Fig. 1-22 and Fig. 1-23).

The main reason is the measurement error arising from the determination of the bubble rise velocity, as already discussed in chapter 1.6.3. The error increases with decreasing superficial liquid velocity (measurement points 111 - 113 of test series III, as well as measurement points 34 - 36 of test series IV). Furthermore, the dependence of the bubble rise velocity on the bubble diameter remains unconsidered. The gas velocity was obtained from a cross-correlation between the two measurement planes of the wire-mesh sensor (chapter 1.5.3). A bubble size-dependent classification of the rise velocity is not yet possible. Thus the calculation of the superficial gas velocity $J_{G,S}$ according to equation (1.36), the dependence of the rise velocity $u_G(r)$ on the bubble size is not considered. Due to the appearance of bubbles of different sizes and as a consequence of this, the modification of the rise velocities for different gas/liquid flows, larger discrepancies between the computed value J_G and the set value can be observed. If bubbles of different sizes and consequently with different rise velocities occur in the flow, then larger differences between the calculated values $J_{G,in}$ and the set value J_G can occur. The effects of the bubble size-dependent rise velocity are examined more deeply in chapter 2.2.

A similar difference between the calculated value $J_{G,in}$ and the set value J_G could also be proved for test series IV, however, at clearly lower level (Fig. 1-22 und Fig. 1-23). Further results for the accuracy test at the determination of the superficial gas velocity are specified in the appendix III, starting from page 195.

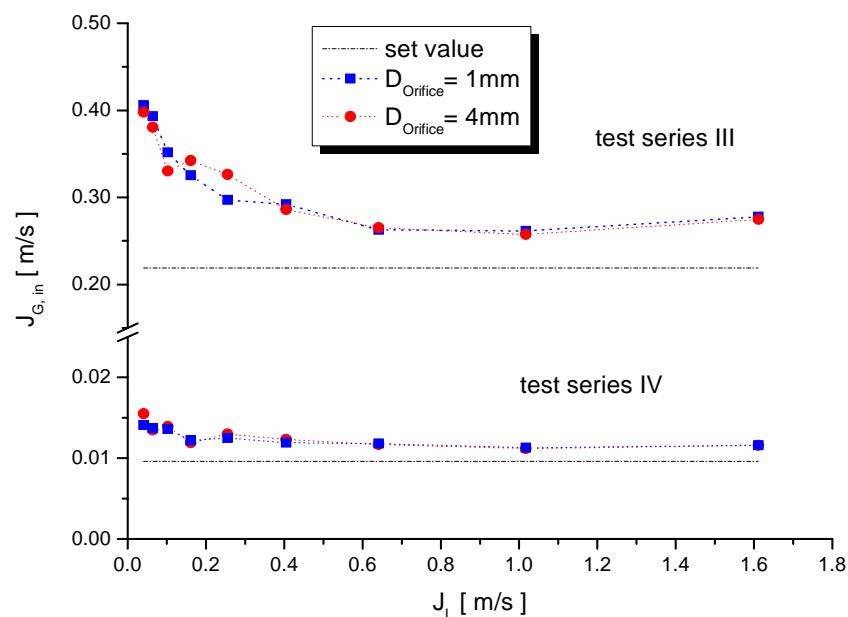


Fig. 1-22 Comparison of the calculated superficial gas velocity $J_{G,in}$ with the constant set value J_G for test series III ($J_G = 0.219$ m/s) and IV ($J_G = 0.0096$ m/s) in dependence on J_L at maximal test section height L/D

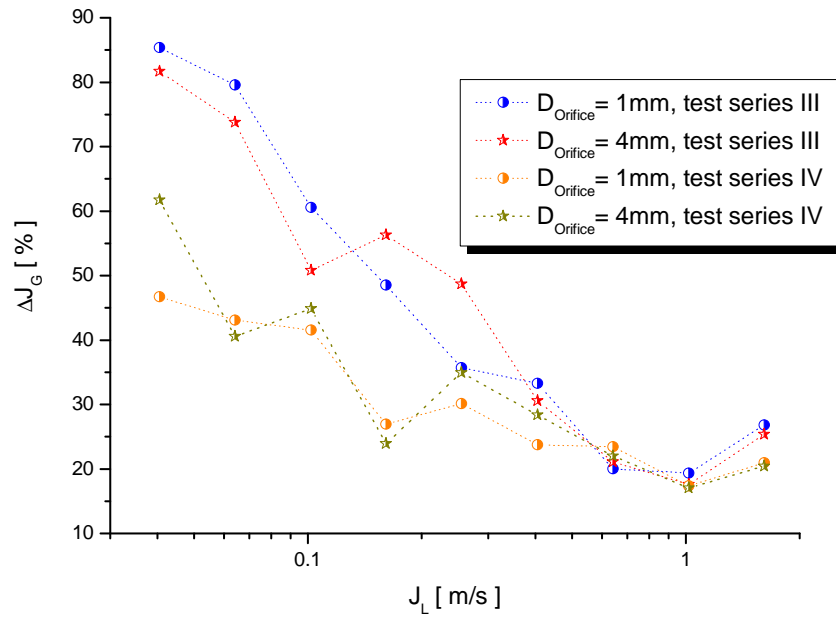


Fig. 1-23 Change of the relative deviation ΔJ_G in dependence on the superficial liquid velocity for the range of the gas injection and at maximum relative test section height L/D for the test series III ($J_G = 0,219$ m/s) and IV ($J_G = 0,0096$ m/s)

2. Results

2.1 Flow patterns

2.1.1 Observed flow patterns

In literature flow patterns in vertical tubes (e.g. Baehr 1996) are usually defined by means of subjective observations. Generally, flow patterns can be categorised basing on characteristic phase distribution in the tube. Objective criteria can be introduced based on the detailed wire-mesh sensor data (s. Prasser et al. 2003). For the present measurements, it is distinguished between bubbly flow, churn-turbulent flow and annular flow. Bubbly flows can be classified additionally in wall- and centre-maximum of the void fraction. According to both Ohnuki et al. (2000) and Prasser et al. (2007), no slug flow (characterised by Taylor bubbles) occurs in the DN200 pipe used.

2.1.2 Criteria for the definition of flow pattern

In the following section, a criterion is introduced, which is used to describe the flow patterns observed in the presented experimental results. The maximum observable diameter $D_{B,max}$ (equivalent diameter of a spherical bubble) serves as such a criterion. A corresponding classification can be done using the bubble size distribution, as well as by visualising of the void fraction. The bubble size distribution for test series I ($J_L = 1.017$ m/s), at a relative test section height of $L/D = 37.7$ and different superficial gas velocities J_G , is shown in Fig. 2-1. In accordance with the virtual side projections view in Fig. 2-2 (1 mm injections) and Fig. 2-3 (4 mm injections), the three flow patterns observed in test series I can be described as follows:

(1) *Bubbly flow*

In the following, a flow is called bubbly flow, if the maximum measured bubble size is smaller than 50 mm ($D_{B,max} < 50$ mm). This flow is characterised by a mono-modal bubble size distribution. The maximum of the bubble size distribution amounts characteristically between 5 and 8 mm. At the maximum scaled test section height and $J_G \leq 0.0574$ m/s, a bubbly flow occurs for all measurements.

As shown in Fig. 2-4, the radial gas volume fraction profiles at the largest L/D have a wall maximum for $J_G \leq 0.0151$ m/s while for $J_G > 0.0151$ m/s a centre-maximum appears.

Similarly, wall maxima of the void fraction always occur close to the gas injection due to the injection through holes in the tube wall. The transition to the profiles of the more or less developed flow (Fig. 2-5) occurs with increasing scaled height L/D . The radial void fraction profiles $\varepsilon(r)$ of all measurement points are represented attached starting from page 99.

(2) Churn-turbulent flow

The churn-turbulent flow is characterised by a bimodal bubble size distribution. In addition to bubble sizes that are similar to the ones in bubbly flows, bigger bubbles with an equivalent diameter from 50 to 500 mm occur. Moreover, a right skewed bubble size distribution develops at larger J_G for the smaller bubble size fraction ($D_B < 50$ mm). As criterion for this flow pattern, $50 \text{ mm} \leq D_{B,\text{max}} \leq 500 \text{ mm}$ was defined. Churn-turbulent flow for test series I occurs at the largest test section height in the range of $0.0898 \text{ m/s} \leq J_G \leq 0.835 \text{ m/s}$. The size of the biggest occurring bubble diameter amounts $D_{B,\text{max}} < 400 \text{ mm}$ (measurement point 151). These bubbles exist not only in the bubble size distribution, but they are also visible in the virtual side projections of the void distribution in Fig. 2-2.

(3) Annular flow

Bimodal bubble size distributions also occur in annular flows. As criterion for this flow pattern, $D_{B,\text{max}} > 500 \text{ mm}$ was defined. An expansion of the average bubble diameter occurs in comparison to the bubbly flow for the smaller bubble size distributions ($D_B < 50$ mm), as well as a right skewed bubble size distribution. Very big gas structures arise with a spherical equivalent diameter from up to about 1 m. By means of the virtual sectional view of the void distribution, in Fig. 2-2 the displacement of liquid in direction of the tube-wall is visible by formation of big interrelated gas structures in the centre of the tube. At measurement point 184 of the test series I, as well as at measurement points 171 and 182 of the test series II, the gas structures are very large and the resulting equivalent diameter is exceeding then 1m. Annular flows occur in the test series I at largest test section height with a superficial gas velocity of $J_G \geq 1.305 \text{ m/s}$.

2.1.3 Dependence of flow pattern on the relative test section height

Alterations of the flow pattern along the bubble rise height occur in the test series I in the range of $0.0898 \text{ m/s} \leq J_G \leq 0.219 \text{ m/s}$. An example of the transition from bubbly flow in the region of gas injection ($L/D = 1.1$) to the churn turbulent flow ($L/D = 39.9$) is indicated at measurement point 118 by means of the bubble size distribution (Fig. 2-6). While in the area of gas injection the biggest bubble diameter is about 50 mm, as result of the coalescence of bubbles, clearly much larger bubbles occur with a $D_{B,\text{max}} = 130 \text{ mm}$ at the L/D of 39.9. The formation of larger bubbles along the test section is also visible by means of the virtual side projections and the sectional views of the void distribution in Fig. 2-7. In these figures, the relation between vertical to horizontal scale is 1:1 i.e. the height is scaled according to average gas phase velocity. There is good agreement between the results of the bubble size distribution with the virtual side projections.

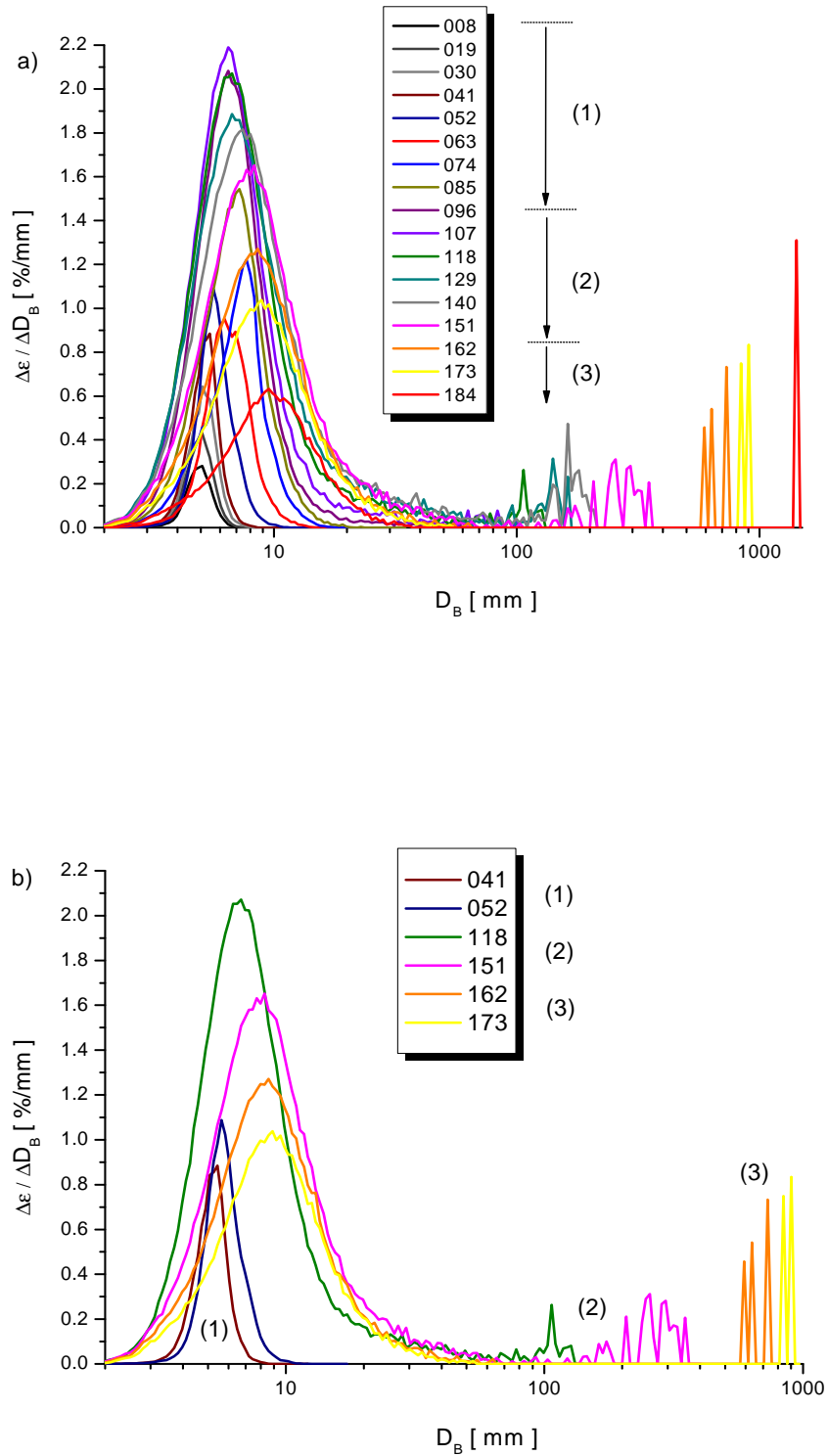


Fig. 2-1 a) Bubble size distributions for different superficial gas velocities J_G (test series I; $J_L = 1.017$ m/s, $D_{\text{Orifice}} = 1$ mm and from measurement point 173 $D_{\text{Orifice}} = 4$ mm, $L/D = 39.7$), b) Selection of some characteristic distributions. The appearance of larger bubble and gas structures is an indication for changed flow patterns.

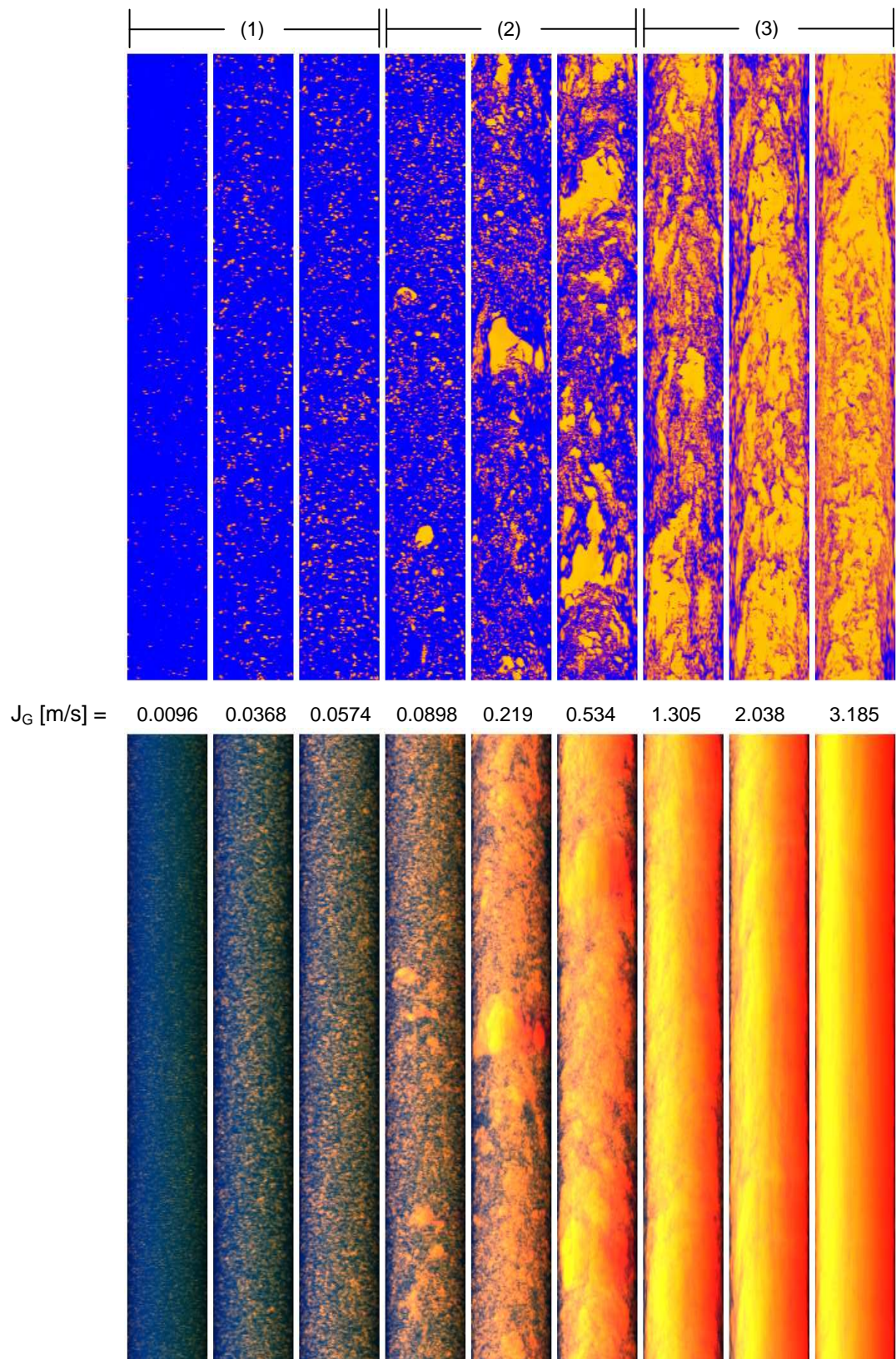


Fig. 2-2 a) Virtual sectional of the void distribution and b) Virtual side projections of the void (air from red to yellow, water = blue) distribution (1) bubbly flow (2) churn-turbulent flow (3) annular flow. Test series I with $D_{\text{Orifice}} = 1$ mm ($D_{\text{Orifice}} = 4$ mm at $J_G = 2.038$ m/s) and maximum L/D . Relation vertical to horizontal scale = 1:1

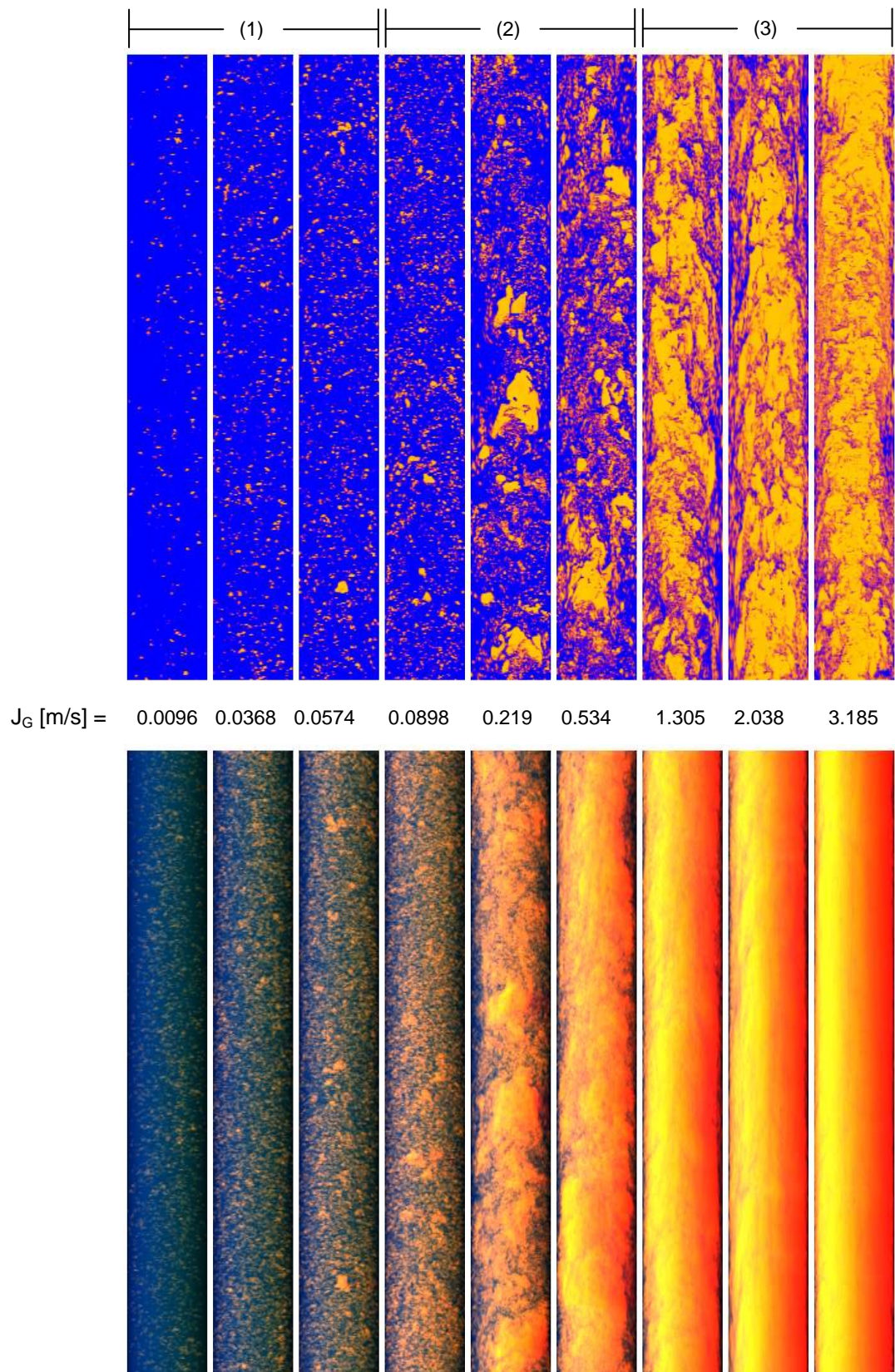


Fig. 2-3 For comparison to Fig. 2-2, test series I with $D_{\text{Orifice}} = 4$ mm is shown here for maximum L/D. (1) bubbly flow (2) churn-turbulent flow (3) annular flow

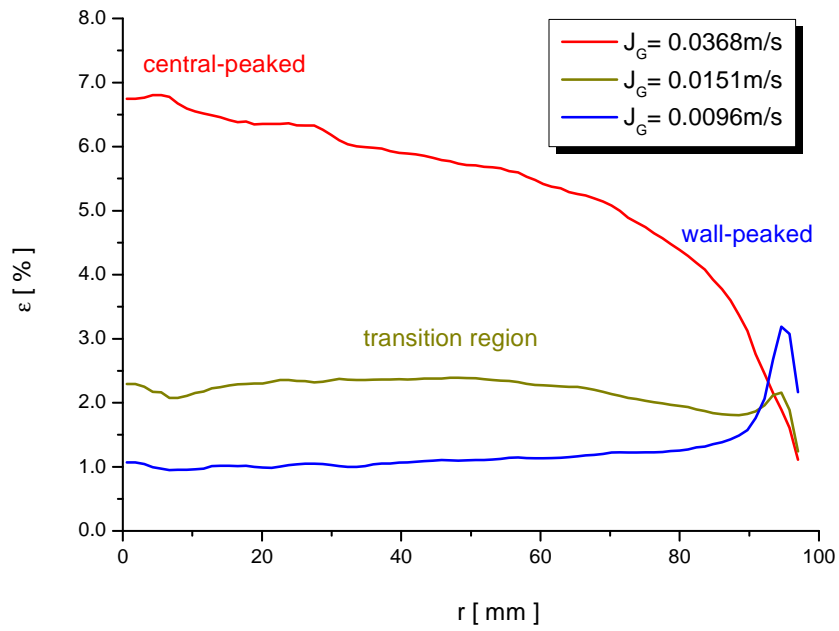


Fig. 2-4 Formation of void fraction maxima during a bubbly flow in dependence on the radius for different superficial gas velocities and constant $J_L = 1.017 \text{ m/s}$ (test series I), maximum test section height and $D_{\text{Orifice}} = 1 \text{ mm}$

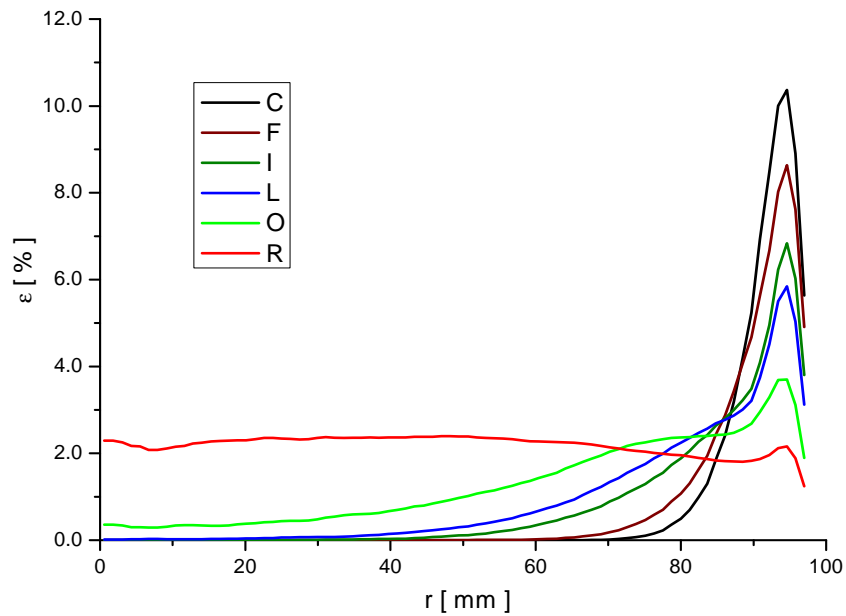


Fig. 2-5 Change of the void fraction peak during bubbly flow along the bubble rise height by the example of the measurement condition 052 ($J_L = 1.017 \text{ m/s}$, $J_G = 0.0151 \text{ m/s}$, $D_{\text{Orifice}} = 1 \text{ mm}$)

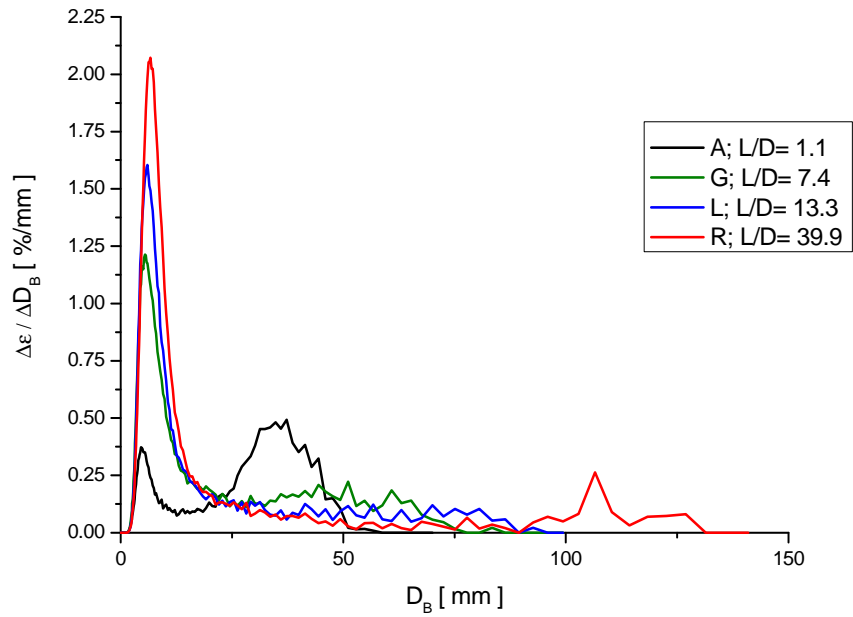


Fig. 2-6 Selection of bubble size distributions in dependence on the height position for measurement point 118. Transition from the bubbly flow at the gas injection with $L/D = 1.1$ to the churn-turbulent flow with $L/D = 39.9$. $D_{\text{Orifice}} = 1 \text{ mm}$

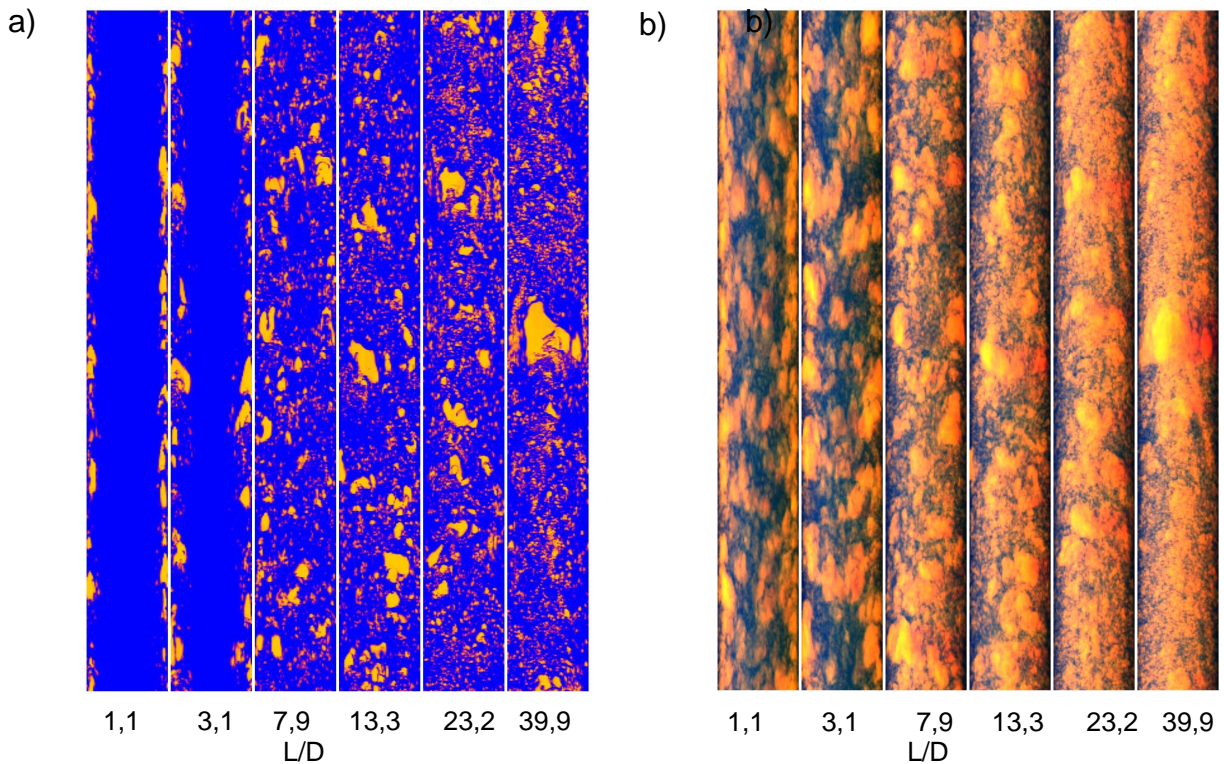


Fig. 2-7 a) Virtual sectional views and b) virtual side projections of the void distribution for different relative test section heights L/D . Measurement point 118 with $J_G = 0.219 \text{ m/s}$ and $J_L = 1.017 \text{ m/s}$. $D_{\text{Orifice}} = 1 \text{ mm}$. Along the rise height, transition from the bubbly to the churn-turbulent flow. Relation vertical to horizontal scale = 1:1

2.1.4 Dependence of the pattern on the diameter of the injection orifices

A change of the flow pattern at maximum L/D caused by the variation of the diameter of the injection from $D_{\text{Orifice}} = 1 \text{ mm}$ to 4 mm was not found. Although the bubble size distribution changes in case of $D_{\text{Orifice}} = 4 \text{ mm}$, particularly during the bubbly flow, the respective flow pattern remains unchanged. The bubble size distributions with $D_{\text{Orifice}} = 1 \text{ mm}$ and 4 mm are represented by their dependence on the relative test section height of L/D for all measurement points in the appendix I.

The influence of D_{Orifice} on the bubble size distribution close to the gas injections is shown for the example of the matrix point 39 of the test series II in Fig. 2-8. Although clearly larger bubbles are formed in case $D_{\text{Orifice}} = 4 \text{ mm}$, the dominate flow pattern, however, does not change ($D_{\text{max}} < 50 \text{ mm}$). In chapter 2.3.1, the influence of the orifice diameter on the position of the bubble size distribution at maximum L/D is discussed more in detail on the basis of the measurement results.

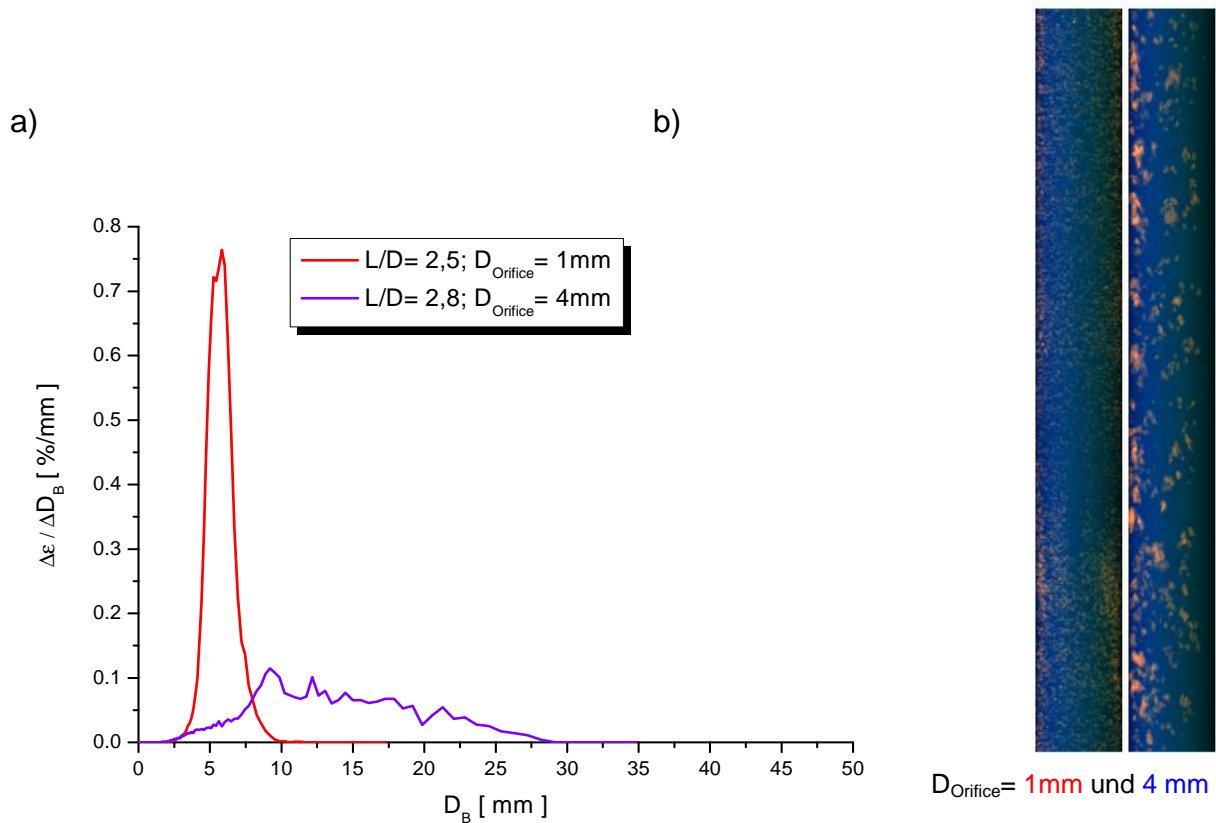


Fig. 2-8 a) Bubble size distribution and b) virtual side projections of the void distribution at matrix point 039, gas injection at different diameters. Relation vertical to horizontal scale = 1:1

2.1.5 Analysis of the flow pattern for the test series II – IV

The changes of the bubble diameter distributions for the test series II ($J_L = 0.405$ m/s) at relative test section height of $L/D = 39.7$ and variable J_G are shown in Fig. 2-9.

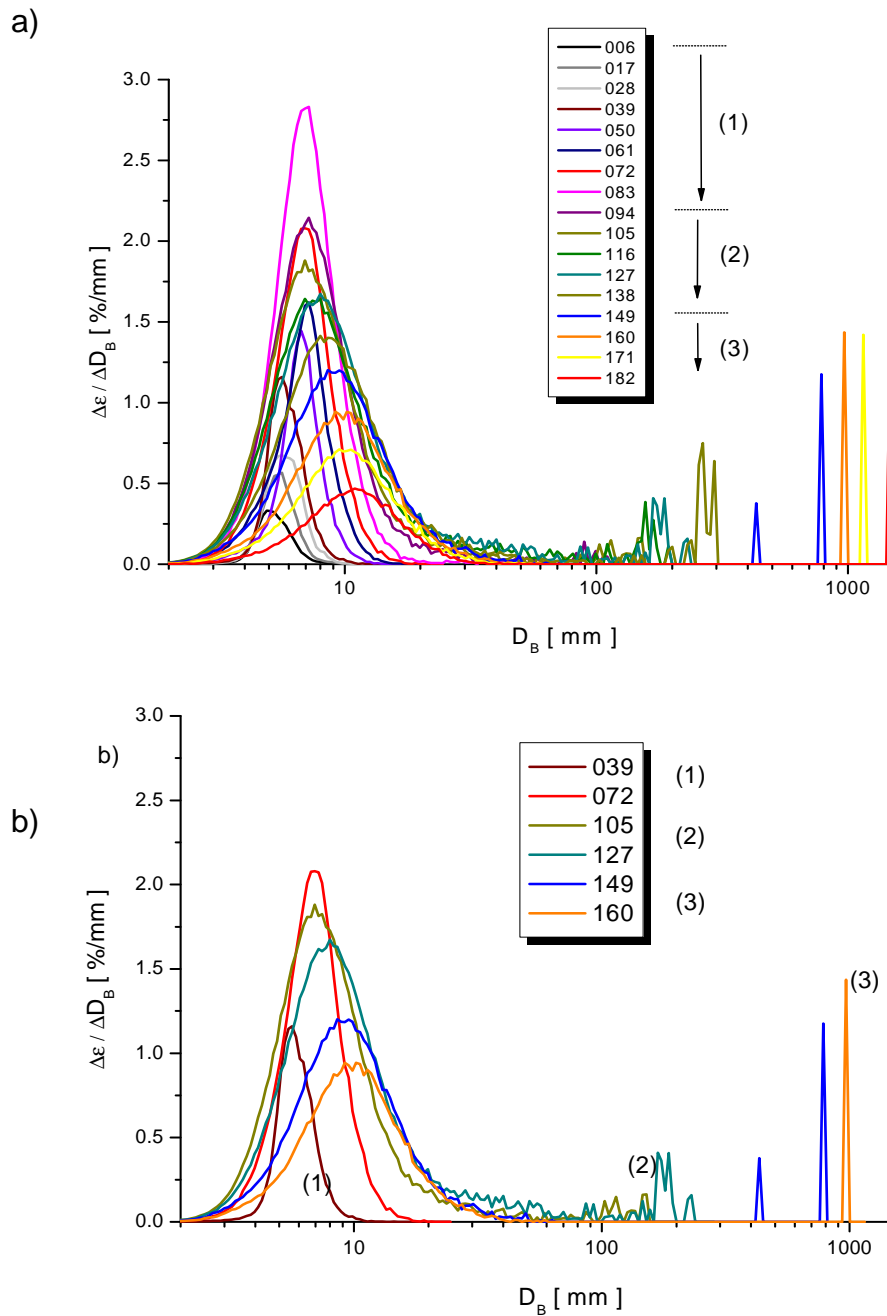


Fig. 2-9 a) Bubble size distributions for different superficial gas velocities J_G (test series II $J_L = 0.405$ m/s, at $L/D = 39.7$ and $D_{\text{Orifice}} = 1$ mm except measurement point 171 for which D_{Orifice} equals to 4 mm), b) Selection of some characteristic distributions. The appearance of larger bubbles and gas structures are an indication for different flow patterns.

Analogous to the bubble size distributions of the test series I, three flow patterns (1)-(3) with the respective characteristic features in the distributions also arise here. The transition from the churn-turbulent flow to the annular flow is observed, in contrast to test series I, already at a superficial gas velocity of $J_G = 0.835$ m/s (Fig. 2-10).

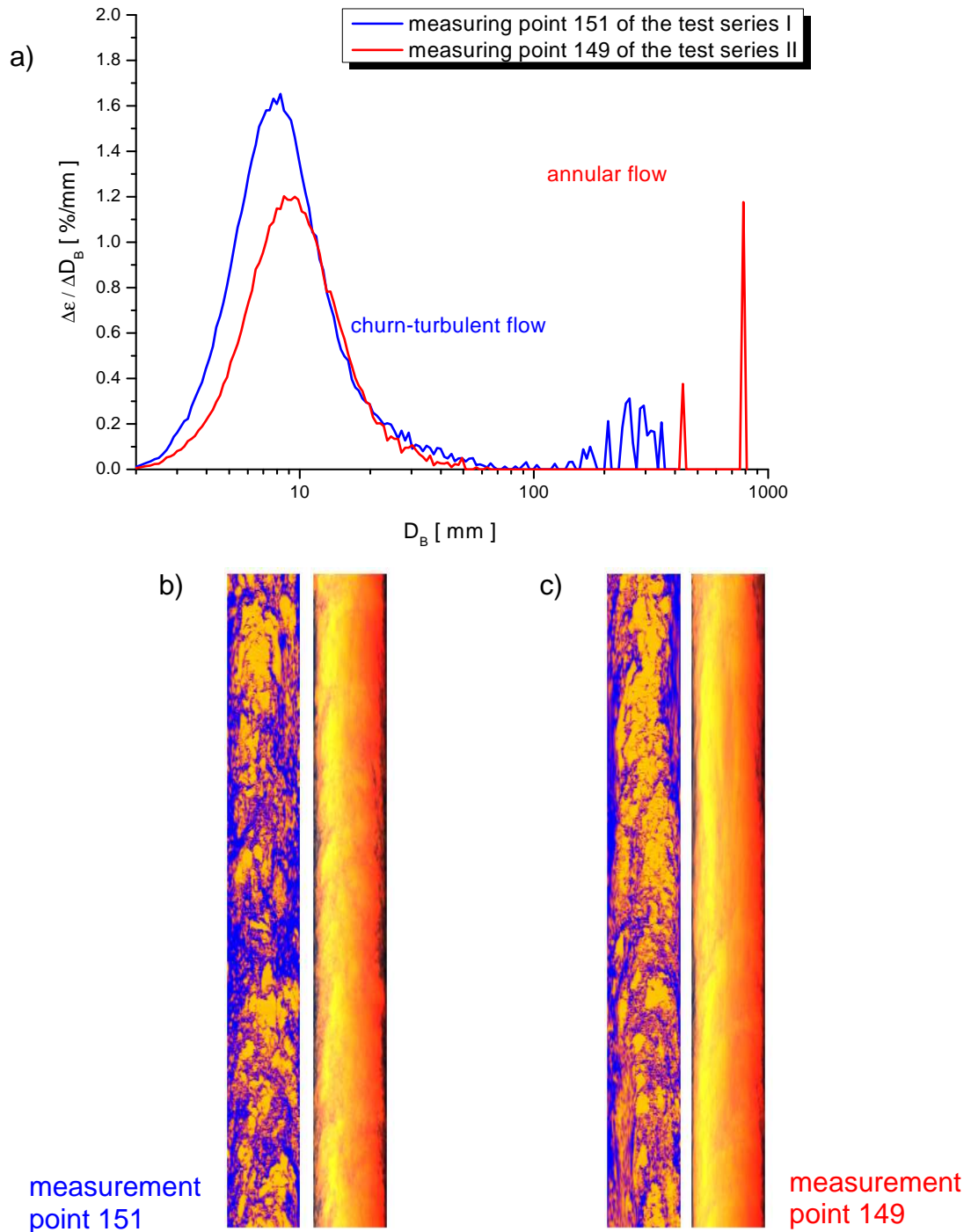


Fig. 2-10 a) Distribution of the bubble diameter at different superficial liquid velocities J_L ; measurement point 151 ($J_L = 1.017$ m/s) and measurement point 149 ($J_L = 0.405$ m/s), for $L/D = 39.7$ and $D_{Orifice} = 1$ mm. Sectional views and virtual side projections of the void distribution with b) churn-turbulent flow and with c) annular flow. Relation vertical to horizontal scale = 1:1

As a consequence of the lower superficial liquid velocity J_L in case of test series II compared to I, larger gas structures are formed, which lead to the formation of annular flow. Developing gas structures with a $D_{B,max} < 400$ mm were observed at a superficial gas velocity of $J_G = 0.835$ m/s in the test series I, whereas significantly larger structures with a $D_{B,max}$ of up to approx. 800 mm (Fig. 2-10 a) are formed in the test series II. The comparison of the sectional views shows the different flow patterns at identical superficial gas velocities J_G (Fig. 2-10 b and c).

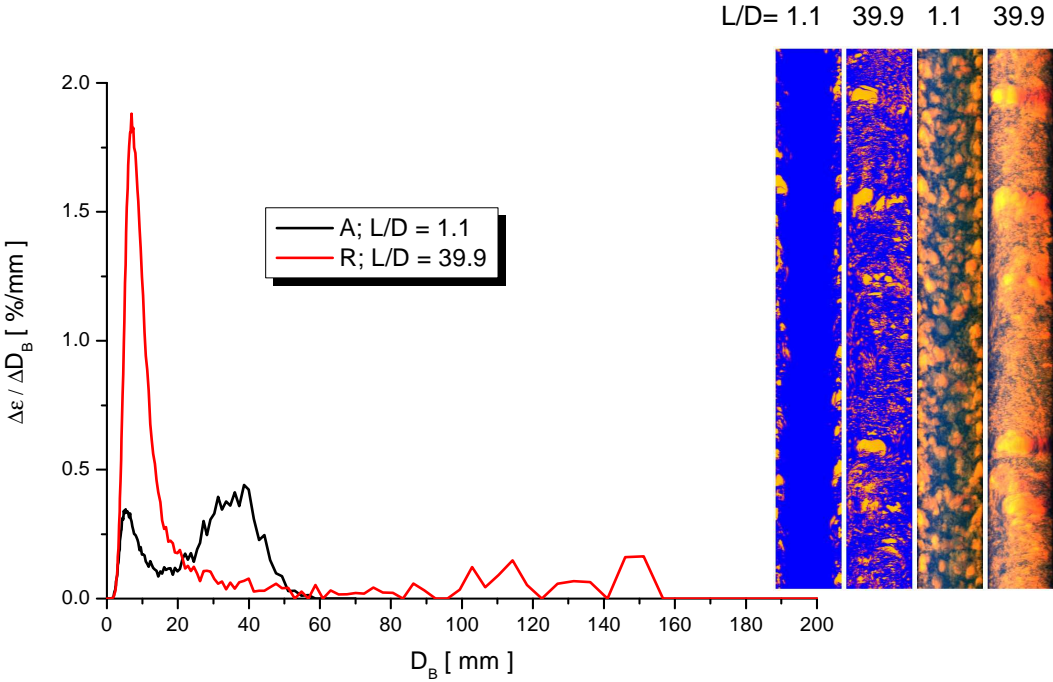


Fig. 2-11 Bubble diameter distribution for the gas injection with $L/D = 1.1$ and at fully developed flow ($L/D = 39.9$) by the example of the measurement point 105 of the test series II ($J_L = 0.405$ m/s). Transition from the bubbly flow to the churn-turbulent flow; $D_{Orifice} = 1$ mm. Sectional views and virtual side projections of the void distribution. Relation vertical to horizontal scale = 1:1

Test series II also proves that the change of the flow pattern occurs during the bubbles' rise for superficial gas velocity 0.0898 m/s and 0.140 m/s. By the example of the matrix point 105, the transition from the bubbly to the churn-turbulent flow during the bubble rise is represented on the basis of the size distribution and the views at Fig. 2-11. Two bubble fractions with average diameters of approx. 5 mm and 35 mm are formed in the range of the gas injection having a maximum diameter of $D_{B,max} \approx 50$ mm. However, due to fragmentation and coalescence a bubble fraction with an average diameter of approx. 7 mm and a broad distribution of large bubble sizes up to $D_B > 140$ mm occur for the largest relative test section height.

The bubble size distributions for test series III ($J_G = 0.219$ m/s), at a relative test section height of $L/D = 39.7$ and different superficial liquid velocities J_L , are represented in Fig. 2-12. Contrary to the bubble size distributions in test series I and II, no changes of the characteristic flow pattern is found.

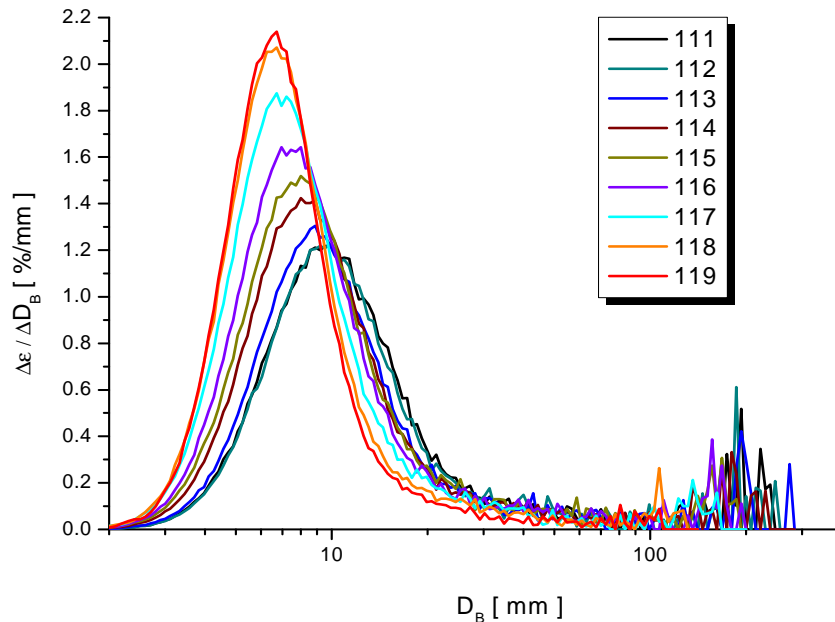


Fig. 2-12 Bubble size distributions for different superficial liquid velocities J_L (test series III, $J_G = 0.219$ m/s, $L/D = 39.7$ and $D_{Orifice} = 1$ mm)

For all measurement points, a churn-turbulent flow exists, which is more or less developed. In addition to the bubble size distribution, typical sectional views and virtual side projections of the void distribution are shown in Fig. 2-13.

Even at matrix point 119 with the highest superficial liquid velocity J_L , pure bubbly flow with a $D_{B,max} < 50$ mm does not occur. The according bubble size distribution (Fig. 2-12) shows a right-inclined frequency distribution with a maximum bubble diameter of $D_{B,max}$ approx. 100 mm. Larger gas structures which develop at lower superficial liquid velocities (measurement point 111-115, 0.0405 m/s $\leq J_L \leq 0.255$ m/s); however cannot be identified in either the bubble size distribution (Fig. 2-12) or the sectional views and virtual side projections of the void distribution for matrix point 119 (Fig. 2-13, $J_L = 1.611$ m/s).

A transition to annular flow is not observed for any of the measurement points due to an insufficiently large superficial gas velocity J_G , which is necessary for the occurrence of annular flow at the selected superficial liquid velocities J_L .

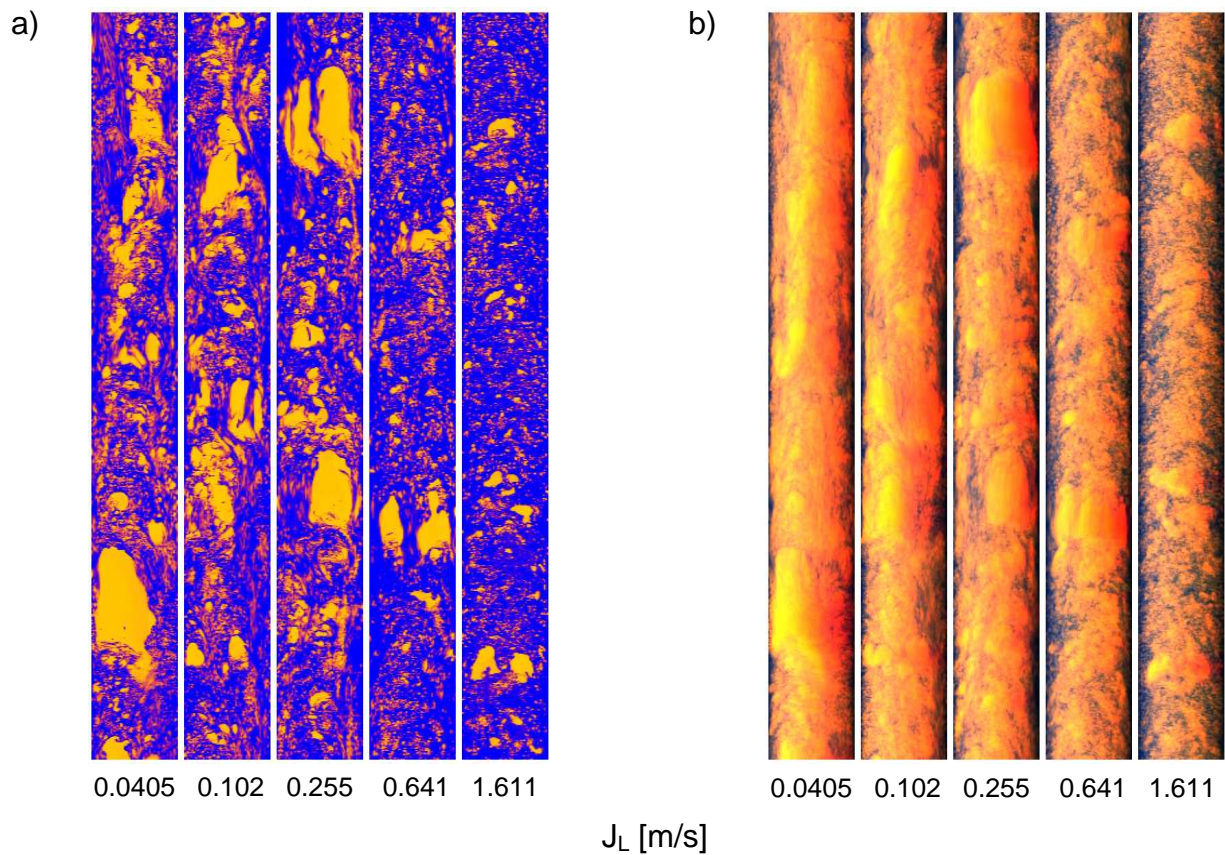


Fig. 2-13 a) Sectional views and b) virtual side projections of the void distribution for test series III ($J_G = 0.219$ m/s, each by $L/D = 39.7$ and $D_{\text{Orifice}} = 1$ mm). Relation vertical to horizontal scale = 1:1

Flow pattern transitions with increasing L/D only appear at measurement points with higher superficial liquid velocities $J_L > 0.405$ m/s (measurement point 117-119). These changes are indicated in the bubble size distribution and the virtual side projections of the gas distribution, as it is discussed by the example of the measurement point 118 of the Fig. 2-6 and Fig. 2-7.

The superficial gas velocity $J_G = 0.0096$ m/s of the test series IV leads, independently on the superficial liquid velocities (0.0405 m/s $\leq J_L \leq 1.611$ m/s) or the bubble rise height, to a bubbly flow without any transition to the churn-turbulent flow (Fig. 2-14) at any measurement point.

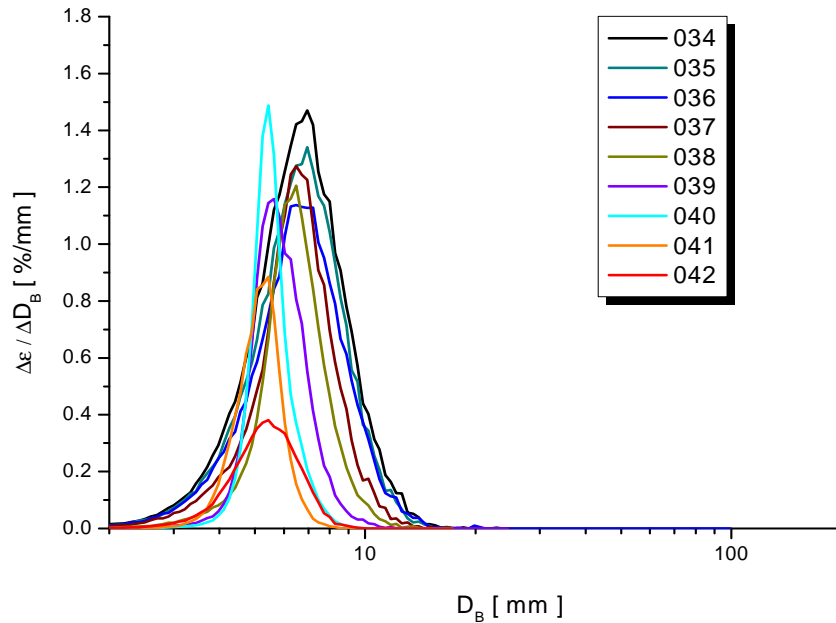


Fig. 2-14 Mono-modal bubble size distributions for different superficial liquid velocities J_L (test series IV, $J_G = 0.0096$ m/s, each with $L/D = 39.7$)

2.1.6 Summary of the observed flow patterns

The results allow to sub divide the measurement matrix into regions of different flows (Table 5). While in the left range of the matrix, the bubbly flow prevails at rather low J_G , the churn-turbulent flow emerges increasingly in the middle and right range, and exclusively at the right edge of the matrix annular flow occurs. Only at measurement points 094-107 and 117-119, as well as at 151 flow pattern transitions along the bubble rise are observed. Thus, the flow pattern changes at measurement points 094-107 and 117-119 from bubbly flow in the range $L/D = 1.1$ into churn-turbulent flow at $L/D = 39.9$.

At measurement point 151, gas structures with a spherical equivalent diameter of $D_B > 500$ mm are detected at $L/D = 1.1$. These gas structures, however, do not develop as a consequence of the forming of an annular flow, but exclusively as a result of the wall injection of the gas. In the pipe centre, no gas structures which are typical for the annular flow are formed at $L/D = 1.1$.

Table 5 Flow pattern for L/D = 39.7. For the coloured fields, a flow pattern transition was observed with increasing L/D.

		Superficial gas velocity J_G [m/s]																				
		0.0025	0.0040	0.0062	0.0096	0.0151	0.0235	0.0368	0.0574	0.0898	0.140	0.219	0.342	0.534	0.835	1.305	2.038	3.185	4.975	7.772	12.14	18.97
Superficial water velocity J_L [m/s]	4.047	011	022	033	044	055	066	077	088	099	110	121	132	143	154	165	176	187	198	209	220	231
	2.554	010	021	032	043	054	065	076	087	098	109	120	131	142	153	164	175	186	197	208	219	230
	1.611	009	020	031	042	053	064	075	086	097	108	119	130	141	152	163	174	185	196	207	218	229
	1.017	008	019	030	041	052	063	074	085	096	107	118	129	140	151	162	173	184	195	206	217	228
	0.641	007	018	029	040	051	062	073	084	095	106	117	128	139	150	161	172	183	194	205	216	227
	0.405	006	017	028	039	050	061	072	083	094	105	116	127	138	149	160	171	182	193	204	215	226
	0.255	005	016	027	038	049	060	071	082	093	104	115	126	137	148	159	170	181	192	203	214	225
	0.161	004	015	026	037	048	059	070	081	092	103	114	125	136	147	158	169	180	191	202	213	224
	0.102	003	014	025	036	047	058	069	080	091	102	113	124	135	146	157	168	179	190	201	212	223
	0.0641	002	013	024	035	046	057	068	079	090	101	112	123	134	145	156	167	178	189	200	211	222
	0.0405	001	012	023	034	045	056	067	078	089	100	111	122	133	144	155	166	177	188	199	210	221

bubbly flow
churn-turbulent flow
annular flow

.....→

2.2 Plausibility of the integral void fraction values

2.2.1 Drift velocity for the validation of experimental results

With the help of the two superposed planes of the wire-mesh sensor, the gas velocity is determined by calculating the cross-correlation functions from the time series of the local instantaneous gas fraction signals at the same mesh points between the measurement planes of the sensor (chapter 1.3). The radial profiles of the gas velocity obtained from the cross-correlations are local averaged values for all bubbles. Additionally to the dependence of the bubble velocity on the radial position, a dependence on the bubble size is also expected. In principle, this could be considered during the evaluation, the statistical uncertainty, however, would be too high. For a reliable determination of gas velocities, longer measurement times would be required due to the dependence of the gas velocity on the radius and the bubble size.

The deviations of the gas volume fluxes calculated from the measurements compared to the appropriate set values, as discussed in chapter 1.7, result from both errors of the measured gas fractions and errors of the measured of the velocities. It can be assumed that the larger errors occur at the velocity measurement. Therefore, in the following, theoretically expected void fraction values will be determined on the basis of drift velocity correlations that are available in the literature and then be compared to measured values.

From the definition of the drift velocity:

$$U_D = U_G - J = J_G / \varepsilon - (J_G + J_L) \quad (2.39)$$

with the volume flow rates (= superficial velocities) J , the void fraction yields:

$$\varepsilon = \frac{J_G}{J_G + J_L + U_D} \quad (2.40)$$

The plausibility check comprises three different assumptions on the drift velocity:

- a) a constant value $U_D = 0.235$ m/s that applies for single bubbles with an equivalent diameter of approx. 6.5 mm; however, the characteristic size range of the bubbles is approx. 4 mm to 10 mm;
- b) an "experimental" value, which is calculated according to equation (2.39) from the measured values for in each case the largest distance between gas injection and measurement plane (1 mm and 4 mm perforations, respectively);
- c) a "weighted" value, which considers both the measured radial profiles and the bubble size distributions (see chapter 2.2.2).

The gas fraction values calculated are represented together with the measured values as a function of the distance between gas injection and the measurement plane, in the appendix I starting from page 99. The dependence of the gas fraction on

L/D occurs, on the one hand, due to the variable pressure, and, on the other hand, due to the change of the drift velocity. In case of comparison a) and b) only the first effect is considered. Thus, the pressure dependence of the gas volume flux is calculated as:

$$J_G(p) = J_{G, \text{Soll}} \frac{p_{\text{Soll}}}{p} \quad (2.41)$$

p stands for the measured pressure near the sensor (at measurement position of pressure PI4-07.1), p_{Soll} is the pressure at the injection position (0.25 MPa) and $J_{G, \text{Soll}}$ is the respective volume flow according to the test matrix (chapter 1.3).

Resulting from this, the gas fraction increases approximately linear with increasing test section length. For large L/D, the gradient usually corresponds to the experimental values with both methods. In case a) a shift between experimental and calculated curves is observed for most of the measurement points. This is avoided by the reference to the experimental value for the maximum L/D ratio (assumption b). There are nevertheless significant deviations within the range of small L/D, which are caused by inlet effects, i.e. the limited validity of the assumption of the constant value for the drift velocity. In order to examine this more exactly, "weighted drift velocities" were used according to assumption c). Their calculation is described more in detail in the following chapter.

2.2.2 Calculation of the weighted drift velocities

The drift flux model is based on the assumption that the cross-section-averaged (one-dimensional) drift velocity is caused by two substantial effects:

- Differences in the radial gas fraction and gas velocity profile affect the average gas velocity. This effect is considered by a so-called profile factor C_0 .
- Local differences of the relative bubble velocities, which mainly depend on the bubble sizes and the bubble density (swarm effect). That is considered by the local drift velocity U_{GL} .

The cross-section-averaged drift velocity is calculated according to:

$$U_D = U_G - J = (C_0 - 1)J + \bar{U}_{GL} \quad (2.42)$$

For the determination of the parameters C_0 and U_{GL} , the cross-section-averaged gas velocity is first determined:

$$\bar{U}_G = \frac{2}{\langle \varepsilon \rangle \cdot R^2} \int_0^R u_G(r) \cdot \varepsilon(r) \cdot r \, dr \quad (2.43)$$

with the cross-section averaged gas fraction:

$$\langle \varepsilon \rangle = \frac{2}{R^2} \int_0^R \varepsilon(r) \cdot r \, dr \quad (2.44)$$

The local gas velocity $u_G(r)$ again depends on the local bubble sizes and the swarm influence. Discrete bubble size distributions are introduced as bubble size classes i , as follows:

$$\bar{U}_G = \frac{2}{\langle \varepsilon \rangle \cdot R^2} \int_0^R \sum_i (u_{G,i}(r) \cdot \varepsilon_i(r)) r dr \quad (2.45)$$

The spatial- and bubble size-dependent gas velocity $u_{G,i}(r)$ might be determined in principle from the experimental data, the statistics, however, is currently not sufficient. For this reason, the velocity is calculated from the local drift velocity of the bubble class i and the local superficial velocity j :

$$u_{G,i}(r) = j(r) + u_{D,i}^{\text{lokal}} \quad (2.46)$$

From equation (2.45) and (2.46), follows:

$$\bar{U}_G = \frac{2}{\langle \varepsilon \rangle R^2} \int_0^R j(r) \cdot \varepsilon(r) r dr + \frac{2}{\langle \varepsilon \rangle R^2} \int_0^R \sum_i (u_{D,i}^{\text{lokal}} \cdot \varepsilon_i(r)) r dr$$

Introducing the parameters C_0 and U_{GL} according to equation (2.42) yields:

$$\bar{U}_G = C_0 J + \bar{U}_{G1} \quad (2.47)$$

$$\text{with } C_0 = \frac{2}{\langle \varepsilon \rangle R^2 \langle j \rangle} \int_0^R j(r) \cdot \varepsilon(r) r dr \quad (2.48)$$

$$\text{and } \bar{U}_{G1} = \frac{2}{\langle \varepsilon \rangle R^2} \int_0^R \sum_i (u_{D,i}^{\text{lokal}} \cdot \varepsilon_i(r)) r dr \quad (2.49)$$

For the calculation of the parameters C_0 and \bar{U}_{G1} the superficial velocity of the two-phase mixture $j(r)$ and the local drift velocity of the bubble class i $u_{D,i}^{\text{lokal}}$ have to be determined, since the profile of the gas volume fraction $\varepsilon(r)$ is known from the experiments.

➤ *Calculation of the local drift velocity of the bubble class i $u_{D,i}^{\text{lokal}}$*

The local drift velocity of the bubble class i can be calculated approximately from the single bubble rise velocity of the appropriate size and a swarm factor:

$$f_{\text{swarm}}(r) = (1 - \varepsilon(r))^{0.25}, \quad (2.50)$$

as follows:

$$u_{D,i}^{\text{lokal}} = (1 - \varepsilon(r)) u_{\text{terminal},i} \cdot f_{\text{swarm}}(r). \quad (2.51)$$

The rise velocity of a single bubble can be determined using the drag coefficient C_D according to:

$$u_{\text{terminal},i} = \sqrt{\frac{4}{3} \cdot \frac{D_B \cdot g}{C_D}} \quad (2.52)$$

The drag factor C_D , for single bubbles largely than 2.6 mm, is calculated basing on the Eötvös-Number:

$$Eo = \frac{g(\rho_f - \rho_B)D_B^2}{\sigma} \quad (2.53)$$

and the following correlation (e.g. Sokolichin, 2004):

$$C_D = \frac{0,622}{\frac{1}{Eo} + 0,235} \quad (2.54)$$

➤ *Calculation of the local volumetric gas flux $j(r)$*

The local volume flux can be calculated according to:

$$j(r) = j_L(r) + j_G(r) = u_L(r)(1 - \varepsilon(r)) + u_G(r)\varepsilon(r) \quad (2.55)$$

Herein the value of the liquid velocity $u_L(r)$ is unknown. Therefore, it is calculated from the measured radial profile of the gas velocity. The average relative velocity dependent on the radial position is given by:

$$u_{\text{rel}}(r) = \frac{f_{\text{Schwarm}}(r)}{\varepsilon(r)} \sum_i (\varepsilon_i(r) \cdot u_{\text{terminal},i}(r)) \quad (2.56)$$

As this calculation method only represents an approximation, a correction factor K is introduced to guarantee the conservation of the liquid mass flow rate. The radial profile of the liquid velocity is calculated according to:

$$u_L(r) = (u_G(r) - u_{\text{rel}}(r)) \cdot K \quad (2.57)$$

Considering the superficial velocity of the water integrated along the piping cross-section:

$$J_L = \frac{2}{R^2} \int_0^R u_L(r) \cdot (1 - \varepsilon(r)) r dr = \frac{2}{R^2} \int_0^R (u_G(r) - u_{\text{rel}}(r)) \cdot K(1 - \varepsilon(r)) r dr \quad (2.58)$$

follows for the correction factor:

$$K = \frac{J_L R^2}{2 \int_0^R (u_G(r) - u_{\text{rel}}(r))(1 - \varepsilon(r)) r dr} \quad (2.59)$$

With the equations (2.42) to (2.59), the computation of the weighted drift velocity can be done all the measurements where the measured values of the gas velocity for all radial positions were acquired.

For all measurement points, where the gas velocity in the centre of the pipe could not be determined due to missing bubbles, a constant value of the gas velocity was accepted as a replacement for the missing radial positions to resolve equation (2.59). This value is formed by the gas velocities, which were based on the radial position r_i , r_{i-1} and r_{i+1} . Whereby, r_i is the radius at which 1 % of the maximum radial gas fraction $\varepsilon(r)$ exists.

Note, that the measured radial gas volume fraction profiles and bubble size distributions used in these calculations are normalised distributions, i.e. the measured absolute values do not influence the results.

2.2.3 Interpretation of the evolution of the gas volume fraction with increasing L/D

In addition to the already mentioned increase of the gas fraction with increasing L/D due to decreasing pressure, it is observed for many measurement points that the curves for small L/D bend either upward (Fig. 2-15 a) or downward (Fig. 2-15 b).

In case of small averaged gas fractions (i.e. matrix points with small gas and large superficial liquid velocities) compared to the usual linear trend higher gas fraction values are observed for small L/D. This increase in gas fraction results from the wall injection of the bubbles. At small gas fraction, the profile of the liquid velocity is only little affected, i.e. close to the wall the liquid velocity is far smaller than in the centre. Therefore, if it is assumed that the relative velocity is only dependent on the bubble size, the gas velocity and in the result the cross-section-averaged drift velocity are consequently also smaller than in case of uniform distributions. The smaller drift velocity causes an increase of the gas fraction.

On the other hand, in case of large gas fractions (i.e. matrix points with large gas and small superficial liquid velocities), there is a substantial influence of the injected gas on the profile of the liquid velocity. The liquid velocities in the wall region are increased and in consequence also the gas velocities have a maximum in this wall region with high gas content, which reduces with increasing L/D. This is clearly identified in the appropriate measured profiles for the gas velocity. Therefore, the cross-section-averaged drift velocity is larger near to the injection and the gas fraction is smaller here.

These described effects are described qualitatively correct according to the calculation of the weighted drift velocities, when considering the above-mentioned effects. However, because of the fact that the calculation also contains some measured values, there is also a dependence of the estimated quantities on these measured values. Nevertheless, since the measured values are only used as weighted distributions, these comparisons make sense. The development of the averaged gas fractions along the tubing height can be explained by means of the above-mentioned effects. However, the comparison also indicates that within the range of the bubbly flow a systematic overestimation of the measured gas fraction obviously exists (see also chapter 1.7).

A calculation of the weighted drift velocities according to the above-mentioned formalism was done for all measurement points, although it is only valid for bubbly

flows. For all measurements, where a churn-turbulent or an annular flow occurred, the validity of the analogy is therefore restricted.

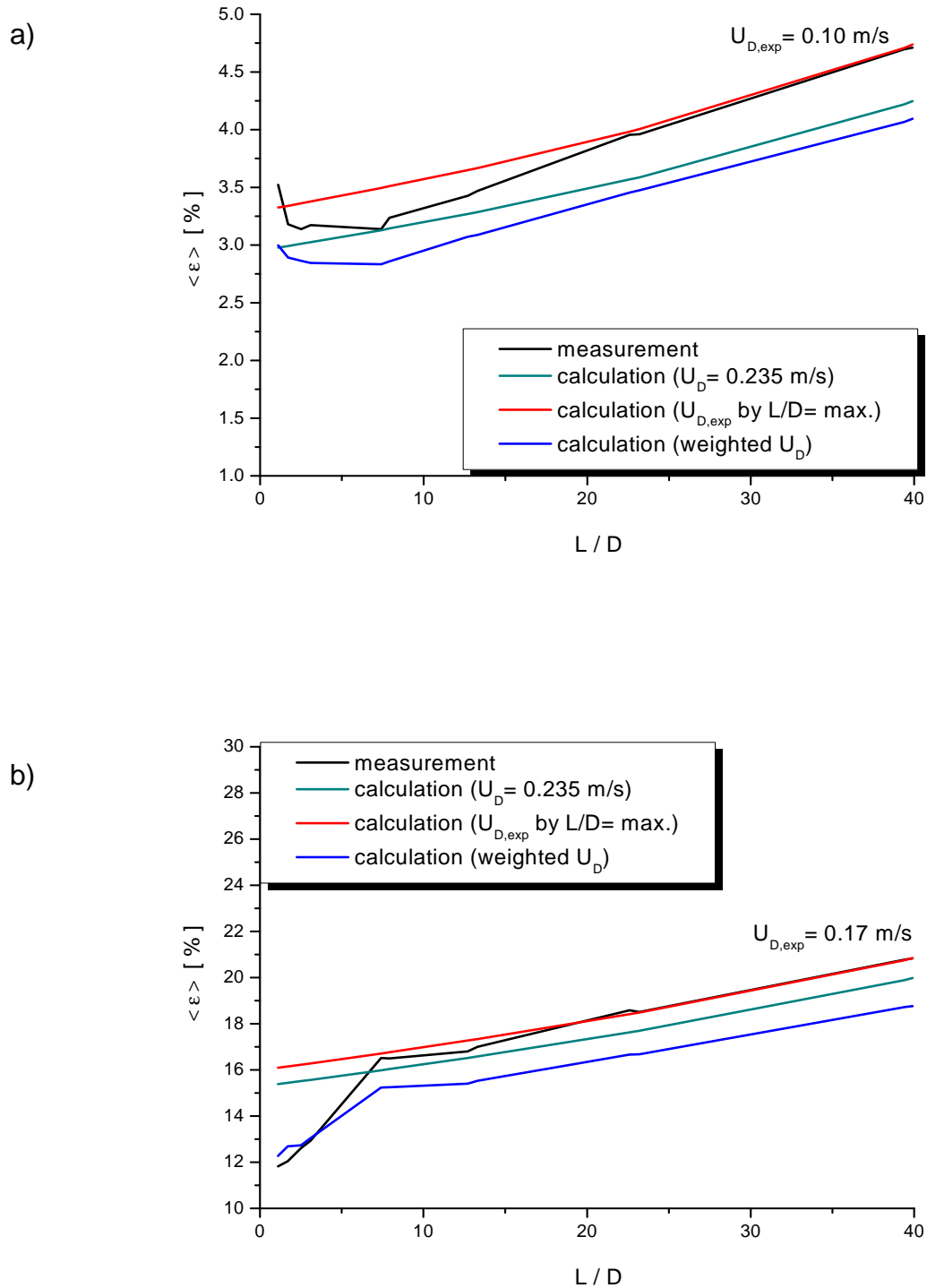


Fig. 2-15 Measured and the calculated gas fraction (different drift velocities as described in chapter 2.2.1) dependent on L/D . Examples of bending the curve in the range of small L/D a) upward at measurement point 074 with $D_{Orifice} = 1$ mm and b) downward at measurement point 118 with $D_{Orifice} = 1$ mm

2.3 Distribution of the bubble diameter

2.3.1 Orifice diameter of the gas injection

The gas injection of the vertical test section enables injection by means of wall orifices with a diameter of $D_{\text{Orifice}} = 1$ or 4 mm, respectively, in order to vary the initial bubble size distribution. Furthermore, the 4 mm orifices of the injection are necessary to realise the high airflow rate (chapter 1.3) required at superficial gas velocities $J_G \geq 2,038$ m/s. In order to be able to assess the influence of the injection diameter at maximum ratio of L/D , the following experimental results are presented.

In the Fig. 2-16, bubble size distributions for different hole diameters of the test section height R ($L/D = 39.9$ and $D_{\text{Orifice}} = 1$ mm) and Q ($L/D = 39.7$ and $D_{\text{Orifice}} = 4$ mm) for matrix points of the test series I are illustrated. While showing significant deviations between the distributions at small superficial gas velocities (J_G until max. 0.015 m/s), they completely disappear starting from a value of $J_G = 0.14$ m/s (measurement point 107). A limit value of $J_G > 0.2$ m/s was indicated for the comparable experiments from previous studies ($D_{\text{Orifice}} = 0.8$ and 6 mm, $J_L = 1.02$ m/s, $L/D = 39.2$). Starting from this value, there is no significant change of the bubble size distribution at the maximum test section length observed for the different injections (Prasser 2002).

In contrast to the test series I, at the test series II differences in the distributions occur only up to a superficial velocity of $J_G = 0.0151$ m/s and disappear nearly completely starting from a velocity of $J_G \geq 0,0368$ m/s (Fig. 2-17). If the superficial gas velocity is further increased, a uniform distribution of the bubble size can be expected at different orifice diameters ($D_{\text{Orifice}} = 1$ mm and 4 mm at maximum L/D).

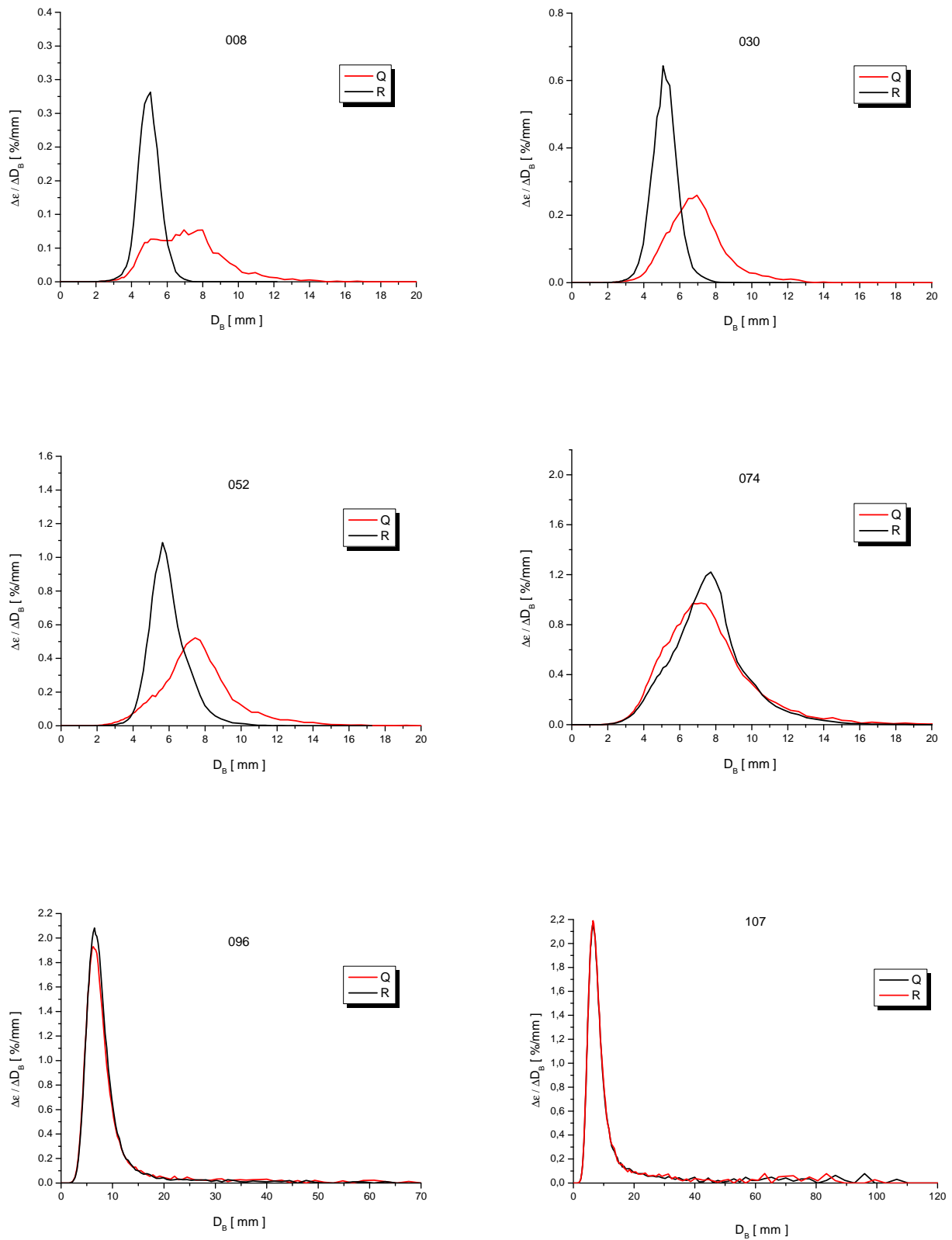


Fig. 2-16 Bubble size distributions for different orifice diameters of the gas injection (test section height R at $L/D = 39.9$ with $D_{\text{Orifice}} = 1$ mm and Q at $L/D = 39.7$ with $D_{\text{Orifice}} = 4$ mm) and different superficial gas velocities J_G from 0.0025 m/s for matrix point 008 to $J_G = 0.14$ m/s for matrix point 107 (test series I)

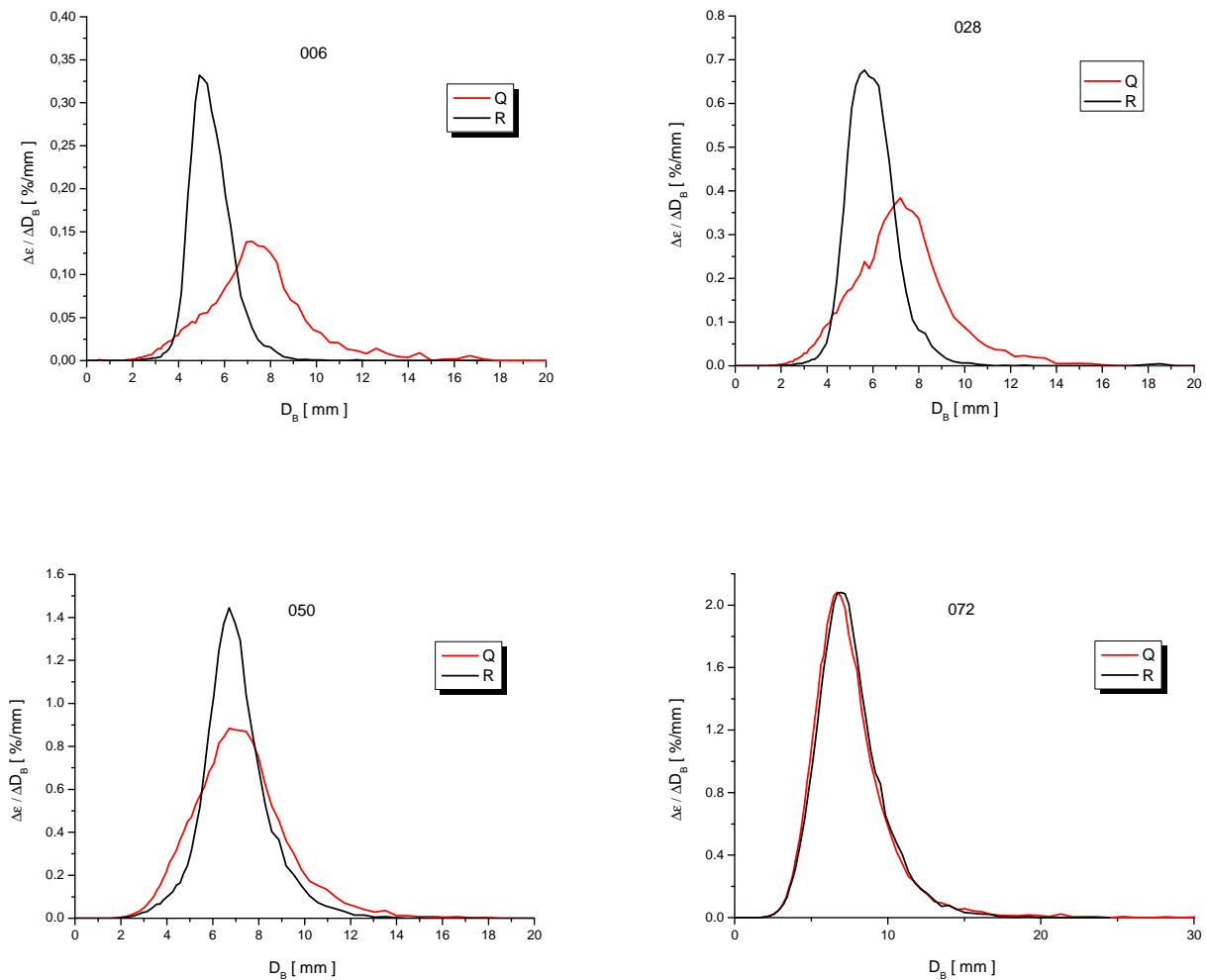


Fig. 2-17 Bubble size distributions for different orifice diameters of the gas injection (test section height R at $L/D = 39.9$ with $D_{\text{Orifice}} = 1$ mm and Q at $L/D = 39.7$ with $D_{\text{Orifice}} = 4$ mm) and different superficial gas velocities J_G from 0.0025 m/s for matrix point 006 to $J_G = 0.0368$ m/s for matrix point 072 (test series II)

2.3.2 Average values of the bubble size distribution

The introduction of average values is a reasonable way for the characterisation of the bubble size distribution. This was done in order to be able to make comparisons on the change of the bubble size caused by variation of the operating conditions or the bubble rise. In contrast to the simple arithmetically averaged value, the median value of a distribution reacts substantially more robust to outliers. Note that the median value must be used in addition to the modal value, mainly for the description of the average bubble sizes in the following analysis.

The bubble size distributions of the test series I-IV, as presented in chapter 2.1, can be used to detect the characteristic average values (Stieß 1994):

⇒ The *median* D_{50} is that bubble size, below those 50 % of all bubble sizes lie.

⇒ The *modal* D_M is at the maximum of the size distribution.

If in the two-phase flow broad distributions with a $D_{B,max} > 50$ mm arise, then in the following, two medians for a defined bubble size range are indicated:

- $2.5 \text{ mm} < D_B \leq 50 \text{ mm} = D_{50,1}$
- $50 \text{ mm} < D_B \leq 500 \text{ mm} = D_{50,2}$

The medians $D_{50,1}$ and $D_{50,2}$ are calculated from the distribution function (distribution sum):

$$Q(D_B) = \int_{D_{B,min}}^{D_B} q(D_B) dD_B \quad \text{with } Q(D_{B, max}) = 1 \quad (2.60)$$

The distribution functions Q of the test series III and the determination of the medians are exemplary presented in the Fig. 2-18. Bubble sizes larger than $D_{50} = 500$ mm are generally not considered for the computation of the median $D_{50,2}$ of all series of measurements, because no statistically useable distribution exists for this size range.

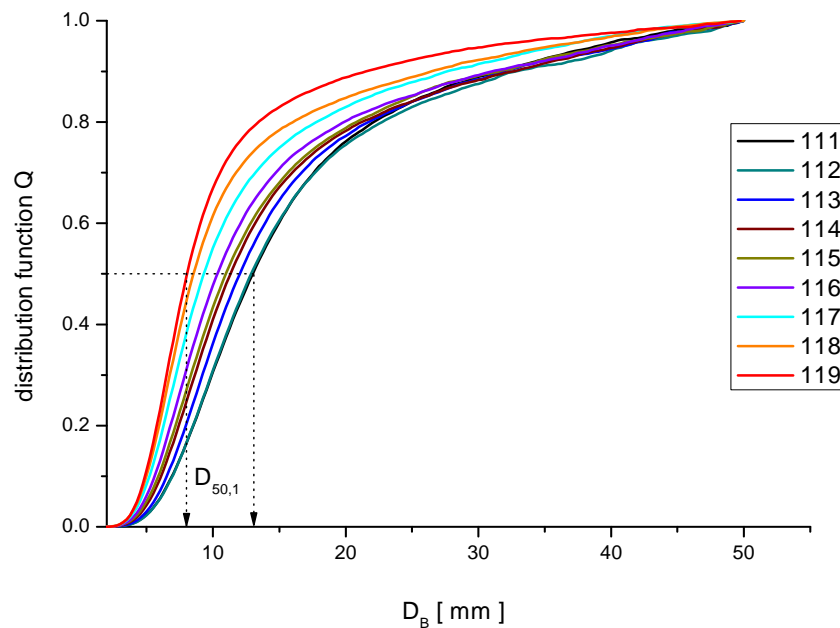


Fig. 2-18 From the distribution function (distribution sum), the median $D_{50,1}$ is determined at $Q = 0.5 (\pm 0.02)$ for different superficial liquid velocities J_L of the test series III, with $J_G = 0.219$ m/s and $D_{Orifice} = 1$ mm, at max. L/D . The resulting median $D_{50,1}$ is between 8.0 mm for the measurement point 119 and 13 mm for the measurement point 111.

The modal D_M as maximum of the bubble size distribution is indicated for all measurement points, exclusively for the size range $2.5 \text{ mm} < D_B < 50$ mm. In the range $D_B > 50$ mm no statistically significant description is possible. The spread of the maximum values of the distribution is too high due to the small number density.

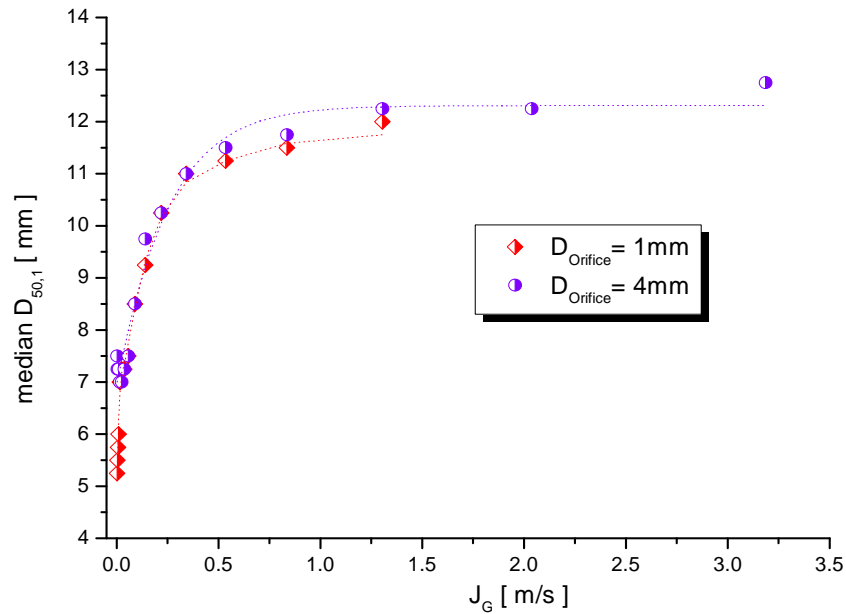


Fig. 2-19 Change of the median $D_{50,1}$ in dependence on the superficial gas velocity J_G of test series II at maximum L/D and different diameters of the perforations for the gas injection

For test series II, the change of the median $D_{50,1}$ is plotted dependent on the superficial gas velocity in the Fig. 2-19. Increases of J_G result in an enlargement of the median up to $D_{50} > 12$ mm for both hole diameters of the gas injection as a consequence of the rising coalescence of the bubbles. While the median changes precipitously for smaller superficial gas velocities ($J_G < 0.8$ m/s), it remains almost constant starting from a value of $J_G \approx 1$ m/s. A further increase of the superficial gas velocity caused an increased generation of larger gas structures within the range of the annular flow. These gas structures, however, are not captured by the median $D_{50,1}$. For the detailed description of the dependence of the median on J_G within the range of smaller superficial gas velocities, the logarithmic representation is chosen in Fig. 1-20. In accordance with the comparative results for bubble size distribution at different orifice diameters $D_{Orifice}$ in chapter 2.3.1, a significant difference in the size of the respective median $D_{50,1}$ only occurs in the range $J_G \leq 0.015$ m/s.

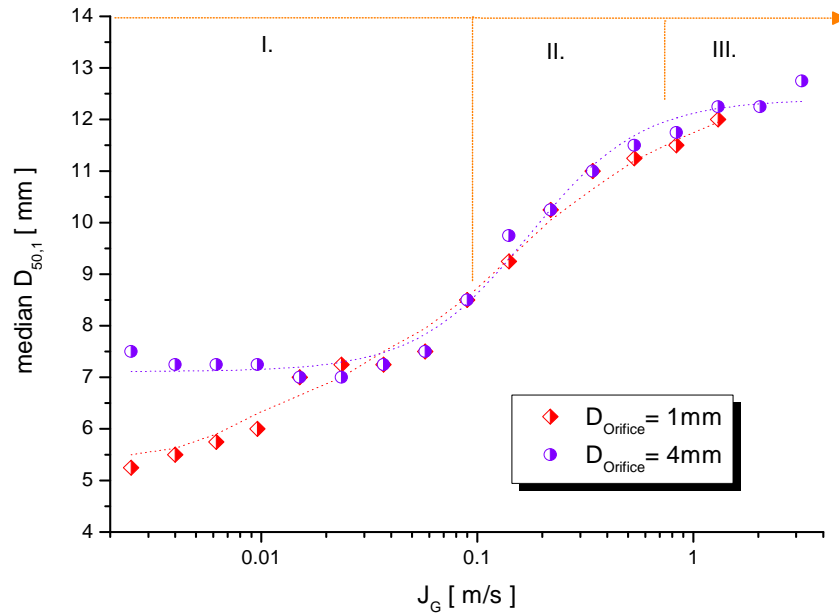


Fig. 2-20 Change of the median $D_{50,1}$ in dependence on the superficial gas velocity J_G of the test series II ($J_L = 0.405$ m/s) at maximum L/D

From the diagrams in Fig. 2-19 and Fig. 1-20, as well as following the criteria on the characteristic flow patterns discussed in chapter 2.1.2, the medians can be assigned to as follows:

- I) bubbly flow: approx. $D_{50,1} = 5 - 8$ mm ($D_{Orifice} = 1$ mm)
 approx. $D_{50,1} = 7 - 8$ mm ($D_{Orifice} = 4$ mm)
- II) churn-turbulent flow: approx. 8 mm $< D_{50,1} < 12$ mm
- III) annular flow: approx. $D_{50,1} \geq 12$ mm

The dependence of the median $D_{50,1}$ on the superficial gas velocity J_G of the test series I displays a course similar to that of test series II (Fig. 2-21). However, as a consequence of the higher superficial liquid velocity (test series I) and an associated reduction of the coalescence with a simultaneous increase of the fragmentation ($\epsilon_{II} > \epsilon_I$) the median $D_{50,1}$ is circa 1.2 mm smaller than the comparable median at test series II ($D_{Orifice} = 4$ mm) starting from $J_G \sim 0.1$ m/s. The influence of the liquid phase on the bubble size distribution can also be described on the basis of the median $D_{50,1}$ of the test series III (variation of J_L with constant J_G). Increases of the superficial liquid velocity cause a reduction of the median $D_{50,1}$ as shown in Fig. 2-22.

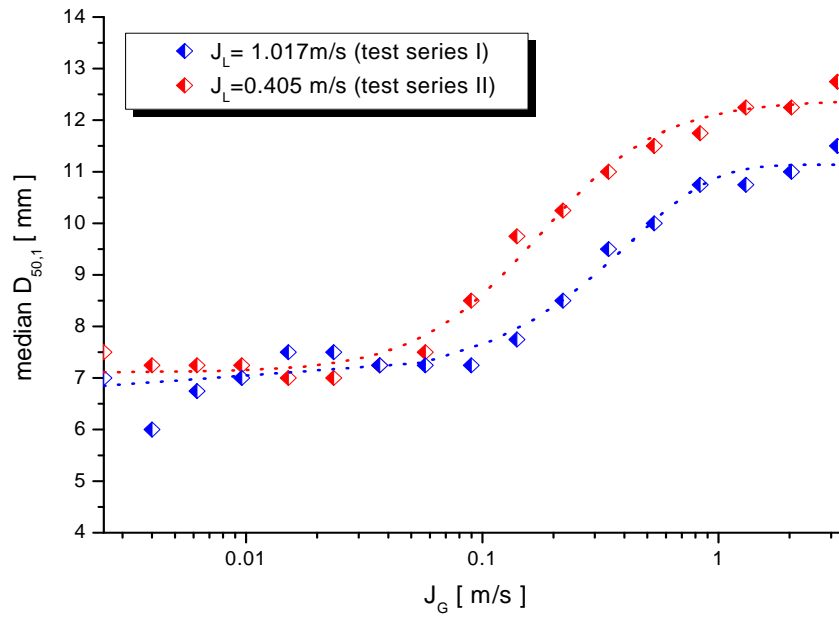


Fig. 2-21 Comparison of the medians $D_{50,1}$ in dependence on the superficial gas velocity J_G for the test series I and II at maximum L/D and $D_{Orifice} = 4$ mm

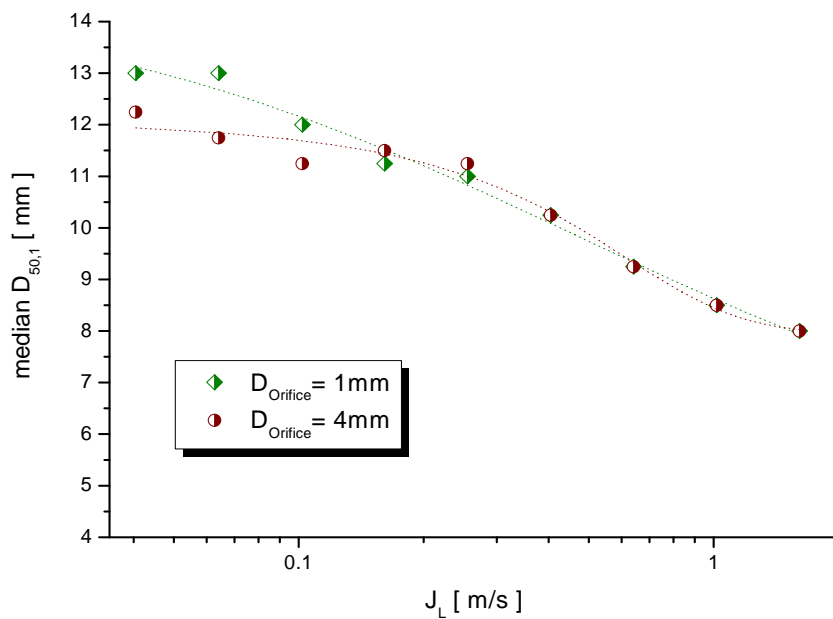


Fig. 2-22 Comparison of the median values of $D_{50,1}$ of the test series III ($J_G = 0,219$ m/s) in dependence on the superficial liquid velocity J_L for different orifice diameters of the gas injection $D_{Orifice}$ at maximum L/D

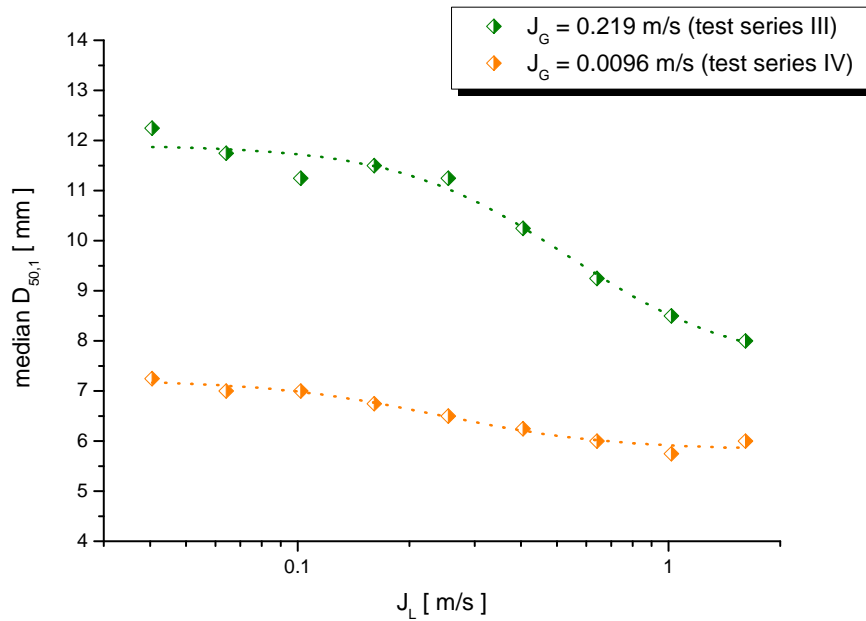


Fig. 2-23 Comparison of the median values of $D_{50,1}$ in dependence on the superficial liquid velocity J_L for the test series III und IV at maximum L/D and $D_{Orifice} = 4$ mm

For this case, the median values of $D_{50,1}$ decrease from approx. $D_{50,1} = 12$ mm to approx. $D_{50,1} = 8$ mm ($D_{Orifice} = 4$ mm), as a consequence of the lower coalescence and higher fragmentation ($\epsilon_{111} > \epsilon_{119}$) for increasing superficial liquid velocities J_L . The influence of the orifice diameter of the gas injection on the median at maximum L/D is limited to superficial liquid velocities lower 0.1 m/s. The test series IV shows a tendentious similar trends ($\epsilon_{036} > \epsilon_{042}$), however, as expected in the range of smaller medians of approx. $6 \text{ mm} \leq D_{50,1} \leq 7.3$ mm (Fig. 2-23).

While for the test series I & II the churn-turbulent flow regime shows maximum medians of approx. $D_{50,1} = 10 - 12$ mm, the median is up to $D_{50,1} = 13$ mm for the churn-turbulent flow regime observed in test series III. This is due to the comparatively smaller superficial liquid velocity and the associated lower fragmentation of the bubbles. Therefore, the median $D_{50,1}$ increases. The transition to the annular flow, however, will not be reached, because the superficial gas velocity of $J_G = 0.219$ m/s is too small.

The bubbly flow regime causes bubbles with medians $D_{50,1}$ of maximal approx. 8 mm at the test series I & II. The results of the test series IV are in accordance with this value, where a maximum median of $D_{50,1} = 7,2$ mm (Fig. 2-23) is observed at $J_L = 0.0405$ m/s. Fig. 2-24 shows the dependence of the median $D_{50,1}$ on the test section length basing on measurement point 050. The continuous reduction of $D_{50,1}$ with increasing L/D is a consequence of turbulence and the subsequent turbulence induced fragmentation. For $L/D \geq 25$, there are no significant changes of the median.

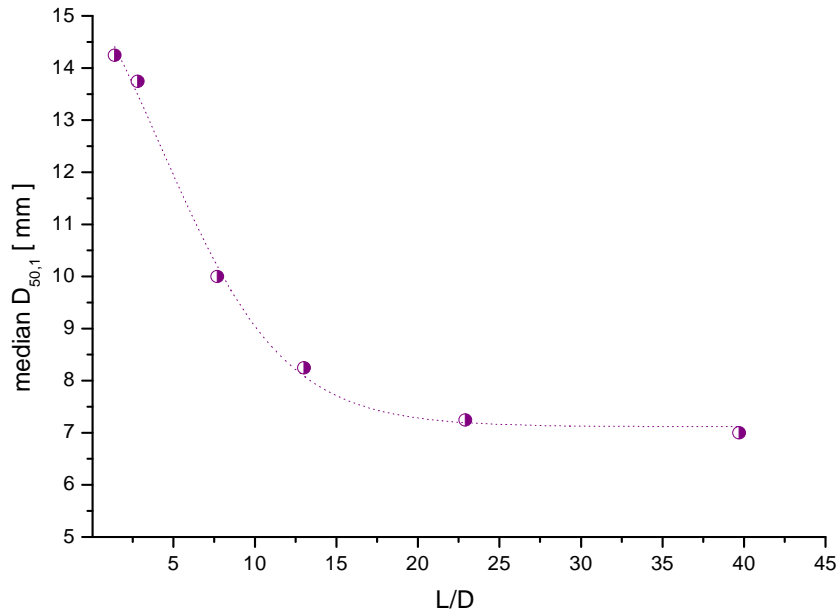


Fig. 2-24 Trend of the median $D_{50,1}$ for measurement point 050 ($J_L = 0.405$ m/s, $J_G = 0.0151$ m/s) along the rise height at $D_{\text{Orifice}} = 4$ mm

The dependence of the median on the test section height can only be used for individual measurement points. If the superficial gas velocity is $J_G < 0.0151$ m/s, the change of the bubble size distribution will be too small for a statistical data evaluation. If J_G exceeds ~ 0.0368 m/s, bimodal velocity distributions form within the range to approx. $L/D \leq 3.1$. However, the gas phase bubble statistics are insufficient for the bubble rise to be related to the median $D_{50,1}$.

For all measurements for which bubbles with a spherical equivalent diameter larger 50 mm occur, the median $D_{50,2}$ increases with the superficial gas velocity and with decreasing superficial liquid velocity. In measurement series IV, the median $D_{50,2}$ is not evaluated, since no gas structures are observed above a bubble diameter of $D_{50,1} > 20$ mm (Fig. 2-14) as a consequence of little coalescence at a relatively small superficial gas velocity ($J_G = 0.0096$ m/s). Fig. 2-25 shows by means of a logarithmical representation the change of the median $D_{50,2}$ with regards to the superficial liquid velocity for the test series III. Large gas structures with a spherical equivalent diameter of up to approx. $D_{50,2} = 200$ mm form at $J_L < 0.0405$ m/s. For a superficial liquid velocity larger 1.611 m/s the size of these bubbles reduce to approx. $D_{50,2} = 80$ mm caused by higher rates of bubble fragmentation (see also Fig. 2-12 and Fig. 2-13).

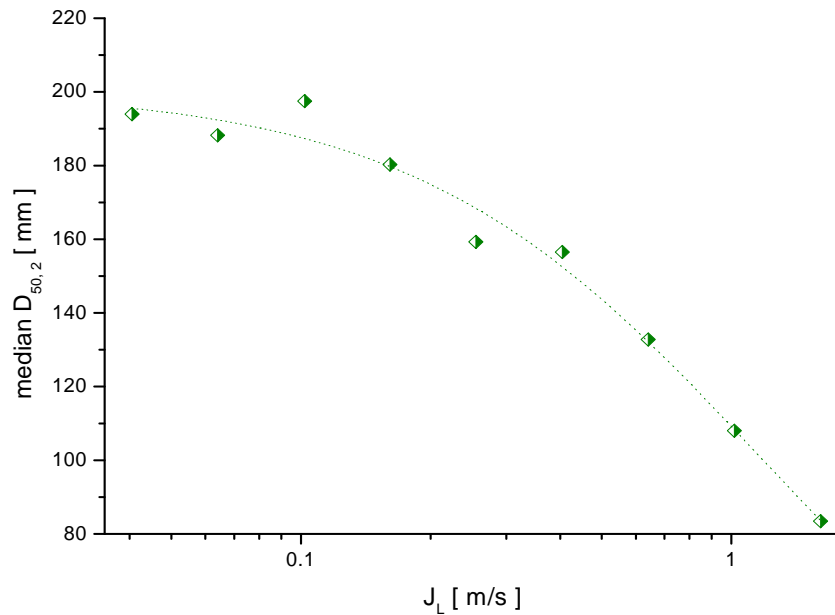


Fig. 2-25 Change of the median $D_{50,2}$ in dependence on the superficial gas velocity J_L of the test series III at maximum L/D and $D_{\text{Orifice}} = 1$ mm

Comparing the medians $D_{50,2}$ for the bubble size of $50 \text{ mm} < D_B < 500 \text{ mm}$ of the test series I and II, two substantial effects can be seen at Fig. 2-26:

- In contrast to the change of the median $D_{50,1}$ (Fig. 2-21), an almost linear rise of $D_{50,2}$ occurs with increasing superficial gas velocity.
- The medians of the test series I are generally smaller, as a consequence of the smaller coalescence and higher fragmentation of the bubbles compared to those of test series II. The reason for this is the larger superficial liquid velocity $J_{L,I} > J_{L,II}$ ($\varepsilon_{II} > \varepsilon_I$).

Significant differences to the trend of the median $D_{50,2}$ with an orifice diameter of the gas injection of $D_{\text{Orifice}} = 4$ mm were not found.

The dependence of the modal D_M on the superficial gas velocity is similar to the median $D_{50,1}$ in all test series. Fig. 2-27 shows the change of the modal D_M and the median $D_{50,1}$ of the test series II with respect to superficial velocity J_G . While the modal and median for superficial gas velocities J_G up to approx. 0.05 m/s don't show significant differences, clear deviations of the average values (up to 2.5 mm) are found for larger superficial gas velocities J_G . This is caused by the different shape of the bubble size distribution for small and large J_G .

Starting from approx. $J_G > 0.1$ m/s, more bubbles with a diameter larger than that of the median occur, which results in an asymmetrical bubble size distribution. The resulting right-skewed distribution, such as represented at measurement point 116 in Fig. 2-28, causes the smaller modal D_M in comparison to the median $D_{50,1}$.

For all four test series, the dependence of the median and modal of the bubble size distribution on the superficial gas velocity and superficial liquid velocity at maximum L/D is presented in the appendix II, starting from page 191.

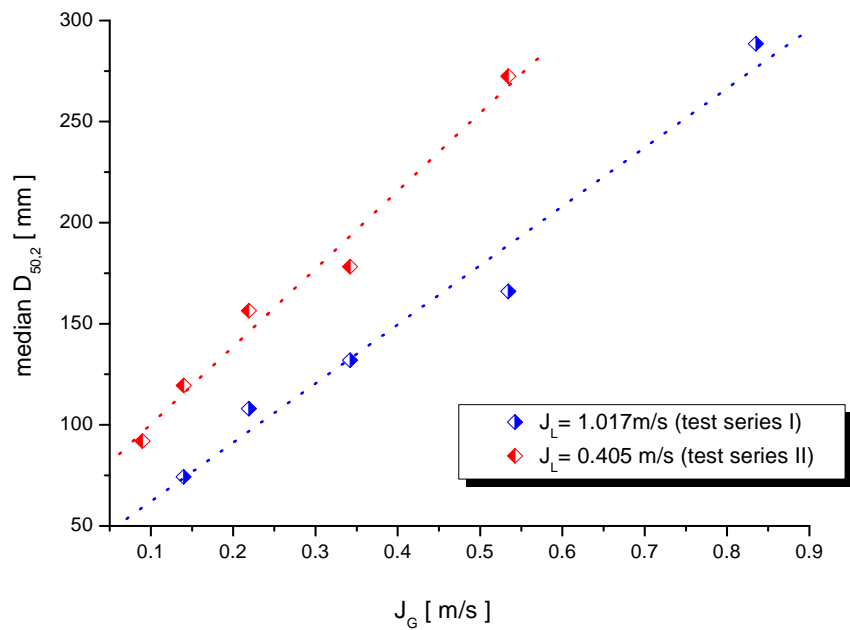


Fig. 2-26 Comparison of median $D_{50,2}$ in dependence on the superficial gas velocity J_G for test series I and II at maximum L/D and $D_{Orifice} = 1$ mm

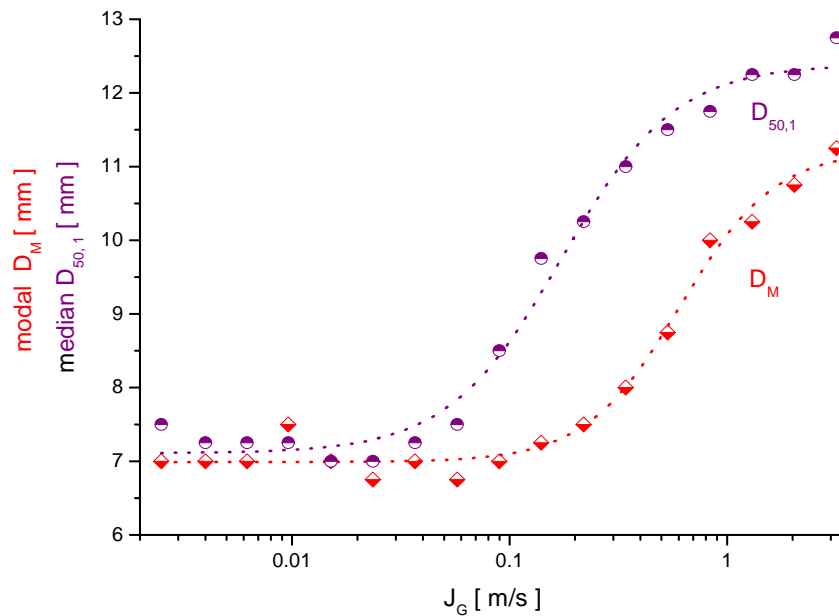


Fig. 2-27 Comparison of the modal D_M and the median $D_{50,1}$ in dependence on the superficial gas velocity J_G for the test series II at maximum L/D and $D_{Orifice} = 4$ mm.

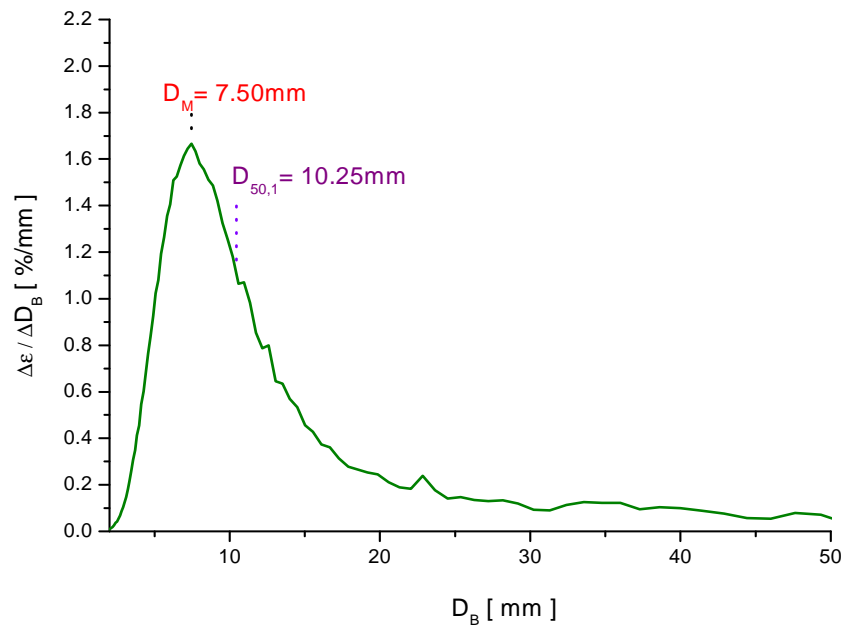


Fig. 2-28 Example of a right-skewed bubble size distribution for bubble diameters up to 50 mm (section of the distribution). Measurement point 116 of the test series II at maximal L/D and $D_{\text{Orifice}} = 4$ mm

3. Conclusions

The extensive experimental results presented in this report provide a high-quality database for air-/water flows in a vertical pipe with a nominal diameter of 200 mm. This database can be used for the development and validation of CFD-like models for two-phase flows, e.g. for bubble coalescence and fragmentation. Experiments are available for bubbly flows, and churn-turbulent, as well as annular flows. In particular, the investigations aim on the evolution of the two-phase flow along the pipe height. Therefore, up to 18 single measurements with varying distances between the gas injection and measurement plane were realised for each of the 92 combinations of gas and water flow rates. Contrary to previous measurements, the pressure at the position of the activated gas injection was kept constant at 0.25 MPa(a). This boundary condition has the advantage that the measured data represent exactly reflect the evolution of the flow along the pipe, i.e. they reflect a configuration at which the gas injection is at a fixed height position, while the measurement plane varies. The water temperature which significantly influences bubble coalescence and fragmentation was kept constant at 30 °C for all measurements. The maximum deviation is 1 K. The primary bubble size was varied by injecting gas through the pipe wall via 1 and 4 mm orifices, respectively.

Important results of this test series are time averaged radial profiles of the gas fraction, and the gas velocity, as well as the time and cross-section averaged bubble size distributions. Furthermore, gas fraction data resolved regarding the bubble size and spatial distribution are presented. For an effective evaluation of the results, the individual tests were grouped into four measurement series, either with a constant superficial gas or water velocity.

As in previous test series, flow patterns were analysed, whereby the classification results from the bubble size. In order to be able to compare the extensive bubble size distributions, median and modal values were used.

A substantial part of these new air/water experiments were quality and plausibility checks of the measured data. As a first step the above mentioned radial profiles and bubble size distributions for different test section lengths were compared to each other for all measurement points and orifice sizes of the gas injection (see Appendix 1). In the result, a clear and consistent trend regarding their evolution with increasing distance from the position of the gas injection was found. As a second check, superficial gas velocities have been reconstructed from the measured radial gas volume fraction and velocity profiles and compared with the setting values, whereby a good agreement could mostly be gained. The reasons for the systematical overestimations in the field of smaller gas fractions are still examined.

In addition, comparisons of the trend of time and cross section averaged gas volume fraction along the pipe height with the theoretically expected values were carried out. For this purpose, averaged drift velocities were calculated considering profile effects as well as the bubble size-dependent rise velocity of single bubbles. Thereby, measured radial gas fraction and velocity profiles, as well as bubble size distributions were used, but they were normalised with their integral values. This minimizes the influence of the measured values on the calculated gas fraction values. These gas fractions well reflect the experimentally determined trend along the pipe height,

particularly that observed close to the gas injection. The small overestimations that particularly occur at low gas fractions are presently analysed.

The influence of the orifice diameter of the gas injection on flow patterns is also discussed in the report. It was verified that differences in the bubble size distribution cannot be determined at superficial water velocities of 0.4 m/s, from a superficial gas velocity of > 0.015 m/s with maximum L/D.

In the currently running TOPFLOW II project, measurements with a fast X-ray tomograph are planned in addition to the ones using a wire-mesh sensor. In this case, no influence of the measurement on the flow is expected. Comparing both measurement methods, the accuracy of the wire-mesh sensors can probably be evaluated more in detail. This possibly should also help to clarify the reasons for the overestimations of the gas fraction for the measurements of bubbly flows with small gas fractions as well as the deviations observed for the reconstructed superficial gas velocities.

4. References

1. Baehr, H. D., Stephan, K. (1996). Wärme-Stoffübergang. Springer Verlag, 2. Auflage, Berlin 1996.
2. Beyer, M., Carl, H., Schütz, P., Pietruske, H., Lenk, S. (2004). Betriebshandbuch für die Mehrzweck-Thermohydraulikversuchsanlage TOPFLOW. FZR-405, Juli 2004.
3. Gnotke, O. (2004). Experimentelle und theoretische Untersuchungen zur Bestimmung von veränderlichen Blasengrößen und Blasengrößenverteilungen in turbulenten Gas-Flüssigkeits-Strömungen. Dissertation am Fachbereich Maschinenbau an der Technischen Universität Darmstadt, April 2004.
4. Gregor, S., Prasser, H.-M., Beyer M. (2006). Thermohydraulische Modellierung der Kondensation von Dampf in einer unterkühlten Flüssigkeitsströmung. FZR-440, Juli 2006.
5. Guet, S., Ooms, G., Oliemans, R. V. A., Mudde, R. F. (2004). Bubble size effect on low liquid input drift-flux parameters. Chemical Engineering Science 59, 3315 – 3329, 2004.
6. Hibiki, T., Ishii, M. (2002). Distribution parameter and drift velocity of drift-flux model in bubbly flow. International Journal of Heat and Mass Transfer 45, 707-721, 2002.
7. Hibiki, T., Ishii, M. (2003). One-dimensional drift-flux model for two-phase flow in a large diameter pipe. International Journal of Heat and Mass Transfer 46, 1773-1790, 2003.
8. Huhn, J., Wolf, J. (1975). Zweiphasenströmung gasförmig/flüssig. Fachbuchverlag Leipzig, 1975.
9. Jakobsen, H. A., Sannaes, B. H., Grevskott, S., Svendsen, H. F. (1997). Modeling of Vertical Bubble-Driven Flows. Industrial Engineering Chemical Research 36, 4052-4074, 1997.
10. Johansen, S. T., Boysan, F. (1988). Fluid Dynamics in Bubble Stirred Ladles: Part II. Mathematical Modeling Metallurgical Transactions B. 19B, 755-764, 1988.
11. Lucas, D., Krepper, E. (2007). CFD models for polydispersed bubbly flows. FZD-486, Sept. 2007.
12. Manera, A., Prasser, H.-M., Van der Hagen, T. H. J. J., Mudde, R. F., de Kruijff, J. M. (2001). A comparison of void-fraction measurements during flashing-induced instabilities obtained with a wire-mesh sensor and a gamma-transmission set-up. 4th International Conference on Multiphase Flow, paper: 436, New Orleans, Louisiana, USA, May 27-June 1, 2001.
13. Matek, W., u. a. (2000). Roloff/Matek Maschinenelemente. Lehr- und Tabellenbuch, Vieweg Verlag, 14. Auflage, Wiesbaden, 2000.

14. Mudde, R. F., Simonin, O. (1999). Two- and Three-Dimensional Simulations of a Bubble Plume Using a Two-Fluid Model. *Chemical Engineering Science* 54, 5061-5069, 1999.
15. Ohnuki, A., Akimoto, H. (2000). Experimental study on transition of flow pattern and phase distribution in upward air-water two-phase flow along a large vertical pipe. *Int. Journal of Multiphase Flow* 26, 367-386, 2000.
16. Pietruske, H., Prasser, H.-M. (2007). Wire-mesh sensors for high-resolving two-phase flow studies at high pressures and temperatures. *Flow Measurement and Instrumentation* 18/2, 87-94, 2007.
17. Prasser, H.-M., Böttger, A., Zschau, J. (1998). A new electrode-mesh tomograph for gas/liquid flows. *Flow Measurement and Instrumentation* 9, 111–119, 1998.
18. Prasser, H.-M., Zschau, J., Peters, D., Pietzsch, G., Taubert, W., Trepte, M. (2000a). Wire-mesh sensor – now 10000 frames per second. Annual report of Institute of Safety Research 1999, FZR-284, ISSN 1437-322X.
19. Prasser, H.-M. (2000b). High-speed measurement of the void fraction distribution in ducts by wire-mesh sensors. International Meeting on Reactor Noise, Athen, 11.-13.10., 2000.
20. Prasser, H.-M., Scholz, D., Zippe, C. (2001). Bubble size measurement using wire-mesh sensors. *Flow Measurement and Instrumentation* 12, 299-312, 2001.
21. Prasser, H.-M., Krepper, E., Lucas, D. (2002). Evolution of the two-phase flow in a vertical tube - decomposition of gas fraction profiles according to bubble size classes using wire-mesh sensors. *International Journal of Thermal Sciences* 41, 17-28, 2002.
22. Prasser, H.-M. (2002). Influence of the Gas Injection on the Void Fraction Profiles and Bubble Size Distributions of a Air-Water Flow in Vertical Pipes. ICMF 2004, Yokohama, Japan, May-June, 2004.
23. Prasser, H.-M., Lucas, D., Krepper, E., Baldauf, D., Böttger, A., Rohde, U., Schütz, P., Weiss, F.-P., Zippe, C., Zippe, W., Zschau, J. (2003). Strömungskarten und Modelle für transiente Zweiphasenströmungen. Abschlußbericht des vom BmWT geförderten zum Forschungsvorhaben 150 1215, Forschungszentrum Dresden-Rossendorf e.V., Institut für Sicherheitsforschung.
24. Prasser, H.-M., Misawa, M., Tiseanu, I. (2005). Comparison between Wire-mesh sensor and ultra-fast X-ray tomograph for an air/water flow in a vertical pipe. *Flow Measurement and Instrumentation* 16, 73-83, 2005.
25. Prasser, H.-M., Beyer, M., Carl, H., Manera, A., Pietruske, H., Schütz, P., Weiß, F.-P. (2006). The multipurpose thermalhydraulic test facility TOPFLOW: an overview on experimental capabilities, instrumentation and results. *Kerntechnik* 71/4, 163-173, 2006.

26. Prasser, H.-M., Beyer, M., Carl, H., Manera, A., Pietruske, H., Schütz, P. (2006). Experimente zu aufwärtsgerichteten Gas/Flüssigkeitsströmungen in vertikalen Rohren. Technischer Fachbericht des vom BmWT geförderten Forschungsvorhaben 150 1265, Forschungszentrum Dresden-Rossendorf e.V., Institut für Sicherheitsforschung.
27. Prasser, H.-M., Lucas, D., Beyer, M., Vallée, C., Krepper, E., Höhne, T., Manera, A., Carl, H., Pietruske, H., Schütz, P., Zaruba, A., Allissa, S., Shi, J.-M., Weiss, F.-P. (2007). Aufbau und Durchführung von Experimenten an der Mehrzweck-Thermohydraulikversuchsanlage TOPFLOW für generische Untersuchungen von Zweiphasenströmungen und die Weiterentwicklung und Validierung von CFD-Codes. Abschlußbericht des vom BmWT geförderten zum Forschungsvorhaben 150 1265, Forschungszentrum Dresden-Rossendorf e.V., Institut für Sicherheitsforschung.
28. Prasser, H.-M., Beyer, M., Carl, H., Manera, A., Pietruske, H., Schütz, P. (2007a). Experiments on upwards gas/liquid flow in vertical pipes, FZD-482, 2007.
29. Prasser, H.-M. (2007b). Evolution of interfacial area concentration in a vertical air-water flow measured by wire-mesh sensors. Nuclear Engineering and Design 237, 1608-1617, 2007.
30. Schaffrath, A., Krüssenberg, A.-K., Weiß, F.-P., Hicken, E.-F., Beyer, M., Carl, H., Prasser, H.-M., Schuster, J., Schütz, P., Tamme, M. (2001). TOPFLOW - a new multipurpose thermalhydraulic test facility for the investigation of steady state and transient two-phase flow phenomena. Kerntechnik 66, 2001.
31. Scholz, D. (2000). Bewertung der Genauigkeit eines Gittersensors zur Visualisierung einer Zweiphasenströmung durch Vergleich mit optischen Hochgeschwindigkeitsaufnahmen. FZR-300, September 2000.
32. Sihana, S. (2002). Bestimmung der Strömungsform von Zweiphasenströmungen mittels Absorption von Röntgenstrahlen und Benutzung von neuronalen Netzen. Dissertation am Fachbereich Prozesswissenschaften der Technischen Universität Berlin, 2002.
33. Sokolichin, A. (2004). Mathematische Modellbildung und numerische Simulation von Gas-Flüssigkeits-Blasenströmung. Habilitation an der Universität Stuttgart 2004.
34. Stieß, M. (1995). Mechanische Verfahrenstechnik Band I, Springer-Verlag Berlin, Heidelberg, New York.
35. Tomiyama, A. (1998). Struggle with Computational Bubble Dynamics. Proceedings of Third Int. Conf. Multiphase Flow, ICMF 1998, Lyon, France, June 8-12, 1998.
36. VDI-Wärmeatlas, 5. Auflage (1988a), Lb1-Lb3.
37. VDI-Wärmeatlas, 5. Auflage (1988b), Lc5-Lc6.

38. Wagner, W., Cooper, J. R., Dittmann, A., Kijima, J., Kretschmar, H.-J., Kruse, A., Mareš, R., Oguchi, K., Sato, H., Stöcker, I., Šifner, O., Takaishi, Y., Tanishita, I., Trübenbach, J., Willkommen, Th. (1997). The IAPWS Industrial Formulation 1997 for the Thermodynamic Properties of Water and Steam. *Journal of Engineering for Gas Turbines and Power* 122, 150-182, 2000.

5. Nomenclature and indexes

5.1 Symbols

Sign	Unit	Description
A	m ²	area
C _D	-	drag coefficient
D	m	diameter
D _M	mm	modal for the bubble size range: 0 - 50 mm
D _{50,1}	mm	median for the bubble size range: 0 - 50 mm
D _{50,2}	mm	median for the bubble size range: 50 - 500 mm
E _o	-	Eötvös-number
f	1/s	frequency
f	-	swarm factor
F	-	factor
g	m/s ²	acceleration due to gravity
g	MPa	gauge pressure
H, h	m	height
h	1/mm	frequency of occurrence
J, j	m/s	cross section and local superficial velocity
k	mm	surface roughness of a pipe, coefficient of pressure drop
ΔL	m	distance between the gas injection and the measurement plane
m	Kg/s	mass flow
n	-	parameter, bubble number
p	Pa	pressure
Q	%	distribution function
R, r	m	radius
rm	m	moment
t	s	time
T	°C	temperature
U	V	voltage
U, u	m/s	cross section and local velocity
D _{D, exp}	m/s	drift velocity, calculated from experimental data at maximum L/D
V	m ³	volume
w	m/s	velocity
X _{LM}	-	LOCKHART/MARTINELLI - parameter
<X>		above the flow cross-section averaged value X
\bar{X}		above the bubble size-averaged value; arithmetical middle value

x	m	coordinate
y	m	coordinate
z	m	coordinate
α	-	part
Φ		two-phase multiplier according to LOCKHART/MARTINELLI
Δ	-	difference
ε	%	volumetric gas fraction
λ	-	pipe friction coefficient
ν	m ² /s	kinematic viscosity
ρ	kg/m ³	density
ζ	-	drag coefficient
σ	N/m	surface tension

5.2 Indices and abbreviations

Sign	Denomination
0	source
1,2	number of measurement planes
a	absolute pressure
b	bubble identification number
B	bubble, bend
CM	centre of mass
D	drift
exp	experimental
F	fluid (two-phase mixture)
G, g	gas
ges	complete
H	hydrostatic
l, L	liquid
i,j,k	inside, index, bubble size class, class
in	gas injection
m	number of concentric ring domain for the azimuthal averaging
Min	minimal
Max	maximal
meas	measurement
N	norm

orifice	diameter of the orifice of the gas injection
P	phase
rel	relative
R	roughness
ü	over pressure
W,l	liquid phase, water
x, y	coordinates

5.3 Abbreviations

Sign	Denomination
BMWi	Bundesministerium für Wirtschaft und Technologie
CFD	C omputational F luid D ynamics
DN	Nominal diameter
FZD	F orschungs Z entrum D resden-Rossendorf e.V.
GS	Wire-mesh sensor
PI	Measurement position of pressure
TOPFLOW	T ransient tw O Phase F LOW test facility
TI	Measurement position of temperature
FIC	Measurement position of mass flow controller

5.4 Figures

Fig. 1-1	General scheme of the thermal hydraulic test facility TOPFLOW; test section circuit and compressed air system are highlighted by colour.....	12
Fig. 1-2	Vertical test section of the TOPFLOW facility with variable gas injection system (DN 200)	14
Fig. 1-3	Injection module of the variable gas injection	14
Fig. 1-4	Variable gas injection with positions of pressure and temperature measurement points	16
Fig. 1-5	Measurement principle of the wire-mesh sensor, simplified scheme of a wire-mesh sensor with 4 x 4 electrodes	22
Fig. 1-6	Construction design of the double low temperature wire-mesh sensor.....	24
Fig. 1-7	Installation of the sensor in the upper range of the test section.....	25
Fig. 1-8	Positions of the relevant measurement points at the test section circuit.....	26
Fig. 1-9	Histogram of the mesh point 43 x 43 for the test point 140	29
Fig. 1-10	Comparison of radially averaged calibration profiles for the test points 140 - green and 182 - red (histogram calibration)	29
Fig. 1-11	Weight coefficients for the cross-section averaging of local gas fractions measured by the wire-mesh sensor	31
Fig. 1-12	Weight coefficients for the cross-section averaging of local gas fractions over a number of ring-shape domains	32
Fig. 1-13	Discretisation error of the determination of the local gas velocities in dependence of the distance between the planes of measurements.....	40
Fig. 1-14	Error for the pressure boundary condition above the wire-mesh sensor for the test series I	43
Fig. 1-15	Error for the pressure boundary condition above the wire-mesh sensor for the test series II	44
Fig. 1-16 & Fig. 1-17	Error for the pressure boundary condition above the wire-mesh sensor for the test series III und IV	44
Fig. 1-18	Comparison of the superficial gas velocity $J_{G,in}$ calculated from experimental data with the set value J_G at maximum L/D for the test series I ($J_L = 1.017$ m/s) with different injection $D_{Orifice} = 1$ and 4 mm	46
Fig. 1-19	Relative deviation of J_G obtained from the measurement compared to the set value of the superficial gas velocity for different diameters of the gas injection at maximum L/D	47
Fig. 1-20	Variation of the relative deviation of J_G obtained from the measurement compared to set value along the relative test section	

	height L/D by the example of the measurement point 140 of the test series I with $D_{\text{orifice}} = 1 \text{ mm}$	47
Fig. 1-21	Variation of the difference ΔJ_G with the superficial gas velocity for the smallest (A) and at maximum (R) relative height L/D (test series I $D_{\text{orifice}} = 1 \text{ mm}$)	48
Fig. 1-22	Comparison of the calculated superficial gas velocity $J_{G,\text{in}}$ with the constant set value J_G for test series III ($J_G = 0.219 \text{ m/s}$) and IV ($J_G = 0.0096 \text{ m/s}$) in dependence on J_L at maximal test section height L/D	49
Fig. 1-23	Change of the relative deviation ΔJ_G in dependence on the superficial liquid velocity for the range of the gas injection and at maximum relative test section height L/D for the test series III ($J_G = 0,219 \text{ m/s}$) and IV ($J_G = 0,0096 \text{ m/s}$)	50
Fig. 2-1	a) Bubble size distributions for different superficial gas velocities J_G (test series I; $J_L = 1.017 \text{ m/s}$, $D_{\text{orifice}} = 1 \text{ mm}$ and from measurement point 173 $D_{\text{orifice}} = 4 \text{ mm}$, $L/D = 39.7$), b) Selection of some characteristic distributions. The appearance of larger bubble and gas structures is an indication for changed flow patterns.	53
Fig. 2-2	a) Virtual sectional of the void distribution and b) Virtual side projections of the void (air from red to yellow, water = blue) distribution (1) bubbly flow (2) churn-turbulent flow (3) annular flow. Test series I with $D_{\text{orifice}} = 1 \text{ mm}$ ($D_{\text{orifice}} = 4 \text{ mm}$ at $J_G = 2.038 \text{ m/s}$) and maximum L/D . Relation vertical to horizontal scale = 1:1	54
Fig. 2-3	For comparison to Fig. 2-2, test series I with $D_{\text{orifice}} = 4 \text{ mm}$ is shown here for maximum L/D . (1) bubbly flow (2) churn-turbulent flow (3) annular flow	55
Fig. 2-4	Formation of void fraction maxima during a bubbly flow in dependence on the radius for different superficial gas velocities and constant $J_L = 1.017 \text{ m/s}$ (test series I), maximum test section height and $D_{\text{orifice}} = 1 \text{ mm}$	56
Fig. 2-5	Change of the void fraction peak during bubbly flow along the bubble rise height by the example of the measurement condition 052 ($J_L = 1.017\text{m/s}$, $J_G = 0.0151 \text{ m/s}$, $D_{\text{orifice}} = 1 \text{ mm}$)	56
Fig. 2-6	Selection of bubble size distributions in dependence on the height position for measurement point 118. Transition from the bubbly flow at the gas injection with $L/D = 1.1$ to the churn-turbulent flow with $L/D = 39.9$. $D_{\text{orifice}} = 1 \text{ mm}$	57
Fig. 2-7	a) Virtual sectional views and b) virtual side projections of the void distribution for different relative test section heights L/D . Measurement point 118 with $J_G = 0.219 \text{ m/s}$ and $J_L = 1.017 \text{ m/s}$. $D_{\text{orifice}} = 1 \text{ mm}$. Along the rise height, transition from the bubbly to the churn-turbulent flow. Relation vertical to horizontal scale = 1:1	57

Fig. 2-8	a) Bubble size distribution and b) virtual side projections of the void distribution at matrix point 039, gas injection at different diameters. Relation vertical to horizontal scale = 1:1	58
Fig. 2-9	a) Bubble size distributions for different superficial gas velocities J_G (test series II $J_L = 0.405$ m/s, at $L/D = 39.7$ and $D_{Orifice} = 1$ mm except measurement point 171 for which $D_{Orifice}$ equals to 4 mm), b) Selection of some characteristic distributions. The appearance of larger bubbles and gas structures are an indication for different flow patterns.....	59
Fig. 2-10	a) Distribution of the bubble diameter at different superficial liquid velocities J_L ; measurement point 151 ($J_L = 1.017$ m/s) and measurement point 149 ($J_L = 0.405$ m/s), for $L/D = 39.7$ and $D_{Orifice} = 1$ mm. Sectional views and virtual side projections of the void distribution with b) churn-turbulent flow and with c) annular flow. Relation vertical to horizontal scale = 1:1	60
Fig. 2-11	Bubble diameter distribution for the gas injection with $L/D = 1.1$ and at fully developed flow ($L/D = 39.9$) by the example of the measurement point 105 of the test series II ($J_L = 0.405$ m/s). Transition from the bubbly flow to the churn-turbulent flow; $D_{Orifice} = 1$ mm. Sectional views and virtual side projections of the void distribution. Relation vertical to horizontal scale = 1:1	61
Fig. 2-12	Bubble size distributions for different superficial liquid velocities J_L (test series III, $J_G = 0.219$ m/s, $L/D = 39.7$ and $D_{Orifice} = 1$ mm).....	62
Fig. 2-13	a) Sectional views and b) virtual side projections of the void distribution for test series III ($J_G = 0.219$ m/s, each by $L/D = 39.7$ and $D_{Orifice} = 1$ mm). Relation vertical to horizontal scale = 1:1	63
Fig. 2-14	Mono-modal bubble size distributions for different superficial liquid velocities J_L (test series IV, $J_G = 0.0096$ m/s, each with $L/D = 39.7$) ...	64
Fig. 2-15	Measured and the calculated gas fraction (different drift velocities as described in chapter 2.2.1) dependent on L/D . Examples of bending the curve in the range of small L/D a) upward at measurement point 074 with $D_{Orifice} = 1$ mm and b) downward at measurement point 118 with $D_{Orifice} = 1$ mm	71
Fig. 2-16	Bubble size distributions for different orifice diameters of the gas injection (test section height R at $L/D = 39.9$ with $D_{Orifice} = 1$ mm and Q at $L/D = 39.7$ with $D_{Orifice} = 4$ mm) and different superficial gas velocities J_G from 0.0025 m/s for matrix point 008 to $J_G = 0.14$ m/s for matrix point 107 (test series I)	73
Fig. 2-17	Bubble size distributions for different orifice diameters of the gas injection (test section height R at $L/D = 39.9$ with $D_{Orifice} = 1$ mm and Q at $L/D = 39.7$ with $D_{Orifice} = 4$ mm) and different superficial gas velocities J_G from 0.0025 m/s for matrix point 006 to $J_G = 0.0368$ m/s for matrix point 072 (test series II)	74
Fig. 2-18	From the distribution function (distribution sum), the median $D_{50,1}$ is determined at $Q = 0.5 (\pm 0.02)$ for different superficial liquid velocities J_L of the test series III, with $J_G = 0.219$ m/s and $D_{Orifice} =$	

	1 mm, at max. L/D. The resulting median $D_{50,1}$ is between 8.0 mm for the measurement point 119 and 13 mm for the measurement point 111.....	75
Fig. 2-19	Change of the median $D_{50,1}$ in dependence on the superficial gas velocity J_G of test series II at maximum L/D and different diameters of the perforations for the gas injection.....	76
Fig. 2-20	Change of the median $D_{50,1}$ in dependence on the superficial gas velocity J_G of the test series II ($J_L = 0.405$ m/s) at maximum L/D.....	77
Fig. 2-21	Comparison of the medians $D_{50,1}$ in dependence on the superficial gas velocity J_G for the test series I and II at maximum L/D and $D_{\text{Orifice}} = 4$ mm	78
Fig. 2-22	Comparison of the median values of $D_{50,1}$ of the test series III ($J_G = 0,219$ m/s) in dependence on the superficial liquid velocity J_L for different orifice diameters of the gas injection D_{Orifice} at maximum L/D.....	78
Fig. 2-23	Comparison of the median values of $D_{50,1}$ in dependence on the superficial liquid velocity J_L for the test series III und IV at maximum L/D and $D_{\text{Orifice}} = 4$ mm	79
Fig. 2-24	Trend of the median $D_{50,1}$ for measurement point 050 ($J_L = 0.405$ m/s, $J_G = 0.0151$ m/s) along the rise height at $D_{\text{Orifice}} = 4$ mm	80
Fig. 2-25	Change of the median $D_{50,2}$ in dependence on the superficial gas velocity J_L of the test series III at maximum L/D and $D_{\text{Orifice}} = 1$ mm	81
Fig. 2-26	Comparison of median $D_{50,2}$ in dependence on the superficial gas velocity J_G for test series I and II at maximum L/D and $D_{\text{Orifice}} = 1$ mm	82
Fig. 2-27	Comparison of the modal D_M and the median $D_{50,1}$ in dependence on the superficial gas velocity J_G for the test series II at maximum L/D and $D_{\text{Orifice}} = 4$ mm.....	82
Fig. 2-28	Example of a right-skewed bubble size distribution for bubble diameters up to 50 mm (section of the distribution). Measurement point 116 of the test series II at maximal L/D and $D_{\text{Orifice}} = 4$ mm.....	83

5.5 Tables

Table 1:	Absolute and relative heights at the test section variable gas injection	15
Table 2:	General experimental matrix of the FZD for vertical pipe flows; test points of the current series are highlighted.....	21
Table 3:	Measurement devices in the test section circuit, which were used during the experiments and for the data evaluation of the air/water series of tests L12	27
Table 4	Number of interpolated azimuthally averaged gas velocities per measurement point and injection length (out of 80 radius rings)	42
Table 5	Flow pattern for $L/D = 39.7$. For the coloured fields, a flow pattern transition was observed with increasing L/D	65

6. Appendix

Starting from page 99 the compilation of the main results for all measurement points is given:

I) Characteristic data of the measurement points.....	99
II) Median and Modal.....	191
III) Additional results of the accuracy check (see chapter 1.7.....	195
IV) Operating data.....	1987
V) Calibration protocols.....	2165
VI) Description of the data files available for the air/water test series L12	2443

Characteristic data for all the measurement points given in the appendix I

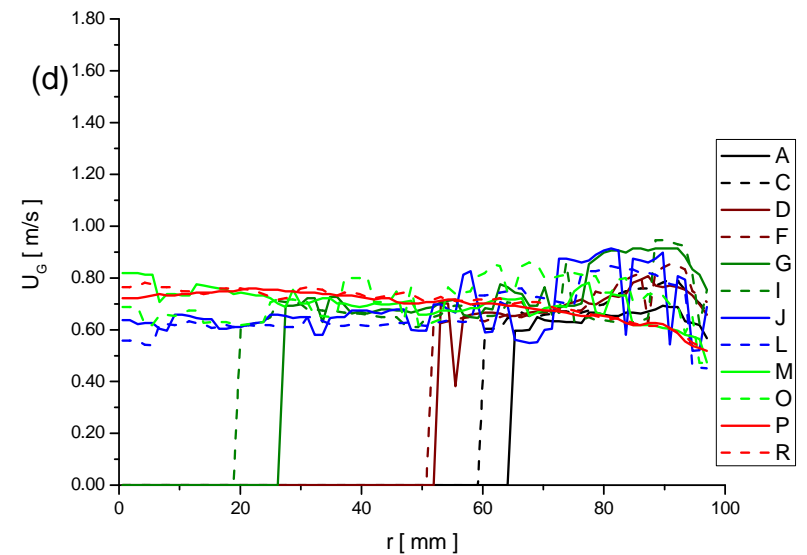
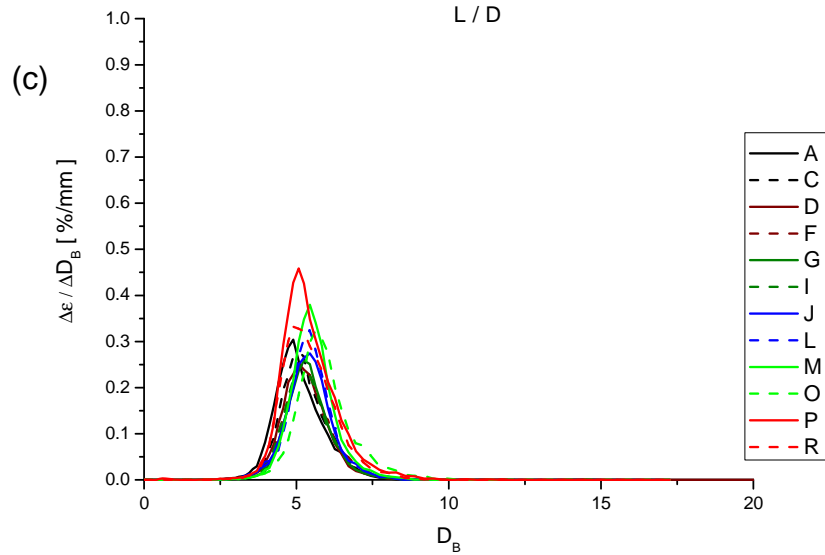
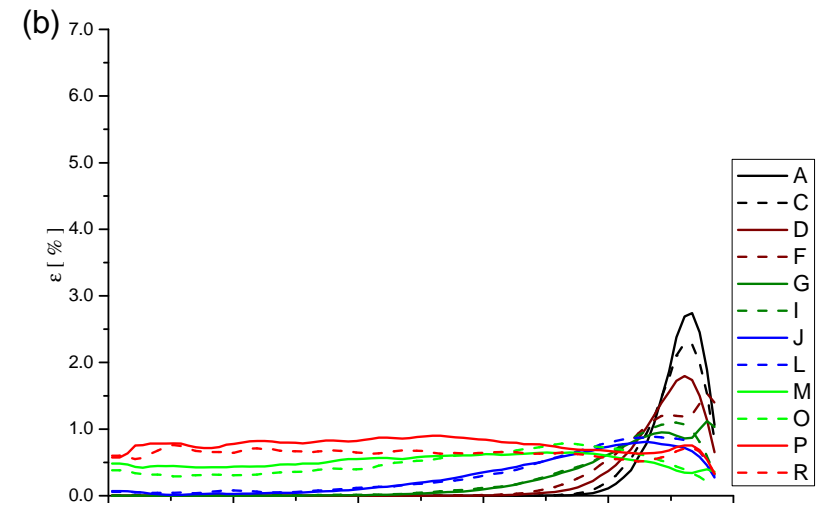
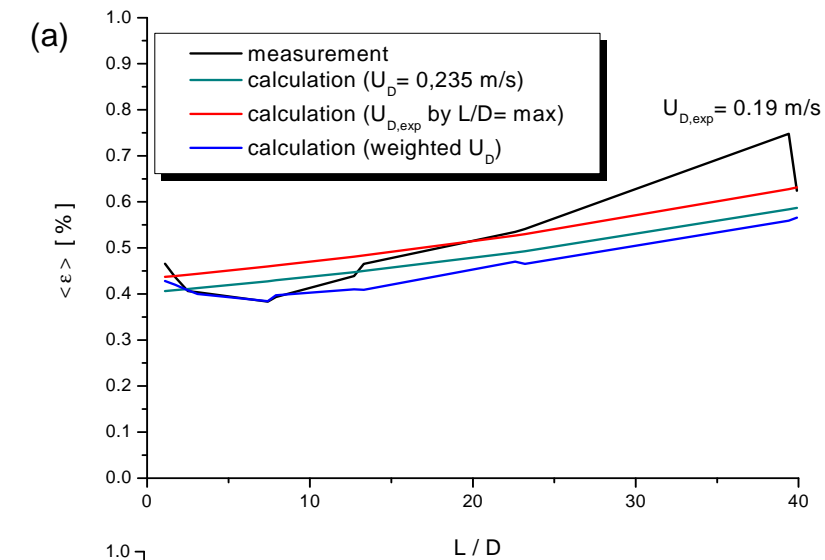
The diagrams are arranged as follows:

- Left top: Comparison of the measured and the calculated gas volume fraction values with three different approaches for the determination of the drift velocity (see page 66).
- Right top: Radial gas volume fraction profiles $\varepsilon(r)$ for different test section heights.
- Left bottom: Distribution of bubble size (D_B).
- Right bottom: Radial profiles of the gas velocity U_G

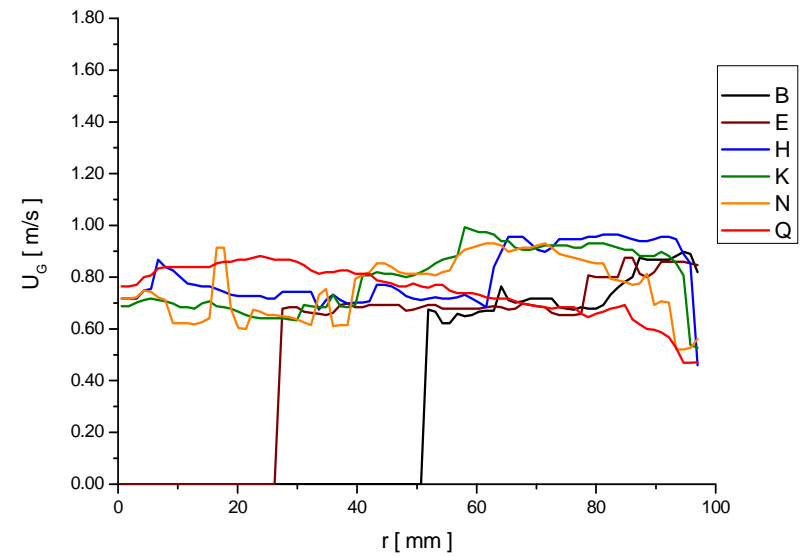
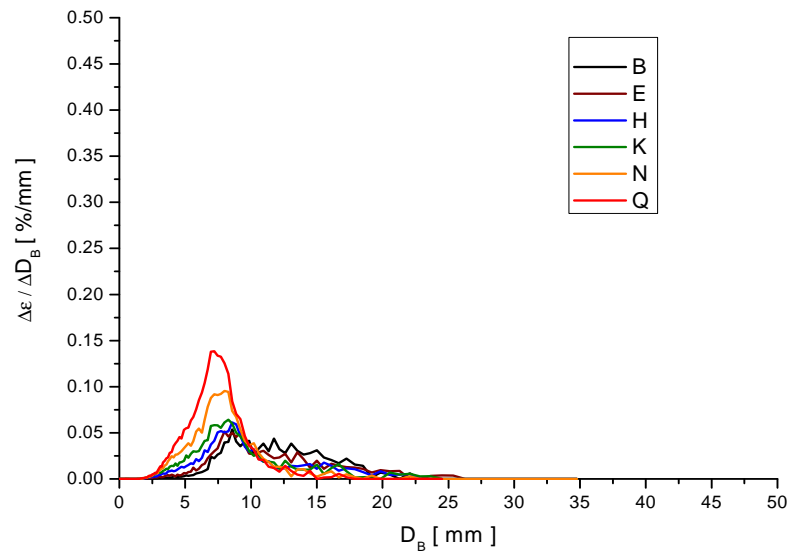
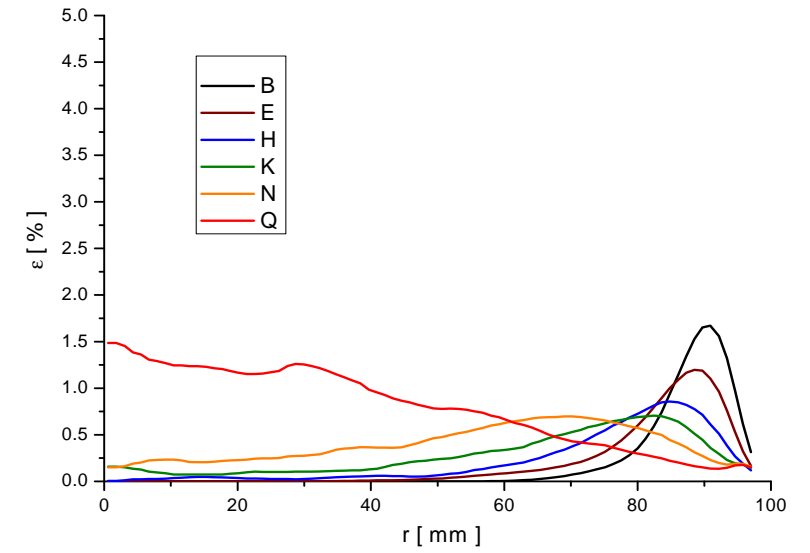
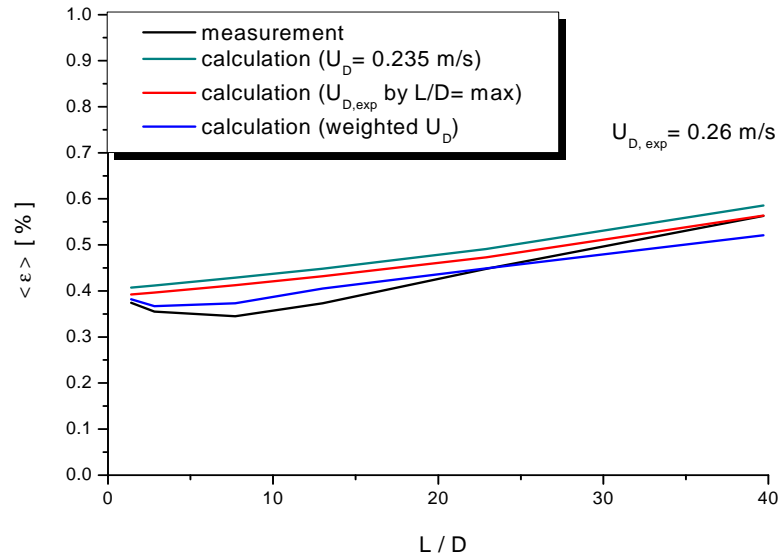
In addition, the difference of the superficial gas velocity to the set value is indicated, ΔJ_G calculated according to eq. (1.38), for the different relative test section heights.

I. Characteristic data of the measurement points

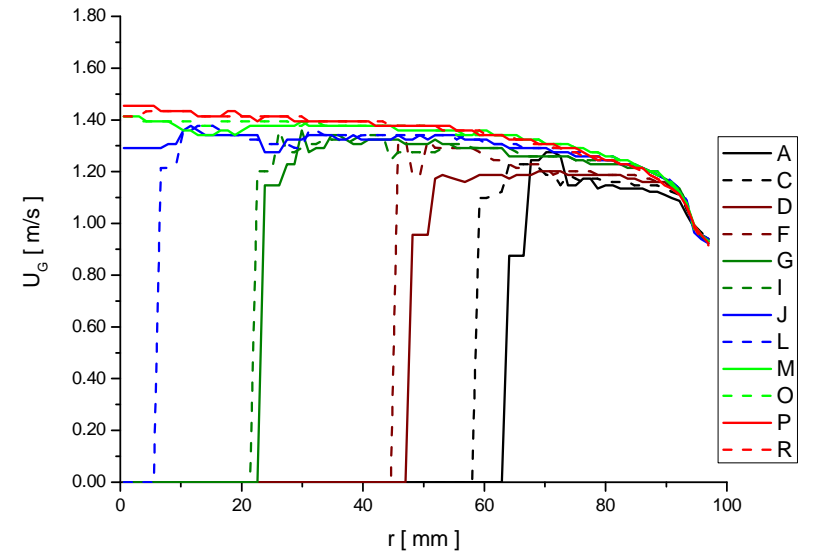
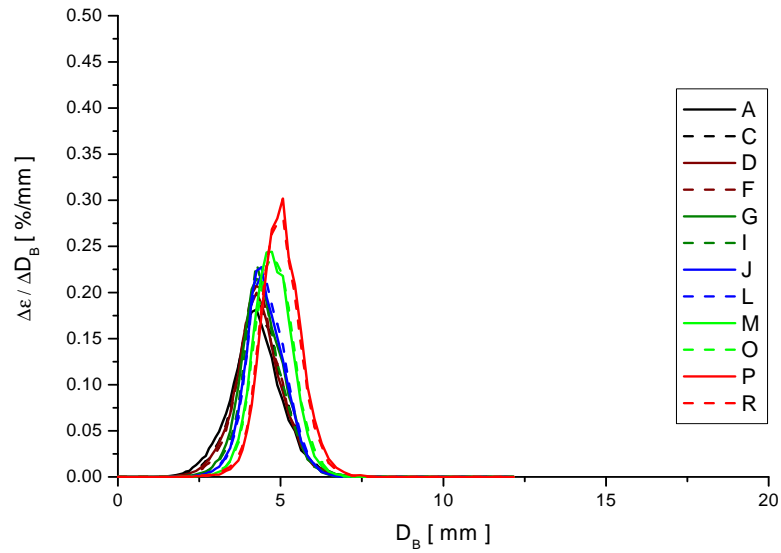
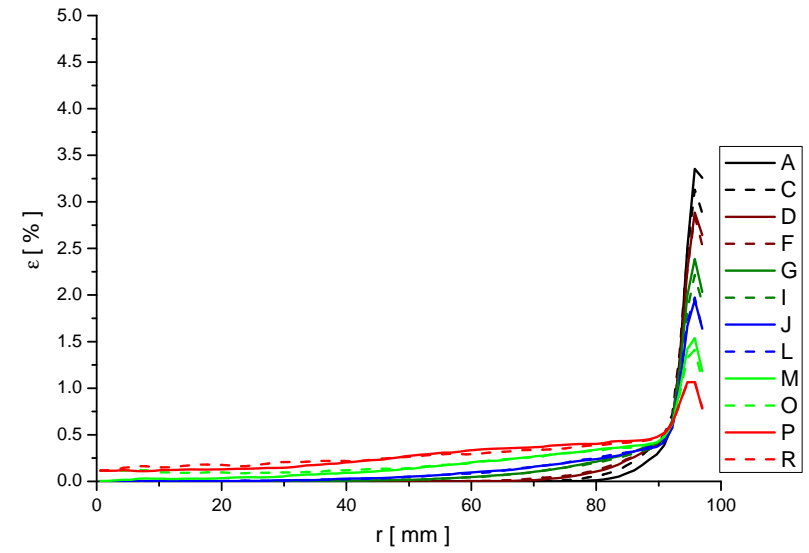
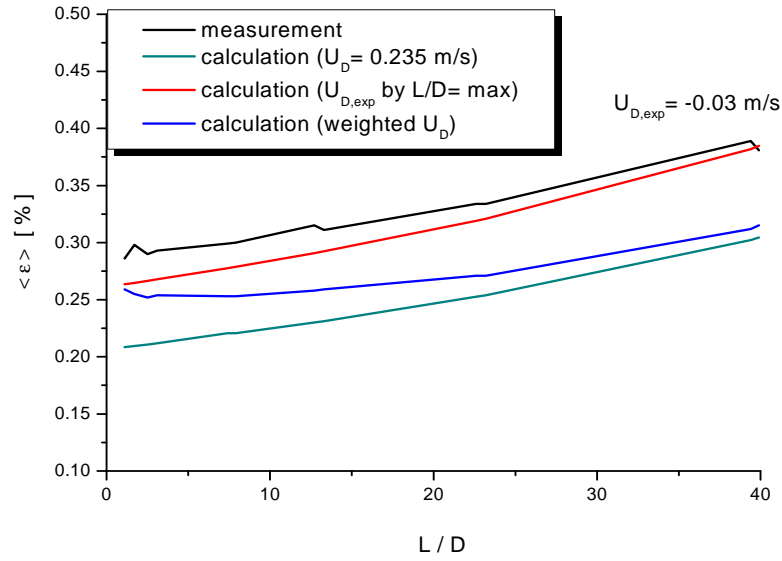
(a) void fraction $\langle \varepsilon \rangle$ (L/D), (b) void fraction ε (r), (c) distribution of bubble diameter (D_B), vertical gas velocity U_G (r)
 measurement point 006 ($J_L = 0.405$ m/s; $J_G = 0.0025$ m/s; $D_{\text{Orifice}} = 1$ mm)



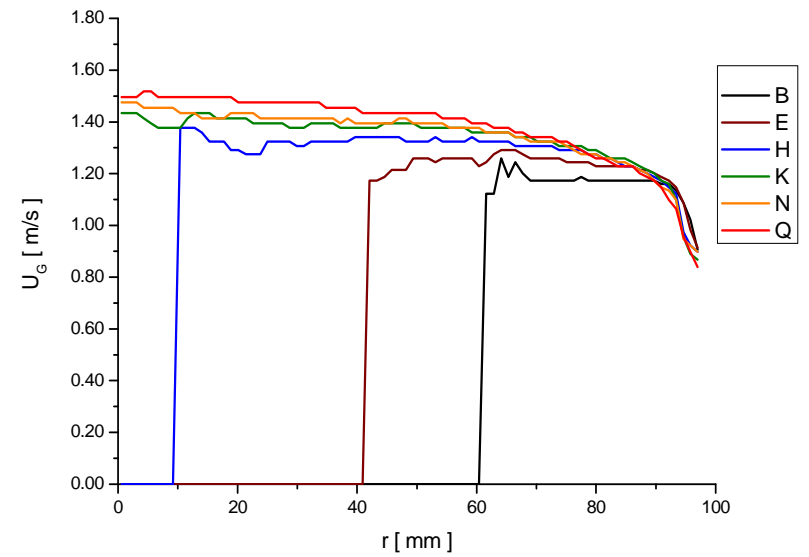
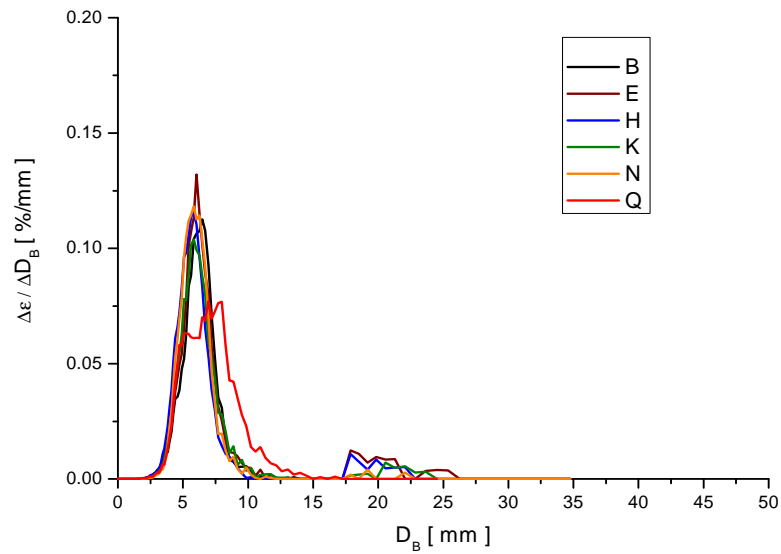
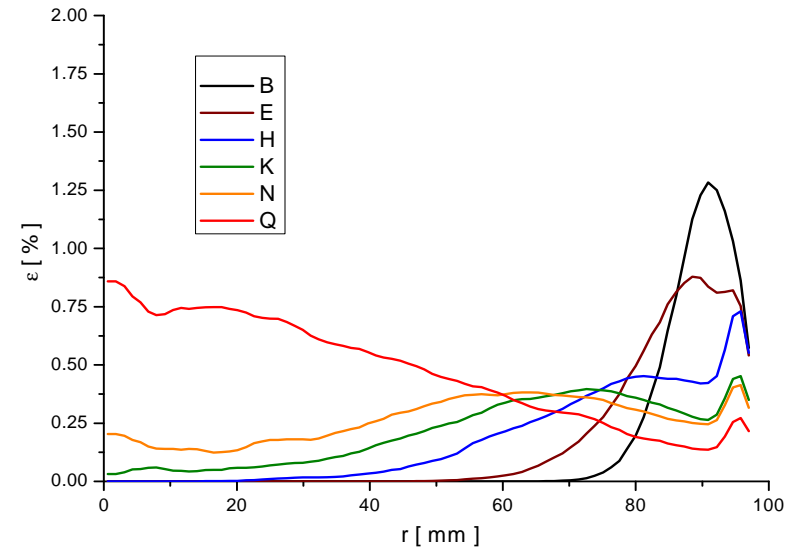
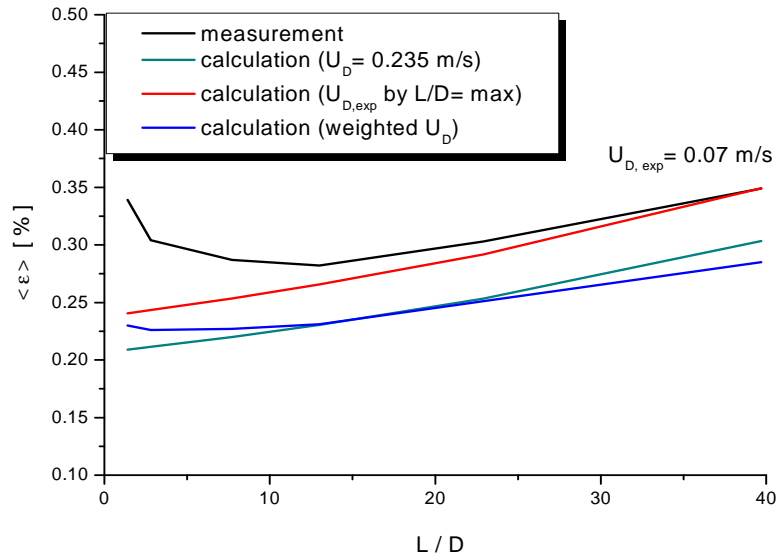
measurement point 006 ($J_L = 0.405$ m/s; $J_G = 0.0025$ m/s; $D_{\text{Orifice}} = 4$ mm)



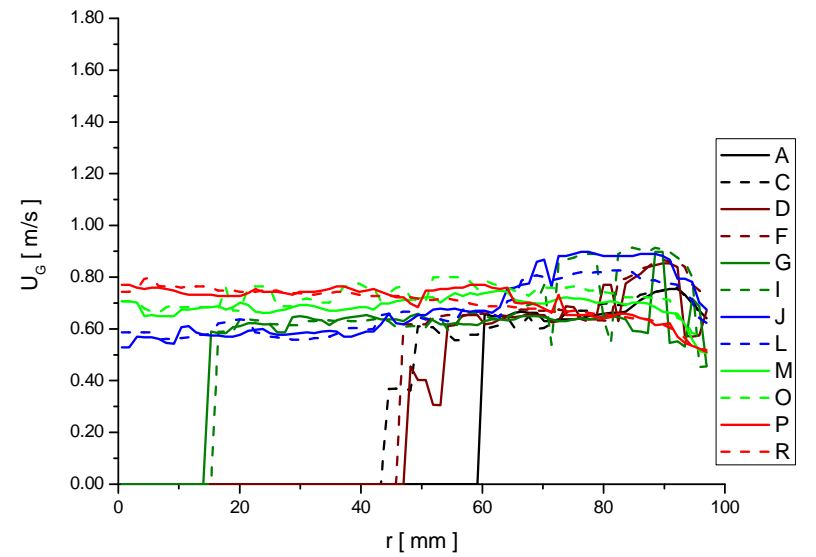
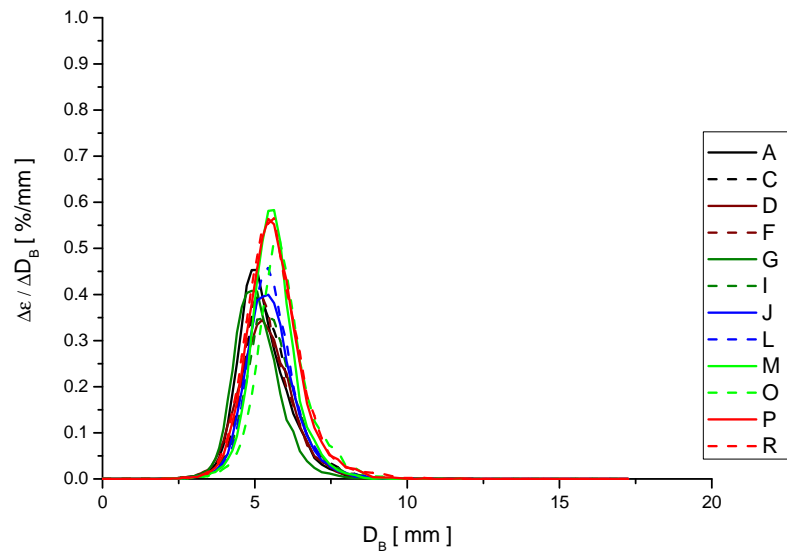
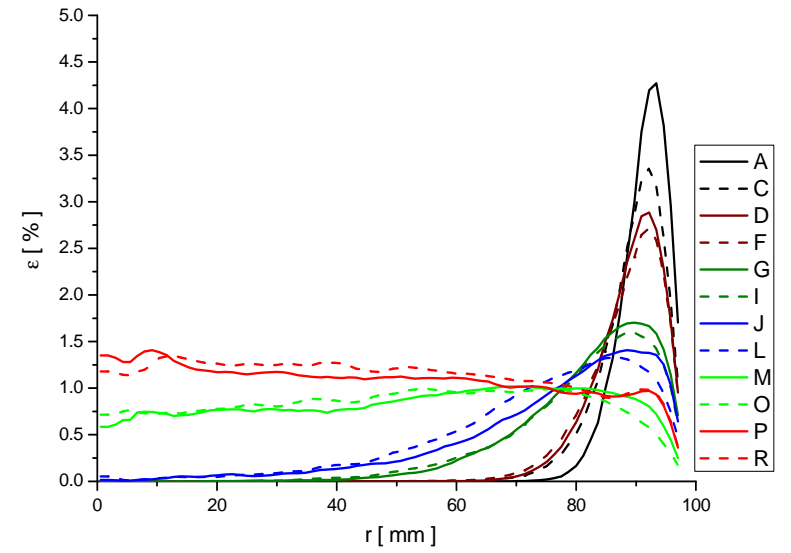
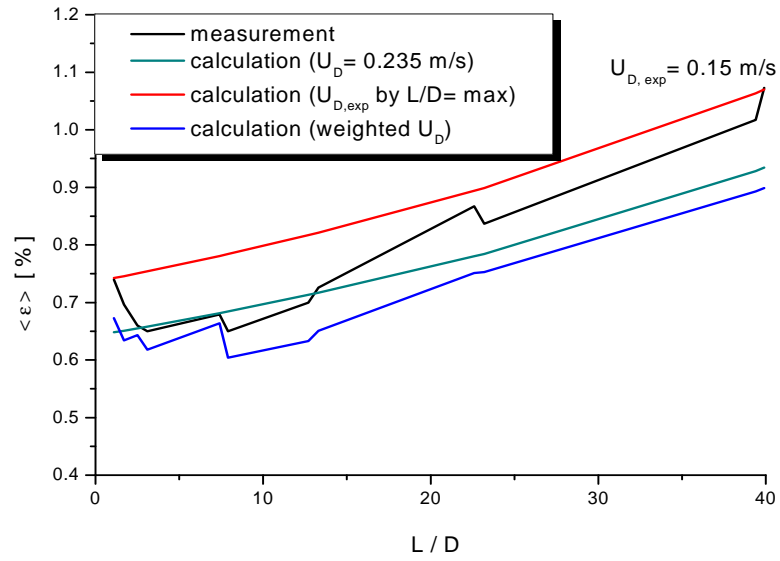
measurement point 008 ($J_L = 1.017$ m/s; $J_G = 0.0025$ m/s; $D_{\text{Orifice}} = 1$ mm)



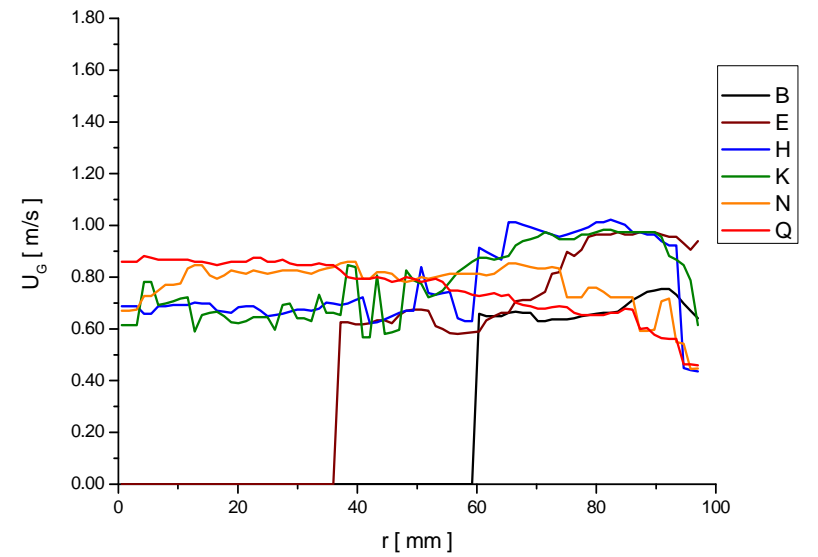
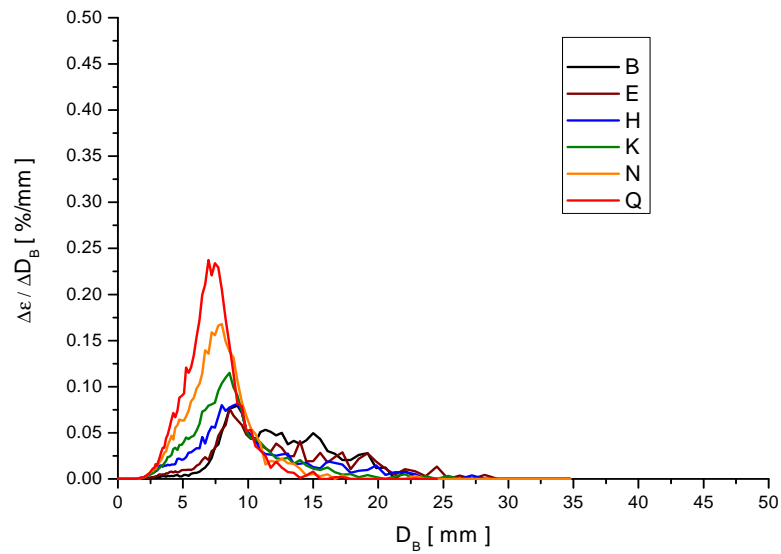
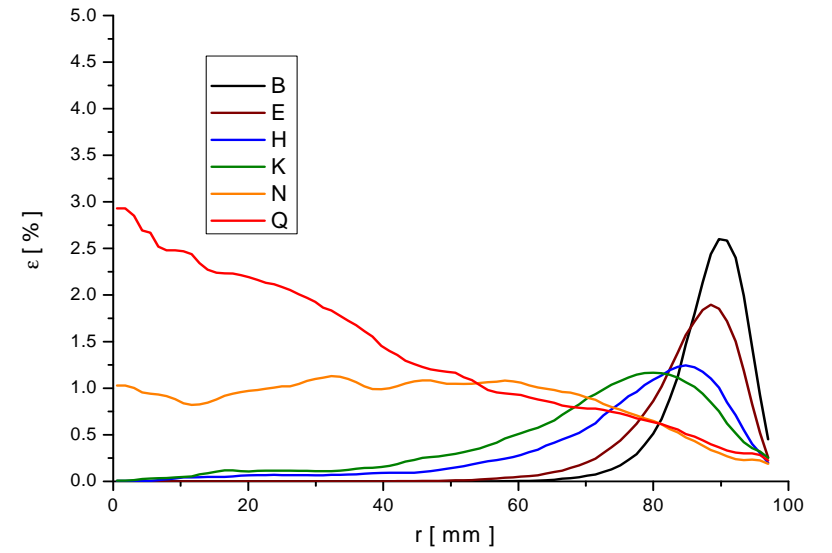
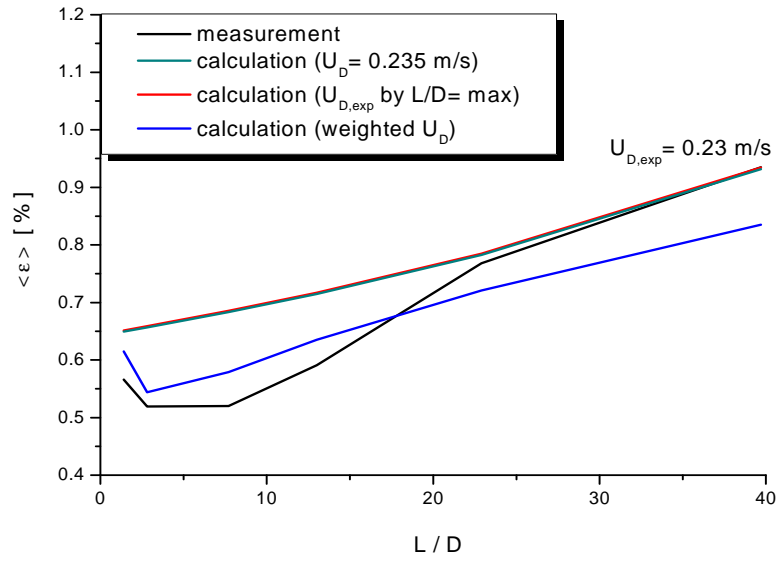
measurement point 008 ($J_L = 1.017 \text{ m/s}$; $J_G = 0.0025 \text{ m/s}$; $D_{\text{Orifice}} = 4 \text{ mm}$)



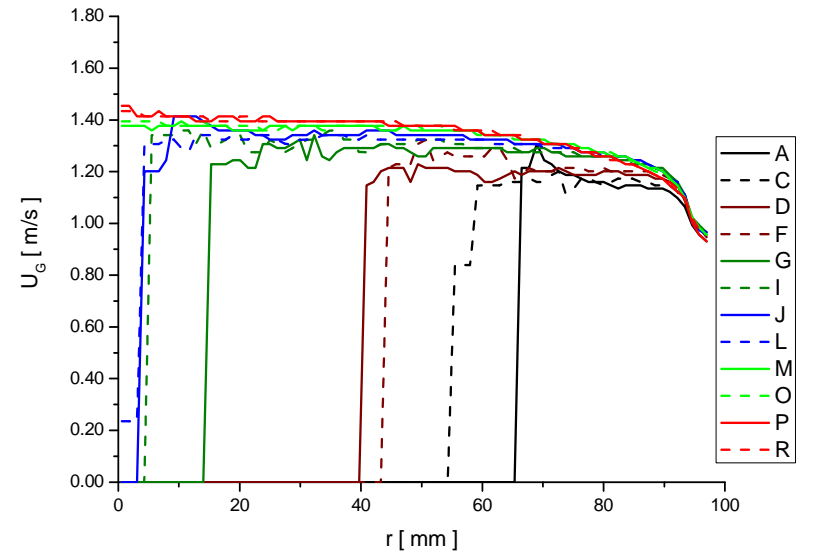
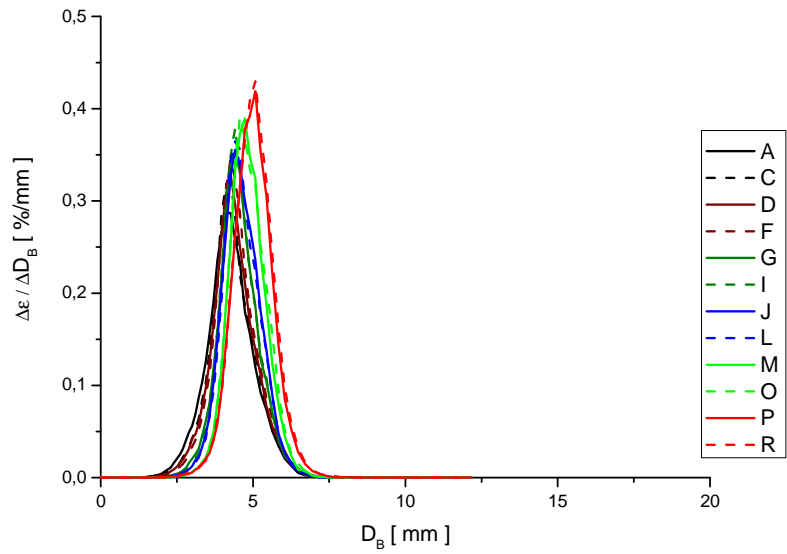
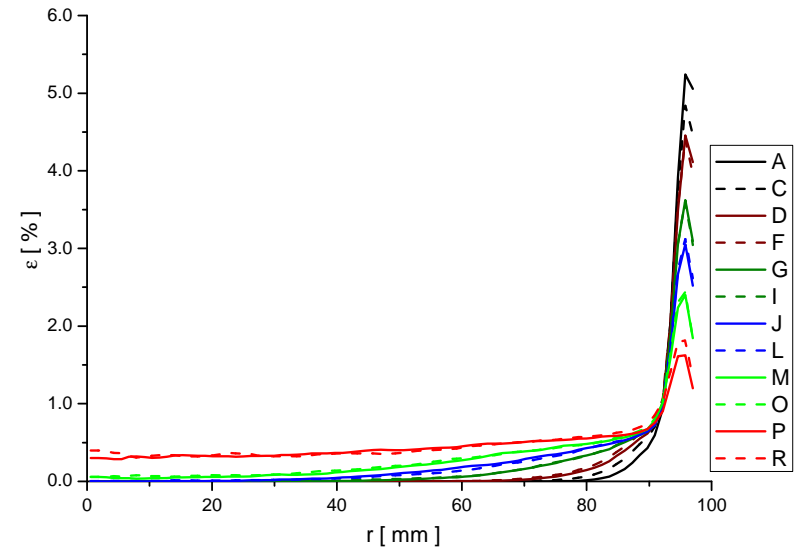
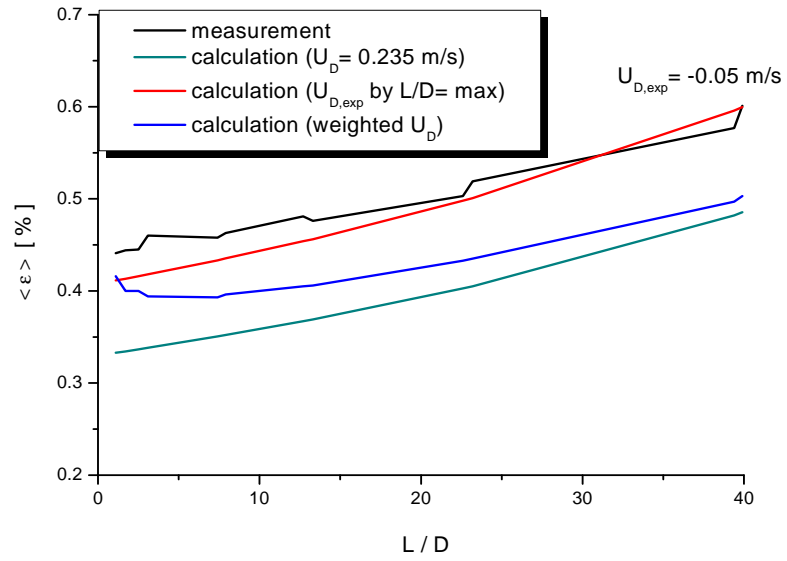
measurement point 017 ($J_L = 0.405$ m/s; $J_G = 0.0040$ m/s; $D_{\text{Orifice}} = 1$ mm)



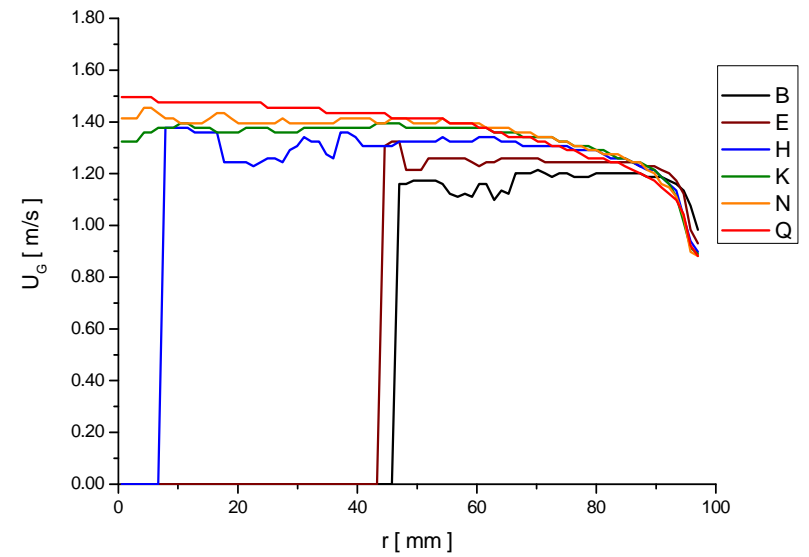
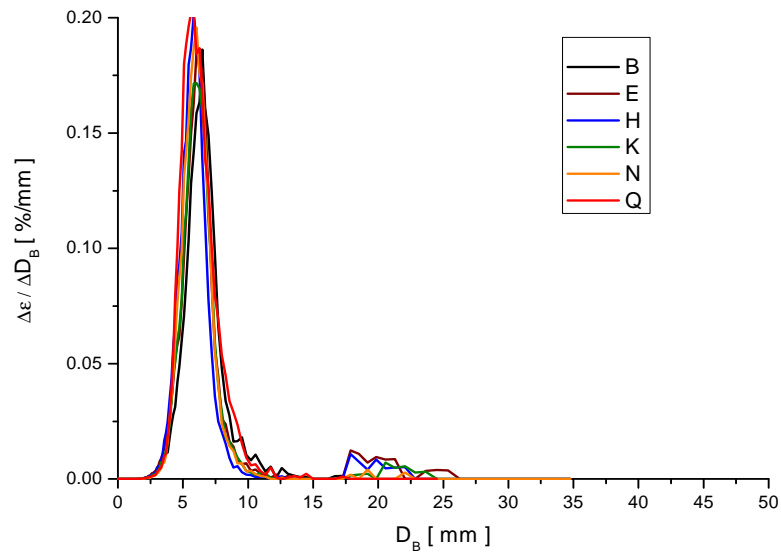
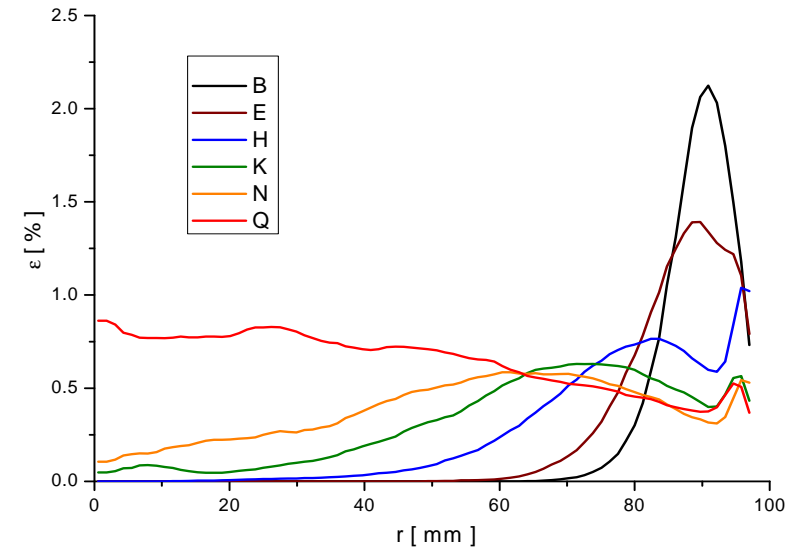
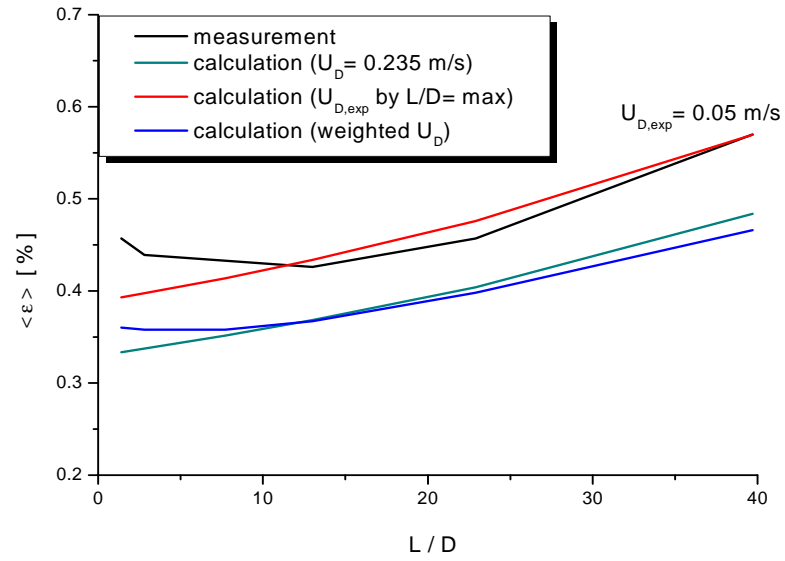
measurement point 017 ($J_L = 0.405$ m/s; $J_G = 0.0040$ m/s; $D_{\text{Orifice}} = 4$ mm)



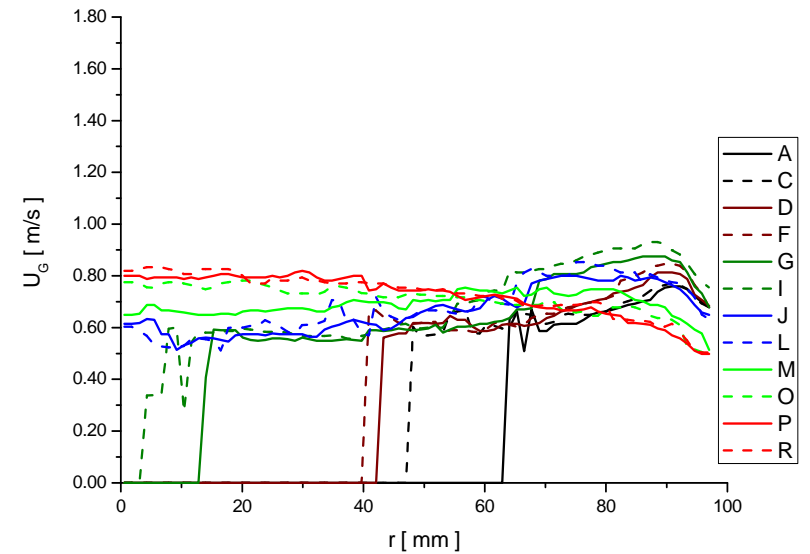
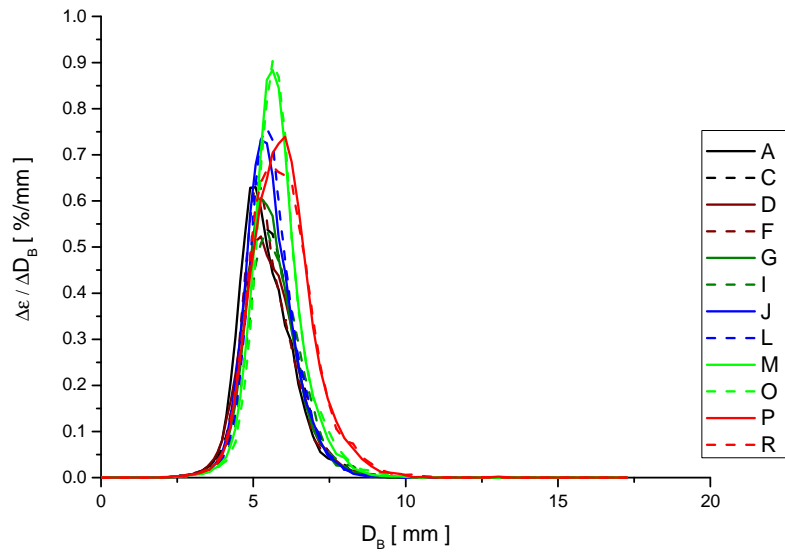
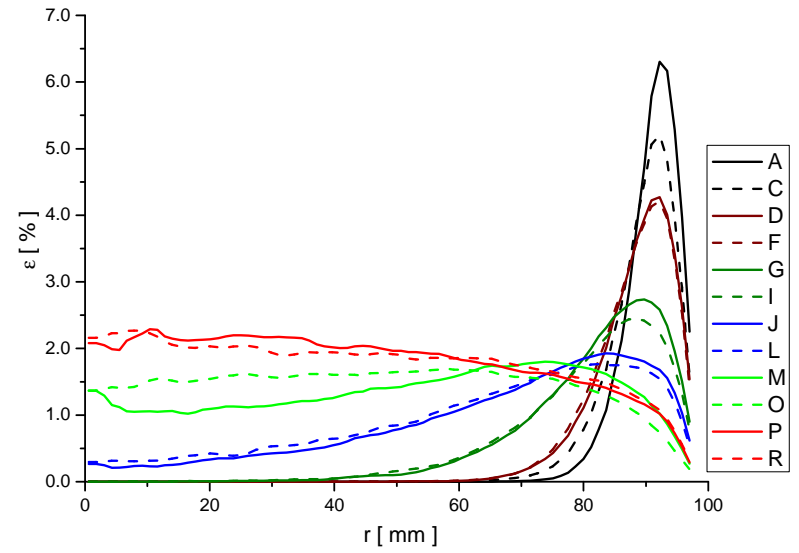
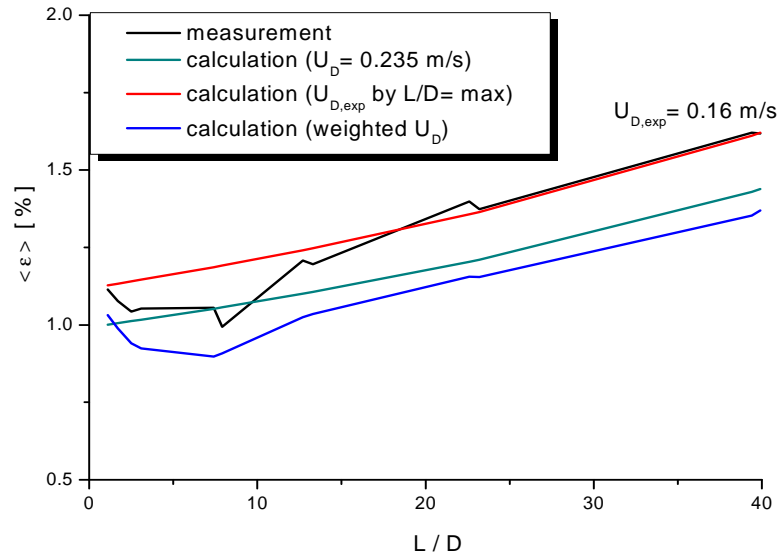
measurement point 019 ($J_L = 1.017$ m/s; $J_G = 0.0040$ m/s; $D_{\text{Orifice}} = 1$ mm)



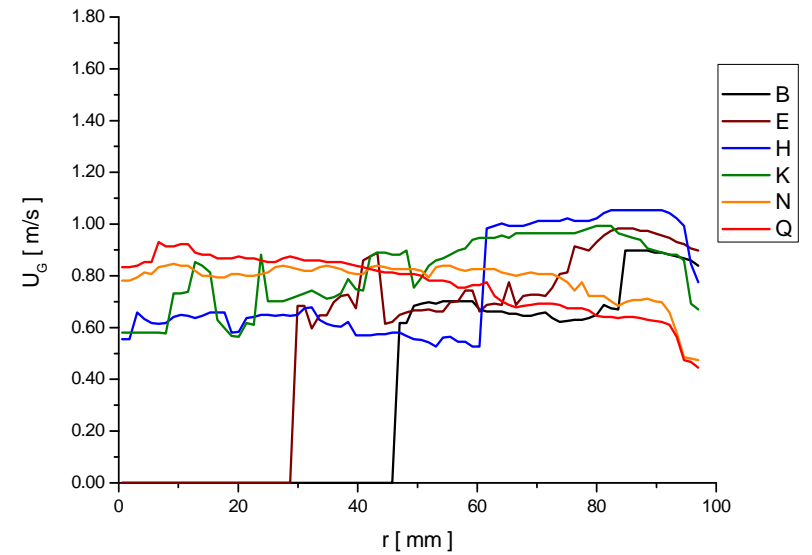
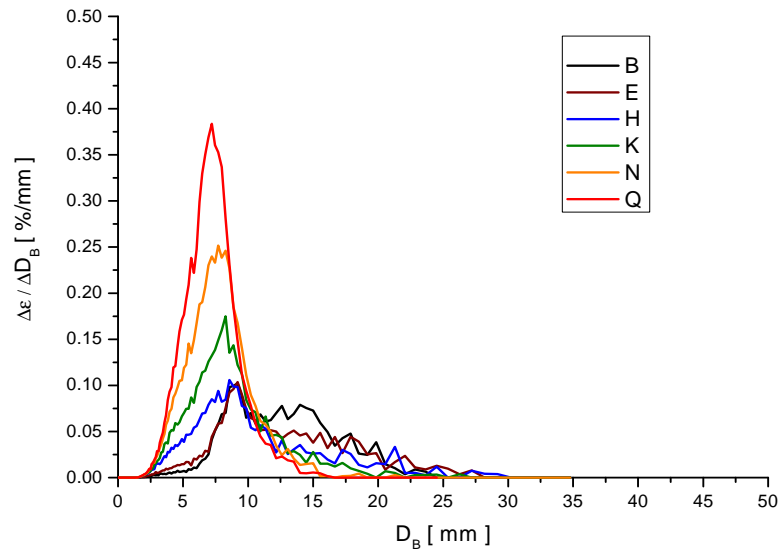
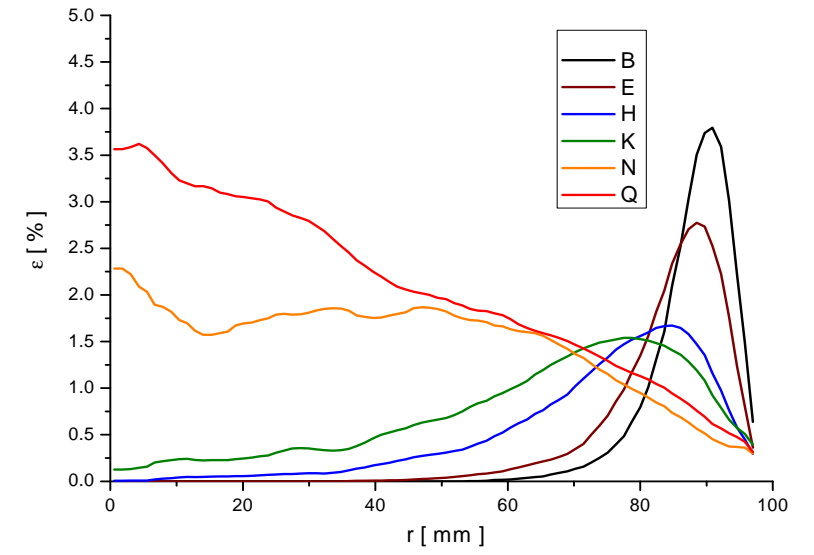
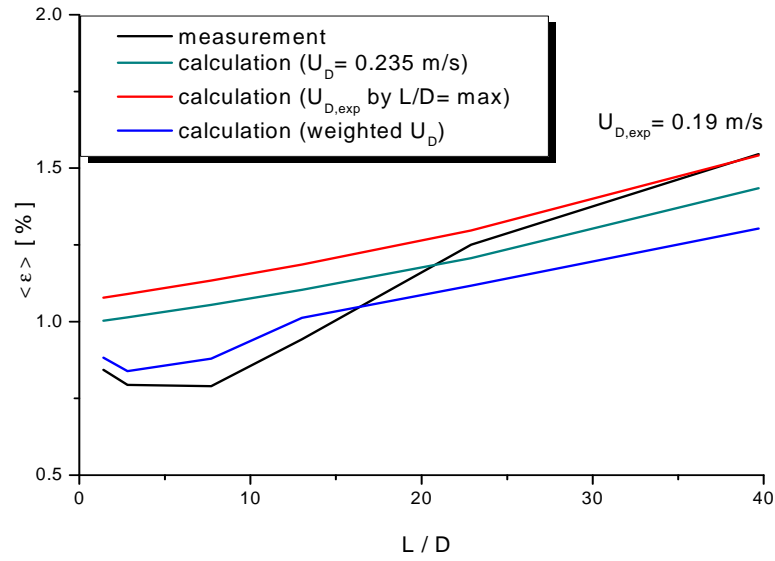
measurement point 019 ($J_L = 1.017$ m/s; $J_G = 0.0040$ m/s; $D_{\text{Orifice}} = 4$ mm)



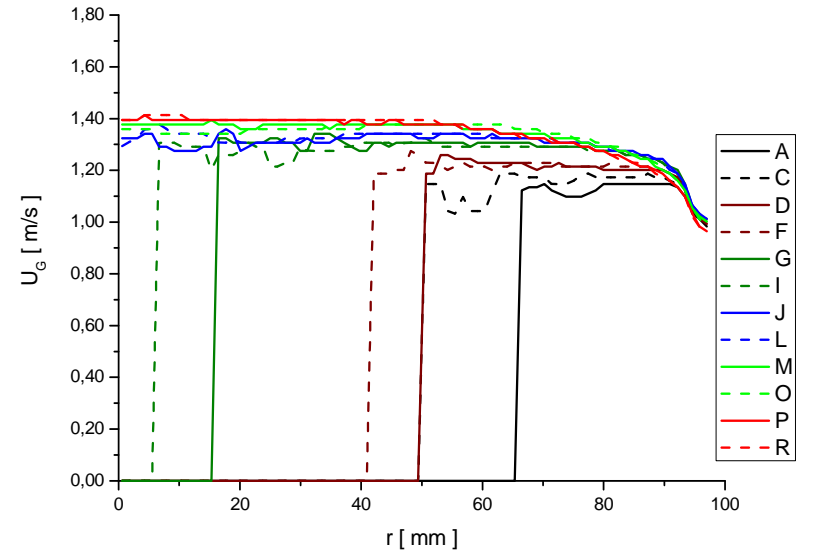
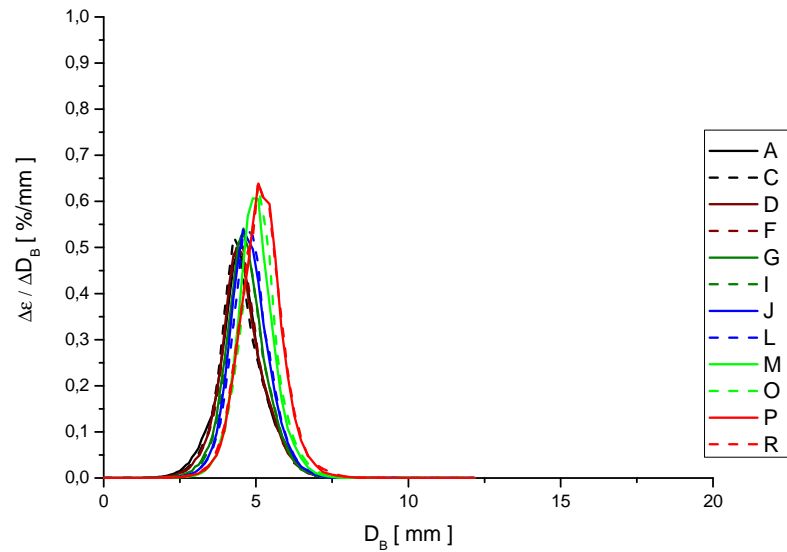
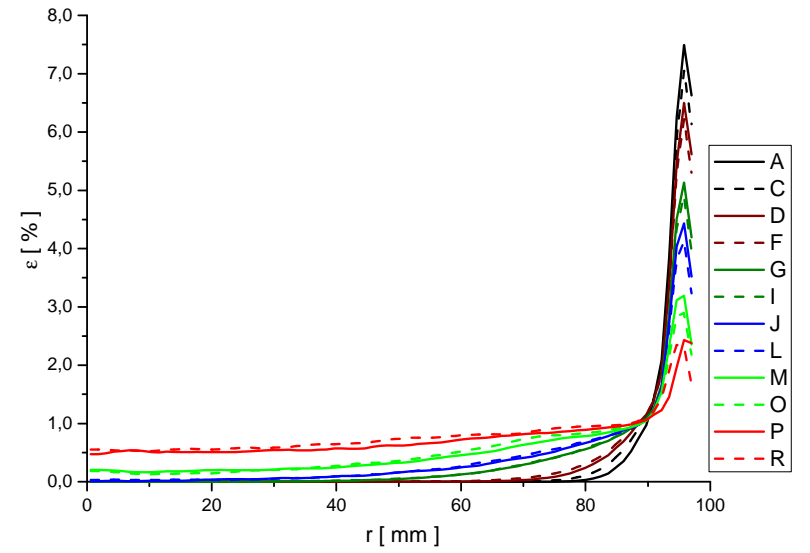
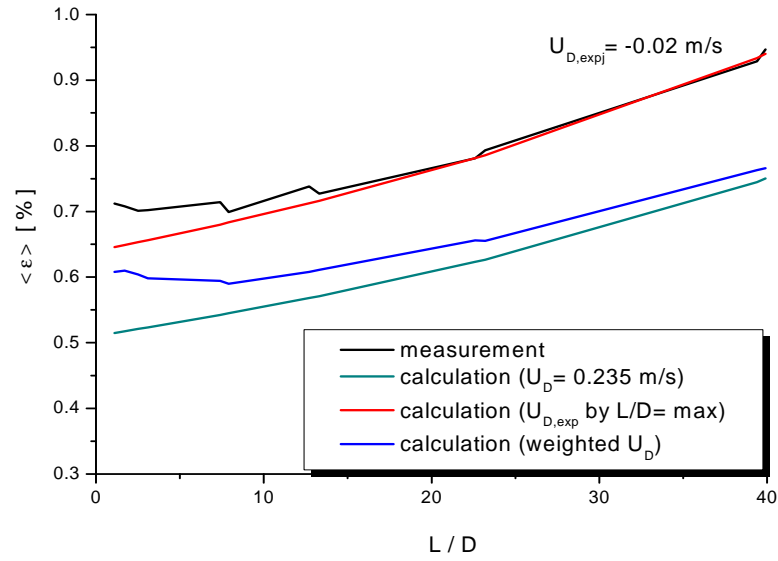
measurement point 028 ($J_L = 0.405$ m/s; $J_G = 0.0062$ m/s; $D_{\text{Orifice}} = 1$ mm)



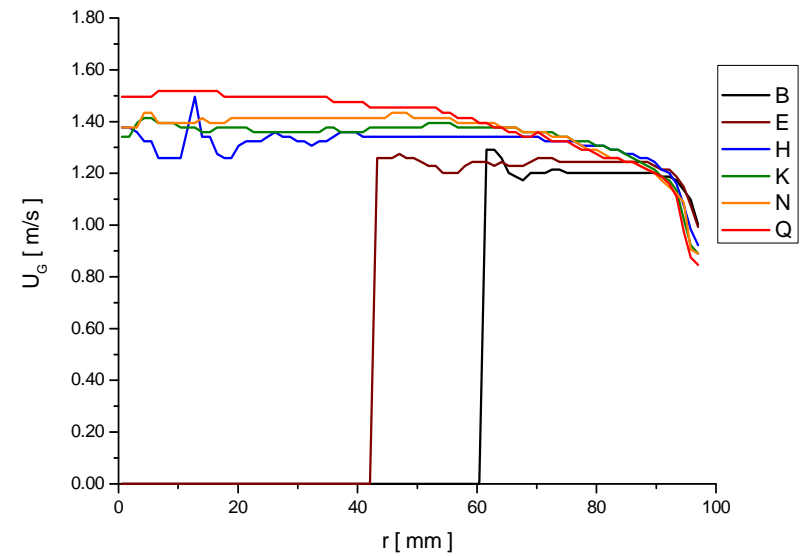
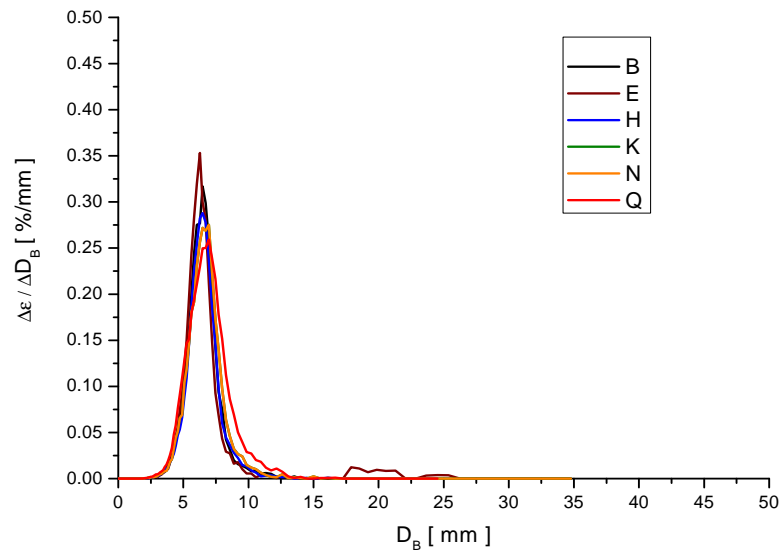
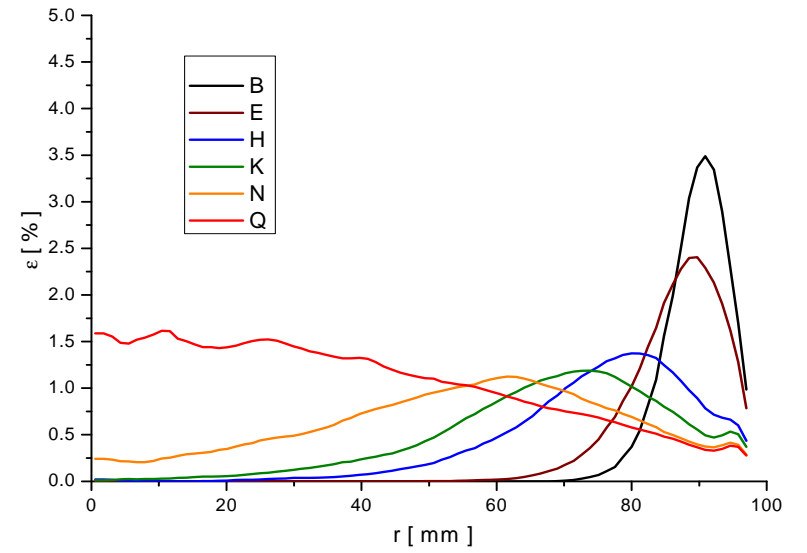
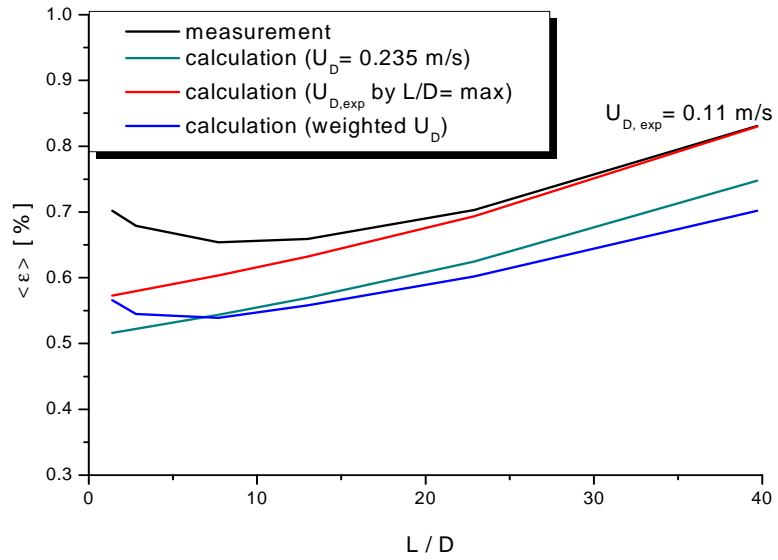
measurement point 028 ($J_L = 0.405$ m/s; $J_G = 0.0062$ m/s; $D_{\text{Orifice}} = 4$ mm)



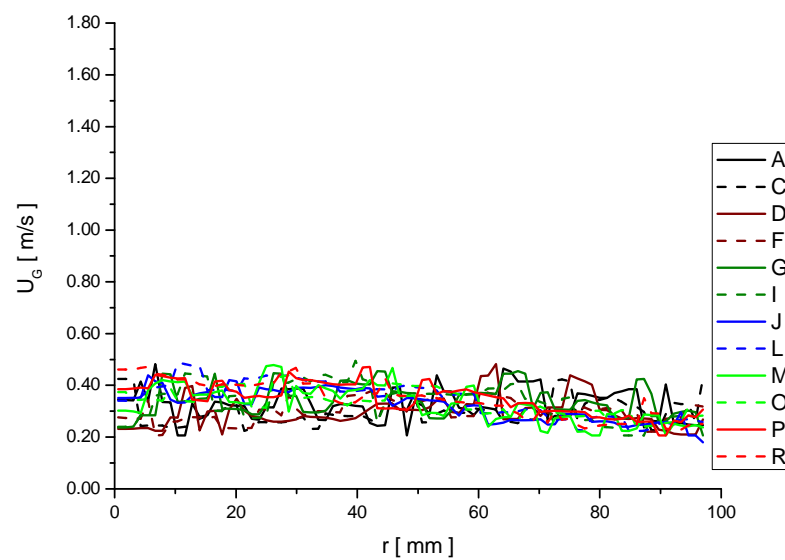
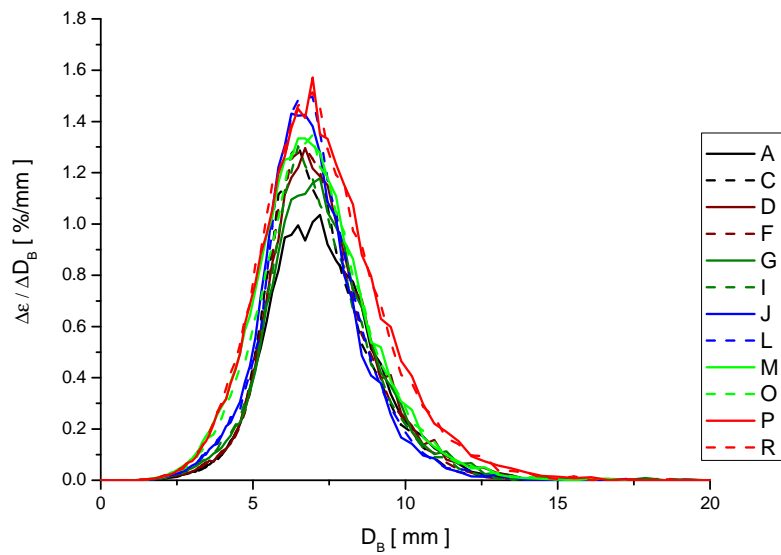
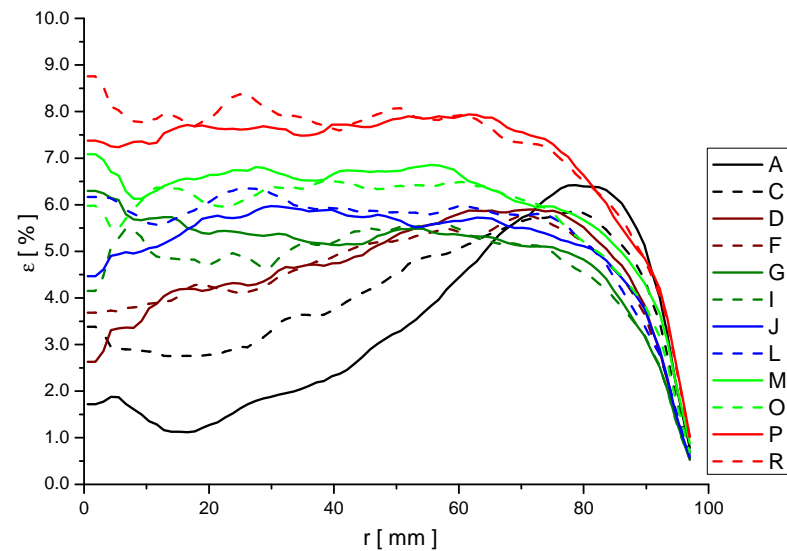
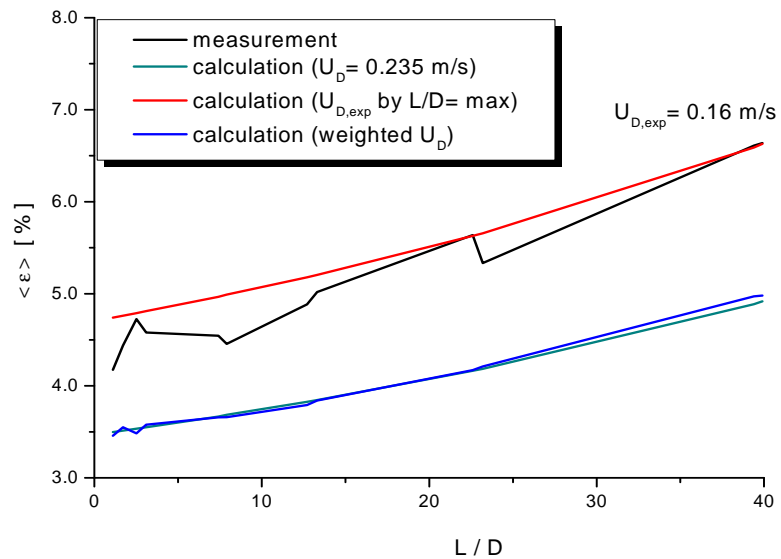
measurement point 030 ($J_L = 1.017$ m/s; $J_G = 0.0062$ m/s; $D_{\text{Orifice}} = 1$ mm)



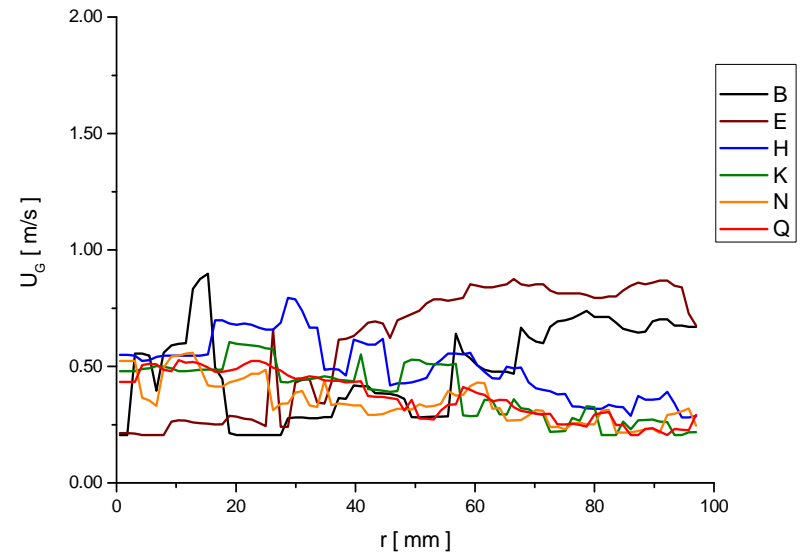
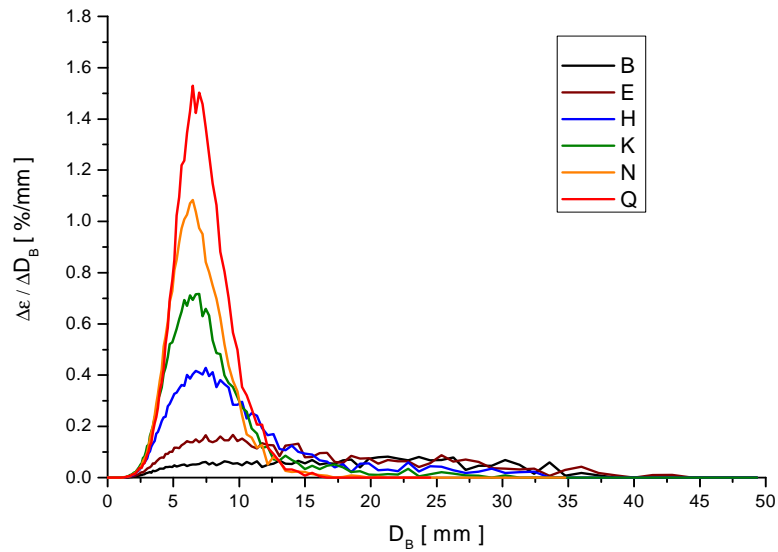
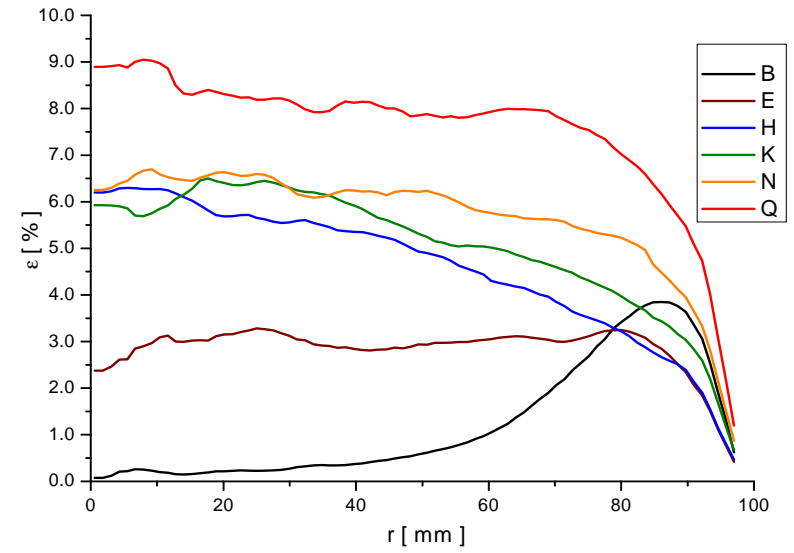
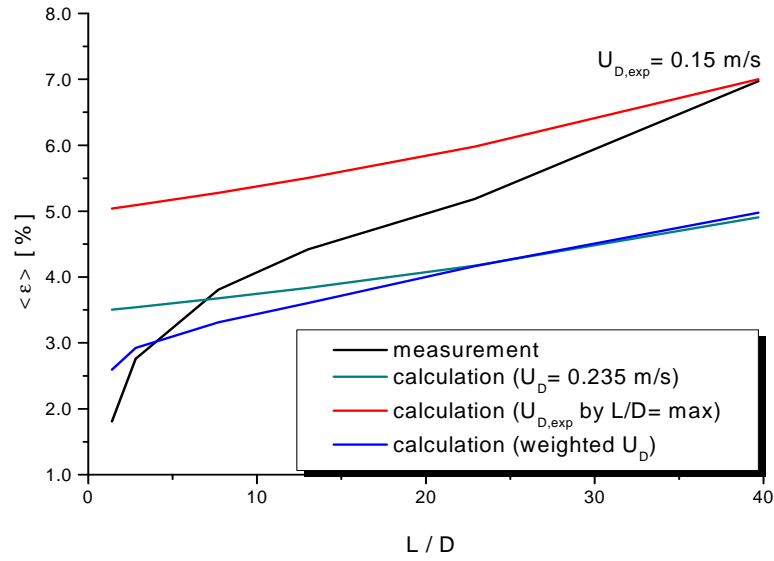
measurement point 030 ($J_L = 1.017$ m/s; $J_G = 0.0062$ m/s; $D_{\text{Orifice}} = 4$ mm)



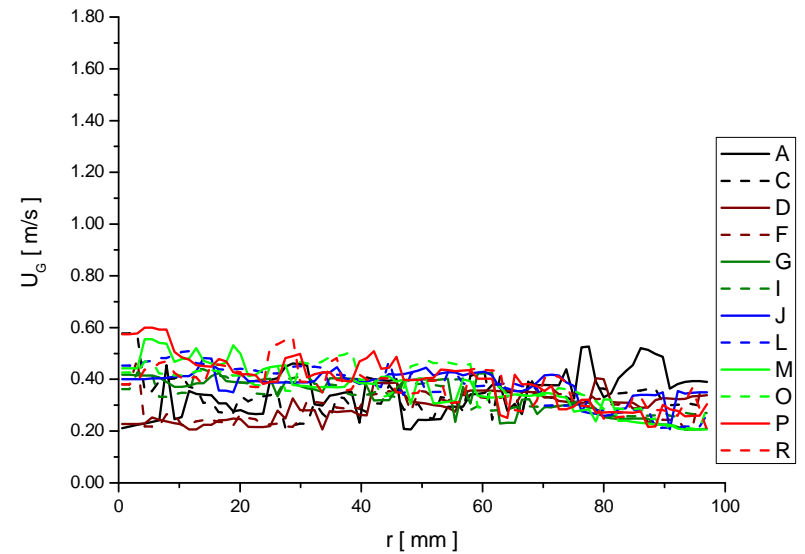
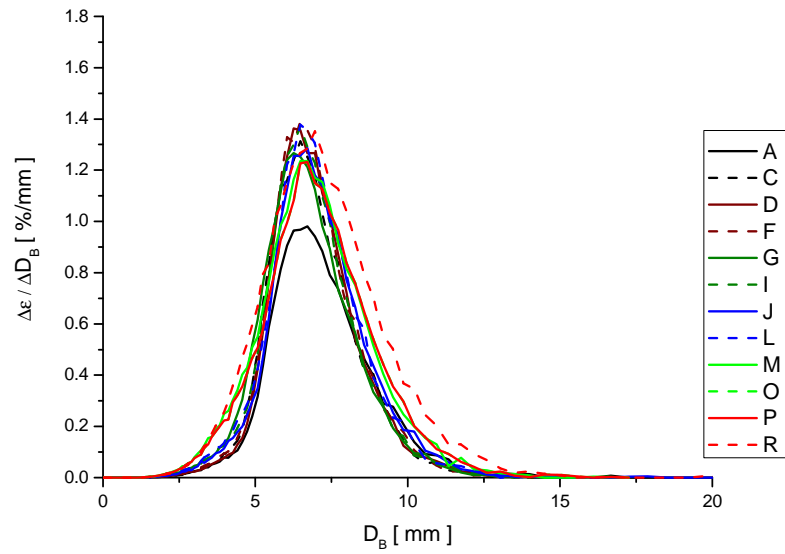
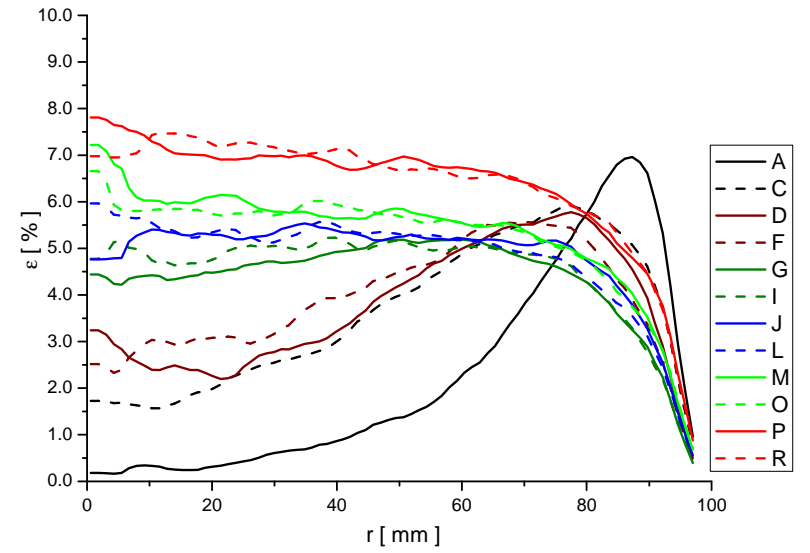
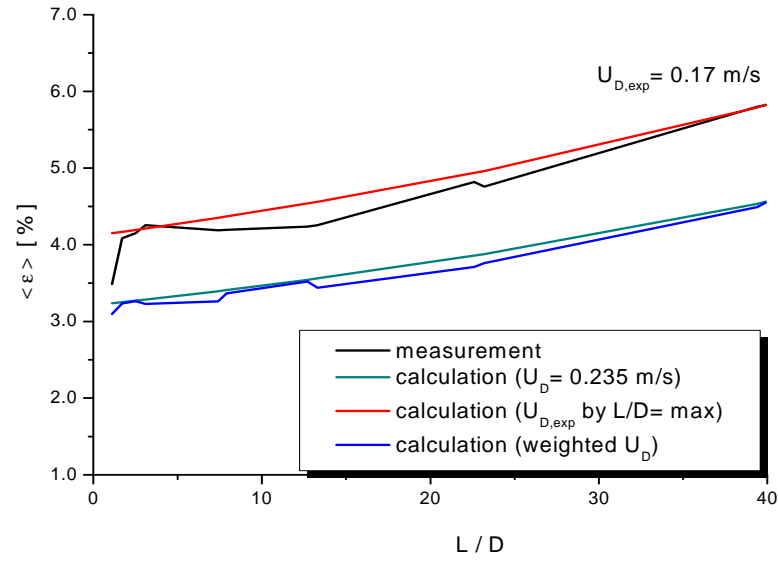
measurement point 034 ($J_L = 0.0405$ m/s; $J_G = 0.0096$ m/s; $D_{\text{Orifice}} = 1$ mm)



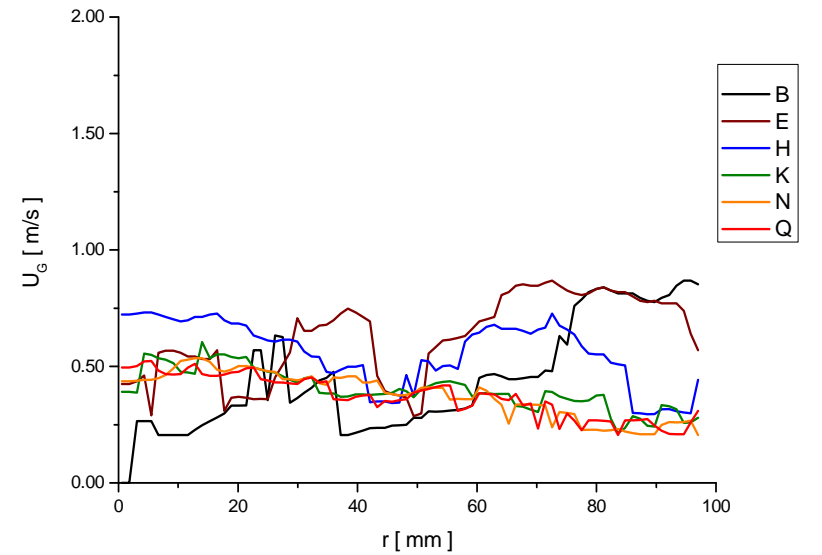
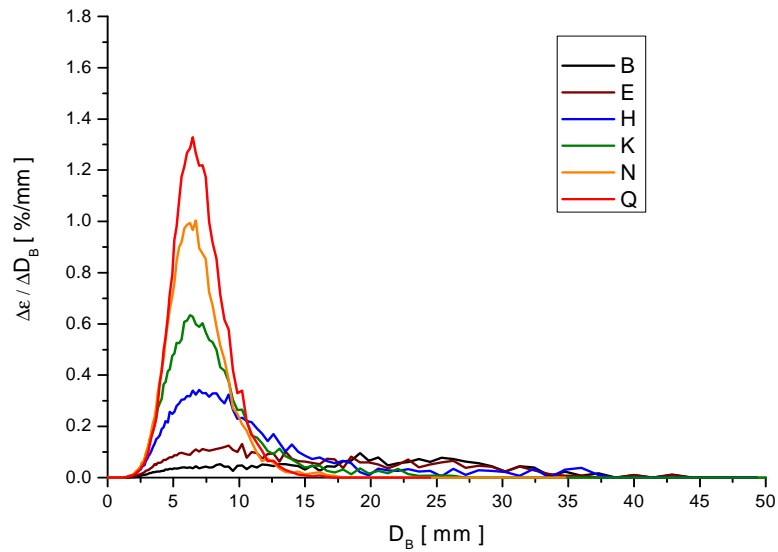
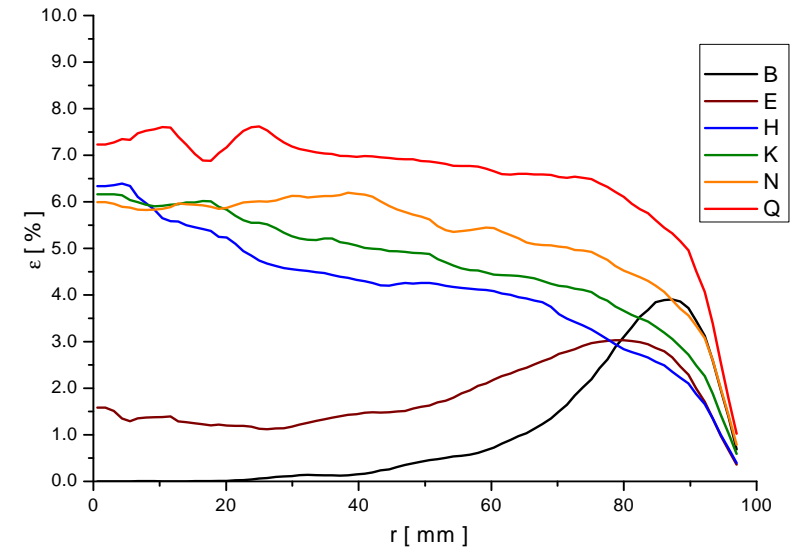
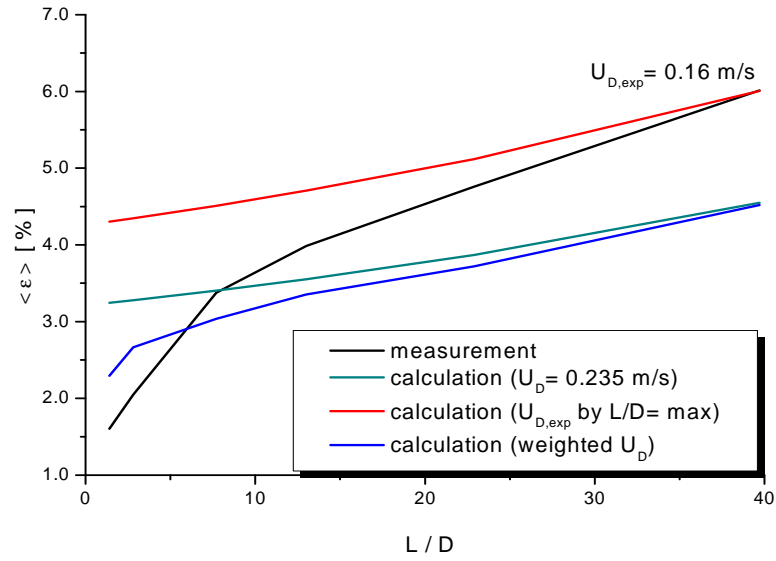
measurement point 034 ($J_L = 0.0405$ m/s; $J_G = 0.0096$ m/s; $D_{\text{Orifice}} = 4$ mm)



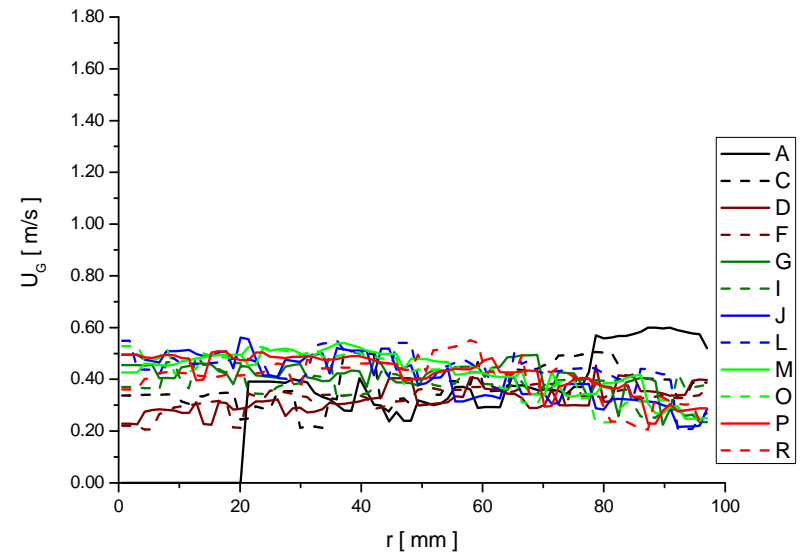
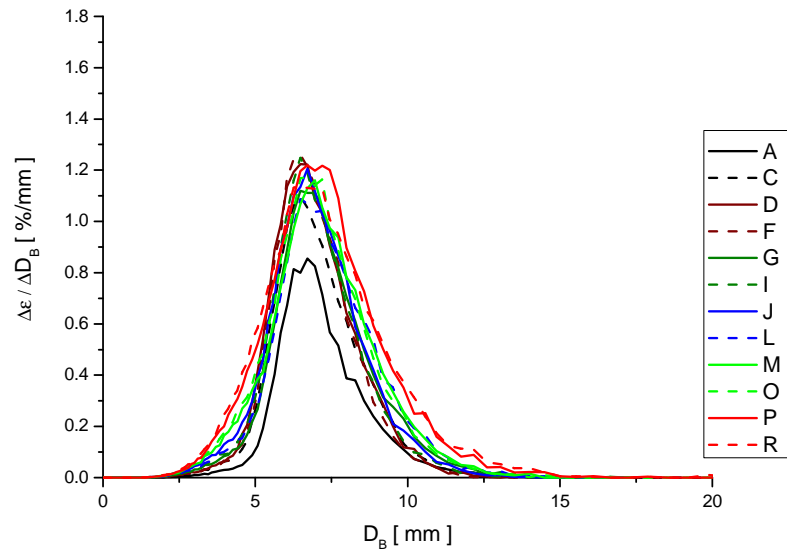
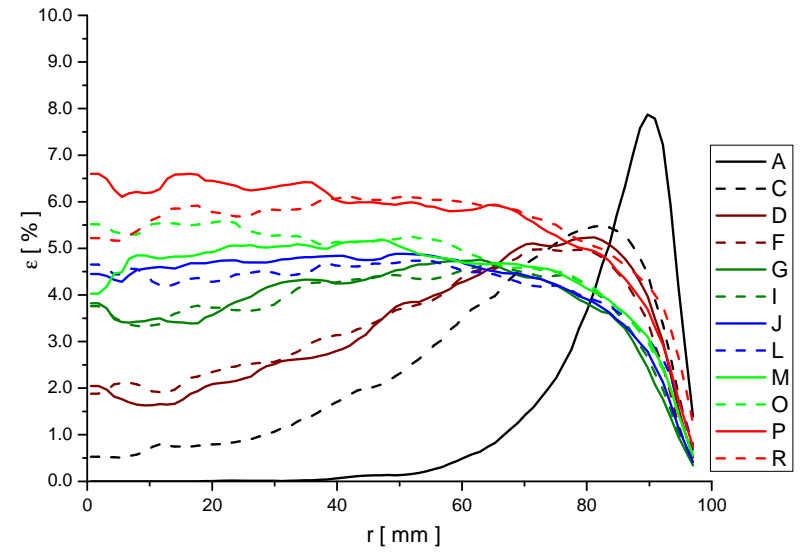
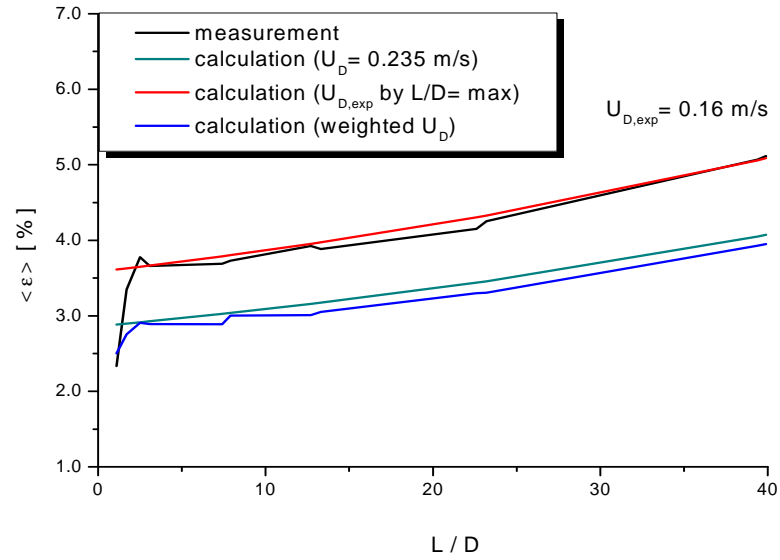
measurement point 035 ($J_L = 0.0641$ m/s; $J_G = 0.0096$ m/s; $D_{\text{Orifice}} = 1$ mm)



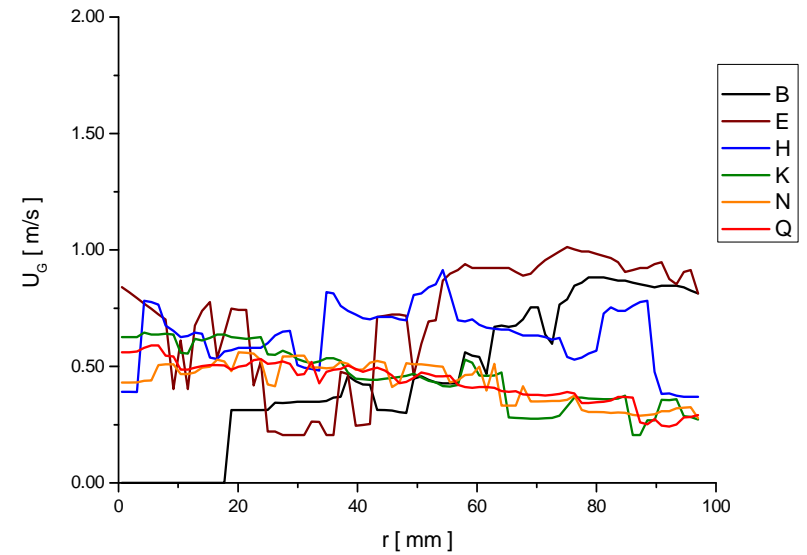
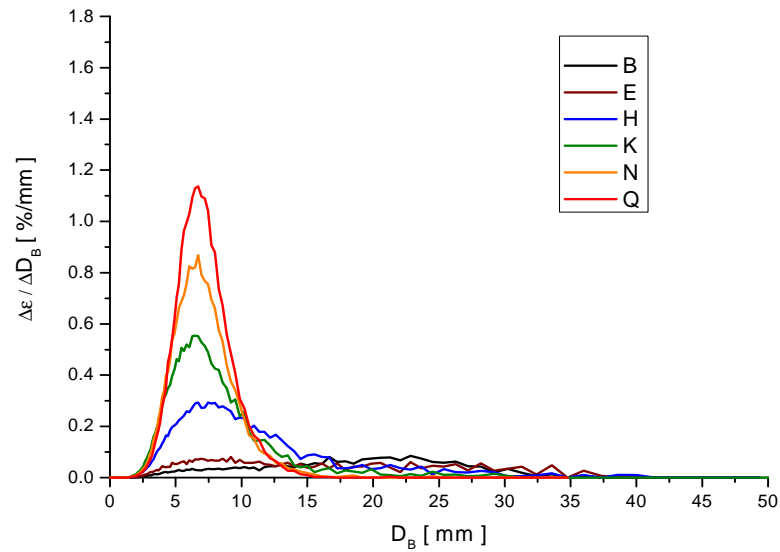
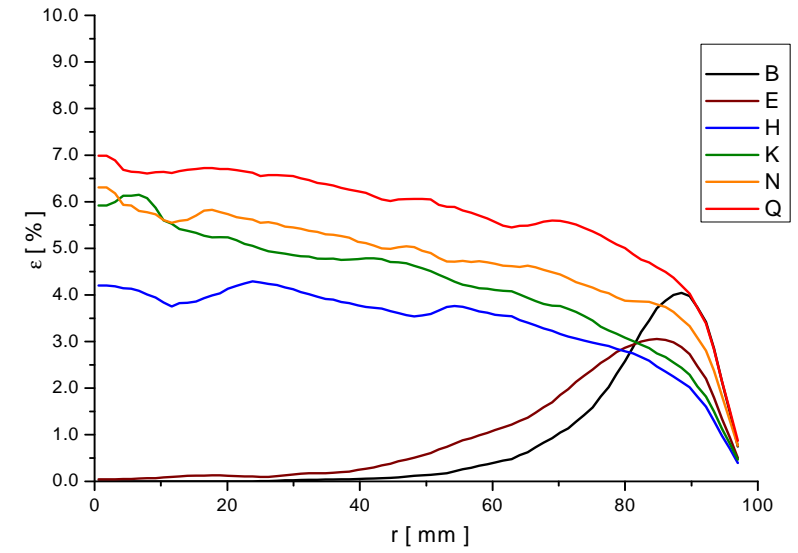
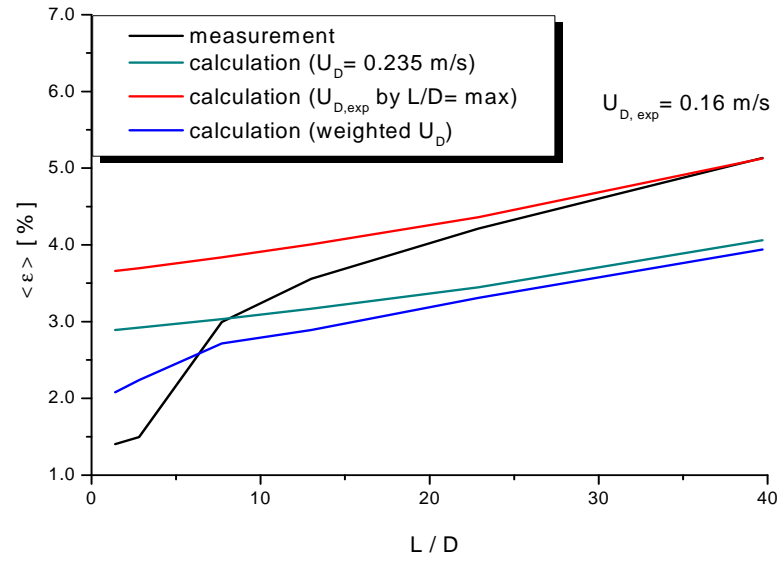
measurement point 035 ($J_L = 0.0641$ m/s; $J_G = 0.0096$ m/s; $D_{\text{Orifice}} = 4$ mm)



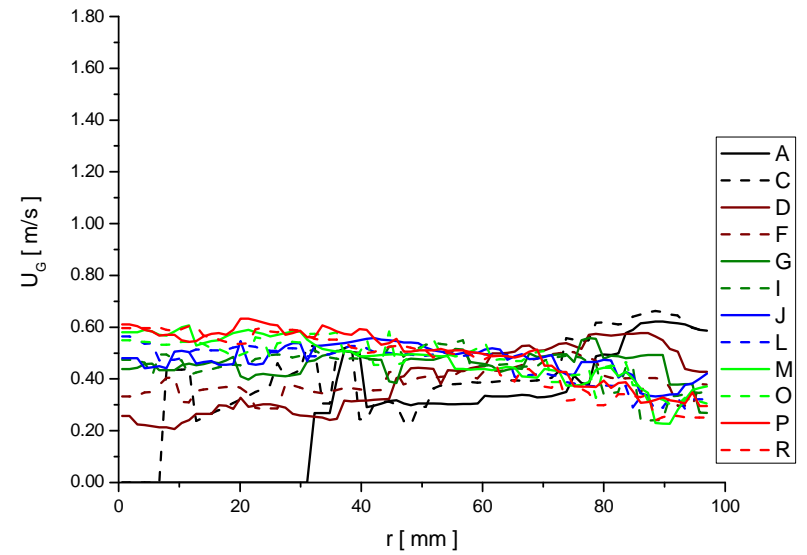
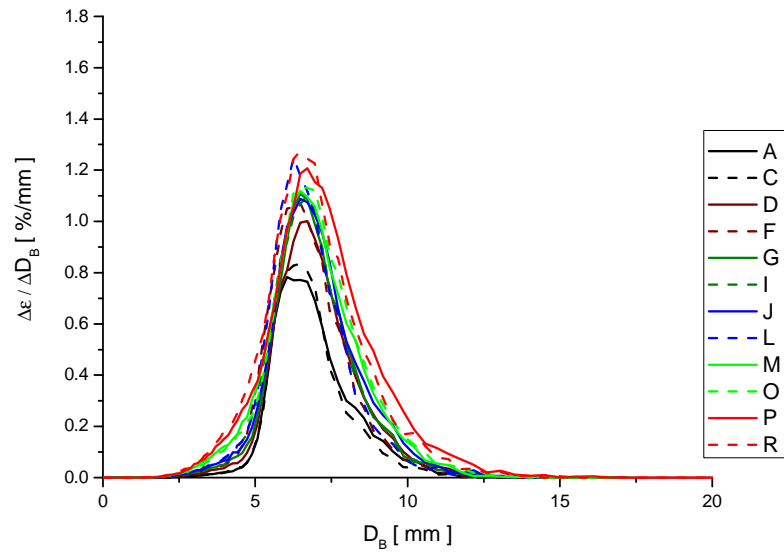
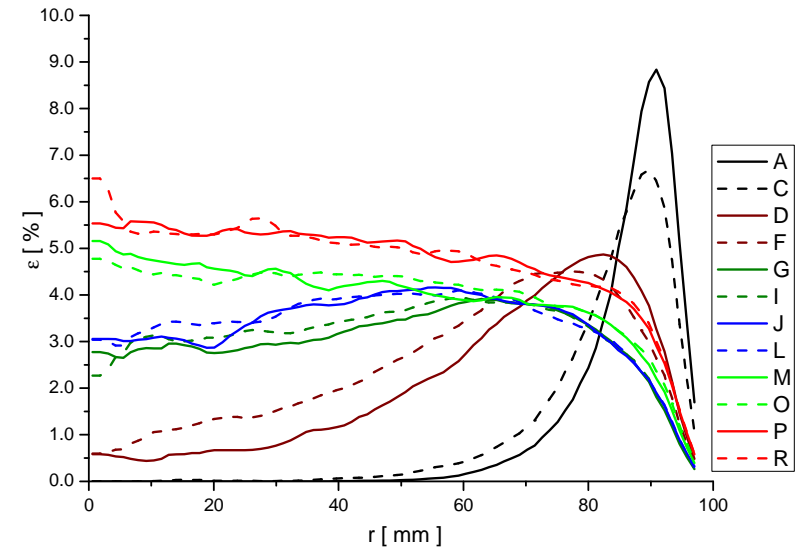
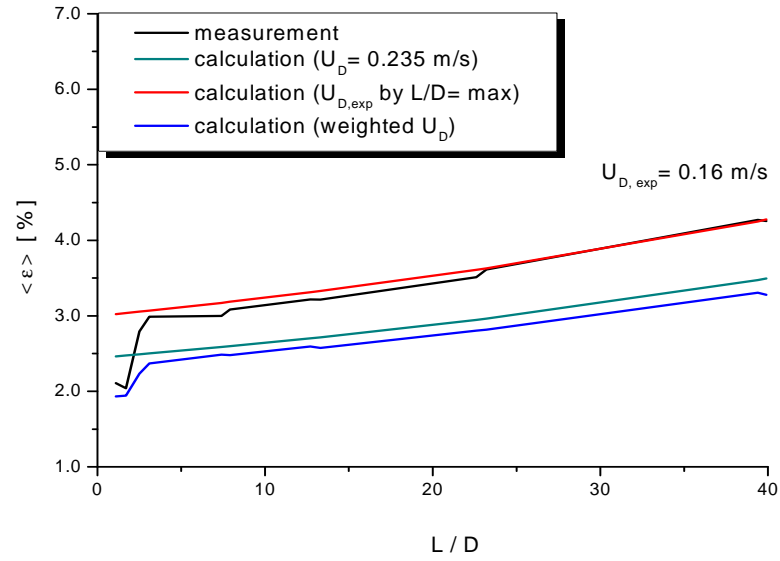
measurement point 036 ($J_L = 0.102$ m/s; $J_G = 0.0096$ m/s; $D_{\text{Orifice}} = 1$ mm)



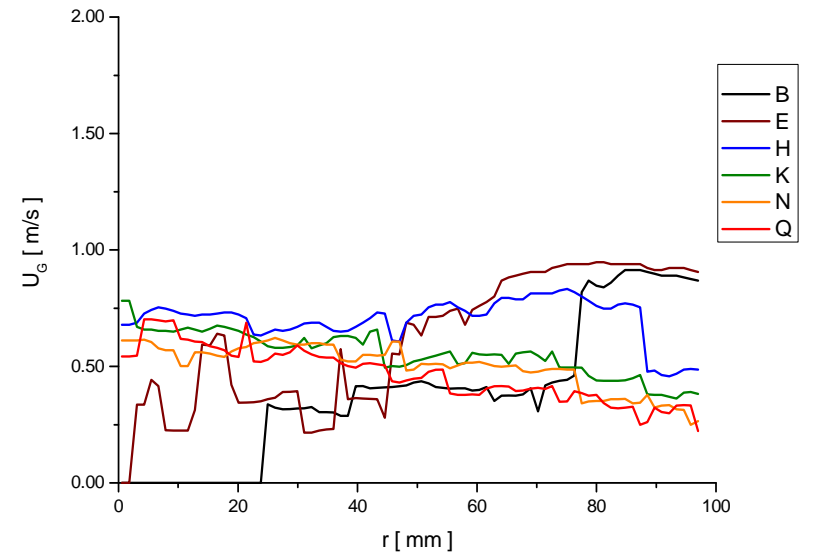
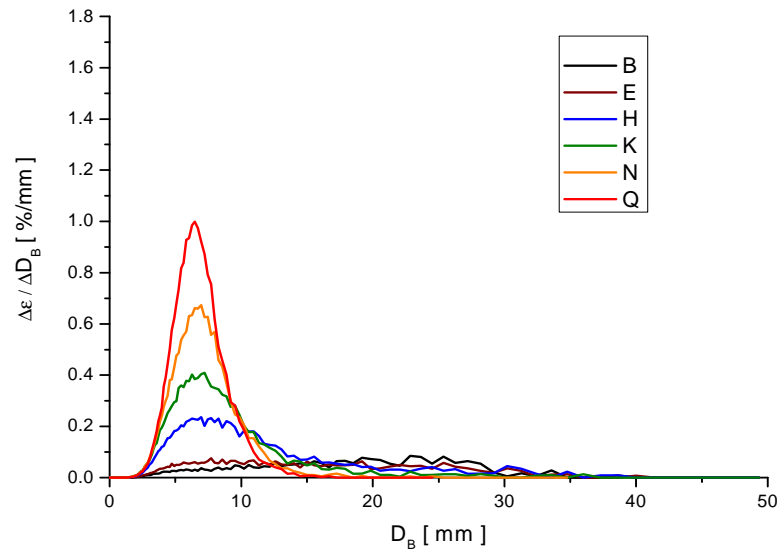
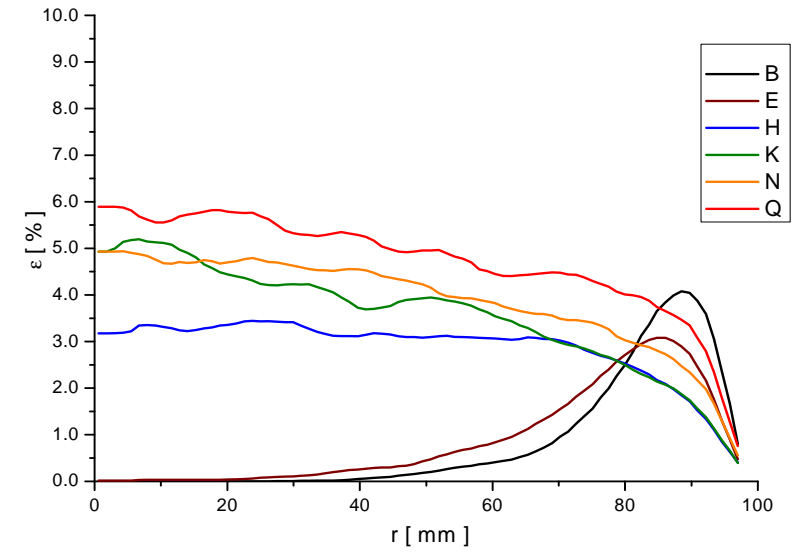
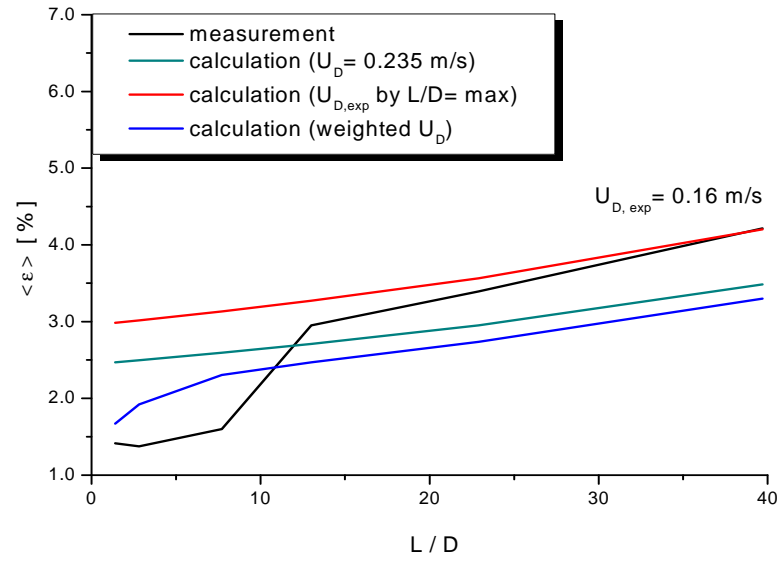
measurement point 036 ($J_L = 0.102$ m/s; $J_G = 0.0096$ m/s; $D_{\text{Orifice}} = 4$ mm)



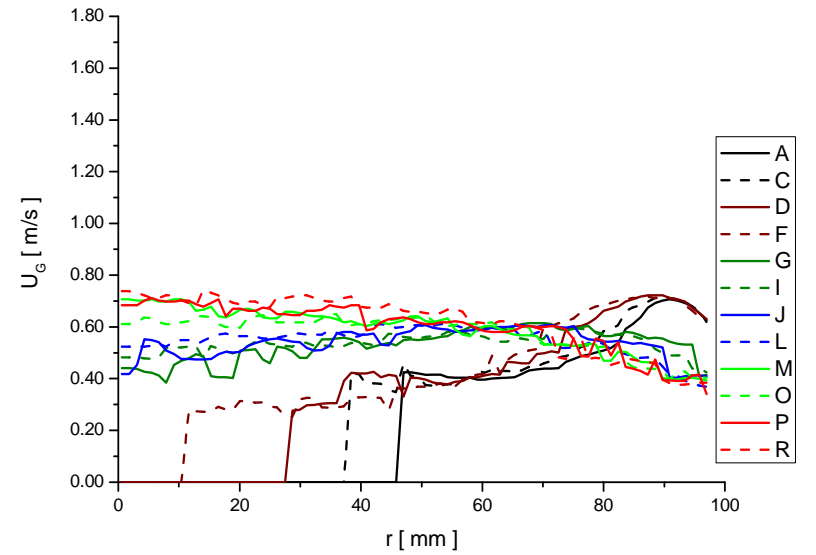
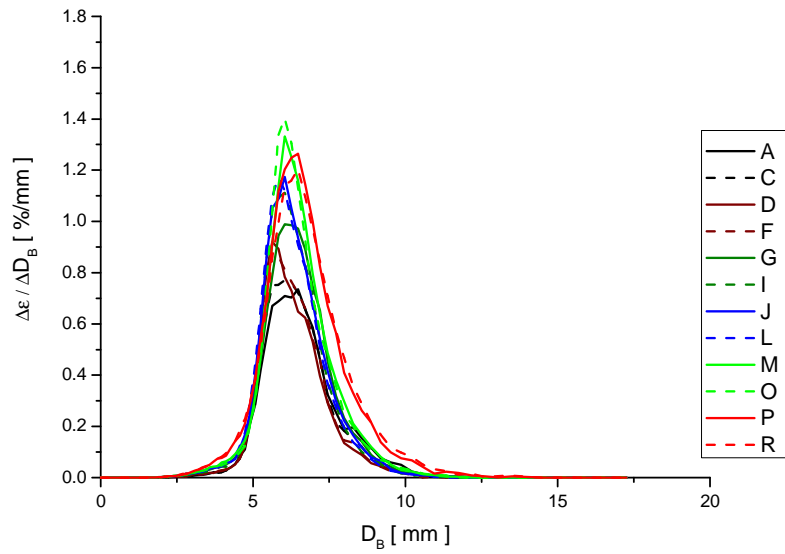
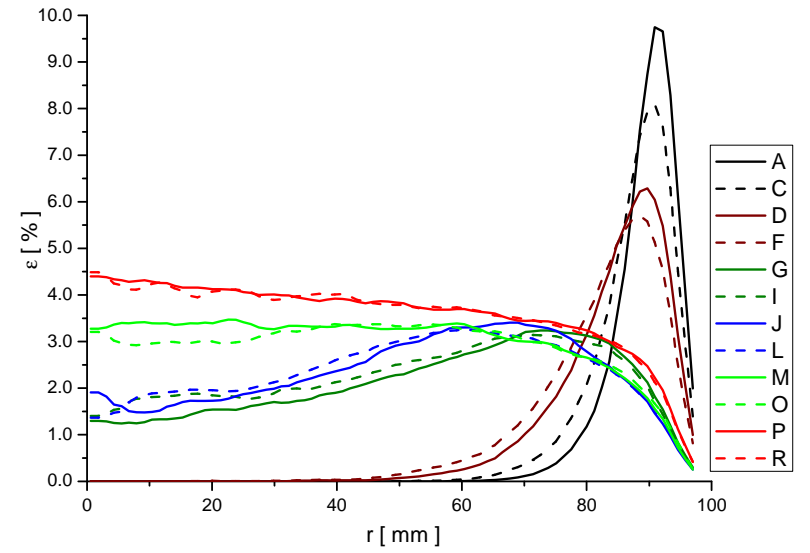
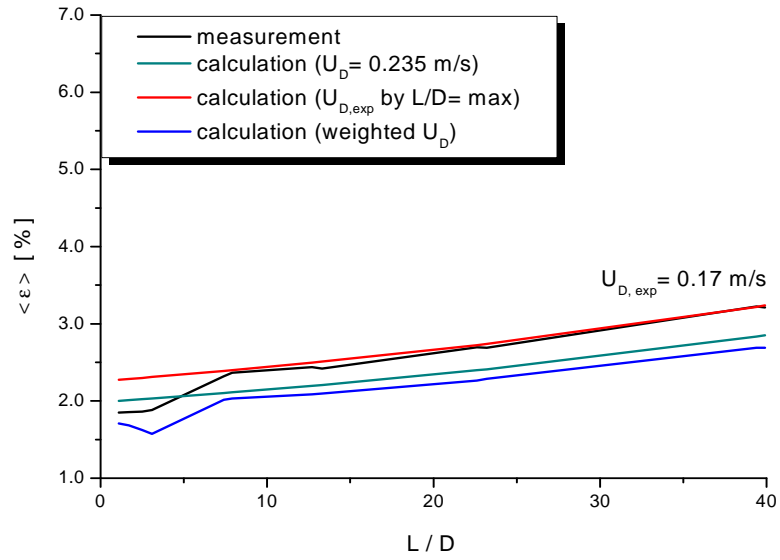
measurement point 037 ($J_L = 0.161$ m/s; $J_G = 0.0096$ m/s; $D_{\text{Orifice}} = 1$ mm)



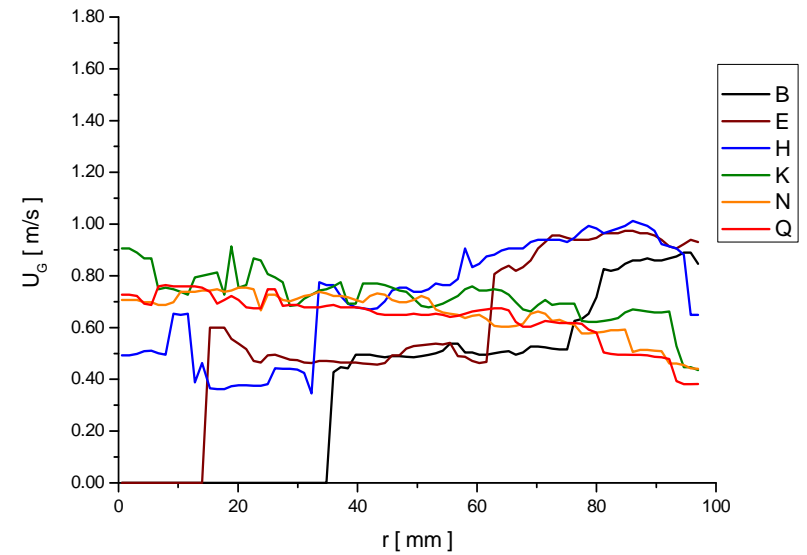
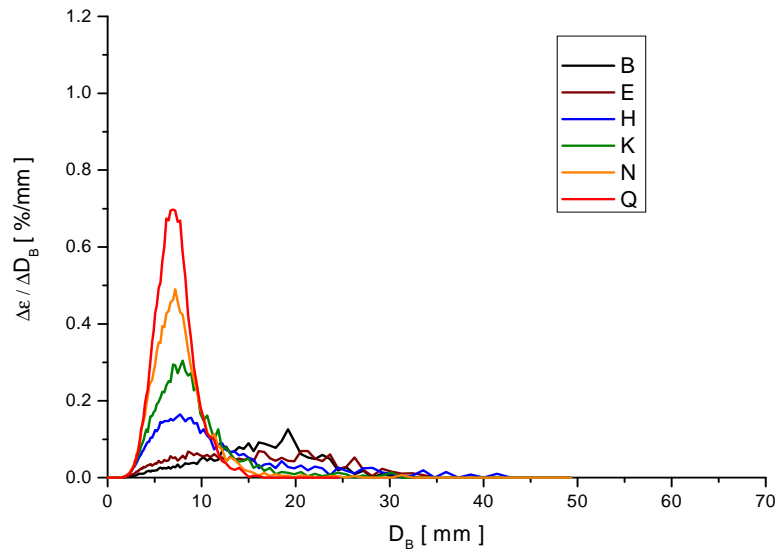
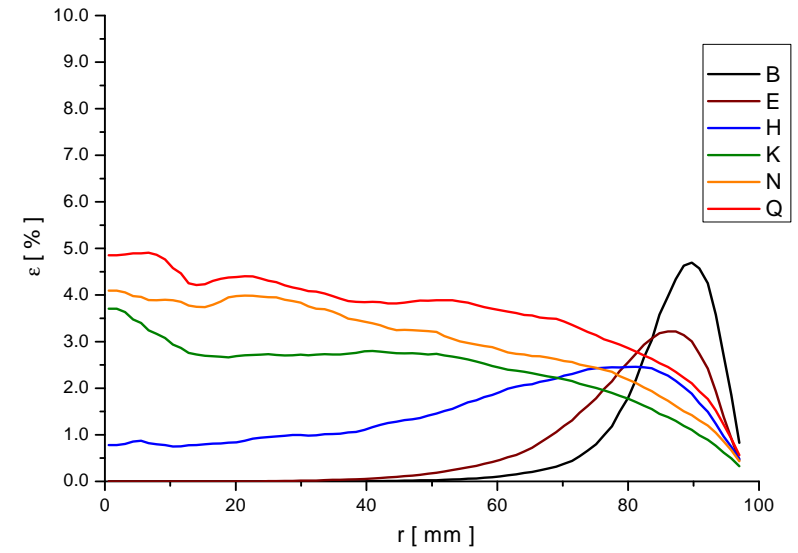
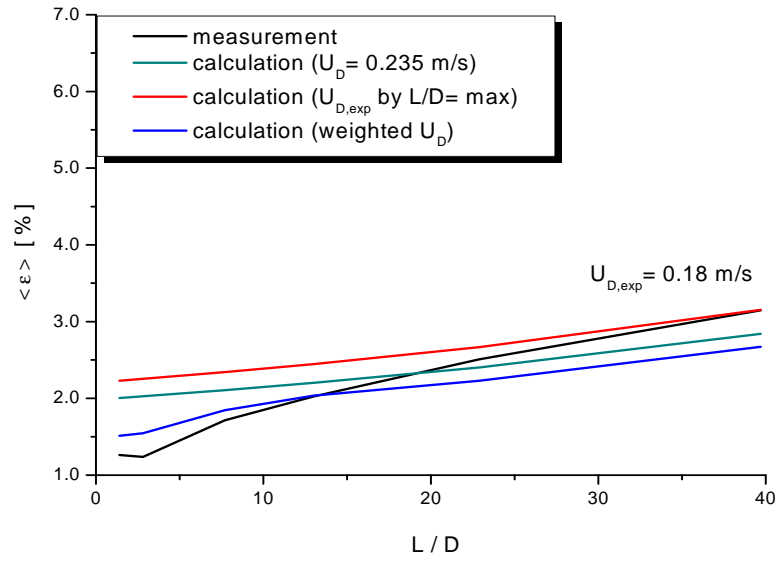
measurement point 037 ($J_L = 0.161$ m/s; $J_G = 0.0096$ m/s; $D_{\text{Orifice}} = 4$ mm)



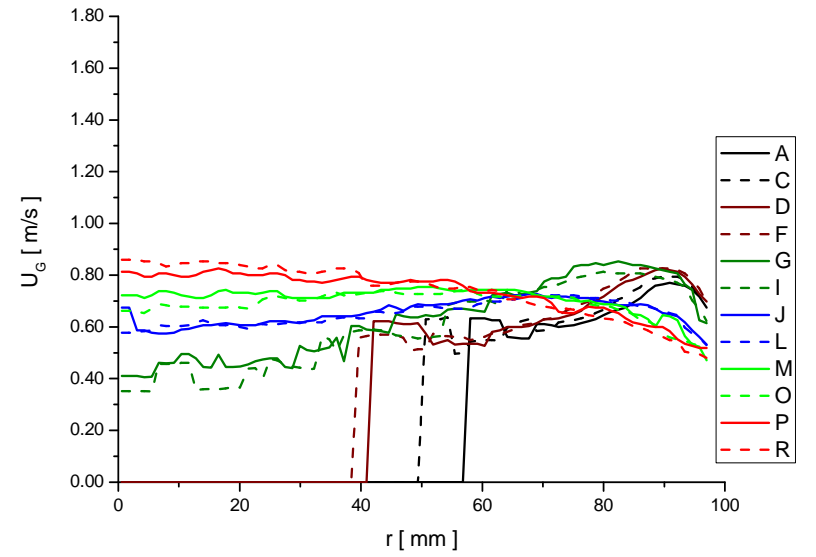
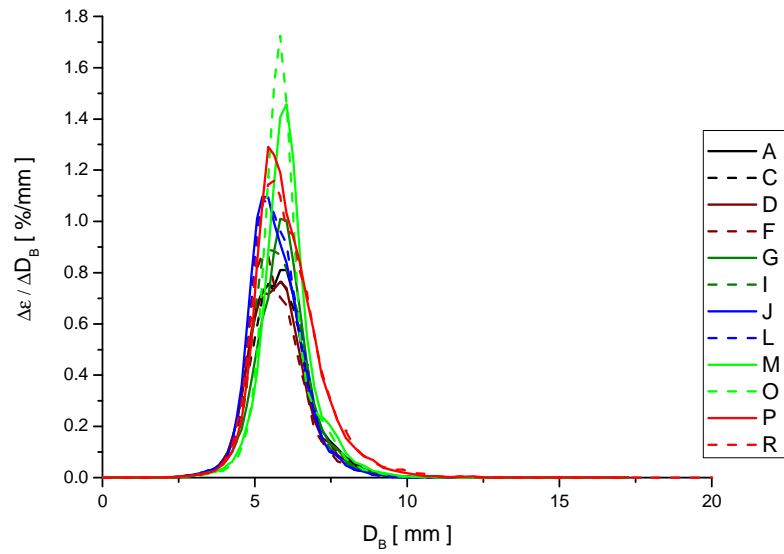
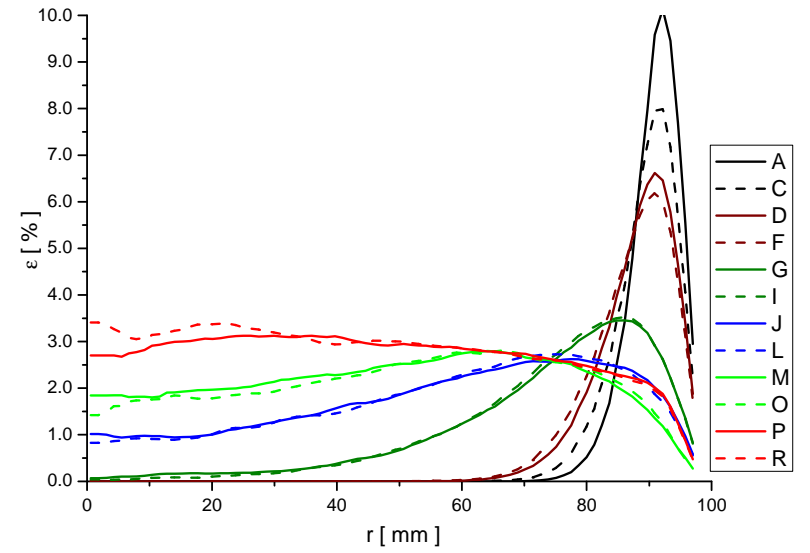
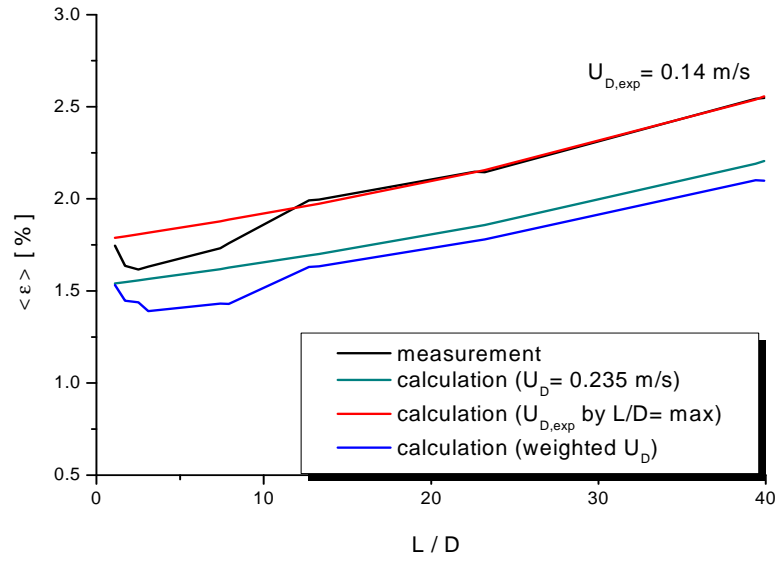
measurement point 038 ($J_L = 0.255$ m/s; $J_G = 0.0096$ m/s; $D_{\text{Orifice}} = 1$ mm)



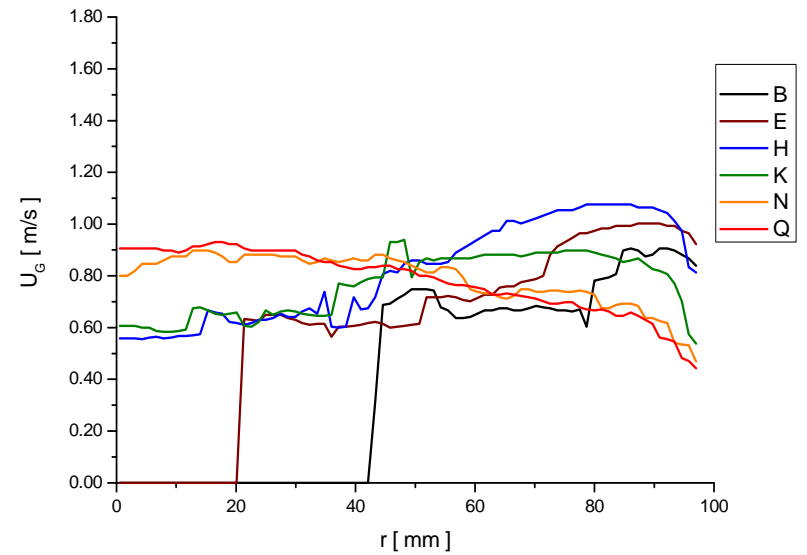
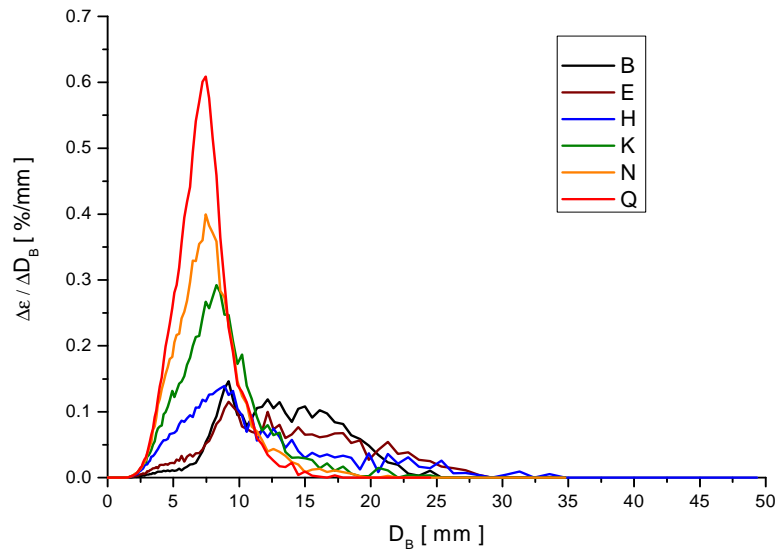
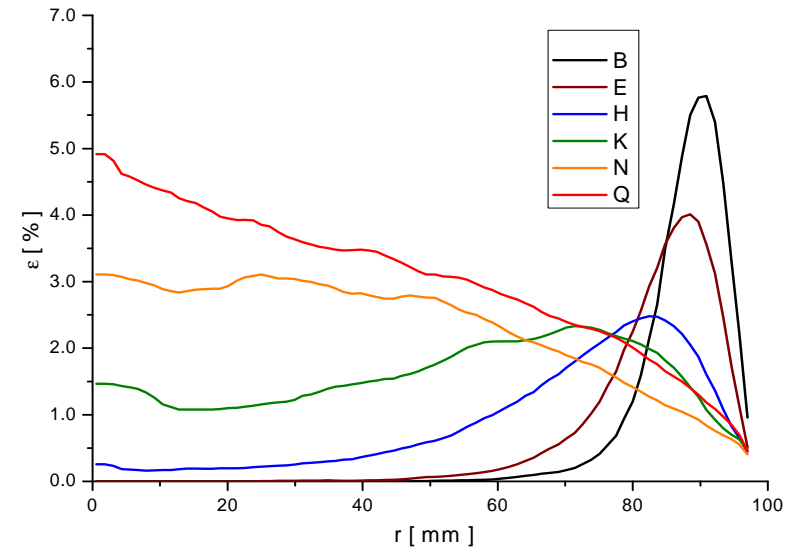
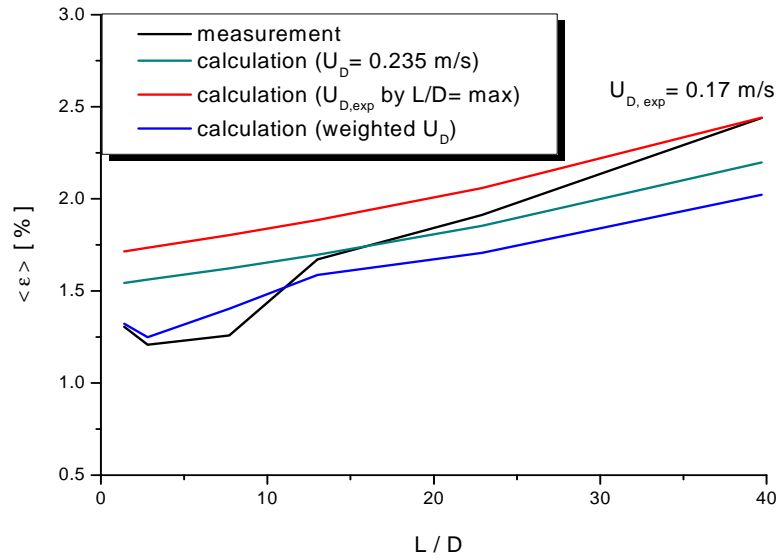
measurement point 038 ($J_L = 0.255$ m/s; $J_G = 0.0096$ m/s; $D_{\text{Orifice}} = 4$ mm)



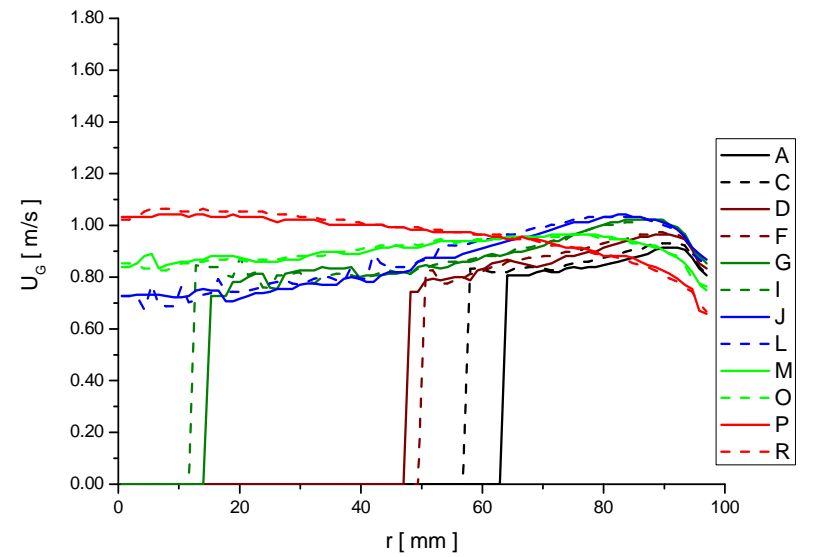
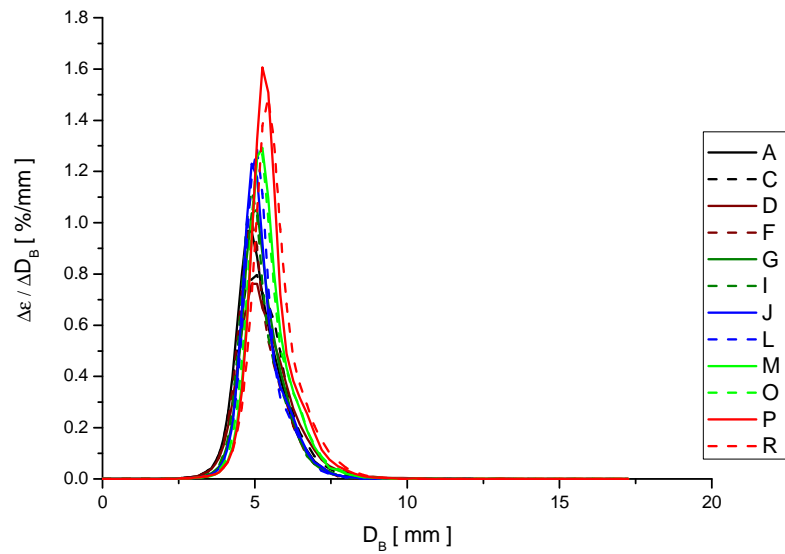
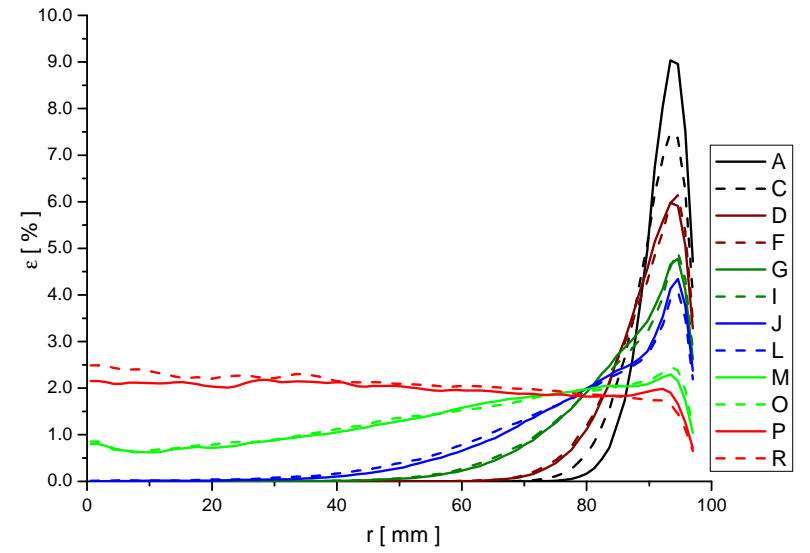
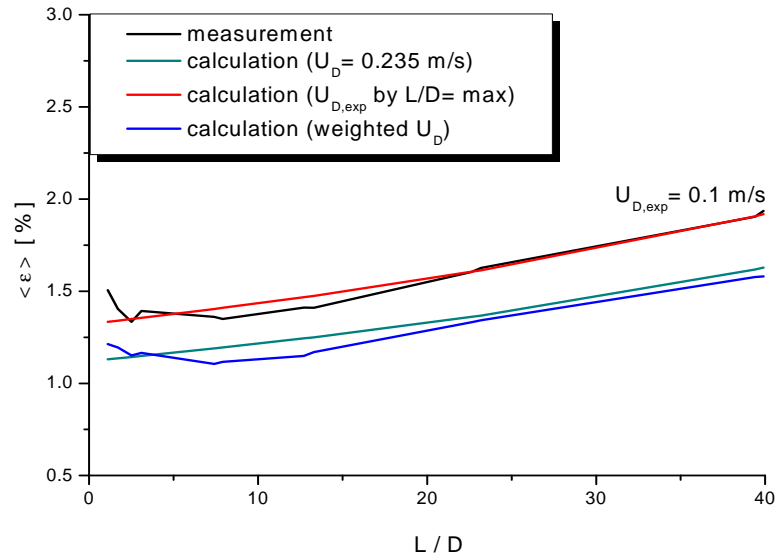
measurement point 039 ($J_L = 0.405$ m/s; $J_G = 0.0096$ m/s; $D_{\text{Orifice}} = 1$ mm)



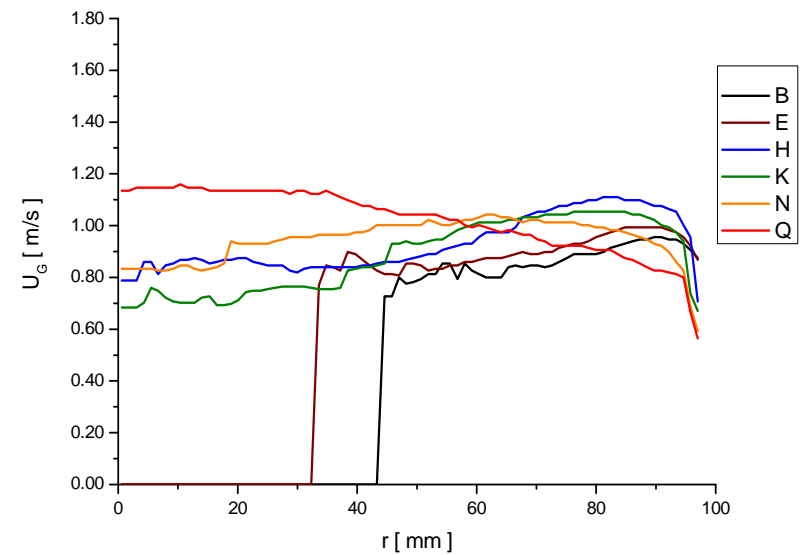
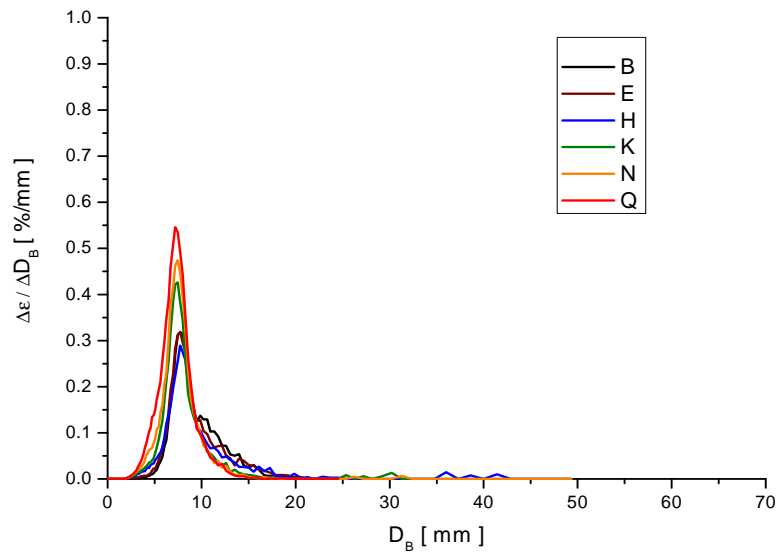
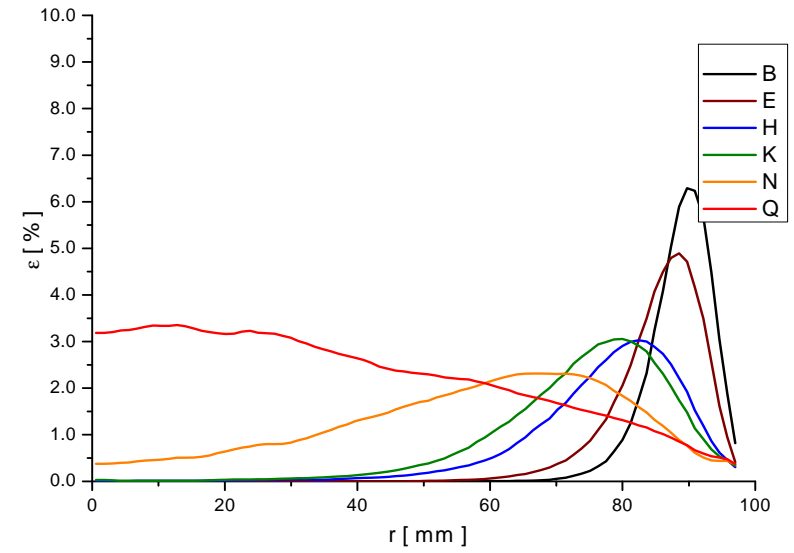
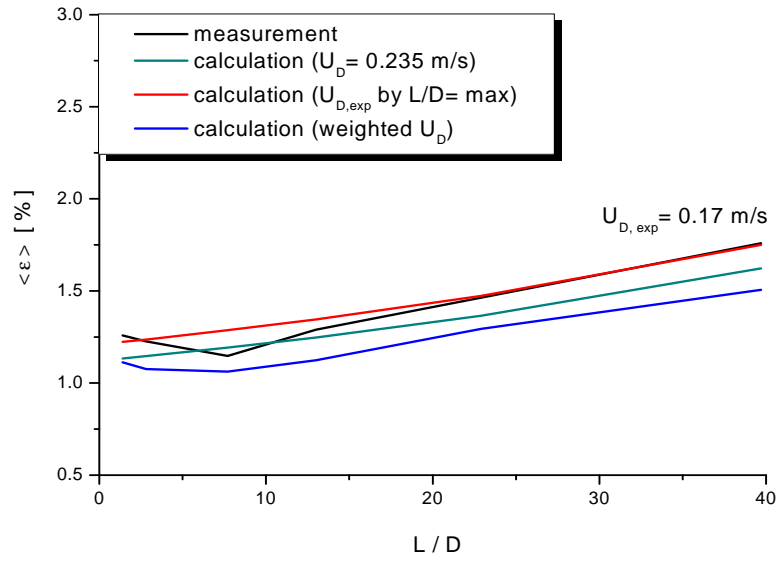
measurement point 039 ($J_L = 0.405$ m/s; $J_G = 0.0096$ m/s; $D_{\text{Orifice}} = 4$ mm)



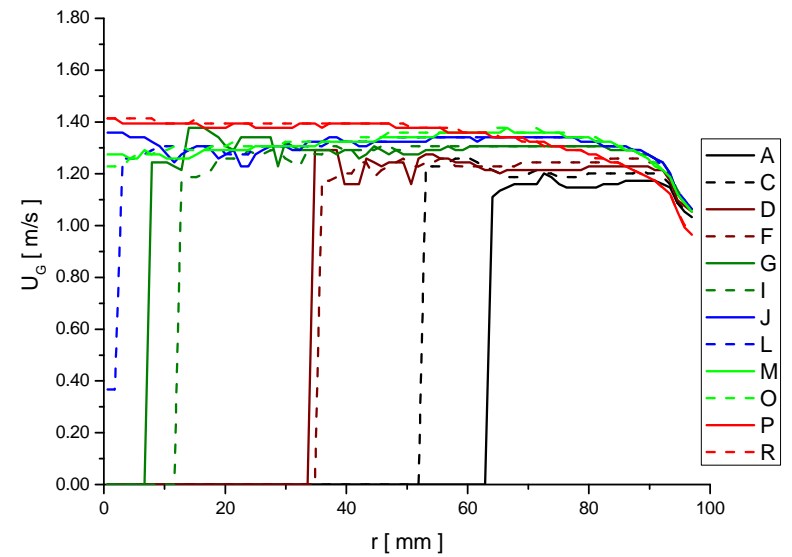
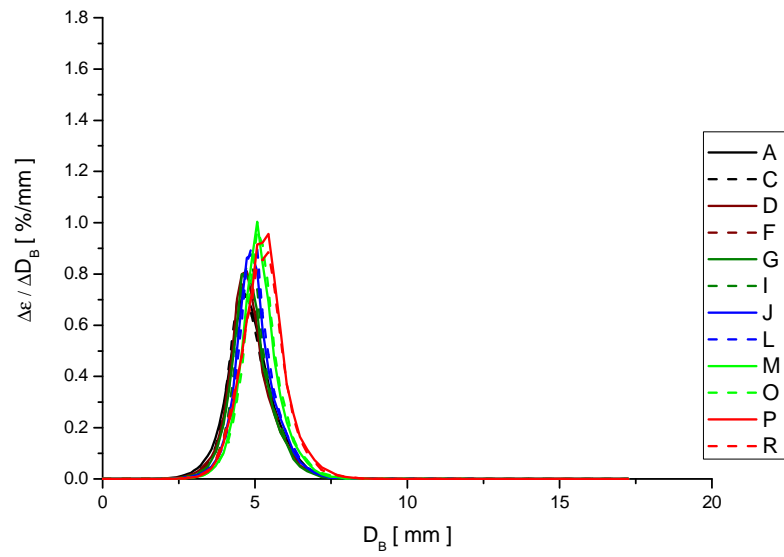
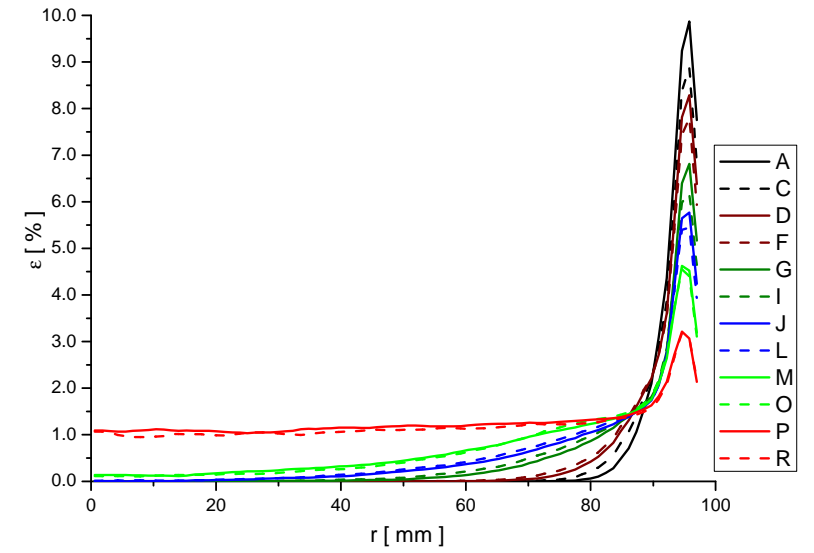
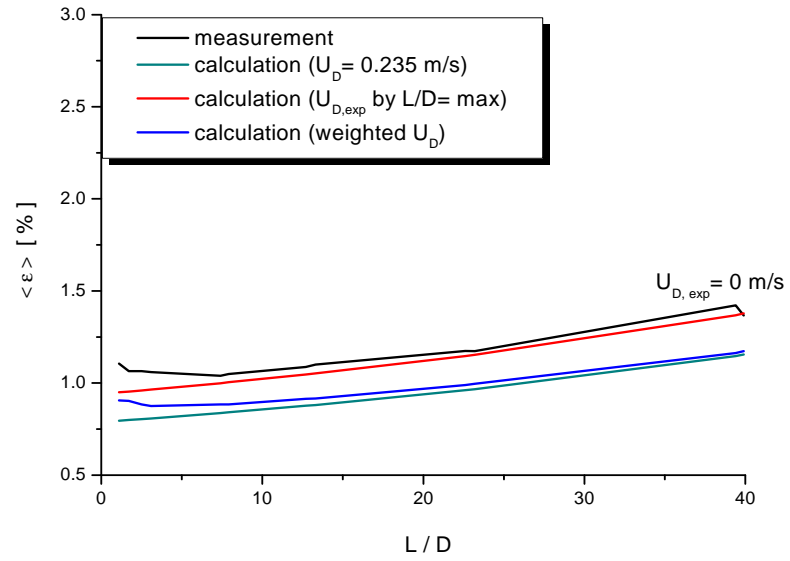
measurement point 040 ($J_L = 0.641$ m/s; $J_G = 0.0096$ m/s; $D_{\text{Orifice}} = 1$ mm)



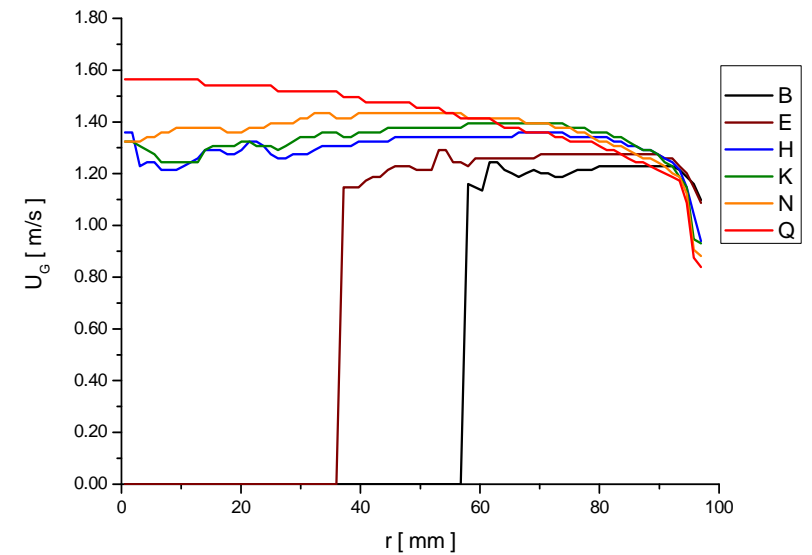
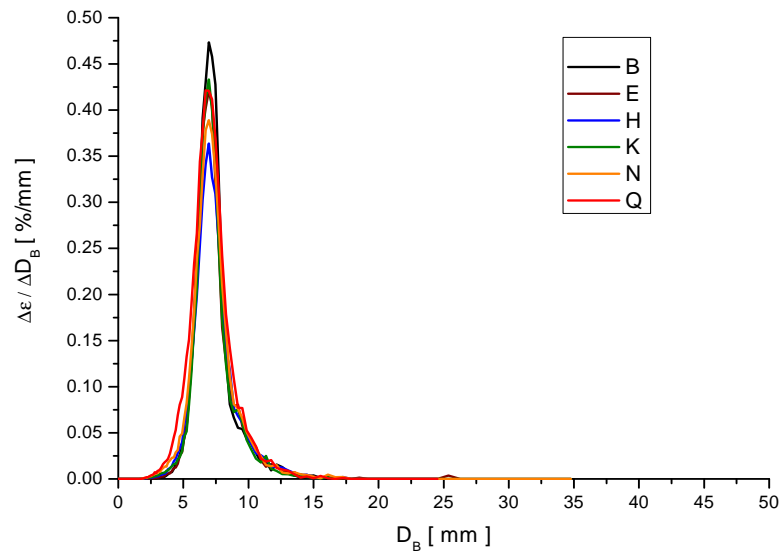
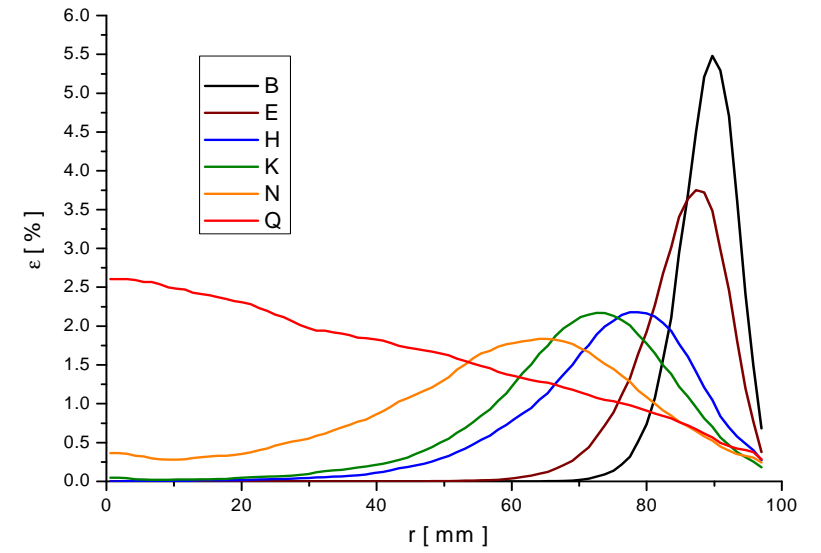
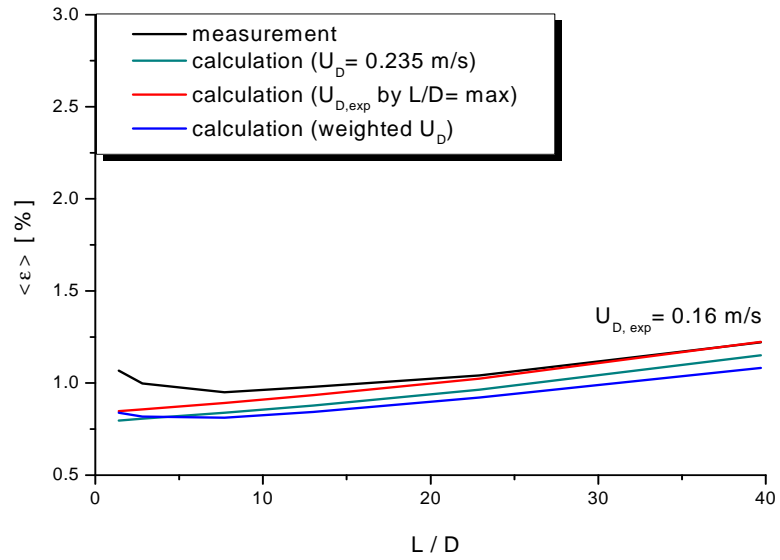
measurement point 040 ($J_L = 0.641$ m/s; $J_G = 0.0096$ m/s; $D_{\text{Orifice}} = 4$ mm)



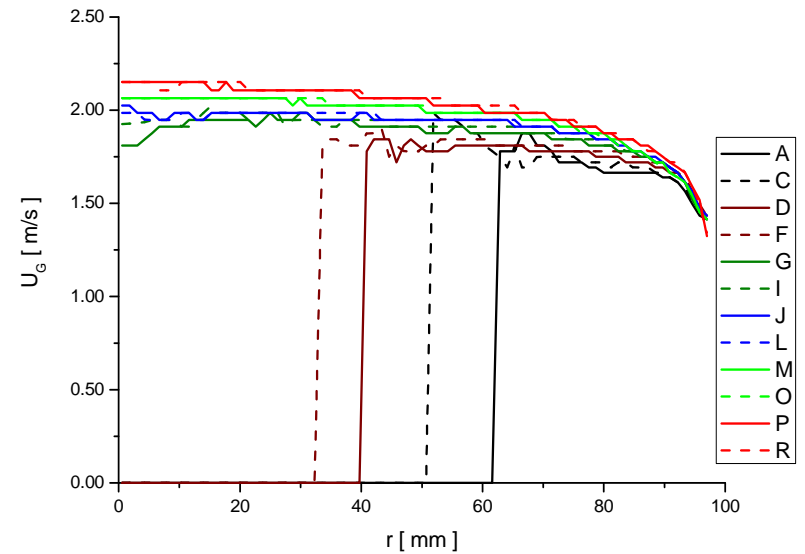
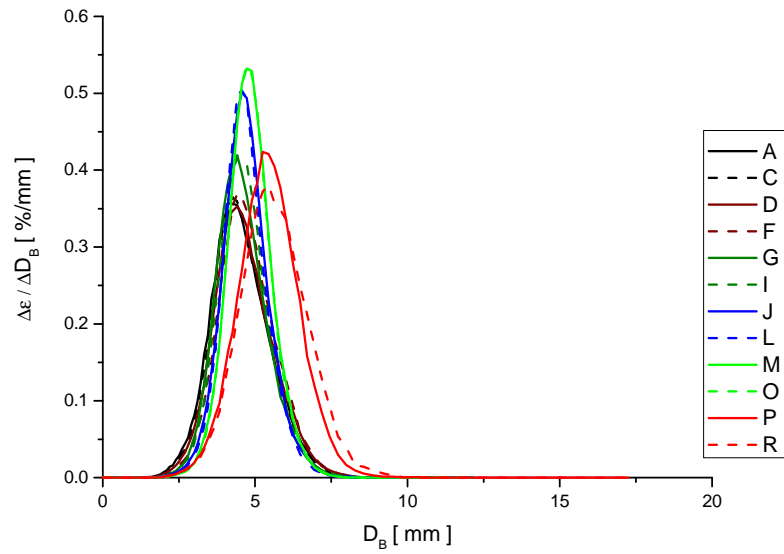
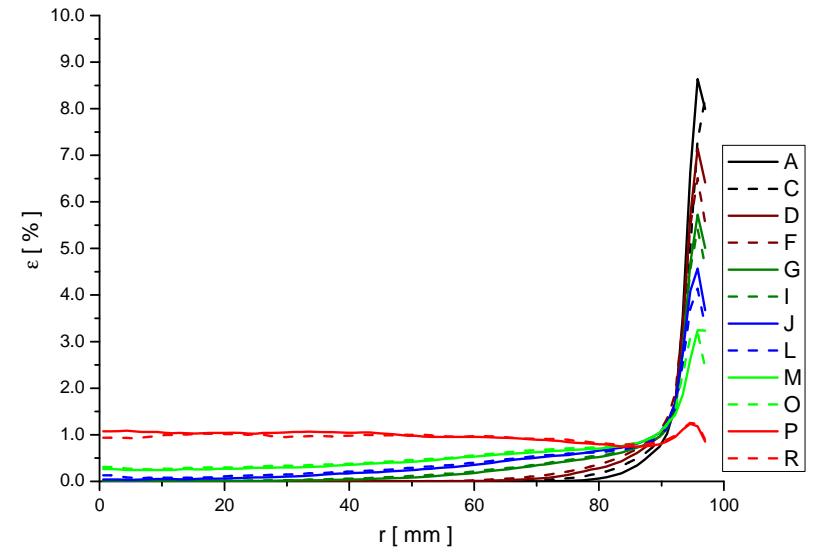
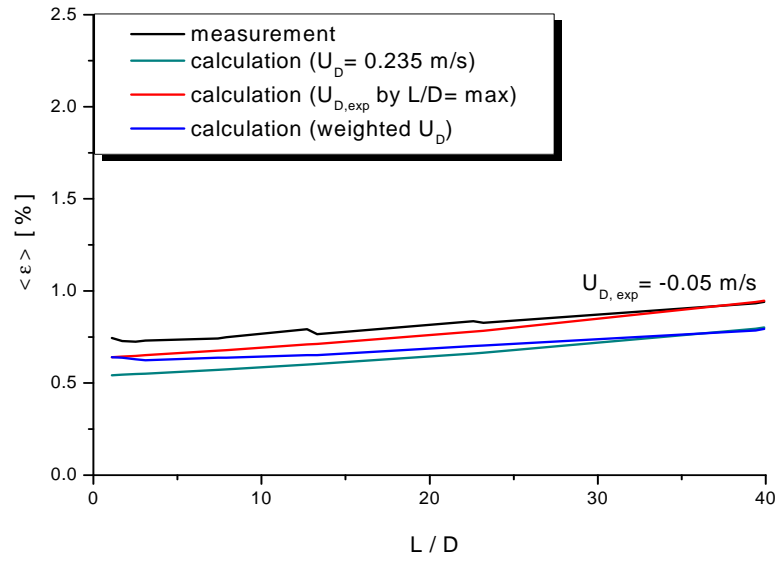
measurement point 041 ($J_L = 1.017$ m/s; $J_G = 0.0096$ m/s; $D_{\text{Orifice}} = 1$ mm)



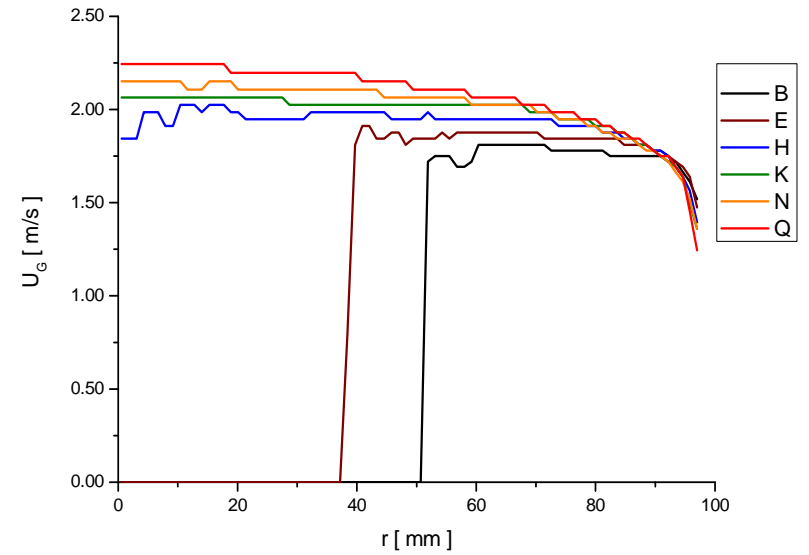
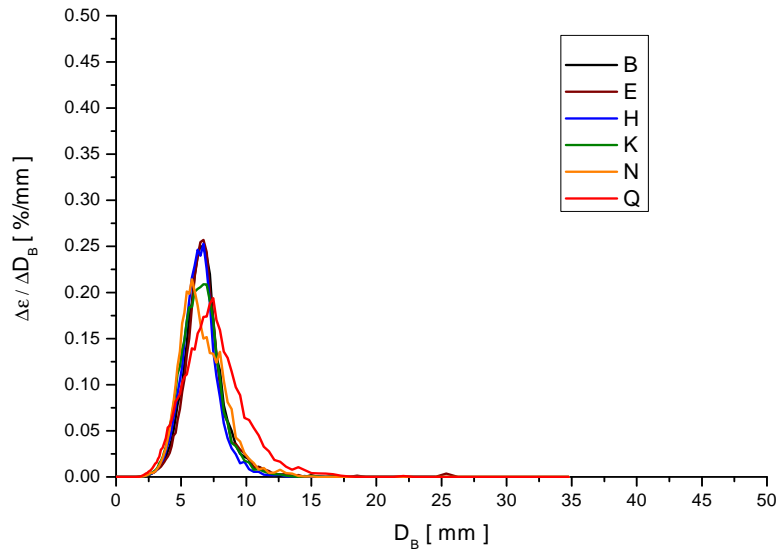
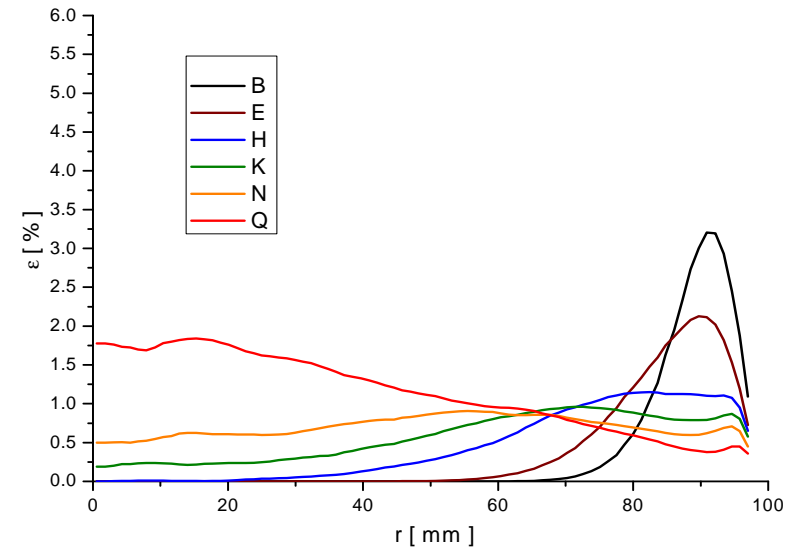
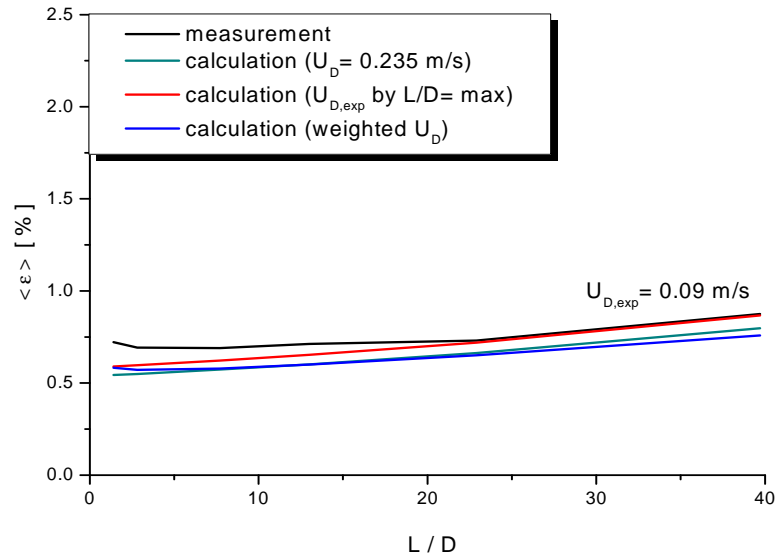
measurement point 041 ($J_L = 1.017$ m/s; $J_G = 0.0096$ m/s; $D_{\text{Orifice}} = 4$ mm)



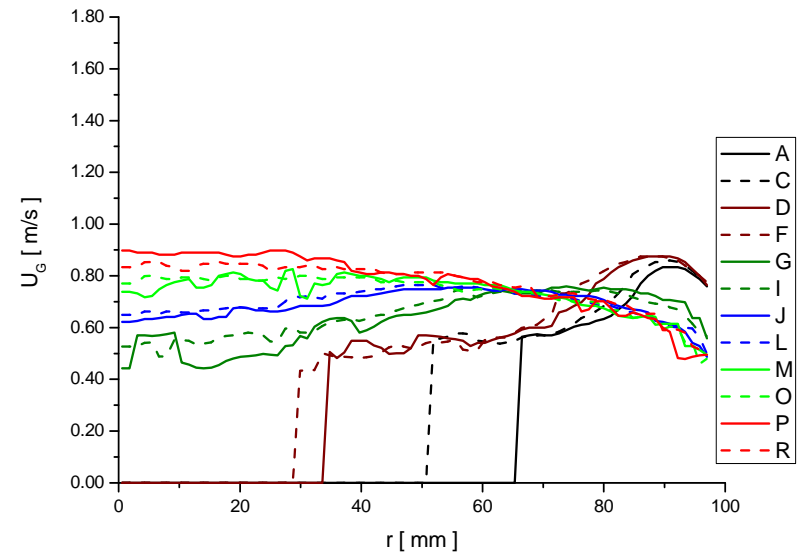
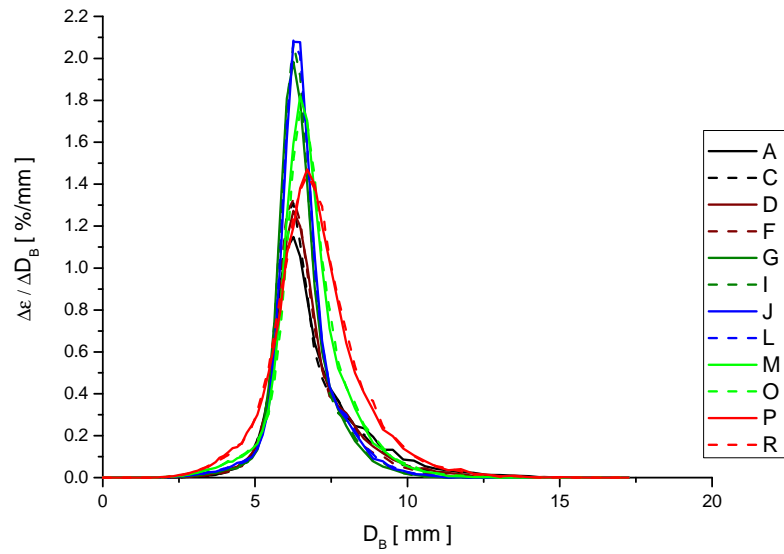
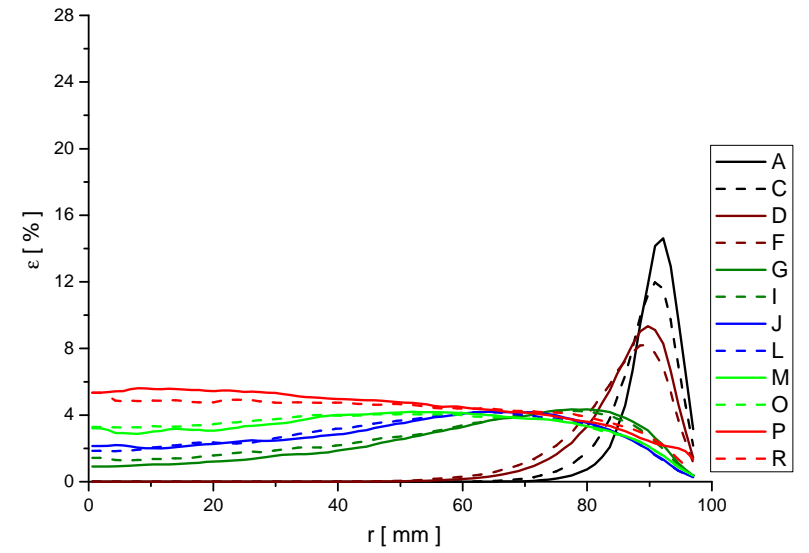
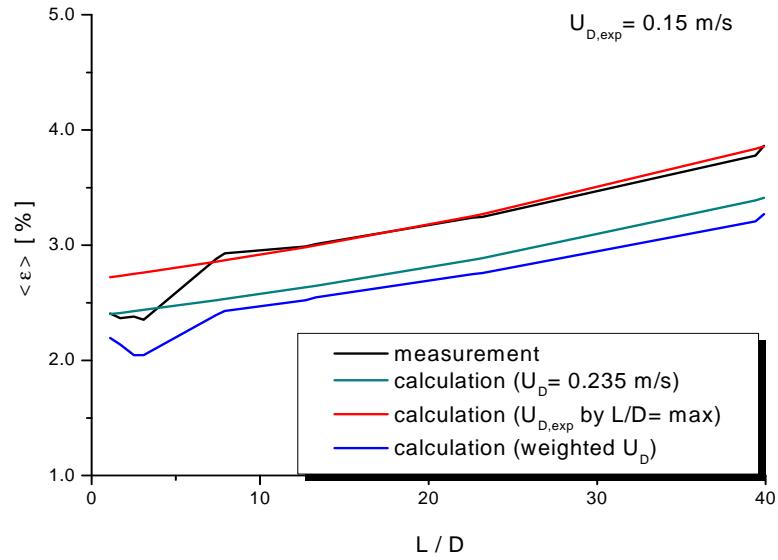
measurement point 042 ($J_L = 1.611$ m/s; $J_G = 0.0096$ m/s; $D_{\text{Orifice}} = 1$ mm)



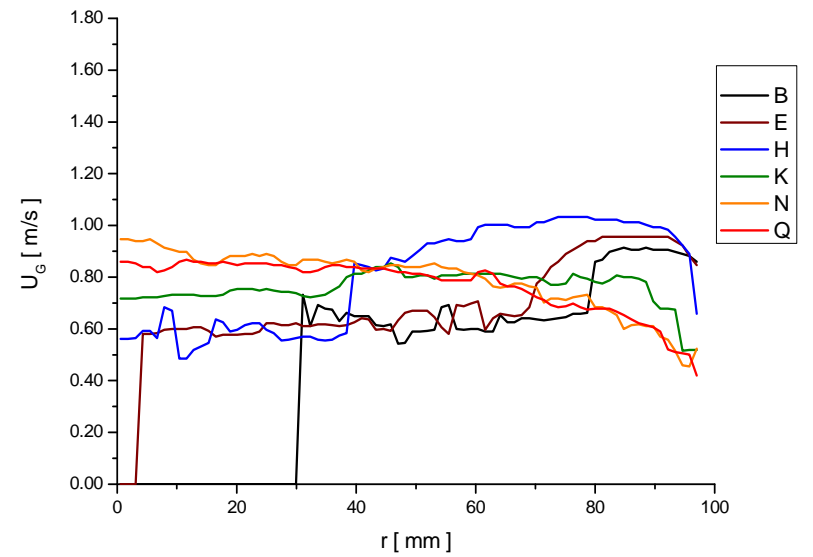
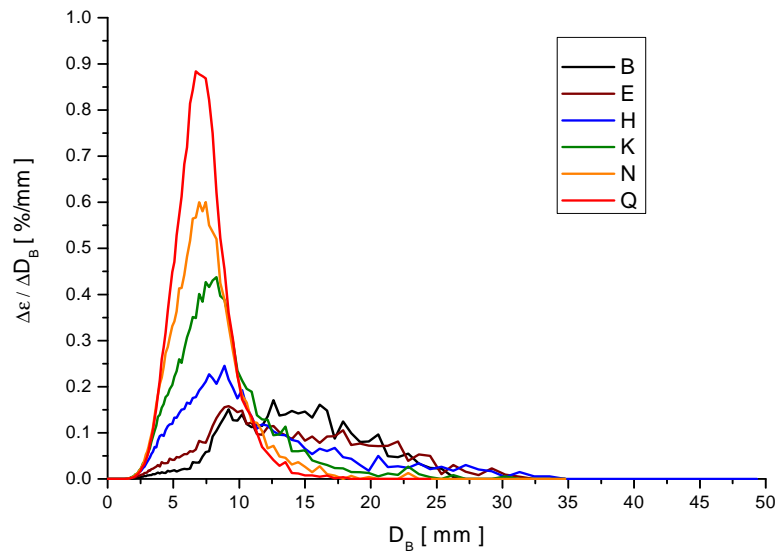
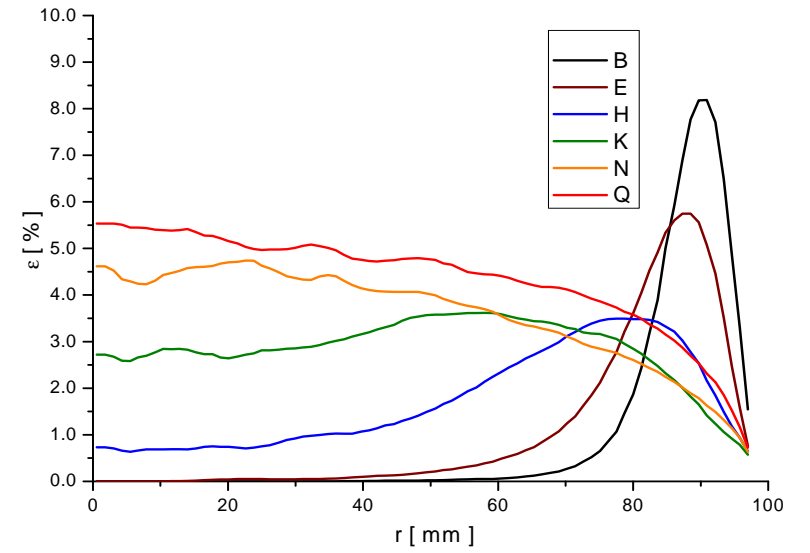
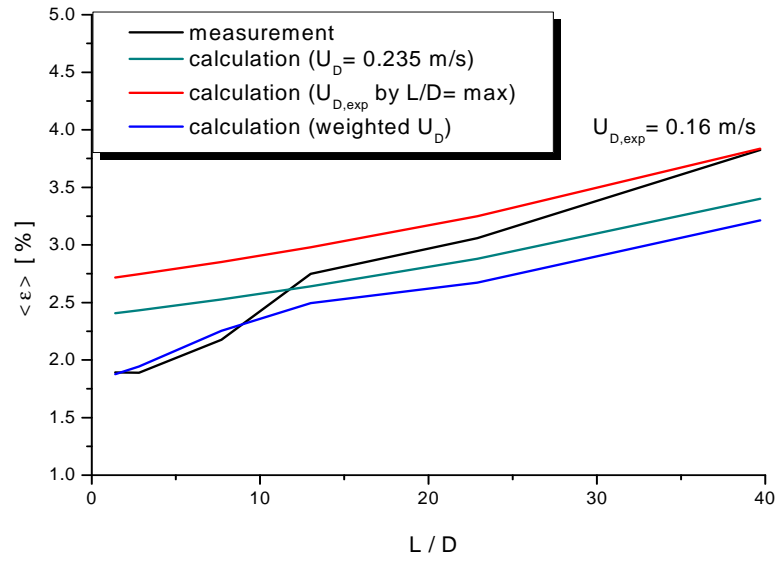
measurement point 042 ($J_L = 1.611$ m/s; $J_G = 0.0096$ m/s; $D_{\text{Orifice}} = 4$ mm)



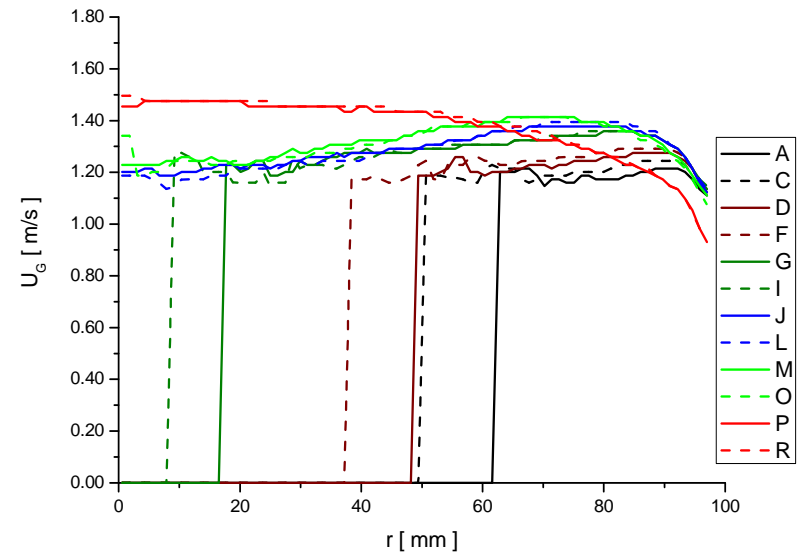
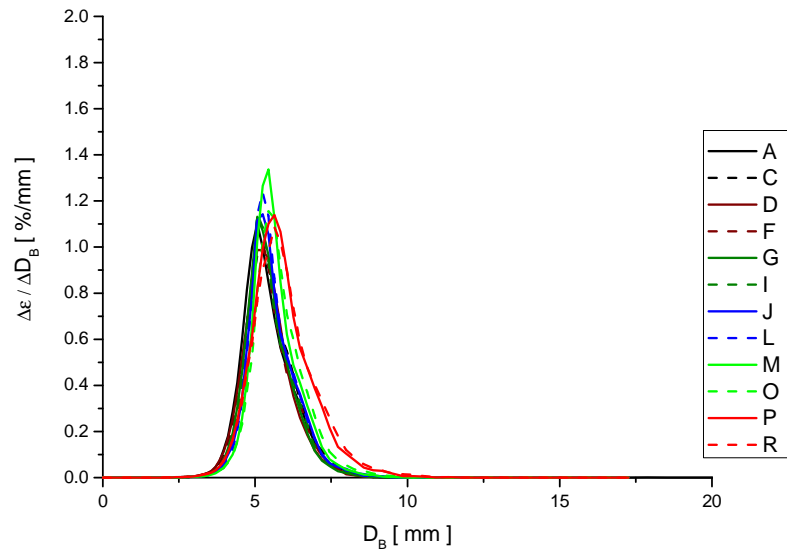
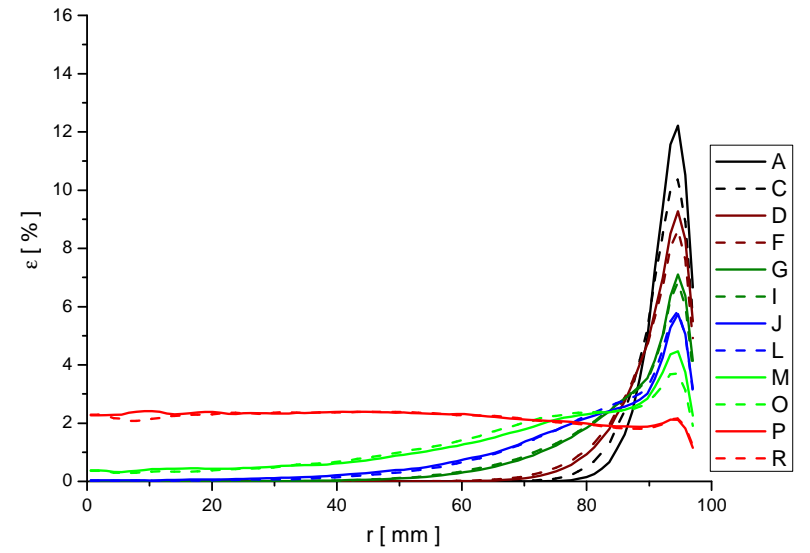
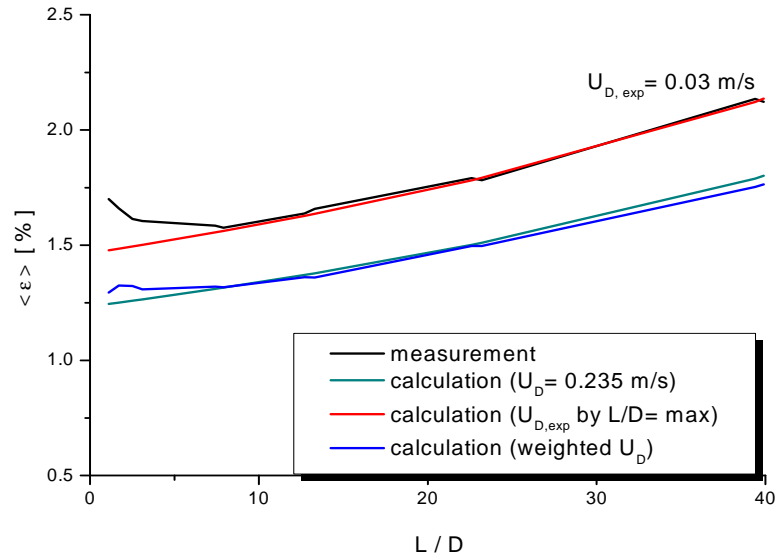
measurement point 050 ($J_L = 0.405$ m/s; $J_G = 0.0151$ m/s; $D_{\text{Orifice}} = 1$ mm)



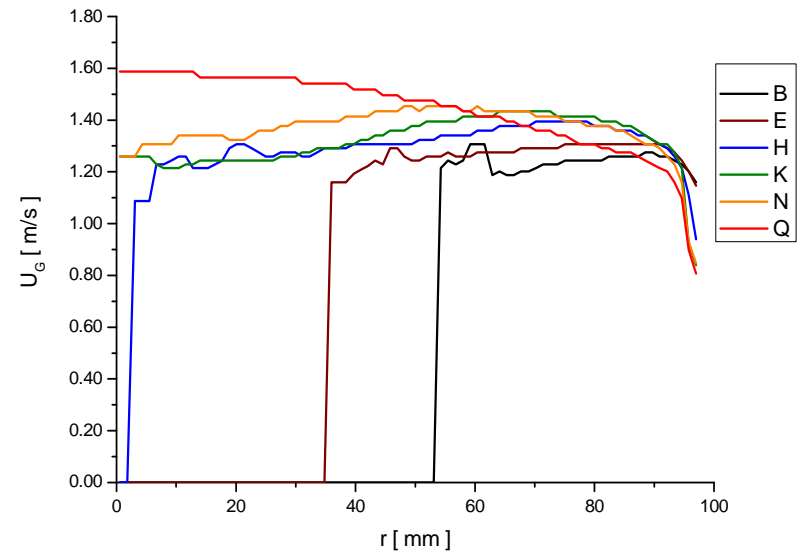
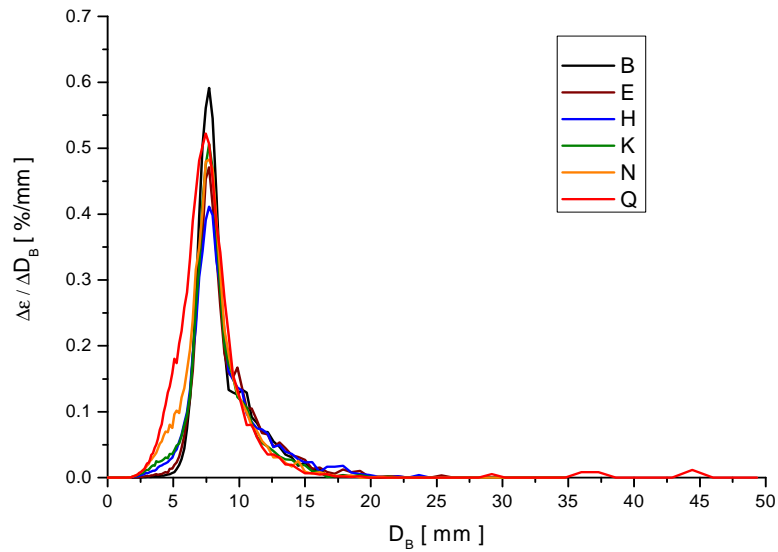
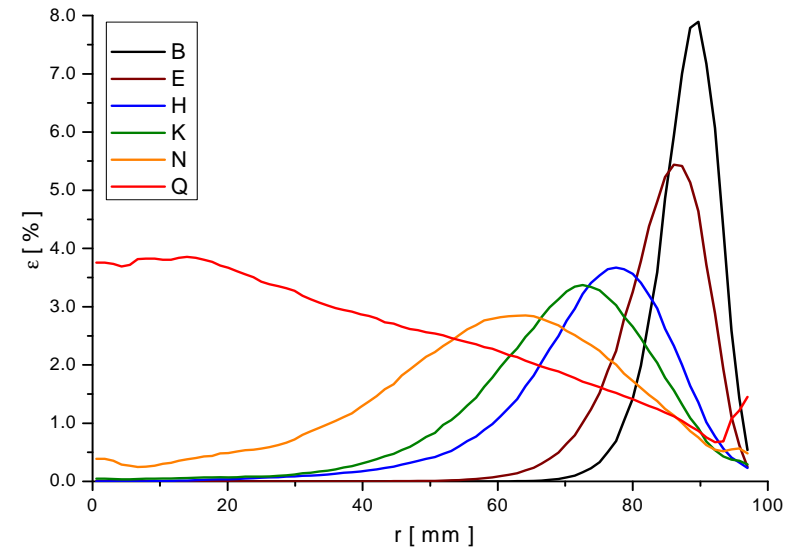
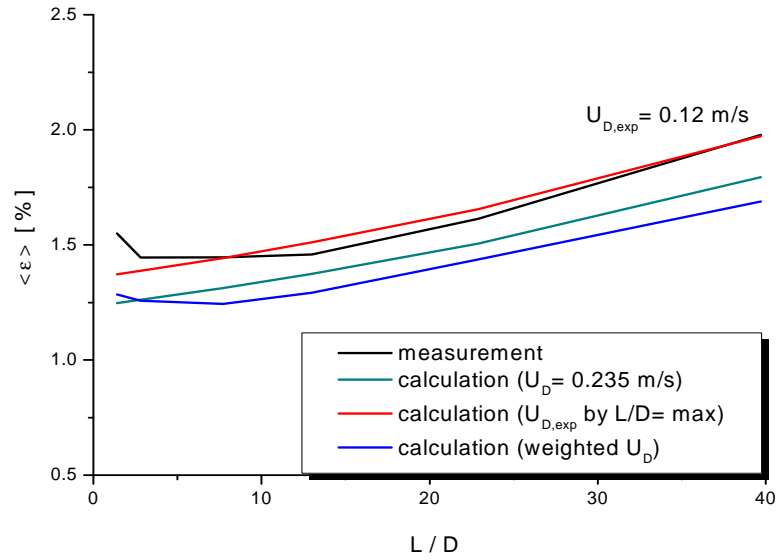
measurement point 050 ($J_L = 0.405$ m/s; $J_G = 0.0151$ m/s; $D_{\text{Orifice}} = 4$ mm)



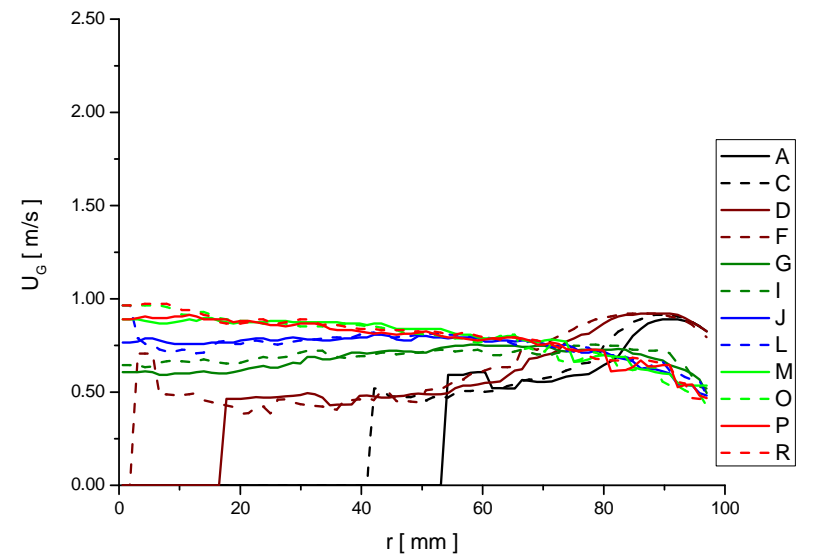
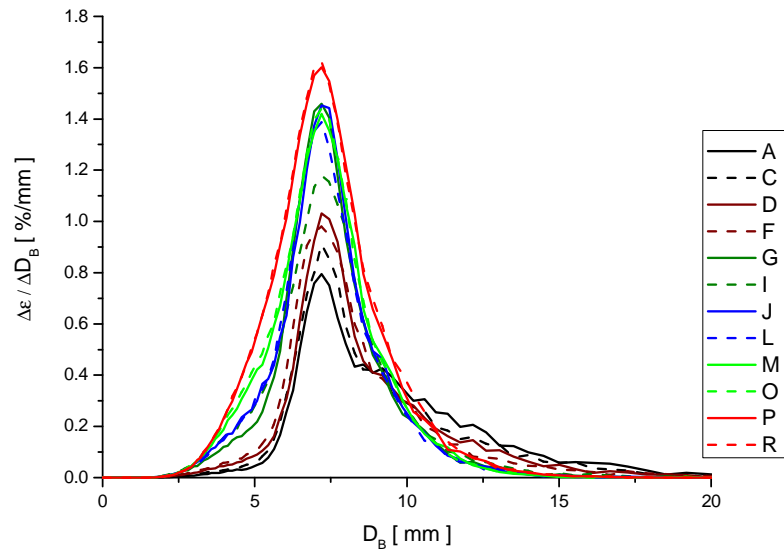
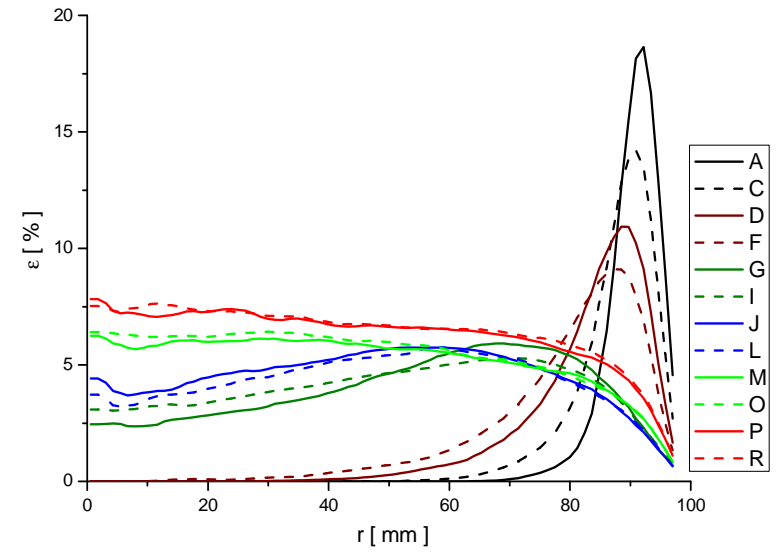
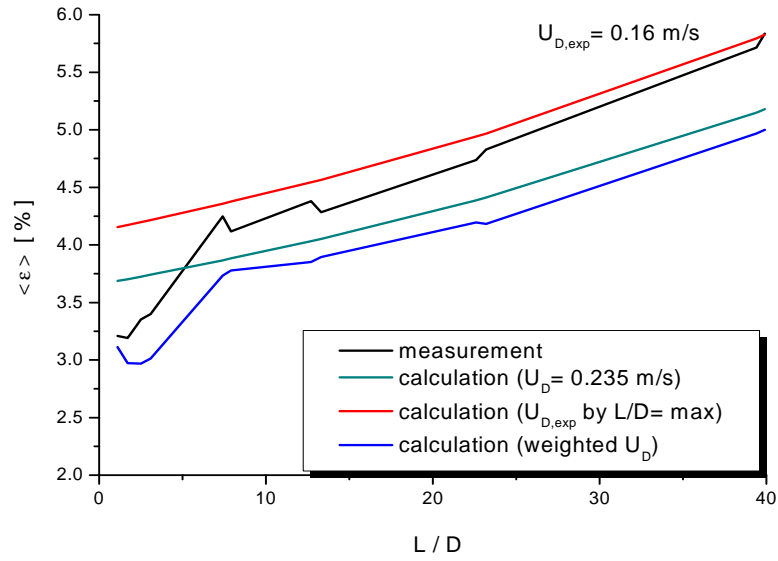
measurement point 052 ($J_L = 1.017$ m/s; $J_G = 0.0151$ m/s; $D_{\text{Orifice}} = 1$ mm)



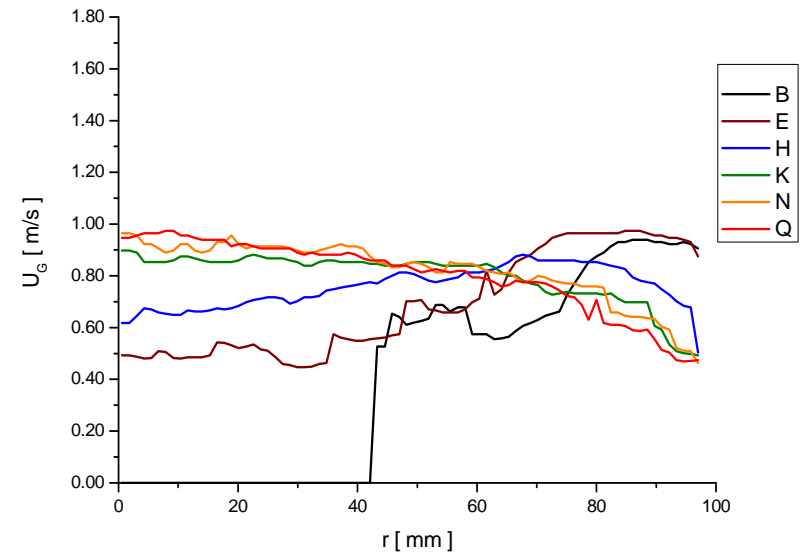
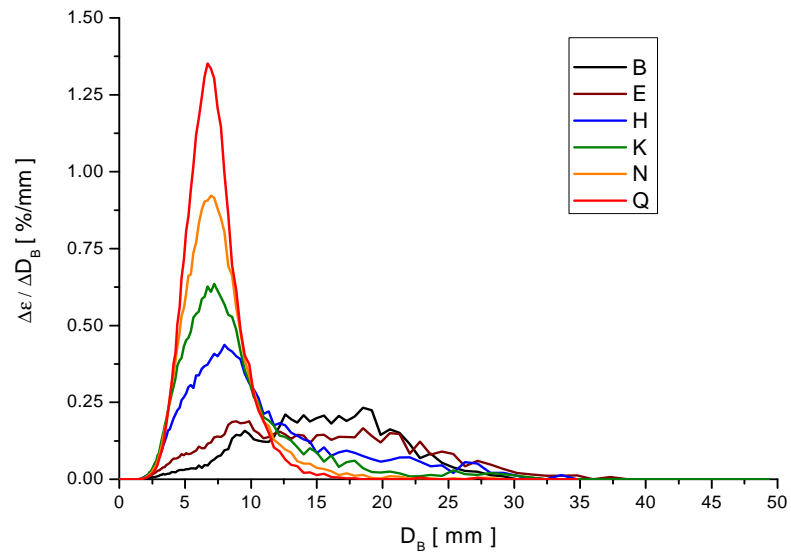
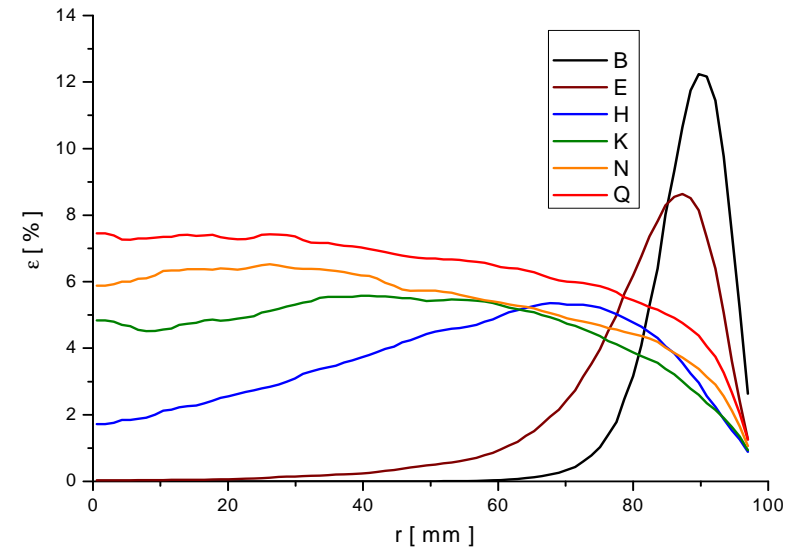
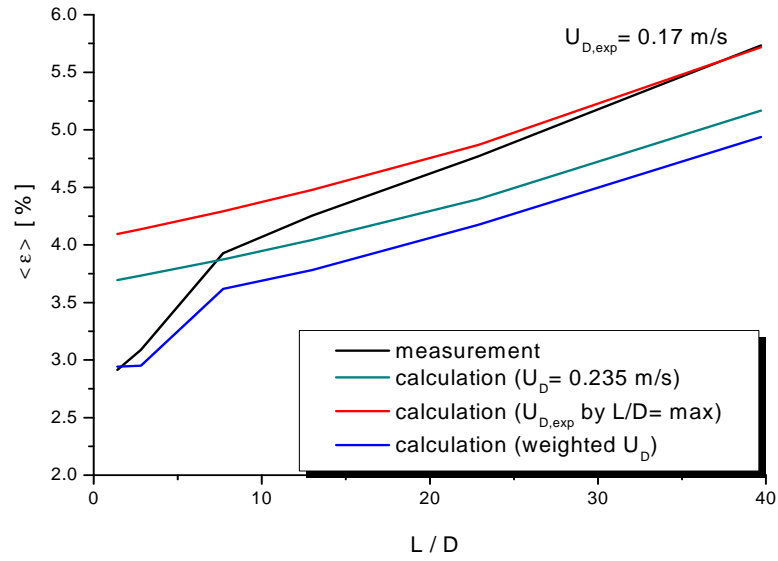
measurement point 052 ($J_L = 1.017$ m/s; $J_G = 0.0151$ m/s; $D_{\text{Orifice}} = 4$ mm)



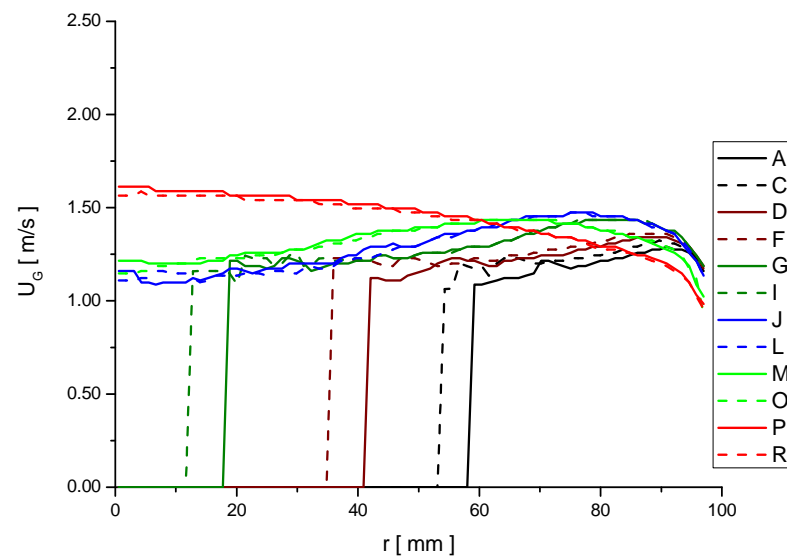
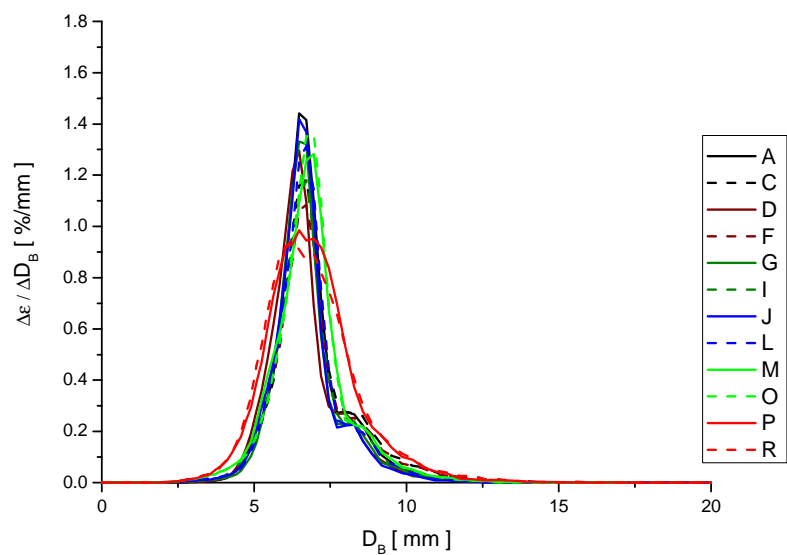
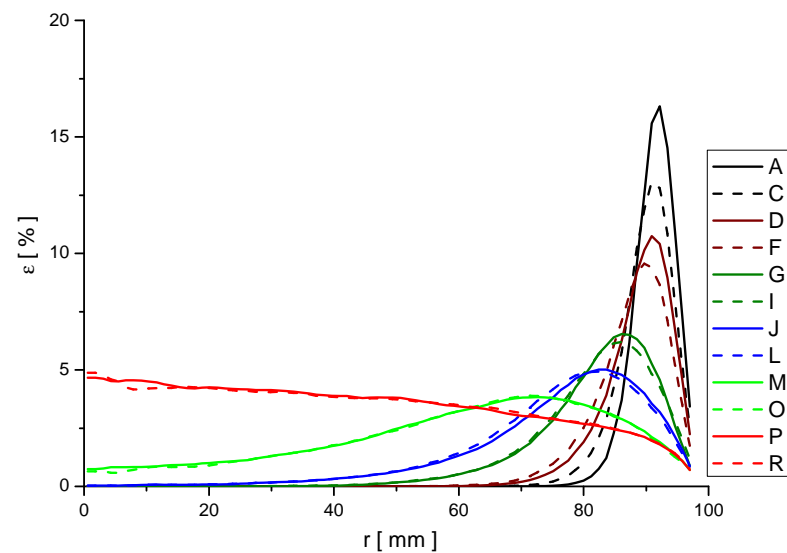
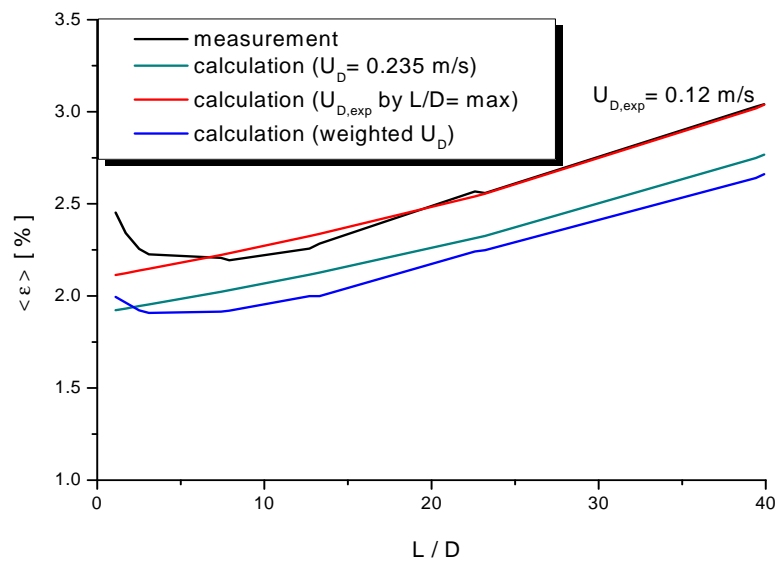
measurement point 061 ($J_L = 0.405$ m/s; $J_G = 0.0235$ m/s; $D_{\text{Orifice}} = 1$ mm)



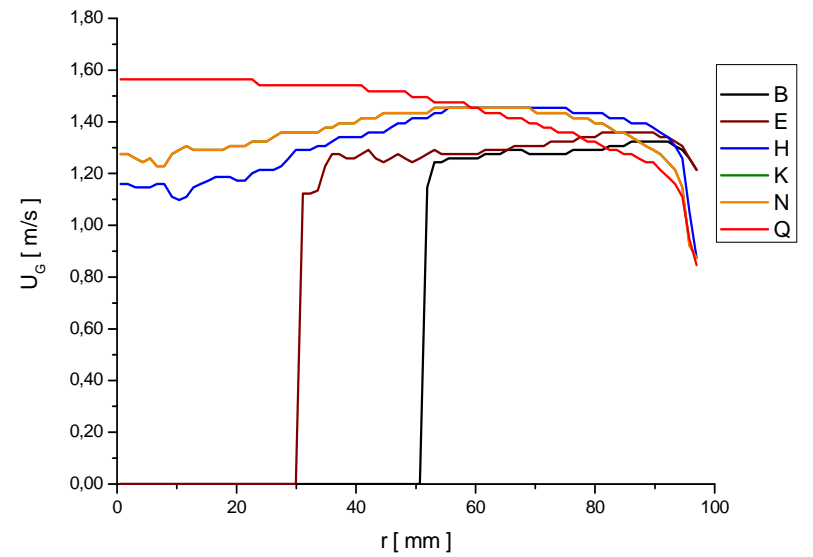
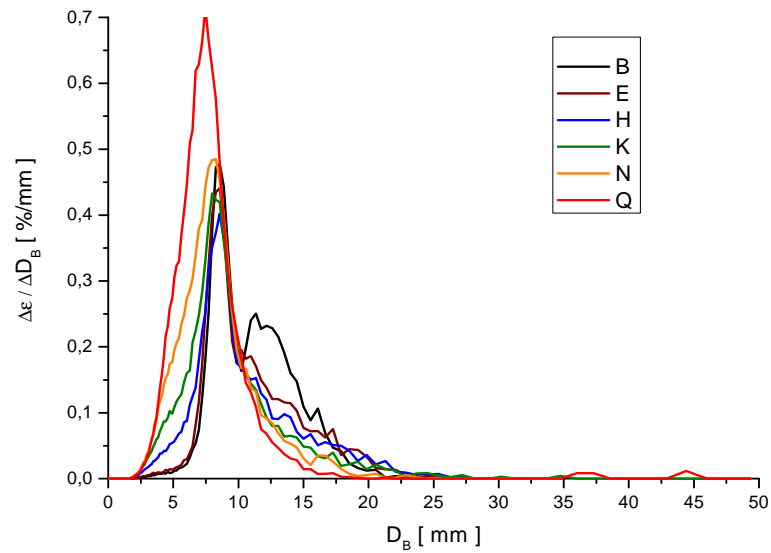
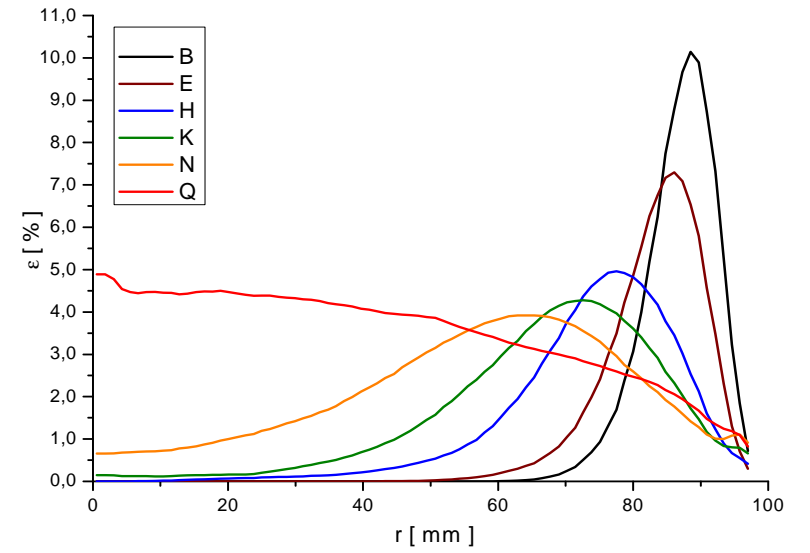
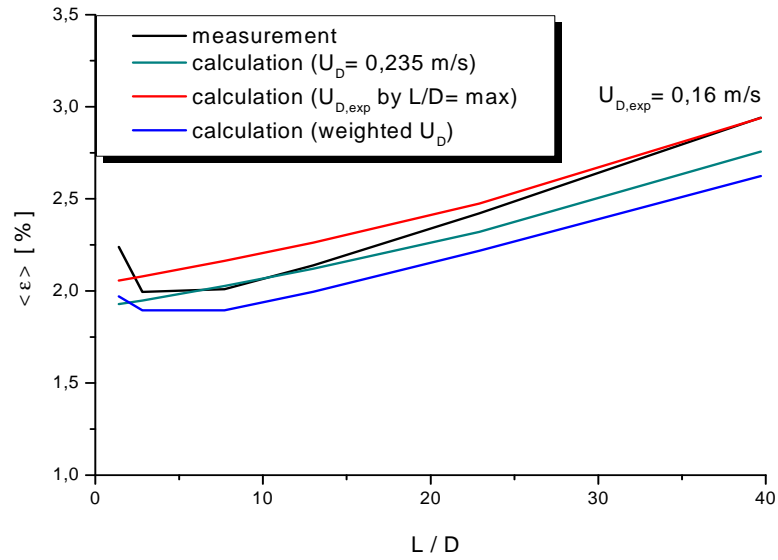
measurement point 061 ($J_L = 0.405$ m/s; $J_G = 0.0235$ m/s; $D_{\text{Orifice}} = 4$ mm)



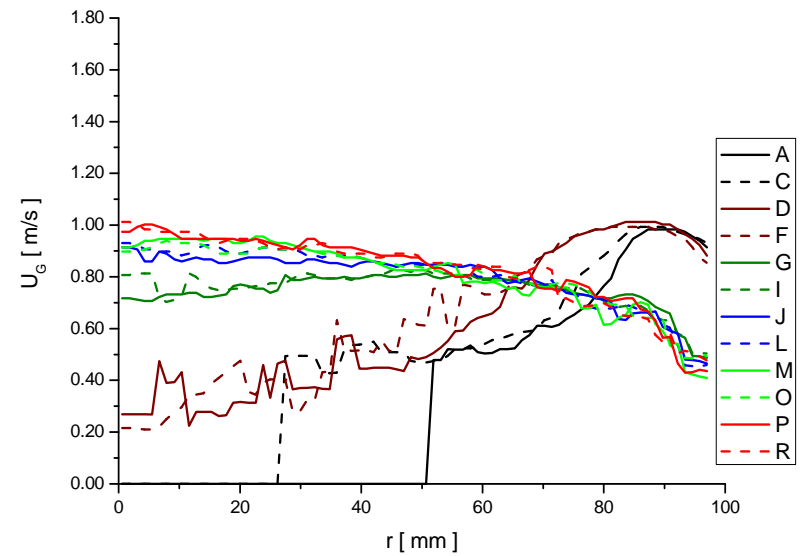
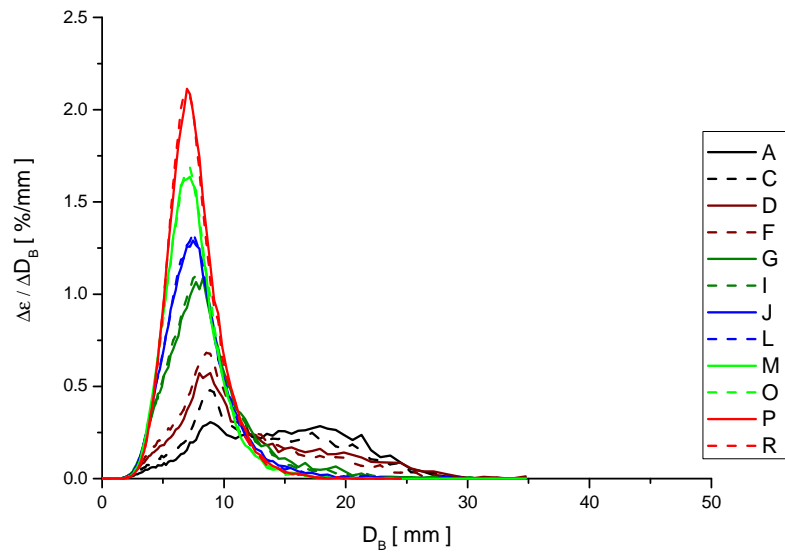
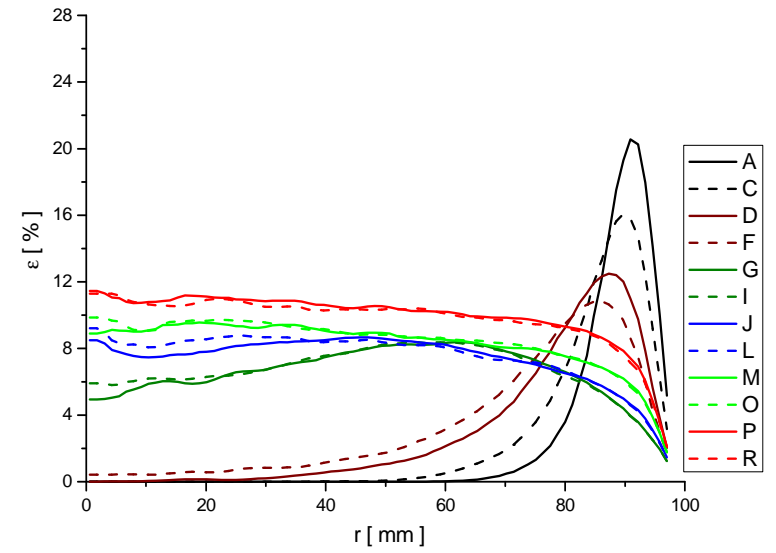
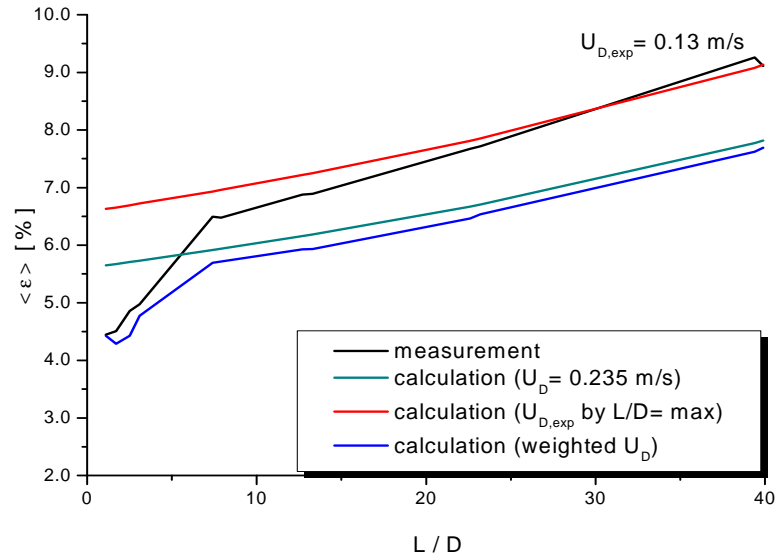
measurement point 063 ($J_L = 1.017$ m/s; $J_G = 0.0235$ m/s; $D_{\text{Orifice}} = 1$ mm)



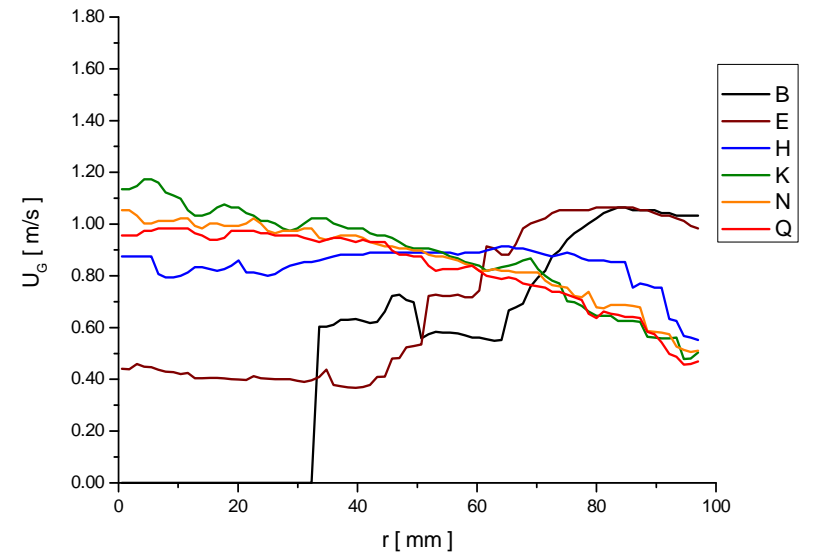
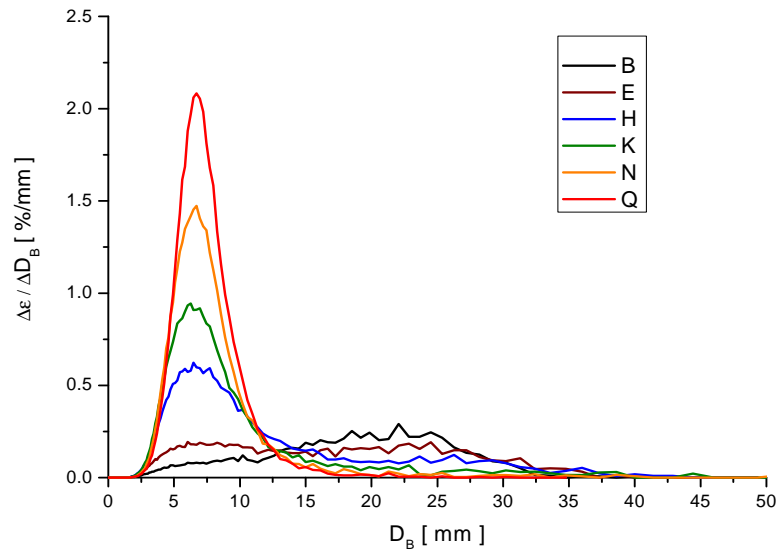
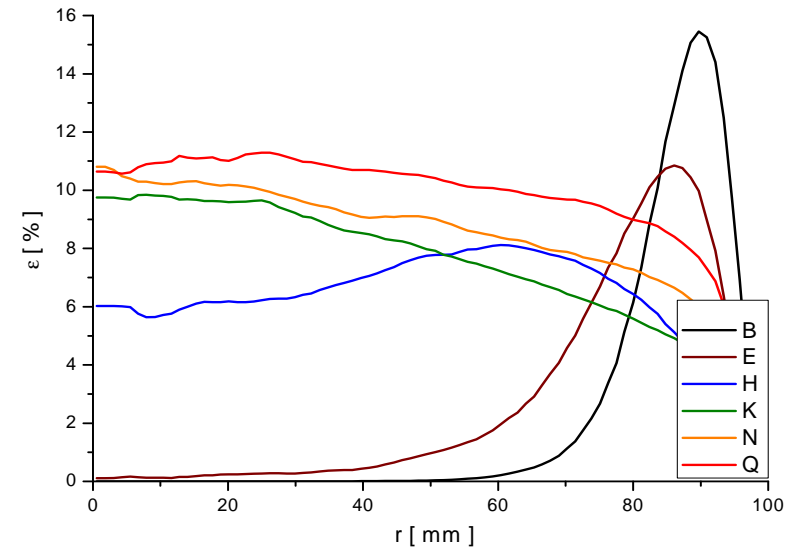
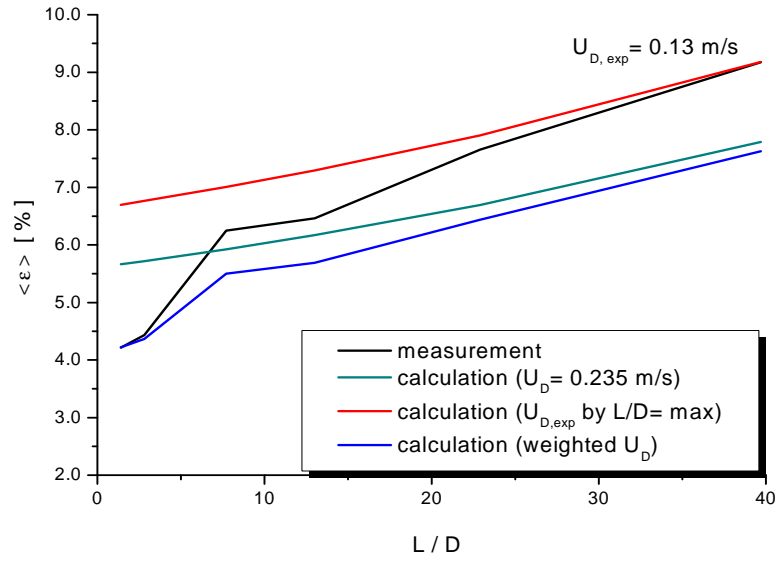
measurement point 063 ($J_L = 1.017$ m/s; $J_G = 0.0235$ m/s; $D_{\text{Orifice}} = 4$ mm)



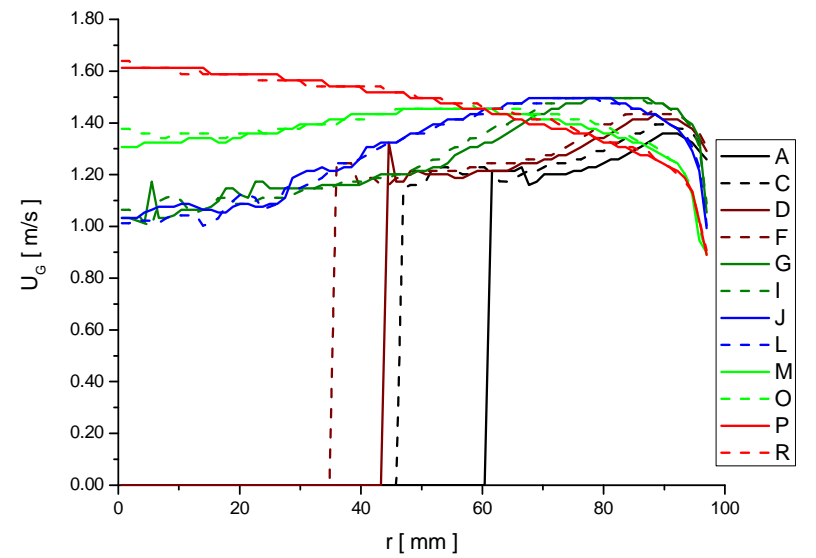
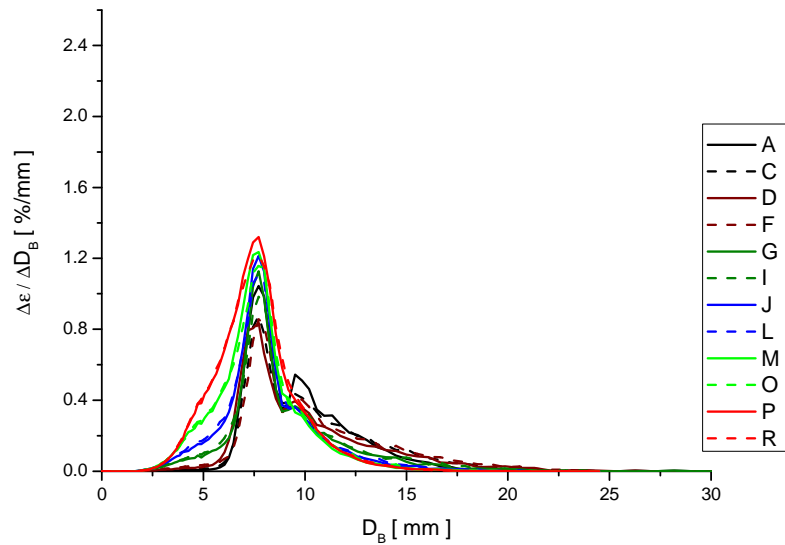
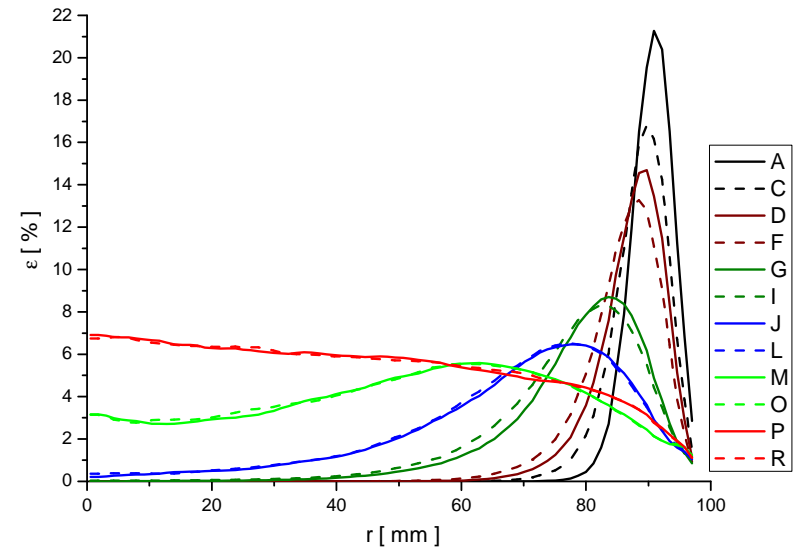
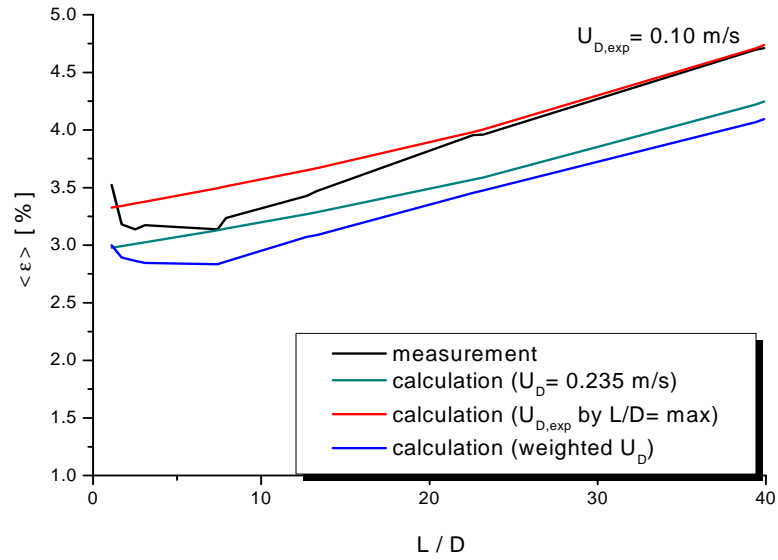
measurement point 072 ($J_L = 0.405$ m/s; $J_G = 0.0368$ m/s; $D_{\text{Orifice}} = 1$ mm)



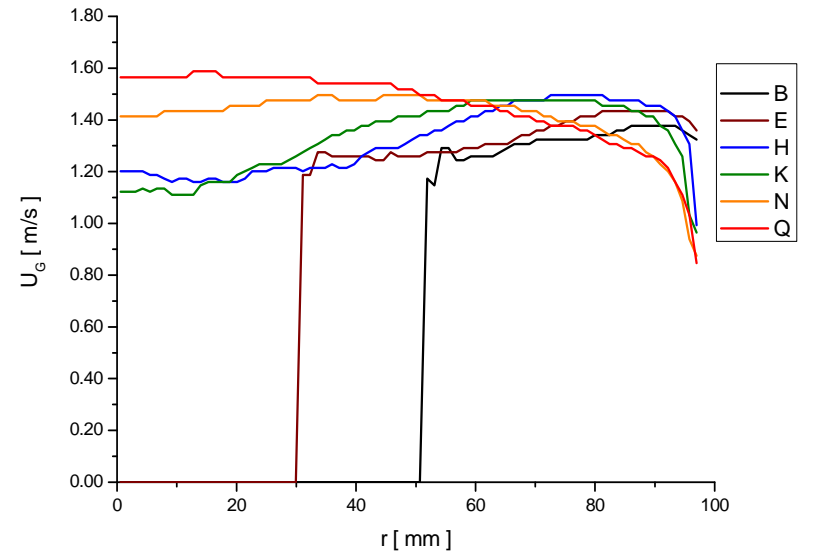
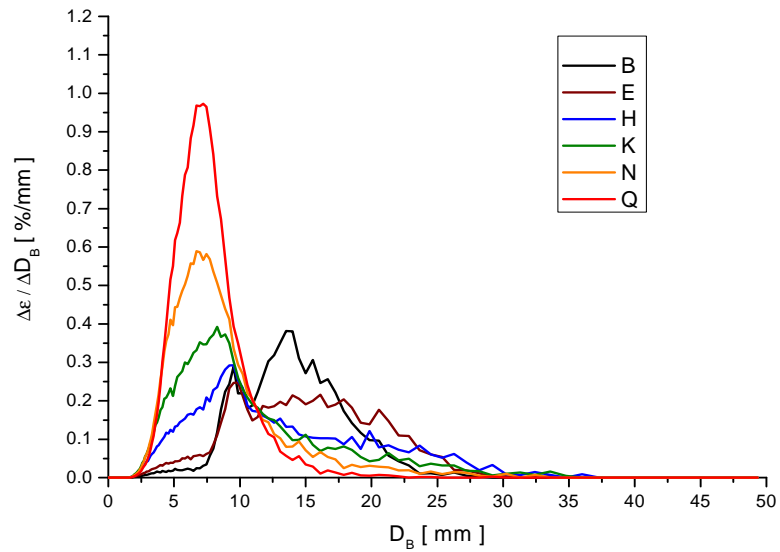
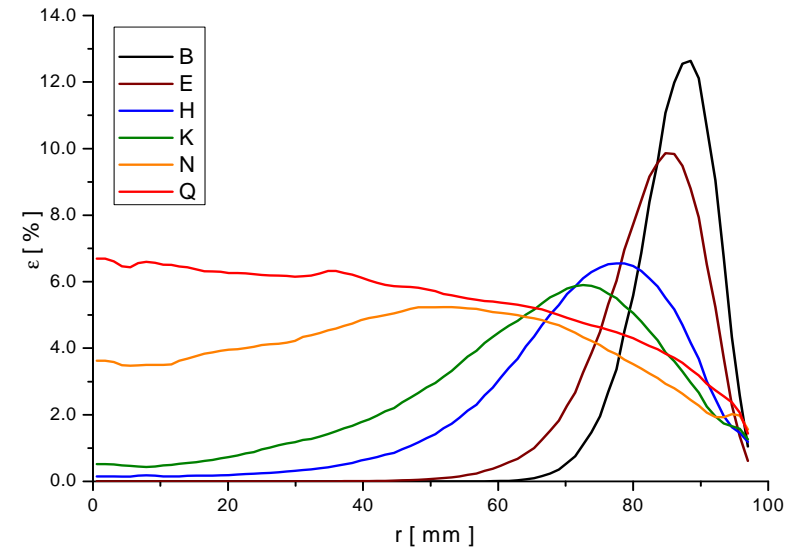
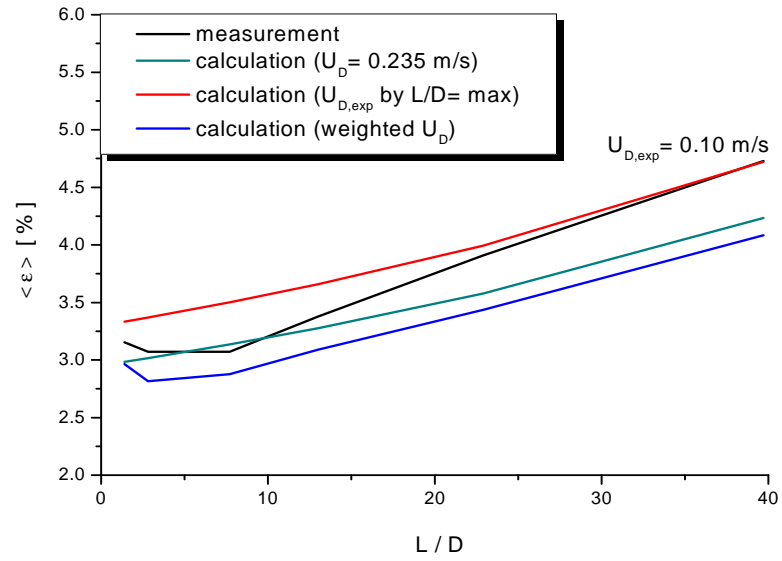
measurement point 072 ($J_L = 0.405$ m/s; $J_G = 0.0368$ m/s; $D_{\text{Orifice}} = 4$ mm)



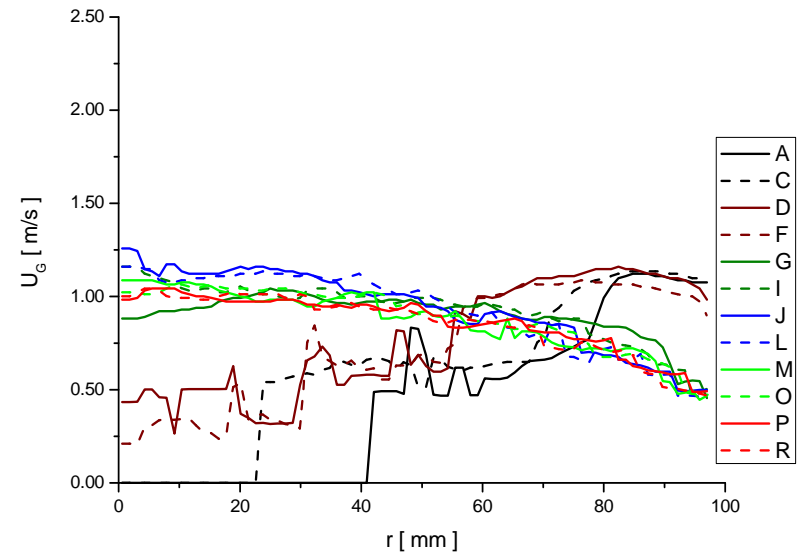
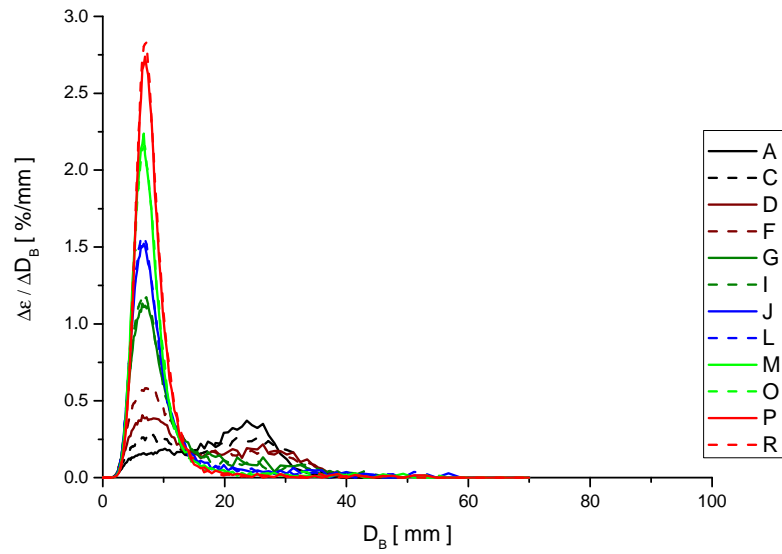
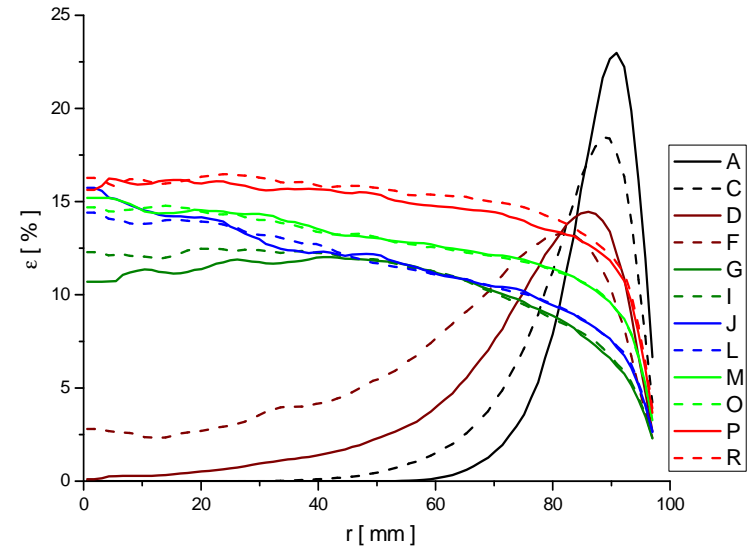
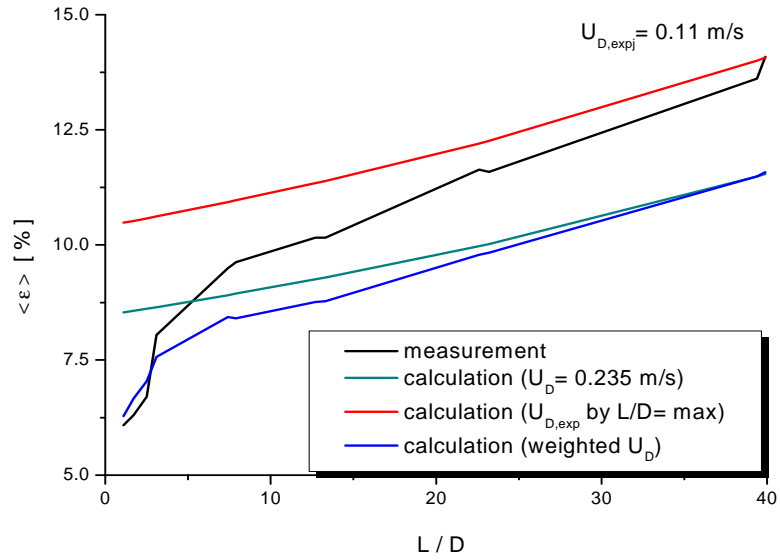
measurement point 074 ($J_L = 1.017$ m/s; $J_G = 0.0368$ m/s; $D_{\text{Orifice}} = 1$ mm)



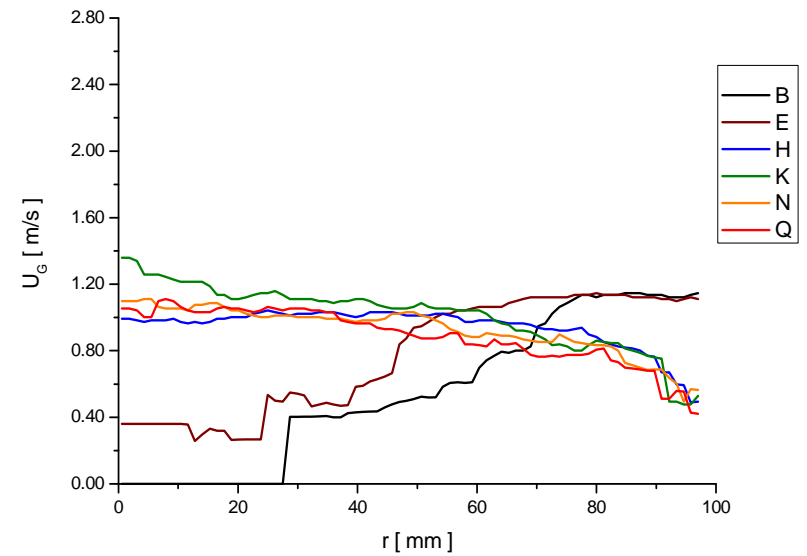
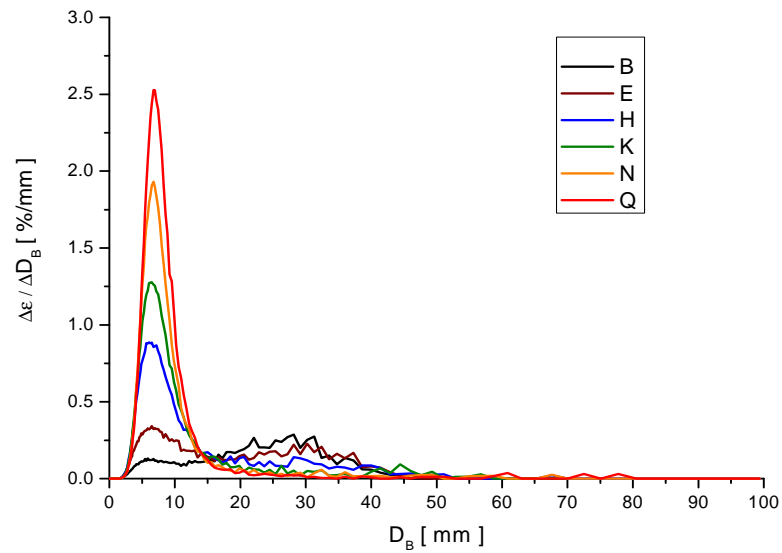
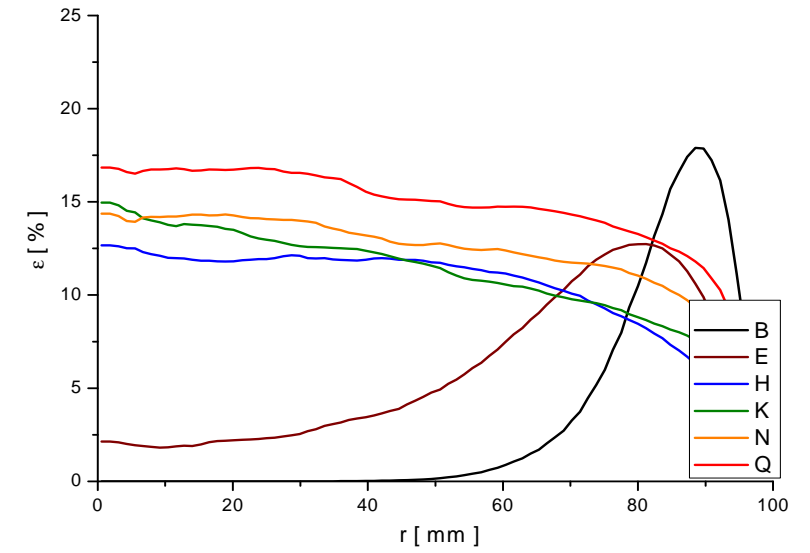
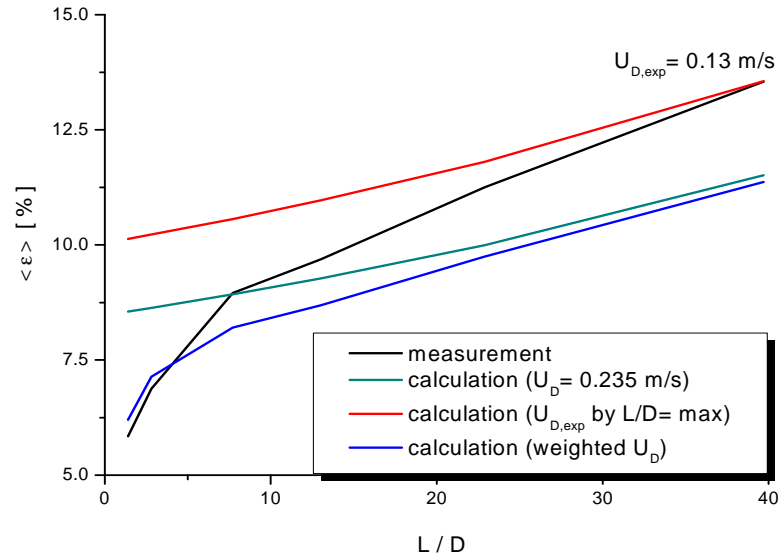
measurement point 074 ($J_L = 1.017$ m/s; $J_G = 0.0368$ m/s; $D_{\text{Orifice}} = 4$ mm)



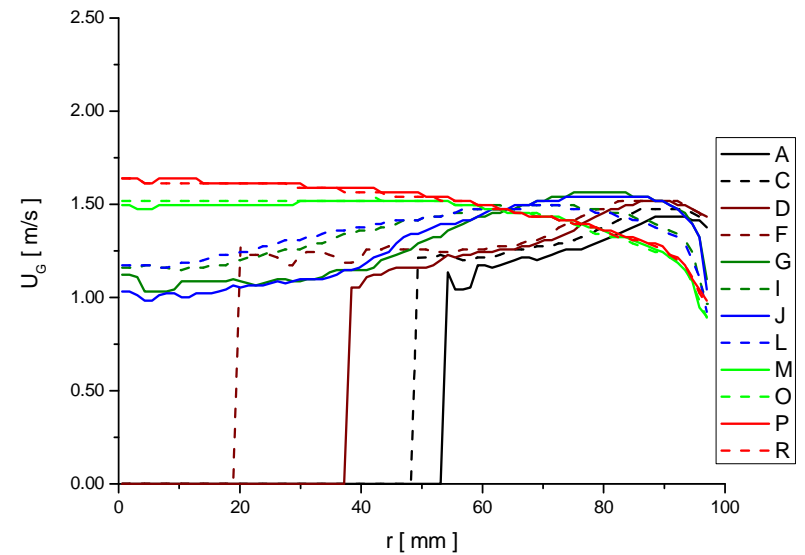
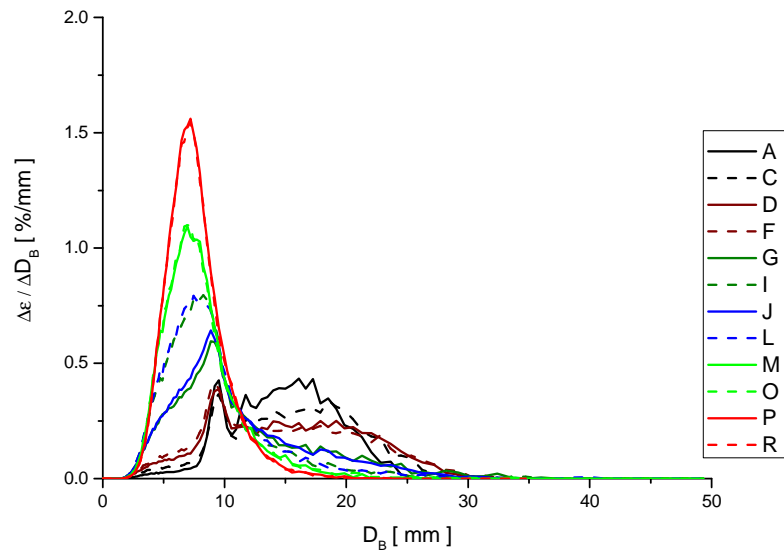
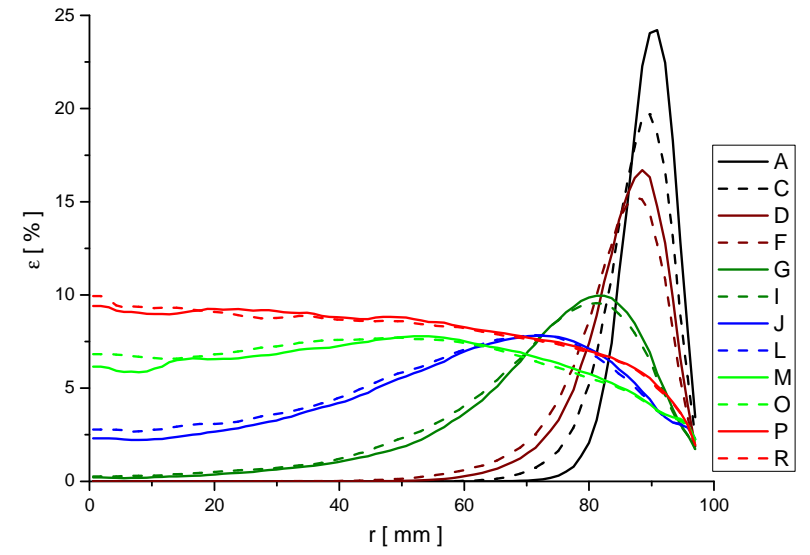
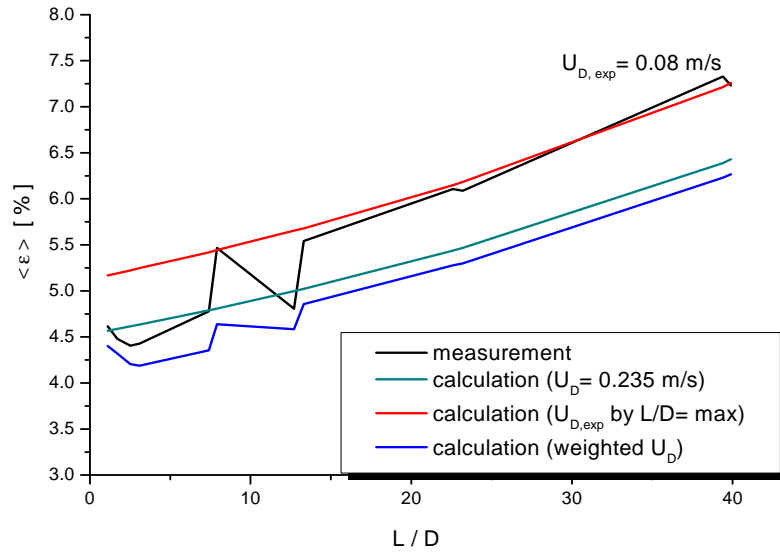
measurement point 083 ($J_L = 0.405$ m/s; $J_G = 0.0574$ m/s; $D_{\text{Orifice}} = 1$ mm)



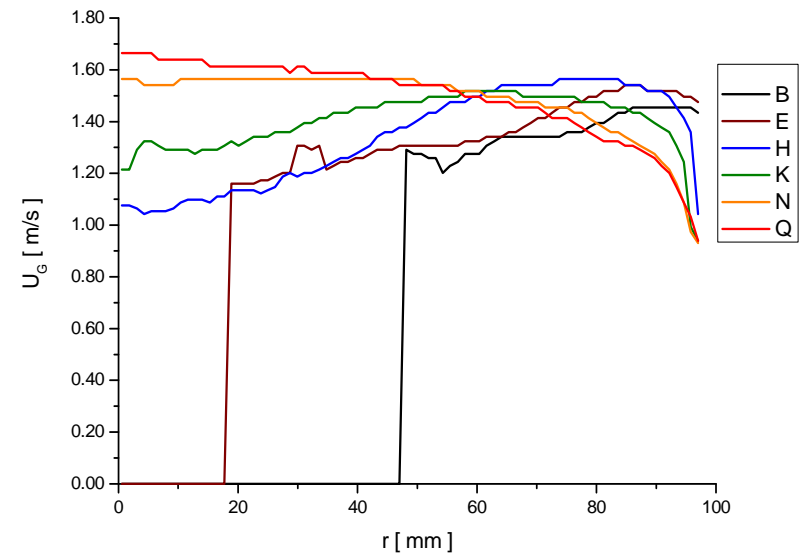
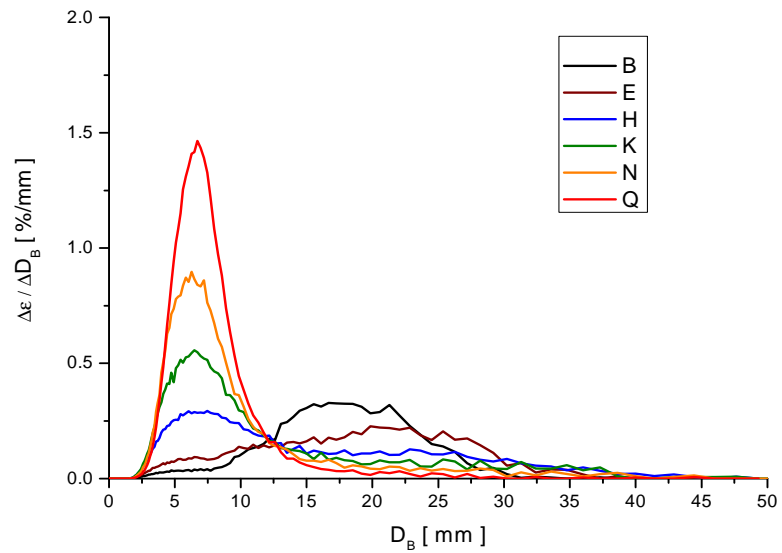
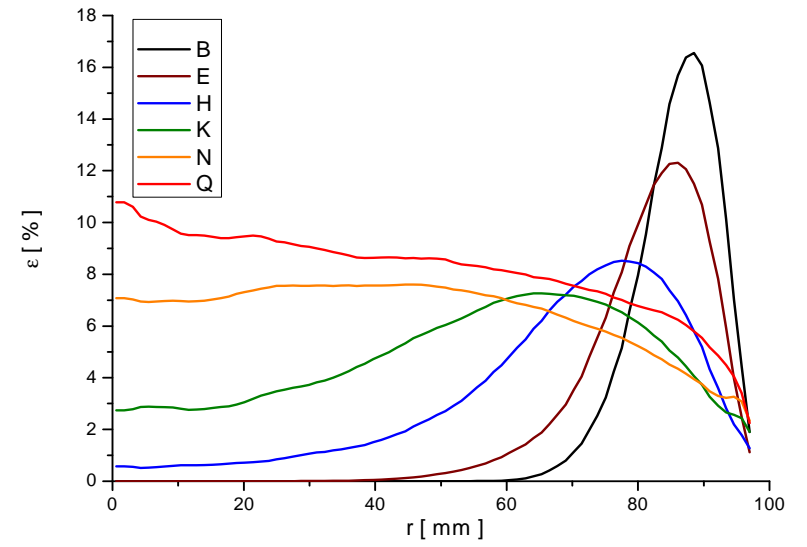
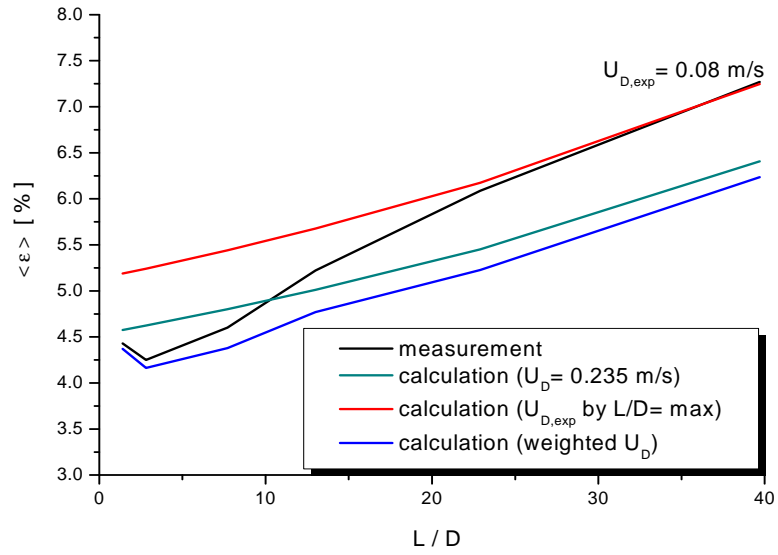
measurement point 083 ($J_L = 0.405$ m/s; $J_G = 0.0574$ m/s; $D_{\text{Orifice}} = 4$ mm)



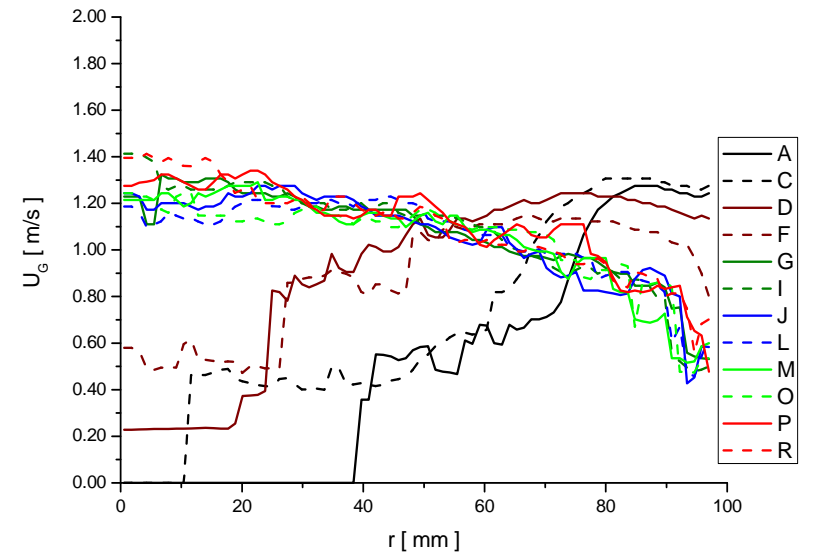
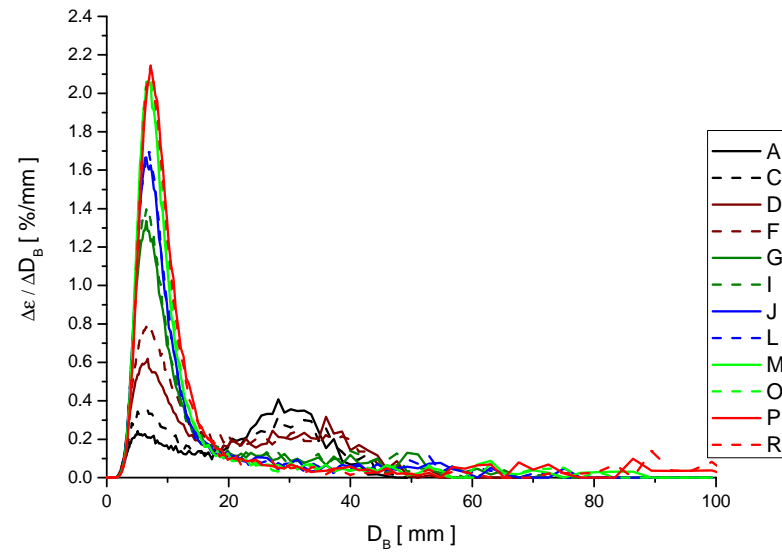
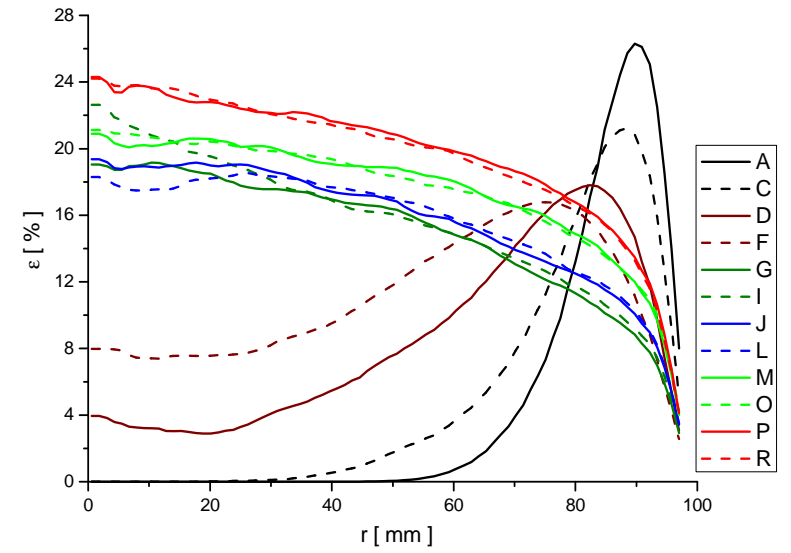
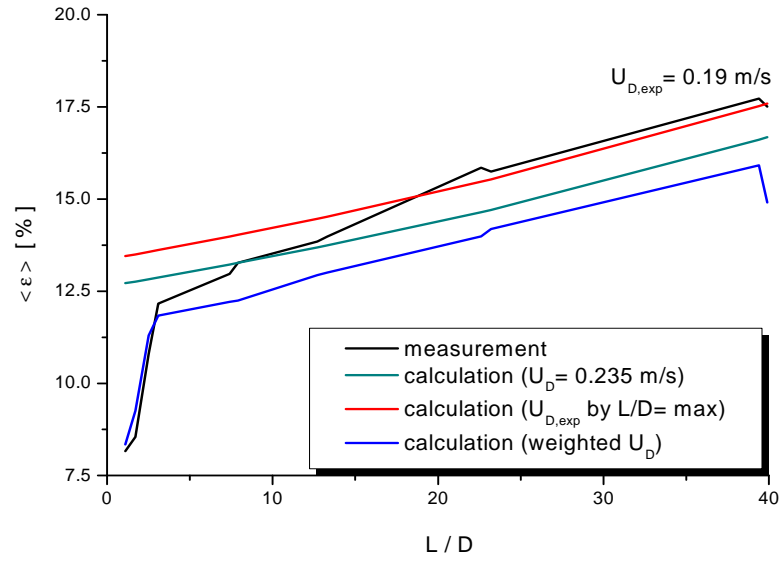
measurement point 085 ($J_L = 1.017$ m/s; $J_G = 0.0574$ m/s; $D_{\text{Orifice}} = 1$ mm)



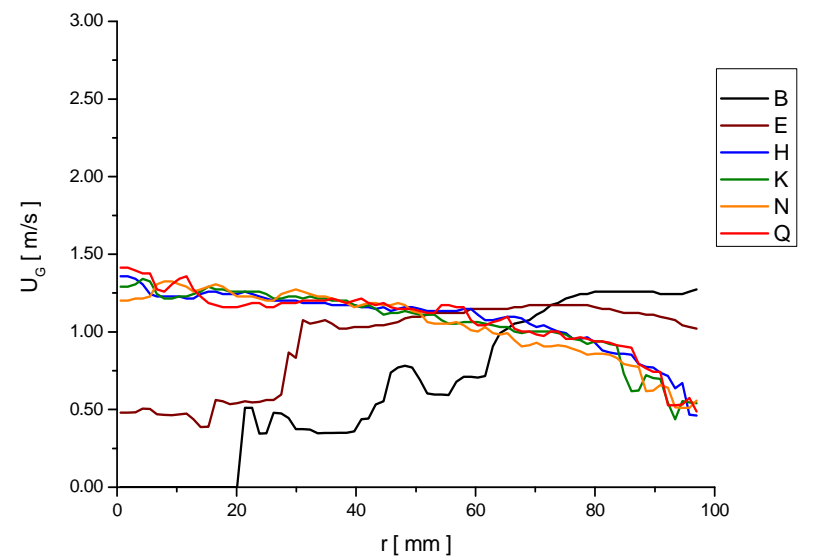
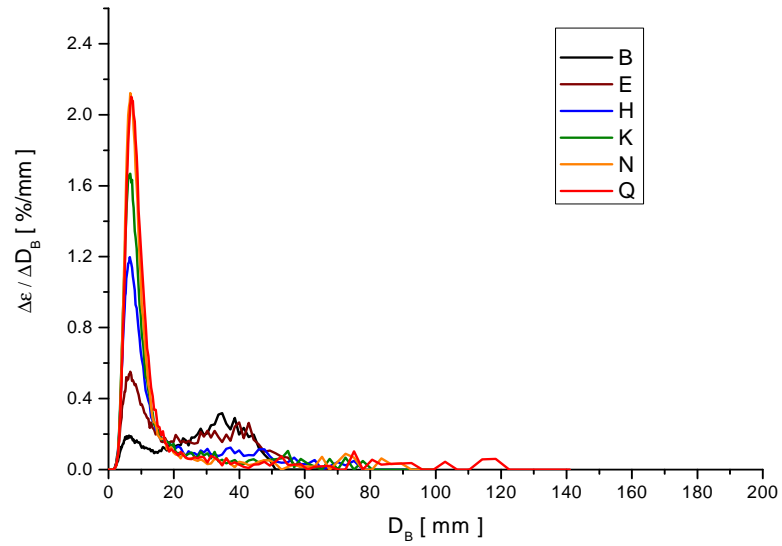
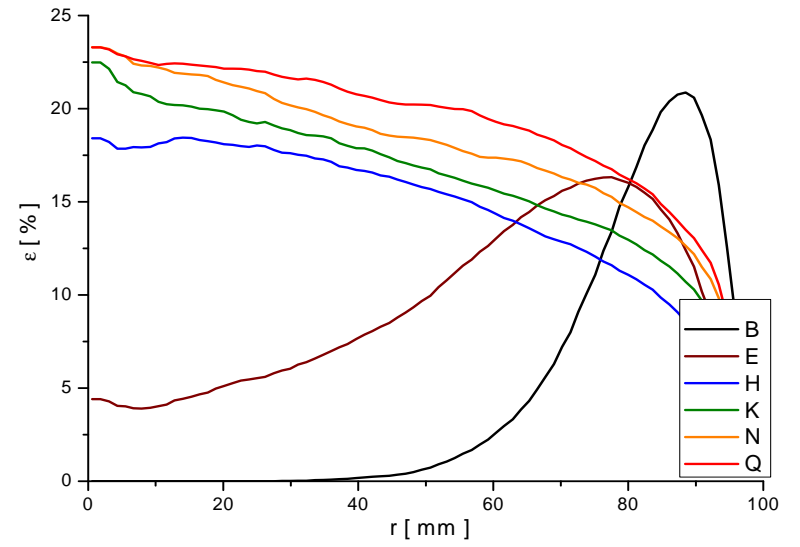
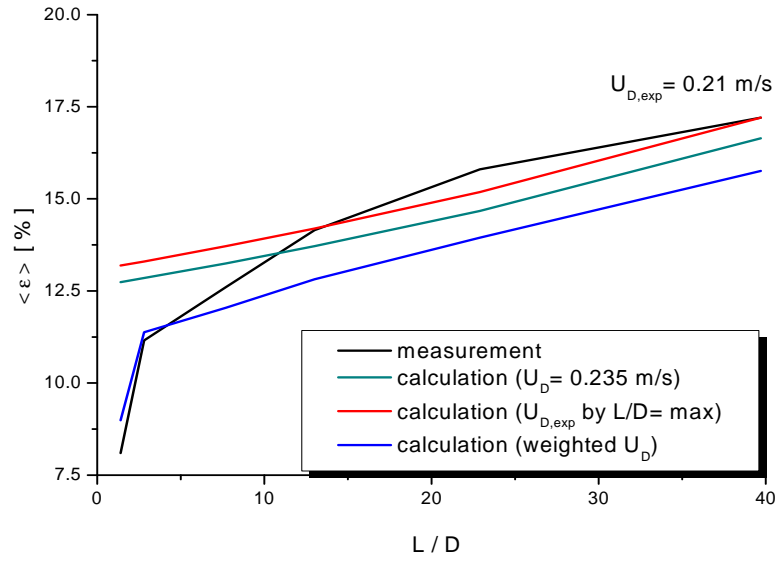
measurement point 085 ($J_L = 1.017$ m/s; $J_G = 0.0574$ m/s; $D_{\text{Orifice}} = 4$ mm)



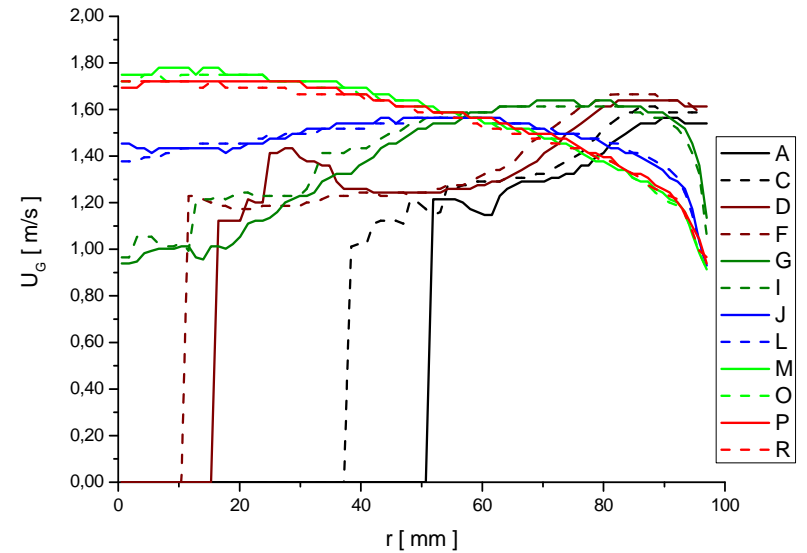
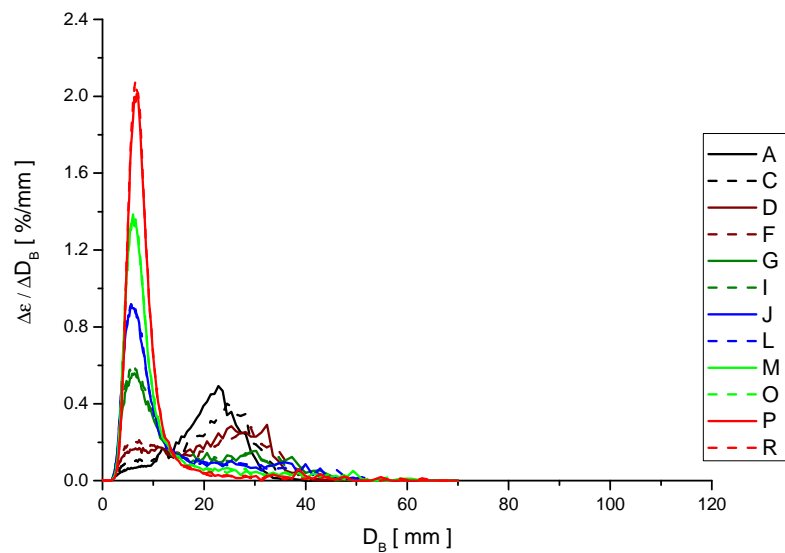
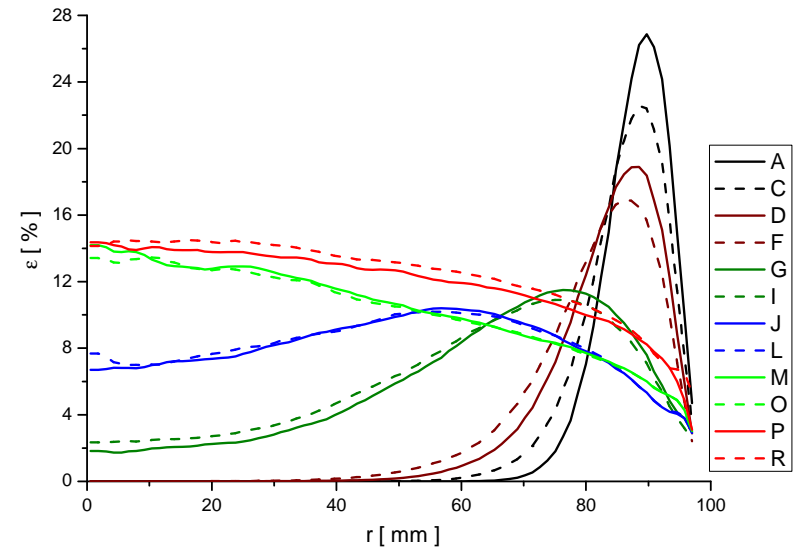
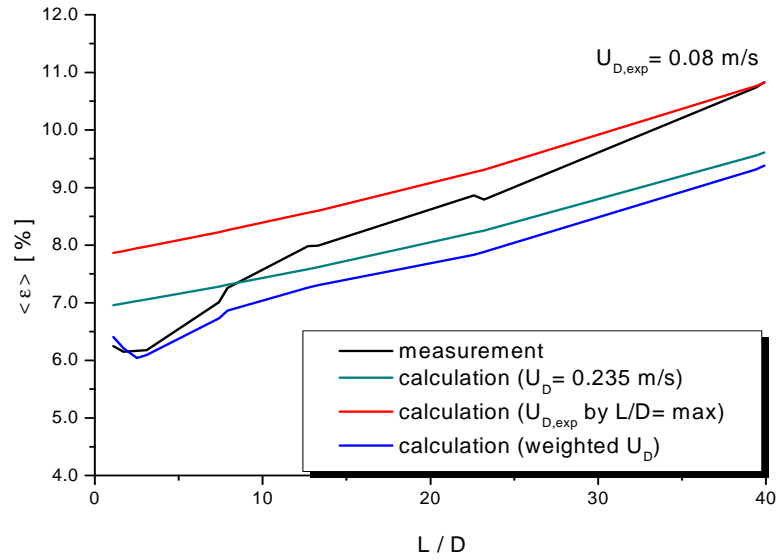
measurement point 094 ($J_L = 0.405$ m/s; $J_G = 0.0898$ m/s; $D_{\text{Orifice}} = 1$ mm)



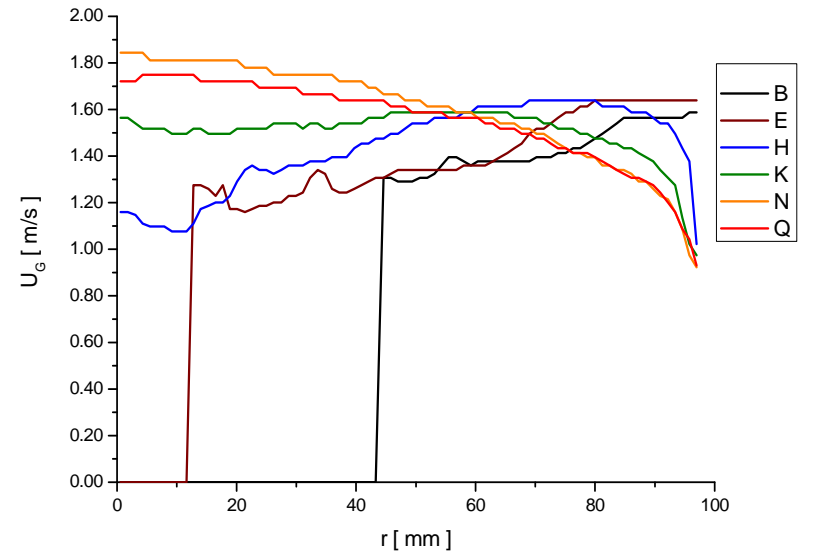
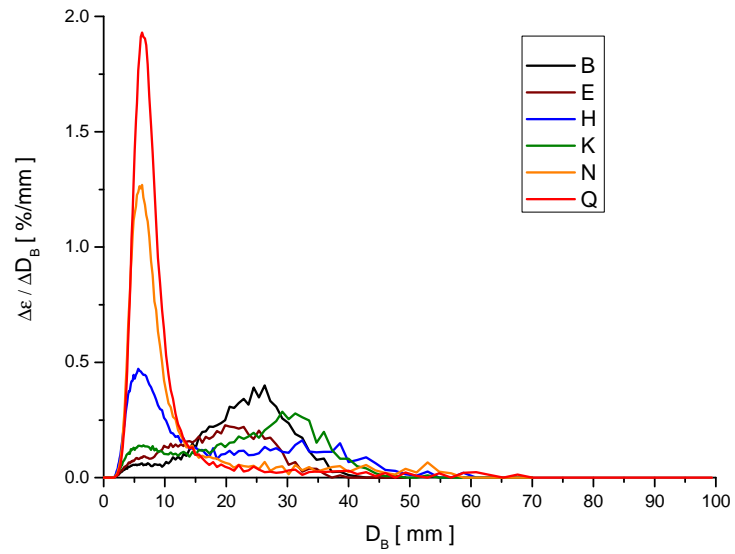
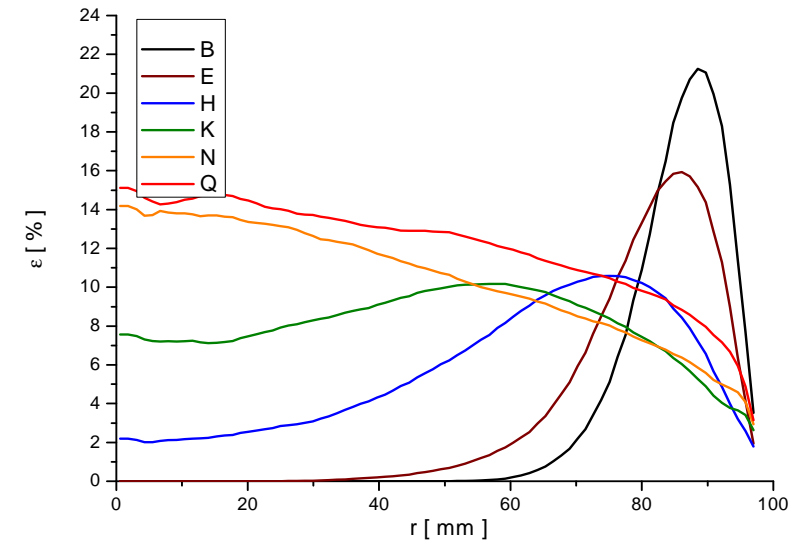
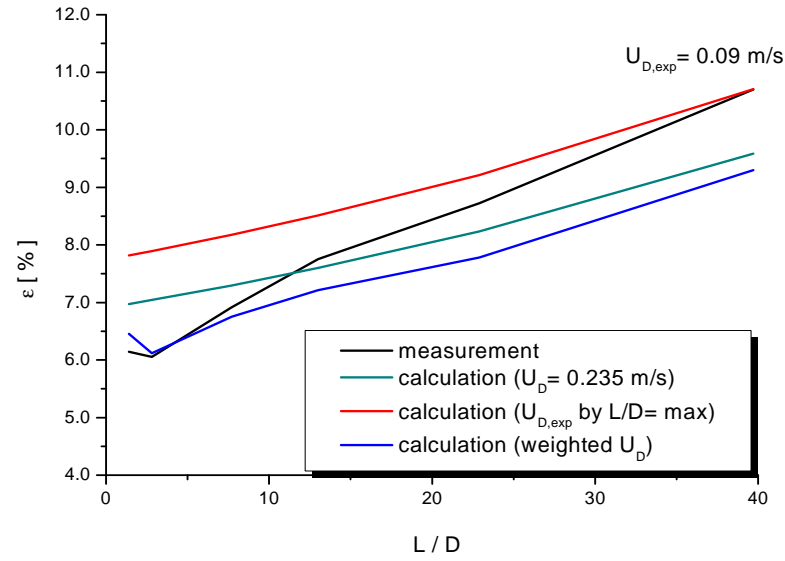
measurement point 094 ($J_L = 0.405$ m/s; $J_G = 0.0898$ m/s; $D_{\text{Orifice}} = 4$ mm)



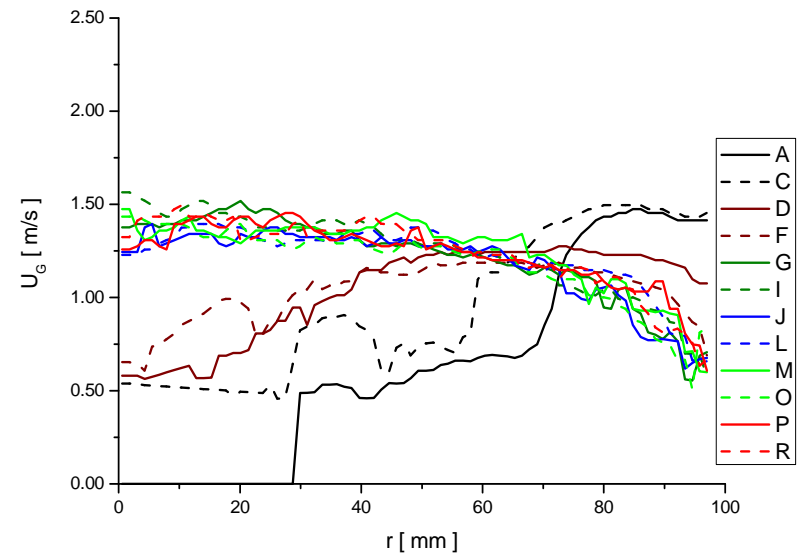
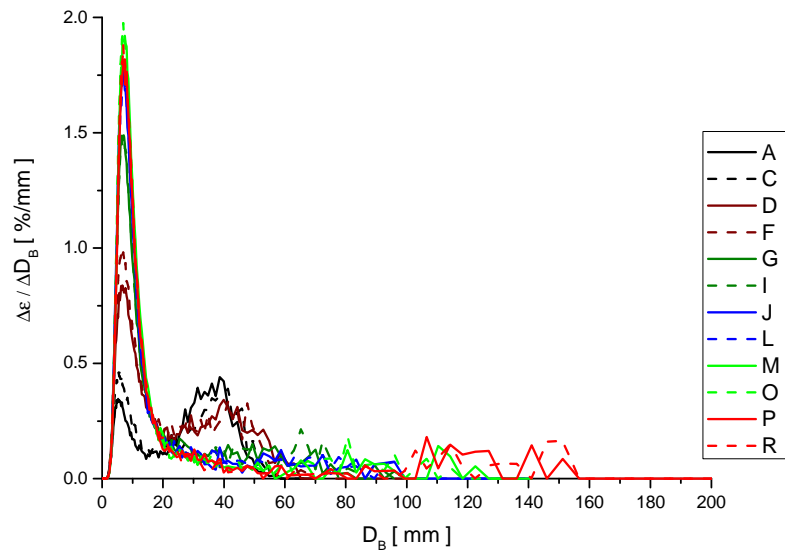
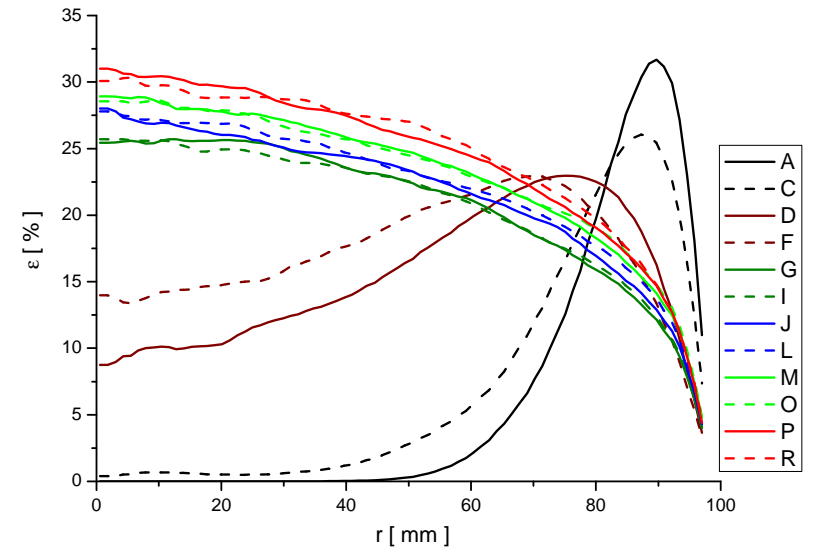
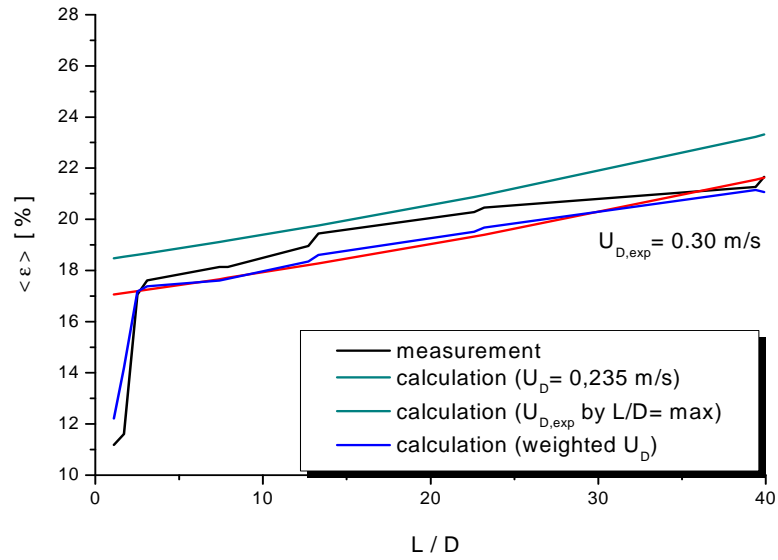
measurement point 096 ($J_L = 1.017$ m/s; $J_G = 0.0898$ m/s; $D_{\text{Orifice}} = 1$ mm)



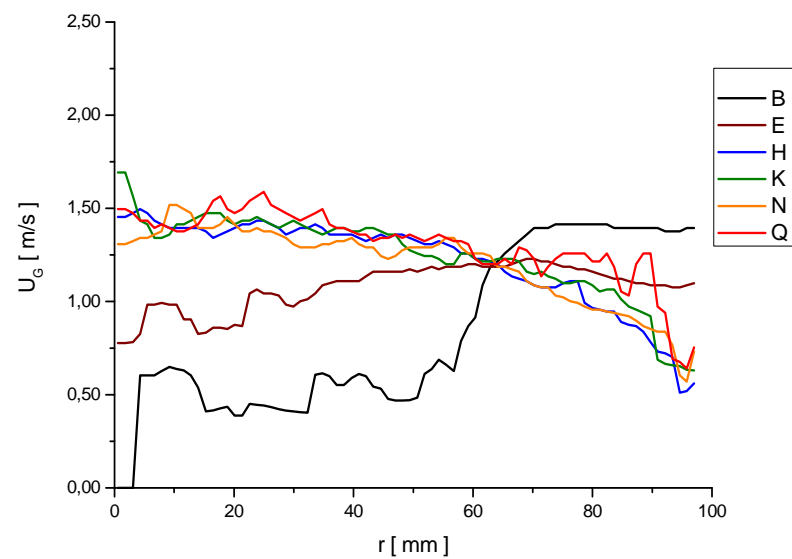
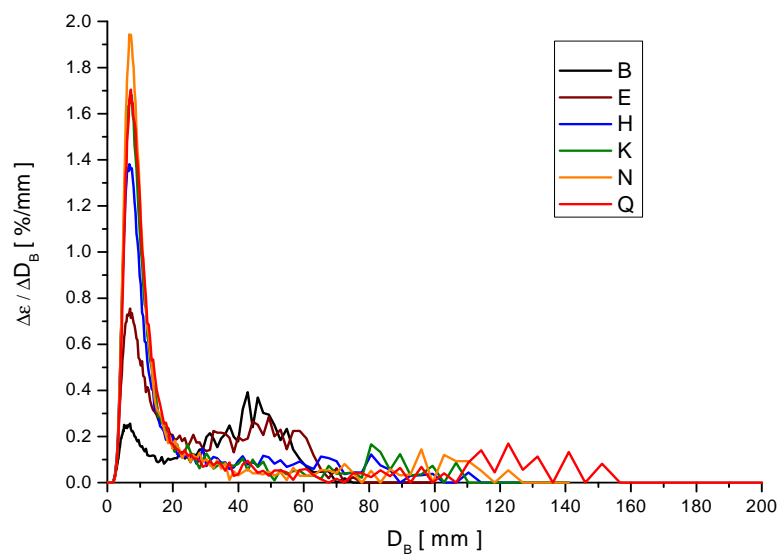
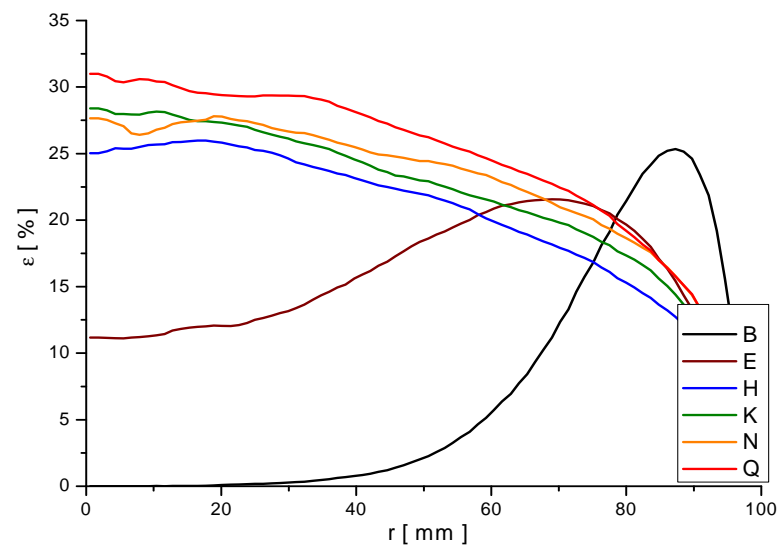
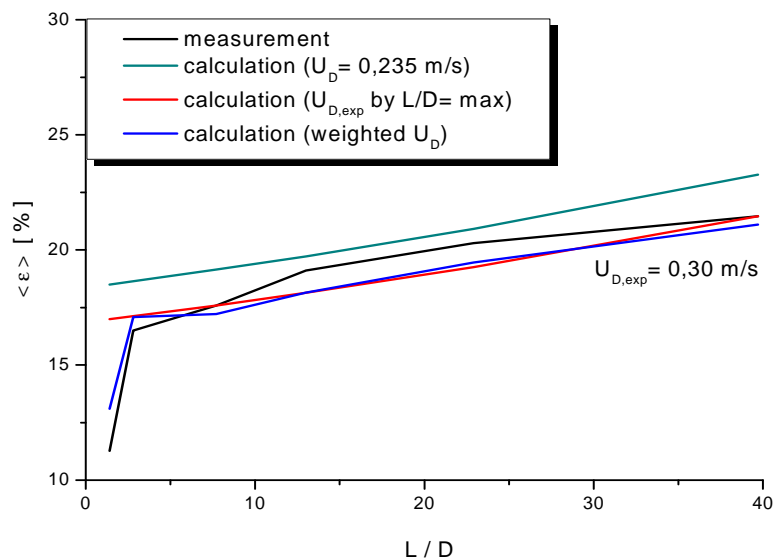
measurement point 096 ($J_L = 1.017$ m/s; $J_G = 0.0898$ m/s; $D_{\text{Orifice}} = 4$ mm)



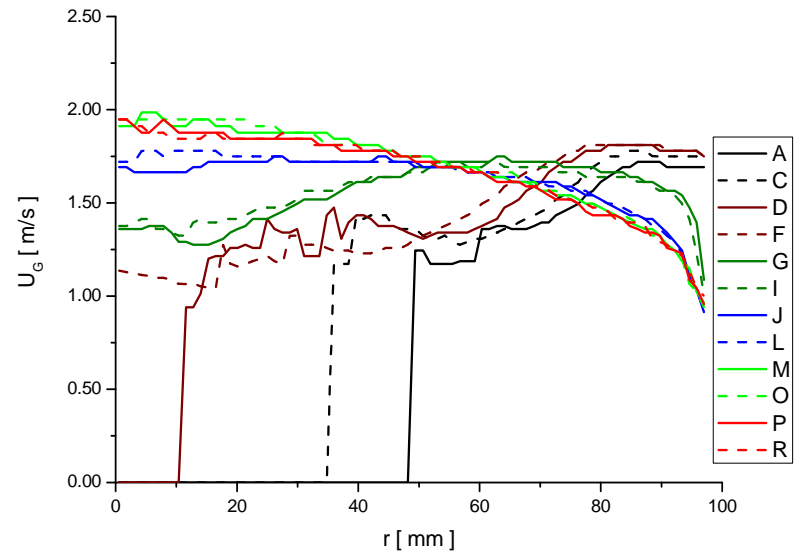
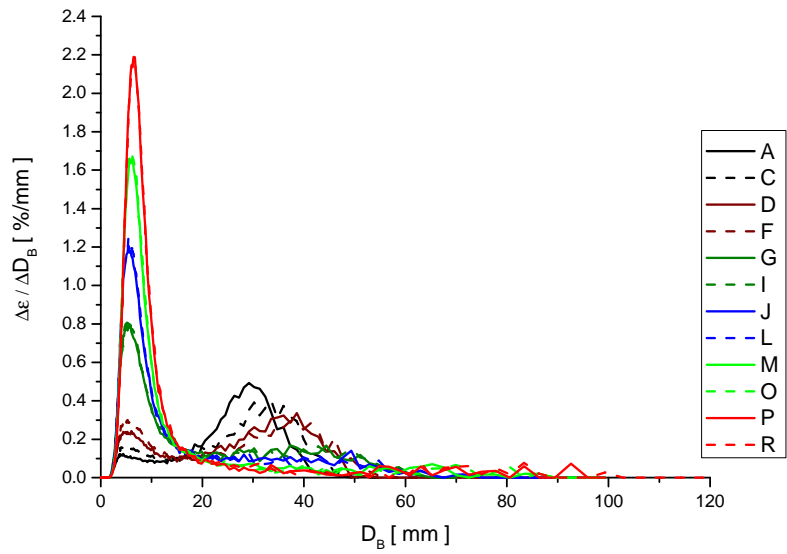
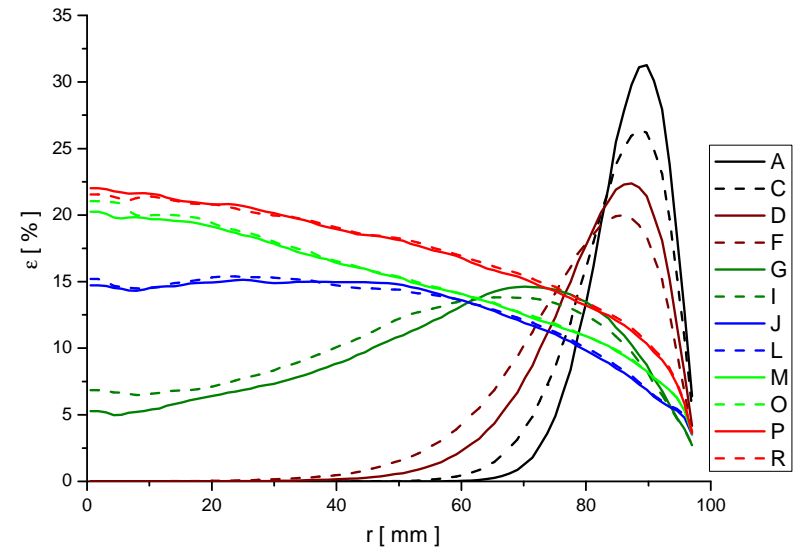
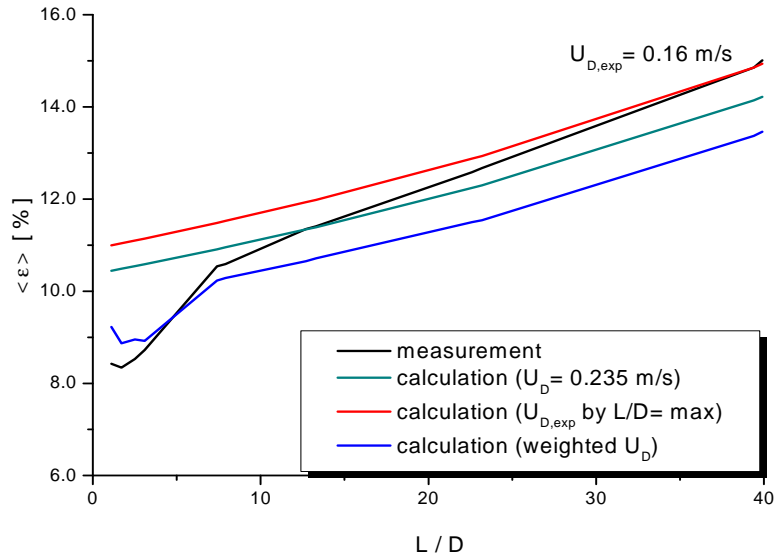
measurement point 105 ($J_L = 0.405$ m/s; $J_G = 0.140$ m/s; $D_{\text{Orifice}} = 1$ mm)



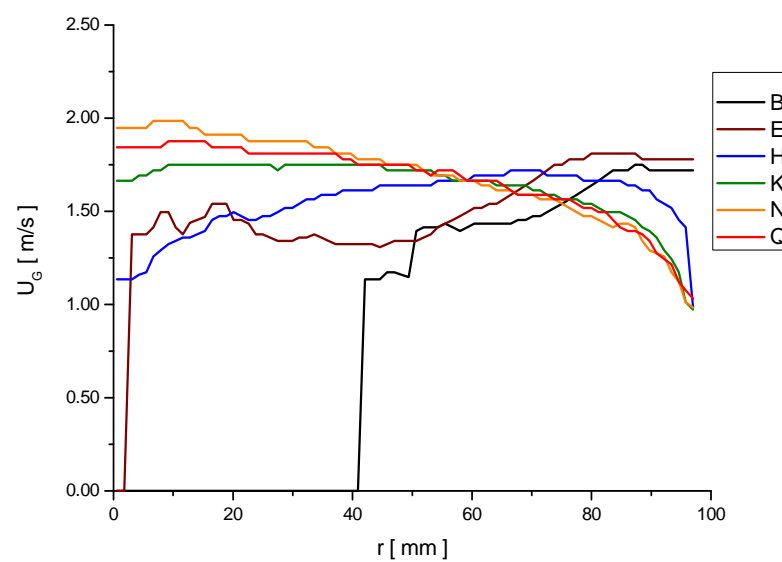
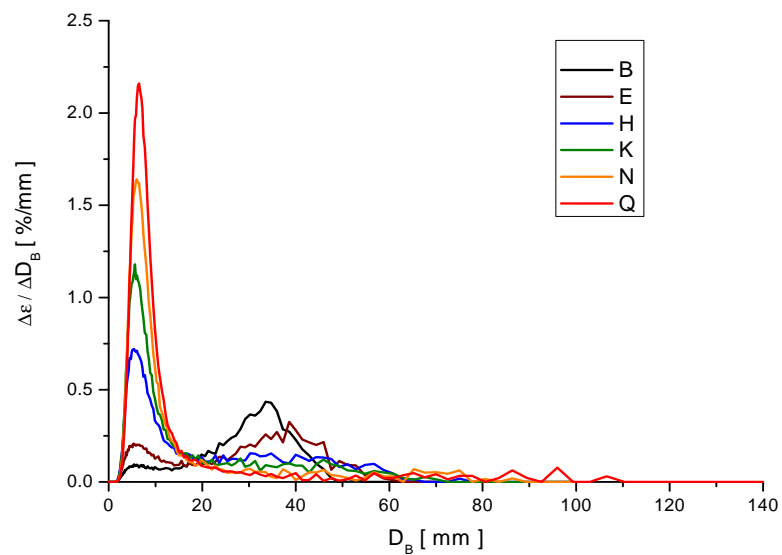
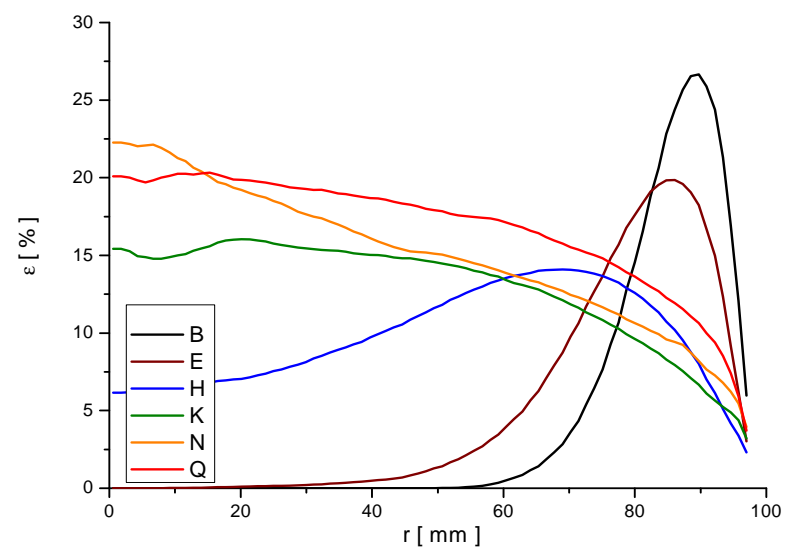
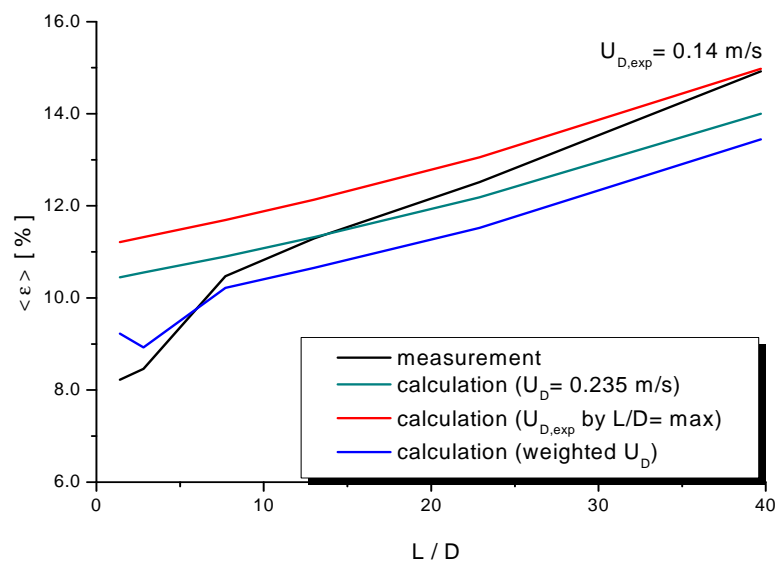
measurement point 105 ($J_L = 0.405$ m/s; $J_G = 0.140$ m/s; $D_{\text{Orifice}} = 4$ mm)



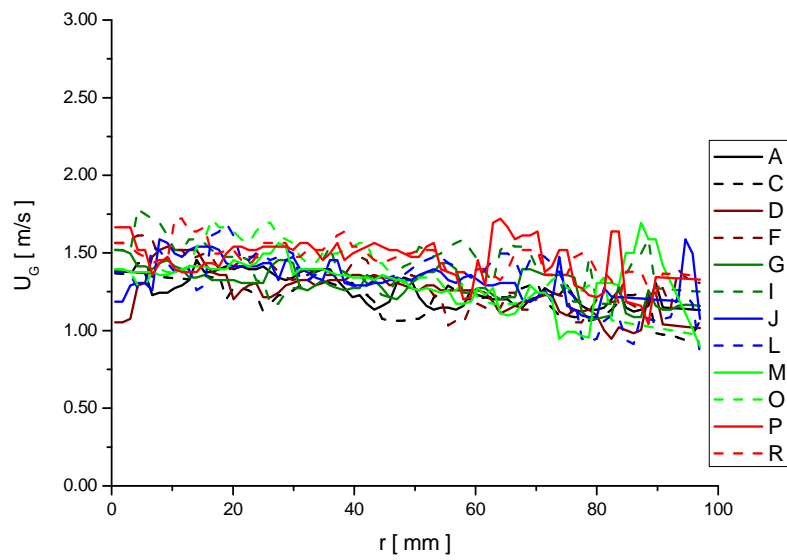
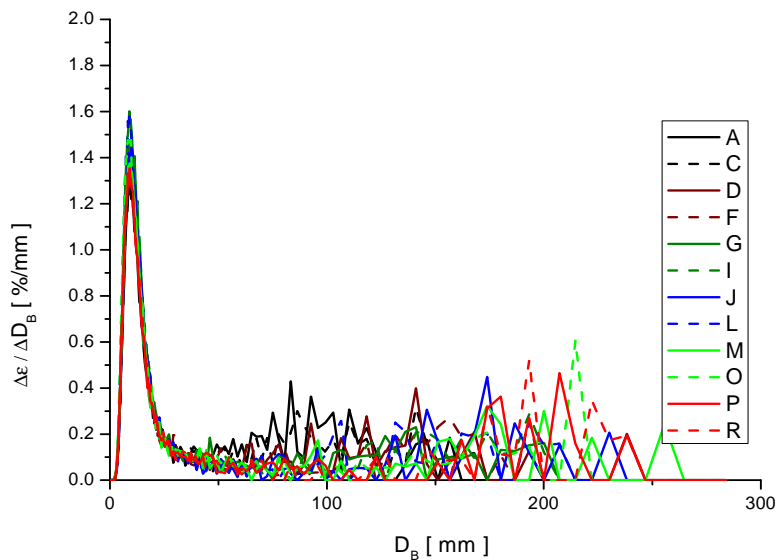
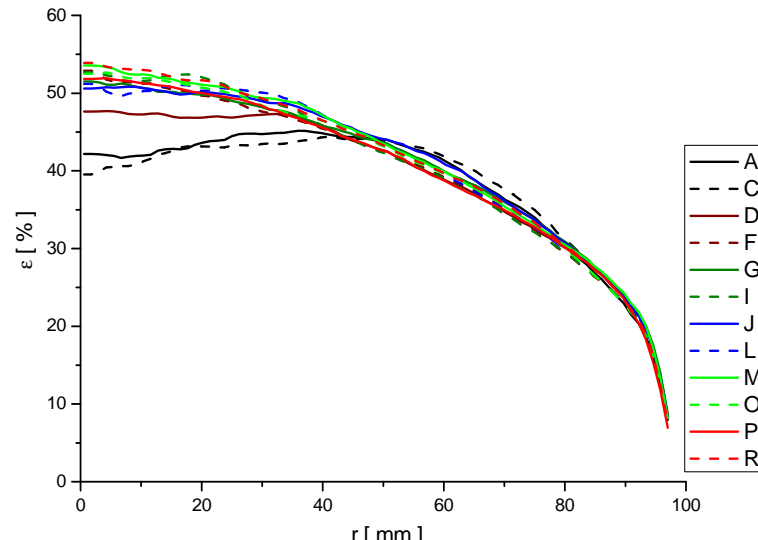
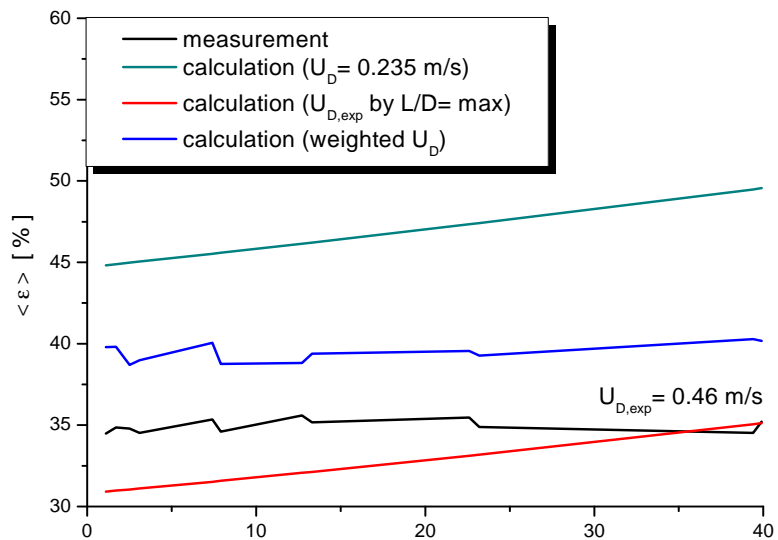
measurement point 107 ($J_L = 1.017$ m/s; $J_G = 0.140$ m/s; $D_{\text{Orifice}} = 1$ mm)



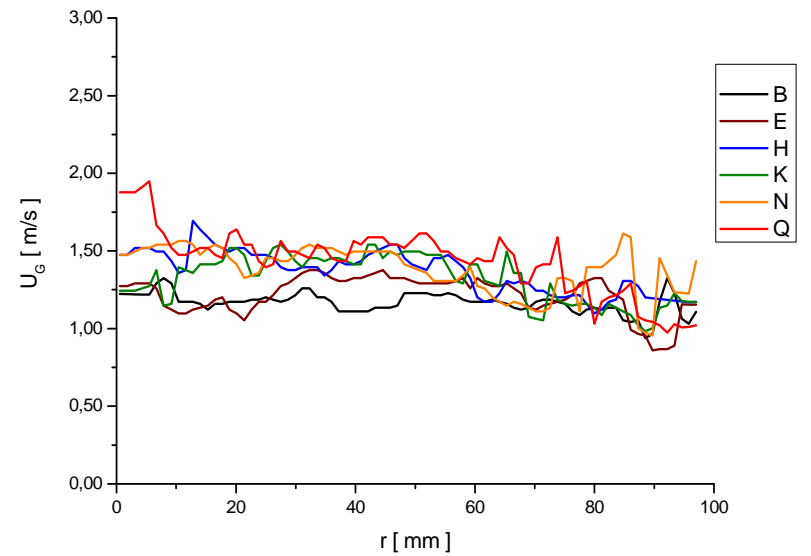
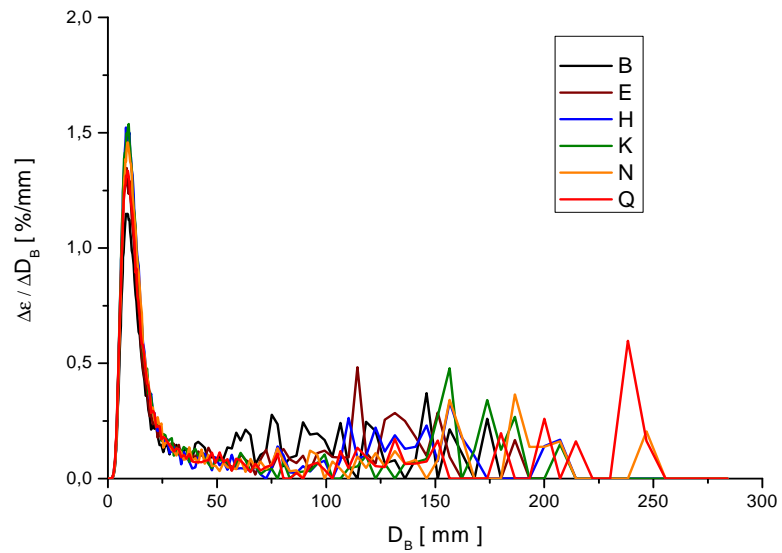
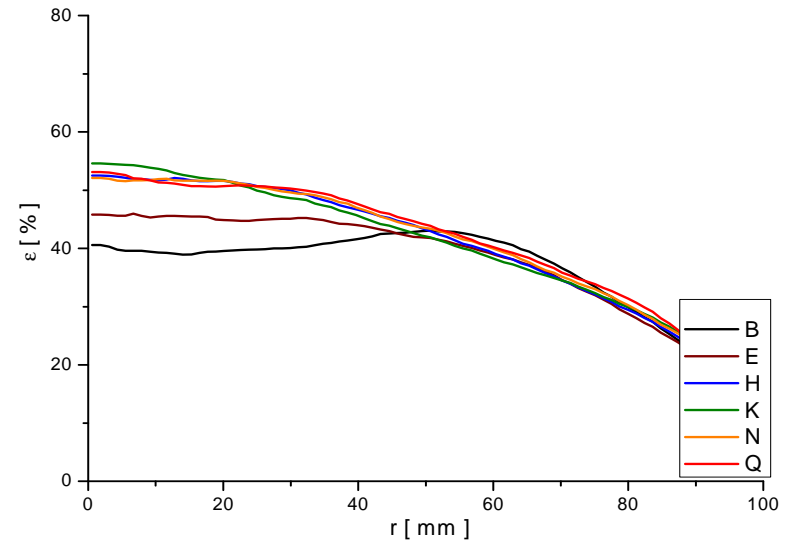
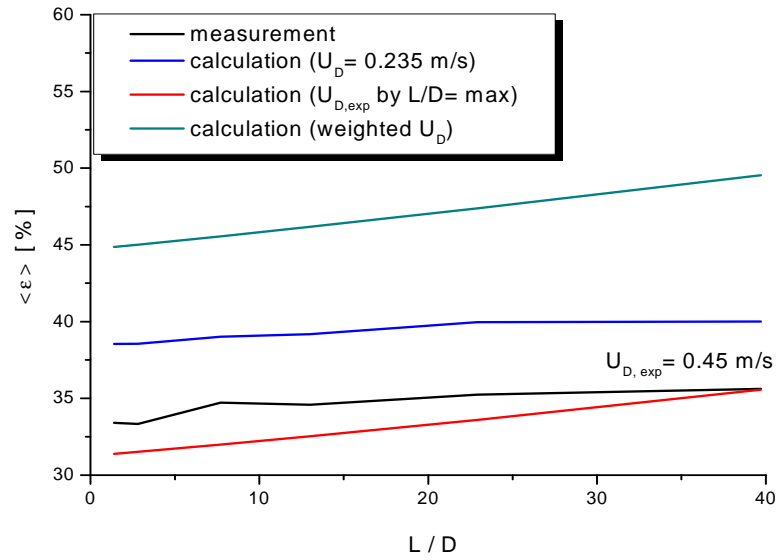
measurement point 107 ($J_L = 1.017$ m/s; $J_G = 0.140$ m/s; $D_{\text{Orifice}} = 4$ mm)



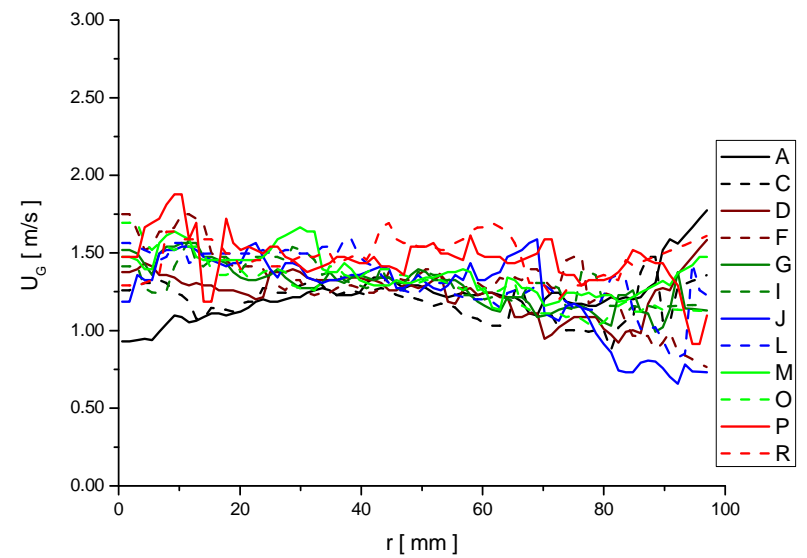
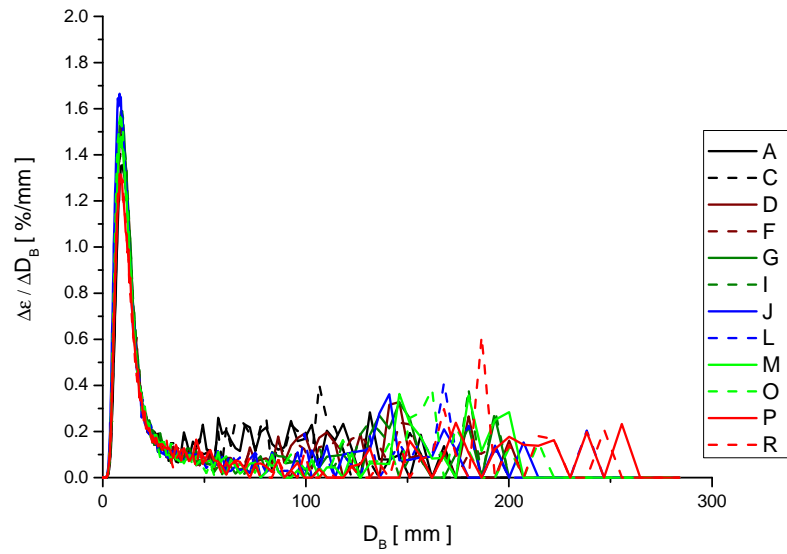
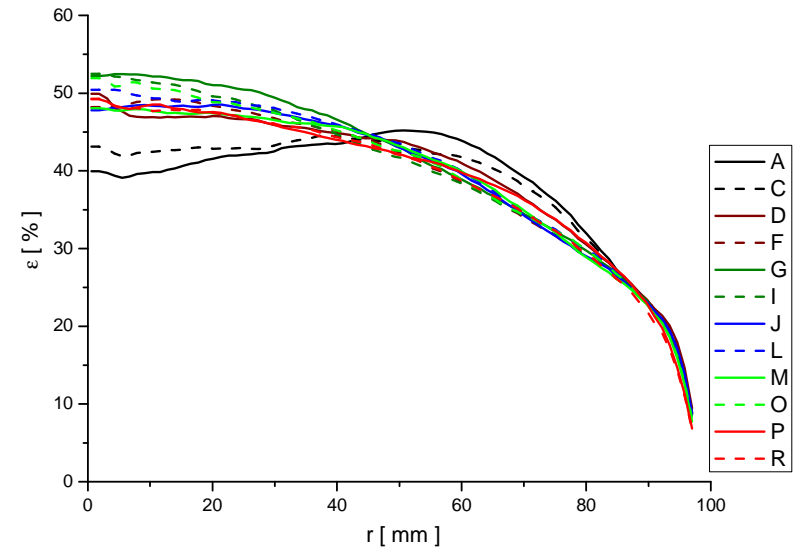
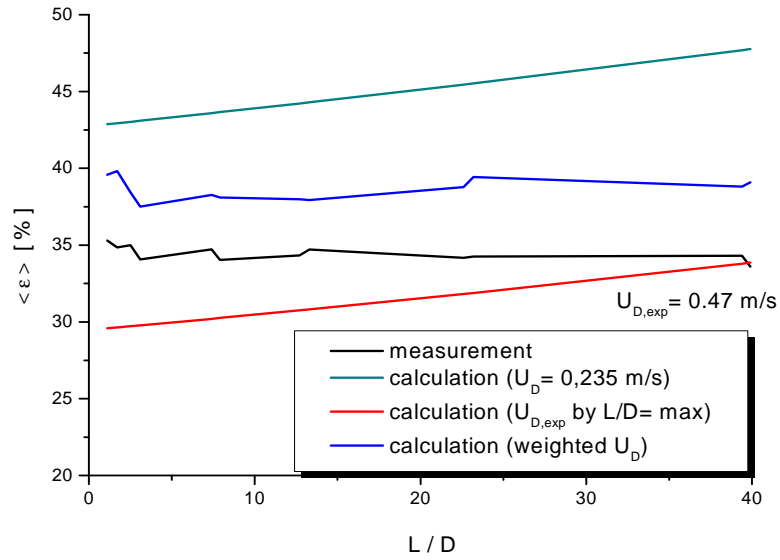
measurement point 111 ($J_L = 0.0405$ m/s; $J_G = 0.219$ m/s; $D_{\text{Orifice}} = 1$ mm)



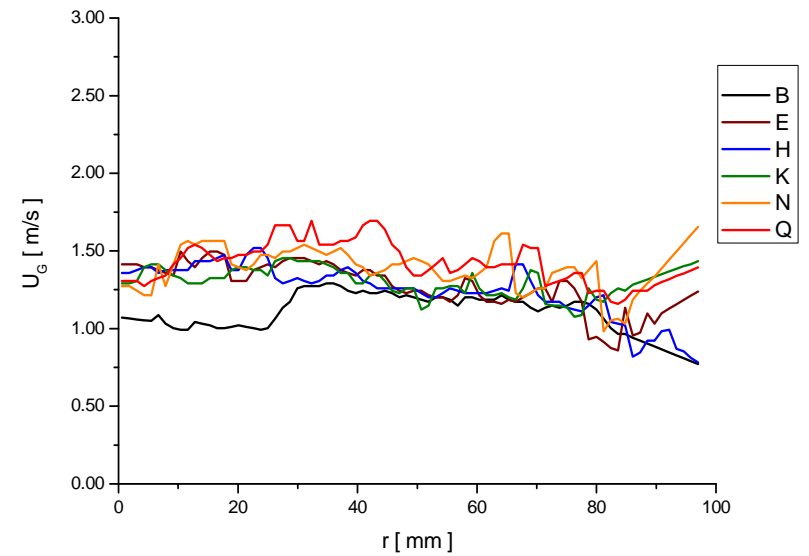
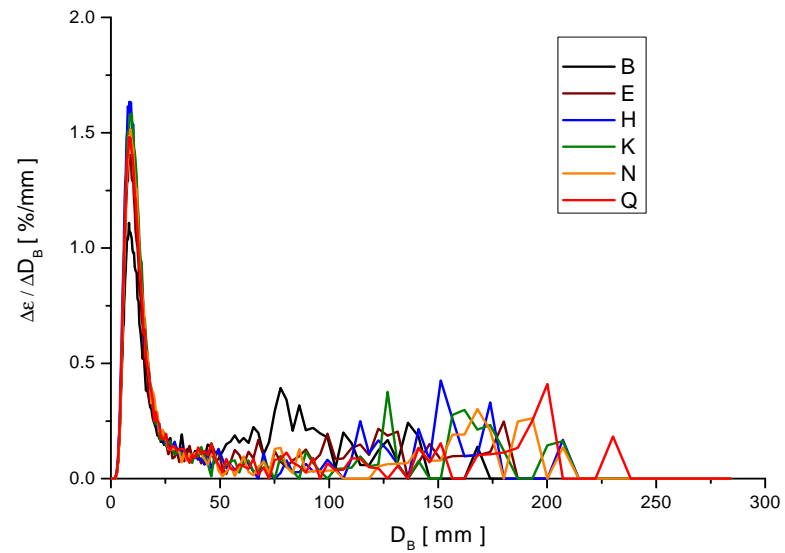
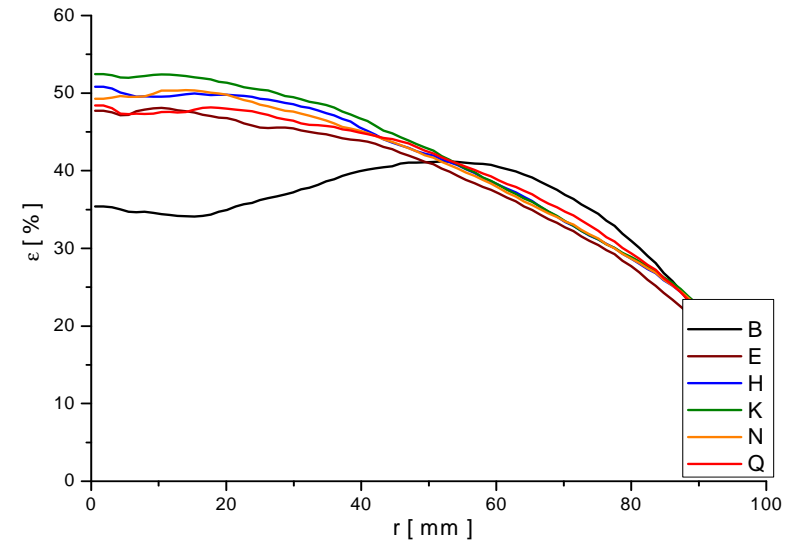
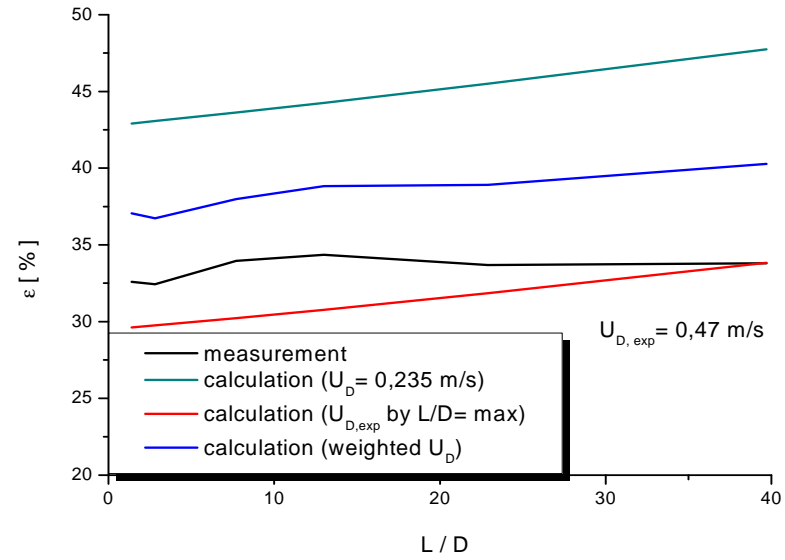
measurement point111 ($J_L = 0.0405$ m/s; $J_G = 0.219$ m/s; $D_{\text{Orifice}} = 4$ mm)



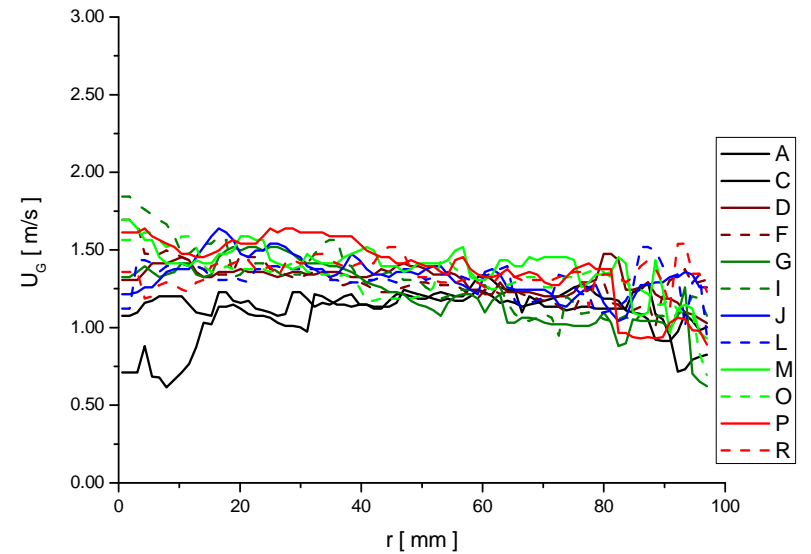
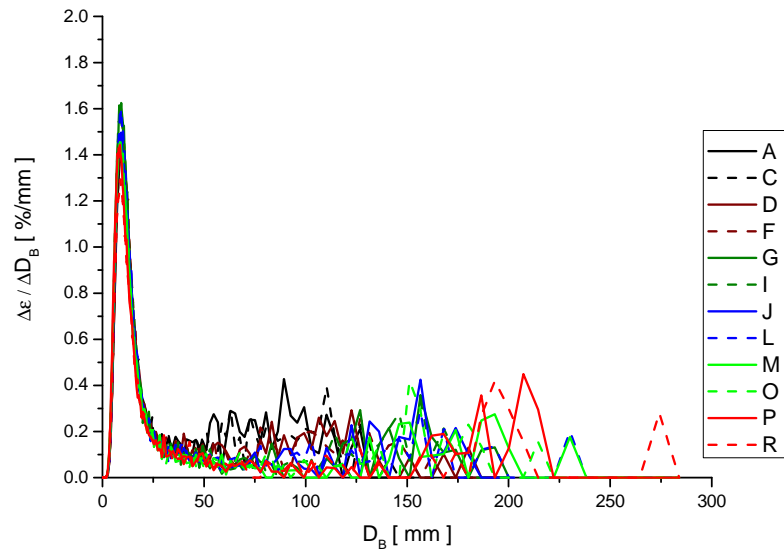
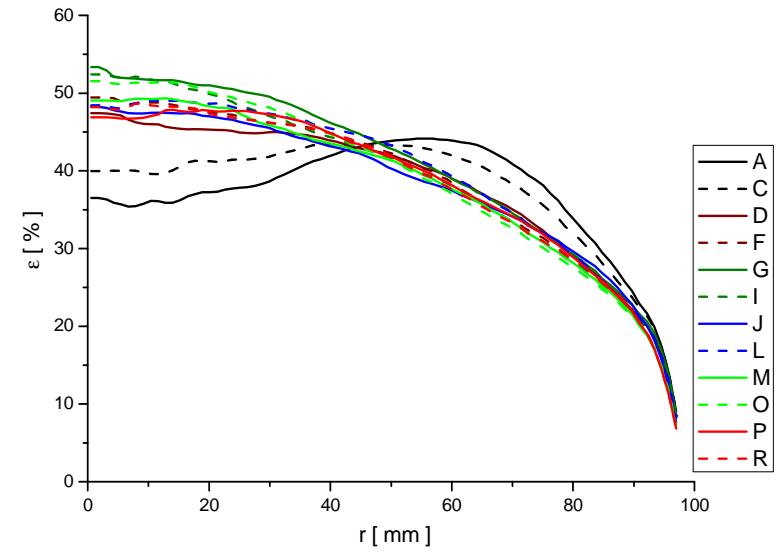
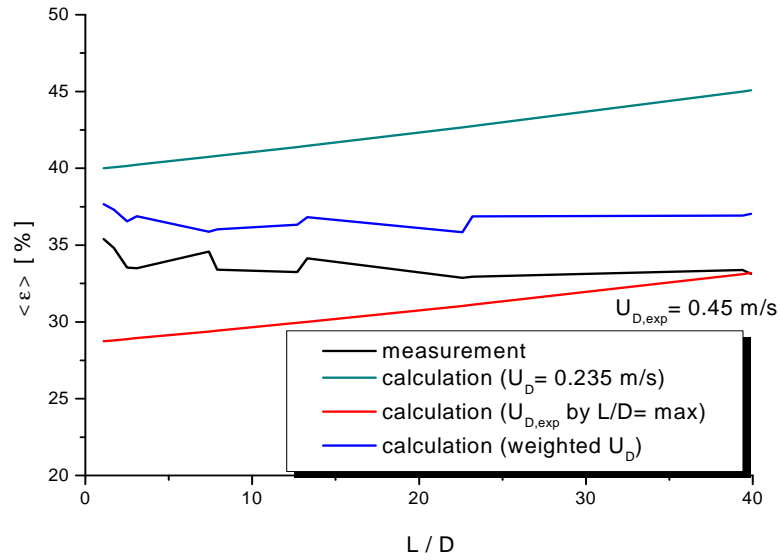
measurement point 112 ($J_L = 0.0641$ m/s; $J_G = 0.219$ m/s; $D_{\text{Orifice}} = 1$ mm)



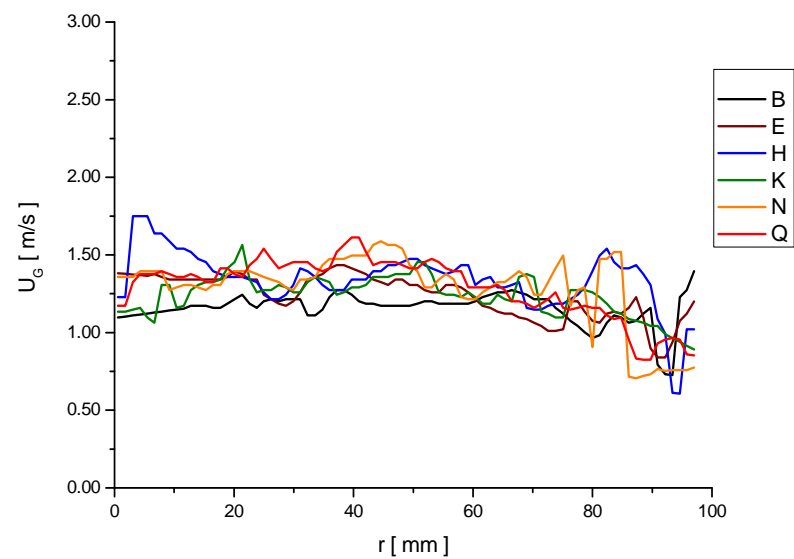
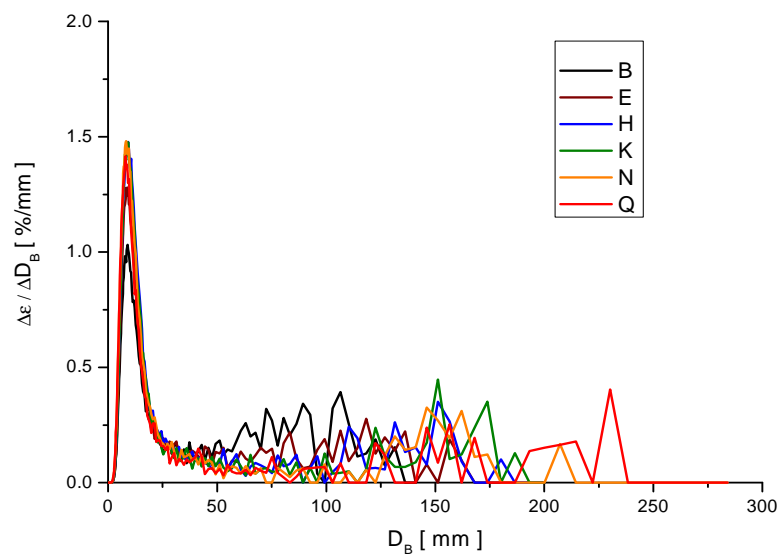
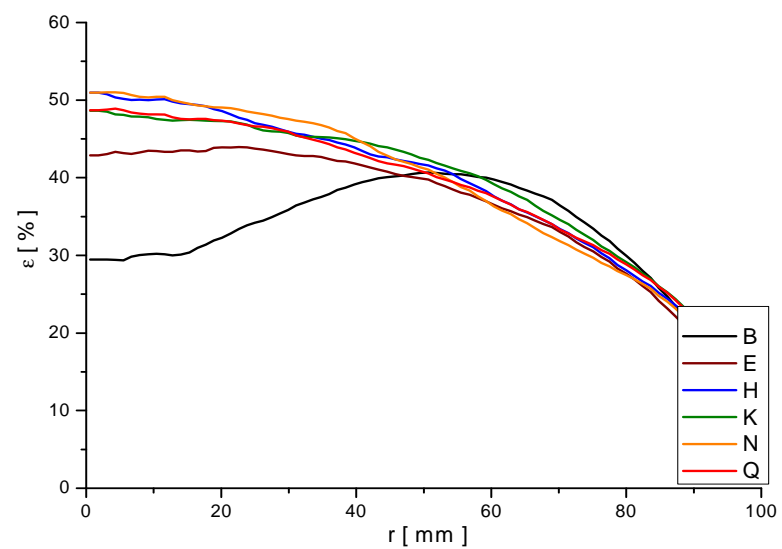
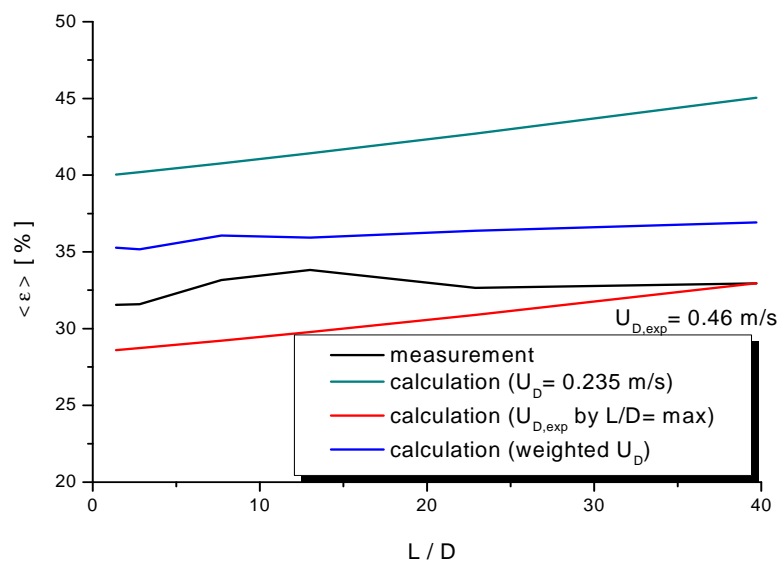
measurement point 112 ($J_L = 0.0641$ m/s; $J_G = 0.219$ m/s; $D_{\text{Orifice}} = 4$ mm)



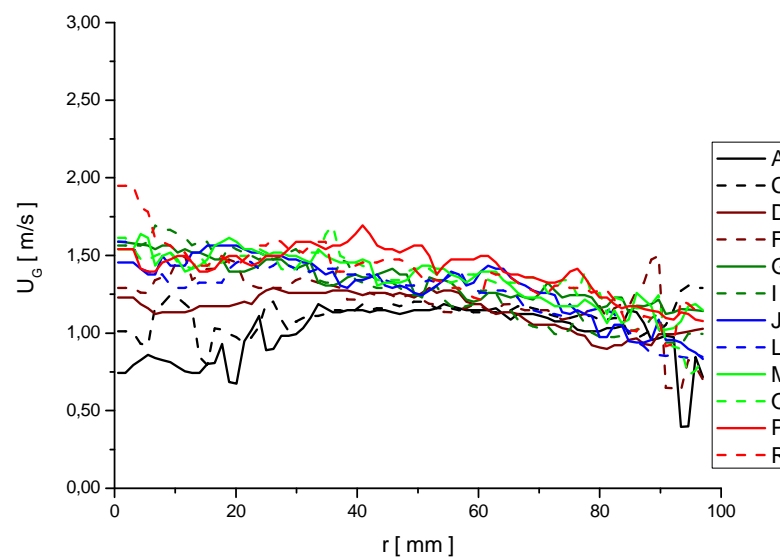
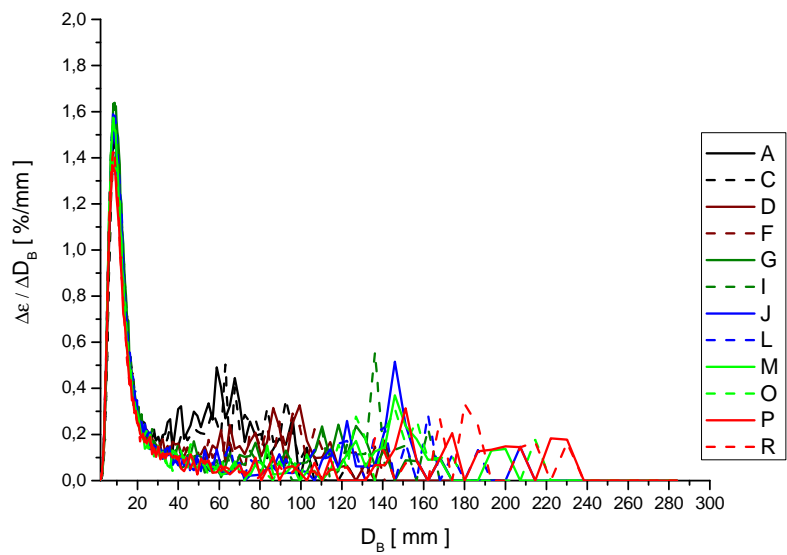
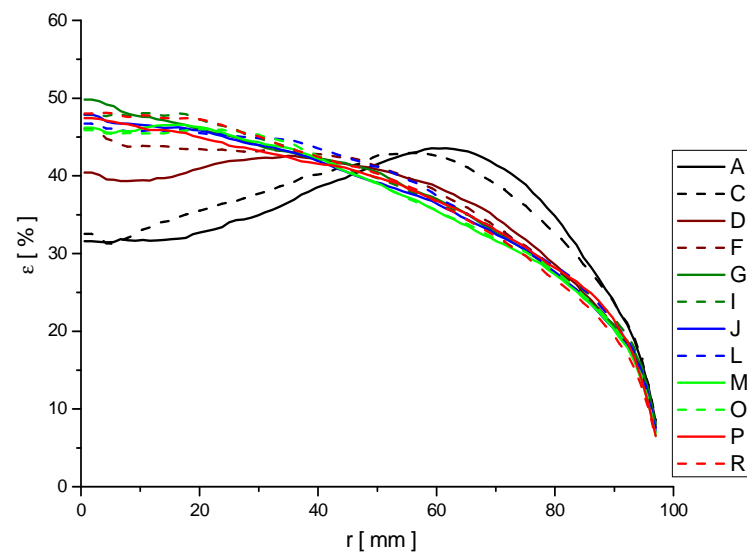
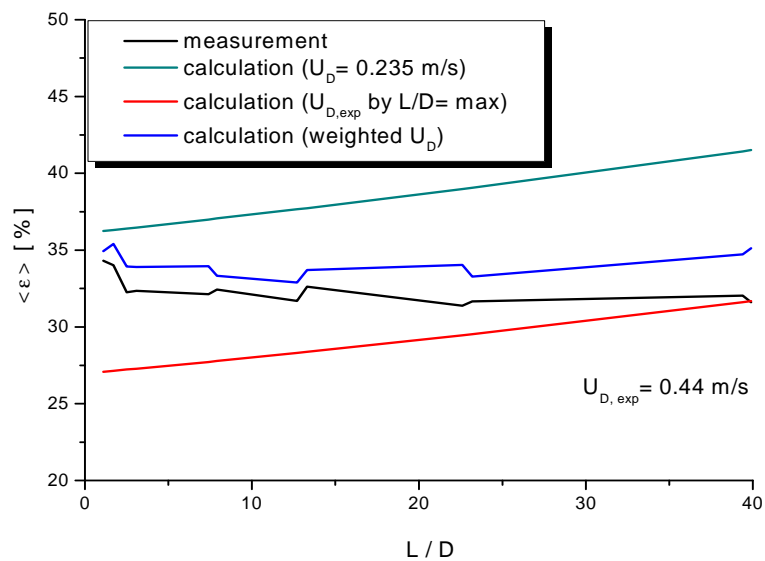
measurement point 113 ($J_L = 0.102$ m/s; $J_G = 0.219$ m/s; $D_{\text{Orifice}} = 1$ mm)



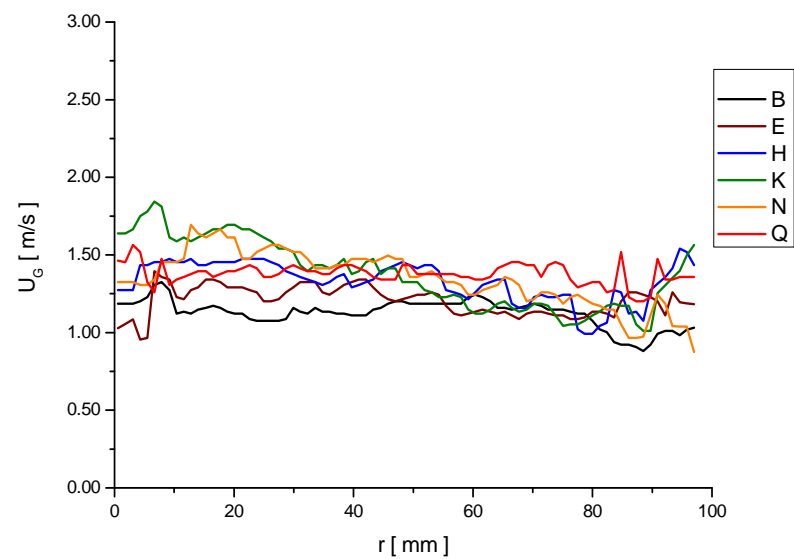
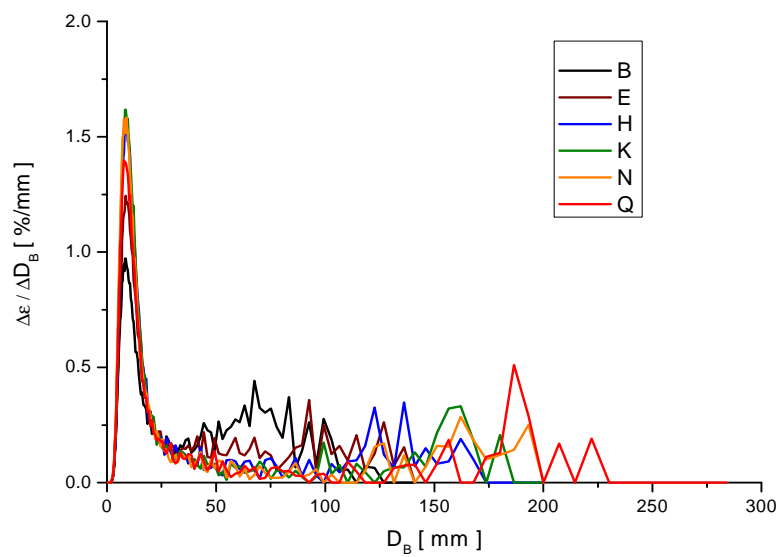
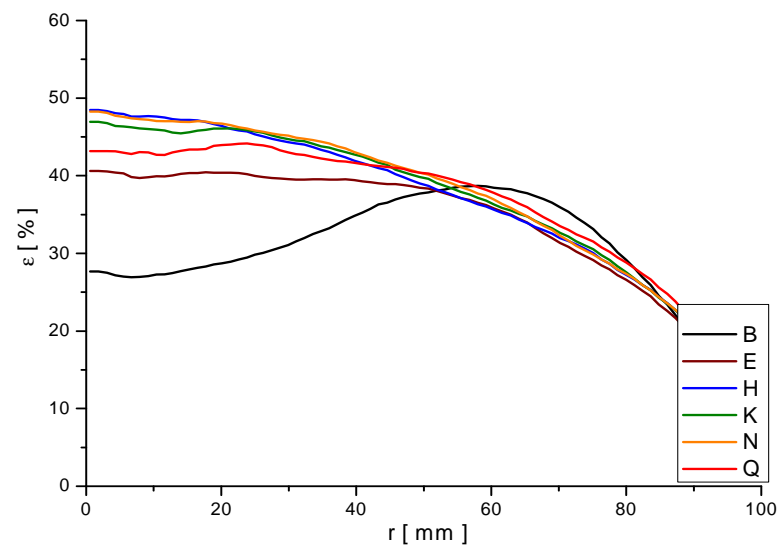
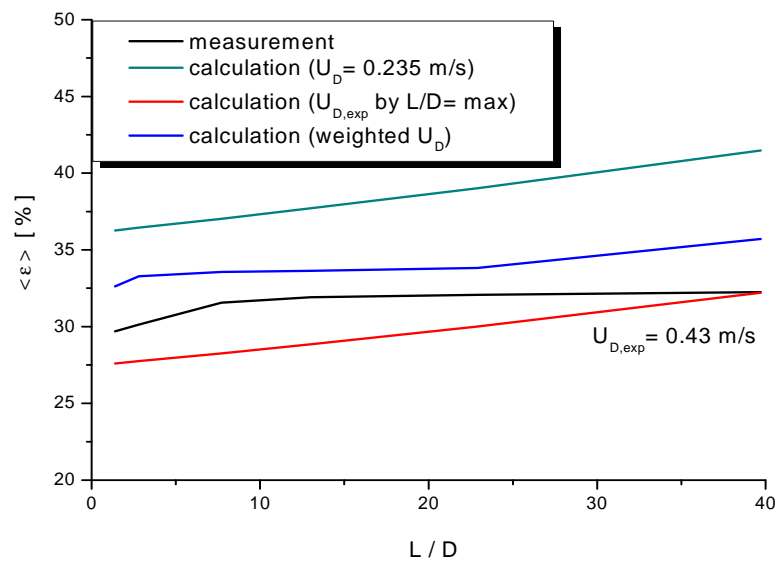
measurement point 113 ($J_L = 0.102$ m/s; $J_G = 0.219$ m/s; $D_{\text{Orifice}} = 4$ mm)



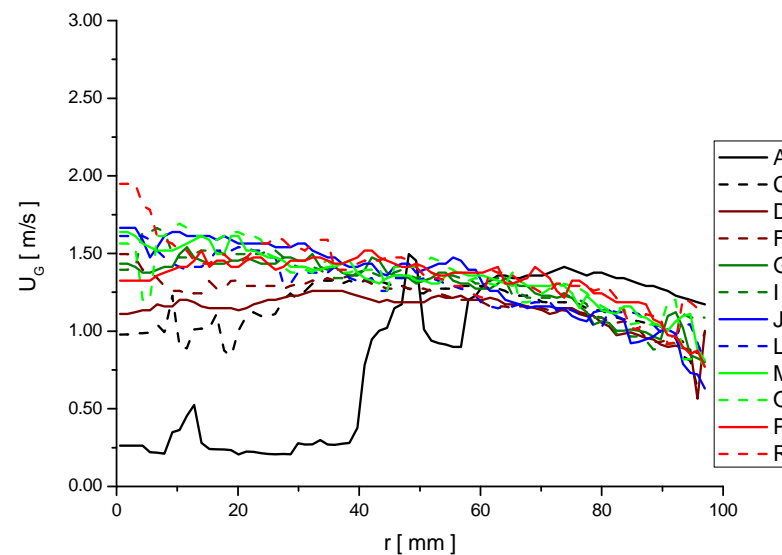
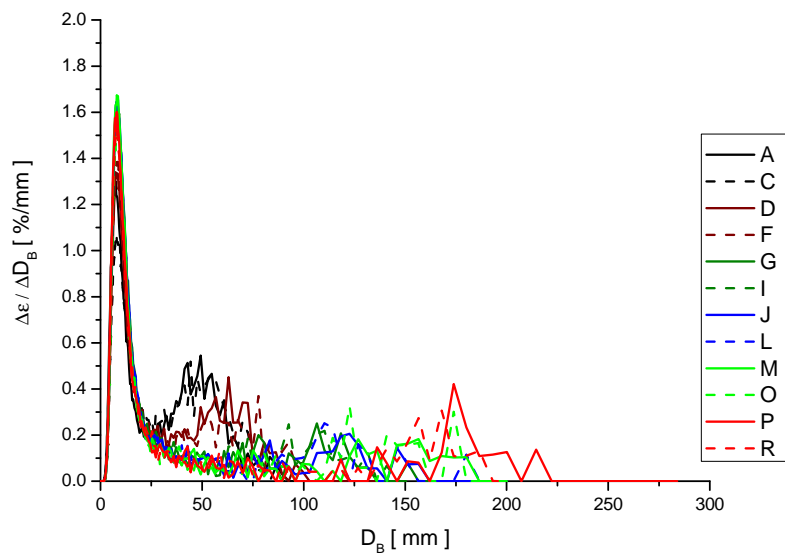
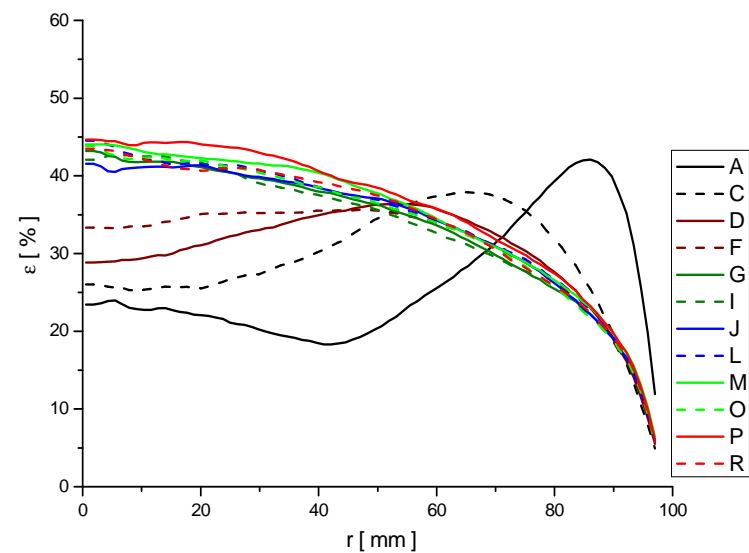
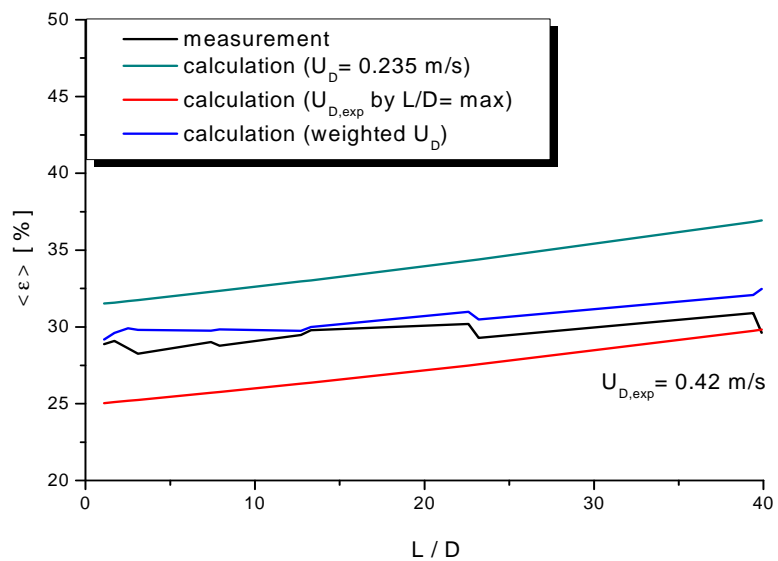
measurement point 114 ($J_L = 0.161$ m/s; $J_G = 0.219$ m/s; $D_{\text{Orifice}} = 1$ mm)



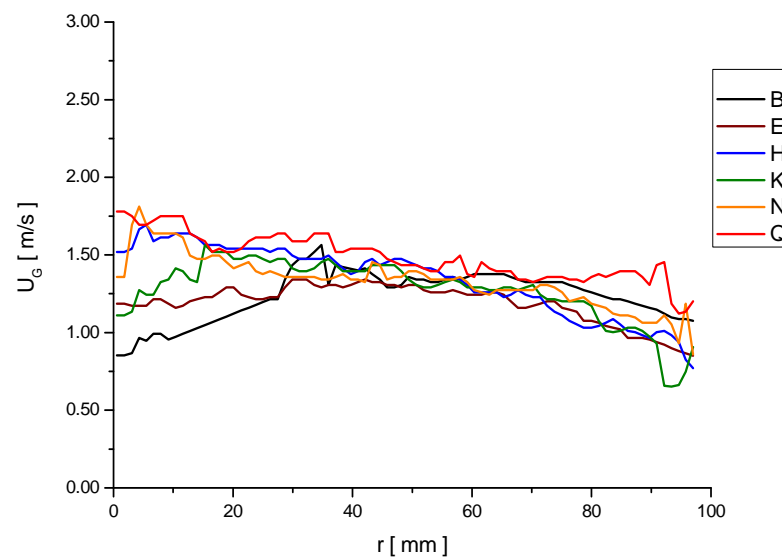
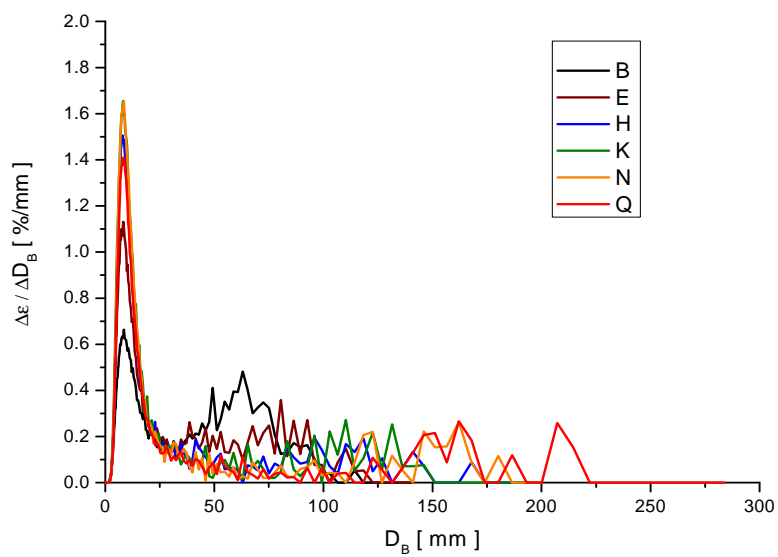
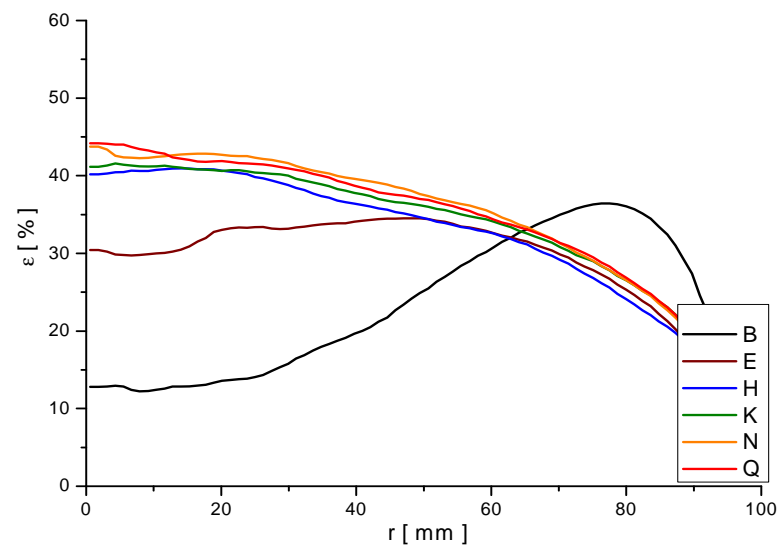
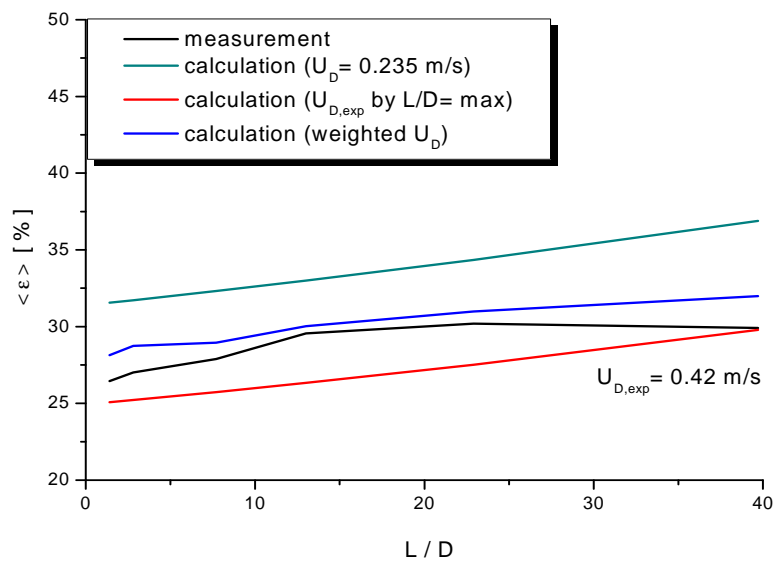
measurement point 114 ($J_L = 0.161$ m/s; $J_G = 0.219$ m/s; $D_{\text{Orifice}} = 4$ mm)



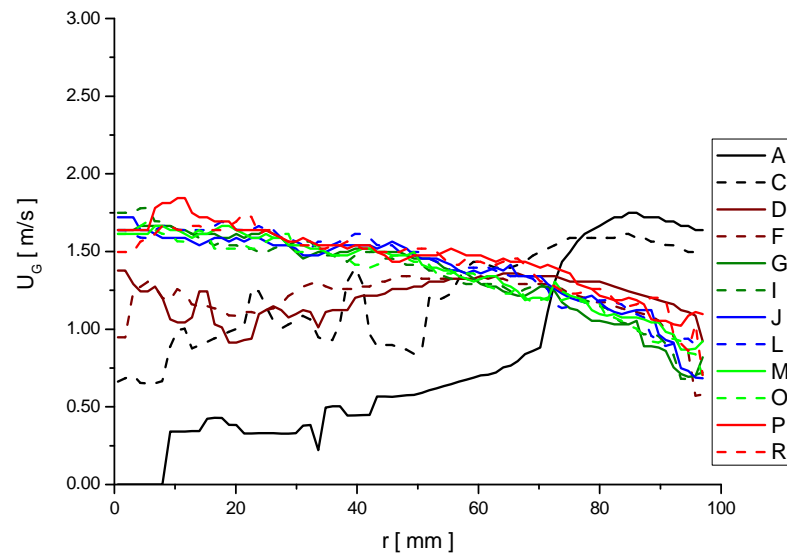
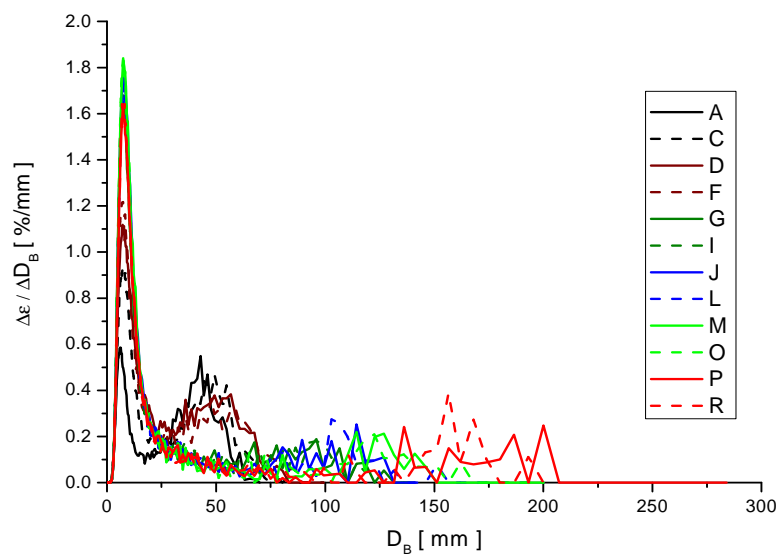
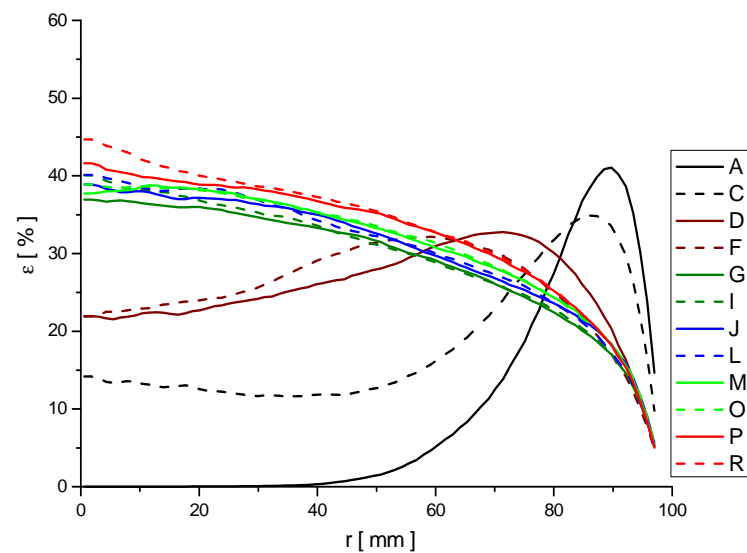
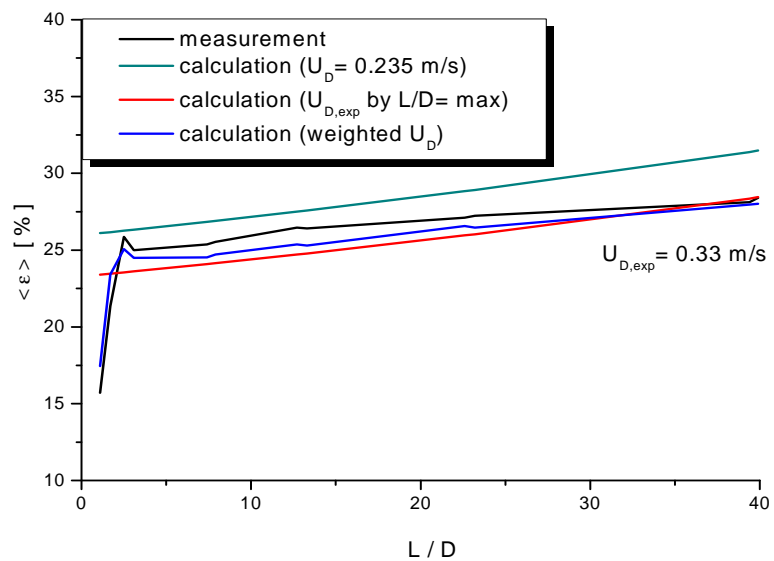
measurement point 115 ($J_L = 0.255$ m/s; $J_G = 0.219$ m/s; $D_{\text{Orifice}} = 1$ mm)



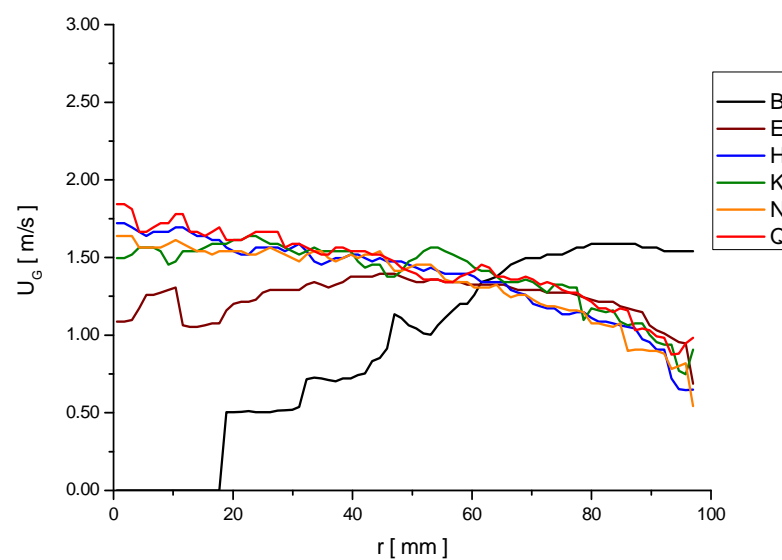
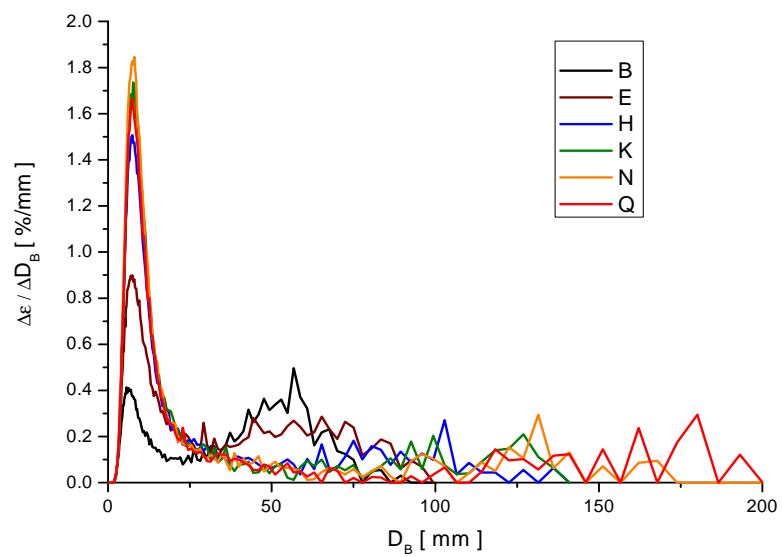
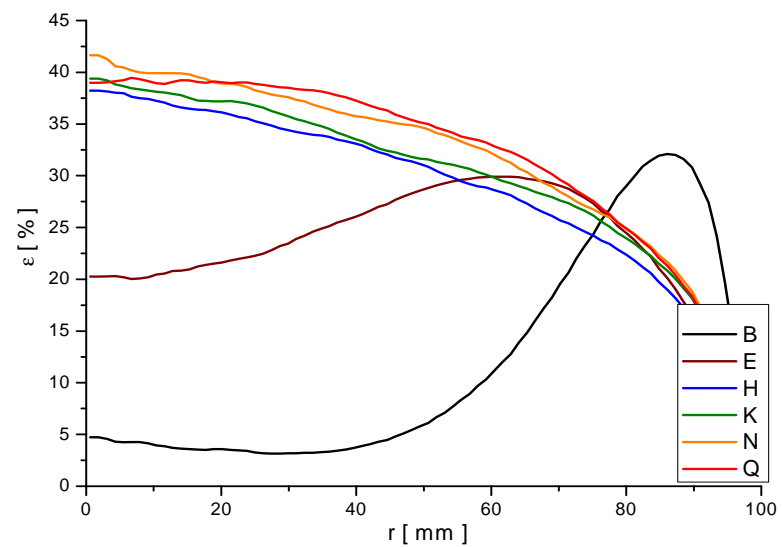
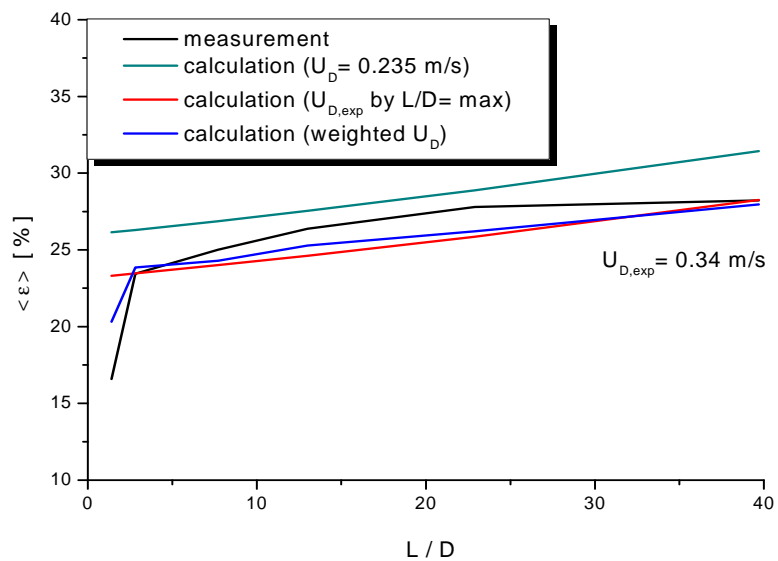
measurement point 115 ($J_L = 0.255$ m/s; $J_G = 0.219$ m/s; $D_{\text{Orifice}} = 4$ mm)



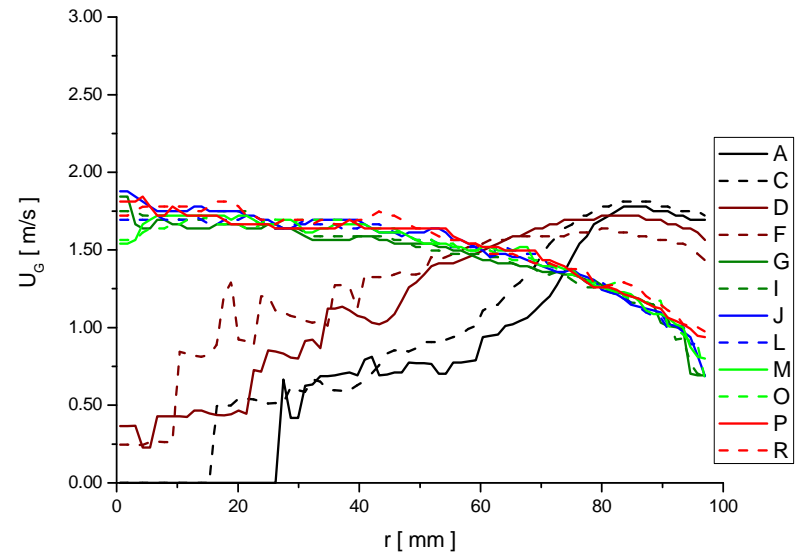
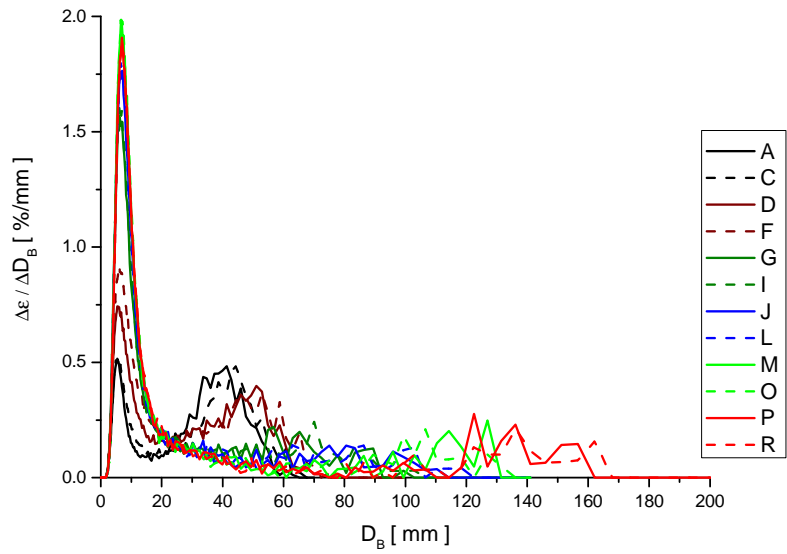
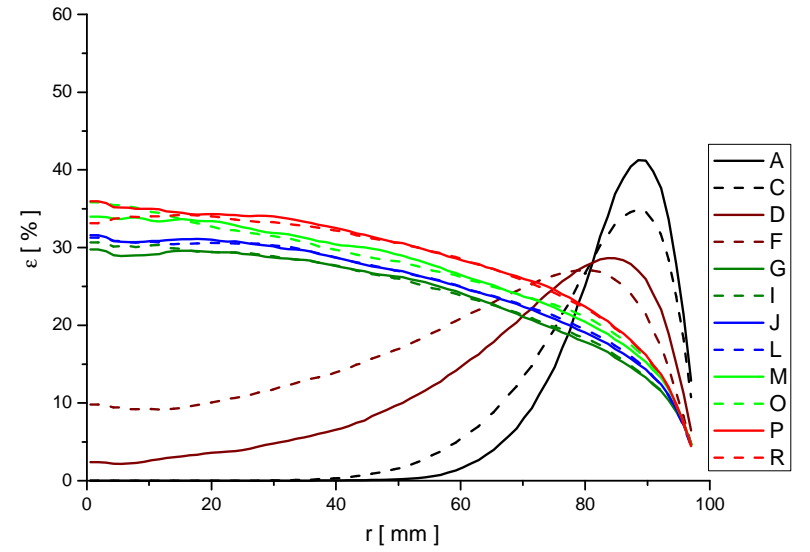
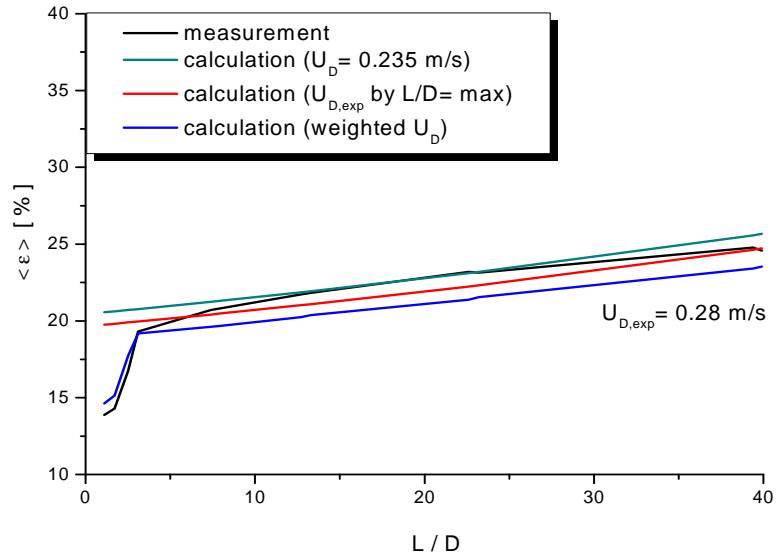
measurement point 116 ($J_L = 0.405$ m/s; $J_G = 0.219$ m/s; $D_{\text{Orifice}} = 1$ mm)



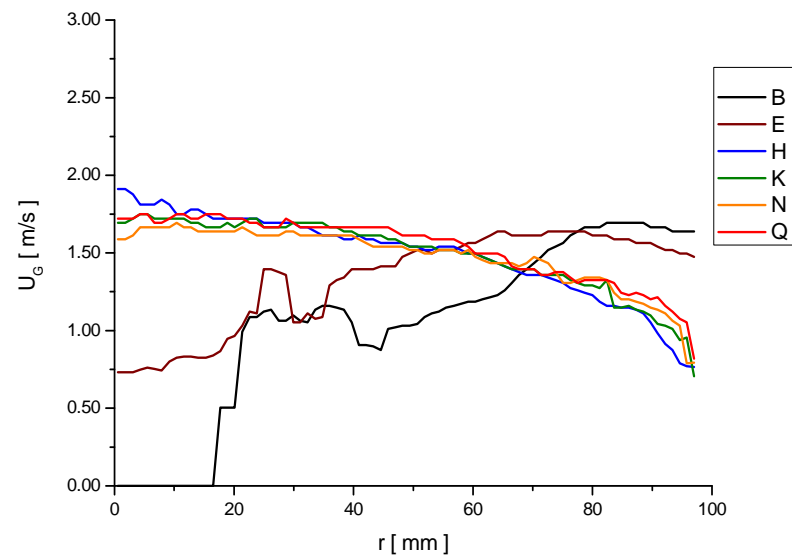
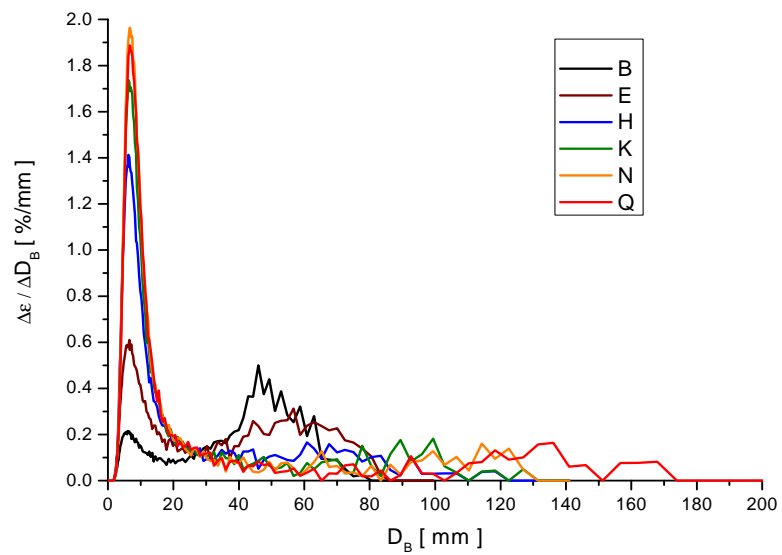
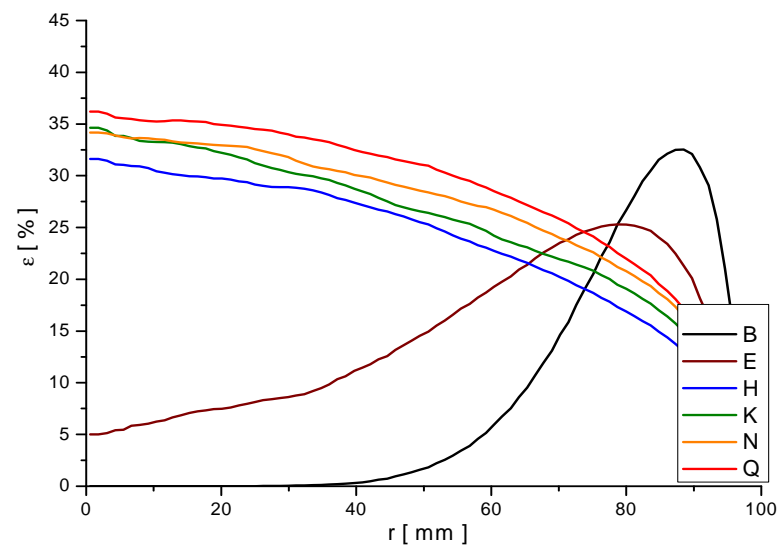
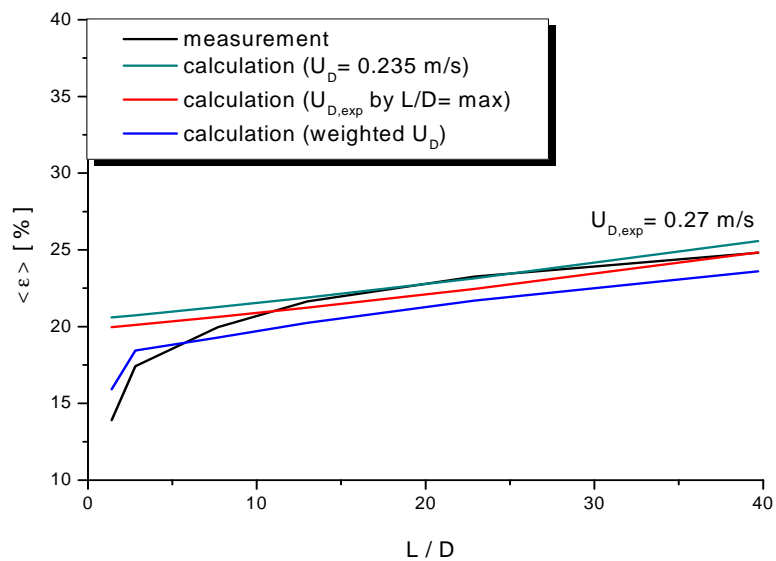
measurement point 116 ($J_L = 0.405$ m/s; $J_G = 0.219$ m/s; $D_{\text{Orifice}} = 4$ mm)



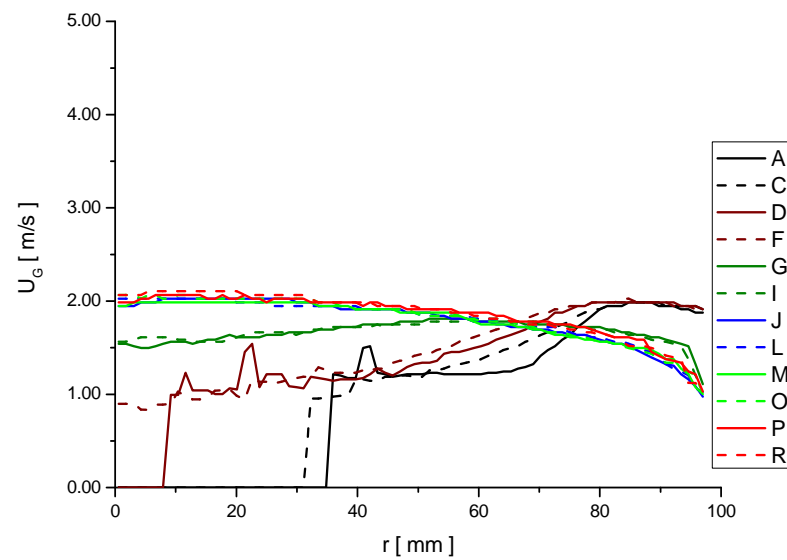
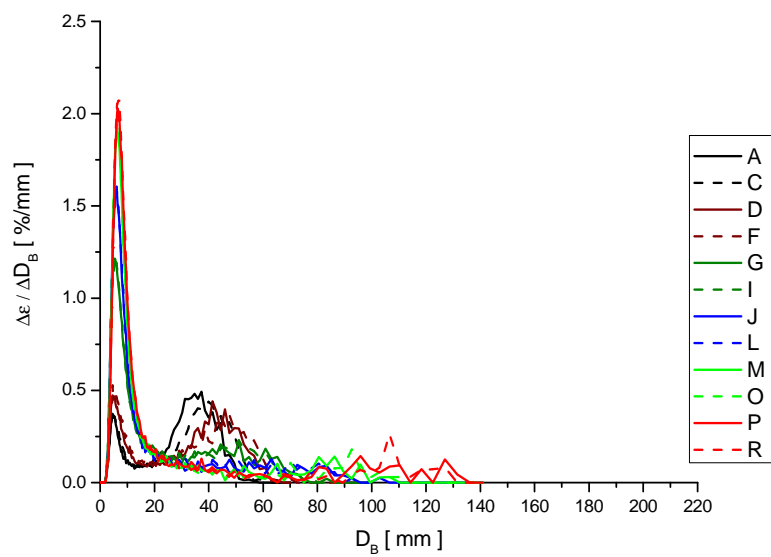
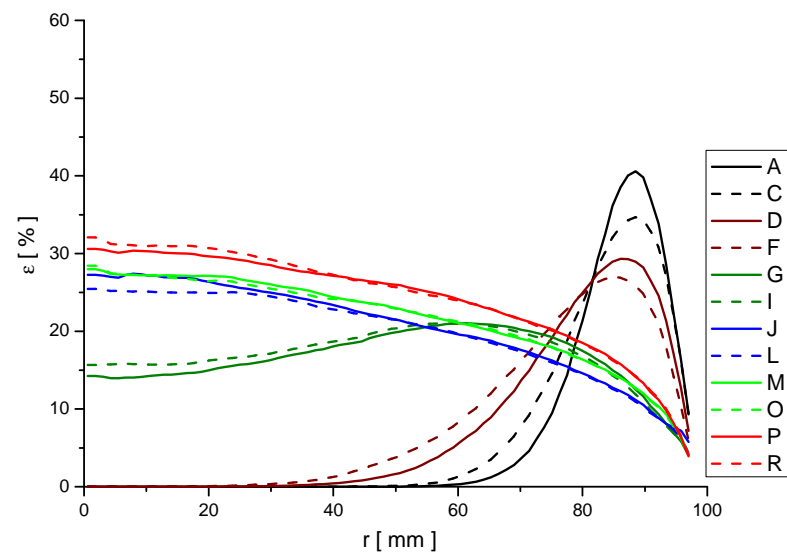
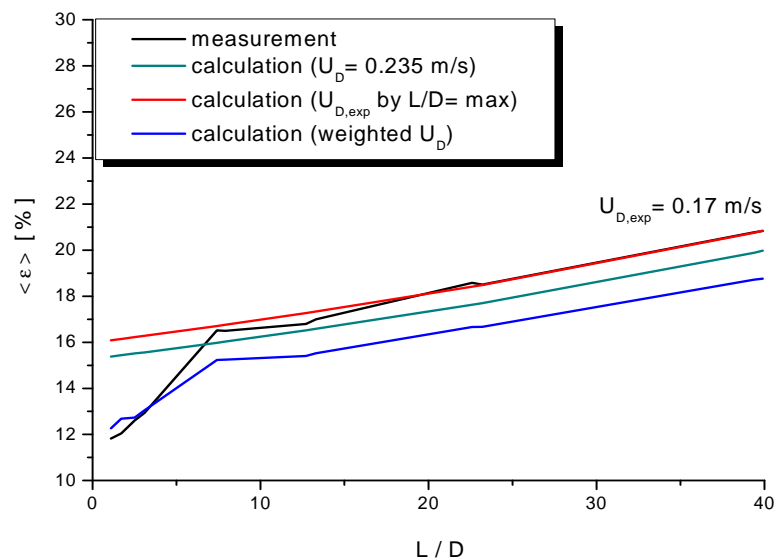
measurement point 117 ($J_L = 0.641$ m/s; $J_G = 0.219$ m/s; $D_{\text{Orifice}} = 1$ mm)



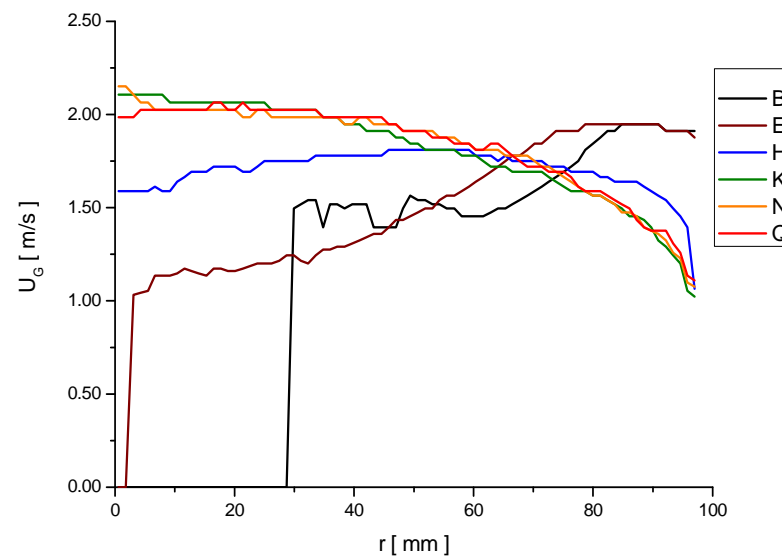
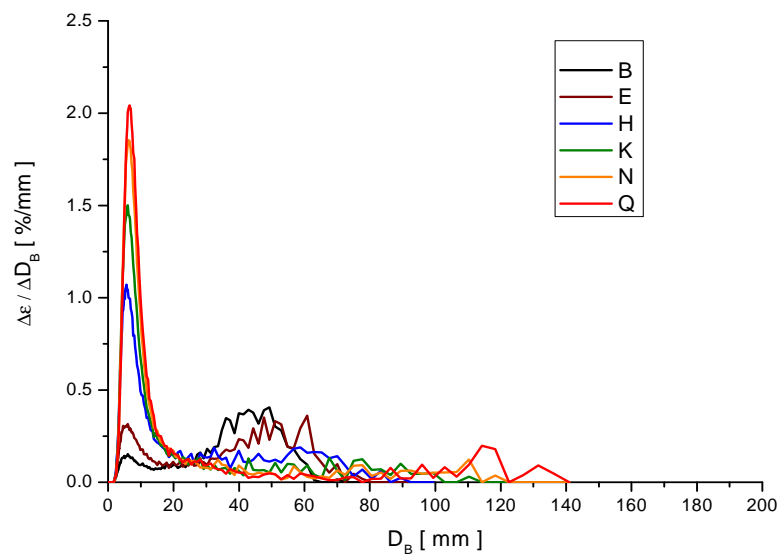
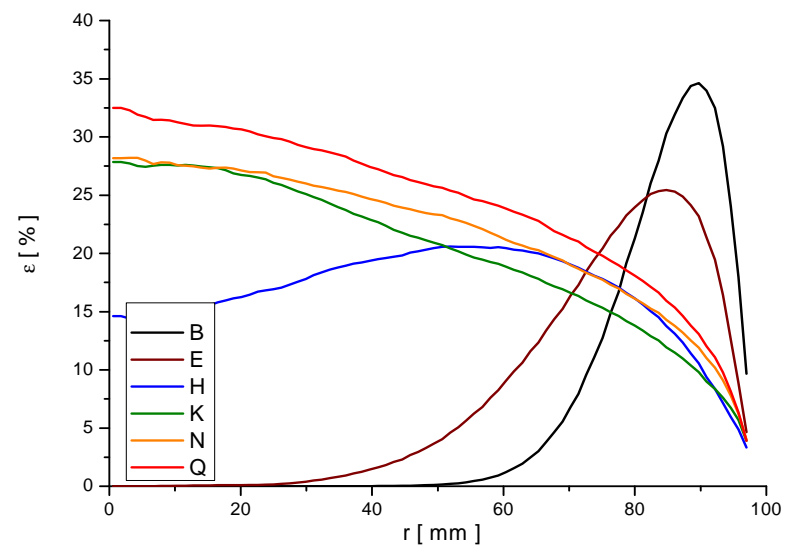
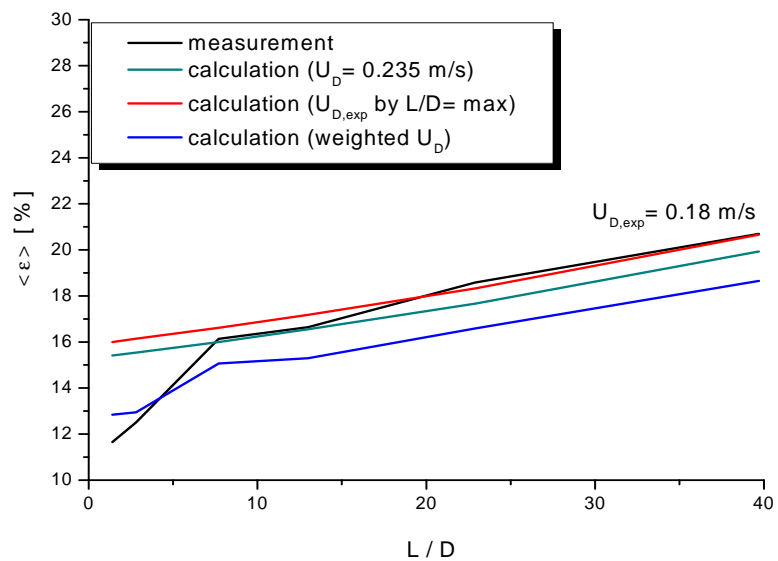
measurement point 117 ($J_L = 0.641$ m/s; $J_G = 0.219$ m/s; $D_{\text{Orifice}} = 4$ mm)



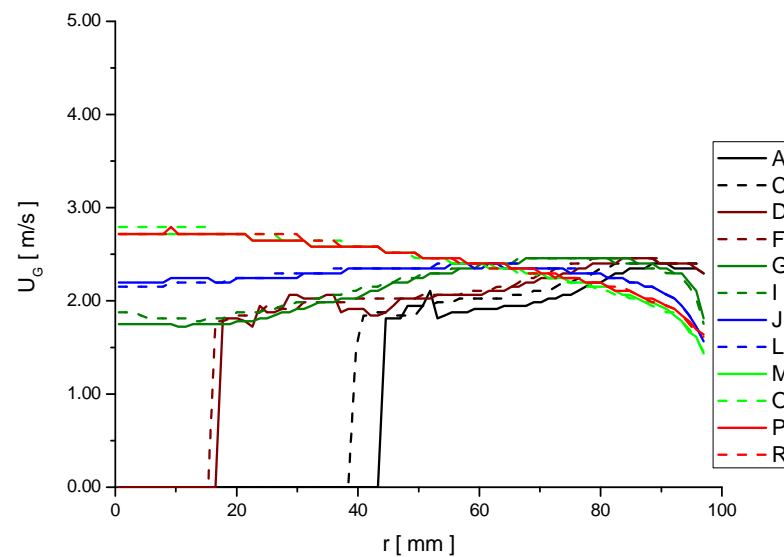
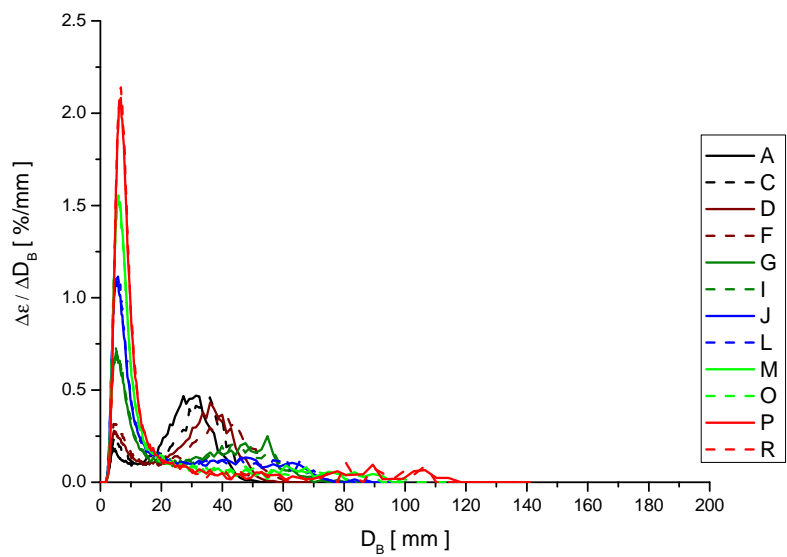
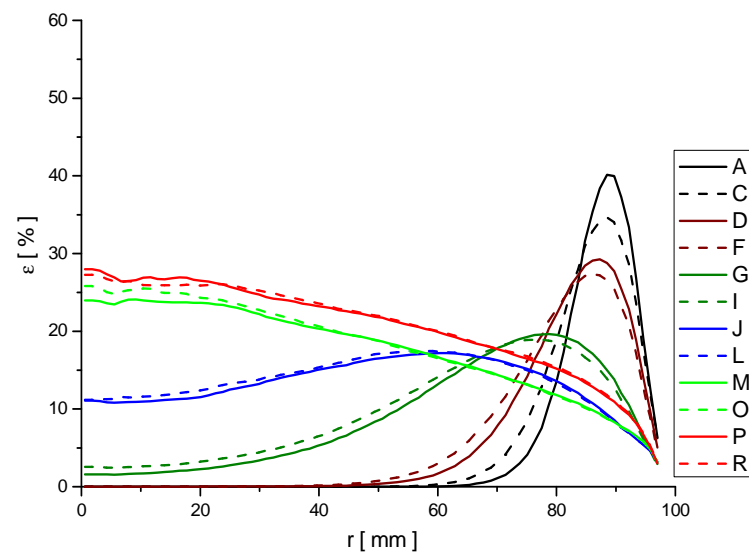
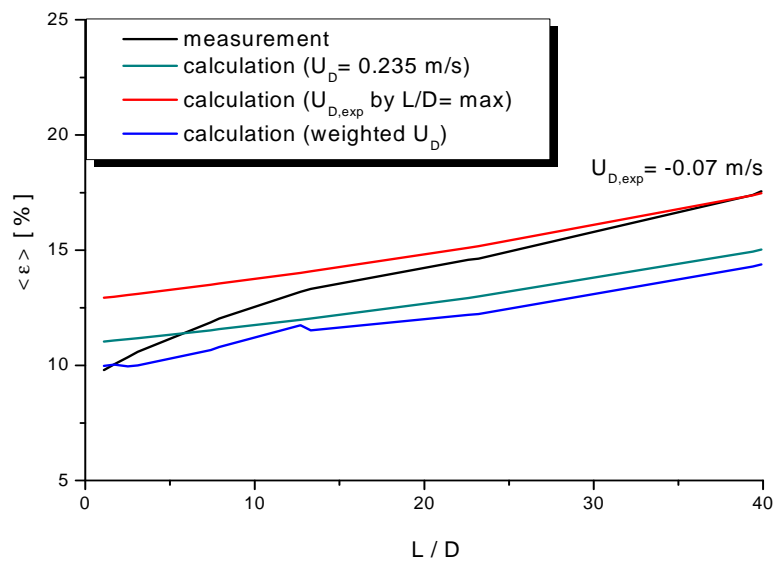
measurement point 118 ($J_L = 1.017$ m/s; $J_G = 0.219$ m/s; $D_{\text{Orifice}} = 1$ mm)



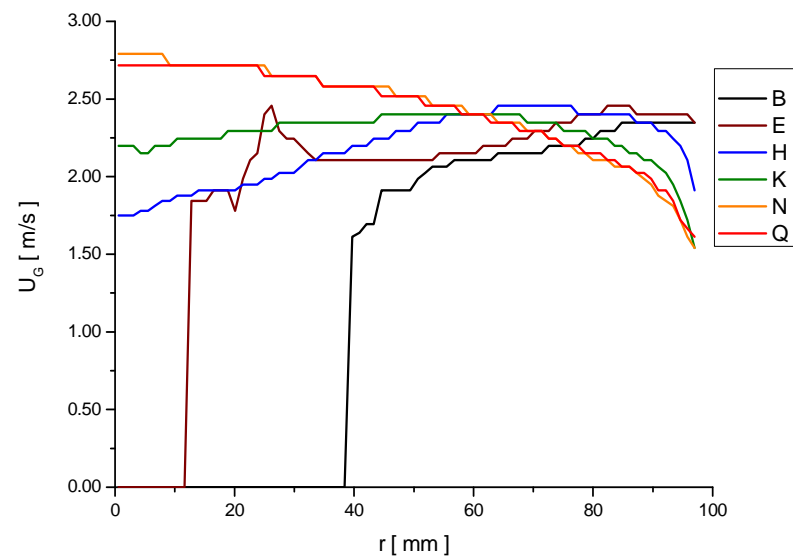
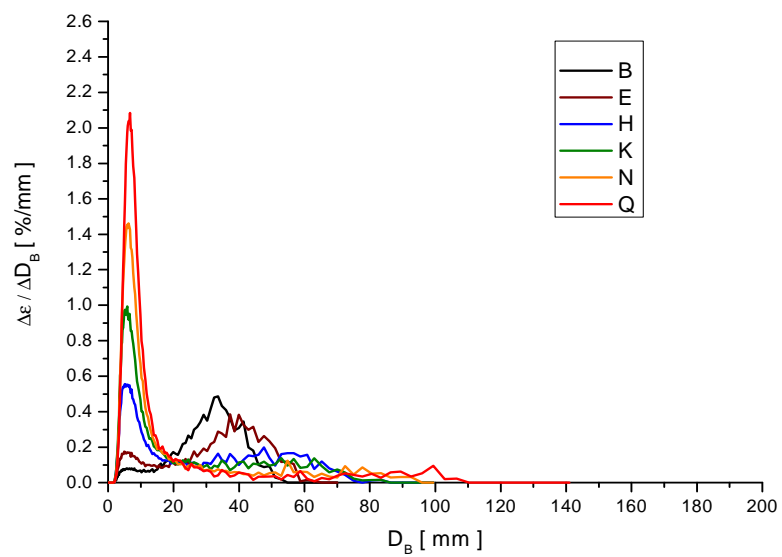
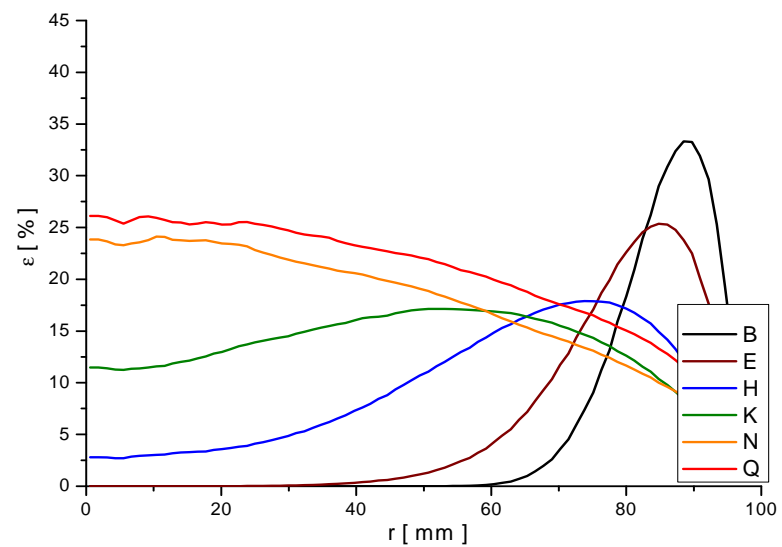
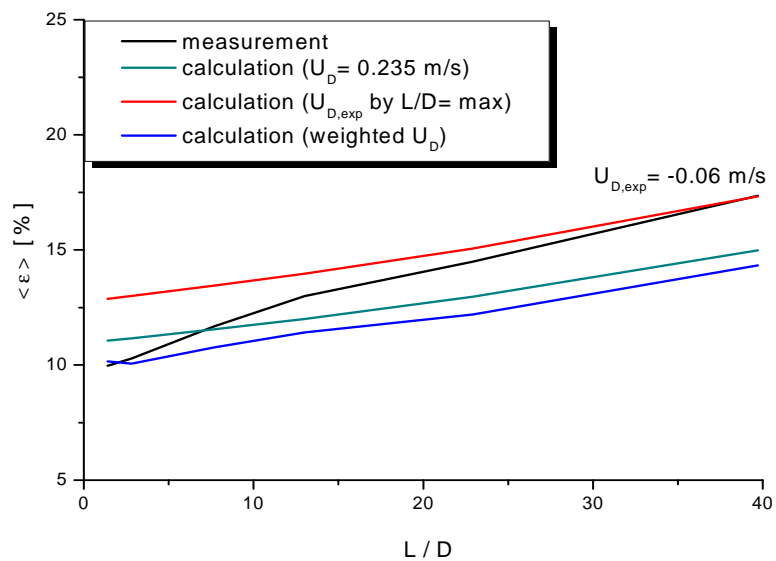
measurement point 118 ($J_L = 1.017$ m/s; $J_G = 0.219$ m/s; $D_{\text{Orifice}} = 4$ mm)



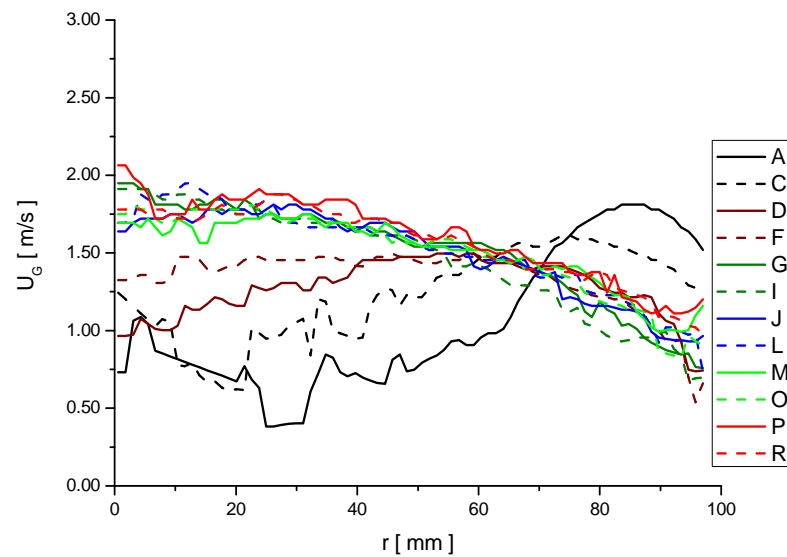
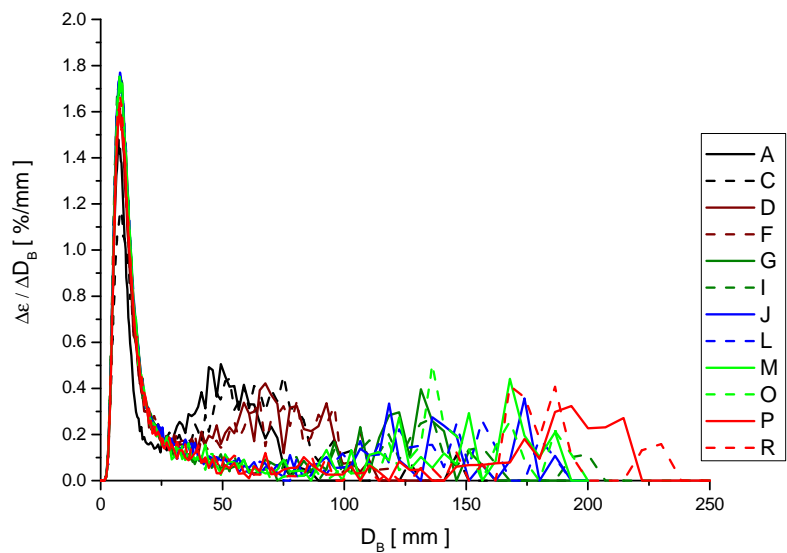
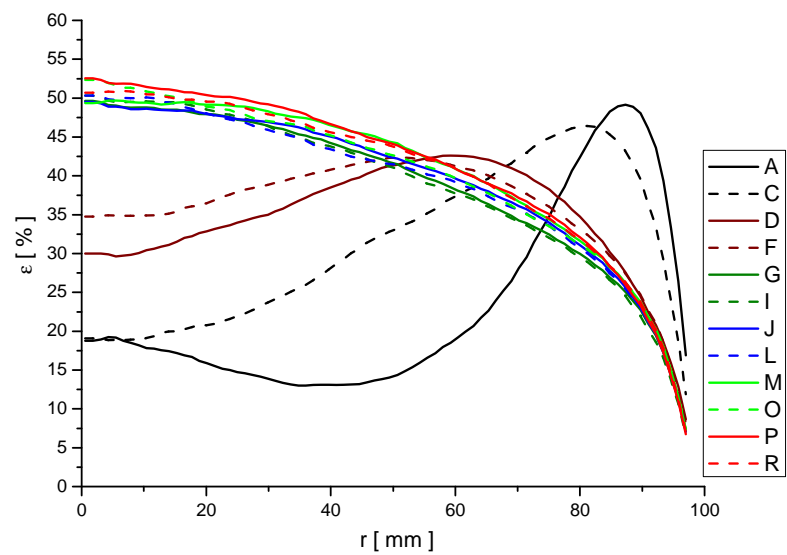
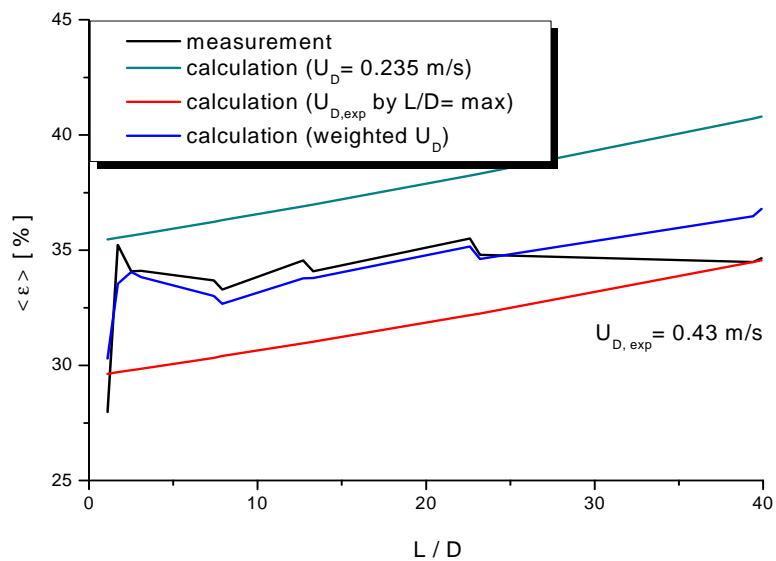
measurement point 119 ($J_L = 1.611$ m/s; $J_G = 0.219$ m/s; $D_{\text{Orifice}} = 1$ mm)



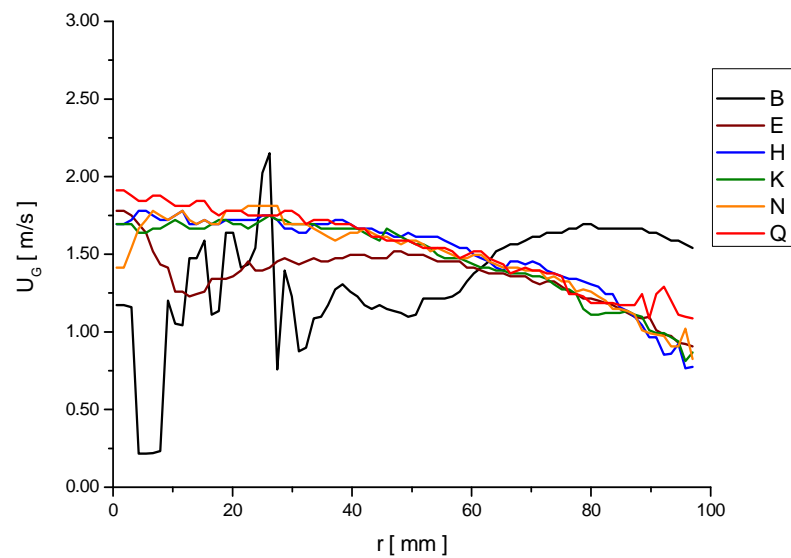
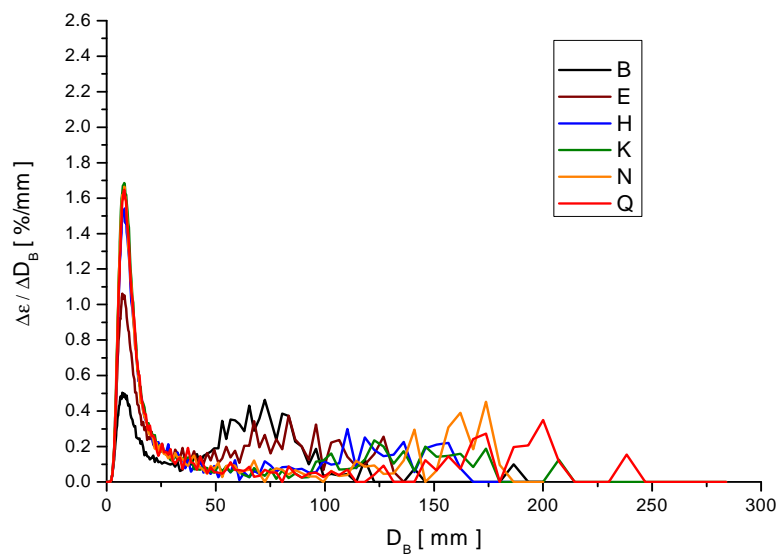
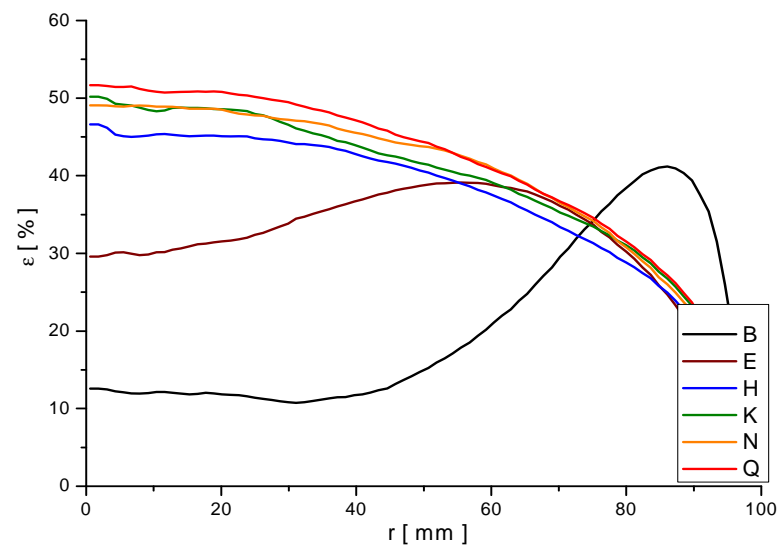
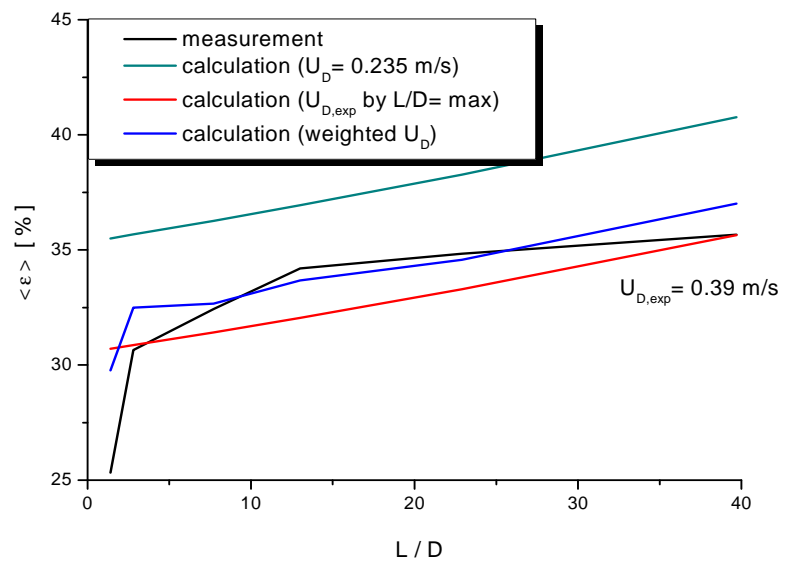
measurement point 119 ($J_L = 1.611$ m/s; $J_G = 0.219$ m/s; $D_{\text{Orifice}} = 4$ mm)



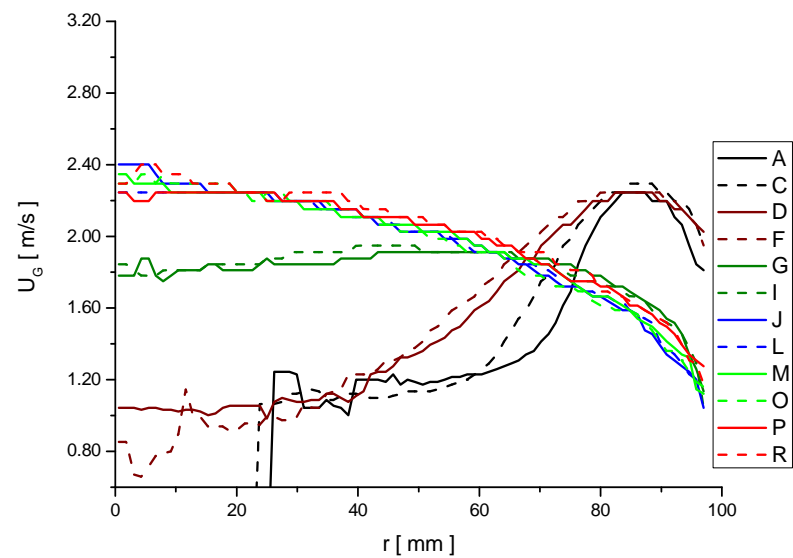
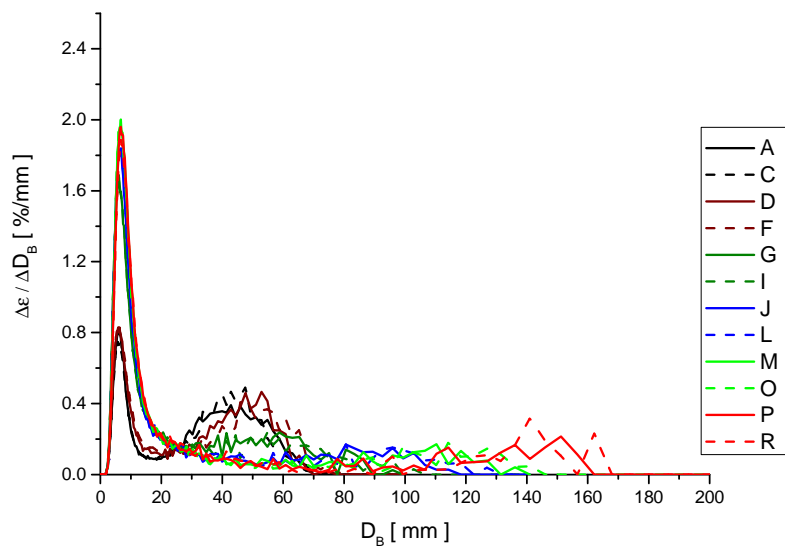
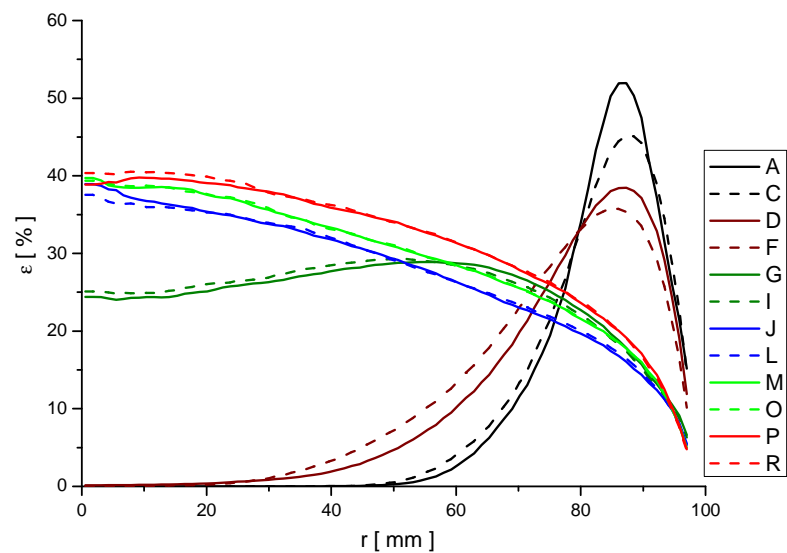
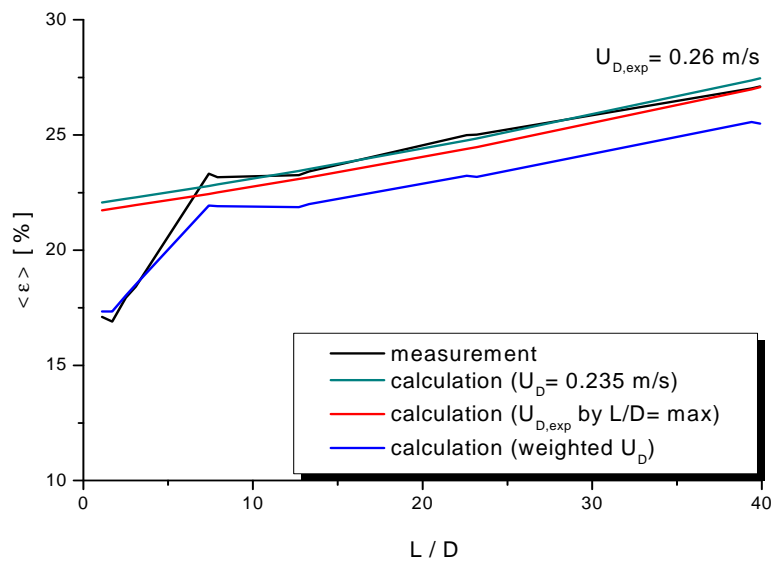
measurement point 127 ($J_L = 0.405$ m/s; $J_G = 0.342$ m/s; $D_{\text{Orifice}} = 1$ mm)



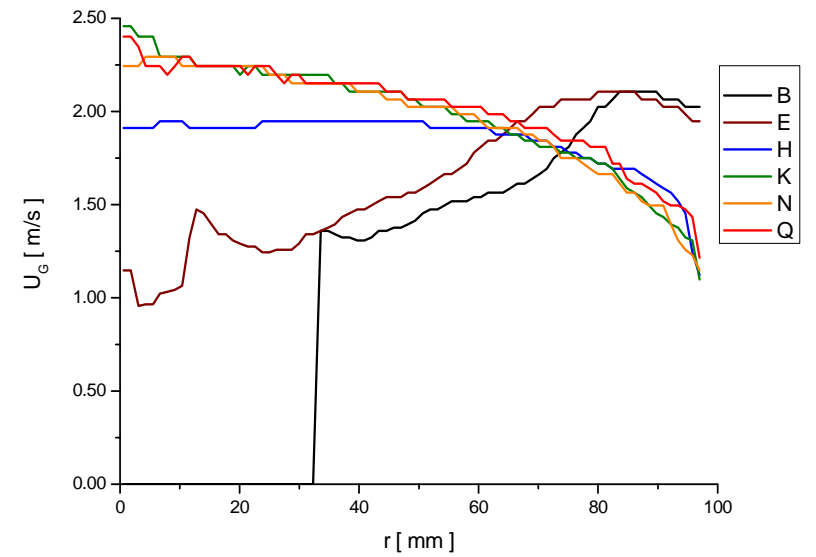
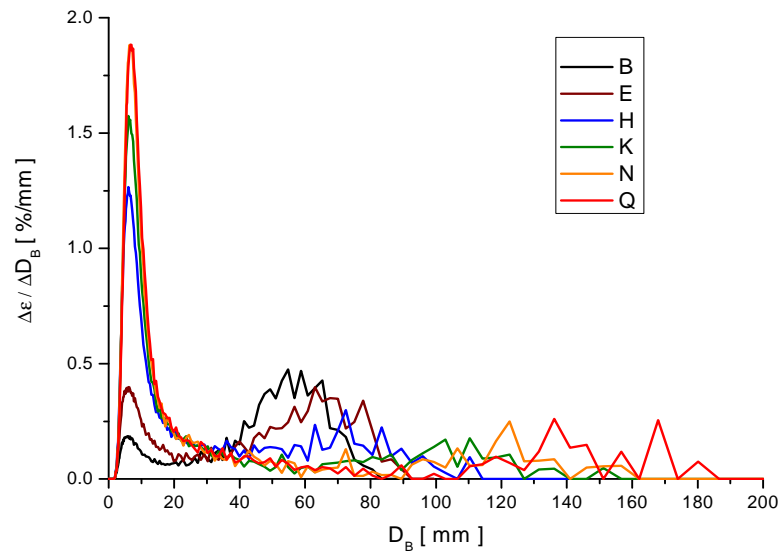
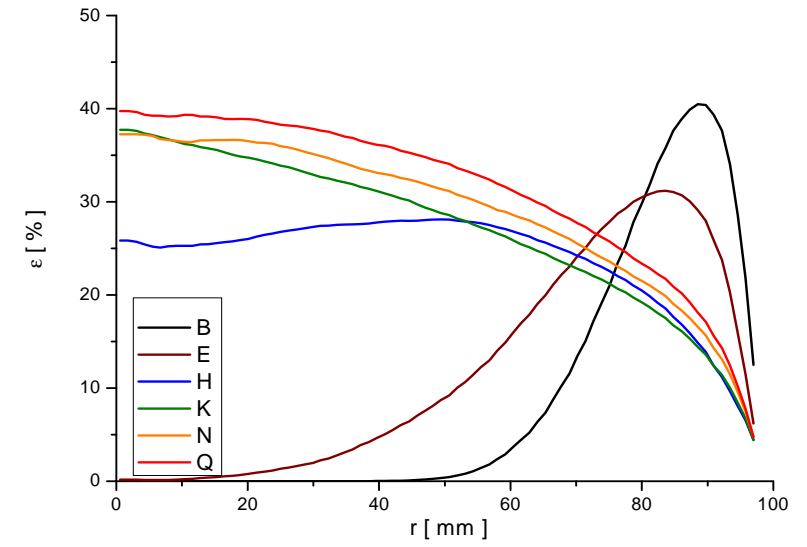
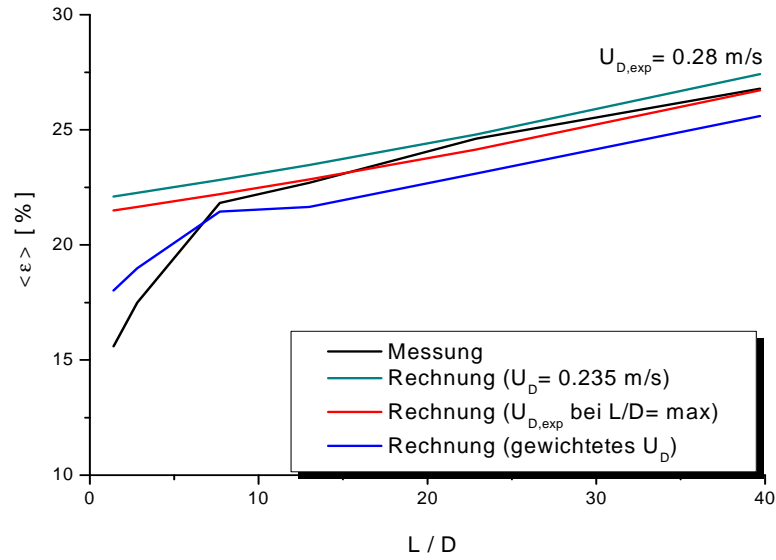
measurement point 127 ($J_L = 0.405$ m/s; $J_G = 0.342$ m/s; $D_{\text{Orifice}} = 4$ mm)



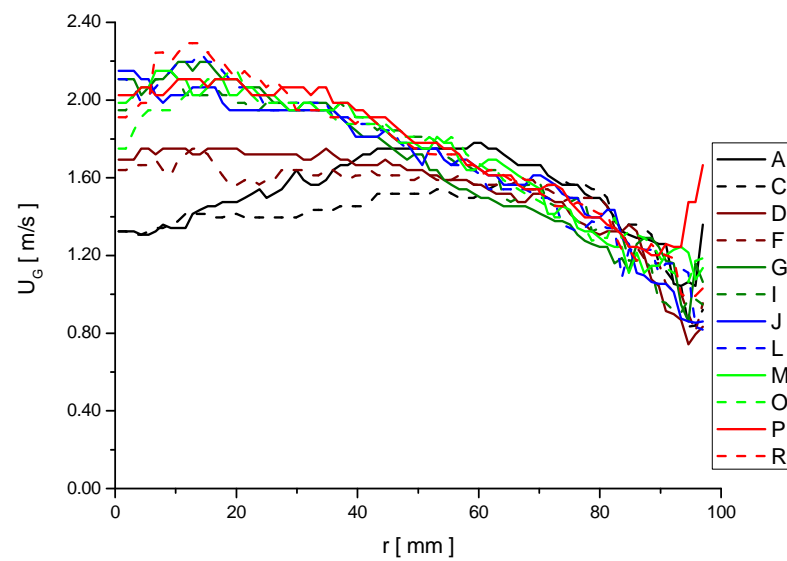
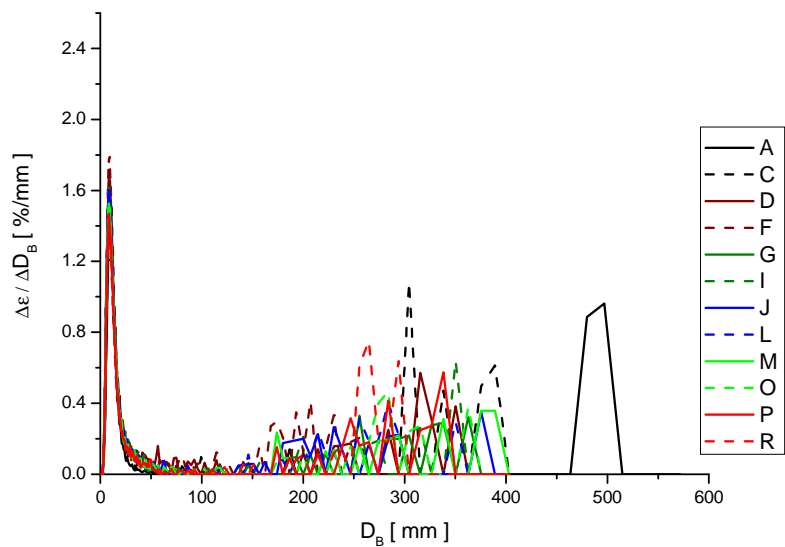
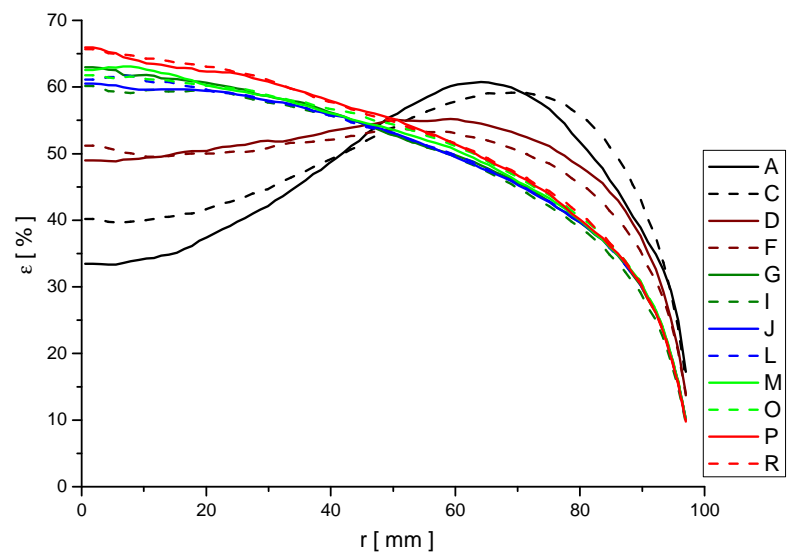
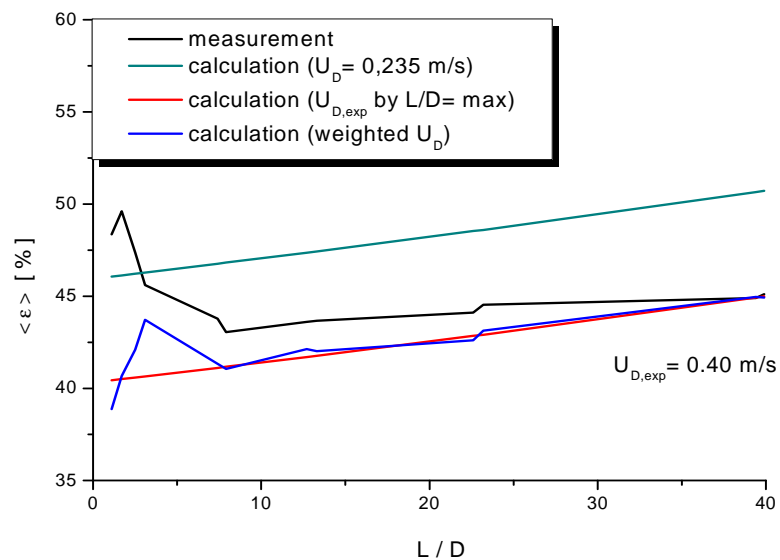
measurement point 129 ($J_L = 1.017$ m/s; $J_G = 0.342$ m/s; $D_{\text{Orifice}} = 1$ mm)



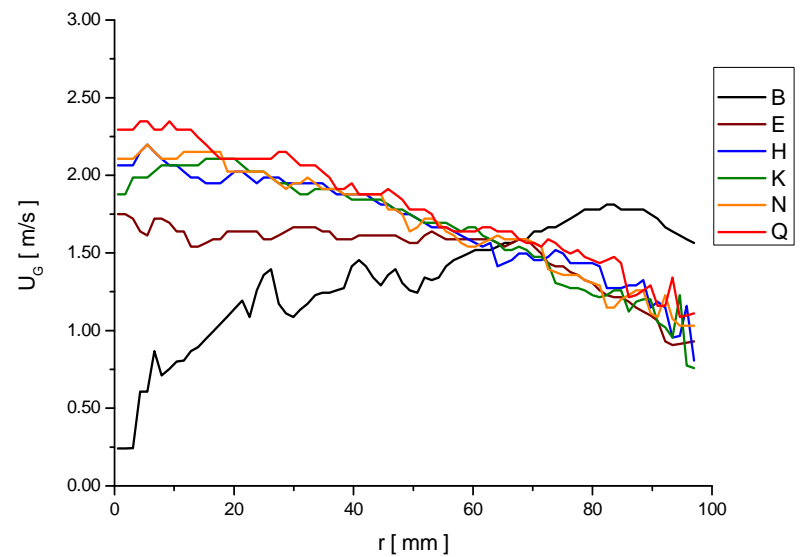
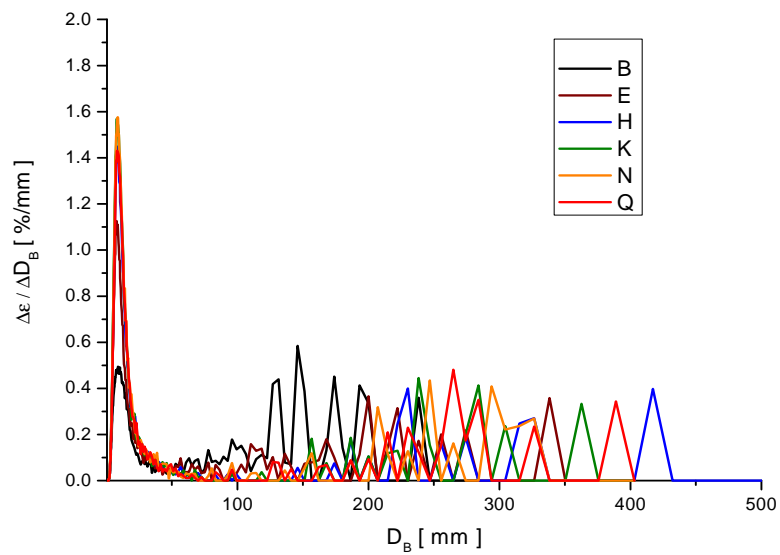
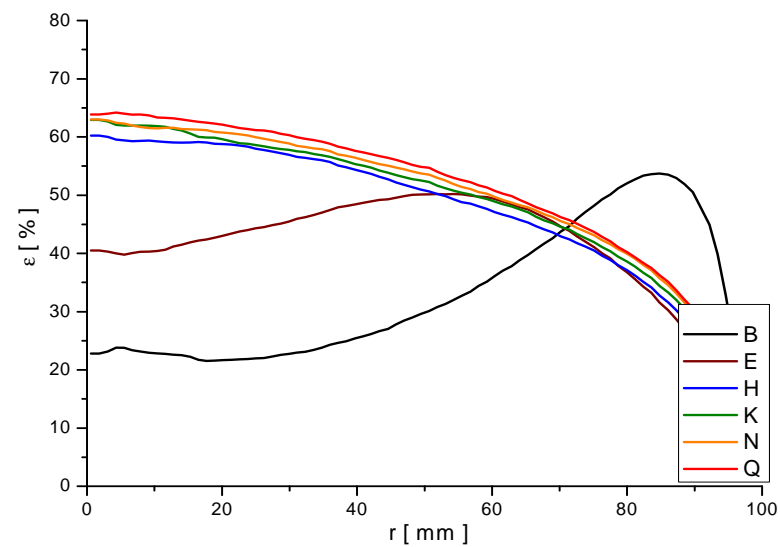
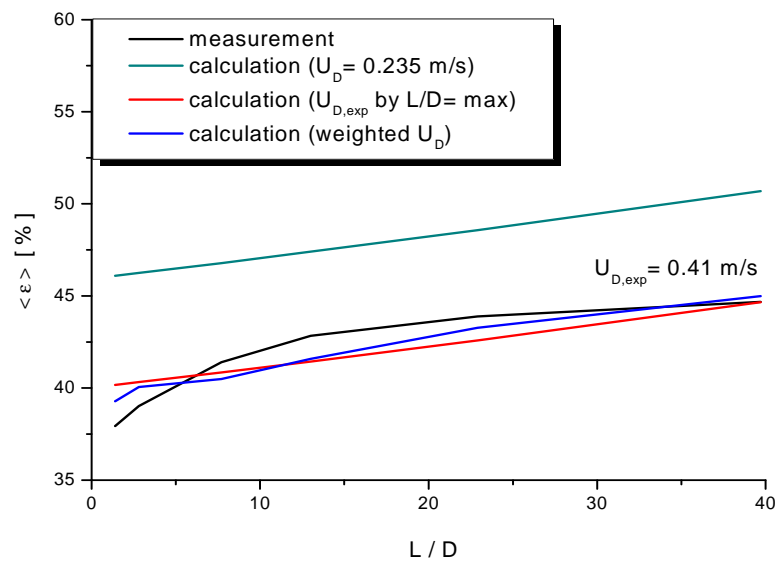
measurement point129 ($J_L = 1.017$ m/s; $J_G = 0.342$ m/s; $D_{\text{Orifice}} = 4$ mm)



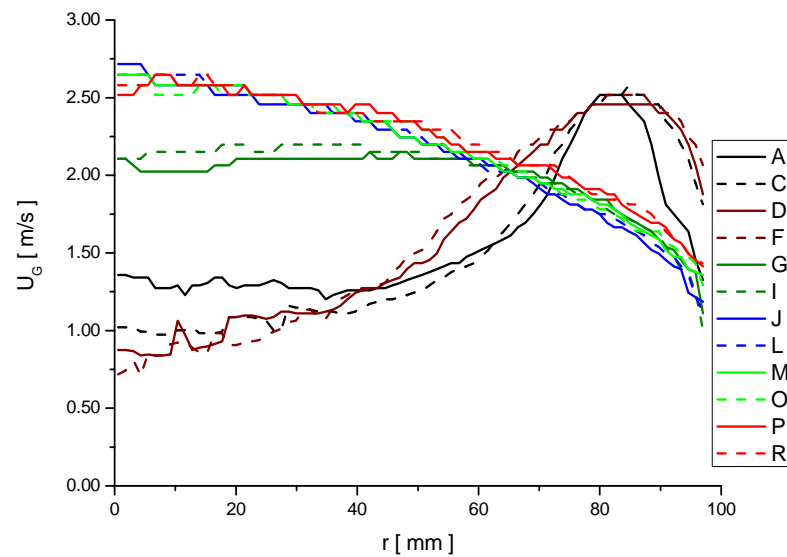
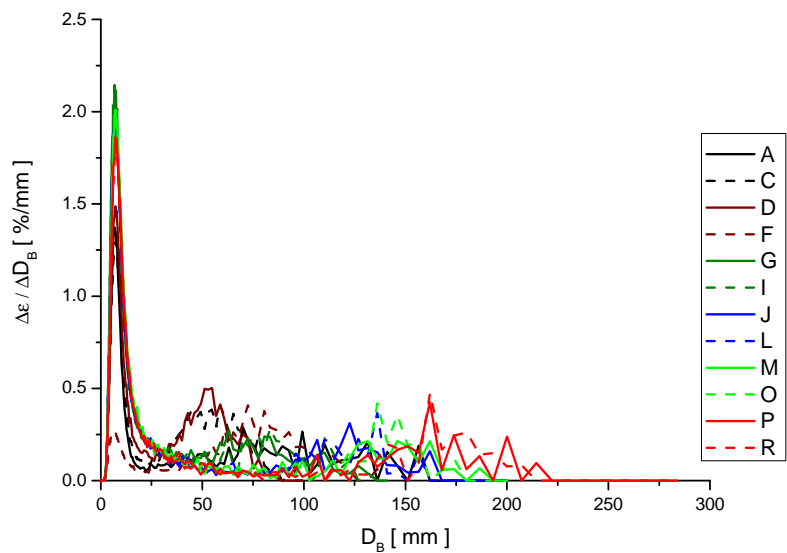
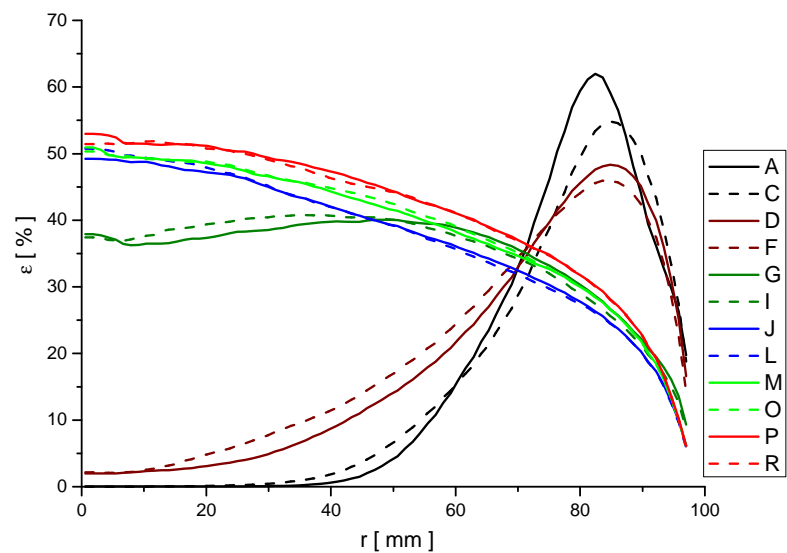
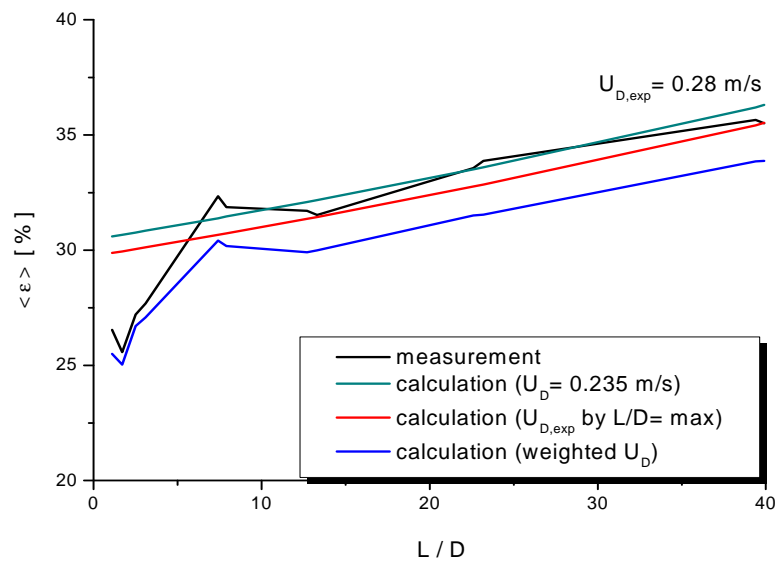
measurement point 138 ($J_L = 0.405$ m/s; $J_G = 0.534$ m/s; $D_{\text{Orifice}} = 1$ mm)



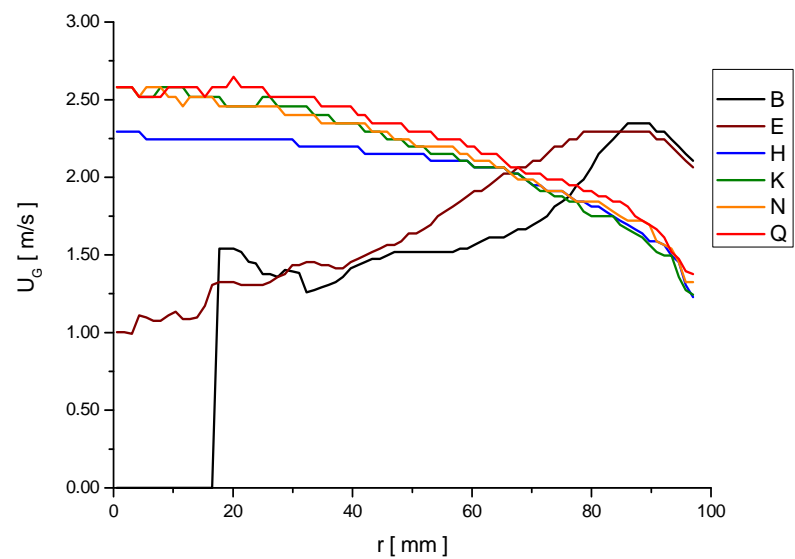
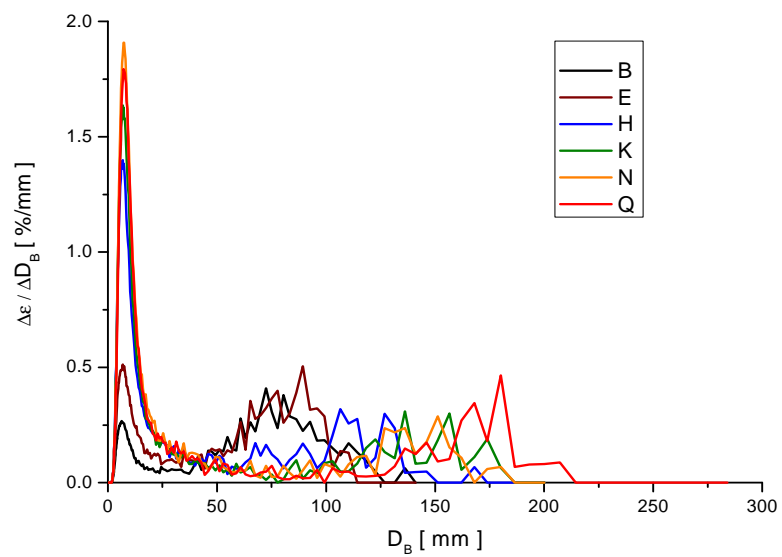
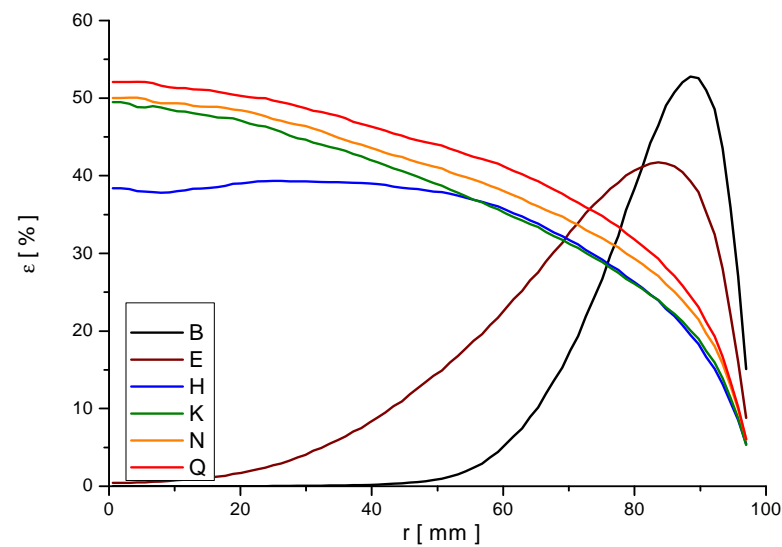
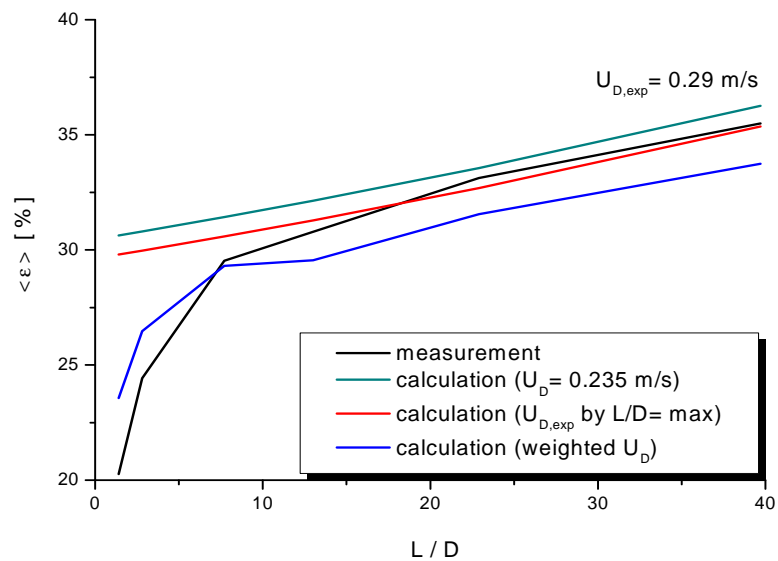
measurement point 138 ($J_L = 0.405$ m/s; $J_G = 0.534$ m/s; $D_{\text{Orifice}} = 4$ mm)



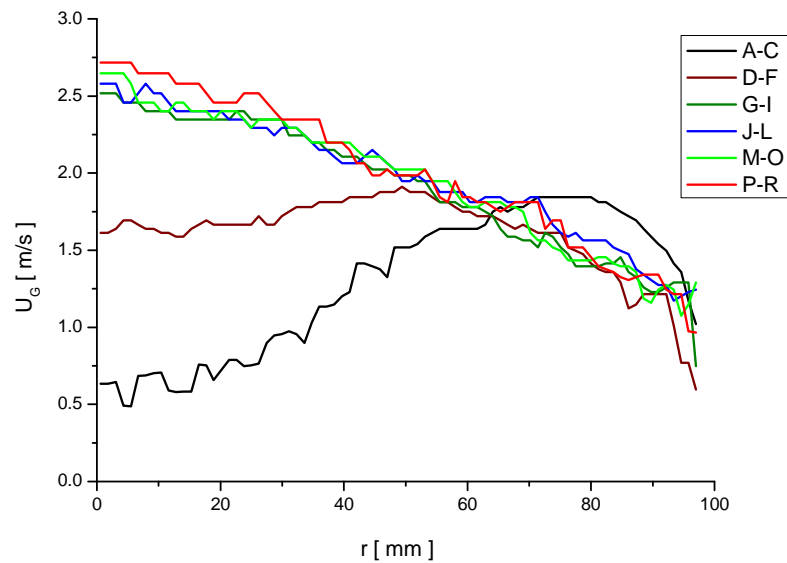
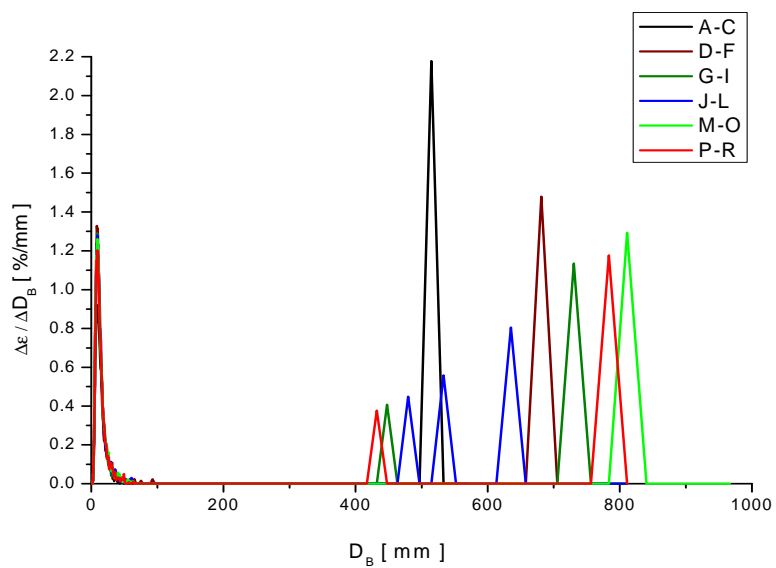
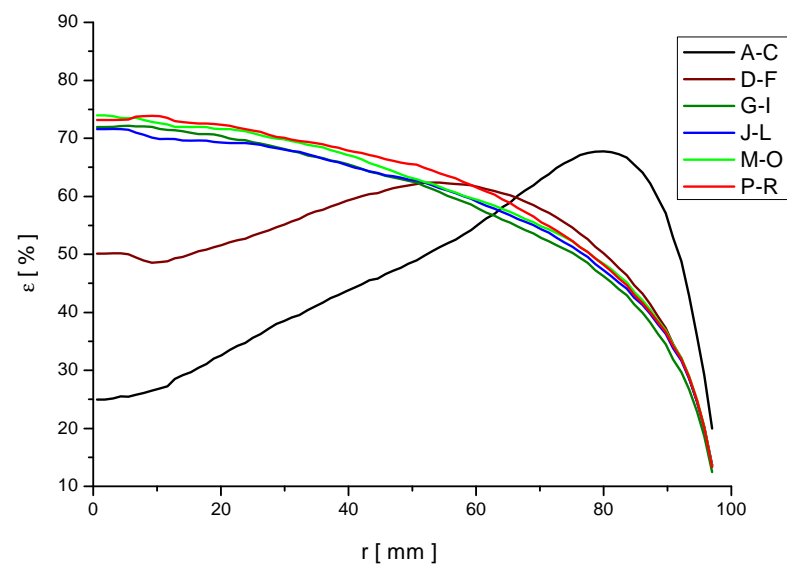
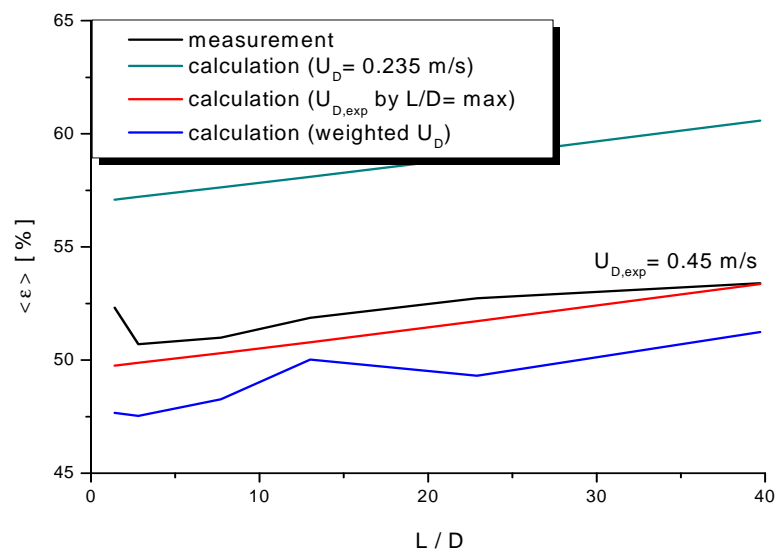
measurement point 140 ($J_L = 1.017$ m/s; $J_G = 0.534$ m/s; $D_{\text{Orifice}} = 1$ mm)



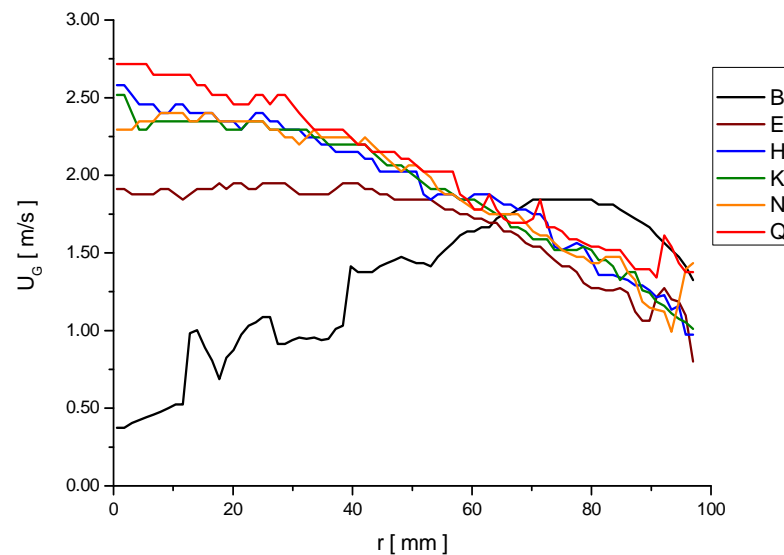
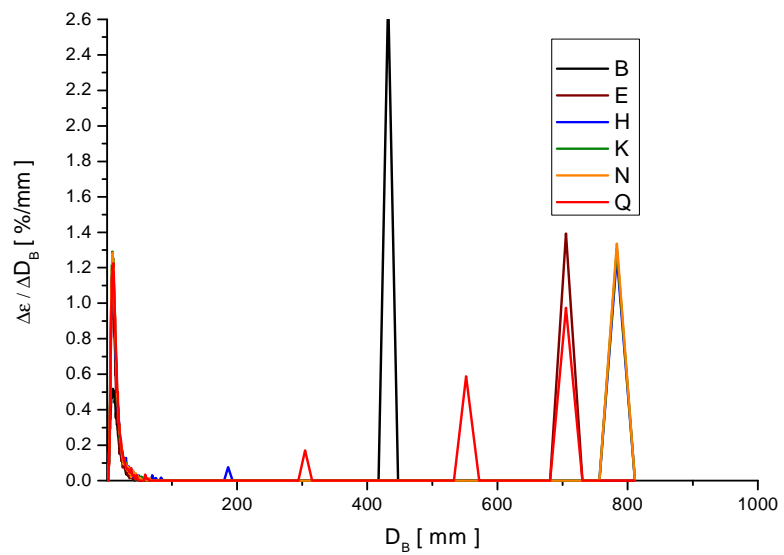
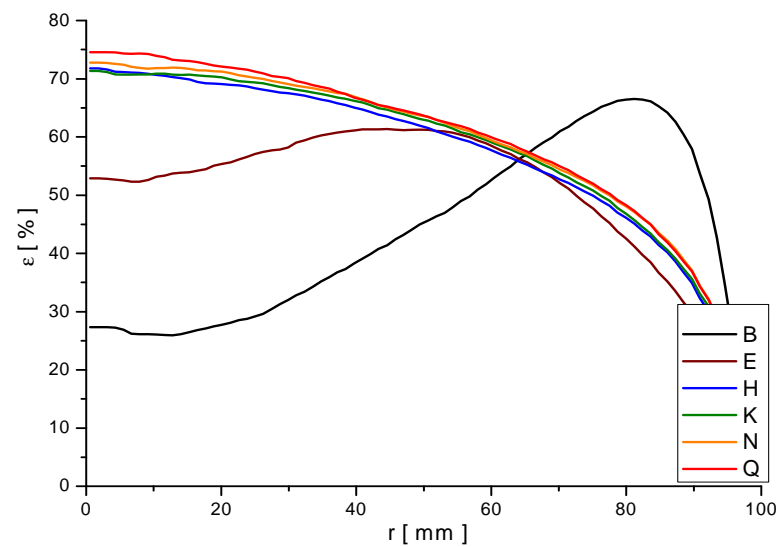
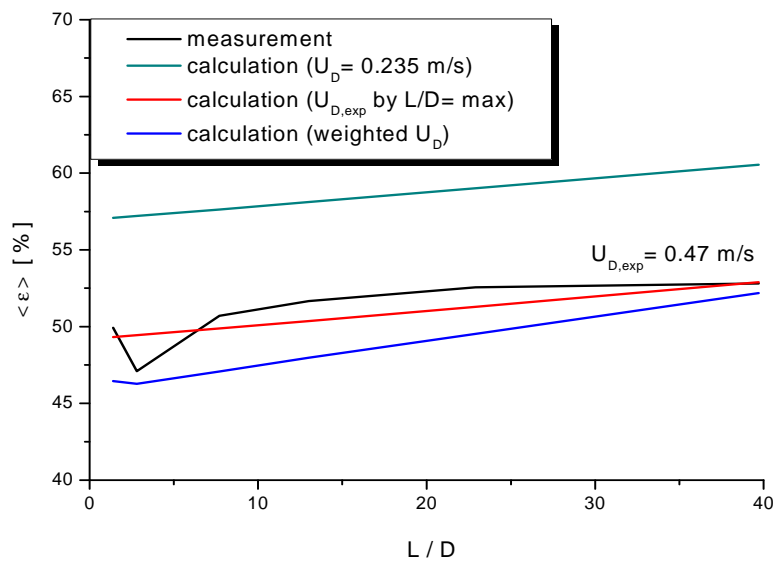
measurement point 140 ($J_L = 1.017$ m/s; $J_G = 0.534$ m/s; $D_{\text{Orifice}} = 4$ mm)



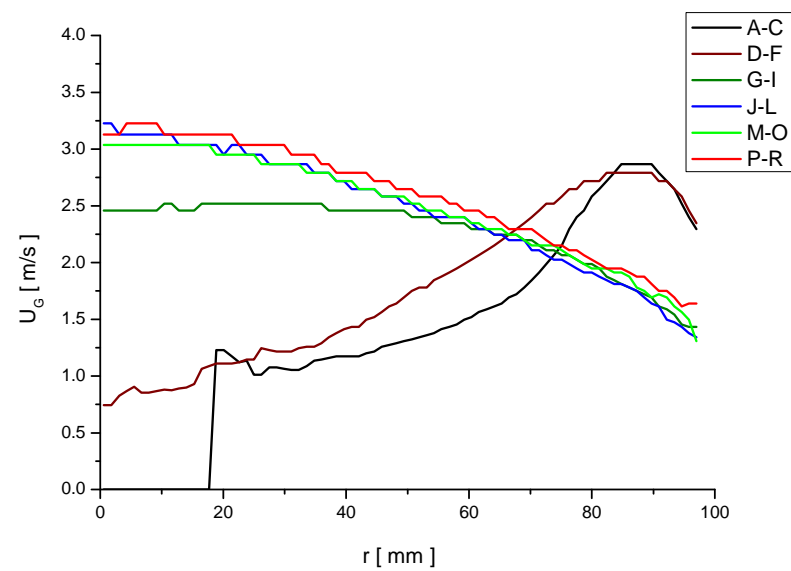
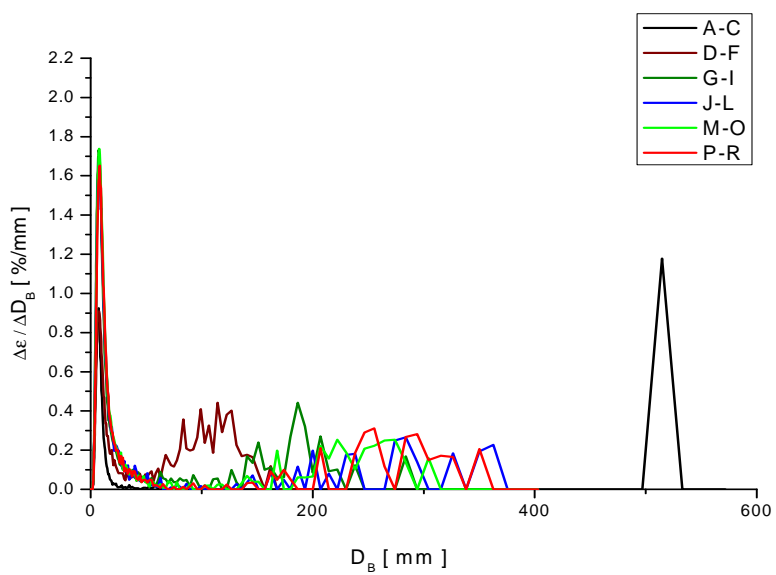
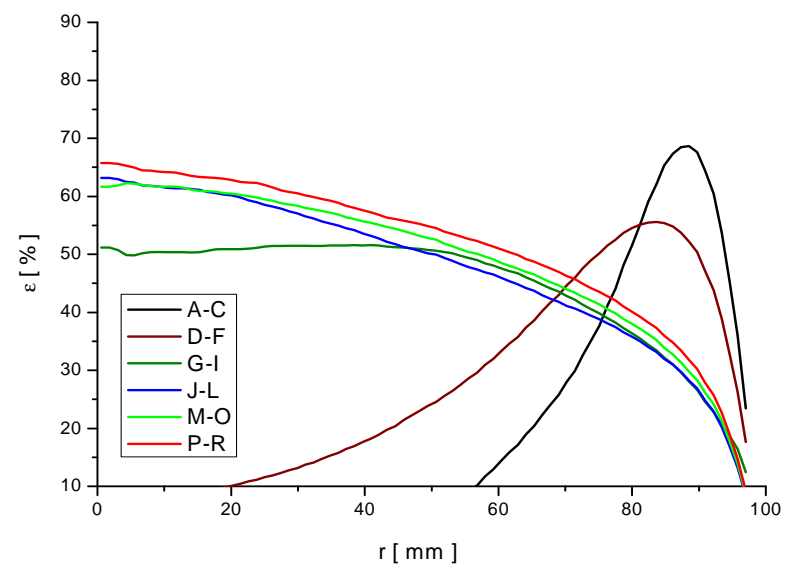
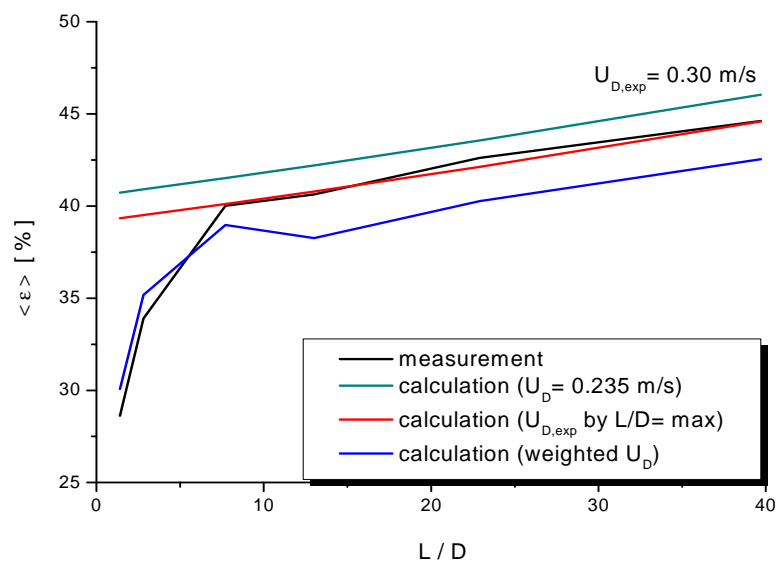
measurement point 149 ($J_L = 0.405$ m/s; $J_G = 0.835$ m/s; $D_{\text{Orifice}} = 1$ mm)



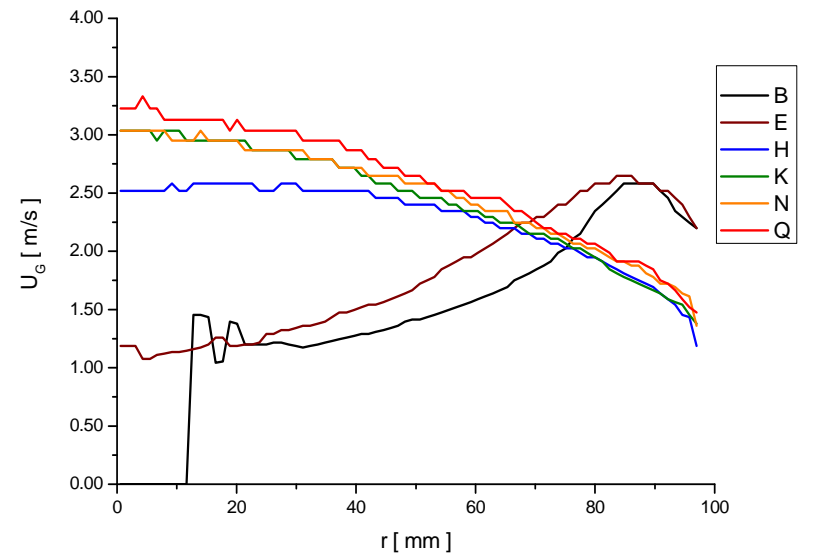
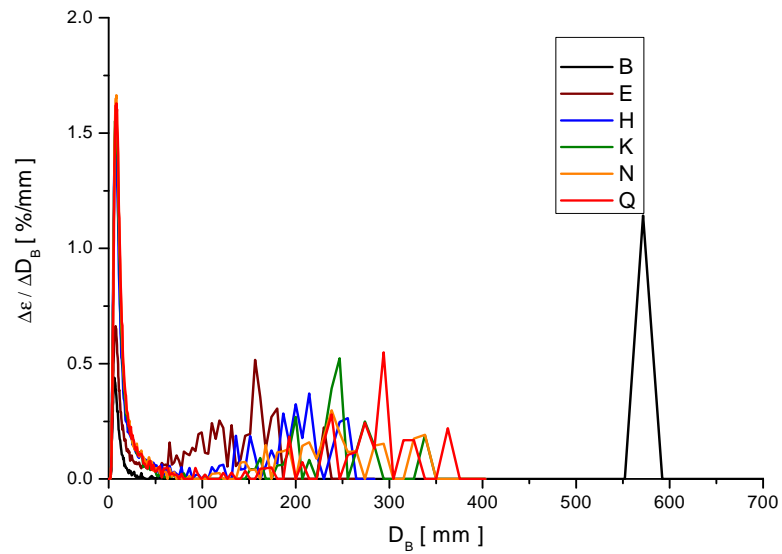
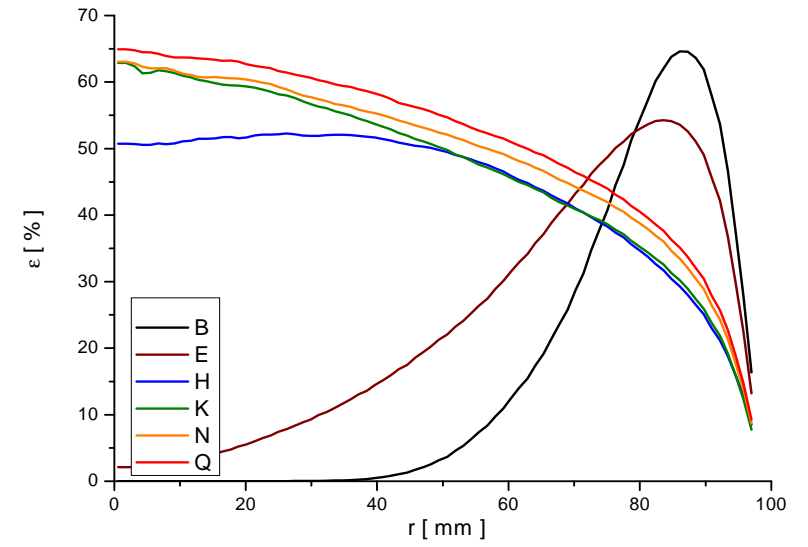
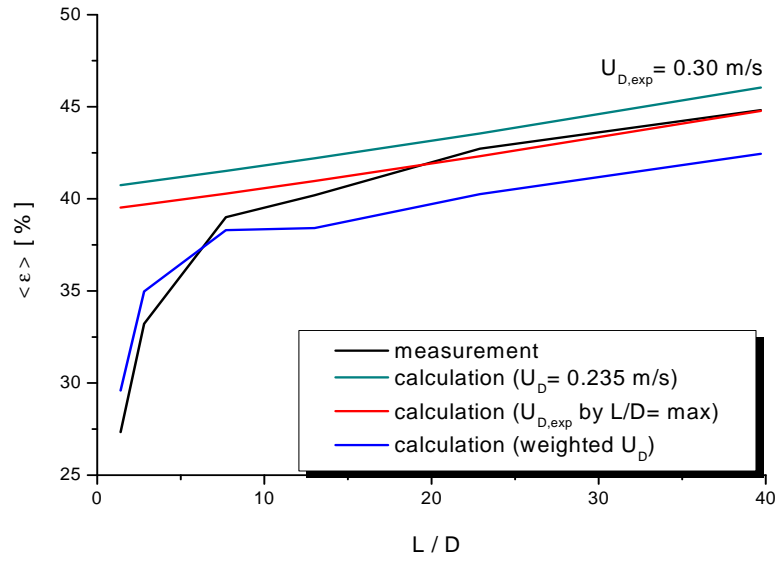
measurement point 149 ($J_L = 0.405$ m/s; $J_G = 0.835$ m/s; $D_{\text{Orifice}} = 4$ mm)



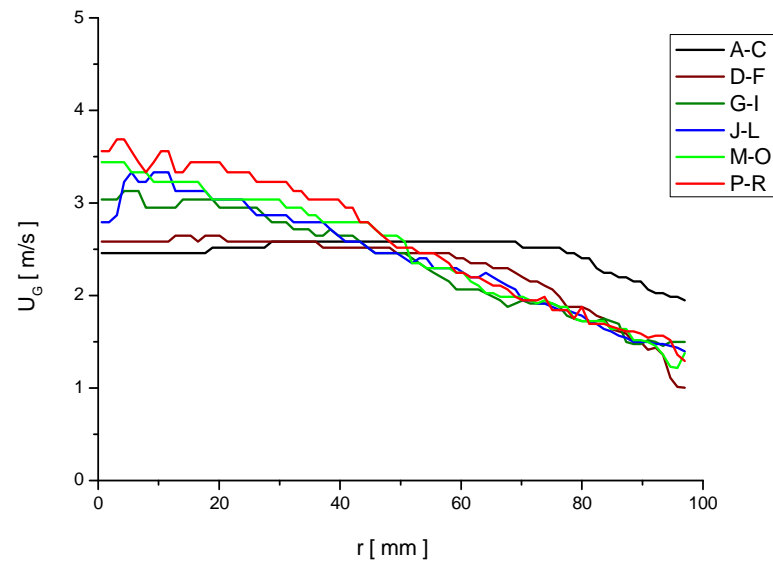
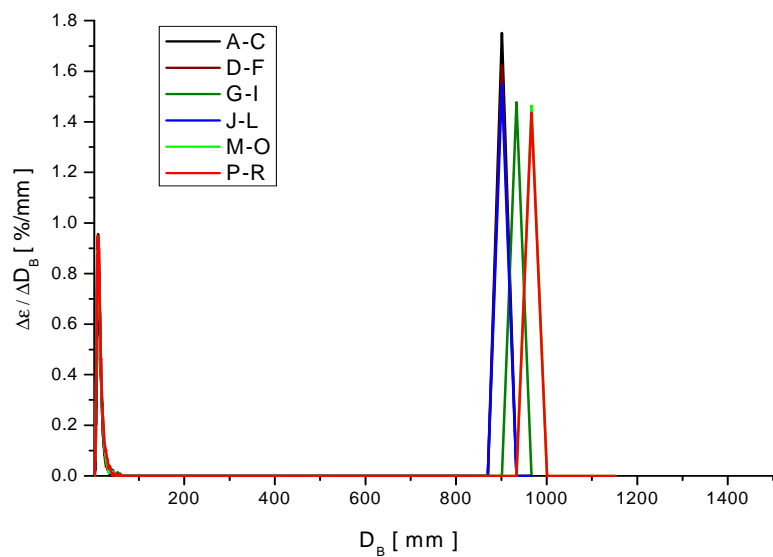
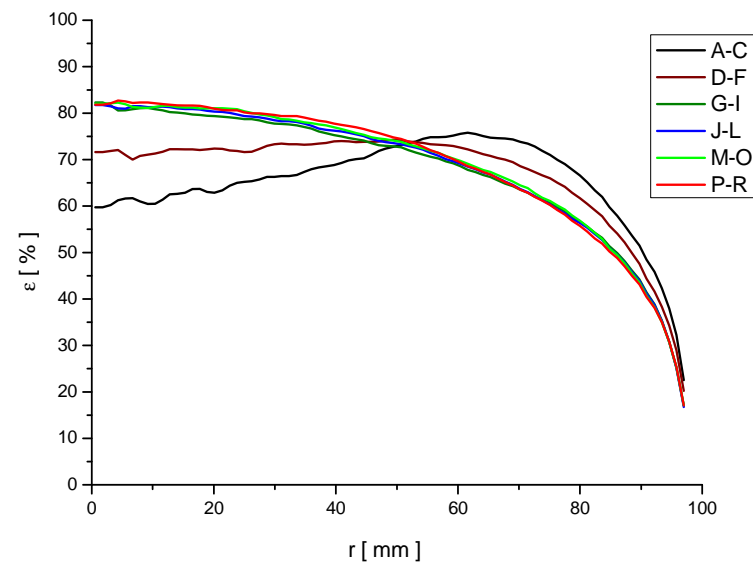
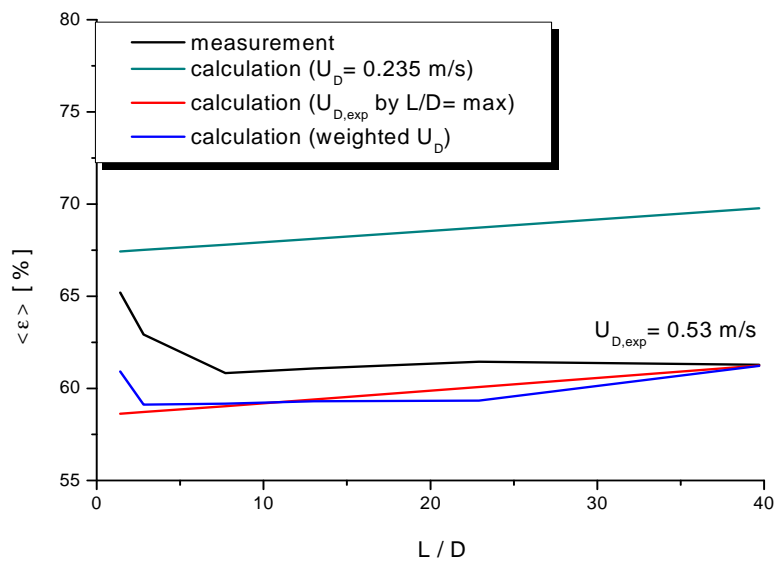
measurement point 151 ($J_L = 1.017$ m/s; $J_G = 0.835$ m/s; $D_{\text{Orifice}} = 1$ mm)



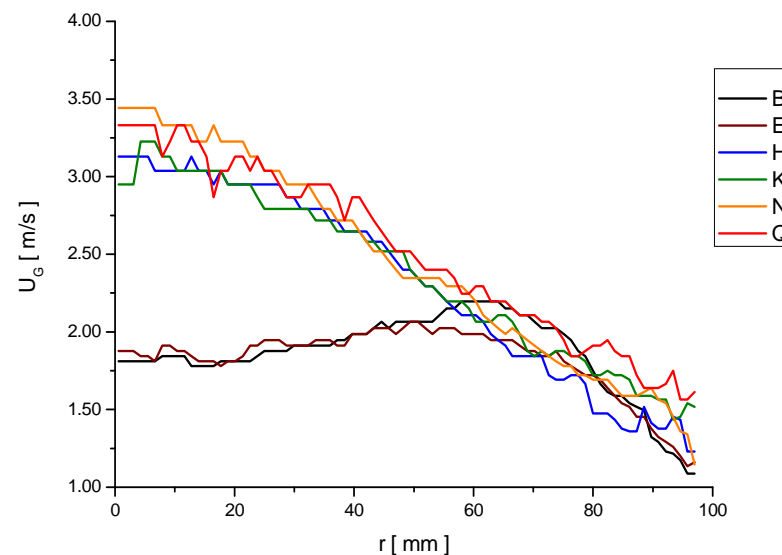
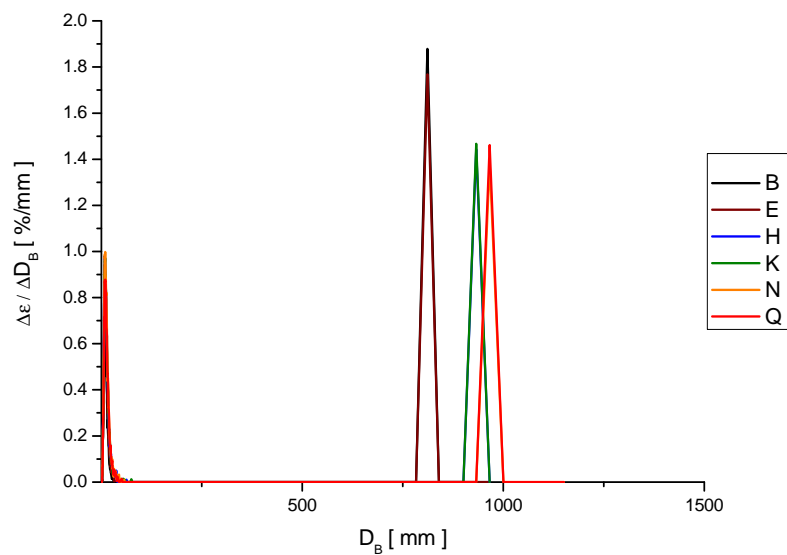
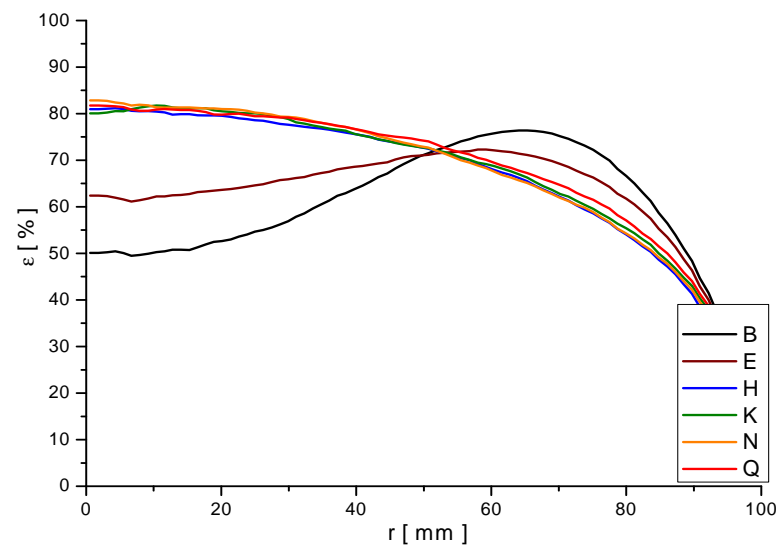
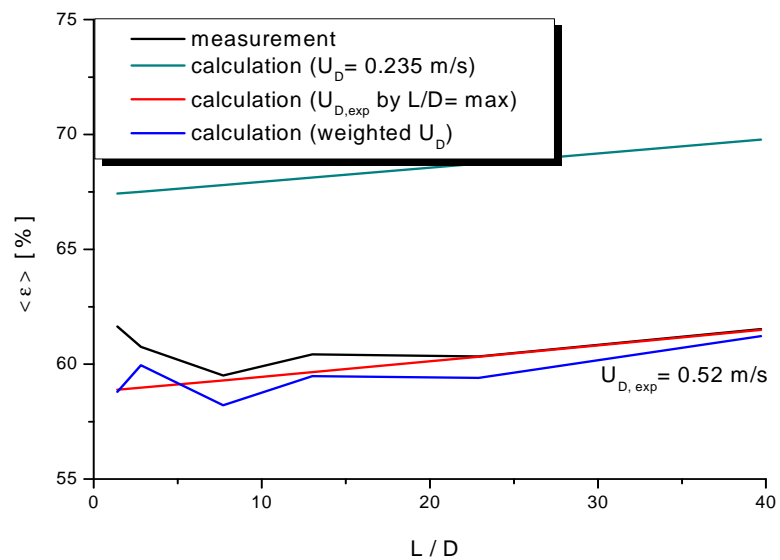
measurement point151 ($J_L = 1.017$ m/s; $J_G = 0.835$ m/s; $D_{\text{Orifice}} = 4$ mm)



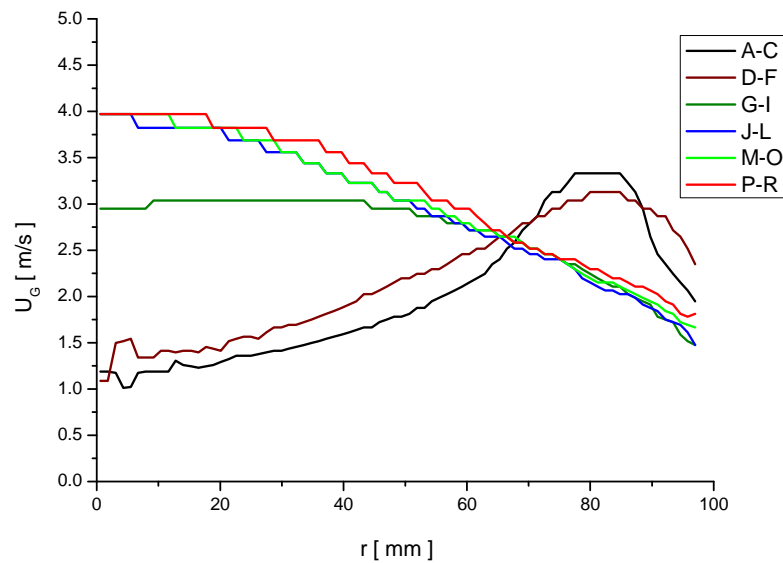
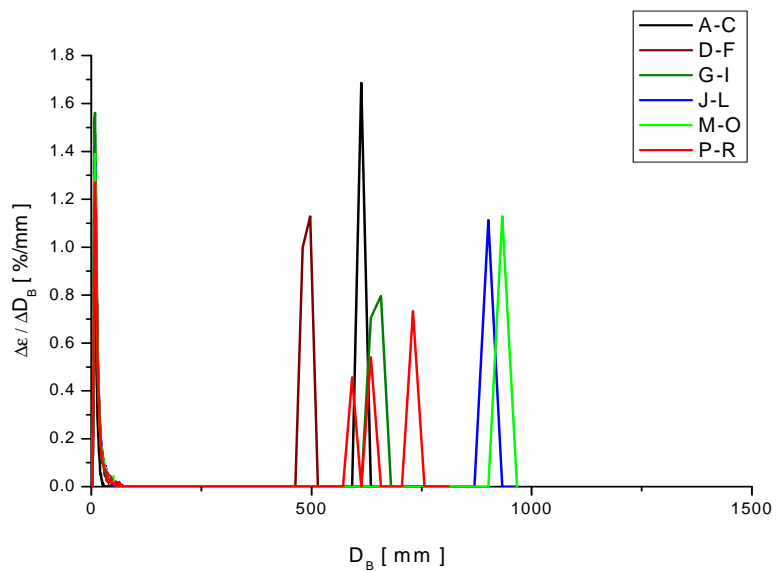
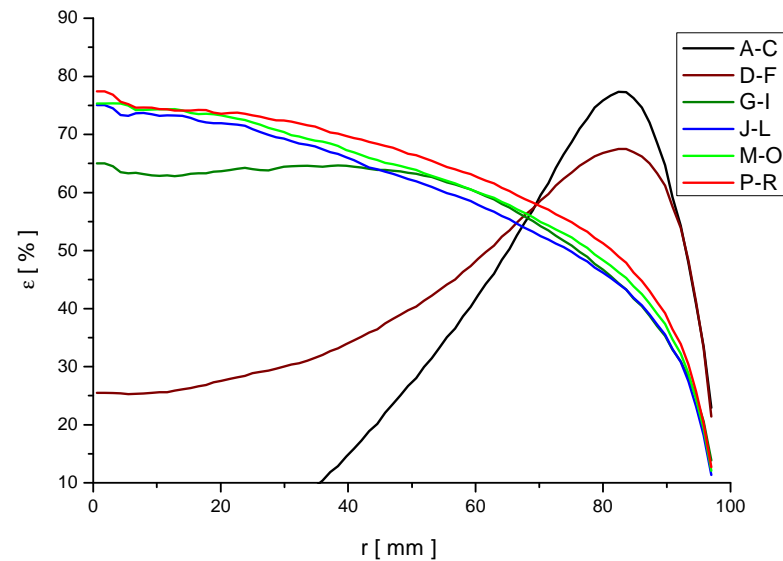
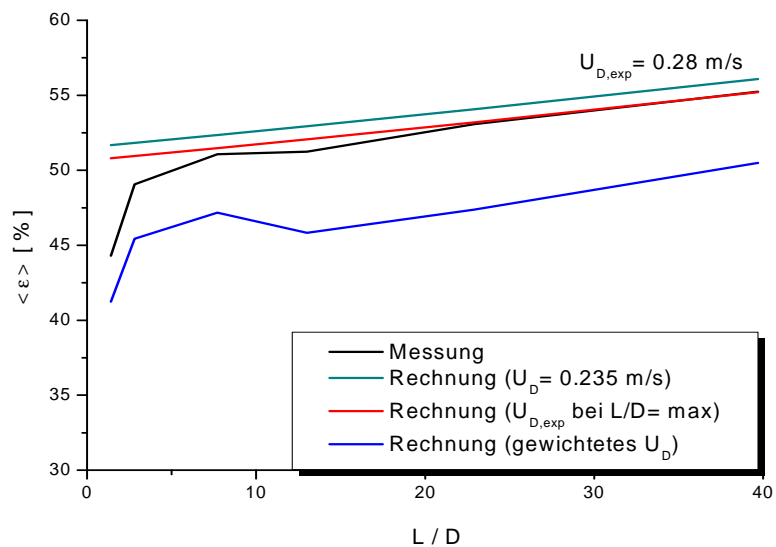
measurement point 160 ($J_L = 0.405$ m/s; $J_G = 1.305$ m/s; $D_{\text{Orifice}} = 1$ mm)



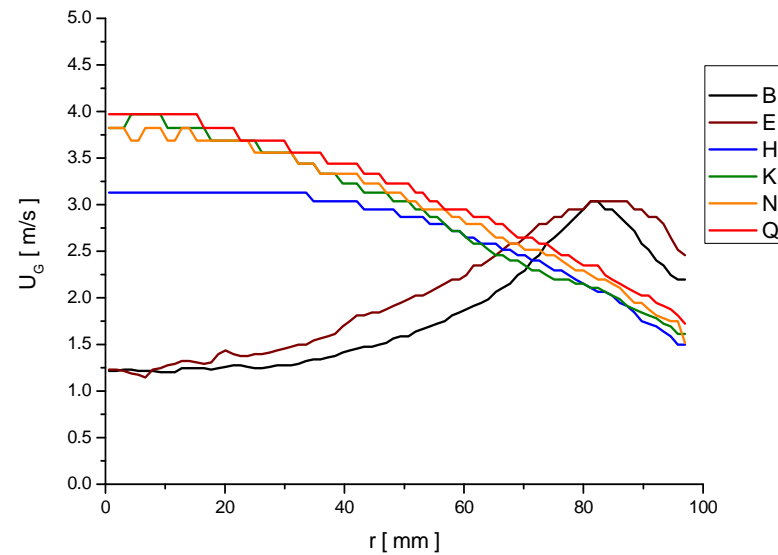
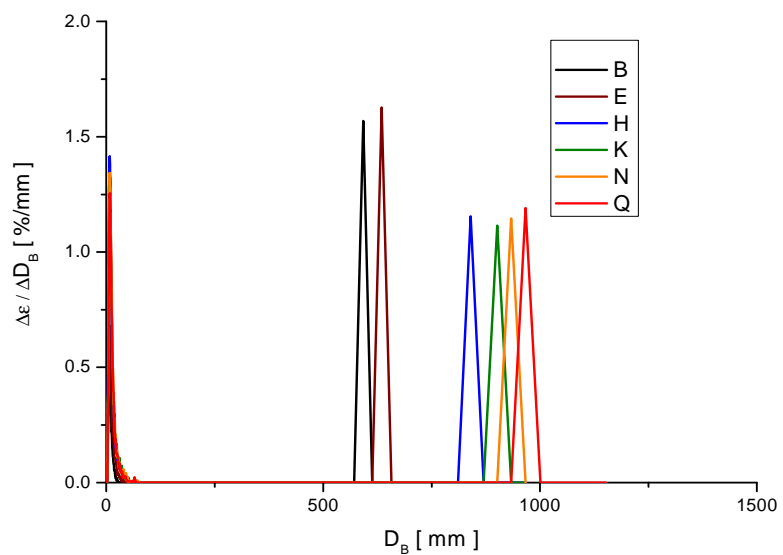
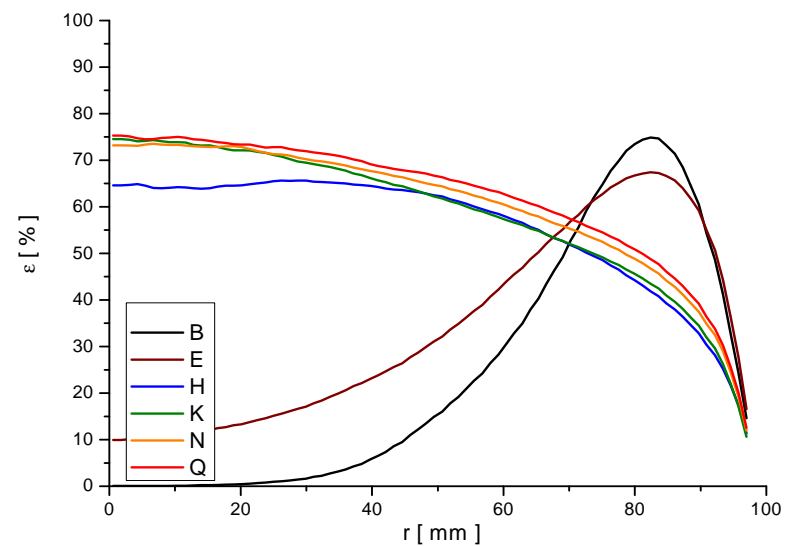
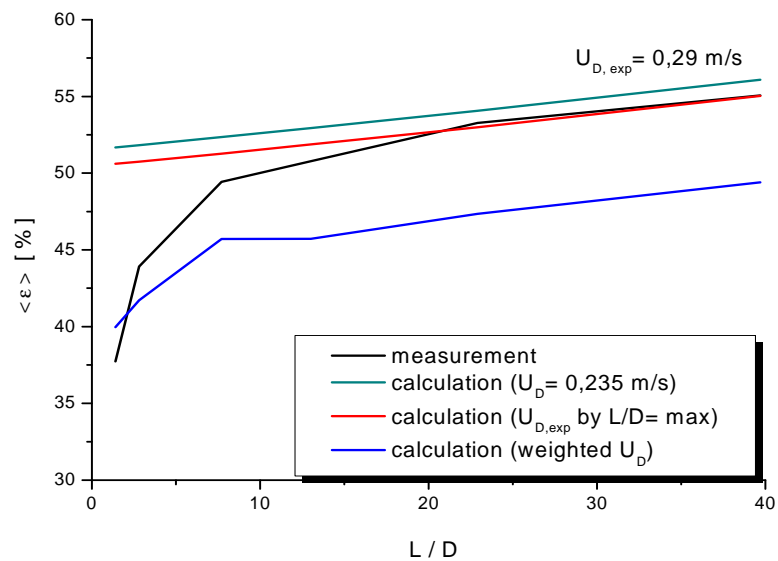
measurement point 160 ($J_L = 0.405$ m/s; $J_G = 1.305$ m/s; $D_{\text{Orifice}} = 4$ mm)



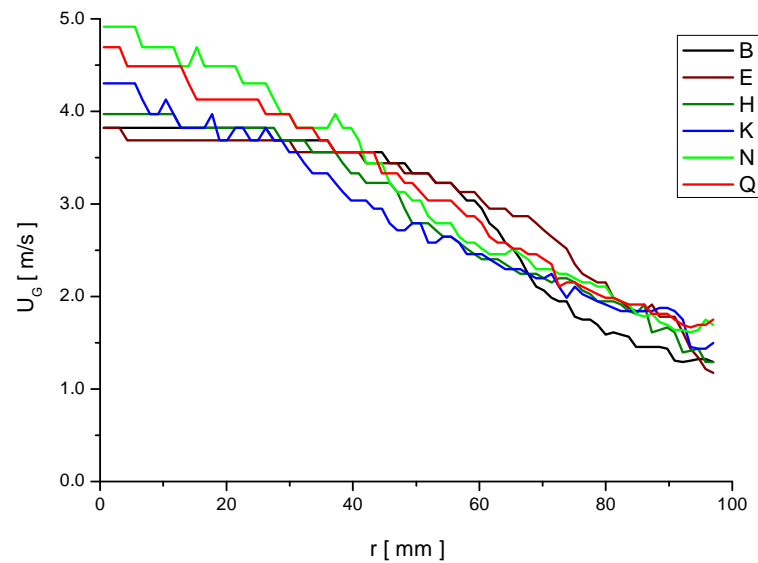
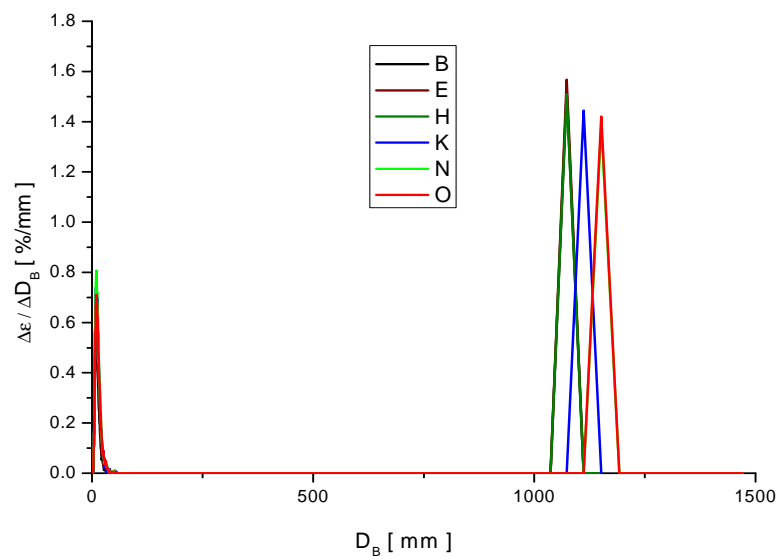
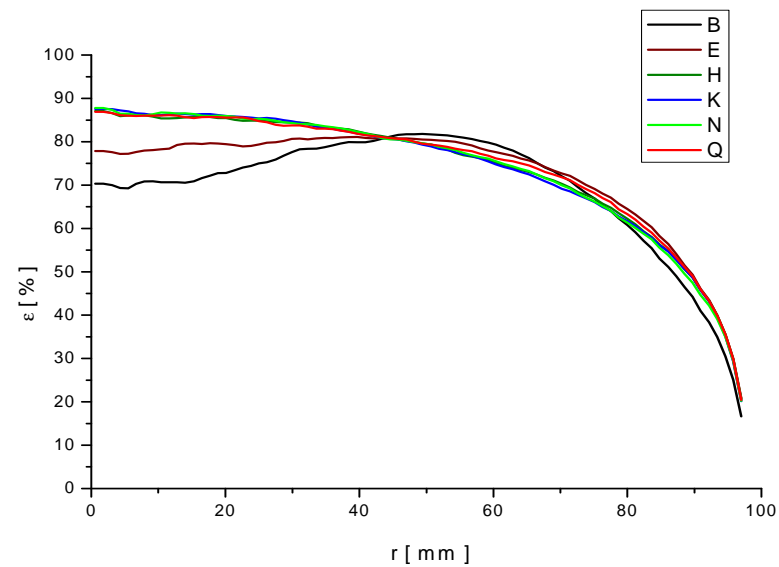
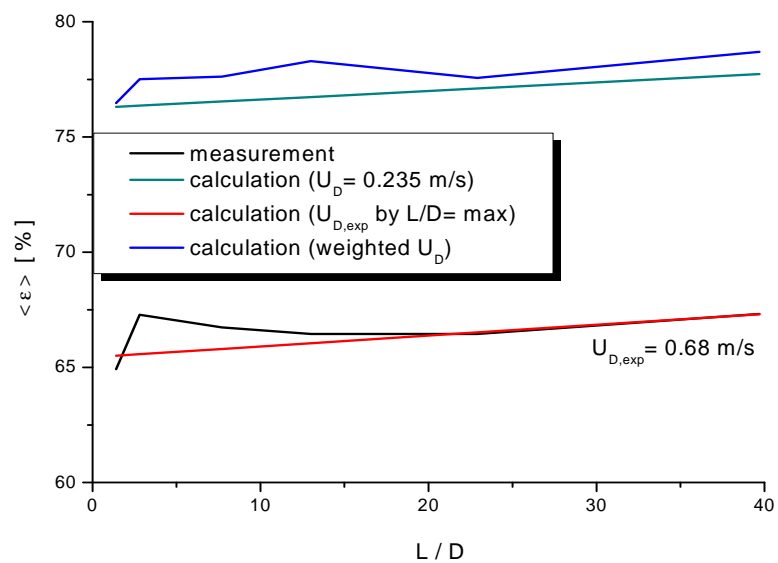
measurement point 162 ($J_L = 1.017$ m/s; $J_G = 1.305$ m/s; $D_{\text{Orifice}} = 1$ mm)



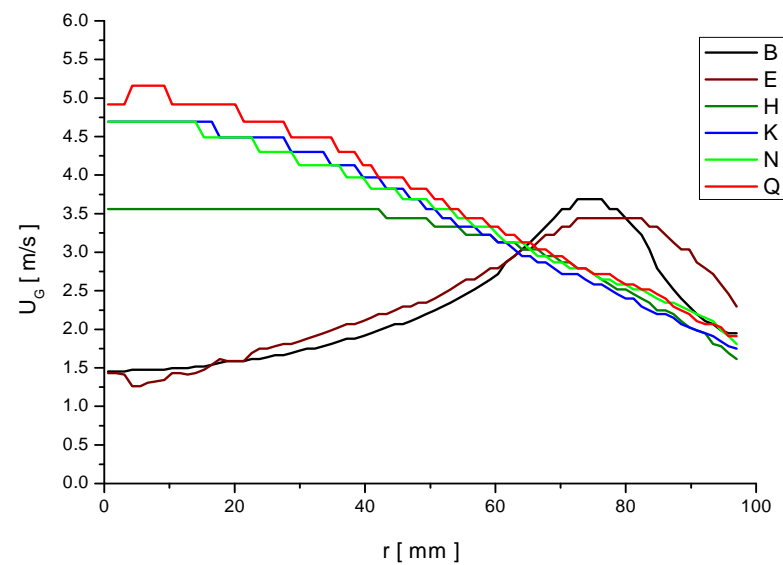
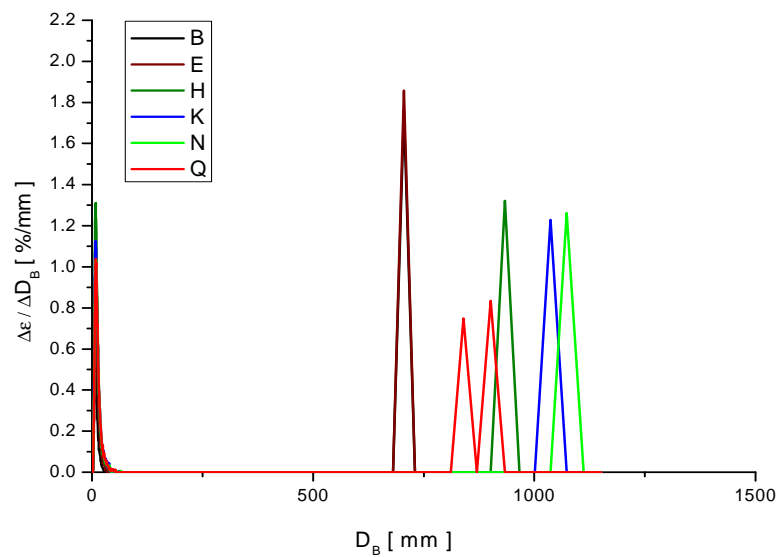
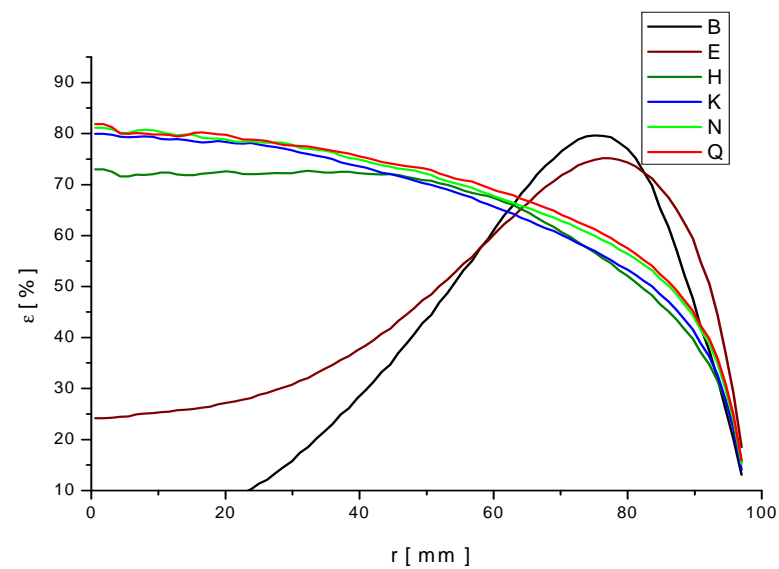
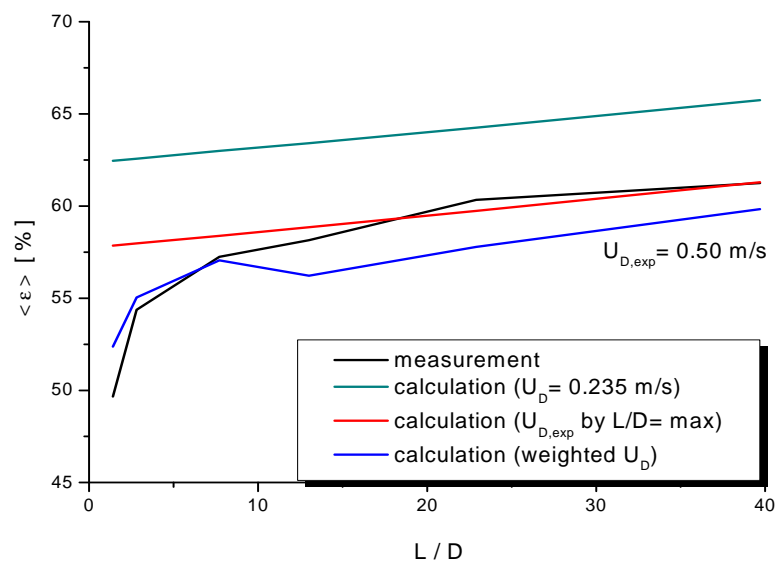
measurement point 162 ($J_L = 1.017$ m/s; $J_G = 1.305$ m/s; $D_{\text{Orifice}} = 4$ mm)



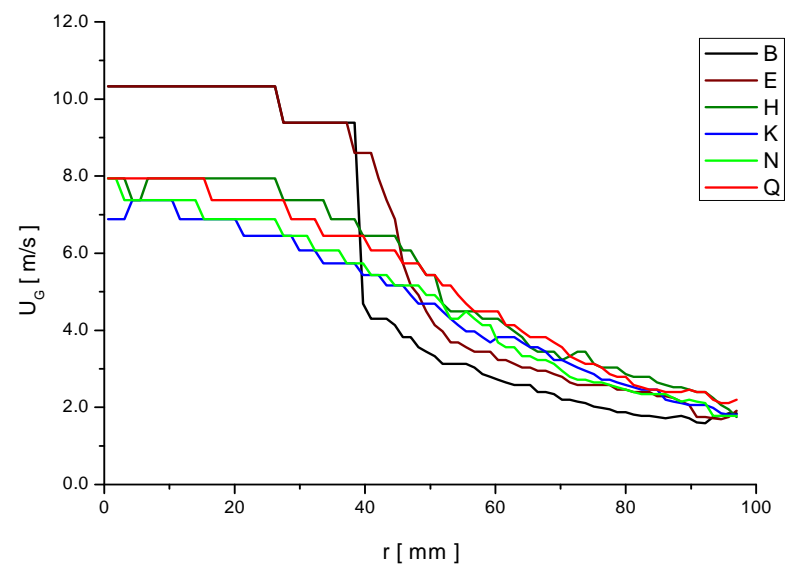
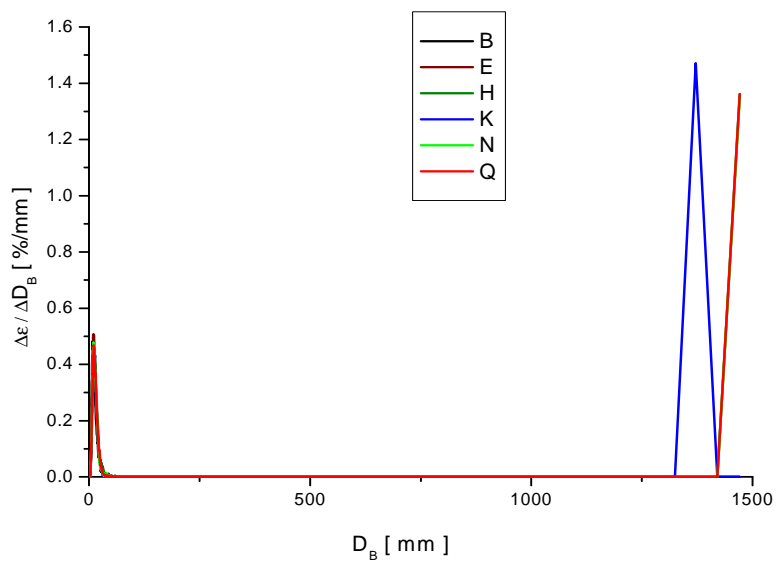
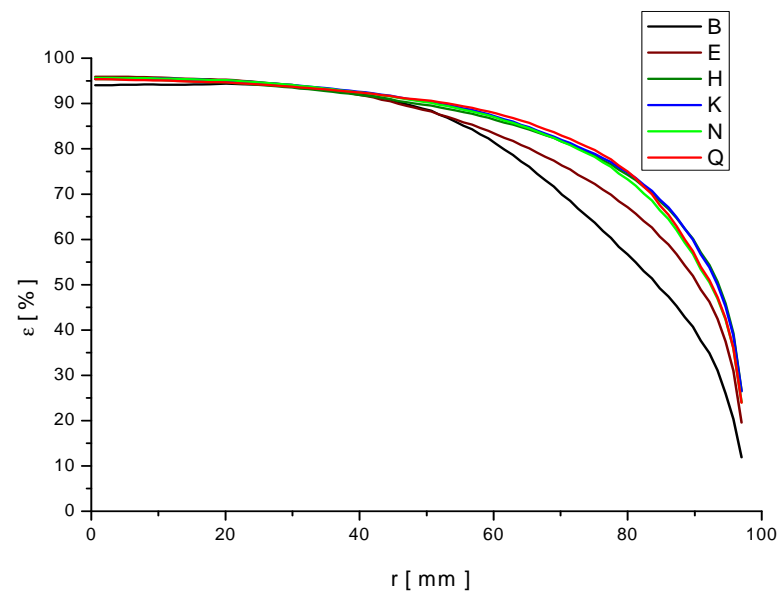
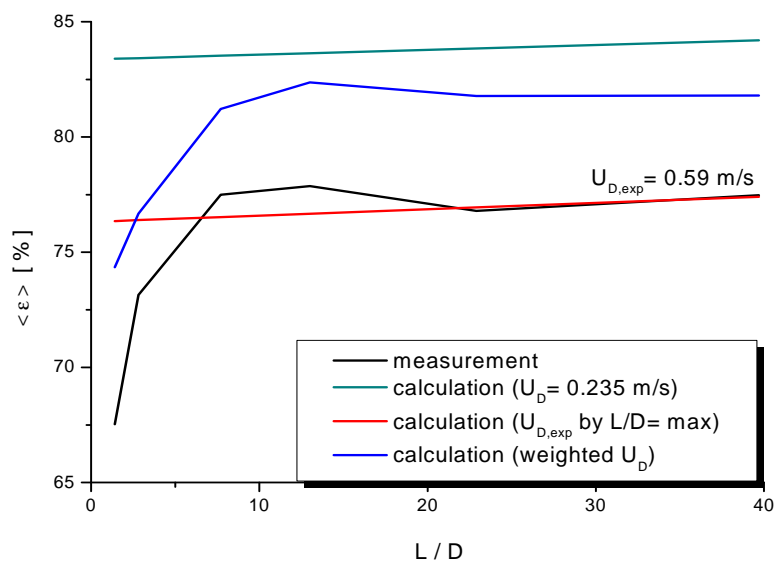
measurement point 171 ($J_L = 0.405$ m/s; $J_G = 2.038$ m/s; $D_{\text{Orifice}} = 4$ mm)



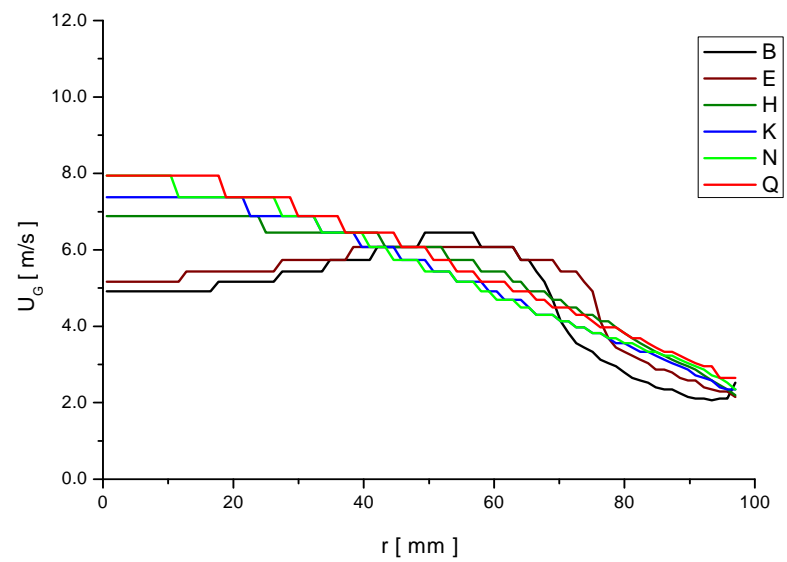
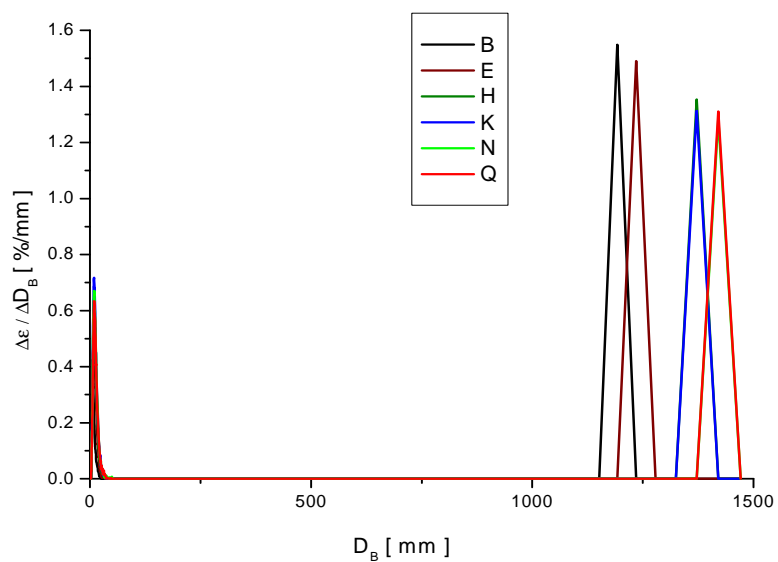
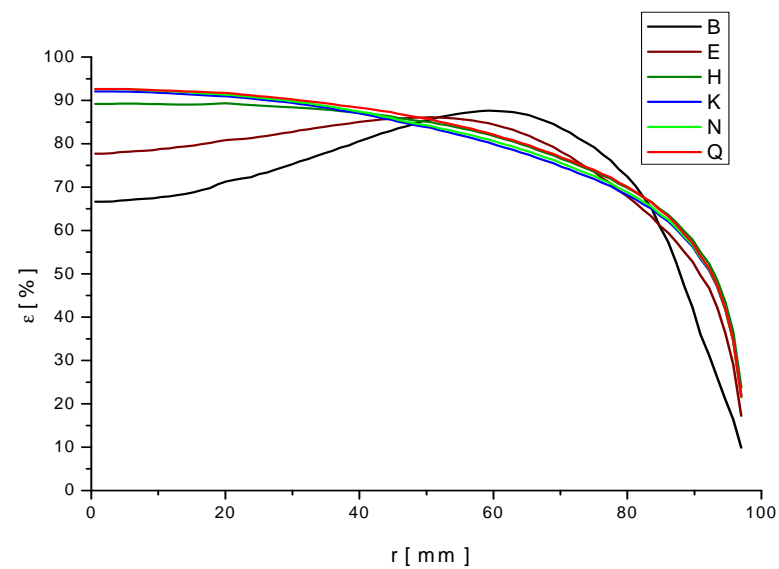
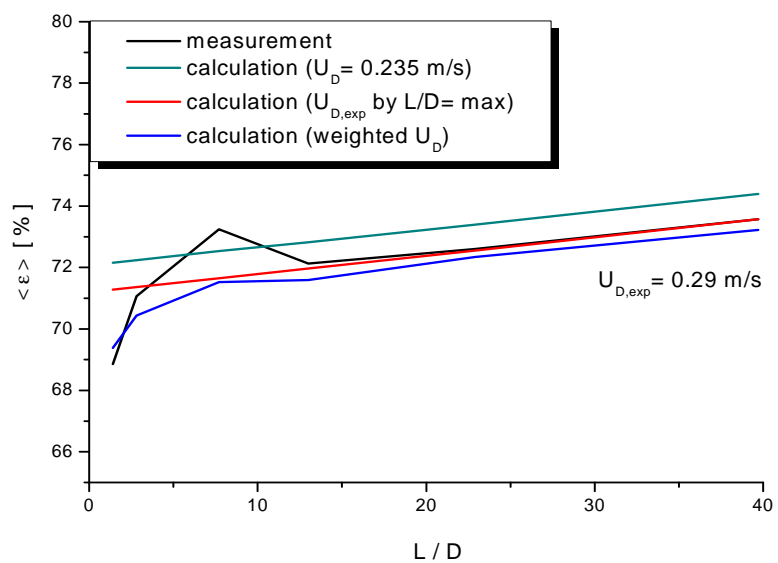
measurement point 173 ($J_L = 1.017$ m/s; $J_G = 2.038$ m/s; $D_{\text{Orifice}} = 4$ mm)



measurement point 182 ($J_L = 0.405$ m/s; $J_G = 3.185$ m/s; $D_{\text{Orifice}} = 4$ mm)

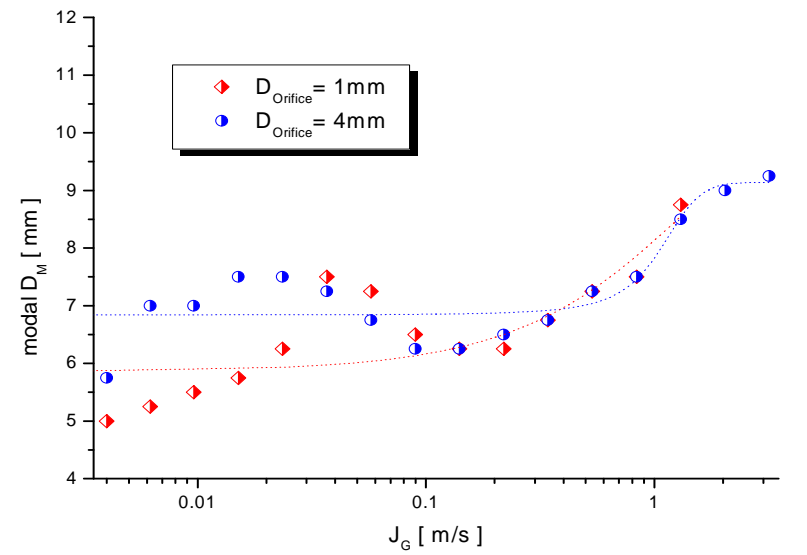
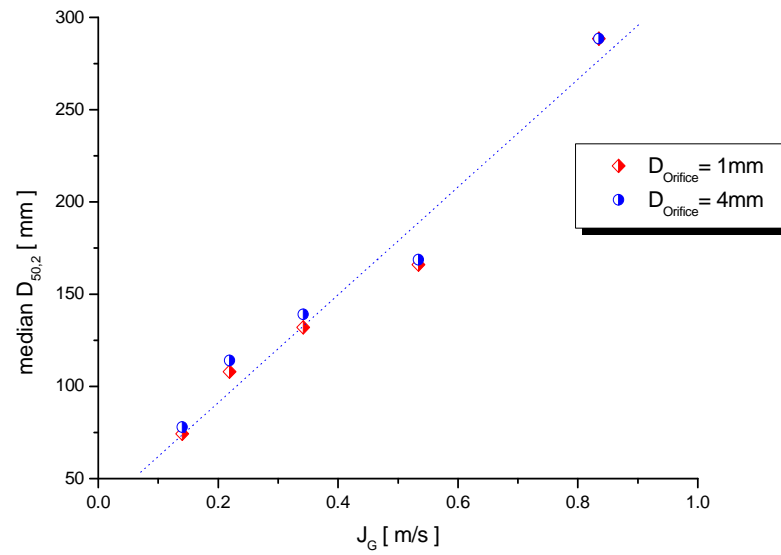
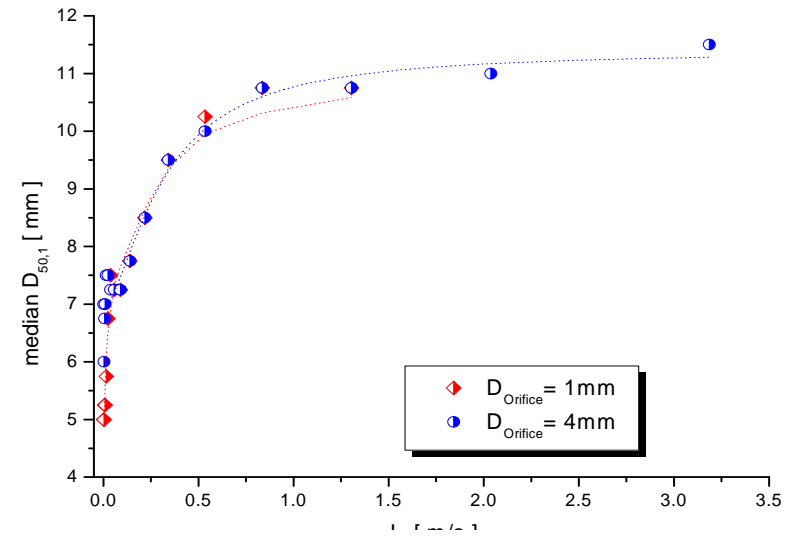
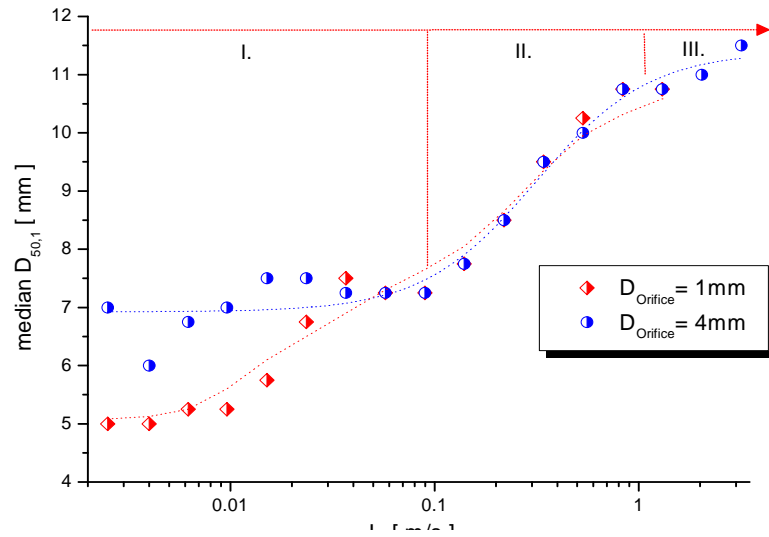


measurement point 184 ($J_L = 1.017$ m/s; $J_G = 3.185$ m/s; $D_{\text{Orifice}} = 4$ mm)

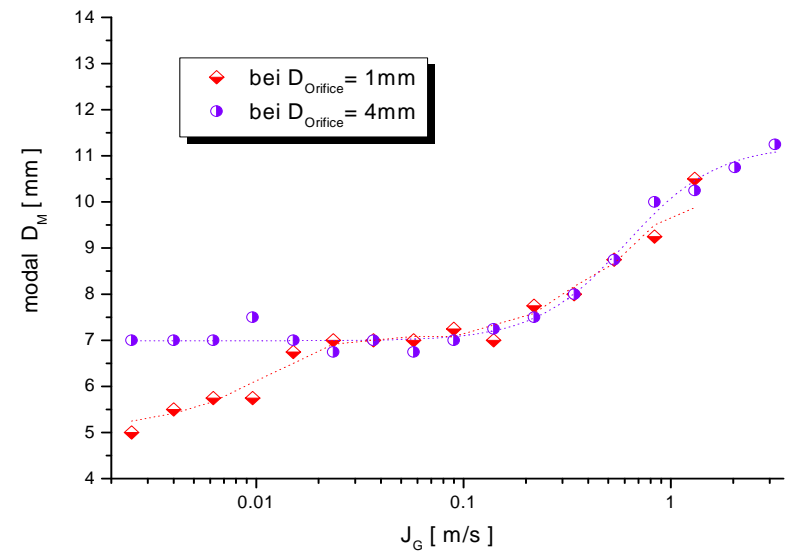
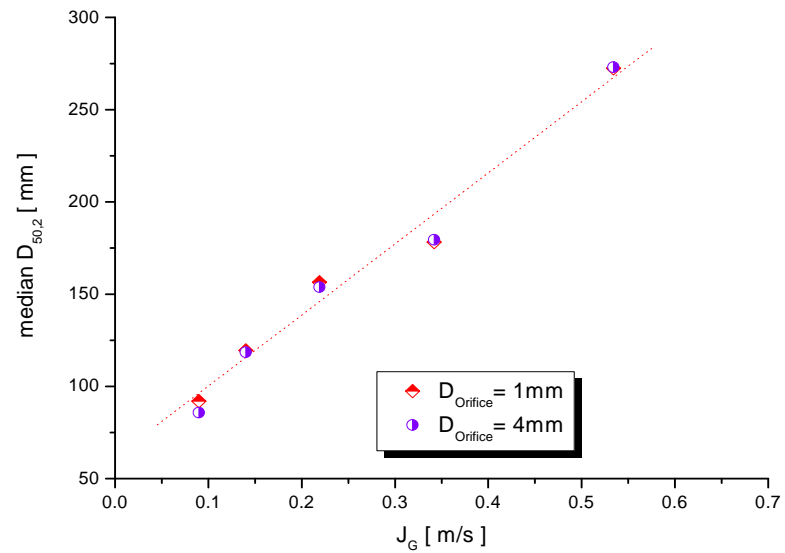
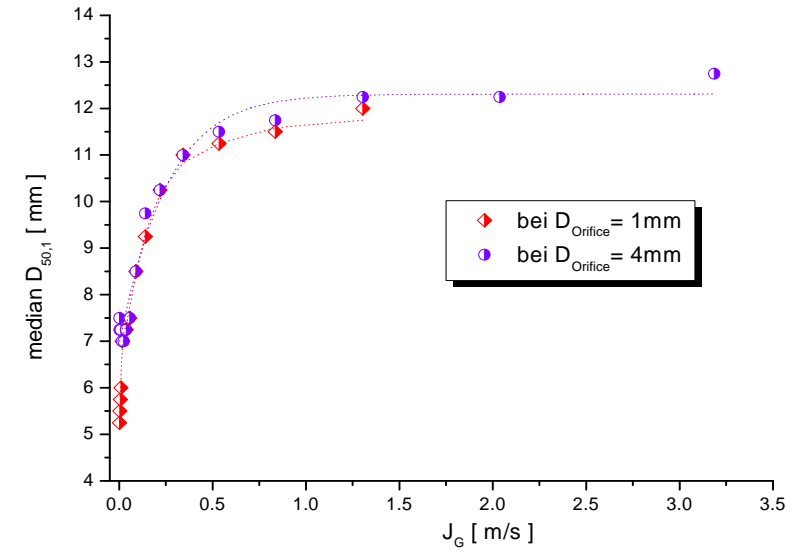
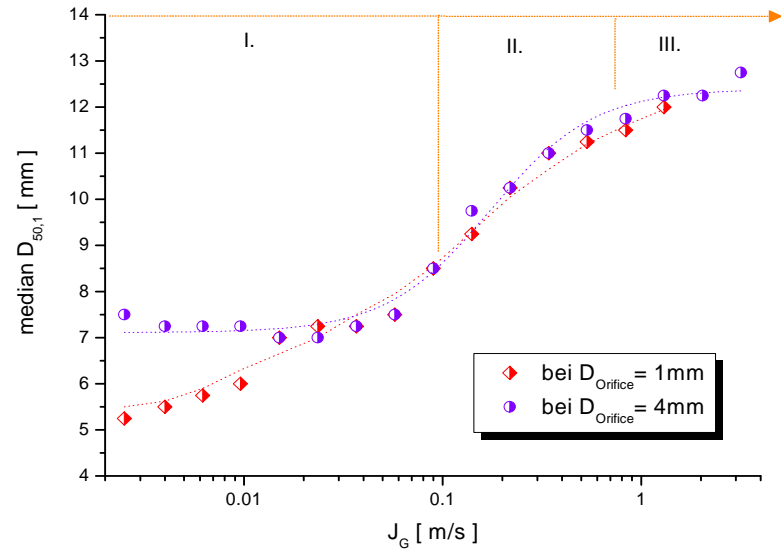


II. Median and Modal

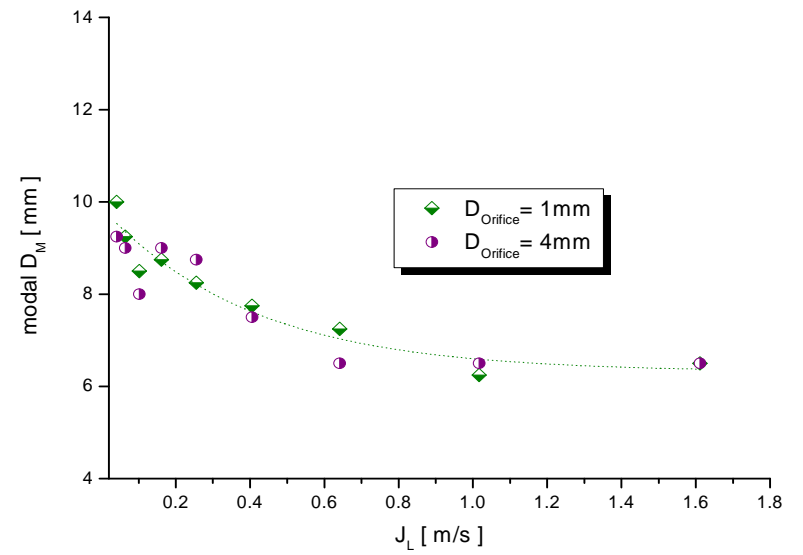
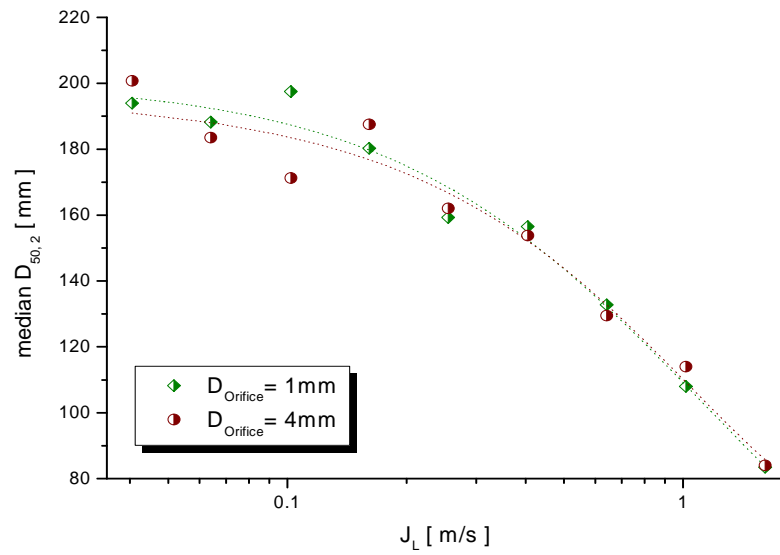
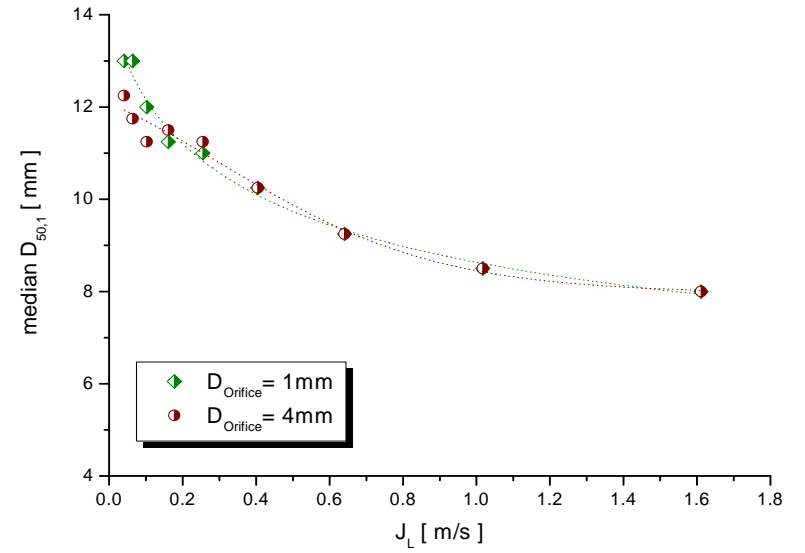
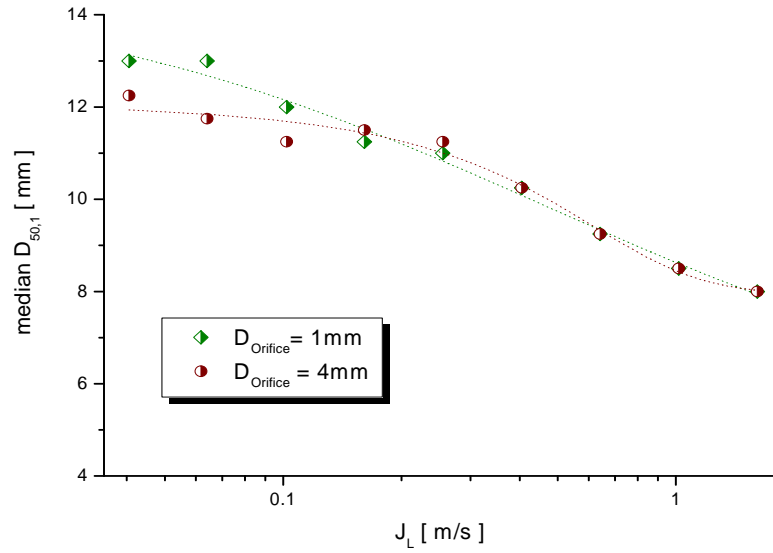
test series I ($J_L = 1.017 \text{ m/s}$)



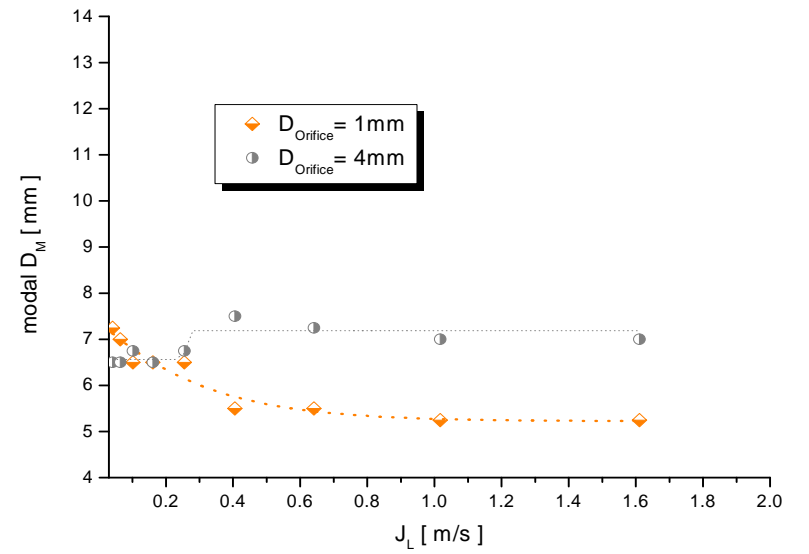
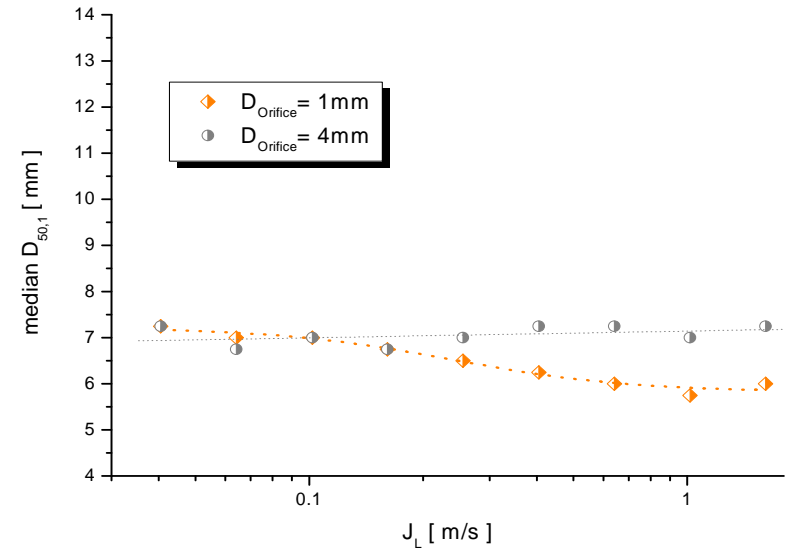
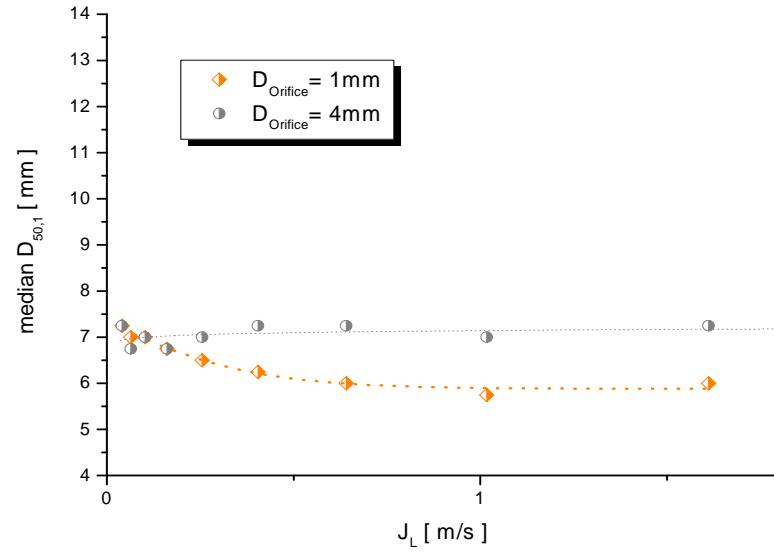
test series II ($J_L = 0.405 \text{ m/s}$)



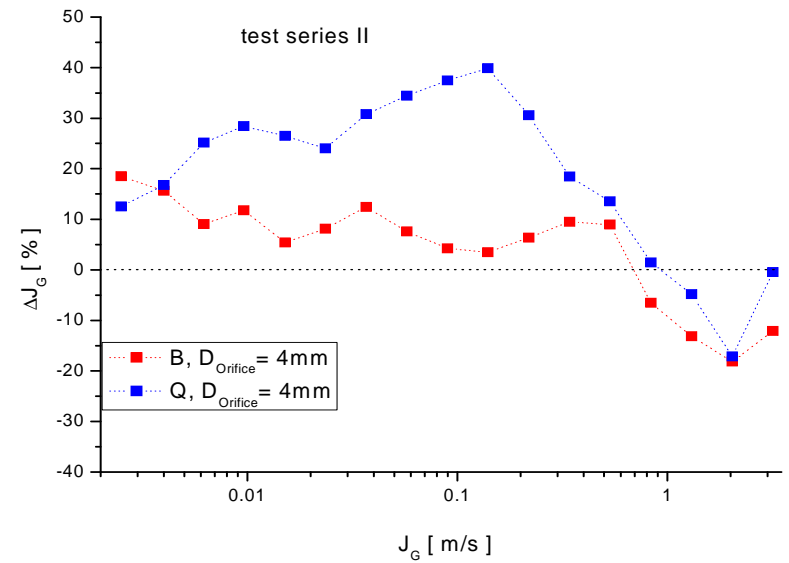
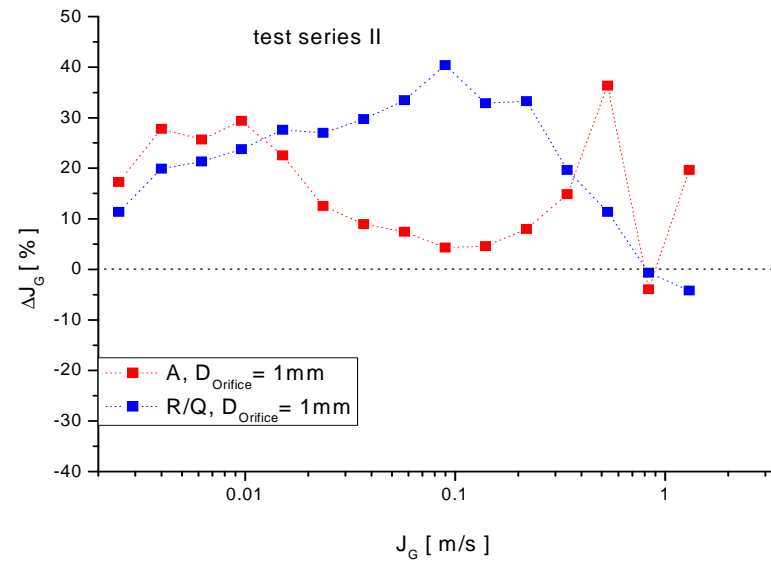
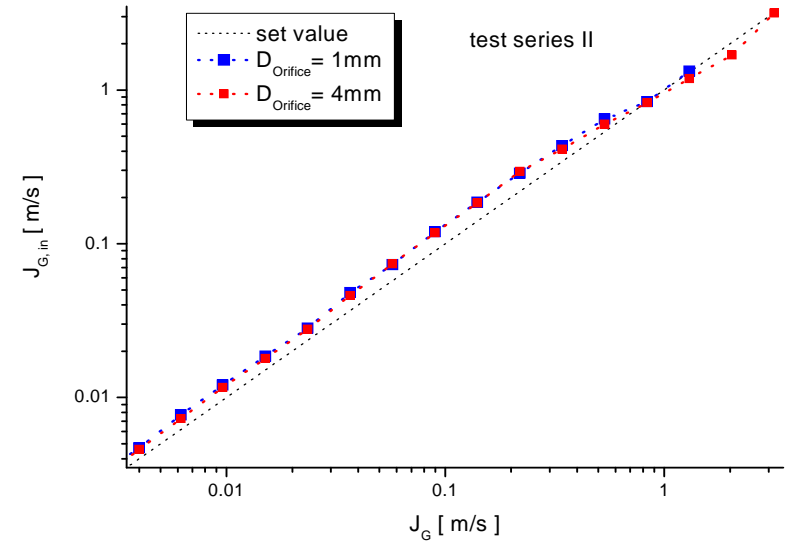
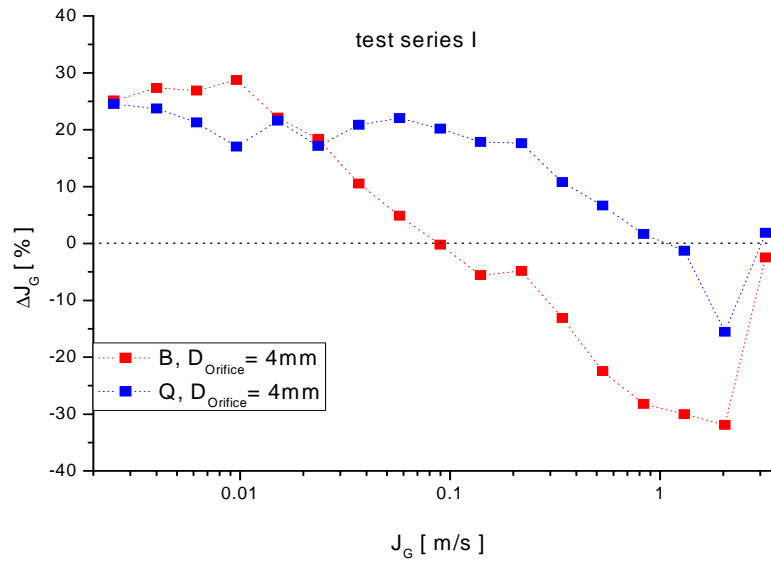
test series III ($J_G = 0.219 \text{ m/s}$)

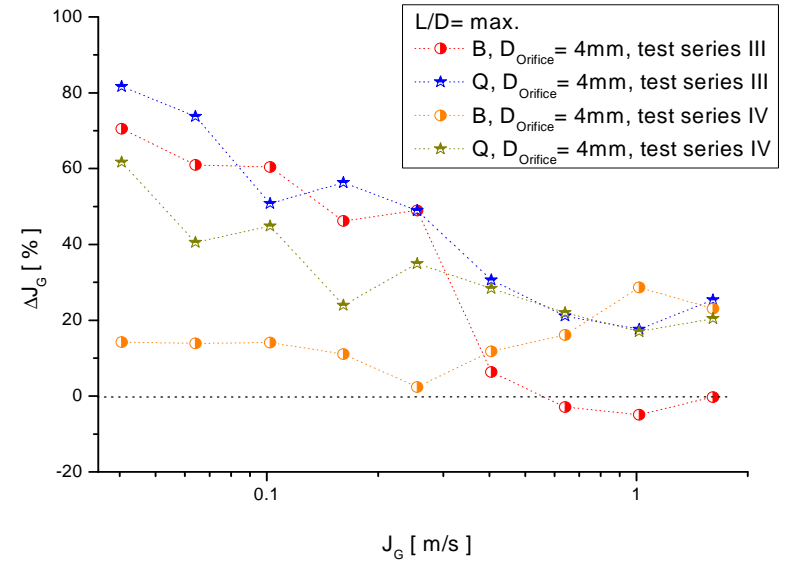
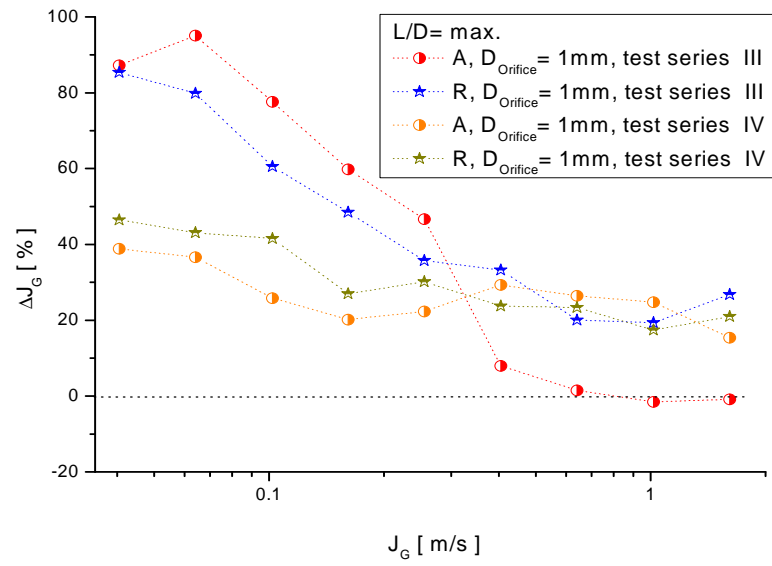


test series IV ($J_G = 0.0096$ m/s)



III. Additional results of the accuracy check (see chapter 1.7)





Appendix IV

Operating data

IV. Operating data

In the following table, the operating data for the measurements of this test series are listed. The columns contain the following information:

Matrix point	Test point according to the test matrix of the FZD (Tab. 2)
Height position	Letter, which characterises the distance between the gas injection and the first measurement plane of the wire-mesh sensor (Fig. 2, Tab. 1)
Pressure at GS (ü) PI4-07 [kPa]	Over pressure set value, which is adjusted at the position PI4-07 above of the wire-mesh sensor, in order to obtain a constant pressure of 0,25 MPa at the gas injection
J_{gas} [m/s] Injection	Set value of the superficial velocity of the gas phase at the gas injection position (Tab. 2)
J_{water} [m/s]	Set value of the superficial velocity of the water phase
V_{gas} [nm ³ /h]	Set value of the gas volume flow at the injection position (0,25 MPa), calculated under normal conditions (cf. chapter 1.3, equation 14)
m_{water} [kg/s]	Set value of the water mass flow
Date	Date of the measurement
File 1 (x)	Name of the raw data file of the first measurement plane in flow direction
File 2 (y)	Name of the raw data file of the second measurement plane in flow direction
DIAdem	Internal number for the synchronisation of the wire-mesh sensor data with the operating data
Operating data (Mean value over 10 s)	Arithmetical mean values over 10 s measurement period for the real operating data
V_{gas} [nm ³ /h]	Actual value of the gas volume flow at the injection position (norm conditions)
M_{water} [kg/s]	Actual value of the water mass flow
t GS [°C]	Actual value of the temperature (TI4-08) above the wire-mesh sensor
p(g) GS [kPa]	Actual value of the over pressure set value at the measurement position PI4-07 above of the wire-mesh sensor

Matrix für Luftversuche TOPFLOW

Normbedingungen: pN [bar] 1.013 D_{innen}: 0.1953 m
 TN [K] 273.15 Fläche: 0.0300 m²
 Einspeisung: Luft pa [bar] 2.5 Dichte_w: 995.7 kg/m³
 Medium t [°C] 30.0 Dichte_g: 2.882 kg/m³

Versuchsserie L12
 Doppelgittersensor in VGE
 1 bzw. 4 mm Randeinspeisung

Matrix-punkt	Höhen-position	Druck am GS (ü) PI4-07 [kPa]	J _{Gas} [m/s] Einspeisung	J _{Wasser} [m/s]	V _{Gas} [nm ³ /h]	m _{Wasser} [kg/s]	Datum	File 1 (x)	File 2 (y)	DIAdem	Betriebsdaten (Mittelwerte über 10 s)			
											V _{Gas} [m ³ /h]	m _{Wasser} [kg/s]	t GS [°C]	p(ü) GS [kPa]
006	A	139.2	0.0025	0.405	0.600	12.081	11.01.2007	L12_195_VGE_A_r01_t30_x.2x64x64.006.mes	L12_195_VGE_A_r01_t30_y.2x64x64.006.mes	5	0.600	12.076	30.4	139.2
006	B	138.7	0.0025	0.405	0.600	12.081	11.01.2007	L12_195_VGE_B_r04_t30_x.2x64x64.006.mes	L12_195_VGE_B_r04_t30_y.2x64x64.006.mes	6	0.599	12.089	30.4	138.7
006	C	138.1	0.0025	0.405	0.600	12.081	11.01.2007	L12_195_VGE_C_r01_t30_x.2x64x64.006.mes	L12_195_VGE_C_r01_t30_y.2x64x64.006.mes	7	0.599	12.066	30.5	138.1
006	D	136.6	0.0025	0.405	0.600	12.081	11.01.2007	L12_195_VGE_D_r01_t30_x.2x64x64.006.mes	L12_195_VGE_D_r01_t30_y.2x64x64.006.mes	4	0.600	12.079	30.3	136.6
006	E	136.0	0.0025	0.405	0.600	12.081	11.01.2007	L12_195_VGE_E_r04_t30_x.2x64x64.006.mes	L12_195_VGE_E_r04_t30_y.2x64x64.006.mes	8	0.599	12.080	30.6	135.9
006	F	135.4	0.0025	0.405	0.600	12.081	11.01.2007	L12_195_VGE_F_r01_t30_x.2x64x64.006.mes	L12_195_VGE_F_r01_t30_y.2x64x64.006.mes	10	0.600	12.086	31.0	135.3
006	G	127.3	0.0025	0.405	0.600	12.081	11.01.2007	L12_195_VGE_G_r01_t30_x.2x64x64.006.mes	L12_195_VGE_G_r01_t30_y.2x64x64.006.mes	11	0.600	12.074	29.4	127.3
006	H	126.8	0.0025	0.405	0.600	12.081	11.01.2007	L12_195_VGE_H_r04_t30_x.2x64x64.006.mes	L12_195_VGE_H_r04_t30_y.2x64x64.006.mes	12	0.599	12.049	29.1	126.8
006	I	126.2	0.0025	0.405	0.600	12.081	11.01.2007	L12_195_VGE_I_r01_t30_x.2x64x64.006.mes	L12_195_VGE_I_r01_t30_y.2x64x64.006.mes	13	0.599	12.078	29.3	126.2
006	J	117.2	0.0025	0.405	0.600	12.081	11.01.2007	L12_195_VGE_J_r01_t30_x.2x64x64.006.mes	L12_195_VGE_J_r01_t30_y.2x64x64.006.mes	14	0.600	12.060	29.4	117.2
006	K	116.6	0.0025	0.405	0.600	12.081	11.01.2007	L12_195_VGE_K_r04_t30_x.2x64x64.006.mes	L12_195_VGE_K_r04_t30_y.2x64x64.006.mes	18	0.599	12.074	29.7	116.6
006	L	116.0	0.0025	0.405	0.600	12.081	11.01.2007	L12_195_VGE_L_r01_t30_x.2x64x64.006.mes	L12_195_VGE_L_r01_t30_y.2x64x64.006.mes	17	0.600	12.083	29.6	116.1
006	M	98.2	0.0025	0.405	0.600	12.081	11.01.2007	L12_195_VGE_M_r01_t30_x.2x64x64.006.mes	L12_195_VGE_M_r01_t30_y.2x64x64.006.mes	20	0.599	12.078	29.7	98.2
006	N	97.7	0.0025	0.405	0.600	12.081	11.01.2007	L12_195_VGE_N_r04_t30_x.2x64x64.006.mes	L12_195_VGE_N_r04_t30_y.2x64x64.006.mes	21	0.600	12.083	29.8	97.6
006	O	97.1	0.0025	0.405	0.600	12.081	11.01.2007	L12_195_VGE_O_r01_t30_x.2x64x64.006.mes	L12_195_VGE_O_r01_t30_y.2x64x64.006.mes	22	0.599	12.082	29.9	97.0
006	P	66.3	0.0025	0.405	0.600	12.081	11.01.2007	L12_195_VGE_P_r01_t30_x.2x64x64.006.mes	L12_195_VGE_P_r01_t30_y.2x64x64.006.mes	23	0.599	12.069	29.9	66.2
006	Q	65.8	0.0025	0.405	0.600	12.081	11.01.2007	L12_195_VGE_Q_r04_t30_x.2x64x64.006.mes	L12_195_VGE_Q_r04_t30_y.2x64x64.006.mes	24	0.600	12.074	30.0	65.7
006	R	65.2	0.0025	0.405	0.600	12.081	11.01.2007	L12_195_VGE_R_r01_t30_x.2x64x64.006.mes	L12_195_VGE_R_r01_t30_y.2x64x64.006.mes	25	0.599	12.078	30.0	65.3
008	A	138.8	0.0025	1.017	0.600	30.336	07.03.2007	L12_195_VGE_A_r01_t30_x.2x64x64.008.mes	L12_195_VGE_A_r01_t30_y.2x64x64.008.mes	1	0.600	30.327	29.4	138.8
008	B	138.3	0.0025	1.017	0.600	30.336	15.06.2007	L12_195_VGE_B_r04_t30_x.2x64x64.008.mes	L12_195_VGE_B_r04_t30_y.2x64x64.008.mes	18	0.600	30.326	30.3	138.2
008	C	137.7	0.0025	1.017	0.600	30.336	07.03.2007	L12_195_VGE_C_r01_t30_x.2x64x64.008.mes	L12_195_VGE_C_r01_t30_y.2x64x64.008.mes	6	0.600	30.318	30.6	137.8
008	D	136.1	0.0025	1.017	0.600	30.336	07.03.2007	L12_195_VGE_D_r01_t30_x.2x64x64.008.mes	L12_195_VGE_D_r01_t30_y.2x64x64.008.mes	7	0.600	30.328	31.0	136.1
008	E	135.5	0.0025	1.017	0.600	30.336	07.03.2007	L12_195_VGE_E_r04_t30_x.2x64x64.008.mes	L12_195_VGE_E_r04_t30_y.2x64x64.008.mes	8	0.600	30.335	29.5	135.4
008	F	135.0	0.0025	1.017	0.600	30.336	07.03.2007	L12_195_VGE_F_r01_t30_x.2x64x64.008.mes	L12_195_VGE_F_r01_t30_y.2x64x64.008.mes	9	0.600	30.330	29.0	135.1
008	G	126.7	0.0025	1.017	0.600	30.336	07.03.2007	L12_195_VGE_G_r01_t30_x.2x64x64.008.mes	L12_195_VGE_G_r01_t30_y.2x64x64.008.mes	12	0.600	30.325	30.2	126.7
008	H	126.2	0.0025	1.017	0.600	30.336	07.03.2007	L12_195_VGE_H_r04_t30_x.2x64x64.008.mes	L12_195_VGE_H_r04_t30_y.2x64x64.008.mes	11	0.600	30.328	29.9	126.2
008	I	125.6	0.0025	1.017	0.600	30.336	15.06.2007	L12_195_VGE_I_r01_t30_x.2x64x64.008.mes	L12_195_VGE_I_r01_t30_y.2x64x64.008.mes	26	0.600	30.324	29.5	125.7
008	J	116.3	0.0025	1.017	0.600	30.336	15.06.2007	L12_195_VGE_J_r01_t30_x.2x64x64.008.mes	L12_195_VGE_J_r01_t30_y.2x64x64.008.mes	27	0.600	30.341	29.7	116.2
008	K	115.8	0.0025	1.017	0.600	30.336	07.03.2007	L12_195_VGE_K_r04_t30_x.2x64x64.008.mes	L12_195_VGE_K_r04_t30_y.2x64x64.008.mes	16	0.600	30.337	29.2	115.7
008	L	115.2	0.0025	1.017	0.600	30.336	15.06.2007	L12_195_VGE_L_r01_t30_x.2x64x64.008.mes	L12_195_VGE_L_r01_t30_y.2x64x64.008.mes	28	0.600	30.328	29.9	115.2
008	M	97.1	0.0025	1.017	0.600	30.336	07.03.2007	L12_195_VGE_M_r01_t30_x.2x64x64.008.mes	L12_195_VGE_M_r01_t30_y.2x64x64.008.mes	19	0.600	30.319	30.2	97.2
008	N	96.5	0.0025	1.017	0.600	30.336	07.03.2007	L12_195_VGE_N_r04_t30_x.2x64x64.008.mes	L12_195_VGE_N_r04_t30_y.2x64x64.008.mes	23	0.600	30.332	30.1	96.5
008	O	96.0	0.0025	1.017	0.600	30.336	07.03.2007	L12_195_VGE_O_r01_t30_x.2x64x64.008.mes	L12_195_VGE_O_r01_t30_y.2x64x64.008.mes	26	0.600	30.360	29.3	95.9
008	P	64.6	0.0025	1.017	0.600	30.336	07.03.2007	L12_195_VGE_P_r01_t30_x.2x64x64.008.mes	L12_195_VGE_P_r01_t30_y.2x64x64.008.mes	27	0.600	30.325	29.5	64.6
008	Q	64.0	0.0025	1.017	0.600	30.336	07.03.2007	L12_195_VGE_Q_r04_t30_x.2x64x64.008.mes	L12_195_VGE_Q_r04_t30_y.2x64x64.008.mes	28	0.600	30.336	29.8	63.9
008	R	63.4	0.0025	1.017	0.600	30.336	07.03.2007	L12_195_VGE_R_r01_t30_x.2x64x64.008.mes	L12_195_VGE_R_r01_t30_y.2x64x64.008.mes	29	0.600	30.335	30.0	63.5
017	A	139.2	0.0040	0.405	0.959	12.081	08.06.2007	L12_195_VGE_A_r01_t30_x.2x64x64.017.mes	L12_195_VGE_A_r01_t30_y.2x64x64.017.mes	1	0.958	12.091	29.1	139.2
017	B	138.7	0.0040	0.405	0.959	12.081	08.06.2007	L12_195_VGE_B_r04_t30_x.2x64x64.017.mes	L12_195_VGE_B_r04_t30_y.2x64x64.017.mes	3	0.959	12.067	29.3	138.7
017	C	138.1	0.0040	0.405	0.959	12.081	08.06.2007	L12_195_VGE_C_r01_t30_x.2x64x64.017.mes	L12_195_VGE_C_r01_t30_y.2x64x64.017.mes	4	0.960	12.094	29.4	138.2
017	D	136.6	0.0040	0.405	0.959	12.081	08.06.2007	L12_195_VGE_D_r01_t30_x.2x64x64.017.mes	L12_195_VGE_D_r01_t30_y.2x64x64.017.mes	7	0.960	12.077	29.8	136.7
017	E	136.0	0.0040	0.405	0.959	12.081	08.06.2007	L12_195_VGE_E_r04_t30_x.2x64x64.017.mes	L12_195_VGE_E_r04_t30_y.2x64x64.017.mes	8	0.960	12.086	30.0	136.0
017	F	135.5	0.0040	0.405	0.959	12.081	08.06.2007	L12_195_VGE_F_r01_t30_x.2x64x64.017.mes	L12_195_VGE_F_r01_t30_y.2x64x64.017.mes	10	0.960	12.075	30.1	135.5
017	G	127.4	0.0040	0.405	0.959	12.081	08.06.2007	L12_195_VGE_G_r01_t30_x.2x64x64.017.mes	L12_195_VGE_G_r01_t30_y.2x64x64.017.mes	11	0.960	12.080	30.3	127.4
017	H	126.8	0.0040	0.405	0.959	12.081	08.06.2007	L12_195_VGE_H_r04_t30_x.2x64x64.017.mes	L12_195_VGE_H_r04_t30_y.2x64x64.017.mes	12	0.960	12.083	30.4	126.8
017	I	126.3	0.0040	0.405	0.959	12.081	08.06.2007	L12_195_VGE_I_r01_t30_x.2x64x64.017.mes	L12_195_VGE_I_r01_t30_y.2x64x64.017.mes	13	0.960	12.092	30.4	126.3
017	J	117.2	0.0040	0.405	0.959	12.081	08.06.2007	L12_195_VGE_J_r01_t30_x.2x64x64.017.mes	L12_195_VGE_J_r01_t30_y.2x64x64.017.mes	14	0.960	12.090	29.8	117.2
017	K	116.7	0.0040	0.405	0.959	12.081	08.06.2007	L12_195_VGE_K_r04_t30_x.2x64x64.017.mes	L12_195_VGE_K_r04_t30_y.2x64x64.017.mes	18	0.960	12.083	29.4	116.8
017	L	116.1	0.0040	0.405	0.959	12.081	08.06.2007	L12_195_VGE_L_r01_t30_x.2x64x64.017.mes	L12_195_VGE_L_r01_t30_y.2x64x64.017.mes	17	0.960	12.069	29.2	116.2
017	M	98.4	0.0040	0.405	0.959	12.081	08.06.2007	L12_195_VGE_M_r01_t30_x.2x64x64.017.mes	L12_195_VGE_M_r01_t30_y.2x64x64.017.mes	22	0.960	12.065	29.6	98.4
017	N	97.8	0.0040	0.405	0.959	12.081	08.06.2007	L12_195_VGE_N_r04_t30_x.2x64x64.017.mes	L12_195_VGE_N_r04_t30_y.2x64x64.017.mes	23	0.960	12.068	29.8	97.8
017	O	97.3	0.0040	0.405	0.959	12.081	08.06.2007	L12_195_VGE_O_r01_t30_x.2x64x64.017.mes	L12_195_VGE_O_r01_t30_y.2x64x64.017.mes	24	0.960	12.068	29.9	97.4
017	P	66.5	0.0040	0.405	0.959	12.081	08.06.2007	L12_195_VGE_P_r01_t30_x.2x64x64.017.mes	L12_195_VGE_P_r01_t30_y.2x64x64.017.mes	25	0.960	12.071	30.0	66.5
017	Q	65.9	0.0040	0.405	0.959	12.081	08.06.2007	L12_195_VGE_Q_r04_t30_x.2x64x64.017.mes	L12_195_VGE_Q_r04_t30_y.2x64x64.017.mes	26	0.960	12.079	30.1	65.9
017	R	65.4	0.0040	0.405	0.959	12.081	08.06.2007	L12_195_VGE_R_r01_t30_x.2x64x64.017.mes	L12_195_VGE_R_r01_t30_y.2x64x64.017.mes	28	0.960	12.079	30.3	65.3

Matrix-punkt	Höhen-position	Druck am GS (ü) PI4-07 [kPa]	J _{Gas} [m/s] Einspeisung	J _{Wasser} [m/s]	V _{Gas} [nm³/h]	m _{Wasser} [kg/s]	Datum	File 1 (x)	File 2 (y)	DIAdem	Betriebsdaten (Mittelwerte über 10 s)			
											V _{Gas} [m³/h]	m _{Wasser} [kg/s]	t _{GS} [°C]	p(ü) GS [kPa]
019	A	138.8	0.0040	1.017	0.959	30.336	15.06.2007	L12_195_VGE_A_r01_t30_x.2x64x64.019.mes	L12_195_VGE_A_r01_t30_y.2x64x64.019.mes	10	2.295	19.110	29.92	139.2
019	B	138.3	0.0040	1.017	0.959	30.336	15.06.2007	L12_195_VGE_B_r04_t30_x.2x64x64.019.mes	L12_195_VGE_B_r04_t30_y.2x64x64.019.mes	12	2.296	19.119	30.0	138.6
019	C	137.7	0.0040	1.017	0.959	30.336	18.06.2007	L12_195_VGE_C_r01_t30_x.2x64x64.019.mes	L12_195_VGE_C_r01_t30_y.2x64x64.019.mes	6	0.959	30.342	30.0	137.7
019	D	136.1	0.0040	1.017	0.959	30.336	18.06.2007	L12_195_VGE_D_r01_t30_x.2x64x64.019.mes	L12_195_VGE_D_r01_t30_y.2x64x64.019.mes	8	0.960	30.339	30.1	136.0
019	E	135.6	0.0040	1.017	0.959	30.336	18.06.2007	L12_195_VGE_E_r04_t30_x.2x64x64.019.mes	L12_195_VGE_E_r04_t30_y.2x64x64.019.mes	9	0.960	30.340	30.3	135.7
019	F	135.0	0.0040	1.017	0.959	30.336	15.06.2007	L12_195_VGE_F_r01_t30_x.2x64x64.019.mes	L12_195_VGE_F_r01_t30_y.2x64x64.019.mes	25	2.295	19.114	29.6	135.4
019	G	126.7	0.0040	1.017	0.959	30.336	18.06.2007	L12_195_VGE_G_r01_t30_x.2x64x64.019.mes	L12_195_VGE_G_r01_t30_y.2x64x64.019.mes	15	0.959	30.340	29.5	126.7
019	H	126.2	0.0040	1.017	0.959	30.336	18.06.2007	L12_195_VGE_H_r04_t30_x.2x64x64.019.mes	L12_195_VGE_H_r04_t30_y.2x64x64.019.mes	16	0.959	30.338	29.1	126.2
019	I	125.6	0.0040	1.017	0.959	30.336	18.06.2007	L12_195_VGE_I_r01_t30_x.2x64x64.019.mes	L12_195_VGE_I_r01_t30_y.2x64x64.019.mes	19	0.959	30.317	29.4	125.6
019	J	116.4	0.0040	1.017	0.959	30.336	18.06.2007	L12_195_VGE_J_r01_t30_x.2x64x64.019.mes	L12_195_VGE_J_r01_t30_y.2x64x64.019.mes	21	0.960	30.330	29.6	116.4
019	K	115.8	0.0040	1.017	0.959	30.336	18.06.2007	L12_195_VGE_K_r04_t30_x.2x64x64.019.mes	L12_195_VGE_K_r04_t30_y.2x64x64.019.mes	22	0.959	30.336	29.8	115.8
019	L	115.3	0.0040	1.017	0.959	30.336	18.06.2007	L12_195_VGE_L_r01_t30_x.2x64x64.019.mes	L12_195_VGE_L_r01_t30_y.2x64x64.019.mes	23	0.959	30.355	30.0	115.3
019	M	97.1	0.0040	1.017	0.959	30.336	18.06.2007	L12_195_VGE_M_r01_t30_x.2x64x64.019.mes	L12_195_VGE_M_r01_t30_y.2x64x64.019.mes	24	0.959	30.329	30.2	97.1
019	N	96.6	0.0040	1.017	0.959	30.336	18.06.2007	L12_195_VGE_N_r04_t30_x.2x64x64.019.mes	L12_195_VGE_N_r04_t30_y.2x64x64.019.mes	25	0.960	30.339	30.3	96.6
019	O	96.0	0.0040	1.017	0.959	30.336	18.06.2007	L12_195_VGE_O_r01_t30_x.2x64x64.019.mes	L12_195_VGE_O_r01_t30_y.2x64x64.019.mes	26	0.960	30.342	30.5	96.0
019	P	64.6	0.0040	1.017	0.959	30.336	18.06.2007	L12_195_VGE_P_r01_t30_x.2x64x64.019.mes	L12_195_VGE_P_r01_t30_y.2x64x64.019.mes	27	0.959	30.340	30.7	64.6
019	Q	64.1	0.0040	1.017	0.959	30.336	18.06.2007	L12_195_VGE_Q_r04_t30_x.2x64x64.019.mes	L12_195_VGE_Q_r04_t30_y.2x64x64.019.mes	28	0.960	30.355	30.8	64.1
019	R	63.5	0.0040	1.017	0.959	30.336	18.06.2007	L12_195_VGE_R_r01_t30_x.2x64x64.019.mes	L12_195_VGE_R_r01_t30_y.2x64x64.019.mes	29	0.960	30.331	30.9	63.5
028	A	139.3	0.0062	0.405	1.487	12.081	15.06.2007	L12_195_VGE_A_r01_t30_x.2x64x64.028.mes	L12_195_VGE_A_r01_t30_y.2x64x64.028.mes	8	1.485	12.081	29.9	139.4
028	B	138.7	0.0062	0.405	1.487	12.081	27.02.2007	L12_195_VGE_B_r04_t30_x.2x64x64.028.mes	L12_195_VGE_B_r04_t30_y.2x64x64.028.mes	7b	1.486	12.078	30.0	138.6
028	C	138.2	0.0062	0.405	1.487	12.081	27.02.2007	L12_195_VGE_C_r01_t30_x.2x64x64.028.mes	L12_195_VGE_C_r01_t30_y.2x64x64.028.mes	6b	1.486	12.075	30.2	138.2
028	D	136.6	0.0062	0.405	1.487	12.081	27.02.2007	L12_195_VGE_D_r01_t30_x.2x64x64.028.mes	L12_195_VGE_D_r01_t30_y.2x64x64.028.mes	5b	1.486	12.074	30.2	136.6
028	E	136.1	0.0062	0.405	1.487	12.081	27.02.2007	L12_195_VGE_E_r04_t30_x.2x64x64.028.mes	L12_195_VGE_E_r04_t30_y.2x64x64.028.mes	4b	1.486	12.079	30.3	136.2
028	F	135.5	0.0062	0.405	1.487	12.081	27.02.2007	L12_195_VGE_F_r01_t30_x.2x64x64.028.mes	L12_195_VGE_F_r01_t30_y.2x64x64.028.mes	3b	1.486	12.085	30.3	135.5
028	G	127.5	0.0062	0.405	1.487	12.081	27.02.2007	L12_195_VGE_G_r01_t30_x.2x64x64.028.mes	L12_195_VGE_G_r01_t30_y.2x64x64.028.mes	16a	1.486	12.073	29.9	127.5
028	H	126.9	0.0062	0.405	1.487	12.081	27.02.2007	L12_195_VGE_H_r04_t30_x.2x64x64.028.mes	L12_195_VGE_H_r04_t30_y.2x64x64.028.mes	14a	1.486	12.069	29.9	126.8
028	I	126.4	0.0062	0.405	1.487	12.081	27.02.2007	L12_195_VGE_I_r01_t30_x.2x64x64.028.mes	L12_195_VGE_I_r01_t30_y.2x64x64.028.mes	13a	1.486	12.096	30.0	126.4
028	J	117.3	0.0062	0.405	1.487	12.081	27.02.2007	L12_195_VGE_J_r01_t30_x.2x64x64.028.mes	L12_195_VGE_J_r01_t30_y.2x64x64.028.mes	12a	1.486	12.073	30.0	117.2
028	K	116.8	0.0062	0.405	1.487	12.081	27.02.2007	L12_195_VGE_K_r04_t30_x.2x64x64.028.mes	L12_195_VGE_K_r04_t30_y.2x64x64.028.mes	11a	1.486	12.079	30.1	116.9
028	L	116.2	0.0062	0.405	1.487	12.081	27.02.2007	L12_195_VGE_L_r01_t30_x.2x64x64.028.mes	L12_195_VGE_L_r01_t30_y.2x64x64.028.mes	10a	1.486	12.076	30.0	116.2
028	M	98.5	0.0062	0.405	1.487	12.081	27.02.2007	L12_195_VGE_M_r01_t30_x.2x64x64.028.mes	L12_195_VGE_M_r01_t30_y.2x64x64.028.mes	6a	1.486	12.082	29.6	98.5
028	N	98.0	0.0062	0.405	1.487	12.081	27.02.2007	L12_195_VGE_N_r04_t30_x.2x64x64.028.mes	L12_195_VGE_N_r04_t30_y.2x64x64.028.mes	5a	1.486	12.080	29.5	98.0
028	O	97.4	0.0062	0.405	1.487	12.081	27.02.2007	L12_195_VGE_O_r01_t30_x.2x64x64.028.mes	L12_195_VGE_O_r01_t30_y.2x64x64.028.mes	4a	1.486	12.071	29.5	97.4
028	P	66.8	0.0062	0.405	1.487	12.081	27.02.2007	L12_195_VGE_P_r01_t30_x.2x64x64.028.mes	L12_195_VGE_P_r01_t30_y.2x64x64.028.mes	3a	1.486	12.103	29.2	66.8
028	Q	66.2	0.0062	0.405	1.487	12.081	27.02.2007	L12_195_VGE_Q_r04_t30_x.2x64x64.028.mes	L12_195_VGE_Q_r04_t30_y.2x64x64.028.mes	2a	1.486	12.084	29.2	66.2
028	R	65.7	0.0062	0.405	1.487	12.081	27.02.2007	L12_195_VGE_R_r01_t30_x.2x64x64.028.mes	L12_195_VGE_R_r01_t30_y.2x64x64.028.mes	1a	1.485	12.091	29.1	65.8
030	A	138.9	0.0062	1.017	1.487	30.336	06.03.2007	L12_195_VGE_A_r01_t30_x.2x64x64.030.mes	L12_195_VGE_A_r01_t30_y.2x64x64.030.mes	29	1.486	30.317	31.0	138.9
030	B	138.3	0.0062	1.017	1.487	30.336	06.03.2007	L12_195_VGE_B_r04_t30_x.2x64x64.030.mes	L12_195_VGE_B_r04_t30_y.2x64x64.030.mes	28	1.486	30.338	30.7	138.4
030	C	137.7	0.0062	1.017	1.487	30.336	06.03.2007	L12_195_VGE_C_r01_t30_x.2x64x64.030.mes	L12_195_VGE_C_r01_t30_y.2x64x64.030.mes	27	1.486	30.330	30.4	137.6
030	D	136.1	0.0062	1.017	1.487	30.336	06.03.2007	L12_195_VGE_D_r01_t30_x.2x64x64.030.mes	L12_195_VGE_D_r01_t30_y.2x64x64.030.mes	24	1.486	30.348	30.2	136.1
030	E	135.6	0.0062	1.017	1.487	30.336	06.03.2007	L12_195_VGE_E_r04_t30_x.2x64x64.030.mes	L12_195_VGE_E_r04_t30_y.2x64x64.030.mes	22	1.486	30.345	29.9	135.5
030	F	135.0	0.0062	1.017	1.487	30.336	06.03.2007	L12_195_VGE_F_r01_t30_x.2x64x64.030.mes	L12_195_VGE_F_r01_t30_y.2x64x64.030.mes	21	1.486	30.344	29.6	135.1
030	G	126.8	0.0062	1.017	1.487	30.336	06.03.2007	L12_195_VGE_G_r01_t30_x.2x64x64.030.mes	L12_195_VGE_G_r01_t30_y.2x64x64.030.mes	16	1.486	30.319	29.7	126.9
030	H	126.2	0.0062	1.017	1.487	30.336	06.03.2007	L12_195_VGE_H_r04_t30_x.2x64x64.030.mes	L12_195_VGE_H_r04_t30_y.2x64x64.030.mes	15	1.486	30.320	31.0	126.3
030	I	125.7	0.0062	1.017	1.487	30.336	06.03.2007	L12_195_VGE_I_r01_t30_x.2x64x64.030.mes	L12_195_VGE_I_r01_t30_y.2x64x64.030.mes	14	1.486	30.337	30.7	125.8
030	J	116.4	0.0062	1.017	1.487	30.336	06.03.2007	L12_195_VGE_J_r01_t30_x.2x64x64.030.mes	L12_195_VGE_J_r01_t30_y.2x64x64.030.mes	13	1.486	30.345	30.2	116.5
030	K	115.9	0.0062	1.017	1.487	30.336	06.03.2007	L12_195_VGE_K_r04_t30_x.2x64x64.030.mes	L12_195_VGE_K_r04_t30_y.2x64x64.030.mes	11	1.486	30.334	29.9	115.8
030	L	115.3	0.0062	1.017	1.487	30.336	06.03.2007	L12_195_VGE_L_r01_t30_x.2x64x64.030.mes	L12_195_VGE_L_r01_t30_y.2x64x64.030.mes	10	1.486	30.331	29.7	115.4
030	M	97.2	0.0062	1.017	1.487	30.336	06.03.2007	L12_195_VGE_M_r01_t30_x.2x64x64.030.mes	L12_195_VGE_M_r01_t30_y.2x64x64.030.mes	9	1.486	30.341	29.3	97.3
030	N	96.7	0.0062	1.017	1.487	30.336	06.03.2007	L12_195_VGE_N_r04_t30_x.2x64x64.030.mes	L12_195_VGE_N_r04_t30_y.2x64x64.030.mes	8	1.486	30.309	29.7	96.7
030	O	96.1	0.0062	1.017	1.487	30.336	06.03.2007	L12_195_VGE_O_r01_t30_x.2x64x64.030.mes	L12_195_VGE_O_r01_t30_y.2x64x64.030.mes	6	1.486	30.332	30.9	96.1
030	P	64.8	0.0062	1.017	1.487	30.336	06.03.2007	L12_195_VGE_P_r01_t30_x.2x64x64.030.mes	L12_195_VGE_P_r01_t30_y.2x64x64.030.mes	5	1.486	30.330	30.7	64.7
030	Q	64.2	0.0062	1.017	1.487	30.336	06.03.2007	L12_195_VGE_Q_r04_t30_x.2x64x64.030.mes	L12_195_VGE_Q_r04_t30_y.2x64x64.030.mes	4	1.486	30.340	30.5	64.2
030	R	63.6	0.0062	1.017	1.487	30.336	06.03.2007	L12_195_VGE_R_r01_t30_x.2x64x64.030.mes	L12_195_VGE_R_r01_t30_y.2x64x64.030.mes	1	1.486	30.369	30.1	63.6

Matrix-punkt	Höhen-position	Druck am GS (ü) PI4-07 [kPa]	J _{Gas} [m/s] Einspeisung	J _{Wasser} [m/s]	V _{Gas} [nm ³ /h]	m _{Wasser} [kg/s]	Datum	File 1 (x)	File 2 (y)	DIAdem	Betriebsdaten (Mittelwerte über 10 s)			
											V _{Gas} [m ³ /h]	m _{Wasser} [kg/s]	t _{GS} [°C]	p(ü) GS [kPa]
034	A	139.6	0.0096	0.041	2.302	1.208	20.03.2007	L12_195_VGE_A_r01_t30_x.2x64x64.034.mes	L12_195_VGE_A_r01_t30_y.2x64x64.034.mes	1	2.296	1.206	29.23	139.5
034	B	139.0	0.0096	0.041	2.302	1.208	20.03.2007	L12_195_VGE_B_r04_t30_x.2x64x64.034.mes	L12_195_VGE_B_r04_t30_y.2x64x64.034.mes	3	2.296	1.208	29.4	138.9
034	C	138.5	0.0096	0.041	2.302	1.208	20.03.2007	L12_195_VGE_C_r01_t30_x.2x64x64.034.mes	L12_195_VGE_C_r01_t30_y.2x64x64.034.mes	5	2.296	1.207	29.4	138.4
034	D	137.0	0.0096	0.041	2.302	1.208	20.03.2007	L12_195_VGE_D_r01_t30_x.2x64x64.034.mes	L12_195_VGE_D_r01_t30_y.2x64x64.034.mes	6	2.296	1.209	29.4	136.9
034	E	136.5	0.0096	0.041	2.302	1.208	20.03.2007	L12_195_VGE_E_r04_t30_x.2x64x64.034.mes	L12_195_VGE_E_r04_t30_y.2x64x64.034.mes	7	2.296	1.206	29.5	136.4
034	F	135.9	0.0096	0.041	2.302	1.208	20.03.2007	L12_195_VGE_F_r01_t30_x.2x64x64.034.mes	L12_195_VGE_F_r01_t30_y.2x64x64.034.mes	9	2.296	1.208	29.6	135.9
034	G	128.1	0.0096	0.041	2.302	1.208	20.03.2007	L12_195_VGE_G_r01_t30_x.2x64x64.034.mes	L12_195_VGE_G_r01_t30_y.2x64x64.034.mes	10	2.296	1.207	29.6	128.2
034	H	127.5	0.0096	0.041	2.302	1.208	20.03.2007	L12_195_VGE_H_r04_t30_x.2x64x64.034.mes	L12_195_VGE_H_r04_t30_y.2x64x64.034.mes	11	2.296	1.206	29.7	127.6
034	I	127.0	0.0096	0.041	2.302	1.208	20.03.2007	L12_195_VGE_I_r01_t30_x.2x64x64.034.mes	L12_195_VGE_I_r01_t30_y.2x64x64.034.mes	13	2.296	1.208	29.8	127.0
034	J	118.2	0.0096	0.041	2.302	1.208	20.03.2007	L12_195_VGE_J_r01_t30_x.2x64x64.034.mes	L12_195_VGE_J_r01_t30_y.2x64x64.034.mes	14	2.296	1.205	29.9	118.1
034	K	117.7	0.0096	0.041	2.302	1.208	20.03.2007	L12_195_VGE_K_r04_t30_x.2x64x64.034.mes	L12_195_VGE_K_r04_t30_y.2x64x64.034.mes	15	2.296	1.207	29.9	117.8
034	L	117.1	0.0096	0.041	2.302	1.208	20.03.2007	L12_195_VGE_L_r01_t30_x.2x64x64.034.mes	L12_195_VGE_L_r01_t30_y.2x64x64.034.mes	16	2.296	1.206	30.0	117.0
034	M	99.9	0.0096	0.041	2.302	1.208	20.03.2007	L12_195_VGE_M_r01_t30_x.2x64x64.034.mes	L12_195_VGE_M_r01_t30_y.2x64x64.034.mes	17	2.296	1.204	30.5	99.7
034	N	99.4	0.0096	0.041	2.302	1.208	20.03.2007	L12_195_VGE_N_r04_t30_x.2x64x64.034.mes	L12_195_VGE_N_r04_t30_y.2x64x64.034.mes	18	2.296	1.208	30.5	99.4
034	O	98.8	0.0096	0.041	2.302	1.208	20.03.2007	L12_195_VGE_O_r01_t30_x.2x64x64.034.mes	L12_195_VGE_O_r01_t30_y.2x64x64.034.mes	19	2.296	1.207	30.6	98.8
034	P	69.0	0.0096	0.041	2.302	1.208	20.03.2007	L12_195_VGE_P_r01_t30_x.2x64x64.034.mes	L12_195_VGE_P_r01_t30_y.2x64x64.034.mes	20	2.296	1.206	30.8	69.0
034	Q	68.4	0.0096	0.041	2.302	1.208	20.03.2007	L12_195_VGE_Q_r04_t30_x.2x64x64.034.mes	L12_195_VGE_Q_r04_t30_y.2x64x64.034.mes	21	2.296	1.198	31.0	68.4
034	R	67.9	0.0096	0.041	2.302	1.208	20.03.2007	L12_195_VGE_R_r01_t30_x.2x64x64.034.mes	L12_195_VGE_R_r01_t30_y.2x64x64.034.mes	22	2.296	1.207	31.0	67.8
035	A	139.6	0.0096	0.064	2.302	1.912	28.06.2007	L12_195_VGE_A_r01_t30_x.2x64x64.035.mes	L12_195_VGE_A_r01_t30_y.2x64x64.035.mes	17	2.296	1.907	30.0	139.6
035	B	139.0	0.0096	0.064	2.302	1.912	28.06.2007	L12_195_VGE_B_r04_t30_x.2x64x64.035.mes	L12_195_VGE_B_r04_t30_y.2x64x64.035.mes	16	2.296	1.908	29.9	139.1
035	C	138.5	0.0096	0.064	2.302	1.912	28.06.2007	L12_195_VGE_C_r01_t30_x.2x64x64.035.mes	L12_195_VGE_C_r01_t30_y.2x64x64.035.mes	9	2.296	1.912	30.9	138.4
035	D	137.0	0.0096	0.064	2.302	1.912	28.06.2007	L12_195_VGE_D_r01_t30_x.2x64x64.035.mes	L12_195_VGE_D_r01_t30_y.2x64x64.035.mes	8	2.295	1.911	30.6	136.9
035	E	136.4	0.0096	0.064	2.302	1.912	28.06.2007	L12_195_VGE_E_r04_t30_x.2x64x64.035.mes	L12_195_VGE_E_r04_t30_y.2x64x64.035.mes	7	2.296	1.912	30.5	136.3
035	F	135.9	0.0096	0.064	2.302	1.912	28.06.2007	L12_195_VGE_F_r01_t30_x.2x64x64.035.mes	L12_195_VGE_F_r01_t30_y.2x64x64.035.mes	5	2.294	1.909	30.4	135.9
035	G	128.0	0.0096	0.064	2.302	1.912	28.06.2007	L12_195_VGE_G_r01_t30_x.2x64x64.035.mes	L12_195_VGE_G_r01_t30_y.2x64x64.035.mes	4	2.295	1.904	30.3	128.0
035	H	127.5	0.0096	0.064	2.302	1.912	28.06.2007	L12_195_VGE_H_r04_t30_x.2x64x64.035.mes	L12_195_VGE_H_r04_t30_y.2x64x64.035.mes	3	2.296	1.908	30.2	127.6
035	I	126.9	0.0096	0.064	2.302	1.912	28.06.2007	L12_195_VGE_I_r01_t30_x.2x64x64.035.mes	L12_195_VGE_I_r01_t30_y.2x64x64.035.mes	2	2.296	1.913	30.1	126.8
035	J	118.1	0.0096	0.064	2.302	1.912	28.06.2007	L12_195_VGE_J_r01_t30_x.2x64x64.035.mes	L12_195_VGE_J_r01_t30_y.2x64x64.035.mes	1	2.295	1.912	30.1	118.1
035	K	117.6	0.0096	0.064	2.302	1.912	25.05.2007	L12_195_VGE_K_r04_t30_x.2x64x64.035.mes	L12_195_VGE_K_r04_t30_y.2x64x64.035.mes	12a	2.296	1.912	29.8	117.7
035	L	117.1	0.0096	0.064	2.302	1.912	25.05.2007	L12_195_VGE_L_r01_t30_x.2x64x64.035.mes	L12_195_VGE_L_r01_t30_y.2x64x64.035.mes	13a	2.296	1.913	29.9	117.1
035	M	99.8	0.0096	0.064	2.302	1.912	25.05.2007	L12_195_VGE_M_r01_t30_x.2x64x64.035.mes	L12_195_VGE_M_r01_t30_y.2x64x64.035.mes	1b	2.296	1.914	30.2	99.8
035	N	99.2	0.0096	0.064	2.302	1.912	25.05.2007	L12_195_VGE_N_r04_t30_x.2x64x64.035.mes	L12_195_VGE_N_r04_t30_y.2x64x64.035.mes	2b	2.296	1.911	30.3	99.3
035	O	98.7	0.0096	0.064	2.302	1.912	25.05.2007	L12_195_VGE_O_r01_t30_x.2x64x64.035.mes	L12_195_VGE_O_r01_t30_y.2x64x64.035.mes	3b	2.296	1.911	30.4	98.8
035	P	68.8	0.0096	0.064	2.302	1.912	25.05.2007	L12_195_VGE_P_r01_t30_x.2x64x64.035.mes	L12_195_VGE_P_r01_t30_y.2x64x64.035.mes	4b	2.296	1.910	30.6	68.8
035	Q	68.2	0.0096	0.064	2.302	1.912	25.05.2007	L12_195_VGE_Q_r04_t30_x.2x64x64.035.mes	L12_195_VGE_Q_r04_t30_y.2x64x64.035.mes	5b	2.296	1.911	30.8	68.4
035	R	67.7	0.0096	0.064	2.302	1.912	25.05.2007	L12_195_VGE_R_r01_t30_x.2x64x64.035.mes	L12_195_VGE_R_r01_t30_y.2x64x64.035.mes	6b	2.296	1.911	30.9	67.8
036	A	139.5	0.0096	0.102	2.302	3.043	28.06.2007	L12_195_VGE_A_r01_t30_x.2x64x64.036.mes	L12_195_VGE_A_r01_t30_y.2x64x64.036.mes	18	2.296	3.044	30.1	139.7
036	B	139.0	0.0096	0.102	2.302	3.043	28.06.2007	L12_195_VGE_B_r04_t30_x.2x64x64.036.mes	L12_195_VGE_B_r04_t30_y.2x64x64.036.mes	14	2.296	3.050	29.8	139.1
036	C	138.4	0.0096	0.102	2.302	3.043	28.06.2007	L12_195_VGE_C_r01_t30_x.2x64x64.036.mes	L12_195_VGE_C_r01_t30_y.2x64x64.036.mes	11	2.296	3.040	29.6	138.4
036	D	136.9	0.0096	0.102	2.302	3.043	21.03.2007	L12_195_VGE_D_r01_t30_x.2x64x64.036.mes	L12_195_VGE_D_r01_t30_y.2x64x64.036.mes	5	2.296	3.042	29.5	137.0
036	E	136.4	0.0096	0.102	2.302	3.043	21.03.2007	L12_195_VGE_E_r04_t30_x.2x64x64.036.mes	L12_195_VGE_E_r04_t30_y.2x64x64.036.mes	6	2.296	3.042	29.6	136.3
036	F	135.8	0.0096	0.102	2.302	3.043	21.03.2007	L12_195_VGE_F_r01_t30_x.2x64x64.036.mes	L12_195_VGE_F_r01_t30_y.2x64x64.036.mes	7	2.296	3.045	29.7	135.7
036	G	127.9	0.0096	0.102	2.302	3.043	21.03.2007	L12_195_VGE_G_r01_t30_x.2x64x64.036.mes	L12_195_VGE_G_r01_t30_y.2x64x64.036.mes	8	2.296	3.040	29.8	127.7
036	H	127.4	0.0096	0.102	2.302	3.043	21.03.2007	L12_195_VGE_H_r04_t30_x.2x64x64.036.mes	L12_195_VGE_H_r04_t30_y.2x64x64.036.mes	10	2.296	3.044	29.9	127.4
036	I	126.9	0.0096	0.102	2.302	3.043	21.03.2007	L12_195_VGE_I_r01_t30_x.2x64x64.036.mes	L12_195_VGE_I_r01_t30_y.2x64x64.036.mes	11	2.296	3.042	30.0	126.9
036	J	118.0	0.0096	0.102	2.302	3.043	21.03.2007	L12_195_VGE_J_r01_t30_x.2x64x64.036.mes	L12_195_VGE_J_r01_t30_y.2x64x64.036.mes	15	2.296	3.043	30.2	118.0
036	K	117.5	0.0096	0.102	2.302	3.043	21.03.2007	L12_195_VGE_K_r04_t30_x.2x64x64.036.mes	L12_195_VGE_K_r04_t30_y.2x64x64.036.mes	13	2.296	3.042	30.1	117.6
036	L	116.9	0.0096	0.102	2.302	3.043	21.03.2007	L12_195_VGE_L_r01_t30_x.2x64x64.036.mes	L12_195_VGE_L_r01_t30_y.2x64x64.036.mes	18	2.296	3.043	30.4	116.9
036	M	99.6	0.0096	0.102	2.302	3.043	21.03.2007	L12_195_VGE_M_r01_t30_x.2x64x64.036.mes	L12_195_VGE_M_r01_t30_y.2x64x64.036.mes	19	2.296	3.041	29.3	99.7
036	N	99.1	0.0096	0.102	2.302	3.043	21.03.2007	L12_195_VGE_N_r04_t30_x.2x64x64.036.mes	L12_195_VGE_N_r04_t30_y.2x64x64.036.mes	20	2.296	3.042	29.6	99.2
036	O	98.5	0.0096	0.102	2.302	3.043	21.03.2007	L12_195_VGE_O_r01_t30_x.2x64x64.036.mes	L12_195_VGE_O_r01_t30_y.2x64x64.036.mes	21	2.296	3.042	29.7	98.5
036	P	68.5	0.0096	0.102	2.302	3.043	21.03.2007	L12_195_VGE_P_r01_t30_x.2x64x64.036.mes	L12_195_VGE_P_r01_t30_y.2x64x64.036.mes	23	2.296	3.043	30.0	68.5
036	Q	68.0	0.0096	0.102	2.302	3.043	21.03.2007	L12_195_VGE_Q_r04_t30_x.2x64x64.036.mes	L12_195_VGE_Q_r04_t30_y.2x64x64.036.mes	24	2.296	3.042	30.2	68.1
036	R	67.4	0.0096	0.102	2.302	3.043	21.03.2007	L12_195_VGE_R_r01_t30_x.2x64x64.036.mes	L12_195_VGE_R_r01_t30_y.2x64x64.036.mes	25	2.296	3.044	30.3	67.3

Matrix-punkt	Höhen-position	Druck am GS (ü) PI4-07 [kPa]	J _{Gas} [m/s] Einspeisung	J _{Wasser} [m/s]	V _{Gas} [nm³/h]	m _{Wasser} [kg/s]	Datum	File 1 (x)	File 2 (y)	DIAdem	Betriebsdaten (Mittelwerte über 10 s)			
											V _{Gas} [m³/h]	m _{Wasser} [kg/s]	t _{GS} [°C]	p(ü) GS [kPa]
037	A	139.5	0.0096	0.161	2.302	4.802	28.06.2007	L12_195_VGE_A_r01_t30_x.2x64x64.037.mes	L12_195_VGE_A_r01_t30_y.2x64x64.037.mes	19	2.296	4.793	30.2	139.5
037	B	138.9	0.0096	0.161	2.302	4.802	28.06.2007	L12_195_VGE_B_r04_t30_x.2x64x64.037.mes	L12_195_VGE_B_r04_t30_y.2x64x64.037.mes	13	2.295	4.798	29.7	138.9
037	C	138.4	0.0096	0.161	2.302	4.802	28.06.2007	L12_195_VGE_C_r01_t30_x.2x64x64.037.mes	L12_195_VGE_C_r01_t30_y.2x64x64.037.mes	12	2.296	4.800	29.6	138.5
037	D	136.9	0.0096	0.161	2.302	4.802	31.05.2007	L12_195_VGE_D_r01_t30_x.2x64x64.037.mes	L12_195_VGE_D_r01_t30_y.2x64x64.037.mes	6	2.296	4.797	30.0	136.8
037	E	136.3	0.0096	0.161	2.302	4.802	31.05.2007	L12_195_VGE_E_r04_t30_x.2x64x64.037.mes	L12_195_VGE_E_r04_t30_y.2x64x64.037.mes	7	2.296	4.795	30.1	136.2
037	F	135.8	0.0096	0.161	2.302	4.802	31.05.2007	L12_195_VGE_F_r01_t30_x.2x64x64.037.mes	L12_195_VGE_F_r01_t30_y.2x64x64.037.mes	8	2.296	4.801	30.3	135.9
037	G	127.9	0.0096	0.161	2.302	4.802	31.05.2007	L12_195_VGE_G_r01_t30_x.2x64x64.037.mes	L12_195_VGE_G_r01_t30_y.2x64x64.037.mes	9	2.296	4.805	30.5	127.9
037	H	127.3	0.0096	0.161	2.302	4.802	31.05.2007	L12_195_VGE_H_r04_t30_x.2x64x64.037.mes	L12_195_VGE_H_r04_t30_y.2x64x64.037.mes	12	2.296	4.795	30.7	127.4
037	I	126.8	0.0096	0.161	2.302	4.802	31.05.2007	L12_195_VGE_I_r01_t30_x.2x64x64.037.mes	L12_195_VGE_I_r01_t30_y.2x64x64.037.mes	13	2.296	4.806	30.8	126.8
037	J	117.9	0.0096	0.161	2.302	4.802	31.05.2007	L12_195_VGE_J_r01_t30_x.2x64x64.037.mes	L12_195_VGE_J_r01_t30_y.2x64x64.037.mes	14	2.296	4.807	29.2	118.0
037	K	117.3	0.0096	0.161	2.302	4.802	31.05.2007	L12_195_VGE_K_r04_t30_x.2x64x64.037.mes	L12_195_VGE_K_r04_t30_y.2x64x64.037.mes	15	2.296	4.794	29.4	117.3
037	L	116.8	0.0096	0.161	2.302	4.802	31.05.2007	L12_195_VGE_L_r01_t30_x.2x64x64.037.mes	L12_195_VGE_L_r01_t30_y.2x64x64.037.mes	16	2.296	4.804	29.6	116.9
037	M	99.4	0.0096	0.161	2.302	4.802	31.05.2007	L12_195_VGE_M_r01_t30_x.2x64x64.037.mes	L12_195_VGE_M_r01_t30_y.2x64x64.037.mes	17	2.296	4.797	29.9	99.5
037	N	98.9	0.0096	0.161	2.302	4.802	31.05.2007	L12_195_VGE_N_r04_t30_x.2x64x64.037.mes	L12_195_VGE_N_r04_t30_y.2x64x64.037.mes	18	2.296	4.801	30.1	99.0
037	O	98.3	0.0096	0.161	2.302	4.802	31.05.2007	L12_195_VGE_O_r01_t30_x.2x64x64.037.mes	L12_195_VGE_O_r01_t30_y.2x64x64.037.mes	19	2.296	4.802	30.3	98.3
037	P	68.2	0.0096	0.161	2.302	4.802	31.05.2007	L12_195_VGE_P_r01_t30_x.2x64x64.037.mes	L12_195_VGE_P_r01_t30_y.2x64x64.037.mes	20	2.296	4.801	30.4	68.2
037	Q	67.6	0.0096	0.161	2.302	4.802	31.05.2007	L12_195_VGE_Q_r04_t30_x.2x64x64.037.mes	L12_195_VGE_Q_r04_t30_y.2x64x64.037.mes	21	2.296	4.809	30.6	67.6
037	R	67.1	0.0096	0.161	2.302	4.802	31.05.2007	L12_195_VGE_R_r01_t30_x.2x64x64.037.mes	L12_195_VGE_R_r01_t30_y.2x64x64.037.mes	24	2.296	4.808	30.7	67.1
038	A	139.4	0.0096	0.255	2.302	7.606	23.03.2007	L12_195_VGE_A_r01_t30_x.2x64x64.038.mes	L12_195_VGE_A_r01_t30_y.2x64x64.038.mes	1	2.296	7.608	29.1	139.3
038	B	138.9	0.0096	0.255	2.302	7.606	23.03.2007	L12_195_VGE_B_r04_t30_x.2x64x64.038.mes	L12_195_VGE_B_r04_t30_y.2x64x64.038.mes	3	2.296	7.606	29.2	138.9
038	C	138.3	0.0096	0.255	2.302	7.606	23.03.2007	L12_195_VGE_C_r01_t30_x.2x64x64.038.mes	L12_195_VGE_C_r01_t30_y.2x64x64.038.mes	4	2.296	7.616	29.3	138.4
038	D	136.8	0.0096	0.255	2.302	7.606	23.03.2007	L12_195_VGE_D_r01_t30_x.2x64x64.038.mes	L12_195_VGE_D_r01_t30_y.2x64x64.038.mes	5	2.296	7.616	29.4	136.8
038	E	136.2	0.0096	0.255	2.302	7.606	23.03.2007	L12_195_VGE_E_r04_t30_x.2x64x64.038.mes	L12_195_VGE_E_r04_t30_y.2x64x64.038.mes	6	2.296	7.607	29.4	136.2
038	F	135.7	0.0096	0.255	2.302	7.606	23.03.2007	L12_195_VGE_F_r01_t30_x.2x64x64.038.mes	L12_195_VGE_F_r01_t30_y.2x64x64.038.mes	7	2.296	7.606	29.5	135.7
038	G	127.7	0.0096	0.255	2.302	7.606	23.03.2007	L12_195_VGE_G_r01_t30_x.2x64x64.038.mes	L12_195_VGE_G_r01_t30_y.2x64x64.038.mes	8	2.296	7.597	29.6	127.7
038	H	127.2	0.0096	0.255	2.302	7.606	23.03.2007	L12_195_VGE_H_r04_t30_x.2x64x64.038.mes	L12_195_VGE_H_r04_t30_y.2x64x64.038.mes	10	2.296	7.611	29.7	127.2
038	I	126.6	0.0096	0.255	2.302	7.606	23.03.2007	L12_195_VGE_I_r01_t30_x.2x64x64.038.mes	L12_195_VGE_I_r01_t30_y.2x64x64.038.mes	11	2.296	7.599	29.7	126.5
038	J	117.7	0.0096	0.255	2.302	7.606	23.03.2007	L12_195_VGE_J_r01_t30_x.2x64x64.038.mes	L12_195_VGE_J_r01_t30_y.2x64x64.038.mes	12	2.296	7.600	30.3	117.6
038	K	117.2	0.0096	0.255	2.302	7.606	23.03.2007	L12_195_VGE_K_r04_t30_x.2x64x64.038.mes	L12_195_VGE_K_r04_t30_y.2x64x64.038.mes	13	2.296	7.604	30.4	117.1
038	L	116.6	0.0096	0.255	2.302	7.606	23.03.2007	L12_195_VGE_L_r01_t30_x.2x64x64.038.mes	L12_195_VGE_L_r01_t30_y.2x64x64.038.mes	15	2.296	7.611	30.5	116.6
038	M	99.1	0.0096	0.255	2.302	7.606	23.03.2007	L12_195_VGE_M_r01_t30_x.2x64x64.038.mes	L12_195_VGE_M_r01_t30_y.2x64x64.038.mes	16	2.296	7.603	30.6	99.0
038	N	98.6	0.0096	0.255	2.302	7.606	23.03.2007	L12_195_VGE_N_r04_t30_x.2x64x64.038.mes	L12_195_VGE_N_r04_t30_y.2x64x64.038.mes	17	2.296	7.604	30.6	98.6
038	O	98.0	0.0096	0.255	2.302	7.606	23.03.2007	L12_195_VGE_O_r01_t30_x.2x64x64.038.mes	L12_195_VGE_O_r01_t30_y.2x64x64.038.mes	18	2.296	7.601	30.7	98.0
038	P	67.7	0.0096	0.255	2.302	7.606	23.03.2007	L12_195_VGE_P_r01_t30_x.2x64x64.038.mes	L12_195_VGE_P_r01_t30_y.2x64x64.038.mes	20	2.296	7.604	30.8	67.8
038	Q	67.2	0.0096	0.255	2.302	7.606	23.03.2007	L12_195_VGE_Q_r04_t30_x.2x64x64.038.mes	L12_195_VGE_Q_r04_t30_y.2x64x64.038.mes	21	2.296	7.604	30.9	67.2
038	R	66.6	0.0096	0.255	2.302	7.606	23.07.2007	L12_195_VGE_R_r01_t30_x.2x64x64.038.mes	L12_195_VGE_R_r01_t30_y.2x64x64.038.mes	22	2.296	7.608	30.9	66.6
039	A	139.3	0.0096	0.405	2.302	12.081	01.06.2007	L12_195_VGE_A_r01_t30_x.2x64x64.039.mes	L12_195_VGE_A_r01_t30_y.2x64x64.039.mes	1	2.296	12.075	30.4	139.2
039	B	138.8	0.0096	0.405	2.302	12.081	01.06.2007	L12_195_VGE_B_r04_t30_x.2x64x64.039.mes	L12_195_VGE_B_r04_t30_y.2x64x64.039.mes	2	2.296	12.090	30.5	138.8
039	C	138.2	0.0096	0.405	2.302	12.081	01.06.2007	L12_195_VGE_C_r01_t30_x.2x64x64.039.mes	L12_195_VGE_C_r01_t30_y.2x64x64.039.mes	3	2.296	12.086	30.5	138.3
039	D	136.7	0.0096	0.405	2.302	12.081	01.06.2007	L12_195_VGE_D_r01_t30_x.2x64x64.039.mes	L12_195_VGE_D_r01_t30_y.2x64x64.039.mes	4	2.296	12.081	30.7	136.8
039	E	136.1	0.0096	0.405	2.302	12.081	01.06.2007	L12_195_VGE_E_r04_t30_x.2x64x64.039.mes	L12_195_VGE_E_r04_t30_y.2x64x64.039.mes	5	2.296	12.073	30.7	136.0
039	F	135.6	0.0096	0.405	2.302	12.081	01.06.2007	L12_195_VGE_F_r01_t30_x.2x64x64.039.mes	L12_195_VGE_F_r01_t30_y.2x64x64.039.mes	6	2.296	12.085	30.8	135.5
039	G	127.6	0.0096	0.405	2.302	12.081	01.06.2007	L12_195_VGE_G_r01_t30_x.2x64x64.039.mes	L12_195_VGE_G_r01_t30_y.2x64x64.039.mes	7	2.296	12.081	30.9	127.6
039	H	127.0	0.0096	0.405	2.302	12.081	01.06.2007	L12_195_VGE_H_r04_t30_x.2x64x64.039.mes	L12_195_VGE_H_r04_t30_y.2x64x64.039.mes	8	2.296	12.084	31.0	127.1
039	I	126.5	0.0096	0.405	2.302	12.081	01.06.2007	L12_195_VGE_I_r01_t30_x.2x64x64.039.mes	L12_195_VGE_I_r01_t30_y.2x64x64.039.mes	9	2.296	12.095	29.5	126.6
039	J	117.5	0.0096	0.405	2.302	12.081	01.06.2007	L12_195_VGE_J_r01_t30_x.2x64x64.039.mes	L12_195_VGE_J_r01_t30_y.2x64x64.039.mes	11	2.296	12.080	29.8	117.4
039	K	116.9	0.0096	0.405	2.302	12.081	01.06.2007	L12_195_VGE_K_r04_t30_x.2x64x64.039.mes	L12_195_VGE_K_r04_t30_y.2x64x64.039.mes	12	2.296	12.086	29.9	116.9
039	L	116.4	0.0096	0.405	2.302	12.081	01.06.2007	L12_195_VGE_L_r01_t30_x.2x64x64.039.mes	L12_195_VGE_L_r01_t30_y.2x64x64.039.mes	13	2.296	12.077	30.0	116.4
039	M	98.8	0.0096	0.405	2.302	12.081	01.06.2007	L12_195_VGE_M_r01_t30_x.2x64x64.039.mes	L12_195_VGE_M_r01_t30_y.2x64x64.039.mes	14	2.295	12.086	30.1	98.7
039	N	98.2	0.0096	0.405	2.302	12.081	01.06.2007	L12_195_VGE_N_r04_t30_x.2x64x64.039.mes	L12_195_VGE_N_r04_t30_y.2x64x64.039.mes	15	2.296	12.074	30.2	98.3
039	O	97.7	0.0096	0.405	2.302	12.081	01.06.2007	L12_195_VGE_O_r01_t30_x.2x64x64.039.mes	L12_195_VGE_O_r01_t30_y.2x64x64.039.mes	16	2.296	12.076	30.3	97.7
039	P	67.2	0.0096	0.405	2.302	12.081	01.06.2007	L12_195_VGE_P_r01_t30_x.2x64x64.039.mes	L12_195_VGE_P_r01_t30_y.2x64x64.039.mes	17	2.296	12.083	30.6	67.2
039	Q	66.6	0.0096	0.405	2.302	12.081	01.06.2007	L12_195_VGE_Q_r04_t30_x.2x64x64.039.mes	L12_195_VGE_Q_r04_t30_y.2x64x64.039.mes	19	2.296	12.079	30.7	66.6
039	R	66.1	0.0096	0.405	2.302	12.081	01.06.2007	L12_195_VGE_R_r01_t30_x.2x64x64.039.mes	L12_195_VGE_R_r01_t30_y.2x64x64.039.mes	20	2.296	12.086	30.8	66.1

Matrix-punkt	Höhen-position	Druck am GS (ü) PI4-07 [kPa]	J _{Gas} [m/s] Einspeisung	J _{Wasser} [m/s]	V _{Gas} [nm³/h]	m _{Wasser} [kg/s]	Datum	File 1 (x)	File 2 (y)	DIAdem	Betriebsdaten (Mittelwerte über 10 s)			
											V _{Gas} [m³/h]	m _{Wasser} [kg/s]	t _{GS} [°C]	p(ü) GS [kPa]
040	A	139.2	0.0096	0.641	2.302	19.120	27.03.2007	L12_195_VGE_A_r01_t30_x.2x64x64.040.mes	L12_195_VGE_A_r01_t30_y.2x64x64.040.mes	26	2.296	19.133	30.4	139.2
040	B	138.6	0.0096	0.641	2.302	19.120	27.03.2007	L12_195_VGE_B_r04_t30_x.2x64x64.040.mes	L12_195_VGE_B_r04_t30_y.2x64x64.040.mes	25	2.296	19.118	30.2	138.6
040	C	138.1	0.0096	0.641	2.302	19.120	27.03.2007	L12_195_VGE_C_r01_t30_x.2x64x64.040.mes	L12_195_VGE_C_r01_t30_y.2x64x64.040.mes	23	2.296	19.110	30.1	138.0
040	D	136.5	0.0096	0.641	2.302	19.120	27.03.2007	L12_195_VGE_D_r01_t30_x.2x64x64.040.mes	L12_195_VGE_D_r01_t30_y.2x64x64.040.mes	22	2.296	19.123	30.0	136.5
040	E	136.0	0.0096	0.641	2.302	19.120	27.03.2007	L12_195_VGE_E_r04_t30_x.2x64x64.040.mes	L12_195_VGE_E_r04_t30_y.2x64x64.040.mes	21	2.296	19.114	29.9	136.0
040	F	135.4	0.0096	0.641	2.302	19.120	27.03.2007	L12_195_VGE_F_r01_t30_x.2x64x64.040.mes	L12_195_VGE_F_r01_t30_y.2x64x64.040.mes	19	2.296	19.121	29.7	135.4
040	G	127.3	0.0096	0.641	2.302	19.120	27.03.2007	L12_195_VGE_G_r01_t30_x.2x64x64.040.mes	L12_195_VGE_G_r01_t30_y.2x64x64.040.mes	17	2.296	19.130	30.5	127.3
040	H	126.8	0.0096	0.641	2.302	19.120	27.03.2007	L12_195_VGE_H_r04_t30_x.2x64x64.040.mes	L12_195_VGE_H_r04_t30_y.2x64x64.040.mes	15	2.296	19.126	30.4	126.8
040	I	126.2	0.0096	0.641	2.302	19.120	27.03.2007	L12_195_VGE_I_r01_t30_x.2x64x64.040.mes	L12_195_VGE_I_r01_t30_y.2x64x64.040.mes	14	2.296	19.120	30.3	126.2
040	J	117.2	0.0096	0.641	2.302	19.120	27.03.2007	L12_195_VGE_J_r01_t30_x.2x64x64.040.mes	L12_195_VGE_J_r01_t30_y.2x64x64.040.mes	12	2.296	19.125	30.2	117.2
040	K	116.6	0.0096	0.641	2.302	19.120	27.03.2007	L12_195_VGE_K_r04_t30_x.2x64x64.040.mes	L12_195_VGE_K_r04_t30_y.2x64x64.040.mes	9	2.296	19.128	30.0	116.6
040	L	116.0	0.0096	0.641	2.302	19.120	27.03.2007	L12_195_VGE_L_r01_t30_x.2x64x64.040.mes	L12_195_VGE_L_r01_t30_y.2x64x64.040.mes	8	2.296	19.119	29.9	116.0
040	M	98.3	0.0096	0.641	2.302	19.120	27.03.2007	L12_195_VGE_M_r01_t30_x.2x64x64.040.mes	L12_195_VGE_M_r01_t30_y.2x64x64.040.mes	7	2.296	19.132	29.7	98.3
040	N	97.7	0.0096	0.641	2.302	19.120	27.03.2007	L12_195_VGE_N_r04_t30_x.2x64x64.040.mes	L12_195_VGE_N_r04_t30_y.2x64x64.040.mes	6	2.296	19.129	29.6	97.7
040	O	97.2	0.0096	0.641	2.302	19.120	27.03.2007	L12_195_VGE_O_r01_t30_x.2x64x64.040.mes	L12_195_VGE_O_r01_t30_y.2x64x64.040.mes	5	2.296	19.117	29.5	97.2
040	P	66.4	0.0096	0.641	2.302	19.120	27.03.2007	L12_195_VGE_P_r01_t30_x.2x64x64.040.mes	L12_195_VGE_P_r01_t30_y.2x64x64.040.mes	4	2.296	19.124	29.2	66.5
040	Q	65.9	0.0096	0.641	2.302	19.120	27.03.2007	L12_195_VGE_Q_r04_t30_x.2x64x64.040.mes	L12_195_VGE_Q_r04_t30_y.2x64x64.040.mes	3	2.296	19.118	29.1	65.9
040	R	65.3	0.0096	0.641	2.302	19.120	27.03.2007	L12_195_VGE_R_r01_t30_x.2x64x64.040.mes	L12_195_VGE_R_r01_t30_y.2x64x64.040.mes	2	2.296	19.122	29.8	65.3
041	A	138.9	0.0096	1.017	2.302	30.336	14.06.2007	L12_195_VGE_A_r01_t30_x.2x64x64.041.mes	L12_195_VGE_A_r01_t30_y.2x64x64.041.mes	46	2.295	30.340	30.5	139.0
041	B	138.3	0.0096	1.017	2.302	30.336	14.06.2007	L12_195_VGE_B_r04_t30_x.2x64x64.041.mes	L12_195_VGE_B_r04_t30_y.2x64x64.041.mes	42	2.295	30.325	29.8	138.3
041	C	137.8	0.0096	1.017	2.302	30.336	14.06.2007	L12_195_VGE_C_r01_t30_x.2x64x64.041.mes	L12_195_VGE_C_r01_t30_y.2x64x64.041.mes	41	2.296	30.347	29.4	137.9
041	D	136.2	0.0096	1.017	2.302	30.336	14.06.2007	L12_195_VGE_D_r01_t30_x.2x64x64.041.mes	L12_195_VGE_D_r01_t30_y.2x64x64.041.mes	40	2.296	30.328	29.3	136.1
041	E	135.6	0.0096	1.017	2.302	30.336	14.06.2007	L12_195_VGE_E_r04_t30_x.2x64x64.041.mes	L12_195_VGE_E_r04_t30_y.2x64x64.041.mes	38	2.296	30.354	29.5	135.6
041	F	135.1	0.0096	1.017	2.302	30.336	14.06.2007	L12_195_VGE_F_r01_t30_x.2x64x64.041.mes	L12_195_VGE_F_r01_t30_y.2x64x64.041.mes	37	2.296	30.331	29.8	135.0
041	G	126.8	0.0096	1.017	2.302	30.336	14.06.2007	L12_195_VGE_G_r01_t30_x.2x64x64.041.mes	L12_195_VGE_G_r01_t30_y.2x64x64.041.mes	31	2.296	30.331	30.6	126.7
041	H	126.3	0.0096	1.017	2.302	30.336	14.06.2007	L12_195_VGE_H_r04_t30_x.2x64x64.041.mes	L12_195_VGE_H_r04_t30_y.2x64x64.041.mes	30	2.296	30.320	30.4	126.2
041	I	125.7	0.0096	1.017	2.302	30.336	14.06.2007	L12_195_VGE_I_r01_t30_x.2x64x64.041.mes	L12_195_VGE_I_r01_t30_y.2x64x64.041.mes	29	2.296	30.340	30.2	125.7
041	J	116.5	0.0096	1.017	2.302	30.336	14.06.2007	L12_195_VGE_J_r01_t30_x.2x64x64.041.mes	L12_195_VGE_J_r01_t30_y.2x64x64.041.mes	24	2.296	30.346	29.4	116.5
041	K	116.0	0.0096	1.017	2.302	30.336	14.06.2007	L12_195_VGE_K_r04_t30_x.2x64x64.041.mes	L12_195_VGE_K_r04_t30_y.2x64x64.041.mes	19	2.296	30.332	29.1	116.0
041	L	115.4	0.0096	1.017	2.302	30.336	14.06.2007	L12_195_VGE_L_r01_t30_x.2x64x64.041.mes	L12_195_VGE_L_r01_t30_y.2x64x64.041.mes	18	2.296	30.340	29.5	115.3
041	M	97.4	0.0096	1.017	2.302	30.336	14.06.2007	L12_195_VGE_M_r01_t30_x.2x64x64.041.mes	L12_195_VGE_M_r01_t30_y.2x64x64.041.mes	12	2.296	30.335	29.6	97.4
041	N	96.8	0.0096	1.017	2.302	30.336	14.06.2007	L12_195_VGE_N_r04_t30_x.2x64x64.041.mes	L12_195_VGE_N_r04_t30_y.2x64x64.041.mes	11	2.296	30.337	29.6	96.8
041	O	96.2	0.0096	1.017	2.302	30.336	14.06.2007	L12_195_VGE_O_r01_t30_x.2x64x64.041.mes	L12_195_VGE_O_r01_t30_y.2x64x64.041.mes	10	2.296	30.343	29.6	96.2
041	P	65.0	0.0096	1.017	2.302	30.336	14.06.2007	L12_195_VGE_P_r01_t30_x.2x64x64.041.mes	L12_195_VGE_P_r01_t30_y.2x64x64.041.mes	9	2.296	30.322	29.7	64.9
041	Q	64.4	0.0096	1.017	2.302	30.336	14.06.2007	L12_195_VGE_Q_r04_t30_x.2x64x64.041.mes	L12_195_VGE_Q_r04_t30_y.2x64x64.041.mes	8	2.296	30.332	29.7	64.4
041	R	63.9	0.0096	1.017	2.302	30.336	14.06.2007	L12_195_VGE_R_r01_t30_x.2x64x64.041.mes	L12_195_VGE_R_r01_t30_y.2x64x64.041.mes	3	2.296	30.333	29.9	64.0
042	A	138.2	0.0096	1.611	2.302	48.054	19.06.2007	L12_195_VGE_A_r01_t30_x.2x64x64.042.mes	L12_195_VGE_A_r01_t30_y.2x64x64.042.mes	6b	2.296	48.063	30.2	138.2
042	B	137.6	0.0096	1.611	2.302	48.054	19.06.2007	L12_195_VGE_B_r04_t30_x.2x64x64.042.mes	L12_195_VGE_B_r04_t30_y.2x64x64.042.mes	5b	2.295	48.029	30.0	137.7
042	C	137.0	0.0096	1.611	2.302	48.054	19.06.2007	L12_195_VGE_C_r01_t30_x.2x64x64.042.mes	L12_195_VGE_C_r01_t30_y.2x64x64.042.mes	1b	2.295	48.049	30.4	137.1
042	D	135.4	0.0096	1.611	2.302	48.054	19.06.2007	L12_195_VGE_D_r01_t30_x.2x64x64.042.mes	L12_195_VGE_D_r01_t30_y.2x64x64.042.mes	30a	2.296	48.077	30.7	135.4
042	E	134.8	0.0096	1.611	2.302	48.054	19.06.2007	L12_195_VGE_E_r04_t30_x.2x64x64.042.mes	L12_195_VGE_E_r04_t30_y.2x64x64.042.mes	25a	2.296	48.061	30.4	134.9
042	F	134.2	0.0096	1.611	2.302	48.054	19.06.2007	L12_195_VGE_F_r01_t30_x.2x64x64.042.mes	L12_195_VGE_F_r01_t30_y.2x64x64.042.mes	24a	2.296	48.050	30.3	134.3
042	G	125.8	0.0096	1.611	2.302	48.054	29.06.2007	L12_195_VGE_G_r01_t30_x.2x64x64.042.mes	L12_195_VGE_G_r01_t30_y.2x64x64.042.mes	6	2.294	48.038	30.0	125.8
042	H	125.2	0.0096	1.611	2.302	48.054	29.06.2007	L12_195_VGE_H_r04_t30_x.2x64x64.042.mes	L12_195_VGE_H_r04_t30_y.2x64x64.042.mes	5	2.295	48.048	29.8	125.1
042	I	124.6	0.0096	1.611	2.302	48.054	29.06.2007	L12_195_VGE_I_r01_t30_x.2x64x64.042.mes	L12_195_VGE_I_r01_t30_y.2x64x64.042.mes	3	2.295	48.049	29.6	124.6
042	J	115.1	0.0096	1.611	2.302	48.054	19.06.2007	L12_195_VGE_J_r01_t30_x.2x64x64.042.mes	L12_195_VGE_J_r01_t30_y.2x64x64.042.mes	17a	2.296	48.053	30.5	115.1
042	K	114.5	0.0096	1.611	2.302	48.054	19.06.2007	L12_195_VGE_K_r04_t30_x.2x64x64.042.mes	L12_195_VGE_K_r04_t30_y.2x64x64.042.mes	14a	2.296	48.056	30.7	114.4
042	L	113.9	0.0096	1.611	2.302	48.054	19.06.2007	L12_195_VGE_L_r01_t30_x.2x64x64.042.mes	L12_195_VGE_L_r01_t30_y.2x64x64.042.mes	13a	2.296	48.073	30.9	113.9
042	M	95.3	0.0096	1.611	2.302	48.054	19.06.2007	L12_195_VGE_M_r01_t30_x.2x64x64.042.mes	L12_195_VGE_M_r01_t30_y.2x64x64.042.mes	12a	2.295	48.040	30.0	95.3
042	N	94.7	0.0096	1.611	2.302	48.054	19.06.2007	L12_195_VGE_N_r04_t30_x.2x64x64.042.mes	L12_195_VGE_N_r04_t30_y.2x64x64.042.mes	10a	2.296	48.065	29.5	94.7
042	O	94.2	0.0096	1.611	2.302	48.054	19.06.2007	L12_195_VGE_O_r01_t30_x.2x64x64.042.mes	L12_195_VGE_O_r01_t30_y.2x64x64.042.mes	6a	2.296	48.065	29.6	94.2
042	P	61.9	0.0096	1.611	2.302	48.054	19.06.2007	L12_195_VGE_P_r01_t30_x.2x64x64.042.mes	L12_195_VGE_P_r01_t30_y.2x64x64.042.mes	5a	2.296	48.052	29.8	61.9
042	Q	61.3	0.0096	1.611	2.302	48.054	19.06.2007	L12_195_VGE_Q_r04_t30_x.2x64x64.042.mes	L12_195_VGE_Q_r04_t30_y.2x64x64.042.mes	3a	2.296	48.061	30.1	61.3
042	R	60.7	0.0096	1.611	2.302	48.054	19.06.2007	L12_195_VGE_R_r01_t30_x.2x64x64.042.mes	L12_195_VGE_R_r01_t30_y.2x64x64.042.mes	1a	2.295	48.057	30.8	60.7

Matrix-punkt	Höhen-position	Druck am GS (ü) PI4-07 [kPa]	J _{Gas} [m/s] Einspeisung	J _{Wasser} [m/s]	V _{Gas} [nm³/h]	m _{Wasser} [kg/s]	Datum	File 1 (x)	File 2 (y)	DIAdem	Betriebsdaten (Mittelwerte über 10 s)			
											V _{Gas} [m³/h]	m _{Wasser} [kg/s]	t _{GS} [°C]	p(ü) GS [kPa]
050	A	139.4	0.0151	0.405	3.621	12.081	23.02.2007	L12_195_VGE_A_r01_t30_x.2x64x64.050.mes	L12_195_VGE_A_r01_t30_y.2x64x64.050.mes	25	3.611	12.094	29.6	139.2
050	B	138.9	0.0151	0.405	3.621	12.081	23.02.2007	L12_195_VGE_B_r04_t30_x.2x64x64.050.mes	L12_195_VGE_B_r04_t30_y.2x64x64.050.mes	24	3.611	12.095	29.6	138.8
050	C	138.3	0.0151	0.405	3.621	12.081	23.02.2007	L12_195_VGE_C_r01_t30_x.2x64x64.050.mes	L12_195_VGE_C_r01_t30_y.2x64x64.050.mes	23	3.611	12.081	29.5	138.2
050	D	136.8	0.0151	0.405	3.621	12.081	23.02.2007	L12_195_VGE_D_r01_t30_x.2x64x64.050.mes	L12_195_VGE_D_r01_t30_y.2x64x64.050.mes	21	3.611	12.079	29.3	136.8
050	E	136.3	0.0151	0.405	3.621	12.081	23.02.2007	L12_195_VGE_E_r04_t30_x.2x64x64.050.mes	L12_195_VGE_E_r04_t30_y.2x64x64.050.mes	19	3.611	12.084	29.2	136.4
050	F	135.7	0.0151	0.405	3.621	12.081	23.02.2007	L12_195_VGE_F_r01_t30_x.2x64x64.050.mes	L12_195_VGE_F_r01_t30_y.2x64x64.050.mes	17	3.611	12.087	29.1	135.6
050	G	127.8	0.0151	0.405	3.621	12.081	23.02.2007	L12_195_VGE_G_r01_t30_x.2x64x64.050.mes	L12_195_VGE_G_r01_t30_y.2x64x64.050.mes	16	3.611	12.104	29.0	127.9
050	H	127.2	0.0151	0.405	3.621	12.081	23.02.2007	L12_195_VGE_H_r04_t30_x.2x64x64.050.mes	L12_195_VGE_H_r04_t30_y.2x64x64.050.mes	15	3.611	12.080	29.9	127.3
050	I	126.7	0.0151	0.405	3.621	12.081	23.02.2007	L12_195_VGE_I_r01_t30_x.2x64x64.050.mes	L12_195_VGE_I_r01_t30_y.2x64x64.050.mes	14	3.611	12.082	30.5	126.8
050	J	117.8	0.0151	0.405	3.621	12.081	23.02.2007	L12_195_VGE_J_r01_t30_x.2x64x64.050.mes	L12_195_VGE_J_r01_t30_y.2x64x64.050.mes	13	3.611	12.077	30.4	117.7
050	K	117.2	0.0151	0.405	3.621	12.081	23.02.2007	L12_195_VGE_K_r04_t30_x.2x64x64.050.mes	L12_195_VGE_K_r04_t30_y.2x64x64.050.mes	12	3.611	12.087	30.3	117.3
050	L	116.7	0.0151	0.405	3.621	12.081	23.02.2007	L12_195_VGE_L_r01_t30_x.2x64x64.050.mes	L12_195_VGE_L_r01_t30_y.2x64x64.050.mes	11	3.610	12.079	30.3	116.8
050	M	99.2	0.0151	0.405	3.621	12.081	23.02.2007	L12_195_VGE_M_r01_t30_x.2x64x64.050.mes	L12_195_VGE_M_r01_t30_y.2x64x64.050.mes	9	3.611	12.077	29.9	99.2
050	N	98.7	0.0151	0.405	3.621	12.081	23.02.2007	L12_195_VGE_N_r04_t30_x.2x64x64.050.mes	L12_195_VGE_N_r04_t30_y.2x64x64.050.mes	8	3.611	12.084	29.8	98.7
050	O	98.1	0.0151	0.405	3.621	12.081	23.02.2007	L12_195_VGE_O_r01_t30_x.2x64x64.050.mes	L12_195_VGE_O_r01_t30_y.2x64x64.050.mes	6	3.611	12.074	29.7	98.1
050	P	67.9	0.0151	0.405	3.621	12.081	23.02.2007	L12_195_VGE_P_r01_t30_x.2x64x64.050.mes	L12_195_VGE_P_r01_t30_y.2x64x64.050.mes	5	3.611	12.074	29.6	68.1
050	Q	67.3	0.0151	0.405	3.621	12.081	23.02.2007	L12_195_VGE_Q_r04_t30_x.2x64x64.050.mes	L12_195_VGE_Q_r04_t30_y.2x64x64.050.mes	4	3.611	12.085	29.4	67.5
050	R	66.8	0.0151	0.405	3.621	12.081	23.02.2007	L12_195_VGE_R_r01_t30_x.2x64x64.050.mes	L12_195_VGE_R_r01_t30_y.2x64x64.050.mes	1	3.610	12.093	29.3	66.9
052	A	138.9	0.0151	1.017	3.621	30.336	22.02.2007	L12_195_VGE_A_r01_t30_x.2x64x64.052.mes	L12_195_VGE_A_r01_t30_y.2x64x64.052.mes	27	3.611	30.331	30.9	138.9
052	B	138.4	0.0151	1.017	3.621	30.336	22.02.2007	L12_195_VGE_B_r04_t30_x.2x64x64.052.mes	L12_195_VGE_B_r04_t30_y.2x64x64.052.mes	26	3.611	30.334	30.5	138.5
052	C	137.8	0.0151	1.017	3.621	30.336	22.02.2007	L12_195_VGE_C_r01_t30_x.2x64x64.052.mes	L12_195_VGE_C_r01_t30_y.2x64x64.052.mes	25	3.611	30.330	30.0	137.8
052	D	136.2	0.0151	1.017	3.621	30.336	15.06.2007	L12_195_VGE_D_r01_t30_x.2x64x64.052.mes	L12_195_VGE_D_r01_t30_y.2x64x64.052.mes	22	3.609	30.346	30.0	136.2
052	E	135.7	0.0151	1.017	3.621	30.336	22.02.2007	L12_195_VGE_E_r04_t30_x.2x64x64.052.mes	L12_195_VGE_E_r04_t30_y.2x64x64.052.mes	23	3.611	30.326	29.5	135.8
052	F	135.1	0.0151	1.017	3.621	30.336	15.06.2007	L12_195_VGE_F_r01_t30_x.2x64x64.052.mes	L12_195_VGE_F_r01_t30_y.2x64x64.052.mes	24	3.611	30.353	29.7	135.2
052	G	126.9	0.0151	1.017	3.621	30.336	22.02.2007	L12_195_VGE_G_r01_t30_x.2x64x64.052.mes	L12_195_VGE_G_r01_t30_y.2x64x64.052.mes	16	3.611	30.339	30.0	126.9
052	H	126.4	0.0151	1.017	3.621	30.336	22.02.2007	L12_195_VGE_H_r04_t30_x.2x64x64.052.mes	L12_195_VGE_H_r04_t30_y.2x64x64.052.mes	14	3.611	30.335	29.4	126.3
052	I	125.8	0.0151	1.017	3.621	30.336	22.02.2007	L12_195_VGE_I_r01_t30_x.2x64x64.052.mes	L12_195_VGE_I_r01_t30_y.2x64x64.052.mes	13	3.611	30.338	29.0	125.7
052	J	116.6	0.0151	1.017	3.621	30.336	22.02.2007	L12_195_VGE_J_r01_t30_x.2x64x64.052.mes	L12_195_VGE_J_r01_t30_y.2x64x64.052.mes	12	3.611	30.338	29.8	116.7
052	K	116.1	0.0151	1.017	3.621	30.336	22.02.2007	L12_195_VGE_K_r04_t30_x.2x64x64.052.mes	L12_195_VGE_K_r04_t30_y.2x64x64.052.mes	11	3.611	30.332	30.6	116.1
052	L	115.5	0.0151	1.017	3.621	30.336	22.02.2007	L12_195_VGE_L_r01_t30_x.2x64x64.052.mes	L12_195_VGE_L_r01_t30_y.2x64x64.052.mes	8	3.611	30.363	30.3	115.5
052	M	97.6	0.0151	1.017	3.621	30.336	22.02.2007	L12_195_VGE_M_r01_t30_x.2x64x64.052.mes	L12_195_VGE_M_r01_t30_y.2x64x64.052.mes	7	3.611	30.340	29.6	97.7
052	N	97.0	0.0151	1.017	3.621	30.336	22.02.2007	L12_195_VGE_N_r04_t30_x.2x64x64.052.mes	L12_195_VGE_N_r04_t30_y.2x64x64.052.mes	6	3.611	30.330	29.4	97.0
052	O	96.4	0.0151	1.017	3.621	30.336	22.02.2007	L12_195_VGE_O_r01_t30_x.2x64x64.052.mes	L12_195_VGE_O_r01_t30_y.2x64x64.052.mes	4	3.611	30.342	29.5	96.3
052	P	65.3	0.0151	1.017	3.621	30.336	22.02.2007	L12_195_VGE_P_r01_t30_x.2x64x64.052.mes	L12_195_VGE_P_r01_t30_y.2x64x64.052.mes	3	3.611	30.332	30.4	65.3
052	Q	64.8	0.0151	1.017	3.621	30.336	22.02.2007	L12_195_VGE_Q_r04_t30_x.2x64x64.052.mes	L12_195_VGE_Q_r04_t30_y.2x64x64.052.mes	2	3.611	30.353	29.6	64.9
052	R	64.2	0.0151	1.017	3.621	30.336	22.02.2007	L12_195_VGE_R_r01_t30_x.2x64x64.052.mes	L12_195_VGE_R_r01_t30_y.2x64x64.052.mes	1	3.610	30.348	29.2	64.3
061	A	139.5	0.0235	0.405	5.636	12.081	16.05.2007	L12_195_VGE_A_r01_t30_x.2x64x64.061.mes	L12_195_VGE_A_r01_t30_y.2x64x64.061.mes	9b	5.655	12.077	30.4	139.6
061	B	139.0	0.0235	0.405	5.636	12.081	16.05.2007	L12_195_VGE_B_r04_t30_x.2x64x64.061.mes	L12_195_VGE_B_r04_t30_y.2x64x64.061.mes	8b	5.652	12.081	30.3	139.1
061	C	138.5	0.0235	0.405	5.636	12.081	16.05.2007	L12_195_VGE_C_r01_t30_x.2x64x64.061.mes	L12_195_VGE_C_r01_t30_y.2x64x64.061.mes	7b	5.653	12.085	30.2	138.6
061	D	137.0	0.0235	0.405	5.636	12.081	16.05.2007	L12_195_VGE_D_r01_t30_x.2x64x64.061.mes	L12_195_VGE_D_r01_t30_y.2x64x64.061.mes	6b	5.652	12.087	30.1	137.0
061	E	136.4	0.0235	0.405	5.636	12.081	16.05.2007	L12_195_VGE_E_r04_t30_x.2x64x64.061.mes	L12_195_VGE_E_r04_t30_y.2x64x64.061.mes	5b	5.656	12.087	29.9	136.5
061	F	135.9	0.0235	0.405	5.636	12.081	16.05.2007	L12_195_VGE_F_r01_t30_x.2x64x64.061.mes	L12_195_VGE_F_r01_t30_y.2x64x64.061.mes	4b	5.656	12.072	29.7	136.0
061	G	128.0	0.0235	0.405	5.636	12.081	16.05.2007	L12_195_VGE_G_r01_t30_x.2x64x64.061.mes	L12_195_VGE_G_r01_t30_y.2x64x64.061.mes	3b	5.652	12.079	30.6	128.2
061	H	127.5	0.0235	0.405	5.636	12.081	16.05.2007	L12_195_VGE_H_r04_t30_x.2x64x64.061.mes	L12_195_VGE_H_r04_t30_y.2x64x64.061.mes	2b	5.647	12.053	30.5	127.6
061	I	126.9	0.0235	0.405	5.636	12.081	16.05.2007	L12_195_VGE_I_r01_t30_x.2x64x64.061.mes	L12_195_VGE_I_r01_t30_y.2x64x64.061.mes	1b	5.651	12.082	30.4	126.8
061	J	118.2	0.0235	0.405	5.636	12.081	16.05.2007	L12_195_VGE_J_r01_t30_x.2x64x64.061.mes	L12_195_VGE_J_r01_t30_y.2x64x64.061.mes	13a	5.655	12.072	30.3	118.5
061	K	117.6	0.0235	0.405	5.636	12.081	16.05.2007	L12_195_VGE_K_r04_t30_x.2x64x64.061.mes	L12_195_VGE_K_r04_t30_y.2x64x64.061.mes	11a	5.651	12.084	30.1	117.5
061	L	117.1	0.0235	0.405	5.636	12.081	16.05.2007	L12_195_VGE_L_r01_t30_x.2x64x64.061.mes	L12_195_VGE_L_r01_t30_y.2x64x64.061.mes	10a	5.652	12.066	30.1	117.3
061	M	99.8	0.0235	0.405	5.636	12.081	16.05.2007	L12_195_VGE_M_r01_t30_x.2x64x64.061.mes	L12_195_VGE_M_r01_t30_y.2x64x64.061.mes	9a	5.652	12.104	30.0	99.8
061	N	99.3	0.0235	0.405	5.636	12.081	16.05.2007	L12_195_VGE_N_r04_t30_x.2x64x64.061.mes	L12_195_VGE_N_r04_t30_y.2x64x64.061.mes	7a	5.651	12.079	29.9	99.2
061	O	98.7	0.0235	0.405	5.636	12.081	16.05.2007	L12_195_VGE_O_r01_t30_x.2x64x64.061.mes	L12_195_VGE_O_r01_t30_y.2x64x64.061.mes	6a	5.653	12.089	29.9	98.7
061	P	68.9	0.0235	0.405	5.636	12.081	16.05.2007	L12_195_VGE_P_r01_t30_x.2x64x64.061.mes	L12_195_VGE_P_r01_t30_y.2x64x64.061.mes	5a	5.656	12.033	29.7	68.8
061	Q	68.3	0.0235	0.405	5.636	12.081	16.05.2007	L12_195_VGE_Q_r04_t30_x.2x64x64.061.mes	L12_195_VGE_Q_r04_t30_y.2x64x64.061.mes	4a	5.654	12.093	29.6	68.2
061	R	67.8	0.0235	0.405	5.636	12.081	16.05.2007	L12_195_VGE_R_r01_t30_x.2x64x64.061.mes	L12_195_VGE_R_r01_t30_y.2x64x64.061.mes	1a	5.653	12.071	29.5	67.8

Matrix-punkt	Höhen-position	Druck am GS (ü) PI4-07 [kPa]	J _{Gas} [m/s] Einspeisung	J _{Wasser} [m/s]	V _{Gas} [nm³/h]	m _{Wasser} [kg/s]	Datum	File 1 (x)	File 2 (y)	DIAdem	Betriebsdaten (Mittelwerte über 10 s)			
											V _{Gas} [m³/h]	m _{Wasser} [kg/s]	t _{GS} [°C]	p(ü) GS [kPa]
063	A	139.0	0.0235	1.017	5.636	30.336	06.06.2007	L12_195_VGE_A_r01_t30_x.2x64x64.063.mes	L12_195_VGE_A_r01_t30_y.2x64x64.063.mes	25b	5.652	30.318	29.9	139.0
063	B	138.4	0.0235	1.017	5.636	30.336	06.06.2007	L12_195_VGE_B_r04_t30_x.2x64x64.063.mes	L12_195_VGE_B_r04_t30_y.2x64x64.063.mes	24b	5.651	30.341	29.7	138.5
063	C	137.9	0.0235	1.017	5.636	30.336	06.06.2007	L12_195_VGE_C_r01_t30_x.2x64x64.063.mes	L12_195_VGE_C_r01_t30_y.2x64x64.063.mes	22b	5.651	30.343	29.5	137.9
063	D	136.3	0.0235	1.017	5.636	30.336	06.06.2007	L12_195_VGE_D_r01_t30_x.2x64x64.063.mes	L12_195_VGE_D_r01_t30_y.2x64x64.063.mes	21b	5.655	30.350	29.2	136.4
063	E	135.8	0.0235	1.017	5.636	30.336	06.06.2007	L12_195_VGE_E_r04_t30_x.2x64x64.063.mes	L12_195_VGE_E_r04_t30_y.2x64x64.063.mes	20b	5.654	30.342	29.4	135.9
063	F	135.2	0.0235	1.017	5.636	30.336	06.06.2007	L12_195_VGE_F_r01_t30_x.2x64x64.063.mes	L12_195_VGE_F_r01_t30_y.2x64x64.063.mes	18b	5.653	30.347	29.6	135.2
063	G	127.1	0.0235	1.017	5.636	30.336	06.06.2007	L12_195_VGE_G_r01_t30_x.2x64x64.063.mes	L12_195_VGE_G_r01_t30_y.2x64x64.063.mes	17b	5.652	30.354	30.2	127.2
063	H	126.5	0.0235	1.017	5.636	30.336	06.06.2007	L12_195_VGE_H_r04_t30_x.2x64x64.063.mes	L12_195_VGE_H_r04_t30_y.2x64x64.063.mes	13b	5.650	30.344	30.7	126.5
063	I	126.0	0.0235	1.017	5.636	30.336	06.06.2007	L12_195_VGE_I_r01_t30_x.2x64x64.063.mes	L12_195_VGE_I_r01_t30_y.2x64x64.063.mes	11b	5.650	30.313	30.8	125.9
063	J	116.8	0.0235	1.017	5.636	30.336	06.06.2007	L12_195_VGE_J_r01_t30_x.2x64x64.063.mes	L12_195_VGE_J_r01_t30_y.2x64x64.063.mes	10b	5.652	30.330	29.6	116.8
063	K	116.3	0.0235	1.017	5.636	30.336	06.06.2007	L12_195_VGE_K_r04_t30_x.2x64x64.063.mes	L12_195_VGE_K_r04_t30_y.2x64x64.063.mes	9b	5.652	30.338	29.4	116.5
063	L	115.7	0.0235	1.017	5.636	30.336	06.06.2007	L12_195_VGE_L_r01_t30_x.2x64x64.063.mes	L12_195_VGE_L_r01_t30_y.2x64x64.063.mes	8b	5.652	30.343	29.2	115.6
063	M	97.9	0.0235	1.017	5.636	30.336	06.06.2007	L12_195_VGE_M_r01_t30_x.2x64x64.063.mes	L12_195_VGE_M_r01_t30_y.2x64x64.063.mes	7b	5.651	30.334	29.6	97.9
063	N	97.3	0.0235	1.017	5.636	30.336	06.06.2007	L12_195_VGE_N_r04_t30_x.2x64x64.063.mes	L12_195_VGE_N_r04_t30_y.2x64x64.063.mes	6b	5.653	30.335	29.9	97.3
063	O	96.8	0.0235	1.017	5.636	30.336	06.06.2007	L12_195_VGE_O_r01_t30_x.2x64x64.063.mes	L12_195_VGE_O_r01_t30_y.2x64x64.063.mes	5b	5.648	30.336	30.2	96.8
063	P	65.8	0.0235	1.017	5.636	30.336	06.06.2007	L12_195_VGE_P_r01_t30_x.2x64x64.063.mes	L12_195_VGE_P_r01_t30_y.2x64x64.063.mes	4b	5.652	30.339	30.9	65.9
063	Q	65.3	0.0235	1.017	5.636	30.336	06.06.2007	L12_195_VGE_Q_r04_t30_x.2x64x64.063.mes	L12_195_VGE_Q_r04_t30_y.2x64x64.063.mes	3b	5.652	30.339	30.7	65.4
063	R	64.7	0.0235	1.017	5.636	30.336	06.06.2007	L12_195_VGE_R_r01_t30_x.2x64x64.063.mes	L12_195_VGE_R_r01_t30_y.2x64x64.063.mes	1a	5.653	30.344	30.4	64.7
072	A	139.7	0.0368	0.405	8.825	12.081	20.02.2007	L12_195_VGE_A_r01_t30_x.2x64x64.072.mes	L12_195_VGE_A_r01_t30_y.2x64x64.072.mes	22	8.977	12.073	31.0	139.7
072	B	139.2	0.0368	0.405	8.825	12.081	20.02.2007	L12_195_VGE_B_r04_t30_x.2x64x64.072.mes	L12_195_VGE_B_r04_t30_y.2x64x64.072.mes	19	8.981	12.088	30.8	139.2
072	C	138.7	0.0368	0.405	8.825	12.081	20.02.2007	L12_195_VGE_C_r01_t30_x.2x64x64.072.mes	L12_195_VGE_C_r01_t30_y.2x64x64.072.mes	18	8.983	12.071	30.8	138.6
072	D	137.2	0.0368	0.405	8.825	12.081	20.02.2007	L12_195_VGE_D_r01_t30_x.2x64x64.072.mes	L12_195_VGE_D_r01_t30_y.2x64x64.072.mes	17	8.981	12.091	30.7	136.9
072	E	136.7	0.0368	0.405	8.825	12.081	20.02.2007	L12_195_VGE_E_r04_t30_x.2x64x64.072.mes	L12_195_VGE_E_r04_t30_y.2x64x64.072.mes	16	8.983	12.092	30.6	136.5
072	F	136.1	0.0368	0.405	8.825	12.081	20.02.2007	L12_195_VGE_F_r01_t30_x.2x64x64.072.mes	L12_195_VGE_F_r01_t30_y.2x64x64.072.mes	15	8.982	12.082	30.3	136.1
072	G	128.4	0.0368	0.405	8.825	12.081	20.02.2007	L12_195_VGE_G_r01_t30_x.2x64x64.072.mes	L12_195_VGE_G_r01_t30_y.2x64x64.072.mes	14	8.981	12.084	30.1	128.2
072	H	127.9	0.0368	0.405	8.825	12.081	20.02.2007	L12_195_VGE_H_r04_t30_x.2x64x64.072.mes	L12_195_VGE_H_r04_t30_y.2x64x64.072.mes	13	8.981	12.080	30.0	127.6
072	I	127.4	0.0368	0.405	8.825	12.081	20.02.2007	L12_195_VGE_I_r01_t30_x.2x64x64.072.mes	L12_195_VGE_I_r01_t30_y.2x64x64.072.mes	12	8.981	12.084	29.9	127.2
072	J	118.7	0.0368	0.405	8.825	12.081	20.02.2007	L12_195_VGE_J_r01_t30_x.2x64x64.072.mes	L12_195_VGE_J_r01_t30_y.2x64x64.072.mes	11	8.981	12.064	29.8	118.7
072	K	118.2	0.0368	0.405	8.825	12.081	20.02.2007	L12_195_VGE_K_r04_t30_x.2x64x64.072.mes	L12_195_VGE_K_r04_t30_y.2x64x64.072.mes	10	8.981	12.083	29.5	118.0
072	L	117.7	0.0368	0.405	8.825	12.081	20.02.2007	L12_195_VGE_L_r01_t30_x.2x64x64.072.mes	L12_195_VGE_L_r01_t30_y.2x64x64.072.mes	9	8.983	12.087	29.4	117.6
072	M	100.8	0.0368	0.405	8.825	12.081	20.02.2007	L12_195_VGE_M_r01_t30_x.2x64x64.072.mes	L12_195_VGE_M_r01_t30_y.2x64x64.072.mes	8	8.983	12.073	29.3	100.8
072	N	100.2	0.0368	0.405	8.825	12.081	20.02.2007	L12_195_VGE_N_r04_t30_x.2x64x64.072.mes	L12_195_VGE_N_r04_t30_y.2x64x64.072.mes	6	8.983	12.083	29.1	100.2
072	O	99.7	0.0368	0.405	8.825	12.081	20.02.2007	L12_195_VGE_O_r01_t30_x.2x64x64.072.mes	L12_195_VGE_O_r01_t30_y.2x64x64.072.mes	5	8.983	12.068	29.0	99.7
072	P	70.4	0.0368	0.405	8.825	12.081	20.02.2007	L12_195_VGE_P_r01_t30_x.2x64x64.072.mes	L12_195_VGE_P_r01_t30_y.2x64x64.072.mes	4	8.979	12.087	30.7	70.6
072	Q	69.9	0.0368	0.405	8.825	12.081	20.02.2007	L12_195_VGE_Q_r04_t30_x.2x64x64.072.mes	L12_195_VGE_Q_r04_t30_y.2x64x64.072.mes	3	8.982	12.076	30.4	70.1
072	R	69.3	0.0368	0.405	8.825	12.081	20.02.2007	L12_195_VGE_R_r01_t30_x.2x64x64.072.mes	L12_195_VGE_R_r01_t30_y.2x64x64.072.mes	2	8.982	12.090	30.2	69.0
074	A	139.1	0.0368	1.017	8.825	30.336	15.06.2007	L12_195_VGE_A_r01_t30_x.2x64x64.074.mes	L12_195_VGE_A_r01_t30_y.2x64x64.074.mes	6	8.850	30.348	30.0	139.1
074	B	138.5	0.0368	1.017	8.825	30.336	21.02.2007	L12_195_VGE_B_r04_t30_x.2x64x64.074.mes	L12_195_VGE_B_r04_t30_y.2x64x64.074.mes	27	8.982	30.349	30.1	138.5
074	C	138.0	0.0368	1.017	8.825	30.336	21.02.2007	L12_195_VGE_C_r01_t30_x.2x64x64.074.mes	L12_195_VGE_C_r01_t30_y.2x64x64.074.mes	25	8.981	30.339	29.8	137.8
074	D	136.4	0.0368	1.017	8.825	30.336	21.02.2007	L12_195_VGE_D_r01_t30_x.2x64x64.074.mes	L12_195_VGE_D_r01_t30_y.2x64x64.074.mes	24	8.982	30.353	29.5	136.2
074	E	135.9	0.0368	1.017	8.825	30.336	21.02.2007	L12_195_VGE_E_r04_t30_x.2x64x64.074.mes	L12_195_VGE_E_r04_t30_y.2x64x64.074.mes	23	8.980	30.350	29.1	136.1
074	F	135.3	0.0368	1.017	8.825	30.336	21.02.2007	L12_195_VGE_F_r01_t30_x.2x64x64.074.mes	L12_195_VGE_F_r01_t30_y.2x64x64.074.mes	22	8.980	30.339	29.7	135.3
074	G	127.2	0.0368	1.017	8.825	30.336	21.02.2007	L12_195_VGE_G_r01_t30_x.2x64x64.074.mes	L12_195_VGE_G_r01_t30_y.2x64x64.074.mes	21	8.984	30.334	30.7	127.1
074	H	126.7	0.0368	1.017	8.825	30.336	21.02.2007	L12_195_VGE_H_r04_t30_x.2x64x64.074.mes	L12_195_VGE_H_r04_t30_y.2x64x64.074.mes	20	8.983	30.344	30.4	126.6
074	I	126.1	0.0368	1.017	8.825	30.336	21.02.2007	L12_195_VGE_I_r01_t30_x.2x64x64.074.mes	L12_195_VGE_I_r01_t30_y.2x64x64.074.mes	19	8.981	30.332	30.2	126.1
074	J	117.1	0.0368	1.017	8.825	30.336	21.02.2007	L12_195_VGE_J_r01_t30_x.2x64x64.074.mes	L12_195_VGE_J_r01_t30_y.2x64x64.074.mes	17	8.984	30.333	29.9	117.3
074	K	116.6	0.0368	1.017	8.825	30.336	21.02.2007	L12_195_VGE_K_r04_t30_x.2x64x64.074.mes	L12_195_VGE_K_r04_t30_y.2x64x64.074.mes	15	8.982	30.338	29.6	116.4
074	L	116.0	0.0368	1.017	8.825	30.336	21.02.2007	L12_195_VGE_L_r01_t30_x.2x64x64.074.mes	L12_195_VGE_L_r01_t30_y.2x64x64.074.mes	13	8.986	30.330	32.9	115.9
074	M	98.3	0.0368	1.017	8.825	30.336	21.02.2007	L12_195_VGE_M_r01_t30_x.2x64x64.074.mes	L12_195_VGE_M_r01_t30_y.2x64x64.074.mes	12	8.980	30.325	30.9	98.6
074	N	97.8	0.0368	1.017	8.825	30.336	21.02.2007	L12_195_VGE_N_r04_t30_x.2x64x64.074.mes	L12_195_VGE_N_r04_t30_y.2x64x64.074.mes	10	8.981	30.341	30.6	97.8
074	O	97.2	0.0368	1.017	8.825	30.336	21.02.2007	L12_195_VGE_O_r01_t30_x.2x64x64.074.mes	L12_195_VGE_O_r01_t30_y.2x64x64.074.mes	9	8.984	30.348	30.5	97.1
074	P	66.5	0.0368	1.017	8.825	30.336	21.02.2007	L12_195_VGE_P_r01_t30_x.2x64x64.074.mes	L12_195_VGE_P_r01_t30_y.2x64x64.074.mes	8	8.983	30.334	30.1	66.6
074	Q	66.0	0.0368	1.017	8.825	30.336	21.02.2007	L12_195_VGE_Q_r04_t30_x.2x64x64.074.mes	L12_195_VGE_Q_r04_t30_y.2x64x64.074.mes	7	8.981	30.325	29.5	66.1
074	R	65.4	0.0368	1.017	8.825	30.336	21.02.2007	L12_195_VGE_R_r01_t30_x.2x64x64.074.mes	L12_195_VGE_R_r01_t30_y.2x64x64.074.mes	6	8.984	30.320	29.2	65.3

Matrix-punkt	Höhen-position	Druck am GS (ü) PI4-07 [kPa]	J _{Gas} [m/s] Einspeisung	J _{Wasser} [m/s]	V _{Gas} [nm³/h]	m _{Wasser} [kg/s]	Datum	File 1 (x)	File 2 (y)	DIAdem	Betriebsdaten (Mittelwerte über 10 s)			
											V _{Gas} [m³/h]	m _{Wasser} [kg/s]	t _{GS} [°C]	p(ü) GS [kPa]
083	A	140.0	0.0574	0.405	13.765	12.081	14.05.2007	L12_195_VGE_A_r01_t30_x.2x64x64.083.mes	L12_195_VGE_A_r01_t30_y.2x64x64.083.mes	25	13.897	12.078	30.4	140.1
083	B	139.5	0.0574	0.405	13.765	12.081	14.05.2007	L12_195_VGE_B_r04_t30_x.2x64x64.083.mes	L12_195_VGE_B_r04_t30_y.2x64x64.083.mes	24	13.896	12.085	30.4	139.6
083	C	139.0	0.0574	0.405	13.765	12.081	14.05.2007	L12_195_VGE_C_r01_t30_x.2x64x64.083.mes	L12_195_VGE_C_r01_t30_y.2x64x64.083.mes	22	13.896	12.072	30.3	138.8
083	D	137.6	0.0574	0.405	13.765	12.081	14.05.2007	L12_195_VGE_D_r01_t30_x.2x64x64.083.mes	L12_195_VGE_D_r01_t30_y.2x64x64.083.mes	21	13.898	12.072	30.2	137.7
083	E	137.0	0.0574	0.405	13.765	12.081	14.05.2007	L12_195_VGE_E_r04_t30_x.2x64x64.083.mes	L12_195_VGE_E_r04_t30_y.2x64x64.083.mes	20	13.893	12.086	30.0	136.7
083	F	136.5	0.0574	0.405	13.765	12.081	14.05.2007	L12_195_VGE_F_r01_t30_x.2x64x64.083.mes	L12_195_VGE_F_r01_t30_y.2x64x64.083.mes	18	13.897	12.080	30.0	136.6
083	G	129.0	0.0574	0.405	13.765	12.081	14.05.2007	L12_195_VGE_G_r01_t30_x.2x64x64.083.mes	L12_195_VGE_G_r01_t30_y.2x64x64.083.mes	17	13.896	12.075	29.8	128.9
083	H	128.5	0.0574	0.405	13.765	12.081	14.05.2007	L12_195_VGE_H_r04_t30_x.2x64x64.083.mes	L12_195_VGE_H_r04_t30_y.2x64x64.083.mes	16	13.896	12.079	30.7	128.6
083	I	128.0	0.0574	0.405	13.765	12.081	14.05.2007	L12_195_VGE_I_r01_t30_x.2x64x64.083.mes	L12_195_VGE_I_r01_t30_y.2x64x64.083.mes	14	13.897	12.075	30.5	128.0
083	J	119.6	0.0574	0.405	13.765	12.081	14.05.2007	L12_195_VGE_J_r01_t30_x.2x64x64.083.mes	L12_195_VGE_J_r01_t30_y.2x64x64.083.mes	13	13.898	12.079	30.5	119.4
083	K	119.1	0.0574	0.405	13.765	12.081	14.05.2007	L12_195_VGE_K_r04_t30_x.2x64x64.083.mes	L12_195_VGE_K_r04_t30_y.2x64x64.083.mes	12	13.897	12.074	30.4	119.2
083	L	118.6	0.0574	0.405	13.765	12.081	14.05.2007	L12_195_VGE_L_r01_t30_x.2x64x64.083.mes	L12_195_VGE_L_r01_t30_y.2x64x64.083.mes	11	13.893	12.066	30.3	118.7
083	M	102.2	0.0574	0.405	13.765	12.081	14.05.2007	L12_195_VGE_M_r01_t30_x.2x64x64.083.mes	L12_195_VGE_M_r01_t30_y.2x64x64.083.mes	8	13.893	12.087	30.2	102.1
083	N	101.6	0.0574	0.405	13.765	12.081	14.05.2007	L12_195_VGE_N_r04_t30_x.2x64x64.083.mes	L12_195_VGE_N_r04_t30_y.2x64x64.083.mes	6	13.894	12.073	30.2	101.6
083	O	101.1	0.0574	0.405	13.765	12.081	14.05.2007	L12_195_VGE_O_r01_t30_x.2x64x64.083.mes	L12_195_VGE_O_r01_t30_y.2x64x64.083.mes	5	13.894	12.074	30.1	101.3
083	P	72.6	0.0574	0.405	13.765	12.081	14.05.2007	L12_195_VGE_P_r01_t30_x.2x64x64.083.mes	L12_195_VGE_P_r01_t30_y.2x64x64.083.mes	4	13.895	12.104	29.4	72.6
083	Q	72.1	0.0574	0.405	13.765	12.081	14.05.2007	L12_195_VGE_Q_r04_t30_x.2x64x64.083.mes	L12_195_VGE_Q_r04_t30_y.2x64x64.083.mes	2	13.894	12.080	29.4	71.8
083	R	71.6	0.0574	0.405	13.765	12.081	14.05.2007	L12_195_VGE_R_r01_t30_x.2x64x64.083.mes	L12_195_VGE_R_r01_t30_y.2x64x64.083.mes	1	13.891	12.088	29.3	71.4
085	A	139.2	0.0574	1.017	13.765	30.336	05.06.2007	L12_195_VGE_A_r01_t30_x.2x64x64.085.mes	L12_195_VGE_A_r01_t30_y.2x64x64.085.mes	41	13.898	30.346	30.6	139.3
085	B	138.7	0.0574	1.017	13.765	30.336	05.06.2007	L12_195_VGE_B_r04_t30_x.2x64x64.085.mes	L12_195_VGE_B_r04_t30_y.2x64x64.085.mes	37	13.897	30.325	29.8	138.8
085	C	138.1	0.0574	1.017	13.765	30.336	05.06.2007	L12_195_VGE_C_r01_t30_x.2x64x64.085.mes	L12_195_VGE_C_r01_t30_y.2x64x64.085.mes	31	13.894	30.331	30.8	137.9
085	D	136.6	0.0574	1.017	13.765	30.336	05.06.2007	L12_195_VGE_D_r01_t30_x.2x64x64.085.mes	L12_195_VGE_D_r01_t30_y.2x64x64.085.mes	30	13.893	30.335	30.6	136.6
085	E	136.1	0.0574	1.017	13.765	30.336	05.06.2007	L12_195_VGE_E_r04_t30_x.2x64x64.085.mes	L12_195_VGE_E_r04_t30_y.2x64x64.085.mes	25	13.893	30.329	30.1	136.2
085	F	135.5	0.0574	1.017	13.765	30.336	05.06.2007	L12_195_VGE_F_r01_t30_x.2x64x64.085.mes	L12_195_VGE_F_r01_t30_y.2x64x64.085.mes	24	13.894	30.323	29.9	135.6
085	G	127.6	0.0574	1.017	13.765	30.336	05.06.2007	L12_195_VGE_G_r01_t30_x.2x64x64.085.mes	L12_195_VGE_G_r01_t30_y.2x64x64.085.mes	19	13.892	30.347	29.6	127.5
085	H	127.0	0.0574	1.017	13.765	30.336	05.06.2007	L12_195_VGE_H_r04_t30_x.2x64x64.085.mes	L12_195_VGE_H_r04_t30_y.2x64x64.085.mes	18	13.895	30.348	29.4	127.1
085	I	126.5	0.0574	1.017	13.765	30.336	05.06.2007	L12_195_VGE_I_r01_t30_x.2x64x64.085.mes	L12_195_VGE_I_r01_t30_y.2x64x64.085.mes	17	13.896	30.320	29.3	126.6
085	J	117.6	0.0574	1.017	13.765	30.336	05.06.2007	L12_195_VGE_J_r01_t30_x.2x64x64.085.mes	L12_195_VGE_J_r01_t30_y.2x64x64.085.mes	16	13.890	30.317	30.1	117.6
085	K	117.0	0.0574	1.017	13.765	30.336	05.06.2007	L12_195_VGE_K_r04_t30_x.2x64x64.085.mes	L12_195_VGE_K_r04_t30_y.2x64x64.085.mes	15	13.896	30.320	30.0	116.9
085	L	116.5	0.0574	1.017	13.765	30.336	05.06.2007	L12_195_VGE_L_r01_t30_x.2x64x64.085.mes	L12_195_VGE_L_r01_t30_y.2x64x64.085.mes	14	13.894	30.347	29.8	116.2
085	M	99.0	0.0574	1.017	13.765	30.336	05.06.2007	L12_195_VGE_M_r01_t30_x.2x64x64.085.mes	L12_195_VGE_M_r01_t30_y.2x64x64.085.mes	13	13.895	30.341	29.1	98.9
085	N	98.5	0.0574	1.017	13.765	30.336	05.06.2007	L12_195_VGE_N_r04_t30_x.2x64x64.085.mes	L12_195_VGE_N_r04_t30_y.2x64x64.085.mes	12	13.886	30.330	29.0	98.5
085	O	97.9	0.0574	1.017	13.765	30.336	05.06.2007	L12_195_VGE_O_r01_t30_x.2x64x64.085.mes	L12_195_VGE_O_r01_t30_y.2x64x64.085.mes	8	13.893	30.340	29.9	97.9
085	P	67.7	0.0574	1.017	13.765	30.336	05.06.2007	L12_195_VGE_P_r01_t30_x.2x64x64.085.mes	L12_195_VGE_P_r01_t30_y.2x64x64.085.mes	6	13.894	30.329	30.5	67.6
085	Q	67.2	0.0574	1.017	13.765	30.336	05.06.2007	L12_195_VGE_Q_r04_t30_x.2x64x64.085.mes	L12_195_VGE_Q_r04_t30_y.2x64x64.085.mes	7	13.895	30.348	30.6	67.1
085	R	66.6	0.0574	1.017	13.765	30.336	05.06.2007	L12_195_VGE_R_r01_t30_x.2x64x64.085.mes	L12_195_VGE_R_r01_t30_y.2x64x64.085.mes	1	13.895	30.342	30.0	66.8
094	A	140.4	0.0898	0.405	21.535	12.081	15.02.2007	L12_195_VGE_A_r01_t30_x.2x64x64.094.mes	L12_195_VGE_A_r01_t30_y.2x64x64.094.mes	23	21.609	12.074	30.2	139.9
094	B	139.9	0.0898	0.405	21.535	12.081	15.02.2007	L12_195_VGE_B_r04_t30_x.2x64x64.094.mes	L12_195_VGE_B_r04_t30_y.2x64x64.094.mes	21	21.592	12.070	30.2	140.0
094	C	139.5	0.0898	0.405	21.535	12.081	15.02.2007	L12_195_VGE_C_r01_t30_x.2x64x64.094.mes	L12_195_VGE_C_r01_t30_y.2x64x64.094.mes	20	21.608	12.085	30.0	140.0
094	D	138.1	0.0898	0.405	21.535	12.081	15.02.2007	L12_195_VGE_D_r01_t30_x.2x64x64.094.mes	L12_195_VGE_D_r01_t30_y.2x64x64.094.mes	19	21.593	12.082	29.9	138.1
094	E	137.6	0.0898	0.405	21.535	12.081	15.02.2007	L12_195_VGE_E_r04_t30_x.2x64x64.094.mes	L12_195_VGE_E_r04_t30_y.2x64x64.094.mes	18	21.610	12.078	29.6	136.9
094	F	137.1	0.0898	0.405	21.535	12.081	15.02.2007	L12_195_VGE_F_r01_t30_x.2x64x64.094.mes	L12_195_VGE_F_r01_t30_y.2x64x64.094.mes	17	21.609	12.094	29.6	136.6
094	G	129.9	0.0898	0.405	21.535	12.081	15.02.2007	L12_195_VGE_G_r01_t30_x.2x64x64.094.mes	L12_195_VGE_G_r01_t30_y.2x64x64.094.mes	15	21.606	12.079	29.3	129.9
094	H	129.4	0.0898	0.405	21.535	12.081	15.02.2007	L12_195_VGE_H_r04_t30_x.2x64x64.094.mes	L12_195_VGE_H_r04_t30_y.2x64x64.094.mes	14	21.609	12.074	29.2	130.0
094	I	128.9	0.0898	0.405	21.535	12.081	15.02.2007	L12_195_VGE_I_r01_t30_x.2x64x64.094.mes	L12_195_VGE_I_r01_t30_y.2x64x64.094.mes	13	21.610	12.071	29.1	129.3
094	J	120.9	0.0898	0.405	21.535	12.081	15.02.2007	L12_195_VGE_J_r01_t30_x.2x64x64.094.mes	L12_195_VGE_J_r01_t30_y.2x64x64.094.mes	12	21.608	12.074	29.0	121.0
094	K	120.4	0.0898	0.405	21.535	12.081	15.02.2007	L12_195_VGE_K_r04_t30_x.2x64x64.094.mes	L12_195_VGE_K_r04_t30_y.2x64x64.094.mes	11	21.610	12.076	30.0	120.8
094	L	119.9	0.0898	0.405	21.535	12.081	15.02.2007	L12_195_VGE_L_r01_t30_x.2x64x64.094.mes	L12_195_VGE_L_r01_t30_y.2x64x64.094.mes	9	21.611	12.089	29.8	120.1
094	M	104.2	0.0898	0.405	21.535	12.081	15.02.2007	L12_195_VGE_M_r01_t30_x.2x64x64.094.mes	L12_195_VGE_M_r01_t30_y.2x64x64.094.mes	8	21.608	12.071	29.7	103.7
094	N	103.7	0.0898	0.405	21.535	12.081	15.02.2007	L12_195_VGE_N_r04_t30_x.2x64x64.094.mes	L12_195_VGE_N_r04_t30_y.2x64x64.094.mes	6	21.610	12.068	29.5	103.3
094	O	103.2	0.0898	0.405	21.535	12.081	15.02.2007	L12_195_VGE_O_r01_t30_x.2x64x64.094.mes	L12_195_VGE_O_r01_t30_y.2x64x64.094.mes	7	21.609	12.080	29.6	103.2
094	P	75.9	0.0898	0.405	21.535	12.081	15.02.2007	L12_195_VGE_P_r01_t30_x.2x64x64.094.mes	L12_195_VGE_P_r01_t30_y.2x64x64.094.mes	5	21.606	12.097	29.4	75.9
094	Q	75.4	0.0898	0.405	21.535	12.081	15.02.2007	L12_195_VGE_Q_r04_t30_x.2x64x64.094.mes	L12_195_VGE_Q_r04_t30_y.2x64x64.094.mes	3	21.608	12.086	29.1	75.6
094	R	75.0	0.0898	0.405	21.535	12.081	15.02.2007	L12_195_VGE_R_r01_t30_x.2x64x64.094.mes	L12_195_VGE_R_r01_t30_y.2x64x64.094.mes	1	21.608	12.084	29.1	74.9

Matrix-punkt	Höhen-position	Druck am GS (ü) PI4-07 [kPa]	J _{Gas} [m/s] Einspeisung	J _{Wasser} [m/s]	V _{Gas} [nm³/h]	m _{Wasser} [kg/s]	Datum	File 1 (x)	File 2 (y)	DIAdem	Betriebsdaten (Mittelwerte über 10 s)			
											V _{Gas} [m³/h]	m _{Wasser} [kg/s]	t _{GS} [°C]	p(ü) GS [kPa]
096	A	139.4	0.0898	1.017	21.535	30.336	15.06.2007	L12_195_VGE_A_r01_t30_x.2x64x64.096.mes	L12_195_VGE_A_r01_t30_y.2x64x64.096.mes	3	21.605	30.330	30.4	139.4
096	B	138.9	0.0898	1.017	21.535	30.336	19.02.2007	L12_195_VGE_B_r04_t30_x.2x64x64.096.mes	L12_195_VGE_B_r04_t30_y.2x64x64.096.mes	40	21.611	30.324	29.8	138.9
096	C	138.3	0.0898	1.017	21.535	30.336	19.02.2007	L12_195_VGE_C_r01_t30_x.2x64x64.096.mes	L12_195_VGE_C_r01_t30_y.2x64x64.096.mes	39	21.609	30.344	29.9	138.0
096	D	136.8	0.0898	1.017	21.535	30.336	19.02.2007	L12_195_VGE_D_r01_t30_x.2x64x64.096.mes	L12_195_VGE_D_r01_t30_y.2x64x64.096.mes	38	21.608	30.322	30.6	136.7
096	E	136.3	0.0898	1.017	21.535	30.336	19.02.2007	L12_195_VGE_E_r04_t30_x.2x64x64.096.mes	L12_195_VGE_E_r04_t30_y.2x64x64.096.mes	36	21.609	30.332	30.4	136.2
096	F	135.8	0.0898	1.017	21.535	30.336	19.02.2007	L12_195_VGE_F_r01_t30_x.2x64x64.096.mes	L12_195_VGE_F_r01_t30_y.2x64x64.096.mes	34	21.607	30.324	29.9	135.6
096	G	128.0	0.0898	1.017	21.535	30.336	19.02.2007	L12_195_VGE_G_r01_t30_x.2x64x64.096.mes	L12_195_VGE_G_r01_t30_y.2x64x64.096.mes	33	21.609	30.339	29.6	128.0
096	H	127.5	0.0898	1.017	21.535	30.336	19.02.2007	L12_195_VGE_H_r04_t30_x.2x64x64.096.mes	L12_195_VGE_H_r04_t30_y.2x64x64.096.mes	30	21.609	30.340	29.1	127.5
096	I	126.9	0.0898	1.017	21.535	30.336	19.02.2007	L12_195_VGE_I_r01_t30_x.2x64x64.096.mes	L12_195_VGE_I_r01_t30_y.2x64x64.096.mes	28	21.609	30.335	29.6	126.8
096	J	118.2	0.0898	1.017	21.535	30.336	19.02.2007	L12_195_VGE_J_r01_t30_x.2x64x64.096.mes	L12_195_VGE_J_r01_t30_y.2x64x64.096.mes	16	21.608	30.336	30.1	118.5
096	K	117.7	0.0898	1.017	21.535	30.336	19.02.2007	L12_195_VGE_K_r04_t30_x.2x64x64.096.mes	L12_195_VGE_K_r04_t30_y.2x64x64.096.mes	15	21.609	30.336	29.9	117.5
096	L	117.2	0.0898	1.017	21.535	30.336	19.02.2007	L12_195_VGE_L_r01_t30_x.2x64x64.096.mes	L12_195_VGE_L_r01_t30_y.2x64x64.096.mes	14	21.610	30.350	29.8	117.1
096	M	100.1	0.0898	1.017	21.535	30.336	19.02.2007	L12_195_VGE_M_r01_t30_x.2x64x64.096.mes	L12_195_VGE_M_r01_t30_y.2x64x64.096.mes	10	21.607	30.336	30.7	100.2
096	N	99.6	0.0898	1.017	21.535	30.336	19.02.2007	L12_195_VGE_N_r04_t30_x.2x64x64.096.mes	L12_195_VGE_N_r04_t30_y.2x64x64.096.mes	9	21.612	30.332	30.5	99.7
096	O	99.1	0.0898	1.017	21.535	30.336	19.02.2007	L12_195_VGE_O_r01_t30_x.2x64x64.096.mes	L12_195_VGE_O_r01_t30_y.2x64x64.096.mes	8	21.607	30.332	30.4	99.5
096	P	69.5	0.0898	1.017	21.535	30.336	19.02.2007	L12_195_VGE_P_r01_t30_x.2x64x64.096.mes	L12_195_VGE_P_r01_t30_y.2x64x64.096.mes	5	21.609	30.327	30.0	69.8
096	Q	68.9	0.0898	1.017	21.535	30.336	19.02.2007	L12_195_VGE_Q_r04_t30_x.2x64x64.096.mes	L12_195_VGE_Q_r04_t30_y.2x64x64.096.mes	3	21.609	30.347	29.8	69.1
096	R	68.4	0.0898	1.017	21.535	30.336	19.02.2007	L12_195_VGE_R_r01_t30_x.2x64x64.096.mes	L12_195_VGE_R_r01_t30_y.2x64x64.096.mes	1	21.610	30.341	29.5	68.1
105	A	141.0	0.1400	0.405	33.574	12.081	10.05.2007	L12_195_VGE_A_r01_t30_x.2x64x64.105.mes	L12_195_VGE_A_r01_t30_y.2x64x64.105.mes	36	33.596	12.076	29.8	140.9
105	B	140.6	0.1400	0.405	33.574	12.081	10.05.2007	L12_195_VGE_B_r04_t30_x.2x64x64.105.mes	L12_195_VGE_B_r04_t30_y.2x64x64.105.mes	34	33.595	12.082	29.7	140.6
105	C	140.1	0.1400	0.405	33.574	12.081	10.05.2007	L12_195_VGE_C_r01_t30_x.2x64x64.105.mes	L12_195_VGE_C_r01_t30_y.2x64x64.105.mes	33	33.595	12.085	29.6	140.3
105	D	138.8	0.1400	0.405	33.574	12.081	10.05.2007	L12_195_VGE_D_r01_t30_x.2x64x64.105.mes	L12_195_VGE_D_r01_t30_y.2x64x64.105.mes	31	33.594	12.081	29.5	138.4
105	E	138.3	0.1400	0.405	33.574	12.081	10.05.2007	L12_195_VGE_E_r04_t30_x.2x64x64.105.mes	L12_195_VGE_E_r04_t30_y.2x64x64.105.mes	30	33.593	12.079	29.4	138.2
105	F	137.9	0.1400	0.405	33.574	12.081	10.05.2007	L12_195_VGE_F_r01_t30_x.2x64x64.105.mes	L12_195_VGE_F_r01_t30_y.2x64x64.105.mes	29	33.594	12.081	29.2	137.7
105	G	131.2	0.1400	0.405	33.574	12.081	10.05.2007	L12_195_VGE_G_r01_t30_x.2x64x64.105.mes	L12_195_VGE_G_r01_t30_y.2x64x64.105.mes	26	33.594	12.090	29.1	130.9
105	H	130.7	0.1400	0.405	33.574	12.081	10.05.2007	L12_195_VGE_H_r04_t30_x.2x64x64.105.mes	L12_195_VGE_H_r04_t30_y.2x64x64.105.mes	25	33.598	12.087	29.0	130.8
105	I	130.2	0.1400	0.405	33.574	12.081	10.05.2007	L12_195_VGE_I_r01_t30_x.2x64x64.105.mes	L12_195_VGE_I_r01_t30_y.2x64x64.105.mes	23	33.592	12.085	29.1	130.4
105	J	122.7	0.1400	0.405	33.574	12.081	10.05.2007	L12_195_VGE_J_r01_t30_x.2x64x64.105.mes	L12_195_VGE_J_r01_t30_y.2x64x64.105.mes	17	33.593	12.069	30.1	122.8
105	K	122.3	0.1400	0.405	33.574	12.081	10.05.2007	L12_195_VGE_K_r04_t30_x.2x64x64.105.mes	L12_195_VGE_K_r04_t30_y.2x64x64.105.mes	20	33.592	12.085	30.2	122.2
105	L	121.8	0.1400	0.405	33.574	12.081	10.05.2007	L12_195_VGE_L_r01_t30_x.2x64x64.105.mes	L12_195_VGE_L_r01_t30_y.2x64x64.105.mes	14	33.595	12.079	29.9	121.8
105	M	107.0	0.1400	0.405	33.574	12.081	10.05.2007	L12_195_VGE_M_r01_t30_x.2x64x64.105.mes	L12_195_VGE_M_r01_t30_y.2x64x64.105.mes	12	33.595	12.071	29.7	107.2
105	N	106.6	0.1400	0.405	33.574	12.081	10.05.2007	L12_195_VGE_N_r04_t30_x.2x64x64.105.mes	L12_195_VGE_N_r04_t30_y.2x64x64.105.mes	9	33.594	12.078	29.5	106.6
105	O	106.1	0.1400	0.405	33.574	12.081	10.05.2007	L12_195_VGE_O_r01_t30_x.2x64x64.105.mes	L12_195_VGE_O_r01_t30_y.2x64x64.105.mes	8	33.595	12.079	29.5	106.3
105	P	80.5	0.1400	0.405	33.574	12.081	10.05.2007	L12_195_VGE_P_r01_t30_x.2x64x64.105.mes	L12_195_VGE_P_r01_t30_y.2x64x64.105.mes	3	33.591	12.085	29.2	80.5
105	Q	80.1	0.1400	0.405	33.574	12.081	10.05.2007	L12_195_VGE_Q_r04_t30_x.2x64x64.105.mes	L12_195_VGE_Q_r04_t30_y.2x64x64.105.mes	2	33.592	12.080	29.1	80.1
105	R	79.6	0.1400	0.405	33.574	12.081	10.05.2007	L12_195_VGE_R_r01_t30_x.2x64x64.105.mes	L12_195_VGE_R_r01_t30_y.2x64x64.105.mes	1	33.592	12.088	29.1	79.6
107	A	139.7	0.1400	1.017	33.574	30.336	04.06.2007	L12_195_VGE_A_r01_t30_x.2x64x64.107.mes	L12_195_VGE_A_r01_t30_y.2x64x64.107.mes	33	33.592	30.337	30.5	139.4
107	B	139.2	0.1400	1.017	33.574	30.336	04.06.2007	L12_195_VGE_B_r04_t30_x.2x64x64.107.mes	L12_195_VGE_B_r04_t30_y.2x64x64.107.mes	28	33.589	30.332	29.7	139.3
107	C	138.7	0.1400	1.017	33.574	30.336	04.06.2007	L12_195_VGE_C_r01_t30_x.2x64x64.107.mes	L12_195_VGE_C_r01_t30_y.2x64x64.107.mes	30	33.593	30.315	30.2	138.7
107	D	137.3	0.1400	1.017	33.574	30.336	04.06.2007	L12_195_VGE_D_r01_t30_x.2x64x64.107.mes	L12_195_VGE_D_r01_t30_y.2x64x64.107.mes	25	33.591	30.326	29.2	137.2
107	E	136.7	0.1400	1.017	33.574	30.336	04.06.2007	L12_195_VGE_E_r04_t30_x.2x64x64.107.mes	L12_195_VGE_E_r04_t30_y.2x64x64.107.mes	24	33.592	30.329	29.0	136.7
107	F	136.2	0.1400	1.017	33.574	30.336	04.06.2007	L12_195_VGE_F_r01_t30_x.2x64x64.107.mes	L12_195_VGE_F_r01_t30_y.2x64x64.107.mes	21	33.593	30.340	28.9	136.2
107	G	128.7	0.1400	1.017	33.574	30.336	04.06.2007	L12_195_VGE_G_r01_t30_x.2x64x64.107.mes	L12_195_VGE_G_r01_t30_y.2x64x64.107.mes	18	33.592	30.328	30.8	128.9
107	H	128.2	0.1400	1.017	33.574	30.336	04.06.2007	L12_195_VGE_H_r04_t30_x.2x64x64.107.mes	L12_195_VGE_H_r04_t30_y.2x64x64.107.mes	17	33.594	30.333	30.7	128.3
107	I	127.7	0.1400	1.017	33.574	30.336	04.06.2007	L12_195_VGE_I_r01_t30_x.2x64x64.107.mes	L12_195_VGE_I_r01_t30_y.2x64x64.107.mes	16	33.592	30.338	30.5	127.8
107	J	119.2	0.1400	1.017	33.574	30.336	04.06.2007	L12_195_VGE_J_r01_t30_x.2x64x64.107.mes	L12_195_VGE_J_r01_t30_y.2x64x64.107.mes	15	33.598	30.340	30.4	119.4
107	K	118.7	0.1400	1.017	33.574	30.336	04.06.2007	L12_195_VGE_K_r04_t30_x.2x64x64.107.mes	L12_195_VGE_K_r04_t30_y.2x64x64.107.mes	14	33.590	30.327	30.3	118.6
107	L	118.2	0.1400	1.017	33.574	30.336	04.06.2007	L12_195_VGE_L_r01_t30_x.2x64x64.107.mes	L12_195_VGE_L_r01_t30_y.2x64x64.107.mes	13	33.589	30.334	30.2	118.2
107	M	101.7	0.1400	1.017	33.574	30.336	04.06.2007	L12_195_VGE_M_r01_t30_x.2x64x64.107.mes	L12_195_VGE_M_r01_t30_y.2x64x64.107.mes	11	33.592	30.339	30.0	101.4
107	N	101.2	0.1400	1.017	33.574	30.336	04.06.2007	L12_195_VGE_N_r04_t30_x.2x64x64.107.mes	L12_195_VGE_N_r04_t30_y.2x64x64.107.mes	10	33.592	30.336	29.9	101.2
107	O	100.7	0.1400	1.017	33.574	30.336	04.06.2007	L12_195_VGE_O_r01_t30_x.2x64x64.107.mes	L12_195_VGE_O_r01_t30_y.2x64x64.107.mes	8	33.590	30.346	29.8	100.9
107	P	72.1	0.1400	1.017	33.574	30.336	04.06.2007	L12_195_VGE_P_r01_t30_x.2x64x64.107.mes	L12_195_VGE_P_r01_t30_y.2x64x64.107.mes	5	33.592	30.341	29.3	72.1
107	Q	71.5	0.1400	1.017	33.574	30.336	04.06.2007	L12_195_VGE_Q_r04_t30_x.2x64x64.107.mes	L12_195_VGE_Q_r04_t30_y.2x64x64.107.mes	3	33.589	30.342	30.2	71.6
107	R	71.0	0.1400	1.017	33.574	30.336	04.06.2007	L12_195_VGE_R_r01_t30_x.2x64x64.107.mes	L12_195_VGE_R_r01_t30_y.2x64x64.107.mes	1	33.589	30.360	30.0	71.1

Matrix-punkt	Höhen-position	Druck am GS (ü) PI4-07 [kPa]	J _{Gas} [m/s] Einspeisung	J _{Wasser} [m/s]	V _{Gas} [nm³/h]	m _{Wasser} [kg/s]	Datum	File 1 (x)	File 2 (y)	DIAdem	Betriebsdaten (Mittelwerte über 10 s)			
											V _{Gas} [m³/h]	m _{Wasser} [kg/s]	t _{GS} [°C]	p(ü) GS [kPa]
111	A	143.9	0.2190	0.041	52.519	1.208	09.03.2007	L12_195_VGE_A_r01_t30_x.2x64x64.111.mes	L12_195_VGE_A_r01_t30_y.2x64x64.111.mes	22	52.525	1.208	30.3	143.5
111	B	143.5	0.2190	0.041	52.519	1.208	09.03.2007	L12_195_VGE_B_r04_t30_x.2x64x64.111.mes	L12_195_VGE_B_r04_t30_y.2x64x64.111.mes	21	52.528	1.208	30.2	143.6
111	C	143.2	0.2190	0.041	52.519	1.208	09.03.2007	L12_195_VGE_C_r01_t30_x.2x64x64.111.mes	L12_195_VGE_C_r01_t30_y.2x64x64.111.mes	20	52.377	1.206	30.1	143.4
111	D	142.3	0.2190	0.041	52.519	1.208	09.03.2007	L12_195_VGE_D_r01_t30_x.2x64x64.111.mes	L12_195_VGE_D_r01_t30_y.2x64x64.111.mes	19	52.528	1.208	30.0	141.8
111	E	142.0	0.2190	0.041	52.519	1.208	09.03.2007	L12_195_VGE_E_r04_t30_x.2x64x64.111.mes	L12_195_VGE_E_r04_t30_y.2x64x64.111.mes	18	52.538	1.207	30.0	142.5
111	F	141.7	0.2190	0.041	52.519	1.208	09.03.2007	L12_195_VGE_F_r01_t30_x.2x64x64.111.mes	L12_195_VGE_F_r01_t30_y.2x64x64.111.mes	17	52.473	1.209	29.9	141.1
111	G	137.1	0.2190	0.041	52.519	1.208	09.03.2007	L12_195_VGE_G_r01_t30_x.2x64x64.111.mes	L12_195_VGE_G_r01_t30_y.2x64x64.111.mes	16	52.535	1.208	29.8	137.0
111	H	136.7	0.2190	0.041	52.519	1.208	09.03.2007	L12_195_VGE_H_r04_t30_x.2x64x64.111.mes	L12_195_VGE_H_r04_t30_y.2x64x64.111.mes	15	52.527	1.206	29.7	136.1
111	I	136.4	0.2190	0.041	52.519	1.208	09.03.2007	L12_195_VGE_I_r01_t30_x.2x64x64.111.mes	L12_195_VGE_I_r01_t30_y.2x64x64.111.mes	14	52.527	1.210	29.7	136.3
111	J	131.2	0.2190	0.041	52.519	1.208	09.03.2007	L12_195_VGE_J_r01_t30_x.2x64x64.111.mes	L12_195_VGE_J_r01_t30_y.2x64x64.111.mes	12	52.523	1.209	29.6	130.9
111	K	130.9	0.2190	0.041	52.519	1.208	09.03.2007	L12_195_VGE_K_r04_t30_x.2x64x64.111.mes	L12_195_VGE_K_r04_t30_y.2x64x64.111.mes	11	52.517	1.207	29.5	131.0
111	L	130.6	0.2190	0.041	52.519	1.208	09.03.2007	L12_195_VGE_L_r01_t30_x.2x64x64.111.mes	L12_195_VGE_L_r01_t30_y.2x64x64.111.mes	9	52.477	1.209	29.4	130.6
111	M	120.4	0.2190	0.041	52.519	1.208	09.03.2007	L12_195_VGE_M_r01_t30_x.2x64x64.111.mes	L12_195_VGE_M_r01_t30_y.2x64x64.111.mes	7	52.535	1.210	29.2	120.9
111	N	120.1	0.2190	0.041	52.519	1.208	09.03.2007	L12_195_VGE_N_r04_t30_x.2x64x64.111.mes	L12_195_VGE_N_r04_t30_y.2x64x64.111.mes	5	52.483	1.206	29.5	120.5
111	O	119.8	0.2190	0.041	52.519	1.208	09.03.2007	L12_195_VGE_O_r01_t30_x.2x64x64.111.mes	L12_195_VGE_O_r01_t30_y.2x64x64.111.mes	4	52.520	1.215	30.6	119.5
111	P	102.2	0.2190	0.041	52.519	1.208	09.03.2007	L12_195_VGE_P_r01_t30_x.2x64x64.111.mes	L12_195_VGE_P_r01_t30_y.2x64x64.111.mes	3	52.543	1.202	30.5	102.0
111	Q	101.8	0.2190	0.041	52.519	1.208	09.03.2007	L12_195_VGE_Q_r04_t30_x.2x64x64.111.mes	L12_195_VGE_Q_r04_t30_y.2x64x64.111.mes	2	52.538	1.213	30.3	101.5
111	R	101.5	0.2190	0.041	52.519	1.208	09.03.2007	L12_195_VGE_R_r01_t30_x.2x64x64.111.mes	L12_195_VGE_R_r01_t30_y.2x64x64.111.mes	1	52.525	1.200	30.2	101.3
112	A	143.6	0.2190	0.064	52.519	1.912	02.04.2007	L12_195_VGE_A_r01_t30_x.2x64x64.112.mes	L12_195_VGE_A_r01_t30_y.2x64x64.112.mes	25	52.542	1.913	30.0	143.9
112	B	143.3	0.2190	0.064	52.519	1.912	02.04.2007	L12_195_VGE_B_r04_t30_x.2x64x64.112.mes	L12_195_VGE_B_r04_t30_y.2x64x64.112.mes	24	52.538	1.912	29.9	143.2
112	C	143.0	0.2190	0.064	52.519	1.912	02.04.2007	L12_195_VGE_C_r01_t30_x.2x64x64.112.mes	L12_195_VGE_C_r01_t30_y.2x64x64.112.mes	23	52.535	1.910	29.9	143.4
112	D	142.1	0.2190	0.064	52.519	1.912	02.04.2007	L12_195_VGE_D_r01_t30_x.2x64x64.112.mes	L12_195_VGE_D_r01_t30_y.2x64x64.112.mes	22	52.535	1.913	29.9	142.0
112	E	141.7	0.2190	0.064	52.519	1.912	02.04.2007	L12_195_VGE_E_r04_t30_x.2x64x64.112.mes	L12_195_VGE_E_r04_t30_y.2x64x64.112.mes	21	52.545	1.911	29.9	141.6
112	F	141.4	0.2190	0.064	52.519	1.912	02.04.2007	L12_195_VGE_F_r01_t30_x.2x64x64.112.mes	L12_195_VGE_F_r01_t30_y.2x64x64.112.mes	20	52.535	1.912	29.8	141.2
112	G	136.6	0.2190	0.064	52.519	1.912	02.04.2007	L12_195_VGE_G_r01_t30_x.2x64x64.112.mes	L12_195_VGE_G_r01_t30_y.2x64x64.112.mes	19	52.403	1.913	29.8	137.0
112	H	136.3	0.2190	0.064	52.519	1.912	02.04.2007	L12_195_VGE_H_r04_t30_x.2x64x64.112.mes	L12_195_VGE_H_r04_t30_y.2x64x64.112.mes	18	52.545	1.913	29.8	136.7
112	I	136.0	0.2190	0.064	52.519	1.912	02.04.2007	L12_195_VGE_I_r01_t30_x.2x64x64.112.mes	L12_195_VGE_I_r01_t30_y.2x64x64.112.mes	17	52.537	1.912	29.8	136.0
112	J	130.6	0.2190	0.064	52.519	1.912	02.04.2007	L12_195_VGE_J_r01_t30_x.2x64x64.112.mes	L12_195_VGE_J_r01_t30_y.2x64x64.112.mes	15	52.530	1.914	29.8	130.6
112	K	130.3	0.2190	0.064	52.519	1.912	02.04.2007	L12_195_VGE_K_r04_t30_x.2x64x64.112.mes	L12_195_VGE_K_r04_t30_y.2x64x64.112.mes	14	52.538	1.913	29.8	130.0
112	L	129.9	0.2190	0.064	52.519	1.912	02.04.2007	L12_195_VGE_L_r01_t30_x.2x64x64.112.mes	L12_195_VGE_L_r01_t30_y.2x64x64.112.mes	13	52.535	1.912	29.7	130.0
112	M	119.4	0.2190	0.064	52.519	1.912	02.04.2007	L12_195_VGE_M_r01_t30_x.2x64x64.112.mes	L12_195_VGE_M_r01_t30_y.2x64x64.112.mes	11	52.548	1.911	29.7	119.4
112	N	119.1	0.2190	0.064	52.519	1.912	02.04.2007	L12_195_VGE_N_r04_t30_x.2x64x64.112.mes	L12_195_VGE_N_r04_t30_y.2x64x64.112.mes	9	52.523	1.914	29.7	118.9
112	O	118.8	0.2190	0.064	52.519	1.912	02.04.2007	L12_195_VGE_O_r01_t30_x.2x64x64.112.mes	L12_195_VGE_O_r01_t30_y.2x64x64.112.mes	5	52.485	1.912	29.7	119.0
112	P	100.6	0.2190	0.064	52.519	1.912	02.04.2007	L12_195_VGE_P_r01_t30_x.2x64x64.112.mes	L12_195_VGE_P_r01_t30_y.2x64x64.112.mes	3	52.542	1.909	29.7	100.6
112	Q	100.2	0.2190	0.064	52.519	1.912	02.04.2007	L12_195_VGE_Q_r04_t30_x.2x64x64.112.mes	L12_195_VGE_Q_r04_t30_y.2x64x64.112.mes	2	52.538	1.915	29.7	100.0
112	R	99.9	0.2190	0.064	52.519	1.912	02.04.2007	L12_195_VGE_R_r01_t30_x.2x64x64.112.mes	L12_195_VGE_R_r01_t30_y.2x64x64.112.mes	1	52.515	1.906	29.6	99.7
113	A	143.3	0.2190	0.102	52.519	3.043	29.03.2007	L12_195_VGE_A_r01_t30_x.2x64x64.113.mes	L12_195_VGE_A_r01_t30_y.2x64x64.113.mes	28	52.523	3.043	30.6	143.0
113	B	143.0	0.2190	0.102	52.519	3.043	29.03.2007	L12_195_VGE_B_r04_t30_x.2x64x64.113.mes	L12_195_VGE_B_r04_t30_y.2x64x64.113.mes	26	52.507	3.043	30.5	143.1
113	C	142.7	0.2190	0.102	52.519	3.043	29.03.2007	L12_195_VGE_C_r01_t30_x.2x64x64.113.mes	L12_195_VGE_C_r01_t30_y.2x64x64.113.mes	24	52.518	3.043	30.4	142.3
113	D	141.7	0.2190	0.102	52.519	3.043	29.03.2007	L12_195_VGE_D_r01_t30_x.2x64x64.113.mes	L12_195_VGE_D_r01_t30_y.2x64x64.113.mes	23	52.535	3.043	30.3	141.7
113	E	141.4	0.2190	0.102	52.519	3.043	29.03.2007	L12_195_VGE_E_r04_t30_x.2x64x64.113.mes	L12_195_VGE_E_r04_t30_y.2x64x64.113.mes	20	52.525	3.042	30.2	141.3
113	F	141.0	0.2190	0.102	52.519	3.043	29.03.2007	L12_195_VGE_F_r01_t30_x.2x64x64.113.mes	L12_195_VGE_F_r01_t30_y.2x64x64.113.mes	18	52.523	3.043	30.1	140.8
113	G	136.0	0.2190	0.102	52.519	3.043	29.03.2007	L12_195_VGE_G_r01_t30_x.2x64x64.113.mes	L12_195_VGE_G_r01_t30_y.2x64x64.113.mes	17	52.522	3.041	30.0	136.2
113	H	135.7	0.2190	0.102	52.519	3.043	29.03.2007	L12_195_VGE_H_r04_t30_x.2x64x64.113.mes	L12_195_VGE_H_r04_t30_y.2x64x64.113.mes	16	52.535	3.044	29.9	135.3
113	I	135.3	0.2190	0.102	52.519	3.043	29.03.2007	L12_195_VGE_I_r01_t30_x.2x64x64.113.mes	L12_195_VGE_I_r01_t30_y.2x64x64.113.mes	15	52.535	3.042	29.8	135.0
113	J	129.7	0.2190	0.102	52.519	3.043	29.03.2007	L12_195_VGE_J_r01_t30_x.2x64x64.113.mes	L12_195_VGE_J_r01_t30_y.2x64x64.113.mes	14	52.518	3.043	29.7	130.0
113	K	129.4	0.2190	0.102	52.519	3.043	29.03.2007	L12_195_VGE_K_r04_t30_x.2x64x64.113.mes	L12_195_VGE_K_r04_t30_y.2x64x64.113.mes	13	52.532	3.041	29.6	129.2
113	L	129.0	0.2190	0.102	52.519	3.043	29.03.2007	L12_195_VGE_L_r01_t30_x.2x64x64.113.mes	L12_195_VGE_L_r01_t30_y.2x64x64.113.mes	12	52.532	3.044	29.3	128.9
113	M	118.0	0.2190	0.102	52.519	3.043	29.03.2007	L12_195_VGE_M_r01_t30_x.2x64x64.113.mes	L12_195_VGE_M_r01_t30_y.2x64x64.113.mes	11	52.522	3.044	30.1	118.6
113	N	117.7	0.2190	0.102	52.519	3.043	29.03.2007	L12_195_VGE_N_r04_t30_x.2x64x64.113.mes	L12_195_VGE_N_r04_t30_y.2x64x64.113.mes	7	52.525	3.045	29.9	117.5
113	O	117.3	0.2190	0.102	52.519	3.043	29.03.2007	L12_195_VGE_O_r01_t30_x.2x64x64.113.mes	L12_195_VGE_O_r01_t30_y.2x64x64.113.mes	6	52.540	3.044	29.9	117.5
113	P	98.3	0.2190	0.102	52.519	3.043	29.03.2007	L12_195_VGE_P_r01_t30_x.2x64x64.113.mes	L12_195_VGE_P_r01_t30_y.2x64x64.113.mes	5	52.520	3.045	29.8	98.7
113	Q	97.9	0.2190	0.102	52.519	3.043	29.03.2007	L12_195_VGE_Q_r04_t30_x.2x64x64.113.mes	L12_195_VGE_Q_r04_t30_y.2x64x64.113.mes	3	52.518	3.046	29.6	97.5
113	R	97.6	0.2190	0.102	52.519	3.043	29.03.2007	L12_195_VGE_R_r01_t30_x.2x64x64.113.mes	L12_195_VGE_R_r01_t30_y.2x64x64.113.mes	1	52.397	3.045	29.5	97.7

Matrix-punkt	Höhen-position	Druck am GS (ü) PI4-07 [kPa]	J _{Gas} [m/s] Einspeisung	J _{Wasser} [m/s]	V _{Gas} [nm³/h]	m _{Wasser} [kg/s]	Datum	File 1 (x)	File 2 (y)	DIAdem	Betriebsdaten (Mittelwerte über 10 s)			
											V _{Gas} [m³/h]	m _{Wasser} [kg/s]	t _{GS} [°C]	p(ü) GS [kPa]
114	A	142.9	0.2190	0.161	52.519	4.802	30.03.2007	L12_195_VGE_A_r01_t30_x.2x64x64.114.mes	L12_195_VGE_A_r01_t30_y.2x64x64.114.mes	33	52.538	4.803	30.3	142.8
114	B	142.6	0.2190	0.161	52.519	4.802	30.03.2007	L12_195_VGE_B_r04_t30_x.2x64x64.114.mes	L12_195_VGE_B_r04_t30_y.2x64x64.114.mes	31	52.522	4.801	30.2	142.3
114	C	142.2	0.2190	0.161	52.519	4.802	30.03.2007	L12_195_VGE_C_r01_t30_x.2x64x64.114.mes	L12_195_VGE_C_r01_t30_y.2x64x64.114.mes	30	52.540	4.802	30.1	141.9
114	D	141.2	0.2190	0.161	52.519	4.802	30.03.2007	L12_195_VGE_D_r01_t30_x.2x64x64.114.mes	L12_195_VGE_D_r01_t30_y.2x64x64.114.mes	29	52.533	4.801	30.0	141.4
114	E	140.8	0.2190	0.161	52.519	4.802	30.03.2007	L12_195_VGE_E_r04_t30_x.2x64x64.114.mes	L12_195_VGE_E_r04_t30_y.2x64x64.114.mes	25	52.548	4.804	29.8	140.8
114	F	140.5	0.2190	0.161	52.519	4.802	30.03.2007	L12_195_VGE_F_r01_t30_x.2x64x64.114.mes	L12_195_VGE_F_r01_t30_y.2x64x64.114.mes	23	52.528	4.802	29.8	140.6
114	G	135.2	0.2190	0.161	52.519	4.802	30.03.2007	L12_195_VGE_G_r01_t30_x.2x64x64.114.mes	L12_195_VGE_G_r01_t30_y.2x64x64.114.mes	22	52.107	4.802	30.7	135.3
114	H	134.8	0.2190	0.161	52.519	4.802	30.03.2007	L12_195_VGE_H_r04_t30_x.2x64x64.114.mes	L12_195_VGE_H_r04_t30_y.2x64x64.114.mes	19	52.528	4.802	30.6	134.8
114	I	134.4	0.2190	0.161	52.519	4.802	30.03.2007	L12_195_VGE_I_r01_t30_x.2x64x64.114.mes	L12_195_VGE_I_r01_t30_y.2x64x64.114.mes	18	52.527	4.803	30.4	134.5
114	J	128.5	0.2190	0.161	52.519	4.802	30.03.2007	L12_195_VGE_J_r01_t30_x.2x64x64.114.mes	L12_195_VGE_J_r01_t30_y.2x64x64.114.mes	17	52.527	4.802	30.4	128.5
114	K	128.1	0.2190	0.161	52.519	4.802	30.03.2007	L12_195_VGE_K_r04_t30_x.2x64x64.114.mes	L12_195_VGE_K_r04_t30_y.2x64x64.114.mes	16	52.528	4.802	30.2	128.2
114	L	127.8	0.2190	0.161	52.519	4.802	30.03.2007	L12_195_VGE_L_r01_t30_x.2x64x64.114.mes	L12_195_VGE_L_r01_t30_y.2x64x64.114.mes	15	52.525	4.803	30.2	127.8
114	M	116.1	0.2190	0.161	52.519	4.802	30.03.2007	L12_195_VGE_M_r01_t30_x.2x64x64.114.mes	L12_195_VGE_M_r01_t30_y.2x64x64.114.mes	11	52.508	4.802	29.9	116.5
114	N	115.8	0.2190	0.161	52.519	4.802	30.03.2007	L12_195_VGE_N_r04_t30_x.2x64x64.114.mes	L12_195_VGE_N_r04_t30_y.2x64x64.114.mes	10	52.248	4.803	29.8	115.8
114	O	115.4	0.2190	0.161	52.519	4.802	30.03.2007	L12_195_VGE_O_r01_t30_x.2x64x64.114.mes	L12_195_VGE_O_r01_t30_y.2x64x64.114.mes	9	52.518	4.802	29.8	115.5
114	P	95.2	0.2190	0.161	52.519	4.802	30.03.2007	L12_195_VGE_P_r01_t30_x.2x64x64.114.mes	L12_195_VGE_P_r01_t30_y.2x64x64.114.mes	3	52.518	4.802	29.5	95.5
114	Q	94.8	0.2190	0.161	52.519	4.802	30.03.2007	L12_195_VGE_Q_r04_t30_x.2x64x64.114.mes	L12_195_VGE_Q_r04_t30_y.2x64x64.114.mes	2	52.537	4.801	29.3	94.8
114	R	94.5	0.2190	0.161	52.519	4.802	30.03.2007	L12_195_VGE_R_r01_t30_x.2x64x64.114.mes	L12_195_VGE_R_r01_t30_y.2x64x64.114.mes	1	52.527	4.803	29.2	94.1
115	A	142.4	0.2190	0.255	52.519	7.606	16.03.2007	L12_195_VGE_A_r01_t30_x.2x64x64.115.mes	L12_195_VGE_A_r01_t30_y.2x64x64.115.mes	26	52.543	7.610	30.2	142.2
115	B	142.0	0.2190	0.255	52.519	7.606	16.03.2007	L12_195_VGE_B_r04_t30_x.2x64x64.115.mes	L12_195_VGE_B_r04_t30_y.2x64x64.115.mes	25	52.528	7.606	30.0	142.1
115	C	141.7	0.2190	0.255	52.519	7.606	16.03.2007	L12_195_VGE_C_r01_t30_x.2x64x64.115.mes	L12_195_VGE_C_r01_t30_y.2x64x64.115.mes	24	52.277	7.606	29.8	141.6
115	D	140.6	0.2190	0.255	52.519	7.606	16.03.2007	L12_195_VGE_D_r01_t30_x.2x64x64.115.mes	L12_195_VGE_D_r01_t30_y.2x64x64.115.mes	23	52.533	7.612	29.6	140.8
115	E	140.2	0.2190	0.255	52.519	7.606	16.03.2007	L12_195_VGE_E_r04_t30_x.2x64x64.115.mes	L12_195_VGE_E_r04_t30_y.2x64x64.115.mes	21	52.537	7.622	29.5	139.9
115	F	139.8	0.2190	0.255	52.519	7.606	16.03.2007	L12_195_VGE_F_r01_t30_x.2x64x64.115.mes	L12_195_VGE_F_r01_t30_y.2x64x64.115.mes	20	52.523	7.629	29.1	140.1
115	G	134.1	0.2190	0.255	52.519	7.606	16.03.2007	L12_195_VGE_G_r01_t30_x.2x64x64.115.mes	L12_195_VGE_G_r01_t30_y.2x64x64.115.mes	19	52.542	7.603	30.4	134.2
115	H	133.7	0.2190	0.255	52.519	7.606	16.03.2007	L12_195_VGE_H_r04_t30_x.2x64x64.115.mes	L12_195_VGE_H_r04_t30_y.2x64x64.115.mes	17	52.537	7.579	30.3	133.4
115	I	133.3	0.2190	0.255	52.519	7.606	16.03.2007	L12_195_VGE_I_r01_t30_x.2x64x64.115.mes	L12_195_VGE_I_r01_t30_y.2x64x64.115.mes	13	52.527	7.589	30.1	132.9
115	J	127.0	0.2190	0.255	52.519	7.606	16.03.2007	L12_195_VGE_J_r01_t30_x.2x64x64.115.mes	L12_195_VGE_J_r01_t30_y.2x64x64.115.mes	12	52.535	7.587	30.0	127.3
115	K	126.6	0.2190	0.255	52.519	7.606	16.03.2007	L12_195_VGE_K_r04_t30_x.2x64x64.115.mes	L12_195_VGE_K_r04_t30_y.2x64x64.115.mes	11	52.547	7.586	30.0	126.9
115	L	126.2	0.2190	0.255	52.519	7.606	16.03.2007	L12_195_VGE_L_r01_t30_x.2x64x64.115.mes	L12_195_VGE_L_r01_t30_y.2x64x64.115.mes	9	52.523	7.599	29.8	126.3
115	M	113.7	0.2190	0.255	52.519	7.606	16.03.2007	L12_195_VGE_M_r01_t30_x.2x64x64.115.mes	L12_195_VGE_M_r01_t30_y.2x64x64.115.mes	8	52.538	7.600	29.6	114.3
115	N	113.3	0.2190	0.255	52.519	7.606	16.03.2007	L12_195_VGE_N_r04_t30_x.2x64x64.115.mes	L12_195_VGE_N_r04_t30_y.2x64x64.115.mes	7	52.533	7.604	29.5	113.2
115	O	112.9	0.2190	0.255	52.519	7.606	16.03.2007	L12_195_VGE_O_r01_t30_x.2x64x64.115.mes	L12_195_VGE_O_r01_t30_y.2x64x64.115.mes	4	52.537	7.609	29.4	112.9
115	P	91.3	0.2190	0.255	52.519	7.606	16.03.2007	L12_195_VGE_P_r01_t30_x.2x64x64.115.mes	L12_195_VGE_P_r01_t30_y.2x64x64.115.mes	3	52.528	7.610	29.3	91.3
115	Q	90.9	0.2190	0.255	52.519	7.606	16.03.2007	L12_195_VGE_Q_r04_t30_x.2x64x64.115.mes	L12_195_VGE_Q_r04_t30_y.2x64x64.115.mes	2	52.532	7.612	29.2	91.7
115	R	90.5	0.2190	0.255	52.519	7.606	16.03.2007	L12_195_VGE_R_r01_t30_x.2x64x64.115.mes	L12_195_VGE_R_r01_t30_y.2x64x64.115.mes	1	52.300	7.600	29.0	90.8
116	A	141.8	0.2190	0.405	52.519	12.081	13.02.2007	L12_195_VGE_A_r01_t30_x.2x64x64.116.mes	L12_195_VGE_A_r01_t30_y.2x64x64.116.mes	26	52.545	12.079	30.1	142.3
116	B	141.4	0.2190	0.405	52.519	12.081	13.02.2007	L12_195_VGE_B_r04_t30_x.2x64x64.116.mes	L12_195_VGE_B_r04_t30_y.2x64x64.116.mes	25	52.553	12.068	30.0	141.0
116	C	141.0	0.2190	0.405	52.519	12.081	13.02.2007	L12_195_VGE_C_r01_t30_x.2x64x64.116.mes	L12_195_VGE_C_r01_t30_y.2x64x64.116.mes	24	52.557	12.075	29.9	141.3
116	D	139.8	0.2190	0.405	52.519	12.081	13.02.2007	L12_195_VGE_D_r01_t30_x.2x64x64.116.mes	L12_195_VGE_D_r01_t30_y.2x64x64.116.mes	21	52.553	12.063	29.7	139.6
116	E	139.4	0.2190	0.405	52.519	12.081	13.02.2007	L12_195_VGE_E_r04_t30_x.2x64x64.116.mes	L12_195_VGE_E_r04_t30_y.2x64x64.116.mes	19	52.550	12.081	31.3	139.4
116	F	139.0	0.2190	0.405	52.519	12.081	13.02.2007	L12_195_VGE_F_r01_t30_x.2x64x64.116.mes	L12_195_VGE_F_r01_t30_y.2x64x64.116.mes	18	52.528	12.096	30.6	138.9
116	G	132.8	0.2190	0.405	52.519	12.081	13.02.2007	L12_195_VGE_G_r01_t30_x.2x64x64.116.mes	L12_195_VGE_G_r01_t30_y.2x64x64.116.mes	16	52.543	12.084	30.3	132.9
116	H	132.4	0.2190	0.405	52.519	12.081	13.02.2007	L12_195_VGE_H_r04_t30_x.2x64x64.116.mes	L12_195_VGE_H_r04_t30_y.2x64x64.116.mes	15	52.533	12.079	30.2	132.8
116	I	132.0	0.2190	0.405	52.519	12.081	13.02.2007	L12_195_VGE_I_r01_t30_x.2x64x64.116.mes	L12_195_VGE_I_r01_t30_y.2x64x64.116.mes	14	52.548	12.081	30.2	132.1
116	J	125.1	0.2190	0.405	52.519	12.081	13.02.2007	L12_195_VGE_J_r01_t30_x.2x64x64.116.mes	L12_195_VGE_J_r01_t30_y.2x64x64.116.mes	12	52.535	12.077	30.1	125.2
116	K	124.7	0.2190	0.405	52.519	12.081	13.02.2007	L12_195_VGE_K_r04_t30_x.2x64x64.116.mes	L12_195_VGE_K_r04_t30_y.2x64x64.116.mes	11	52.537	12.063	30.0	123.9
116	L	124.3	0.2190	0.405	52.519	12.081	13.02.2007	L12_195_VGE_L_r01_t30_x.2x64x64.116.mes	L12_195_VGE_L_r01_t30_y.2x64x64.116.mes	9	52.547	12.098	29.8	124.3
116	M	110.8	0.2190	0.405	52.519	12.081	13.02.2007	L12_195_VGE_M_r01_t30_x.2x64x64.116.mes	L12_195_VGE_M_r01_t30_y.2x64x64.116.mes	8	52.548	12.082	29.7	110.9
116	N	110.4	0.2190	0.405	52.519	12.081	13.02.2007	L12_195_VGE_N_r04_t30_x.2x64x64.116.mes	L12_195_VGE_N_r04_t30_y.2x64x64.116.mes	7	52.548	12.071	29.6	110.0
116	O	110.0	0.2190	0.405	52.519	12.081	13.02.2007	L12_195_VGE_O_r01_t30_x.2x64x64.116.mes	L12_195_VGE_O_r01_t30_y.2x64x64.116.mes	6	52.548	12.063	29.5	109.8
116	P	86.7	0.2190	0.405	52.519	12.081	13.02.2007	L12_195_VGE_P_r01_t30_x.2x64x64.116.mes	L12_195_VGE_P_r01_t30_y.2x64x64.116.mes	4	52.558	12.086	29.3	86.9
116	Q	86.3	0.2190	0.405	52.519	12.081	13.02.2007	L12_195_VGE_Q_r04_t30_x.2x64x64.116.mes	L12_195_VGE_Q_r04_t30_y.2x64x64.116.mes	3	52.523	12.082	29.2	86.1
116	R	85.8	0.2190	0.405	52.519	12.081	13.02.2007	L12_195_VGE_R_r01_t30_x.2x64x64.116.mes	L12_195_VGE_R_r01_t30_y.2x64x64.116.mes	2	52.515	12.078	29.1	85.6

Matrix- punkt	Höhen- position	Druck am GS (ü) PI4-07 [kPa]	J _{Gas} [m/s] Einspeisung	J _{Wasser} [m/s]	V _{Gas} [nm³/h]	m _{Wasser} [kg/s]	Datum	File 1 (x)	File 2 (y)	DIAdem	Betriebsdaten (Mittelwerte über 10 s)			
											V _{Gas} [m³/h]	m _{Wasser} [kg/s]	t _{GS} [°C]	p(ü) GS [kPa]
117	A	141.1	0.2190	0.641	52.519	19.120	14.03.2007	L12_195_VGE_A_r01_t30_x.2x64x64.117.mes	L12_195_VGE_A_r01_t30_y.2x64x64.117.mes	26	52.527	19.128	29.9	141.0
117	B	140.6	0.2190	0.641	52.519	19.120	14.03.2007	L12_195_VGE_B_r04_t30_x.2x64x64.117.mes	L12_195_VGE_B_r04_t30_y.2x64x64.117.mes	25	52.540	19.120	29.8	140.8
117	C	140.2	0.2190	0.641	52.519	19.120	14.03.2007	L12_195_VGE_C_r01_t30_x.2x64x64.117.mes	L12_195_VGE_C_r01_t30_y.2x64x64.117.mes	24	52.535	19.116	29.6	140.0
117	D	138.9	0.2190	0.641	52.519	19.120	14.03.2007	L12_195_VGE_D_r01_t30_x.2x64x64.117.mes	L12_195_VGE_D_r01_t30_y.2x64x64.117.mes	23	52.540	19.111	29.5	138.9
117	E	138.5	0.2190	0.641	52.519	19.120	14.03.2007	L12_195_VGE_E_r04_t30_x.2x64x64.117.mes	L12_195_VGE_E_r04_t30_y.2x64x64.117.mes	22	52.542	19.139	29.4	138.5
117	F	138.0	0.2190	0.641	52.519	19.120	14.03.2007	L12_195_VGE_F_r01_t30_x.2x64x64.117.mes	L12_195_VGE_F_r01_t30_y.2x64x64.117.mes	20	52.538	19.117	29.0	137.8
117	G	131.4	0.2190	0.641	52.519	19.120	14.03.2007	L12_195_VGE_G_r01_t30_x.2x64x64.117.mes	L12_195_VGE_G_r01_t30_y.2x64x64.117.mes	19	52.535	19.127	29.3	131.6
117	H	130.9	0.2190	0.641	52.519	19.120	14.03.2007	L12_195_VGE_H_r04_t30_x.2x64x64.117.mes	L12_195_VGE_H_r04_t30_y.2x64x64.117.mes	18	52.393	19.138	29.1	130.9
117	I	130.5	0.2190	0.641	52.519	19.120	14.03.2007	L12_195_VGE_I_r01_t30_x.2x64x64.117.mes	L12_195_VGE_I_r01_t30_y.2x64x64.117.mes	16	52.548	19.124	29.7	130.5
117	J	123.1	0.2190	0.641	52.519	19.120	14.03.2007	L12_195_VGE_J_r01_t30_x.2x64x64.117.mes	L12_195_VGE_J_r01_t30_y.2x64x64.117.mes	15	52.530	19.130	30.2	123.5
117	K	122.6	0.2190	0.641	52.519	19.120	14.03.2007	L12_195_VGE_K_r04_t30_x.2x64x64.117.mes	L12_195_VGE_K_r04_t30_y.2x64x64.117.mes	12	52.373	19.113	30.1	122.5
117	L	122.2	0.2190	0.641	52.519	19.120	14.03.2007	L12_195_VGE_L_r01_t30_x.2x64x64.117.mes	L12_195_VGE_L_r01_t30_y.2x64x64.117.mes	11	52.525	19.137	30.0	122.2
117	M	107.6	0.2190	0.641	52.519	19.120	14.03.2007	L12_195_VGE_M_r01_t30_x.2x64x64.117.mes	L12_195_VGE_M_r01_t30_y.2x64x64.117.mes	10	52.545	19.117	29.8	107.8
117	N	107.2	0.2190	0.641	52.519	19.120	14.03.2007	L12_195_VGE_N_r04_t30_x.2x64x64.117.mes	L12_195_VGE_N_r04_t30_y.2x64x64.117.mes	9	52.517	19.118	29.7	107.2
117	O	106.7	0.2190	0.641	52.519	19.120	14.03.2007	L12_195_VGE_O_r01_t30_x.2x64x64.117.mes	L12_195_VGE_O_r01_t30_y.2x64x64.117.mes	5	52.525	19.121	29.6	107.0
117	P	81.6	0.2190	0.641	52.519	19.120	14.03.2007	L12_195_VGE_P_r01_t30_x.2x64x64.117.mes	L12_195_VGE_P_r01_t30_y.2x64x64.117.mes	4	52.533	19.113	29.5	81.6
117	Q	81.1	0.2190	0.641	52.519	19.120	14.03.2007	L12_195_VGE_Q_r04_t30_x.2x64x64.117.mes	L12_195_VGE_Q_r04_t30_y.2x64x64.117.mes	3	52.520	19.130	29.2	81.3
117	R	80.7	0.2190	0.641	52.519	19.120	14.03.2007	L12_195_VGE_R_r01_t30_x.2x64x64.117.mes	L12_195_VGE_R_r01_t30_y.2x64x64.117.mes	2	52.560	19.127	29.2	80.6
118	A	140.2	0.2190	1.017	52.519	30.336	14.02.2007	L12_195_VGE_A_r01_t30_x.2x64x64.118.mes	L12_195_VGE_A_r01_t30_y.2x64x64.118.mes	23	52.572	30.335	29.8	140.0
118	B	139.7	0.2190	1.017	52.519	30.336	14.02.2007	L12_195_VGE_B_r04_t30_x.2x64x64.118.mes	L12_195_VGE_B_r04_t30_y.2x64x64.118.mes	22	52.557	30.328	30.7	139.4
118	C	139.2	0.2190	1.017	52.519	30.336	14.02.2007	L12_195_VGE_C_r01_t30_x.2x64x64.118.mes	L12_195_VGE_C_r01_t30_y.2x64x64.118.mes	20	52.155	30.330	30.3	138.9
118	D	137.8	0.2190	1.017	52.519	30.336	14.02.2007	L12_195_VGE_D_r01_t30_x.2x64x64.118.mes	L12_195_VGE_D_r01_t30_y.2x64x64.118.mes	19	52.557	30.349	30.0	137.6
118	E	137.3	0.2190	1.017	52.519	30.336	14.02.2007	L12_195_VGE_E_r04_t30_x.2x64x64.118.mes	L12_195_VGE_E_r04_t30_y.2x64x64.118.mes	18	52.560	30.343	29.6	137.6
118	F	136.9	0.2190	1.017	52.519	30.336	14.02.2007	L12_195_VGE_F_r01_t30_x.2x64x64.118.mes	L12_195_VGE_F_r01_t30_y.2x64x64.118.mes	17	52.558	30.328	29.4	136.5
118	G	129.7	0.2190	1.017	52.519	30.336	14.02.2007	L12_195_VGE_G_r01_t30_x.2x64x64.118.mes	L12_195_VGE_G_r01_t30_y.2x64x64.118.mes	16	52.565	30.333	30.4	129.8
118	H	129.2	0.2190	1.017	52.519	30.336	14.02.2007	L12_195_VGE_H_r04_t30_x.2x64x64.118.mes	L12_195_VGE_H_r04_t30_y.2x64x64.118.mes	15	52.552	30.331	30.1	129.2
118	I	128.7	0.2190	1.017	52.519	30.336	14.02.2007	L12_195_VGE_I_r01_t30_x.2x64x64.118.mes	L12_195_VGE_I_r01_t30_y.2x64x64.118.mes	14	52.552	30.315	29.9	128.8
118	J	120.7	0.2190	1.017	52.519	30.336	14.02.2007	L12_195_VGE_J_r01_t30_x.2x64x64.118.mes	L12_195_VGE_J_r01_t30_y.2x64x64.118.mes	13	52.557	30.346	29.7	121.2
118	K	120.2	0.2190	1.017	52.519	30.336	14.02.2007	L12_195_VGE_K_r04_t30_x.2x64x64.118.mes	L12_195_VGE_K_r04_t30_y.2x64x64.118.mes	12	52.577	30.332	29.5	120.0
118	L	119.7	0.2190	1.017	52.519	30.336	14.02.2007	L12_195_VGE_L_r01_t30_x.2x64x64.118.mes	L12_195_VGE_L_r01_t30_y.2x64x64.118.mes	11	52.560	30.331	29.0	119.8
118	M	104.0	0.2190	1.017	52.519	30.336	14.02.2007	L12_195_VGE_M_r01_t30_x.2x64x64.118.mes	L12_195_VGE_M_r01_t30_y.2x64x64.118.mes	8	52.563	30.345	30.7	104.3
118	N	103.5	0.2190	1.017	52.519	30.336	14.02.2007	L12_195_VGE_N_r04_t30_x.2x64x64.118.mes	L12_195_VGE_N_r04_t30_y.2x64x64.118.mes	7	52.568	30.342	30.7	103.5
118	O	103.1	0.2190	1.017	52.519	30.336	14.02.2007	L12_195_VGE_O_r01_t30_x.2x64x64.118.mes	L12_195_VGE_O_r01_t30_y.2x64x64.118.mes	5	52.553	30.348	30.5	103.1
118	P	75.9	0.2190	1.017	52.519	30.336	14.02.2007	L12_195_VGE_P_r01_t30_x.2x64x64.118.mes	L12_195_VGE_P_r01_t30_y.2x64x64.118.mes	3	52.555	30.330	29.7	75.8
118	Q	75.4	0.2190	1.017	52.519	30.336	14.02.2007	L12_195_VGE_Q_r04_t30_x.2x64x64.118.mes	L12_195_VGE_Q_r04_t30_y.2x64x64.118.mes	2	52.535	30.330	29.5	75.4
118	R	74.9	0.2190	1.017	52.519	30.336	14.02.2007	L12_195_VGE_R_r01_t30_x.2x64x64.118.mes	L12_195_VGE_R_r01_t30_y.2x64x64.118.mes	1	52.567	30.335	29.3	75.2
119	A	138.9	0.2190	1.611	52.519	48.054	08.03.2007	L12_195_VGE_A_r01_t30_x.2x64x64.119.mes	L12_195_VGE_A_r01_t30_y.2x64x64.119.mes	32	52.540	48.040	30.6	138.7
119	B	138.4	0.2190	1.611	52.519	48.054	08.03.2007	L12_195_VGE_B_r04_t30_x.2x64x64.119.mes	L12_195_VGE_B_r04_t30_y.2x64x64.119.mes	29	52.532	48.046	30.3	138.5
119	C	137.8	0.2190	1.611	52.519	48.054	08.03.2007	L12_195_VGE_C_r01_t30_x.2x64x64.119.mes	L12_195_VGE_C_r01_t30_y.2x64x64.119.mes	28	52.542	48.060	29.6	137.9
119	D	136.3	0.2190	1.611	52.519	48.054	15.06.2007	L12_195_VGE_D_r01_t30_x.2x64x64.119.mes	L12_195_VGE_D_r01_t30_y.2x64x64.119.mes	21	52.488	48.045	30.6	136.2
119	E	135.8	0.2190	1.611	52.519	48.054	08.03.2007	L12_195_VGE_E_r04_t30_x.2x64x64.119.mes	L12_195_VGE_E_r04_t30_y.2x64x64.119.mes	24	52.530	48.035	30.1	135.7
119	F	135.3	0.2190	1.611	52.519	48.054	08.03.2007	L12_195_VGE_F_r01_t30_x.2x64x64.119.mes	L12_195_VGE_F_r01_t30_y.2x64x64.119.mes	22	52.520	48.045	31.1	135.6
119	G	127.5	0.2190	1.611	52.519	48.054	08.03.2007	L12_195_VGE_G_r01_t30_x.2x64x64.119.mes	L12_195_VGE_G_r01_t30_y.2x64x64.119.mes	21	52.533	48.039	30.7	127.5
119	H	126.9	0.2190	1.611	52.519	48.054	08.03.2007	L12_195_VGE_H_r04_t30_x.2x64x64.119.mes	L12_195_VGE_H_r04_t30_y.2x64x64.119.mes	20	52.520	48.069	30.3	126.8
119	I	126.4	0.2190	1.611	52.519	48.054	08.03.2007	L12_195_VGE_I_r01_t30_x.2x64x64.119.mes	L12_195_VGE_I_r01_t30_y.2x64x64.119.mes	19	52.527	48.047	29.9	126.1
119	J	117.7	0.2190	1.611	52.519	48.054	08.03.2007	L12_195_VGE_J_r01_t30_x.2x64x64.119.mes	L12_195_VGE_J_r01_t30_y.2x64x64.119.mes	16	52.528	48.054	29.3	117.5
119	K	117.1	0.2190	1.611	52.519	48.054	08.03.2007	L12_195_VGE_K_r04_t30_x.2x64x64.119.mes	L12_195_VGE_K_r04_t30_y.2x64x64.119.mes	14	52.530	48.045	29.3	117.2
119	L	116.6	0.2190	1.611	52.519	48.054	08.03.2007	L12_195_VGE_L_r01_t30_x.2x64x64.119.mes	L12_195_VGE_L_r01_t30_y.2x64x64.119.mes	11	52.537	48.041	30.8	116.7
119	M	99.5	0.2190	1.611	52.519	48.054	08.03.2007	L12_195_VGE_M_r01_t30_x.2x64x64.119.mes	L12_195_VGE_M_r01_t30_y.2x64x64.119.mes	10	52.532	48.048	29.6	99.4
119	N	98.9	0.2190	1.611	52.519	48.054	08.03.2007	L12_195_VGE_N_r04_t30_x.2x64x64.119.mes	L12_195_VGE_N_r04_t30_y.2x64x64.119.mes	8	52.527	48.026	29.2	99.1
119	O	98.4	0.2190	1.611	52.519	48.054	08.03.2007	L12_195_VGE_O_r01_t30_x.2x64x64.119.mes	L12_195_VGE_O_r01_t30_y.2x64x64.119.mes	7	52.518	48.042	29.4	98.4
119	P	68.7	0.2190	1.611	52.519	48.054	08.03.2007	L12_195_VGE_P_r01_t30_x.2x64x64.119.mes	L12_195_VGE_P_r01_t30_y.2x64x64.119.mes	4	52.527	48.046	30.2	68.5
119	Q	68.2	0.2190	1.611	52.519	48.054	08.03.2007	L12_195_VGE_Q_r04_t30_x.2x64x64.119.mes	L12_195_VGE_Q_r04_t30_y.2x64x64.119.mes	3	52.447	48.044	29.7	68.3
119	R	67.6	0.2190	1.611	52.519	48.054	08.03.2007	L12_195_VGE_R_r01_t30_x.2x64x64.119.mes	L12_195_VGE_R_r01_t30_y.2x64x64.119.mes	2	52.532	48.067	29.4	67.6

Matrix-punkt	Höhen-position	Druck am GS (ü) PI4-07 [kPa]	J _{Gas} [m/s] Einspeisung	J _{Wasser} [m/s]	V _{Gas} [nm³/h]	m _{Wasser} [kg/s]	Datum	File 1 (x)	File 2 (y)	DIAdem	Betriebsdaten (Mittelwerte über 10 s)			
											V _{Gas} [m³/h]	m _{Wasser} [kg/s]	t _{GS} [°C]	p(ü) GS [kPa]
127	A	142.8	0.3420	0.405	82.016	12.081	23.04.2007	L12_195_VGE_A_r01_t30_x.2x64x64.127.mes	L12_195_VGE_A_r01_t30_y.2x64x64.127.mes	25	81.927	12.076	30.5	142.6
127	B	142.4	0.3420	0.405	82.016	12.081	23.04.2007	L12_195_VGE_B_r04_t30_x.2x64x64.127.mes	L12_195_VGE_B_r04_t30_y.2x64x64.127.mes	24	81.932	12.077	30.4	142.8
127	C	142.0	0.3420	0.405	82.016	12.081	23.04.2007	L12_195_VGE_C_r01_t30_x.2x64x64.127.mes	L12_195_VGE_C_r01_t30_y.2x64x64.127.mes	23	81.910	12.076	30.4	142.1
127	D	141.0	0.3420	0.405	82.016	12.081	23.04.2007	L12_195_VGE_D_r01_t30_x.2x64x64.127.mes	L12_195_VGE_D_r01_t30_y.2x64x64.127.mes	22	81.908	12.085	30.3	141.2
127	E	140.6	0.3420	0.405	82.016	12.081	23.04.2007	L12_195_VGE_E_r04_t30_x.2x64x64.127.mes	L12_195_VGE_E_r04_t30_y.2x64x64.127.mes	21	81.913	12.076	30.3	140.7
127	F	140.3	0.3420	0.405	82.016	12.081	23.04.2007	L12_195_VGE_F_r01_t30_x.2x64x64.127.mes	L12_195_VGE_F_r01_t30_y.2x64x64.127.mes	20	81.908	12.079	30.2	140.5
127	G	134.9	0.3420	0.405	82.016	12.081	23.04.2007	L12_195_VGE_G_r01_t30_x.2x64x64.127.mes	L12_195_VGE_G_r01_t30_y.2x64x64.127.mes	19	81.908	12.070	30.1	134.5
127	H	134.5	0.3420	0.405	82.016	12.081	23.04.2007	L12_195_VGE_H_r04_t30_x.2x64x64.127.mes	L12_195_VGE_H_r04_t30_y.2x64x64.127.mes	18	81.918	12.095	30.1	134.4
127	I	134.1	0.3420	0.405	82.016	12.081	23.04.2007	L12_195_VGE_I_r01_t30_x.2x64x64.127.mes	L12_195_VGE_I_r01_t30_y.2x64x64.127.mes	17	81.920	12.102	30.0	134.2
127	J	128.1	0.3420	0.405	82.016	12.081	23.04.2007	L12_195_VGE_J_r01_t30_x.2x64x64.127.mes	L12_195_VGE_J_r01_t30_y.2x64x64.127.mes	13	81.920	12.076	29.7	128.6
127	K	127.7	0.3420	0.405	82.016	12.081	23.04.2007	L12_195_VGE_K_r04_t30_x.2x64x64.127.mes	L12_195_VGE_K_r04_t30_y.2x64x64.127.mes	12	81.898	12.079	29.7	127.6
127	L	127.4	0.3420	0.405	82.016	12.081	23.04.2007	L12_195_VGE_L_r01_t30_x.2x64x64.127.mes	L12_195_VGE_L_r01_t30_y.2x64x64.127.mes	11	81.918	12.077	29.6	127.8
127	M	115.5	0.3420	0.405	82.016	12.081	23.04.2007	L12_195_VGE_M_r01_t30_x.2x64x64.127.mes	L12_195_VGE_M_r01_t30_y.2x64x64.127.mes	10	81.918	12.068	29.5	115.7
127	N	115.2	0.3420	0.405	82.016	12.081	23.04.2007	L12_195_VGE_N_r04_t30_x.2x64x64.127.mes	L12_195_VGE_N_r04_t30_y.2x64x64.127.mes	9	81.900	12.082	29.5	115.6
127	O	114.8	0.3420	0.405	82.016	12.081	23.04.2007	L12_195_VGE_O_r01_t30_x.2x64x64.127.mes	L12_195_VGE_O_r01_t30_y.2x64x64.127.mes	8	81.903	12.080	29.4	115.1
127	P	94.3	0.3420	0.405	82.016	12.081	23.04.2007	L12_195_VGE_P_r01_t30_x.2x64x64.127.mes	L12_195_VGE_P_r01_t30_y.2x64x64.127.mes	7	81.905	12.089	29.3	94.1
127	Q	93.9	0.3420	0.405	82.016	12.081	23.04.2007	L12_195_VGE_Q_r04_t30_x.2x64x64.127.mes	L12_195_VGE_Q_r04_t30_y.2x64x64.127.mes	6	81.907	12.094	29.3	94.0
127	R	93.6	0.3420	0.405	82.016	12.081	23.04.2007	L12_195_VGE_R_r01_t30_x.2x64x64.127.mes	L12_195_VGE_R_r01_t30_y.2x64x64.127.mes	2	81.903	12.071	29.3	93.7
127	P	94.3	0.3420	0.405	82.016	12.081	26.07.2007	L12_195_VGE_P_r01_t30_x.2x64x64.127.mes	L12_195_VGE_P_r01_t30_y.2x64x64.127.mes	5	81.980	12.084	29.3	94.1
127	Q	93.9	0.3420	0.405	82.016	12.081	26.07.2007	L12_195_VGE_Q_r04_t30_x.2x64x64.127.mes	L12_195_VGE_Q_r04_t30_y.2x64x64.127.mes	2	82.002	12.089	29.2	93.7
127	R	93.6	0.3420	0.405	82.016	12.081	26.07.2007	L12_195_VGE_R_r01_t30_x.2x64x64.127.mes	L12_195_VGE_R_r01_t30_y.2x64x64.127.mes	4	82.020	12.076	29.3	93.5
129	A	140.8	0.3420	1.017	82.016	30.336	21.05.2007	L12_195_VGE_A_r01_t30_x.2x64x64.129.mes	L12_195_VGE_A_r01_t30_y.2x64x64.129.mes	30	81.963	30.334	30.4	140.6
129	B	140.4	0.3420	1.017	82.016	30.336	21.05.2007	L12_195_VGE_B_r04_t30_x.2x64x64.129.mes	L12_195_VGE_B_r04_t30_y.2x64x64.129.mes	27	81.958	30.362	30.1	140.5
129	C	139.9	0.3420	1.017	82.016	30.336	21.05.2007	L12_195_VGE_C_r01_t30_x.2x64x64.129.mes	L12_195_VGE_C_r01_t30_y.2x64x64.129.mes	25	81.927	30.308	29.8	139.6
129	D	138.6	0.3420	1.017	82.016	30.336	21.05.2007	L12_195_VGE_D_r01_t30_x.2x64x64.129.mes	L12_195_VGE_D_r01_t30_y.2x64x64.129.mes	24	81.922	30.343	29.5	138.6
129	E	138.2	0.3420	1.017	82.016	30.336	21.05.2007	L12_195_VGE_E_r04_t30_x.2x64x64.129.mes	L12_195_VGE_E_r04_t30_y.2x64x64.129.mes	22	81.953	30.355	29.4	138.3
129	F	137.7	0.3420	1.017	82.016	30.336	21.05.2007	L12_195_VGE_F_r01_t30_x.2x64x64.129.mes	L12_195_VGE_F_r01_t30_y.2x64x64.129.mes	21	81.953	30.323	29.7	137.7
129	G	131.1	0.3420	1.017	82.016	30.336	21.05.2007	L12_195_VGE_G_r01_t30_x.2x64x64.129.mes	L12_195_VGE_G_r01_t30_y.2x64x64.129.mes	20	81.952	30.351	30.3	131.7
129	H	130.6	0.3420	1.017	82.016	30.336	21.05.2007	L12_195_VGE_H_r04_t30_x.2x64x64.129.mes	L12_195_VGE_H_r04_t30_y.2x64x64.129.mes	17	81.943	30.335	30.8	130.5
129	I	130.2	0.3420	1.017	82.016	30.336	21.05.2007	L12_195_VGE_I_r01_t30_x.2x64x64.129.mes	L12_195_VGE_I_r01_t30_y.2x64x64.129.mes	19	81.982	30.340	30.7	130.3
129	J	122.7	0.3420	1.017	82.016	30.336	21.05.2007	L12_195_VGE_J_r01_t30_x.2x64x64.129.mes	L12_195_VGE_J_r01_t30_y.2x64x64.129.mes	15	81.925	30.347	30.4	122.7
129	K	122.3	0.3420	1.017	82.016	30.336	21.05.2007	L12_195_VGE_K_r04_t30_x.2x64x64.129.mes	L12_195_VGE_K_r04_t30_y.2x64x64.129.mes	14	81.943	30.320	30.1	122.5
129	L	121.8	0.3420	1.017	82.016	30.336	21.05.2007	L12_195_VGE_L_r01_t30_x.2x64x64.129.mes	L12_195_VGE_L_r01_t30_y.2x64x64.129.mes	13	81.955	30.356	29.9	122.1
129	M	107.2	0.3420	1.017	82.016	30.336	21.05.2007	L12_195_VGE_M_r01_t30_x.2x64x64.129.mes	L12_195_VGE_M_r01_t30_y.2x64x64.129.mes	12	81.943	30.332	29.6	107.6
129	N	106.8	0.3420	1.017	82.016	30.336	21.05.2007	L12_195_VGE_N_r04_t30_x.2x64x64.129.mes	L12_195_VGE_N_r04_t30_y.2x64x64.129.mes	11	81.952	30.341	29.3	106.9
129	O	106.3	0.3420	1.017	82.016	30.336	21.05.2007	L12_195_VGE_O_r01_t30_x.2x64x64.129.mes	L12_195_VGE_O_r01_t30_y.2x64x64.129.mes	10	81.950	30.339	29.3	106.5
129	P	81.0	0.3420	1.017	82.016	30.336	21.05.2007	L12_195_VGE_P_r01_t30_x.2x64x64.129.mes	L12_195_VGE_P_r01_t30_y.2x64x64.129.mes	5	81.942	30.346	29.4	81.3
129	Q	80.6	0.3420	1.017	82.016	30.336	21.05.2007	L12_195_VGE_Q_r04_t30_x.2x64x64.129.mes	L12_195_VGE_Q_r04_t30_y.2x64x64.129.mes	1	81.947	30.335	30.9	80.6
129	R	80.1	0.3420	1.017	82.016	30.336	21.05.2007	L12_195_VGE_R_r01_t30_x.2x64x64.129.mes	L12_195_VGE_R_r01_t30_y.2x64x64.129.mes	3	81.955	30.330	30.3	80.2
138	A	143.9	0.5340	0.405	128.06	12.081	12.02.2007	L12_195_VGE_A_r01_t30_x.2x64x64.138.mes	L12_195_VGE_A_r01_t30_y.2x64x64.138.mes	25	128.207	12.072	30.2	144.5
138	B	143.6	0.5340	0.405	128.06	12.081	12.02.2007	L12_195_VGE_B_r04_t30_x.2x64x64.138.mes	L12_195_VGE_B_r04_t30_y.2x64x64.138.mes	24	128.243	12.065	30.2	144.8
138	C	143.3	0.5340	0.405	128.06	12.081	12.02.2007	L12_195_VGE_C_r01_t30_x.2x64x64.138.mes	L12_195_VGE_C_r01_t30_y.2x64x64.138.mes	23	128.078	12.082	30.1	142.9
138	D	142.4	0.5340	0.405	128.06	12.081	12.02.2007	L12_195_VGE_D_r01_t30_x.2x64x64.138.mes	L12_195_VGE_D_r01_t30_y.2x64x64.138.mes	22	127.953	12.073	30.1	142.8
138	E	142.1	0.5340	0.405	128.06	12.081	12.02.2007	L12_195_VGE_E_r04_t30_x.2x64x64.138.mes	L12_195_VGE_E_r04_t30_y.2x64x64.138.mes	20	128.467	12.092	30.0	142.4
138	F	141.8	0.5340	0.405	128.06	12.081	12.02.2007	L12_195_VGE_F_r01_t30_x.2x64x64.138.mes	L12_195_VGE_F_r01_t30_y.2x64x64.138.mes	19	128.048	12.084	30.0	141.4
138	G	137.2	0.5340	0.405	128.06	12.081	12.02.2007	L12_195_VGE_G_r01_t30_x.2x64x64.138.mes	L12_195_VGE_G_r01_t30_y.2x64x64.138.mes	17	128.205	12.094	29.9	136.1
138	H	136.9	0.5340	0.405	128.06	12.081	12.02.2007	L12_195_VGE_H_r04_t30_x.2x64x64.138.mes	L12_195_VGE_H_r04_t30_y.2x64x64.138.mes	16	128.060	12.073	29.8	136.6
138	I	136.6	0.5340	0.405	128.06	12.081	12.02.2007	L12_195_VGE_I_r01_t30_x.2x64x64.138.mes	L12_195_VGE_I_r01_t30_y.2x64x64.138.mes	15	128.190	12.088	29.7	136.1
138	J	131.5	0.5340	0.405	128.06	12.081	12.02.2007	L12_195_VGE_J_r01_t30_x.2x64x64.138.mes	L12_195_VGE_J_r01_t30_y.2x64x64.138.mes	14	127.130	12.087	29.6	132.1
138	K	131.2	0.5340	0.405	128.06	12.081	12.02.2007	L12_195_VGE_K_r04_t30_x.2x64x64.138.mes	L12_195_VGE_K_r04_t30_y.2x64x64.138.mes	13	128.087	12.069	29.6	131.8
138	L	130.9	0.5340	0.405	128.06	12.081	12.02.2007	L12_195_VGE_L_r01_t30_x.2x64x64.138.mes	L12_195_VGE_L_r01_t30_y.2x64x64.138.mes	12	128.187	12.085	29.6	130.4
138	M	120.9	0.5340	0.405	128.06	12.081	12.02.2007	L12_195_VGE_M_r01_t30_x.2x64x64.138.mes	L12_195_VGE_M_r01_t30_y.2x64x64.138.mes	11	128.352	12.075	29.5	121.4
138	N	120.6	0.5340	0.405	128.06	12.081	12.02.2007	L12_195_VGE_N_r04_t30_x.2x64x64.138.mes	L12_195_VGE_N_r04_t30_y.2x64x64.138.mes	10	128.250	12.088	29.5	120.8
138	O	120.3	0.5340	0.405	128.06	12.081	12.02.2007	L12_195_VGE_O_r01_t30_x.2x64x64.138.mes	L12_195_VGE_O_r01_t30_y.2x64x64.138.mes	9	128.242	12.082	29.5	120.3
138	P	103.0	0.5340	0.405	128.06	12.081	12.02.2007	L12_195_VGE_P_r01_t30_x.2x64x64.138.mes	L12_195_VGE_P_r01_t30_y.2x64x64.138.mes	6	128.227	12.080	29.2	102.9
138	Q	102.7	0.5340	0.405	128.06	12.081	12.02.2007	L12_195_VGE_Q_r04_t30_x.2x64x64.138.mes	L12_195_VGE_Q_r04_t30_y.2x64x64.138.mes	5	127.975	12.091	29.2	102.9
138	R	102.4	0.5340	0.405	128.06	12.081	12.02.2007	L12_195_VGE_R_r01_t30_x.2x64x64.138.mes	L12_195_VGE_R_r01_t30_y.2x64x64.138.mes	2	128.233	12.076	29.2	102.6

Matrix-punkt	Höhen-position	Druck am GS (ü) PI4-07 [kPa]	J _{Gas} [m/s] Einspeisung	J _{Wasser} [m/s]	V _{Gas} [nm³/h]	m _{Wasser} [kg/s]	Datum	File 1 (x)	File 2 (y)	DIAdem	Betriebsdaten (Mittelwerte über 10 s)			
											V _{Gas} [m³/h]	m _{Wasser} [kg/s]	t _{GS} [°C]	p(ü) GS [kPa]
140	A	141.6	0.5340	1.017	128.06	30.336	01.02.2007	L12_195_VGE_A_r01_t30_x.2x64x64.140.mes	L12_195_VGE_A_r01_t30_y.2x64x64.140.mes	35	127.835	30.340	30.3	141.8
140	B	141.2	0.5340	1.017	128.06	30.336	01.02.2007	L12_195_VGE_B_r04_t30_x.2x64x64.140.mes	L12_195_VGE_B_r04_t30_y.2x64x64.140.mes	32	127.535	30.324	29.8	141.1
140	C	140.8	0.5340	1.017	128.06	30.336	01.02.2007	L12_195_VGE_C_r01_t30_x.2x64x64.140.mes	L12_195_VGE_C_r01_t30_y.2x64x64.140.mes	30	127.492	30.316	29.5	140.8
140	D	139.7	0.5340	1.017	128.06	30.336	01.02.2007	L12_195_VGE_D_r01_t30_x.2x64x64.140.mes	L12_195_VGE_D_r01_t30_y.2x64x64.140.mes	28	127.488	30.327	30.3	140.3
140	E	139.3	0.5340	1.017	128.06	30.336	01.02.2007	L12_195_VGE_E_r04_t30_x.2x64x64.140.mes	L12_195_VGE_E_r04_t30_y.2x64x64.140.mes	25	127.373	30.338	30.4	139.7
140	F	138.8	0.5340	1.017	128.06	30.336	01.02.2007	L12_195_VGE_F_r01_t30_x.2x64x64.140.mes	L12_195_VGE_F_r01_t30_y.2x64x64.140.mes	24	127.507	30.342	30.2	138.7
140	G	132.8	0.5340	1.017	128.06	30.336	01.02.2007	L12_195_VGE_G_r01_t30_x.2x64x64.140.mes	L12_195_VGE_G_r01_t30_y.2x64x64.140.mes	23	127.515	30.328	30.0	133.6
140	H	132.4	0.5340	1.017	128.06	30.336	01.02.2007	L12_195_VGE_H_r04_t30_x.2x64x64.140.mes	L12_195_VGE_H_r04_t30_y.2x64x64.140.mes	22	127.370	30.348	29.8	132.5
140	I	132.0	0.5340	1.017	128.06	30.336	01.02.2007	L12_195_VGE_I_r01_t30_x.2x64x64.140.mes	L12_195_VGE_I_r01_t30_y.2x64x64.140.mes	20	127.502	30.338	29.6	132.0
140	J	125.3	0.5340	1.017	128.06	30.336	01.02.2007	L12_195_VGE_J_r01_t30_x.2x64x64.140.mes	L12_195_VGE_J_r01_t30_y.2x64x64.140.mes	19	127.433	30.320	29.4	125.3
140	K	124.9	0.5340	1.017	128.06	30.336	01.02.2007	L12_195_VGE_K_r04_t30_x.2x64x64.140.mes	L12_195_VGE_K_r04_t30_y.2x64x64.140.mes	18	127.340	30.343	29.3	124.3
140	L	124.5	0.5340	1.017	128.06	30.336	01.02.2007	L12_195_VGE_L_r01_t30_x.2x64x64.140.mes	L12_195_VGE_L_r01_t30_y.2x64x64.140.mes	16	127.482	30.329	29.0	124.5
140	M	111.3	0.5340	1.017	128.06	30.336	01.02.2007	L12_195_VGE_M_r01_t30_x.2x64x64.140.mes	L12_195_VGE_M_r01_t30_y.2x64x64.140.mes	14	126.850	30.332	30.6	111.1
140	N	110.9	0.5340	1.017	128.06	30.336	01.02.2007	L12_195_VGE_N_r04_t30_x.2x64x64.140.mes	L12_195_VGE_N_r04_t30_y.2x64x64.140.mes	13	127.375	30.320	30.4	110.8
140	O	110.5	0.5340	1.017	128.06	30.336	01.02.2007	L12_195_VGE_O_r01_t30_x.2x64x64.140.mes	L12_195_VGE_O_r01_t30_y.2x64x64.140.mes	12	127.525	30.342	30.0	109.6
140	P	87.7	0.5340	1.017	128.06	30.336	01.02.2007	L12_195_VGE_P_r01_t30_x.2x64x64.140.mes	L12_195_VGE_P_r01_t30_y.2x64x64.140.mes	10	127.465	30.336	29.7	87.3
140	Q	87.2	0.5340	1.017	128.06	30.336	01.02.2007	L12_195_VGE_Q_r04_t30_x.2x64x64.140.mes	L12_195_VGE_Q_r04_t30_y.2x64x64.140.mes	9	127.463	30.329	29.7	87.3
140	R	86.8	0.5340	1.017	128.06	30.336	01.02.2007	L12_195_VGE_R_r01_t30_x.2x64x64.140.mes	L12_195_VGE_R_r01_t30_y.2x64x64.140.mes	5	127.378	30.321	29.5	86.8
149	A	145.0	0.8350	0.405	200.24	12.081	11.05.2007	L12_195_VGE_AC_r01_t30_x.2x64x64.149.mes	L12_195_VGE_AC_r01_t30_y.2x64x64.149.mes	16	200.045	12.089	29.7	144.9
149	B	144.8	0.8350	0.405	200.24	12.081	11.05.2007	L12_195_VGE_B_r04_t30_x.2x64x64.149.mes	L12_195_VGE_B_r04_t30_y.2x64x64.149.mes	17	200.222	12.076	29.7	144.4
149	C	144.5	0.8350	0.405	200.24	12.081								
149	D	143.8	0.8350	0.405	200.24	12.081	11.05.2007	L12_195_VGE_DF_r01_t30_x.2x64x64.149.mes	L12_195_VGE_DF_r01_t30_y.2x64x64.149.mes	12	200.392	12.071	29.6	144.1
149	E	143.6	0.8350	0.405	200.24	12.081	11.05.2007	L12_195_VGE_E_r04_t30_x.2x64x64.149.mes	L12_195_VGE_E_r04_t30_y.2x64x64.149.mes	13	200.297	12.088	29.6	143.7
149	F	143.3	0.8350	0.405	200.24	12.081								
149	G	139.7	0.8350	0.405	200.24	12.081	11.05.2007	L12_195_VGE_GI_r01_t30_x.2x64x64.149.mes	L12_195_VGE_GI_r01_t30_y.2x64x64.149.mes	9	200.443	12.073	29.5	139.3
149	H	139.4	0.8350	0.405	200.24	12.081	11.05.2007	L12_195_VGE_H_r04_t30_x.2x64x64.149.mes	L12_195_VGE_H_r04_t30_y.2x64x64.149.mes	11	200.303	12.074	29.6	139.0
149	I	139.2	0.8350	0.405	200.24	12.081								
149	J	135.1	0.8350	0.405	200.24	12.081	11.05.2007	L12_195_VGE_JL_r01_t30_x.2x64x64.149.mes	L12_195_VGE_JL_r01_t30_y.2x64x64.149.mes	6	200.425	12.074	29.5	134.4
149	K	134.8	0.8350	0.405	200.24	12.081	11.05.2007	L12_195_VGE_K_r04_t30_x.2x64x64.149.mes	L12_195_VGE_K_r04_t30_y.2x64x64.149.mes	7	200.015	12.077	29.5	135.7
149	L	134.6	0.8350	0.405	200.24	12.081								
149	M	126.6	0.8350	0.405	200.24	12.081	11.05.2007	L12_195_VGE_MO_r01_t30_x.2x64x64.149.mes	L12_195_VGE_MO_r01_t30_y.2x64x64.149.mes	4	200.030	12.080	29.3	126.8
149	N	126.3	0.8350	0.405	200.24	12.081	11.05.2007	L12_195_VGE_N_r04_t30_x.2x64x64.149.mes	L12_195_VGE_N_r04_t30_y.2x64x64.149.mes	5	200.340	12.089	29.3	126.9
149	O	126.1	0.8350	0.405	200.24	12.081								
149	P	112.2	0.8350	0.405	200.24	12.081	11.05.2007	L12_195_VGE_PR_r01_t30_x.2x64x64.149.mes	L12_195_VGE_PR_r01_t30_y.2x64x64.149.mes	1	200.453	12.088	29.3	112.5
149	Q	111.9	0.8350	0.405	200.24	12.081	11.05.2007	L12_195_VGE_Q_r04_t30_x.2x64x64.149.mes	L12_195_VGE_Q_r04_t30_y.2x64x64.149.mes	2	200.207	12.087	29.3	111.9
149	R	111.7	0.8350	0.405	200.24	12.081								
151	A	142.6	0.8350	1.017	200.24	30.336	15.05.2007	L12_195_VGE_AC_r01_t30_x.2x64x64.151.mes	L12_195_VGE_AC_r01_t30_y.2x64x64.151.mes	23	200.235	30.327	30.1	142.9
151	B	142.2	0.8350	1.017	200.24	30.336	15.05.2007	L12_195_VGE_B_r04_t30_x.2x64x64.151.mes	L12_195_VGE_B_r04_t30_y.2x64x64.151.mes	24	199.980	30.336	30.1	142.3
151	C	141.9	0.8350	1.017	200.24	30.336								
151	D	140.9	0.8350	1.017	200.24	30.336	15.05.2007	L12_195_VGE_DF_r01_t30_x.2x64x64.151.mes	L12_195_VGE_DF_r01_t30_y.2x64x64.151.mes	19	200.428	30.332	29.6	140.8
151	E	140.5	0.8350	1.017	200.24	30.336	15.05.2007	L12_195_VGE_E_r04_t30_x.2x64x64.151.mes	L12_195_VGE_E_r04_t30_y.2x64x64.151.mes	20	200.292	30.331	29.7	140.4
151	F	140.2	0.8350	1.017	200.24	30.336								
151	G	134.9	0.8350	1.017	200.24	30.336	15.05.2007	L12_195_VGE_GI_r01_t30_x.2x64x64.151.mes	L12_195_VGE_GI_r01_t30_y.2x64x64.151.mes	15	200.342	30.336	29.3	134.4
151	H	134.6	0.8350	1.017	200.24	30.336	15.05.2007	L12_195_VGE_H_r04_t30_x.2x64x64.151.mes	L12_195_VGE_H_r04_t30_y.2x64x64.151.mes	17	200.745	30.341	29.4	134.8
151	I	134.2	0.8350	1.017	200.24	30.336								
151	J	128.4	0.8350	1.017	200.24	30.336	15.05.2007	L12_195_VGE_JL_r01_t30_x.2x64x64.151.mes	L12_195_VGE_JL_r01_t30_y.2x64x64.151.mes	11	200.008	30.338	30.7	128.3
151	K	128.0	0.8350	1.017	200.24	30.336	15.05.2007	L12_195_VGE_K_r04_t30_x.2x64x64.151.mes	L12_195_VGE_K_r04_t30_y.2x64x64.151.mes	14	199.973	30.337	30.7	128.2
151	L	127.6	0.8350	1.017	200.24	30.336								
151	M	116.2	0.8350	1.017	200.24	30.336	15.05.2007	L12_195_VGE_MO_r01_t30_x.2x64x64.151.mes	L12_195_VGE_MO_r01_t30_y.2x64x64.151.mes	6	199.977	30.330	30.2	116.5
151	N	115.8	0.8350	1.017	200.24	30.336	15.05.2007	L12_195_VGE_N_r04_t30_x.2x64x64.151.mes	L12_195_VGE_N_r04_t30_y.2x64x64.151.mes	8	200.315	30.331	30.4	115.8
151	O	115.4	0.8350	1.017	200.24	30.336								
151	P	95.5	0.8350	1.017	200.24	30.336	15.05.2007	L12_195_VGE_PR_r01_t30_x.2x64x64.151.mes	L12_195_VGE_PR_r01_t30_y.2x64x64.151.mes	1	200.410	30.306	29.9	95.6
151	Q	95.2	0.8350	1.017	200.24	30.336	15.05.2007	L12_195_VGE_Q_r04_t30_x.2x64x64.151.mes	L12_195_VGE_Q_r04_t30_y.2x64x64.151.mes	3	200.085	30.347	30.1	95.4
151	R	94.8	0.8350	1.017	200.24	30.336								

Matrix-punkt	Höhen-position	Druck am GS (ü) PI4-07 [kPa]	J _{Gas} [m/s] Einspeisung	J _{Wasser} [m/s]	V _{Gas} [nm³/h]	m _{Wasser} [kg/s]	Datum	File 1 (x)	File 2 (y)	DIAdem	Betriebsdaten (Mittelwerte über 10 s)				
											V _{Gas} [m³/h]	m _{Wasser} [kg/s]	t _{GS} [°C]	p(ü) GS [kPa]	
160	A	146.1	1.3050	0.405	312.95	12.081	30.01.2007	L12_195_VGE_AC_r01_t30_x.2x64x64.160.mes	L12_195_VGE_AC_r01_t30_y.2x64x64.160.mes	11b	310.595	12.066	29.7	146.1	
160	B	145.9	1.3050	0.405	312.95	12.081	30.01.2007	L12_195_VGE_B_r04_t30_x.2x64x64.160.mes	L12_195_VGE_B_r04_t30_y.2x64x64.160.mes	12b	312.612	12.083	29.7	145.2	
160	C	145.7	1.3050	0.405	312.95	12.081									
160	D	145.2	1.3050	0.405	312.95	12.081	30.01.2007	L12_195_VGE_DF_r01_t30_x.2x64x64.160.mes	L12_195_VGE_DF_r01_t30_y.2x64x64.160.mes	9b	310.645	12.059	29.5	145.4	
160	E	145.0	1.3050	0.405	312.95	12.081	30.01.2007	L12_195_VGE_E_r04_t30_x.2x64x64.160.mes	L12_195_VGE_E_r04_t30_y.2x64x64.160.mes	10b	312.580	12.076	29.6	144.7	
160	F	144.8	1.3050	0.405	312.95	12.081									
160	G	142.0	1.3050	0.405	312.95	12.081	30.01.2007	L12_195_VGE_GI_r01_t30_x.2x64x64.160.mes	L12_195_VGE_GI_r01_t30_y.2x64x64.160.mes	6b	310.570	12.057	29.5	142.3	
160	H	141.8	1.3050	0.405	312.95	12.081	30.01.2007	L12_195_VGE_H_r04_t30_x.2x64x64.160.mes	L12_195_VGE_H_r04_t30_y.2x64x64.160.mes	7b	312.848	12.072	29.5	143.1	
160	I	141.6	1.3050	0.405	312.95	12.081									
160	J	138.4	1.3050	0.405	312.95	12.081	30.01.2007	L12_195_VGE_JL_r01_t30_x.2x64x64.160.mes	L12_195_VGE_JL_r01_t30_y.2x64x64.160.mes	4b	310.622	12.073	29.4	138.7	
160	K	138.2	1.3050	0.405	312.95	12.081	30.01.2007	L12_195_VGE_K_r04_t30_x.2x64x64.160.mes	L12_195_VGE_K_r04_t30_y.2x64x64.160.mes	5b	312.528	12.072	29.4	138.9	
160	L	138.0	1.3050	0.405	312.95	12.081									
160	M	131.8	1.3050	0.405	312.95	12.081	30.01.2007	L12_195_VGE_MO_r01_t30_x.2x64x64.160.mes	L12_195_VGE_MO_r01_t30_y.2x64x64.160.mes	1a	311.982	12.061	29.3	130.3	
160	N	131.6	1.3050	0.405	312.95	12.081	30.01.2007	L12_195_VGE_N_r04_t30_x.2x64x64.160.mes	L12_195_VGE_N_r04_t30_y.2x64x64.160.mes	2a	312.797	12.080	29.3	132.0	
160	O	131.5	1.3050	0.405	312.95	12.081									
160	P	120.7	1.3050	0.405	312.95	12.081	30.01.2007	L12_195_VGE_PR_r01_t30_x.2x64x64.160.mes	L12_195_VGE_PR_r01_t30_y.2x64x64.160.mes	4a	312.308	12.065	29.3	119.0	
160	Q	120.5	1.3050	0.405	312.95	12.081	30.01.2007	L12_195_VGE_Q_r04_t30_x.2x64x64.160.mes	L12_195_VGE_Q_r04_t30_y.2x64x64.160.mes	3b	312.812	12.087	29.3	119.0	
160	R	120.3	1.3050	0.405	312.95	12.081									
162	A	143.6	1.3050	1.017	312.95	30.336	29.01.2007	L12_195_VGE_AC_r01_t30_x.2x64x64.162.mes	L12_195_VGE_AC_r01_t30_y.2x64x64.162.mes	14	312.727	30.325	30.1	144.0	
162	B	143.3	1.3050	1.017	312.95	30.336	29.01.2007	L12_195_VGE_B_r04_t30_x.2x64x64.162.mes	L12_195_VGE_B_r04_t30_y.2x64x64.162.mes	15	312.758	30.327	30.1	143.5	
162	C	143.0	1.3050	1.017	312.95	30.336									
162	D	142.2	1.3050	1.017	312.95	30.336	29.01.2007	L12_195_VGE_DF_r01_t30_x.2x64x64.162.mes	L12_195_VGE_DF_r01_t30_y.2x64x64.162.mes	11	311.215	30.327	29.7	141.2	
162	E	141.9	1.3050	1.017	312.95	30.336	29.01.2007	L12_195_VGE_E_r04_t30_x.2x64x64.162.mes	L12_195_VGE_E_r04_t30_y.2x64x64.162.mes	12	312.800	30.336	29.8	142.2	
162	F	141.6	1.3050	1.017	312.95	30.336									
162	G	137.2	1.3050	1.017	312.95	30.336	29.01.2007	L12_195_VGE_GI_r01_t30_x.2x64x64.162.mes	L12_195_VGE_GI_r01_t30_y.2x64x64.162.mes	9	312.497	30.324	29.4	136.0	
162	H	136.9	1.3050	1.017	312.95	30.336	29.01.2007	L12_195_VGE_H_r04_t30_x.2x64x64.162.mes	L12_195_VGE_H_r04_t30_y.2x64x64.162.mes	10	312.530	30.322	29.6	135.6	
162	I	136.6	1.3050	1.017	312.95	30.336									
162	J	131.6	1.3050	1.017	312.95	30.336	29.01.2007	L12_195_VGE_JL_r01_t30_x.2x64x64.162.mes	L12_195_VGE_JL_r01_t30_y.2x64x64.162.mes	7	312.223	30.325	29.5	131.5	
162	K	131.3	1.3050	1.017	312.95	30.336	29.01.2007	L12_195_VGE_K_r04_t30_x.2x64x64.162.mes	L12_195_VGE_K_r04_t30_y.2x64x64.162.mes	8	312.765	30.328	29.6	132.4	
162	L	131.0	1.3050	1.017	312.95	30.336									
162	M	121.4	1.3050	1.017	312.95	30.336	29.01.2007	L12_195_VGE_MO_r01_t30_x.2x64x64.162.mes	L12_195_VGE_MO_r01_t30_y.2x64x64.162.mes	5	312.158	30.311	29.3	122.8	
162	N	121.1	1.3050	1.017	312.95	30.336	29.01.2007	L12_195_VGE_N_r04_t30_x.2x64x64.162.mes	L12_195_VGE_N_r04_t30_y.2x64x64.162.mes	6	312.508	30.327	29.4	120.7	
162	O	120.8	1.3050	1.017	312.95	30.336									
162	P	104.0	1.3050	1.017	312.95	30.336	29.01.2007	L12_195_VGE_PR_r01_t30_x.2x64x64.162.mes	L12_195_VGE_PR_r01_t30_y.2x64x64.162.mes	2	312.452	30.299	29.1	103.8	
162	Q	103.7	1.3050	1.017	312.95	30.336	29.01.2007	L12_195_VGE_Q_r04_t30_x.2x64x64.162.mes	L12_195_VGE_Q_r04_t30_y.2x64x64.162.mes	4	312.748	30.335	29.2	102.2	
162	R	103.4	1.3050	1.017	312.95	30.336									
171	A	147.0	2.0380	0.405	488.74	12.081									
171	B	146.9	2.0380	0.405	488.74	12.081	02.02.2007	L12_195_VGE_B_r04_t30_x.2x64x64.171.mes	L12_195_VGE_B_r04_t30_y.2x64x64.171.mes	22	485.362	12.054	29.9	146.6	
171	C	146.7	2.0380	0.405	488.74	12.081									
171	D	146.3	2.0380	0.405	488.74	12.081									
171	E	146.2	2.0380	0.405	488.74	12.081	02.02.2007	L12_195_VGE_E_r04_t30_x.2x64x64.171.mes	L12_195_VGE_E_r04_t30_y.2x64x64.171.mes	17	485.303	12.068	29.7	145.6	
171	F	146.0	2.0380	0.405	488.74	12.081									
171	G	143.9	2.0380	0.405	488.74	12.081									
171	H	143.8	2.0380	0.405	488.74	12.081	02.02.2007	L12_195_VGE_H_r04_t30_x.2x64x64.171.mes	L12_195_VGE_H_r04_t30_y.2x64x64.171.mes	16	485.767	12.090	29.7	143.3	
171	I	143.6	2.0380	0.405	488.74	12.081									
171	J	141.2	2.0380	0.405	488.74	12.081									
171	K	141.1	2.0380	0.405	488.74	12.081	02.02.2007	L12_195_VGE_K_r04_t30_x.2x64x64.171.mes	L12_195_VGE_K_r04_t30_y.2x64x64.171.mes	9	485.220	12.067	29.6	142.0	
171	L	140.9	2.0380	0.405	488.74	12.081									
171	M	136.3	2.0380	0.405	488.74	12.081									
171	N	136.1	2.0380	0.405	488.74	12.081	02.02.2007	L12_195_VGE_N_r04_t30_x.2x64x64.171.mes	L12_195_VGE_N_r04_t30_y.2x64x64.171.mes	8	485.835	12.092	29.6	134.7	
171	O	136.0	2.0380	0.405	488.74	12.081									
171	P	127.9	2.0380	0.405	488.74	12.081									
171	Q	127.8	2.0380	0.405	488.74	12.081	02.02.2007	L12_195_VGE_Q_r04_t30_x.2x64x64.171.mes	L12_195_VGE_Q_r04_t30_y.2x64x64.171.mes	2	485.825	12.093	29.6	127.9	
171	R	127.6	2.0380	0.405	488.74	12.081									

Matrix-punkt	Höhen-position	Druck am GS (ü) PI4-07 [kPa]	J _{Gas} [m/s] Einspeisung	J _{Wasser} [m/s]	V _{Gas} [nm³/h]	m _{Wasser} [kg/s]	Datum	File 1 (x)	File 2 (y)	DIAdem	Betriebsdaten (Mittelwerte über 10 s)			
											V _{Gas} [m³/h]	m _{Wasser} [kg/s]	t _{GS} [°C]	p(ü) GS [kPa]
173	A	144.6	2.0380	1.017	488.74	30.336								
173	B	144.3	2.0380	1.017	488.74	30.336	02.02.2007	L12_195_VGE_B_r04_t30_x.2x64x64.173.mes	L12_195_VGE_B_r04_t30_y.2x64x64.173.mes	21	485.818	30.361	29.9	143.0
173	C	144.1	2.0380	1.017	488.74	30.336								
173	D	143.4	2.0380	1.017	488.74	30.336								
173	E	143.1	2.0380	1.017	488.74	30.336	02.02.2007	L12_195_VGE_E_r04_t30_x.2x64x64.173.mes	L12_195_VGE_E_r04_t30_y.2x64x64.173.mes	19	485.313	30.323	29.8	143.1
173	F	142.9	2.0380	1.017	488.74	30.336								
173	G	139.3	2.0380	1.017	488.74	30.336								
173	H	139.0	2.0380	1.017	488.74	30.336	02.02.2007	L12_195_VGE_H_r04_t30_x.2x64x64.173.mes	L12_195_VGE_H_r04_t30_y.2x64x64.173.mes	12	485.790	30.350	29.8	138.4
173	I	138.8	2.0380	1.017	488.74	30.336								
173	J	134.7	2.0380	1.017	488.74	30.336								
173	K	134.5	2.0380	1.017	488.74	30.336	02.02.2007	L12_195_VGE_K_r04_t30_x.2x64x64.173.mes	L12_195_VGE_K_r04_t30_y.2x64x64.173.mes	10	485.318	30.338	29.7	134.9
173	L	134.2	2.0380	1.017	488.74	30.336								
173	M	126.3	2.0380	1.017	488.74	30.336								
173	N	126.1	2.0380	1.017	488.74	30.336	02.02.2007	L12_195_VGE_N_r04_t30_x.2x64x64.173.mes	L12_195_VGE_N_r04_t30_y.2x64x64.173.mes	6	485.293	30.314	29.8	126.5
173	O	125.8	2.0380	1.017	488.74	30.336								
173	P	112.1	2.0380	1.017	488.74	30.336								
173	Q	111.8	2.0380	1.017	488.74	30.336	02.02.2007	L12_195_VGE_Q_r04_t30_x.2x64x64.173.mes	L12_195_VGE_Q_r04_t30_y.2x64x64.173.mes	4	485.285	30.345	29.7	111.6
173	R	111.6	2.0380	1.017	488.74	30.336								
182	A	147.7	3.1850	0.405	763.80	12.081								
182	B	147.5	3.1850	0.405	763.80	12.081	26.01.2007	L12_195_VGE_B_r04_t30_x.2x64x64.182.mes	L12_195_VGE_B_r04_t30_y.2x64x64.182.mes	7b	763.957	12.096	29.3	148.5
182	C	147.4	3.1850	0.405	763.80	12.081								
182	D	147.1	3.1850	0.405	763.80	12.081								
182	E	147.0	3.1850	0.405	763.80	12.081	26.01.2007	L12_195_VGE_E_r04_t30_x.2x64x64.182.mes	L12_195_VGE_E_r04_t30_y.2x64x64.182.mes	6b	763.887	12.059	29.4	147.7
182	F	146.9	3.1850	0.405	763.80	12.081								
182	G	145.3	3.1850	0.405	763.80	12.081								
182	H	145.2	3.1850	0.405	763.80	12.081	26.01.2007	L12_195_VGE_H_r04_t30_x.2x64x64.182.mes	L12_195_VGE_H_r04_t30_y.2x64x64.182.mes	1b	763.923	12.086	30.0	145.8
182	I	145.1	3.1850	0.405	763.80	12.081								
182	J	143.3	3.1850	0.405	763.80	12.081								
182	K	143.2	3.1850	0.405	763.80	12.081	26.01.2007	L12_195_VGE_K_r04_t30_x.2x64x64.182.mes	L12_195_VGE_K_r04_t30_y.2x64x64.182.mes	10a	763.953	12.088	29.1	143.0
182	L	143.1	3.1850	0.405	763.80	12.081								
182	M	139.6	3.1850	0.405	763.80	12.081								
182	N	139.5	3.1850	0.405	763.80	12.081	26.01.2007	L12_195_VGE_N_r04_t30_x.2x64x64.182.mes	L12_195_VGE_N_r04_t30_y.2x64x64.182.mes	6a	763.763	12.078	29.4	139.2
182	O	139.4	3.1850	0.405	763.80	12.081								
182	P	133.4	3.1850	0.405	763.80	12.081								
182	Q	133.3	3.1850	0.405	763.80	12.081	26.01.2007	L12_195_VGE_Q_r04_t30_x.2x64x64.182.mes	L12_195_VGE_Q_r04_t30_y.2x64x64.182.mes	5a	764.033	12.051	30.0	133.2
182	R	133.2	3.1850	0.405	763.80	12.081								
184	A	145.3	3.1850	1.017	763.80	30.336								
184	B	145.1	3.1850	1.017	763.80	30.336	26.01.2007	L12_195_VGE_B_r04_t30_x.2x64x64.184.mes	L12_195_VGE_B_r04_t30_y.2x64x64.184.mes	8b	763.653	30.336	29.5	147.1
184	C	144.9	3.1850	1.017	763.80	30.336								
184	D	144.3	3.1850	1.017	763.80	30.336								
184	E	144.1	3.1850	1.017	763.80	30.336	26.01.2007	L12_195_VGE_E_r04_t30_x.2x64x64.184.mes	L12_195_VGE_E_r04_t30_y.2x64x64.184.mes	3b	763.920	30.349	30.0	145.4
184	F	143.9	3.1850	1.017	763.80	30.336								
184	G	140.9	3.1850	1.017	763.80	30.336								
184	H	140.7	3.1850	1.017	763.80	30.336	26.01.2007	L12_195_VGE_H_r04_t30_x.2x64x64.184.mes	L12_195_VGE_H_r04_t30_y.2x64x64.184.mes	2b	763.817	30.330	30.0	140.9
184	I	140.5	3.1850	1.017	763.80	30.336								
184	J	137.2	3.1850	1.017	763.80	30.336								
184	K	137.0	3.1850	1.017	763.80	30.336	26.01.2007	L12_195_VGE_K_r04_t30_x.2x64x64.184.mes	L12_195_VGE_K_r04_t30_y.2x64x64.184.mes	9a	763.763	30.307	29.3	138.4
184	L	136.8	3.1850	1.017	763.80	30.336								
184	M	130.4	3.1850	1.017	763.80	30.336								
184	N	130.2	3.1850	1.017	763.80	30.336	26.01.2007	L12_195_VGE_N_r04_t30_x.2x64x64.184.mes	L12_195_VGE_N_r04_t30_y.2x64x64.184.mes	8a	763.580	30.328	29.4	130.4
184	O	130.0	3.1850	1.017	763.80	30.336								
184	P	118.8	3.1850	1.017	763.80	30.336								
184	Q	118.6	3.1850	1.017	763.80	30.336	26.01.2007	L12_195_VGE_Q_r04_t30_x.2x64x64.184.mes	L12_195_VGE_Q_r04_t30_y.2x64x64.184.mes	4a	763.697	30.325	30.4	118.6
184	R	118.4	3.1850	1.017	763.80	30.336								

Appendix V

Calibration protocols

POLYNOMIAL FUNCTIONS

== Calculation method ==

The polynomial functions are calculated using the collection of measuring points listed in the results on the calibration certificate as a source, excluding the result at zero flow (0%).

The "Least Square method" is used for the polynomial fit, resulting in a polynomial of the 3rd degree that will accurately describe the calibration curve.

== Identifications ==

Serial number : M1206151A
 Model number : F-106CI-FZD-03-V
 Certificate no. : BHTG04/387873
 Flow (*) : 1000 m3n/h AiR *(FIC 4-10)*

== Polynomial description ==

Scaled polynomial for flow : $y = A + Bx + Cx^2 + Dx^3$
 Scaled polynomial for setpoint (only applicable for controllers) : $z = E + Fy + Gy^2 + Hy^3$

in which: x = output signal [mA]
 y = flow [m3n/h]
 z = setpoint signal [mA]
 A / H = calculated parameters

Unscaled polynomial for flow (only applicable for FLOW-BUS devices) : $y = A + Bx + Cx^2 + Dx^3$
 Unscaled polynomial for setpoint (only applicable for FLOW-BUS controllers) : $z = E + Fy + Gy^2 + Hy^3$

in which: x = output signal [%FS/100]
 y = flow [%FS/100]
 z = setpoint signal [%FS/100]
 A / H = calculated parameters

== Calculated polynomial parameters ==

Scaled polynomial:		Unscaled polynomial:	
A = -2.4012E+02	E = +4.0057E+00	A = -3.0726E - 04	E = +3.5784E - 04
B = +5.8618E+01	F = +1.6347E - 02	B = +9.7793E - 01	F = +1.0217E+00
C = +3.7567E - 01	G = -1.0136E - 06	C = +6.3994E - 02	G = -6.3348E - 02
D = -1.0474E - 02	H = +6.8095E - 10	D = -4.2903E - 02	H = +4.2559E - 02

== Notes ==

* Reference conditions of flow unit: 0.00 °C, 1013.25 hPa (a).

CALIBRATION CERTIFICATE

We herewith certify that the instrument mentioned below has been calibrated in accordance with the stated values and conditions. The calibration standards used are traceable to national standards of the Dutch Weights & Measures (NMI).

== Identifications ==

	<u>Calibrated Instrument</u>	<u>Calibration Standard</u>
Type :	Flow meter	Turbine meter
Serial number :	M1206151A	80038
Model number :	F-106CI-FZD-03-V	FTM T-1600-TD
Certificate no. :	BHTG04/387873	NMi/G1S3760

F104-10

== Conditions ==

	<u>Customer</u>		<u>Calibration</u>
Fluid :	AiR	Fluid :	AiR
Pressure :	5.5 bar (g)	Pressure :	0.0 bar (g)
Temperature :	15..25 °C	Temperature :	20.9 °C
Flow (*) :	1000 m3n/h	Room temperature :	20.9 °C
Output range :	4 - 20 mA	Atm. pressure :	1003 hPa

== Results ==

Nominal Flow Setting	Calibrated Output Signal	Customer Flow(*)	
0.0 %	4.032 mA	0.0000	m3n/h
10.0 %	5.601 mA	98.01	m3n/h
20.0 %	7.201 mA	197.8	m3n/h
40.0 %	10.402 mA	398.4	m3n/h
60.0 %	13.599 mA	600.0	m3n/h
80.0 %	16.804 mA	801.5	m3n/h
95.0 %	19.078 mA	942.1	m3n/h

== Notes ==

* Reference conditions of flow units: 0.00 °C, 1013.25 hPa (a).

Maximum calibrated flow is 95%.

Calibrator : H.V.

Date : 02-10-2006

Signed :

QC :

POLYNOMIAL FUNCTIONS

== Calculation method ==

The polynomial functions are calculated using the collection of measuring points listed in the results on the calibration certificate as a source, excluding the result at zero flow (0%).

The "Least Square method" is used for the polynomial fit, resulting in a polynomial of the 3rd degree that will accurately describe the calibration curve.

== Identifications ==

Serial number : M1206032A
 Model number : F-206BI-FGD-99-V
 Certificate no. : BHTG04/388850
 Flow (*) : 500 m³/h Air *(FIC 4-11)*

== Polynomial description ==

Scaled polynomial for flow : $y = A + Bx + Cx^2 + Dx^3$
 Scaled polynomial for setpoint (only applicable for controllers) : $z = E + Fy + Gy^2 + Hy^3$

in which: x = output signal [mA]
 y = flow [m³/h]
 z = setpoint signal [mA]
 A / H = calculated parameters

Unscaled polynomial for flow (only applicable for FLOW-BUS devices) : $y = A + Bx + Cx^2 + Dx^3$
 Unscaled polynomial for setpoint (only applicable for FLOW-BUS controllers) : $z = E + Fy + Gy^2 + Hy^3$

in which: x = output signal [%FS/100]
 y = flow [%FS/100]
 z = setpoint signal [%FS/100]
 A / H = calculated parameters

== Calculated polynomial parameters ==

Scaled polynomial:		Unscaled polynomial:	
A = -9.5306E+01	E = +3.9682E+00	A = +2.1354E - 03	E = -1.9882E - 03
B = +1.9912E+01	F = +3.5682E - 02	B = +8.8605E - 01	F = +1.1151E+00
C = +1.1916E+00	G = -2.5106E - 05	C = +3.8531E - 01	G = -3.9228E - 01
D = -3.6590E - 02	H = +3.9282E - 08	D = -2.9974E - 01	H = +3.0689E - 01

== Notes ==

* Reference conditions of flow unit: 0.00 °C, 1013.25 hPa (a).

CALIBRATION CERTIFICATE

We herewith certify that the instrument mentioned below has been calibrated in accordance with the stated values and conditions. The calibration standards used are traceable to national standards of the Dutch Weights & Measures (NMI).

== Identifications ==

	Calibrated Instrument	Calibration Standard
Type :	Flow controller	Turbine meter
Serial number :	M1206032A	80038
Model number :	F-206BI-FGD-99-V	FTM T-1600-TD
Certificate no. :	BHTG04/388850	NMI/G1S3760

FIC 4-11

== Conditions ==

	Customer		Calibration
Fluid :	AiR	Fluid :	AiR
Pressure :	5.5 bar (g)	Pressure :	0.0 bar (g)
Temperature :	15..25 °C	Temperature :	22.9 °C
Flow (*) :	500 m3n/h	Room temperature :	22.9 °C
Output range :	4 - 20 mA	Atm. pressure :	1007 hPa

== Results ==

Nominal Flow Setting	Calibrated Output Signal	Customer Flow(*)	
0.0 %	4.032 mA	0.0000	m3n/h
10.0 %	5.596 mA	46.67	m3n/h
20.0 %	7.198 mA	96.78	m3n/h
40.0 %	10.399 mA	199.2	m3n/h
60.0 %	13.597 mA	303.4	m3n/h
80.0 %	16.804 mA	402.9	m3n/h
90.0 %	18.400 mA	446.2	m3n/h

== Notes ==

* Reference conditions of flow units: 0.00 °C, 1013.25 hPa (a).

Maximum calibrated flow is 90%.

Calibrator : H.V.

Date : 04-10-2006

Signed :

QC :

POLYNOMIAL FUNCTIONS

== Calculation method ==

The polynomial functions are calculated using the collection of measuring points listed in the results on the calibration certificate as a source, excluding the result at zero flow (0%).

The "Least Square method" is used for the polynomial fit, resulting in a polynomial of the 3rd degree that will accurately describe the calibration curve.

== Identifications ==

Serial number : M1206032B
 Model number : F-203AC-FGB-44-V
 Certificate no. : BHTG22/384269
 Flow (*) : 50 m3n/h AiR (FIC 4-12)

== Polynomial description ==

Scaled polynomial for flow : $y = A + Bx + Cx^2 + Dx^3$
 Scaled polynomial for setpoint (only applicable for controllers) : $z = E + Fy + Gy^2 + Hy^3$

in which: x = output signal [mA]
 y = flow [m3n/h]
 z = setpoint signal [mA]
 A / H = calculated parameters

Unscaled polynomial for flow (only applicable for FLOW-BUS devices) : $y = A + Bx + Cx^2 + Dx^3$
 Unscaled polynomial for setpoint (only applicable for FLOW-BUS controllers) : $z = E + Fy + Gy^2 + Hy^3$

in which: x = output signal [%FS/100]
 y = flow [%FS/100]
 z = setpoint signal [%FS/100]
 A / H = calculated parameters

== Calculated polynomial parameters ==

Scaled polynomial:		Unscaled polynomial:	
A = -1.4008E+01	E = +4.0280E+00	A = -2.2335E-03	E = +1.7476E-03
B = +3.6846E+00	F = +3.0453E-01	B = +1.0538E+00	F = +9.5167E-01
C = -5.9982E-02	G = +1.1509E-03	C = -1.9394E-01	G = +1.7983E-01
D = +1.8419E-03	H = -1.8030E-05	D = +1.5089E-01	H = -1.4086E-01

== Notes ==

* Reference conditions of flow unit: 0.00 °C, 1013.25 hPa (a).

CALIBRATION CERTIFICATE

We herewith certify that the instrument mentioned below has been calibrated in accordance with the stated values and conditions. The calibration standards used are traceable to national standards of the Dutch Weights & Measures (NMI).

== Identifications ==

	Calibrated Instrument	Calibration Standard
Type :	Flow controller	Rotor meter
Serial number :	M1206032B	80236
Model number :	F-203AC-FGB-44-V	FRM R-100-TD
Certificate no. :	BHTG22/384269	Nmi/G1S3283

F104-12

== Conditions ==

	Customer		Calibration
Fluid :	AiR	Fluid :	AiR
Pressure :	5.5 bar (g)	Pressure :	6.5 bar (a)
Temperature :	15..25 °C	Temperature :	23.5 °C
Flow (*) :	50 m3n/h	Room temperature :	23.5 °C
Output range :	4 - 20 mA	Atm. pressure :	1005 hPa

== Results ==

Nominal Flow Setting	Calibrated Output Signal	Customer Flow(*)	
0.0 %	4.032 mA	0.0000	m3n/h
10.0 %	5.606 mA	5.079	m3n/h
20.0 %	7.201 mA	10.12	m3n/h
40.0 %	10.401 mA	19.88	m3n/h
60.0 %	13.602 mA	29.66	m3n/h
80.0 %	16.802 mA	39.70	m3n/h
100.0 %	20.001 mA	50.43	m3n/h

== Notes ==

* Reference conditions of flow units: 0.00 °C, 1013.25 hPa (a).

Calibrator : M.Se.

Date : 15-09-2006

Signed : 

QC : 

POLYNOMIAL FUNCTIONS

Calculation method

The polynomial functions are calculated using the collection of measuring points listed in the results on the calibration certificate as a source, excluding the result at zero flow (0%).

The "Least Square method" is used for the polynomial fit, resulting in a polynomial of the 3rd degree that will accurately describe the calibration curve.

Identifications

Serial number : M1206032C
 Model number : F-202AC-FGB-33-V
 Certificate no. : WAGNER/012943
 Flow (*) : 5 m3n/h AiR *(FIC 4-13)*

Polynomial description

Scaled polynomial for flow : $y = A + Bx + Cx^2 + Dx^3$
 Scaled polynomial for setpoint (only applicable for controllers) : $z = E + Fy + Gy^2 + Hy^3$

in which: $x =$ output signal [mA]
 $y =$ flow [m3n/h]
 $z =$ setpoint signal [mA]
 A / H = calculated parameters

Unscaled polynomial for flow (only applicable for FLOW-BUS devices) : $y = A + Bx + Cx^2 + Dx^3$
 Unscaled polynomial for setpoint (only applicable for FLOW-BUS controllers) : $z = E + Fy + Gy^2 + Hy^3$

in which: $x =$ output signal [%FS/100]
 $y =$ flow [%FS/100]
 $z =$ setpoint signal [%FS/100]
 A / H = calculated parameters

Calculated polynomial parameters

Scaled polynomial:		Unscaled polynomial:	
A = -1.4053E +00	E = +4.0310E +00	A = -2.1057E -03	E = +1.9405E -03
B = +3.6894E -01	F = +3.0160E +00	B = +1.0597E +00	F = +9.4251E -01
C = -5.7328E -03	G = +1.1765E -01	C = -1.8998E -01	G = +1.8382E -01
D = +1.6851E -04	H = -1.7083E -02	D = +1.3805E -01	H = -1.3346E -01

Notes

* Reference conditions of flow unit: 0.00 °C, 1013.25 hPa (a).

CALIBRATION CERTIFICATE

We herewith certify that the instrument mentioned below has been calibrated in accordance with the stated values and conditions. The calibration standards used are traceable to national standards of the Dutch Weights & Measures (NMI).

Identifications

	<u>Calibrated Instrument</u>	<u>Calibration Standard</u>
Type :	Flow controller	Rotor meter
Serial number :	M1206032C	9721314D
Model number :	F-202AC-FGB-33-V	FRM R-025-TD
Certificate no. :	WAGNER/012943	NMi/G1S5817

FIC 4-13

Conditions

	<u>Customer</u>		<u>Calibration</u>
Fluid :	AiR	Fluid :	AiR
Pressure :	5.5 bar (g)	Pressure :	4.0 bar (g)
Temperature :	25 °C	Temperature :	22.2 °C
Flow (*) :	5 m3n/h	Room temperature :	22.2 °C
Output range :	4 - 20 mA	Atm. pressure :	1009 hPa

Results

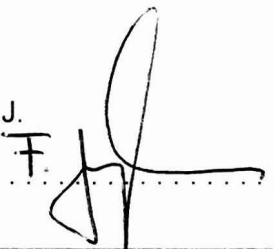
Nominal Flow Setting	Calibrated Output Signal	Customer Flow(*)
0.0 %	4.032 mA	0.0000 m3n/h
10.0 %	5.600 mA	0.5093 m3n/h
20.0 %	7.200 mA	1.019 m3n/h
40.0 %	10.400 mA	2.000 m3n/h
60.0 %	13.600 mA	2.975 m3n/h
80.0 %	16.800 mA	3.975 m3n/h
100.0 %	20.000 mA	5.028 m3n/h

Notes

* Reference conditions of flow units: 0.00 °C, 1013.25 hPa (a).

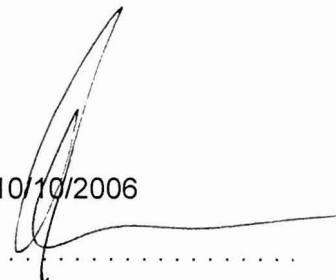
Calibrator : F.J.

Signed :



Date : 10/10/2006

QC :



Messumformer-Typ:	Smar LD 301
Serien-Nr.:	51131
Serien-Nr.Messzelle:	60906
Messbereich:	-2486,42 kPa bis 2486,42 kPa
Messgrenze (Untere/Obere):	-2486,42 kPa / 2486,42 kPa
Messspanne (Min/Max)	62,16 kPa bis 2486,42
Eingestellter Messanfang:	0,00 kPa
Eingestelltes Messende:	250,0 kPa
Eingestellte Messspanne:	250,0 kPa
Ausgangssignal:	4-20 mA linear
Gerätebezeichnung:	PI 4-07.1
Vergleichsgerät/Messgerät/Gerätenummer:	UNOMAT MCX/1910
Vergleichsgerät/Druckmodul/Gerätenumm	MCX-PM/1194
Kalibrierdatum:Vergleichsgerät	20.06.2006

Ausgang: 4-20 mA (2...10VDC über 220 Ω Prüfwiderstand)

Prüf- Druck kPa	Prüf- Druck %	Soll mA	Ist mA	Messabweichung %
0,000	0	4,000	4,051	1,28
50,000	20	7,200	7,231	0,43
100,000	40	10,400	10,440	0,38
150,000	60	13,600	13,645	0,33
200,000	80	16,800	16,834	0,20
250,000	100	20,000	19,956	-0,22

Prüf- Druck kPa	Prüf- Druck %	Soll mA	Ist mA	Messabweichung %
250,000	100	20,000	19,947	-0,27
200,000	80	16,800	16,822	0,13
150,000	60	13,600	13,641	0,30
100,000	40	10,400	10,425	0,24
50,000	20	7,200	7,241	0,57
0,000	0	4,000	4,062	1,55

Kalibrierdatum: 07.02.2007
 Kalibriert von: Lindner,Klaus
 Bemerkung:

Messaufnehmer	Thermoelement Typ K
Serien-Nr.:	367
Messbereich:	-270°C bis +1200°C
Messstellenbezeichnung:	TI 4-08
Vergleichsgerät: Temperaturgeber/Gerätenummer	Metallblockkalibrator Jupiter 650SN / 181031/2
Vergleichsgerät: Thermometer/Gerätenummer	Platinthermoelement / 181031/2
Kalibrierdatum:Vergleichsgerät-Temperatur	10.10.2006
Vergleichsgerät: Temperaturgeber/Gerätenummer	MCX / 1910
Kalibrierdatum:Vergleichsgerät-Temperatur	20.06.2006
Analog / Digitalwandler	PhoenixContact IB IL TEMP 2 UTH / 33268369
Kalibrierdatum:Vergleichsgerät-Temperaturgeber	20.06.2006

Thermoelement			Analog/Digitalwandler			max. Ab- weichung
Temperatur in °C			Temperatur in °C			
Soll	Ist	Differenz	Soll	Ist	Differenz	°C
50,0	49,9	-0,1	50,0	49,6	-0,4	-0,5
100,0	100,2	0,2	100,0	99,7	-0,3	-0,1
150,0	150,2	0,2	150,0	149,9	-0,1	0,1
200,0	200,0	0,0	200,0	200,1	0,1	0,1
250,0	250,2	0,2	250,0	250,1	0,1	0,3
300,0	300,1	0,1	300,0	300,2	0,2	0,3

Kalibrierdatum: A/D Wandler 18.10.2006
 Kalibrierdatum:Thermoelemen 18.10.2006

Kalibriert von: Lindner,Klaus
 Bemerkung:

Messaufnehmer	Thermoelement Typ K
Serien-Nr.:	897
Messbereich:	-270°C bis +1200°C
Messstellenbezeichnung:	TI 4-410
Vergleichsgerät: Temperaturgeber/Gerätenummer	Metallblockkalibrator Jupiter 650SN / 181031/2
Vergleichsgerät: Thermometer/Gerätenummer	Platinthermoelement / 181031/2
Kalibrierdatum: Vergleichsgerät-Temperatur	10.10.2006
Vergleichsgerät: Temperaturgeber/Gerätenummer	MCX / 1910
Vergleichsgerät: Thermometer/Gerätenummer	20.06.2006
Analog / Digitawandler	PhoenixContact IB IL TEMP 2 UTH / 33277813

Thermoelement gemeinsam mit
Analog/Digitalwandler

Temperatur in °C		
Soll	Ist	Differenz
35,0	35,0	0,0
40,0	40,0	0,0
50,0	50,0	0,0

max. Ab-
weichung

°C
0,0
0,0
0,0

Kalibrierdatum: A/D Wandler
Kalibrierdatum: Thermoelement

16.11.2006

Kalibriert von: Lindner, Klaus
Bemerkung:

Messaufnehmer	Thermoelement Typ K
Serien-Nr.:	873
Messbereich:	-270°C bis +1200°C
Messstellenbezeichnung:	TI 4-411
Vergleichsgerät: Temperaturgeber/Gerätenummer	Metallblockkalibrator Jupiter 650SN / 181031/2
Vergleichsgerät: Thermometer/Gerätenummer	Platinthermoelement / 181031/2
Kalibrierdatum: Vergleichsgerät-Temperatur	10.10.2006
Vergleichsgerät: Temperaturgeber/Gerätenummer	MCX / 1910
Vergleichsgerät: Thermometer/Gerätenummer	20.06.2006
Analog / Digitawandler	PhoenixContact IB IL TEMP 2 UTH / 33277486

Thermoelement gemeinsam mit
Analog/Digitalwandler

max. Ab-
weichung

Temperatur in °C			°C
Soll	Ist	Differenz	
35,0	35,0	0,0	0,0
40,0	40,0	0,0	0,0
50,0	50,0	0,0	0,0

Kalibrierdatum: A/D Wandler 16.11.2006
Kalibrierdatum: Thermoelement

Kalibriert von: Lindner, Klaus
Bemerkung:

Messaufnehmer	Thermoelement Typ K
Serien-Nr.:	895
Messbereich:	-270°C bis +1200°C
Messstellenbezeichnung:	TI 4-412
Vergleichsgerät: Temperaturgeber/Gerätenummer	Metallblockkalibrator Jupiter 650SN / 181031/2
Vergleichsgerät: Thermometer/Gerätenummer	Platinthermoelement / 181031/2
Kalibrierdatum: Vergleichsgerät-Temperatur	10.10.2006
Vergleichsgerät: Temperaturgeber/Gerätenummer	MCX / 1910
Vergleichsgerät: Thermometer/Gerätenummer	20.06.2006
Analog / Digitawandler	PhoenixContact IB IL TEMP 2 UTH / 33277486

Thermoelement gemeinsam mit
Analog/Digitalwandler

max. Ab-
weichung

Temperatur in °C			
Soll	Ist	Differenz	°C
35,0	35,1	0,1	0,1
40,0	39,9	-0,1	-0,1
50,0	49,9	-0,1	-0,1

Kalibrierdatum: A/D Wandler
Kalibrierdatum: Thermoelement

16.11.2006

Kalibriert von: Lindner, Klaus
Bemerkung:

Messaufnehmer	Thermoelement Typ K
Serien-Nr.:	894
Messbereich:	-270°C bis +1200°C
Messstellenbezeichnung:	TI 4-413
Vergleichsgerät: Temperaturgeber/Gerätenummer	Metallblockkalibrator Jupiter 650SN / 181031/2
Vergleichsgerät: Thermometer/Gerätenummer	Platinthermoelement / 181031/2
Kalibrierdatum: Vergleichsgerät-Temperatur	16.11.2006
Vergleichsgerät: Temperaturgeber/Gerätenummer	MCX / 1910
Kalibrierdatum: Thermometer/Gerätenummer	20.06.2006
Analog / Digitawandler	PhoenixContact IB IL TEMP 2 UTH / 33277185

Thermoelement gemeinsam mit
Analog/Digitalwandler

max. Ab-
weichung

Temperatur in °C			°C
Soll	Ist	Differenz	
35,0	35,0	0,0	0,0
40,0	40,0	0,0	0,0
50,0	50,1	0,1	0,1

Kalibrierdatum: A/D Wandler 16.11.2006
Kalibrierdatum: Thermoelement

Kalibriert von: Lindner, Klaus
Bemerkung:



GE Infrastructure
Sensing

CALIBRATION
CERTIFICATE

Druck Nederland B.V.
Zuideinde 37, 2991 LJ
Postbus 232, 2990 AE, Barendrecht,
The Netherlands

T 0180 - 611 555, F 0180 - 618 131
druck.nl@druck.com, www.gesensing.com

Page 1 of 3

Certificate Number: 20060036 D

Customer

Name

Forschungszentrum Rossendorf

Address

01314 DRESDEN

Your reference

n.a.

Our order number

4008659

Instrument

Manufacturer

GE Druck

Type

MCX

Serial Number

1910

Identification Number

n.a.

Reference Standard

Manufacturer and type

Druck DPI 515

Druck DPI 150

Serial Number

51500850

2252346

Calibration Due

12 Oct. 2006

18 Jan. 2007

Environmental conditions

Temperature

20 °C ± 1 °C

Relative Humidity

40-70%

Date of calibration: 20 June 2006

Date of signing : 20 June 2006

P. de Greef
Deputy head of laboratory

A.G. v.d. Berghe
Head of laboratory

The measurements have been checked using
standards which are traceable to international
standards

Druck Nederland B.V. is a member of the
International Geophysical Institute (IGI)



Range 0 to 10000 mbar g.

Type Sensor PM
Serial number sensor 1194

As Found / Left

Applied pressure mbar g.	Instrument reading mbar g.	Deviation mbar g.
0.00	0.0	0.00
2000.00	2001.5	1.50
4000.00	4001.2	1.20
6000.00	5998.1	-1.90
8000.00	7995.4	-4.60
10000.00	9994.3	-5.70
8000.00	7996.6	-3.40
6000.00	5999.8	-0.20
4000.00	4002.6	2.60
2000.00	2002.0	2.00
0.00	0.0	0.00

Max. deviation 0.050 % of Reading

Comment:



Range 0 to 120 bar g.

Type Sensor PM
Serial number sensor 1194

As Found

Applied pressure bar g.	Instrument reading bar g.	Deviation bar g.
0.0000	0.000	0.0000
20.0000	19.977	-0.0230
40.0000	39.955	-0.0450
60.0000	59.934	-0.0660
80.0000	79.922	-0.0780
100.0000	99.889	-0.1110
120.0000	119.866	-0.1340
100.0000	99.894	-0.1060
80.0000	79.929	-0.0710
60.0000	59.942	-0.0580
40.0000	39.965	-0.0350
20.0000	19.985	-0.0150
0.0000	0.005	0.0050

Max. deviation 0.102 % of Reading

Comment:

As Left

Applied pressure bar g.	Instrument reading bar g.	Deviation bar g.
0.0000	0.000	0.0000
20.0000	20.003	0.0030
40.0000	40.003	0.0030
60.0000	60.006	0.0060
80.0000	80.014	0.0140
100.0000	100.035	0.0350
120.0000	120.027	0.0270
100.0000	100.038	0.0380
80.0000	80.030	0.0300
60.0000	60.026	0.0260
40.0000	40.013	0.0130
20.0000	20.006	0.0060
0.00000	0.004	0.0040

Max. deviation 0.026 % of Reading



GE Industrial Sensing

Druck Nederland B.V.
Zuideinde 37, 2991 LJ
Postbus 232, 2990 AE, Barendrecht,
The Netherlands

T 0180 - 611 555, F 0180 - 618 131
druck.nl@druck.com, www.gesensing.com

CALIBRATION CERTIFICATE

Page 1 of 6

Certificate Number: 20060057 E

Customer	
Name	Forschungszentrum Rossendorf
Address	01314 DRESDEN
Your reference	N.A.
Our ordernumber	4008659
Instrument	
Manufacturer	GE Druck
Type	MCX
Serial number	1910
ID number	N.A.
Results	AS-LEFT
Remarks	
Environmental conditions	
Temperature	20 °C ± 1 °C
Relative Humidity	40-70 %

Date of calibration: 20 June 2006

Approval


P. de Greef
Deputy head of laboratory

The measurements have been executed using standards which are traceable to (inter)national standards.

This certificate is issued provided that Druck Nederland B.V. does not assume any liability



Reference Standards

<u>Manufacturer</u>	<u>Model</u>	<u>Serial Number</u>	<u>Certificate Number</u>	<u>Due Date</u>
ALMEMO	2290-3 TEMPERATURE INDICATOR	942599	2003/020	10/6/2008
DATRON	1281 DIGITAL MULTIMETER	43394	06-1030	24/1/2007
FLUKE	5500 CALIBRATOR	7820027	F1282003	26/3/2007
FLUKE	PM6680B COUNTER	SM785650	645446	6/1/2009

Test Results

<u>Range</u>	<u>Output</u>	<u>Measured</u>	<u>Lower limit</u>	<u>Upper limit</u>
<i>CURRENT MEASURE</i>				
<i>52mA Range</i>				
	0.0000 mA	0.001 mA	-0.006 mA	0.006 mA
	3.9999 mA	4.001 mA	3.994 mA	4.006 mA
	7.9998 mA	8.002 mA	7.993 mA	8.006 mA
	11.9998 mA	12.002 mA	11.993 mA	12.006 mA
	15.9997 mA	16.002 mA	15.993 mA	16.007 mA
	20.0003 mA	20.003 mA	19.993 mA	20.007 mA
	35.0013 mA	35.003 mA	34.994 mA	35.009 mA
	50.0017 mA	50.004 mA	49.993 mA	50.010 mA
<i>CURRENT GENERATE</i>				
<i>24 mA Range</i>				
	0.0000 mA	0.001 mA	-0.007 mA	0.007 mA
	4.0000 mA	4.000 mA	3.993 mA	4.007 mA
	8.0000 mA	8.000 mA	7.993 mA	8.007 mA
	12.0000 mA	12.000 mA	11.993 mA	12.007 mA
	16.0000 mA	16.000 mA	15.993 mA	16.007 mA
	20.0000 mA	20.001 mA	19.993 mA	20.007 mA
<i>DC VOLTAGE MEASURE</i>				
<i>100mV Range</i>				
	0.0005 mV	0.000 mV	-0.005 mV	0.005 mV
	24.9997 mV	24.999 mV	24.994 mV	25.006 mV
	49.9991 mV	49.999 mV	49.992 mV	50.006 mV
	74.9988 mV	75.000 mV	74.991 mV	75.007 mV
	98.9984 mV	99.000 mV	98.989 mV	99.007 mV
<i>DC VOLTAGE MEASURE</i>				
<i>600mV Range</i>				
	199.999 mV	200.00 mV	199.94 mV	200.06 mV
	399.998 mV	400.01 mV	399.92 mV	400.08 mV
	589.997 mV	590.01 mV	589.90 mV	590.10 mV
<i>DC VOLTAGE MEASURE</i>				

The measurements have been executed using standards which are traceable to (inter)national standards.

This certificate is issued provided that Druck Nederland BV does not assume any liability



Test Results

<u>Range</u>	<u>Output</u>	<u>Measured</u>	<u>Lower limit</u>	<u>Upper limit</u>	
<i>6V Range</i>					
	0.00000 V	0.0000 V	-0.0004 V	0.0004 V	
	1.99999 V	2.0000 V	1.9994 V	2.0005 V	
	3.99999 V	4.0001 V	3.9993 V	4.0007 V	
	5.89997 V	5.9001 V	5.8991 V	5.9008 V	
<i>DC VOLTAGE MEASURE</i>					
<i>60V Range</i>					
	6.1000 V	6.100 V	6.095 V	6.105 V	
	9.9999 V	10.000 V	9.994 V	10.005 V	
	29.9998 V	30.000 V	29.993 V	30.007 V	
	59.0003 V	59.002 V	58.990 V	59.010 V	
<i>DC VOLTAGE GENERATE</i>					
<i>100 mV Range</i>					
	0.0000 mV	-0.000 mV	-0.005 mV	0.005 mV	
	25.0000 mV	25.000 mV	24.994 mV	25.006 mV	
	50.0000 mV	50.001 mV	49.993 mV	50.007 mV	
	75.0000 mV	75.000 mV	74.992 mV	75.008 mV	
	99.0000 mV	98.999 mV	98.991 mV	99.009 mV	
<i>DC VOLTAGE GENERATE</i>					
<i>12 V Range</i>					
	0.00000 V	0.0001 V	-0.0004 V	0.0004 V	
	2.00000 V	2.0000 V	1.9995 V	2.0005 V	
	4.00000 V	4.0001 V	3.9994 V	4.0006 V	
	8.00000 V	8.0001 V	7.9993 V	8.0007 V	
	10.00000 V	10.0001 V	9.9992 V	10.0008 V	
	11.50000 V	11.5000 V	11.4991 V	11.5009 V	
<i>FREQUENCY MEASURE</i>					
<i>655Hz Range at 1 Volt</i>					
	1.001 Hz	1.00 Hz	1.00 Hz	0.99 Hz	1.01 Hz
	5.999 Hz	6.00 Hz	6.00 Hz	5.99 Hz	6.01 Hz
	59.999 Hz	60.00 Hz	60.00 Hz	59.99 Hz	60.01 Hz
	649.992 Hz	650.00 Hz	650.00 Hz	649.94 Hz	650.04 Hz
<i>FREQUENCY MEASURE</i>					
<i>1310Hz Range at 1 Volt</i>					
	659.99 Hz	660.0 Hz	660.0 Hz	659.9 Hz	660.1 Hz
	899.98 Hz	900.0 Hz	900.0 Hz	899.9 Hz	900.1 Hz
	1299.98 Hz	1300.0 Hz	1300.0 Hz	1299.9 Hz	1300.1 Hz
<i>FREQUENCY MEASURE</i>					
<i>10000Hz Range at 1 Volt</i>					
	1499.9725 kHz	1500 Hz	1500.000 kHz	1498.973 kHz	1500.973 kHz
	2999.9465 kHz	3000 Hz	3000.000 kHz	2998.947 kHz	3000.947 kHz

The measurements have been executed using standards which are traceable to international standards.

This certificate is issued provided that Druck Nederland B.V. does not assume any liability



Test Results

<u>Range</u>	<u>Output</u>		<u>Measured</u>	<u>Lower limit</u>	<u>Upper limit</u>
	5999.8976 kHz	6000 Hz	6000.000 kHz	5998.898 kHz	6000.898 kHz
	9989.8356 kHz	9990 Hz	9990.000 kHz	9988.836 kHz	9990.836 kHz

PULSE GENERATE

100 Hz Range at 1 Volt

1.000 Hz	1.00 Hz	1.00 Hz	0.99 Hz	1.01 Hz
25.000 Hz	25.00 Hz	25.00 Hz	24.99 Hz	25.01 Hz
50.000 Hz	50.00 Hz	50.00 Hz	49.99 Hz	50.01 Hz
75.000 Hz	75.00 Hz	75.00 Hz	74.99 Hz	75.01 Hz
99.000 Hz	99.00 Hz	99.00 Hz	98.99 Hz	99.01 Hz

PULSE GENERATE

10000 Hz Range at 1 Volt

110.0000 kHz	110 Hz	110.036 kHz	109.000 kHz	111.000 kHz
1000.0000 kHz	1000 Hz	999.977 kHz	999.000 kHz	1001.000 kHz
5000.0000 kHz	5000 Hz	4999.758 kHz	4999.000 kHz	5001.000 kHz
9990.0000 kHz	9990 Hz	9989.159 kHz	9989.000 kHz	9991.000 kHz

RESISTANCE MEASURE

400 Ohm Range

10.000 Ohm	9.98 Ohm	9.93 Ohm	10.07 Ohm
90.000 Ohm	89.98 Ohm	89.93 Ohm	90.07 Ohm
200.000 Ohm	199.98 Ohm	199.93 Ohm	200.07 Ohm
300.000 Ohm	299.99 Ohm	299.93 Ohm	300.07 Ohm
390.000 Ohm	389.99 Ohm	389.93 Ohm	390.07 Ohm

RESISTANCE MEASURE

2000 Ohm Range

500.00 Ohm	500.0 Ohm	499.4 Ohm	500.6 Ohm
1000.00 Ohm	1000.0 Ohm	999.4 Ohm	1000.6 Ohm
1500.00 Ohm	1500.0 Ohm	1499.4 Ohm	1500.6 Ohm
1990.00 Ohm	1990.1 Ohm	1989.4 Ohm	1990.6 Ohm

RESISTANCE GENERATE

400 Ohm Range

10.000 Ohm	10.00 Ohm	9.91 Ohm	10.09 Ohm
90.000 Ohm	90.00 Ohm	89.91 Ohm	90.09 Ohm
200.000 Ohm	200.01 Ohm	199.91 Ohm	200.09 Ohm
300.000 Ohm	300.00 Ohm	299.91 Ohm	300.09 Ohm
390.000 Ohm	389.99 Ohm	389.91 Ohm	390.09 Ohm

RESISTANCE GENERATE

2000 Ohm Range

500.00 Ohm	500.1 Ohm	499.4 Ohm	500.6 Ohm
1000.00 Ohm	1000.1 Ohm	999.4 Ohm	1000.6 Ohm
1500.00 Ohm	1500.2 Ohm	1499.4 Ohm	1500.6 Ohm
1990.00 Ohm	1990.1 Ohm	1989.4 Ohm	1990.6 Ohm

The measurements have been executed using standards which are traceable to international standards.

This certificate is issued provided that Druck Nederland BV does not assume any liability



Test Results

<u>Range</u>	<u>Output</u>	<u>Measured</u>	<u>Lower limit</u>	<u>Upper limit</u>
<i>RTD Pt100 MEASURE ITS-90</i>				
<i>850 °C Range</i>				
-190.000 °C	190.00 degC	-189.97 °C	-190.23 °C	-189.77 °C
0.000 °C	0.00 degC	-0.05 °C	-0.23 °C	0.23 °C
100.000 °C	100.00 degC	99.94 °C	99.77 °C	100.23 °C
500.000 °C	500.00 degC	500.13 °C	499.77 °C	500.23 °C
800.000 °C	800.00 degC	800.12 °C	799.77 °C	800.23 °C
<i>RTD Pt100 GENERATE ITS-90</i>				
<i>50 °C Range, true and nominal value are in °C</i>				
-190.000 °C	22.83 Ohms	-190.08 °C	-190.28 °C	-189.72 °C
0.000 °C	100 Ohms	-0.03 °C	-0.28 °C	0.28 °C
20.000 °C	107.79 Ohms	19.98 °C	19.72 °C	20.28 °C
160.000 °C	161.05 Ohms	159.95 °C	159.72 °C	160.28 °C
500.000 °C	280.98 Ohms	499.84 °C	499.72 °C	500.28 °C
830.000 °C	384.6 Ohms	829.95 °C	829.72 °C	830.28 °C
<i>THERMOCOUPLE TYPE K MEASURE ITS-90</i>				
<i>1372 °C Range</i>				
-220.00 °C	-220.0 °C	-220.1 °C	-220.5 °C	-219.5 °C
0.00 °C	0.0 °C	0.0 °C	-0.2 °C	0.2 °C
300.00 °C	300.0 °C	300.0 °C	299.8 °C	300.2 °C
900.00 °C	900.0 °C	900.0 °C	899.8 °C	900.2 °C
1360.00 °C	1360.0 °C	1360.0 °C	1359.8 °C	1360.2 °C
<i>THERMOCOUPLE TYPE J MEASURE ITS-90</i>				
<i>1200 °C Range</i>				
-200.00 °C	-200.0 °C	-200.0 °C	-200.2 °C	-199.8 °C
0.00 °C	0.0 °C	0.0 °C	-0.2 °C	0.2 °C
300.00 °C	300.0 °C	300.0 °C	299.8 °C	300.2 °C
600.00 °C	600.0 °C	600.0 °C	599.8 °C	600.2 °C
1180.00 °C	1180.0 °C	1180.0 °C	1179.8 °C	1180.2 °C
<i>THERMOCOUPLE TYPE T MEASURE ITS-90</i>				
<i>400 °C Range</i>				
-240.00 °C	-240.0 °C	-240.1 °C	-240.6 °C	-239.4 °C
-180.00 °C	-180.0 °C	-180.1 °C	-180.6 °C	-179.4 °C
0.00 °C	0.0 °C	0.0 °C	-0.2 °C	0.2 °C
100.00 °C	100.0 °C	100.0 °C	99.8 °C	100.2 °C
390.00 °C	390.0 °C	389.9 °C	389.8 °C	390.2 °C
<i>THERMOCOUPLE TYPE K GENERATE ITS-90</i>				
<i>1372 °C Range, true and nominal value are in °C</i>				
-190.00 °C	-5730 μV	-189.9 °C	-190.5 °C	-189.5 °C
0.00 °C	0 μV	-0.0 °C	-0.5 °C	0.5 °C
300.00 °C	12209 μV	299.9 °C	299.8 °C	300.2 °C

The measurements have been executed using standards which are traceable to international standards

This certificate is issued provided that Druck Nederland BV does not assume any liability



Test Results

<u>Range</u>	<u>Output</u>	<u>Measured</u>	<u>Lower limit</u>	<u>Upper limit</u>
	900.00 °C	37326 μV	900.0 °C	899.8 °C
	1370.00 °C	54819 μV	1369.9 °C	1369.8 °C
<i>THERMOCOUPLE TYPE J GENERATE ITS-90</i>				
<i>1200 °C Range, true and nominal value are in °C</i>				
	-200.00 °C	-7890 μV	-200.0 °C	-200.2 °C
	0.00 °C	0 μV	-0.0 °C	-0.2 °C
	300.00 °C	16326 μV	300.0 °C	299.8 °C
	600.00 °C	33102 μV	600.0 °C	599.8 °C
	1180.00 °C	68406 μV	1180.0 °C	1179.8 °C
<i>THERMOCOUPLE TYPE T GENERATE ITS-90</i>				
<i>400 °C Range, true and nominal value are in °C</i>				
	-240.00 °C	-6105 μV	-240.0 °C	-240.6 °C
	-170.00 °C	-5070 μV	-169.9 °C	-170.3 °C
	0.00 °C	0 μV	-0.0 °C	-0.2 °C
	100.00 °C	4279 μV	99.9 °C	99.8 °C
	390.00 °C	20255 μV	390.0 °C	389.8 °C
<i>INTERNAL COLD JUNCTION</i>				
<i>Measure T/C</i>				
	23.760 °C	23.76 °C	23.70 °C	23.36 °C
<i>Simulation T/C</i>				
	23.455 °C	23.455 °C	23.40 °C	23.06 °C

The measurements have been executed using standards which are traceable to international standards

This certificate is issued provided that Druck Nederland B.V. does not assume any liability

DEUTSCHER KALIBRIERDIENST

Kalibrierlaboratorium für Temperatur
Calibration laboratory for temperature

DKD

Akkreditiert durch die / *accredited by the*

Akkreditierungsstelle des DKD bei der

PHYSIKALISCH-TECHNISCHEN BUNDESANSTALT (PTB)



Deutscher
 Akkreditierungs
 Rat
DAR
 DKD-K-19001



Klasmeier

Kalibrier- und Messtechnik GmbH
 Browertsraße 39
 36039 Fulda

Kalibrierschein
Calibration Certificate

Kalibrierzeichen
Calibration label

936
DKD-K-19001
2006-10

Gegenstand <i>Object</i>	Metallblock-Kalibrator
Hersteller <i>Manufacturer</i>	ISOTECH Isothermal Technology Ltd.
Typ <i>Type</i>	Jupiter 650SN
Fabrikat/Serien-Nr. <i>Serial number</i>	181031/2 + 181031/2
Auftraggeber <i>Customer</i>	Forschungszentrum Rossendorf e.V. Postfach 510119 D-01314 Dresden
Auftragsnummer <i>Order No.</i>	4537/06
Anzahl der Seiten des Kalibrierscheines <i>Number of pages of the certificate</i>	4
Datum der Kalibrierung <i>Date of calibration</i>	10.10.2006

Dieser Kalibrierschein dokumentiert die Rückführung auf nationale Normale zur Darstellung der Einheiten in Übereinstimmung mit dem Internationalen Einheitensystem (SI).

Der DKD ist Unterzeichner der multi-lateralen Übereinkommen der European co-operation for Accreditation (EA) und der International Laboratory Accreditation Cooperation (ILAC) zur gegenseitigen Anerkennung der Kalibrierscheine.

Für die Einhaltung einer angemessenen Frist zur Wiederholung der Kalibrierung ist der Benutzer verantwortlich.

This calibration certificate documents the traceability to national standards, which realize the units of measurement according to the International System of Units (SI).

The DKD is signatory to the multilateral agreements of the European co-operation for Accreditation (EA) and of the International Laboratory Accreditation Cooperation (ILAC) for the mutual recognition of calibration certificates.

The user is obliged to have the object recalibrated at appropriate intervals.

Dieser Kalibrierschein darf nur vollständig und unverändert weiterverbreitet werden. Auszüge oder Änderungen bedürfen der Genehmigung sowohl der Akkreditierungsstelle des DKD als auch des ausstellenden Kalibrierlaboratoriums. Kalibrierscheine ohne Unterschrift und Stempel haben keine Gültigkeit.

This calibration certificate may not be reproduced other than in full except with the permission of both the Accreditation Body of the DKD and the issuing laboratory. Calibration certificates without signature and seal are not valid.

Stempel <i>Seal</i>	Datum <i>Date</i>	Stellv. Leiter des Kalibrierlaboratoriums <i>Deputy Head of the calibration laboratory</i>	Bearbeiter <i>Person in charge</i>
	11.10.2006	 Dipl.-Ing. (FH) Thomas Klasmeier	 Boris Kalb

Klasmeier Kalibrier- und Messtechnik GmbH, Browerstraße 39, 36039 Fulda, Tel./Fax 0661-55011 / 57498

1. Kalibriergegenstand

Der Kalibriergegenstand ist ein Block-Kalibrator für den Temperaturbereich von 50 bis 650 °C. Der Metallblock (Einsatz) enthält verschiedene Bohrungen mit unterschiedlichen Durchmessern zur Aufnahme der Thermometer, die kalibriert werden sollen, und eine Bohrung mit 3,5 mm Durchmesser zur Aufnahme des zum Kalibrator gehörenden Normal-Thermometers. Das Normalthermometer wird in 4-Leiter-Schaltung angeschlossen. Die maximale Einbautiefe der Thermometer beträgt 140 mm.

2. Meßbedingungen

Bei der Kalibrierung wurden folgende Bedingungen eingehalten:

- Der Kopf des Blocks wurde während der Kalibrierung mit Mineralwolle zusätzlich thermisch isoliert.
- Am Regler wurden keine Offsets eingestellt.
- Am Temperatur-Indikator wurden keine Offsets eingestellt.
- Alle Thermometer sind maximal eingetaucht.

Die im DKD-Kalibrierlaboratorium benutzte Temperaturskala ist die Internationale Temperaturskala von 1990 (ITS-90).

Das zur Kalibrierung verwendete Normal-Widerstandsthermometer Ser.-Nr. 25582/3 ist rückführbar auf nationale Normale, ebenso die Widerstandsmeßeinrichtung T.T.I. 2 Ser.-Nr. 141162/1.

2.1 Umgebungsbedingungen

Die Umgebungstemperatur betrug $23\text{ °C} \pm 5\text{ °C}$.

Die Netzspannung, an der der Kalibrator angeschlossen war, betrug 230 V (Wechselspannung 50 Hz).

3. Kalibrierverfahren

Grundlage für die Kalibrierung ist die DKD-Richtlinie für die Kalibrierung von Temperatur-Block-Kalibratoren (DKD-R-5-4, und der ISOTECH-Jupiter Untersuchungsbericht).

Entsprechend o. gen. Richtlinie wurden die Kalibrierung an 5 Temperaturwerten vorgenommen, die beginnend bei 100 °C sich in Schritten bis 600°C und wieder fallend auf 100°C erstreckten. Die Messungen erfolgten nach Temperaturstabilisierung am jeweiligen Kalibrierpunkt über einen Zeitraum von 10 min (siehe Meßschrieb).

4. Kalibrierergebnisse

Die Kalibrierergebnisse sind in der nachfolgenden Tabelle angegeben. Dabei sind in den ersten beiden Spalten die Soll- und Ist-Werte des Temperatur-Reglers aufgeführt, in der dritten Spalte die mit einem Normal-Widerstandsthermometer gemessene richtige Temperatur am Boden einer Bohrung des Blocks (Kalibriertemperatur) und in der vierten Spalte die Anzeige des Temperatur-Indikators des Kalibrators in Verbindung mit dem zugehörigen Thermometer.

Die Meßwerte, die für die Kalibrierpunkte in den beiden Meßzyklen erhalten wurden, sind als Mittelwert angegeben. Die fünfte Spalte enthält die Meßunsicherheit der Kalibrierung.

Regler		Kalibrier-Temperatur	angezeigte Temperatur Temp.-Indik. in Verb. mit Thermometer Ser.-Nr. 181031/2	Mess- unsicherheit
Sollwert in °C	Istwert in °C	in °C	in °C	in ±K
100	100	99,972	100,0	0,2
200	200	199,804	199,8	0,3
400	400	399,763	400,0	0,5
500	500	499,78	500,2	1,0
600	600	599,869	600,3	1,0

5. Messunsicherheit

Die angegebenen Messunsicherheiten setzen sich zusammen aus den Messunsicherheiten des verwendeten Normals, des Kalibrierverfahrens und den über Voruntersuchungen bekannten Meßunsicherheitsanteilen, die aus der Temperaturverteilung im Block, den Wärmeübergangsbedingungen in den Bohrungen des Blocks, der Länge des Widerstandselements im Widerstandsthermometer, der thermischen Belastung durch unterschiedliche Anzahl von Prüflingen und der Kurzzeitstabilität des Thermometers Ser.-Nr. 181031/2 in Verbindung mit dem Temperatur-Indikator des Block-Kalibrators resultieren.

Angegeben ist die erweiterte Messunsicherheit, die sich aus der Standardmessunsicherheit durch Multiplikation mit dem Erweiterungsfaktor $k = 2$ ergibt. Sie wurde gemäß DKD-3 ermittelt. Der Wert der Messgröße liegt mit einer Wahrscheinlichkeit von 95% im zugeordneten Werteintervall.

Hinweise zum Einsatz von Temperatur-Blockkalibratoren

Durch den Kalibrierschein eines DKD-Kalibrierlabors wird bestätigt, daß der Temperatur-Blockkalibrator die hohen Anforderungen an die Kalibrierbarkeit eines solchen Gerätes erfüllt, wie sie in der DKD-Richtlinie R5-4 festgelegt sind. Dennoch sind beim Einsatz des Kalibrators die folgenden Punkte zu beachten:

Die Kalibrierung von Temperatur Blockkalibratoren bezieht sich vorwiegend auf die Temperatur des Festkörperblocks. Die Temperatur des im Block zu kalibrierenden Thermometers kann von dieser Temperatur abweichen. Der kalibrierte Metallblockkalibrator ist ein Arbeitsnormal mit einer zertifizierten Messunsicherheit. Die Kalibrierung fand in einem DKD-Kalibrierlaboratorium unter optimalen Bedingungen statt. Der Einsatz des Kalibrators zur Kalibrierung von Temperaturfühler führt daher zu einer Erhöhung der Meßunsicherheit. Falls im Kalibrierschein nichts anderes angegeben ist, muß sichergestellt sein, daß

- das Meßelement sich in der homogenen Temperaturzone befindet.
- der Innendurchmesser der im Kalibrator benutzten Bohrung (evt. der Hülse) im Temperaturbereich -80°C bis 660°C maximal 0,5 mm und im Temperaturbereich 660°C bis 1300°C maximal 1,0 mm größer ist als der Außendurchmesser des zu kalibrierenden Thermometers.
- die Eintauchtiefe des zu kalibrierenden Thermometers mindestens das 15-fache des Außendurchmessers des zu kalibrierenden Thermometers beträgt.
- das zu kalibrierende Thermometer einen Außendurchmesser $d \leq 6\text{mm}$ hat.

Bitte achten Sie besonders darauf, ob bei der Kalibrierung Ihres Temperatur-Blockkalibrators ein Wärmeträgermittel eingesetzt wurde. Wenn dies der Fall ist, so gilt die Kalibrierung nur bei Einsatz des Kalibrators mit einem entsprechenden Wärmeträgermittel.

Bei der Kalibrierung von Thermometern mit Außendurchmesser $d > 6\text{mm}$ ist eine zusätzliche Meßabweichung durch Wärmeableitung zu berücksichtigen. Falls solche Messungen durchgeführt werden sollen, so kann die zusätzliche Wärmeableitung für den bei Ihnen untersuchten Thermometertyp von Ihrem DKD-Kalibrierlabor bestimmt werden. Ein guter Test auf mögliche Wärmeleitfehler besteht darin, zu kontrollieren, ob sich die Anzeige des prüfenden Thermometers ändert, wenn es um 20mm angehoben wird. Beiträge zur Meßunsicherheit, die durch das von Ihnen zu kalibrierende Thermometer bedingt sind. (z.B. Inhomogenitäten von Thermoelementen), sind ebenfalls nicht in der Meßunsicherheit des Kalibrators enthalten.

Maßgeblich für die Kalibrierung sind die Angaben im Kalibrierschein, nicht die Herstellerangaben. Sprechen Sie bitte unbedingt vor der Kalibrierung die Einsatz- und Kalibrierbedingungen mit Ihrem DKD-Kalibrierlabor ab.

Wenn im Kalibrierschein nichts anderes angegeben ist, muß (unabhängig von Herstellerangaben) sichergestellt sein, daß

- der Kalibrator in vertikaler Stellung betrieben wird.
- keine zusätzlichen thermischen Isolierungen benutzt werden
- die Umgebungstemperatur $(23 \pm 5)^\circ\text{C}$ beträgt.

Zur Überprüfung von Temperatur-Blockkalibratoren wird empfohlen, regelmäßige Kontrollmessungen mit einem kalibrierten Thermometer vorzunehmen. Ohne Kontrollmessungen mit einem kalibrierten Thermometer wird eine jährliche Rekalibrierung des Temperatur-Blockkalibrators dringend empfohlen.

ISOTECH-Untersuchungsberichte können unter: www.klasmeier.com/untersuchungsberichte heruntergeladen werden.

Appendix VI

**Description of the data files available for the air/water test series
L12**

VI. Description of the data files available for the air/water test series L12

VI.1 Name convention for the data files

The measurement data and the results of the evaluation are stored in files with the following structure:

NNN_DDD_VVV_YY_rzz_tcc_d.1x64x64.pkt.typ;

The letter combinations have the following meaning:

- NNN - Identification number of the test series (L12 – air/water experiments in the test section variable gas injection),
- DDD - Inner diameter of the test section in mm – 195 stands for 195.3 mm,
- VVV - Configuration of the test section, in this case VGE for variable gas injection,
- YY - Position of gas injection one or two letters are possible, respectively. Compare with Fig. 2, Tab. 1 and chapter 1.3,
- rzz - Gas injection using 72 x 1 mm orifices (rzz = r01) or 32 x 4 mm orifices (rzz = r04),
- t30 - Temperature of water in the test section: 30 °C ± 1 K,
- d - Either x for the data of the first measurement plane in direction of flow or y for the second,
- 2x64x64 - A two plane sensor with 64 x 64 mesh electrons is used,
- pkt - Test or matrix point corresponding Tab. 2,
- typ - Filetyp, cf. Tab. VI.1.

VI.2 Description of the data files

Tab. VI.1: File types available for the test series L12

File typ	Description	Format
*.a	Geometric characteristics of all identified bubbles (chapter: 1.5.4, short info: VI.3)	ASCII
*.b	Matrix with the bubble identification numbers (chapter: 1.5.4)	binary
*.epsr	Time averaged gas fraction for all cross points of the wire-mesh sensor, table with two columns containing distance of the point from the centre of the pipe and the respective gas fraction (chapter: 1.5.2, file structure: VI.4)	ASCII
*.epsrad_80	Time and azimuthally (inside of 80 radius domains) averaged gas fraction (chapter: 1.5.2, file structure: VI.5)	ASCII
*.epsrad_80_bub	Information of the *.epsrad_80-files partitioned in bubble classes (chapter: 1.5.5, file structure: VI.6)	ASCII
*.epsxy	Time averaged gas fraction for all cross points of the wire-mesh sensor as matrix (chapter: 1.5.2, file structure: VI.7)	ASCII
*.his_lin	Bubble size distribution referring to linear bubble classes (chapter: 1.5.5, file structure: VI.8)	ASCII
*.his_lin_r	Bubble size distribution referring to linear bubble	ASCII

	classes partitioned in 80 radius domains (chapter: 1.5.5, file structure: VI.9)	
*.his_log	Bubble size distribution referring to logarithmic bubble classes (chapter: 1.5.5, file structure: VI.10)	ASCII
*.log	File with all information about the evaluation programmes and the parameters used	ASCII
*.mes	Measurement data, generated by the electronics of the wire-mesh sensor and the measurement software	binary
*.ud	Weighted drift velocities (chapter: 2.2.1, file structure: VI.11)	ASCII
*.uw	Calibration matrix for all cross points of the wire-mesh sensor (chapter: 1.5.1, file structure: VI.12)	ASCII
*.uwrad_80	Azimuthally (partitioned in 80 radius discs) averaged calibrating values from *.uw (chapter: 1.5.1, file structure: VI.13)	ASCII
*.v	Gas fraction values for the single cross points of the wire-mesh sensor for all measurement frames, value between 0 and 100 % (chapter: 1.5.1)	binär
*.v00	Local gas velocities, table with two columns containing the distance of the measurement point from the centre of the pipe and the respective velocity, only for internal usage (chapter: 1.5.3, file structure: VI.14)	ASCII
*.vel	Local azimuthally (80 radius domains) averaged gas velocities (chapter: 1.5.3, file structure: VI.15)	ASCII

VI.3 Geometrical bubble characteristics

Tab. VI.2 Part of a *.a file (bubble characteristics)

bb	im	jm	km	ifront	jfront	kfront	iback	jback	kback	rmi	rmj	rmk	rmxy	max	v	rv	n	deps	rxymax
[-]	[ms]	[mm]	[mm]	[ms]	[mm]	[mm]	[ms]	[mm]	[mm]	[ms]	[mm]	[mm]	[mm]	[%]	[ms*mm ²]	[s ³ (ms*mm ²) ²]	[-]	[%]	[mm]
1	3.6	18.7	132.2	0.4	15.0	120.0	9.6	21.0	135.0	5.4	13.1	13.0	18.4	100	1348.93	6.85	888	0.0004527	9.031
2	18.0	98.2	103.1	0.4	21.0	102.0	52.0	36.0	135.0	23.9	97.0	72.5	121.1	100	304569.4	41.74	1358	0.1022072	55.256
3	6.0	165.9	44.1	0.4	147.0	51.0	15.6	177.0	48.0	9.2	15.6	13.4	20.6	100	3991.92	9.84	2134	0.0013396	12.017
4	8.5	27.5	66.7	0.4	18.0	66.0	16.0	42.0	72.0	8.7	16.3	12.9	20.8	100	3754.53	9.64	1964	0.0012599	10.822
5	14.9	93.6	25.1	9.2	93.0	24.0	19.2	99.0	24.0	5.7	10.2	8.4	13.2	100	1180.37	6.56	667	0.0003961	7.183
6	...																		

The *.a – files contain a table (Tab VI.2), which summarises for all identify bubbles:

- bb - Bubble identification number,
- im, jm, km - Coordinates of the centre of the bubble in i – flow direction and j, k – measurement cross-section,
- ifront, jfront, kfront - Coordinates of the bubble front,
- iback, jback, kback - Coordinate of the bubble back,
- rmi, rmj, rmk - Moments of the bubble in i – flow direction and j, k – measurement cross-section,

rmxy -	Radial moment of the bubble in measurement cross-section plane,
max -	Maximum of the gas fraction of the bubble,
v -	Bubble volume,
rv -	Radius of a volume equivalent sphere,
n -	Number volume elements occupied by the bubble,
deps -	Part of the gas fraction per bubble referring to the total flow volume,
rxymax -	Maximal circle equivalent radius of the bubble in the measurement plane.

In the second line of the table VI.2, the units for the bubble characteristics are given. It is indicated once again that with the bubble characteristics contrary to the gas fraction calculation, the index *i* refers to the serial number of the frames (time axis or *z*-direction), and the indices *j* and *k* apply to the measurement cross-section, respectively. All characteristics in direction of the time axis are given in time unities (ms).

VI.4 Time averaged gas fraction distribution

The ASCII files *.epsr contain the local time averaged gas fractions presented by two columns: The left column contains the radial distance of each individual measurement point (*x*, *y*) from axis of the pipe in mm while in the right column contains the gas fraction in percent. The order depends on the alignment of the measurement points of the wire-mesh sensor. 64 x 64 points are listed in a series, whereas the points outside of the measurement cross-section have a gas fraction of 0.00 %. The left-hand side of Table VI.3 shows an excerpt of a *.epsr file. The table presents 20 measurement points for an electrode at the edge of the wire-mesh sensor. Two points at the upper and at the lower end are outside of the sensor.

Tab. VI.3 Part of gas fraction files *.epsr and *.epsrad_80

.....	0.6 51.439
100.601 0.00	1.8 51.439
99.612 0.00	3.1 51.475
98.704 1.36	4.3 51.519
97.880 3.13	5.5 51.403
97.142 6.25	6.7 51.433
96.491 8.56	7.9 51.564
95.930 9.97	9.2 51.695
95.459 12.97	10.4 51.851
95.082 14.27	11.6 51.890
94.797 13.94	12.8 51.726
94.607 14.91	14.0 51.554
94.512 16.05	15.3 51.449
94.512 16.81	16.5 51.428
94.607 15.61	17.7 51.337
94.797 14.72	18.9 51.004
95.082 13.24	20.1 50.789
95.459 12.15	21.4 50.684
95.930 10.09	22.6 50.596
96.491 8.45	23.8 50.460
97.142 5.61	25.0 50.117
97.880 4.06	26.2 49.974
98.704 3.11	27.5 49.713
99.612 0.00	28.7 49.375
100.601 0.00	29.9 49.118
.....
Part of a *.epsr-file	Part of a epsrad_80 file

VI.5 Time and azimuthally averaged gas fraction distributions

This file (*.epsrad_80) contains time and azimuthally averaged gas fraction information for 80 concentric rings of the same width. Column 1 contains the distance [mm] of the respective ring from the centre of the pipe. The right column contains the appropriate gas fraction in percent [%]. The right-hand side of Tab. VI.3 shows a detail of this file. These radial gas fraction profiles are presented graphically in the appendix I.

VI.6 Time and azimuthally averaged gas fraction distribution decomposed into bubble classes

In this file (*.epsrad_80_bub), in addition to the information contained in the *.epsrad_80-files, there are four columns, in which the azimuthally and time averaged gas fraction is decomposed into the bubble classes (see Tab. VI.4). The size of the individual bubble classes is indicated in mm in the table head. The sum of the gas fractions over the four classes results in the total gas fraction in the column eps_all.

Tab. VI.4 Part of a *.epsrad_80_bub file

r	eps_all	0.0 <	4.0 <	5.8 <	7.0 <	200.0
mm	%	%	%	%	%	%
0.6	51.27	0.20	0.76	0.97	49.34	
1.8	51.27	0.20	0.76	0.97	49.34	
3.1	51.30	0.20	0.77	1.00	49.34	
4.3	51.34	0.20	0.78	1.03	49.32	
5.5	51.22	0.21	0.78	1.03	49.21	
6.7	51.25	0.21	0.78	1.00	49.26	
7.9	51.37	0.20	0.79	1.00	49.37	
9.2	51.48	0.20	0.79	1.00	49.49	
10.4	51.61	0.20	0.78	1.00	49.63	
.....						

VI.7 Time averaged gas fraction distribution

The files (*.epsxy) contain the time averaged volumetric gas fractions in percent [%] as matrix for all the measurement cross-section (64 x 64 values). Fig. VI.1 shows a detailed view of this matrix. In this presentation, the points outside of the pipe cross-section also have the value 0.00 %.

0.00	0.00	0.00	0.00	0.00	0.00	0.00	0.00	0.00	0.00	0.00	0.00	0.00	0.00	0.00	0.00	0.00	0.00
0.00	0.00	0.00	0.00	0.00	0.00	0.00	0.00	0.00	0.00	0.00	0.00	0.00	0.00	0.00	0.00	0.00	0.00	0.00
0.00	0.00	0.00	0.00	0.00	0.00	0.00	0.00	0.00	0.00	0.00	0.00	0.00	0.00	0.00	0.00	0.00	0.00	0.70
0.00	0.00	0.00	0.00	0.00	0.00	0.00	0.00	0.00	0.00	0.00	0.00	0.00	0.00	0.00	0.00	1.68	4.85	11.10
0.00	0.00	0.00	0.00	0.00	0.00	0.00	0.00	0.00	0.00	0.00	0.00	0.00	0.00	0.00	0.72	3.05	9.54	14.49
0.00	0.00	0.00	0.00	0.00	0.00	0.00	0.00	0.00	0.00	0.00	0.00	0.00	0.00	0.00	1.64	5.50	12.31	17.41
0.00	0.00	0.00	0.00	0.00	0.00	0.00	0.00	0.00	0.00	0.00	0.00	1.89	7.96	14.98	18.85	23.32	24.92	26.92
0.00	0.00	0.00	0.00	0.00	0.00	0.00	0.00	0.00	0.00	0.00	0.00	3.21	10.29	16.23	19.37	21.99	24.87	27.67
0.00	0.00	0.00	0.00	0.00	0.00	0.00	0.00	0.00	0.00	0.00	0.00	3.36	10.96	16.53	19.79	22.58	24.78	27.98
0.00	0.00	0.00	0.00	0.00	0.00	0.00	0.00	0.00	0.00	0.00	3.06	10.31	16.22	19.83	21.98	24.56	27.68	30.60
0.00	0.00	0.00	0.00	0.00	0.00	0.00	2.43	10.75	16.10	21.03	23.77	24.79	27.33	29.64	31.07	33.42	34.74	
0.00	0.00	0.00	0.00	0.00	0.00	0.64	8.40	15.66	20.19	23.17	26.07	28.06	29.02	30.82	32.34	33.71	35.29	
0.00	0.00	0.00	0.00	0.10	7.42	15.18	20.52	23.23	25.85	28.05	29.74	30.76	31.78	32.60	34.96	35.58		
0.00	0.00	0.00	0.00	5.60	14.37	19.71	23.72	26.08	27.78	30.12	32.35	33.23	32.49	34.34	35.91	37.41		
0.00	0.00	0.00	0.00	2.80	12.20	18.78	23.12	25.53	28.71	30.65	31.53	34.36	33.29	34.06	36.45	36.83	38.44	
0.00	0.00	0.00	0.00	7.11	15.93	20.69	24.06	28.32	29.65	32.58	33.63	35.15	35.39	36.42	36.99	39.06	39.53	
0.00	0.00	0.00	3.03	13.68	19.19	23.29	27.39	30.63	31.34	33.41	34.47	36.25	37.33	37.73	38.98	40.38	40.29	
0.00	0.00	0.00	8.57	18.04	21.84	25.67	29.48	31.95	33.86	35.02	36.34	37.60	39.05	39.48	40.66	40.87	39.40	
0.00	0.00	3.61	14.25	21.12	26.01	28.41	31.09	32.86	35.34	36.78	38.41	38.73	40.35	39.67	40.55	41.14	40.28	
0.00	0.00	7.43	18.02	24.67	27.91	29.51	32.74	33.86	36.45	38.01	39.03	38.98	41.17	41.08	40.91	40.99	42.05	

0.00 1.93 11.77 20.31 25.91 29.55 30.74 33.69 35.55 37.08 37.29 39.58 41.10 41.33 41.87 42.27 41.35 42.27
0.00 4.43 15.19 22.52 26.78 29.13 31.32 34.86 35.92 38.10 38.94 39.15 40.66 40.18 40.65 42.10 41.90 42.84
0.00 8.20 18.29 23.26 27.12 30.03 32.36 35.57 35.98 38.31 39.15 40.46 41.13 40.92 41.72 42.09 41.60 42.96
0.53 11.17 20.14 24.69 28.03 30.29 33.01 36.54 36.15 38.33 39.93 39.64 40.67 41.12 42.30 43.31 42.67 43.16
2.93 12.80 21.76 26.42 29.93 31.73 33.68 35.76 36.78 38.02 38.96 39.83 40.68 43.07 42.64 43.84 43.83 44.90
4.96 15.00 21.77 27.13 31.22 32.95 34.64 37.44 38.07 38.06 39.51 40.67 41.61 42.90 44.06 44.91 44.98 44.64
7.33 16.06 23.12 28.44 31.97 33.95 35.89 36.59 37.47 38.11 39.19 40.84 41.45 41.37 43.65 45.87 45.14 44.74
9.04 17.42 23.93 28.37 31.82 33.62 35.70 37.70 37.65 38.20 39.35 41.14 43.38 43.27 45.44 46.71 45.85 45.64
10.21 18.41 24.72 27.19 30.58 33.17 35.88 37.14 37.54 38.92 39.92 41.87 44.15 43.09 45.51 46.71 46.93 45.65
11.26 19.42 24.76 27.60 30.63 32.71 35.78 37.24 37.77 39.13 40.00 42.07 42.89 43.71 46.17 46.15 46.22 47.01
11.82 19.83 24.52 27.07 30.50 32.88 35.10 35.86 36.71 38.12 40.98 42.84 43.83 44.20 45.00 47.07 46.24 45.35
13.03 19.26 23.99 26.96 30.27 31.95 34.83 35.84 37.48 38.44 41.09 42.85 43.86 43.38 44.53 45.38 45.74 46.28
.....

Fig. VI.1 Visualisation time averaged gas fractions over a quarter of the measurement cross-section from a *.epsxy file

VI.8 Bubble size distribution for a linear bubble class width

These files (* his_lin) contain a table as shown at tab. VI.5.

Tab. VI.5 Bubble size distribution for linear bubble class width from the file *.his_lin

d	hdxy	hdrelxy	hdnxy	hdv	hdrelv	hdnv
[mm]	[%/mm]	[1/mm]	[1/mm/s]	[%/mm]	[1/mm]	[1/mm/s]
0.00	0.0000	0.0000	59.60	0.0000	0.0000	25.20
0.25	0.0000	0.0001	59.20	0.0000	0.0000	31.20
0.50	0.0002	0.0011	168.00	0.0000	0.0000	33.20
0.75	0.0005	0.0022	167.20	0.0001	0.0003	76.00
1.00	0.0011	0.0055	248.00	0.0001	0.0007	127.60
1.25	0.0021	0.0103	310.40	0.0004	0.0019	176.00
1.50	0.0051	0.0252	597.60	0.0009	0.0045	250.80
1.75	0.0133	0.0655	1182.00	0.0033	0.0161	551.60
2.00	0.0335	0.1643	2222.00	0.0106	0.0523	1231.60
2.25	0.0503	0.2468	2492.40	0.0227	0.1113	1927.60
2.50	0.0686	0.3365	2664.80	0.0357	0.1750	2224.00
2.75	0.0996	0.4889	3211.20	0.0564	0.2770	2732.80
3.00	0.1274	0.6252	3452.00	0.0812	0.3988	3059.20
.....						

The single columns include the following information (see also chapter 1.5.5):

- d – Bubble diameter in mm
- hd – Gas fraction of the bubbles of this class referring to bubble class width (0,25 mm) in %/mm
- hdrel – hd related to the total gas fraction in 1/mm
- hdn – Number of bubbles in respective class referring to the class width and the sum of measurement time 1/(mm*s)

These three distributions are available related to the area equivalent bubble diameter for the largest cross-section area of the bubble in the measurement plane (xy) and basing on the volume equivalent bubble diameter (v), respectively. For the calculation of the volume equivalent parameters, the local gas velocities are used, in order to convert the time coordinate from the *.a- files into a geometrical length.

VI.9 Bubble size distribution for linear bubble class widths distributed in ring domains

These files (*.his_lin_r) contain for each of the 80 rings a table, as shown in tab. VI.5. The minimum and maximum radius of the ring is given above each table. At the end, a table with the integral bubble size distributions is added, which correspond to the distributions in the file *.his_lin.

VI.10 Bubble size distribution for logarithmic bubble class widths

The *.his_log files contain the same bubble size distributions as the *.his_lin files (cf. chapter VI.8), but in this case the bubble class width increases logarithmically starting from a diameter of 3 mm. For smaller bubbles, a linear class width of 0.1 mm is used. Appendix I includes the graphical presentation of the bubble size distributions basing on the *.his_log files.

Tab. VI.6 Example for nubble size distribution for logarithmic bubble class widths from a *.his_log file

d [mm]	hdx [%/mm]	hdrelx [1/mm]	hdnxy [%/mm/s]	hdv [%/mm]	hdrelv [1/mm]	hdnv [%/mm/s]
.....						
2.50	0.0696	0.3416	2882.00	0.0288	0.1412	1971.00
2.60	0.0664	0.3261	2503.00	0.0382	0.1875	2331.00
2.70	0.0848	0.4165	3009.00	0.0461	0.2264	2549.00
2.80	0.0940	0.4612	3055.00	0.0545	0.2674	2716.00
2.90	0.1056	0.5183	3241.00	0.0627	0.3077	2825.00
3.00	0.1212	0.5949	3533.62	0.0730	0.3586	2951.55
3.11	0.1288	0.6324	3376.85	0.0849	0.4166	3103.95
3.22	0.1276	0.6265	2992.83	0.0976	0.4789	3203.98
3.33	0.1402	0.6880	2968.25	0.1098	0.5388	3234.49
3.45	0.1568	0.7696	3042.70	0.1197	0.5876	3194.02
3.57	0.1563	0.7674	2786.43	0.1380	0.6773	3306.48
3.70	0.1726	0.8473	2829.40	0.1506	0.7395	3257.98
3.83	0.1688	0.8285	2546.78	0.1624	0.7972	3157.65
3.97	0.1919	0.9422	2660.76	0.1723	0.8459	3037.73
4.11	0.2001	0.9824	2567.87	0.1905	0.9349	3022.71
4.26	0.1988	0.9760	2316.66	0.1899	0.9323	2714.98
4.41	0.2034	0.9986	2223.62	0.2129	1.0449	2735.58
4.57	0.2231	1.0952	2176.03	0.2103	1.0323	2430.59
4.73	0.2299	1.1287	2018.06	0.2265	1.1117	2372.51
4.90	0.2288	1.1231	1860.94	0.2311	1.1345	2177.41
5.07	0.2291	1.1244	1684.00	0.2417	1.1866	2046.05
5.25	0.2518	1.2359	1684.88	0.2487	1.2210	1896.56
.....						

VI.11 Weighted drift velocities

The *.ud files contain the results of the calculation of the weighted drift velocities. The theoretical basis for the calculations is described in detail in chapter 2.2.2. The files contain a table (example: Tab. VI.7) with the following information:

- r – Radius of the ring domain used in each case for azimuthally averaging (cf. Fig. 12) in mm,
- f – Swarm factor,
- urel – Calculated values of the azimuthally averaged relative velocities between both phases in m/s,
- ul – Calculated values of the azimuthally averaged velocities of the liquid phase in m/s,
- jl – Calculated values of the azimuthally averaged superficial velocity of the liquid phase in m/s,
- lg – Calculated values of the azimuthally averaged superficial gas velocity in m/s.

Tab. VI.7 Intermediate results for the calculation of the weighted drift velocities

r	f	urel	ul	jl	lg
mm	-	m/s	m/s	m/s	m/s
0.6	1.6581	0.5428	2.0364	0.9889	1.3276
1.8	1.6581	0.5428	2.0364	0.9889	1.3276
3.1	1.6589	0.5430	2.0362	0.9880	1.3286
4.3	1.6600	0.5436	2.0356	0.9869	1.3297
5.5	1.6572	0.5446	2.0346	0.9888	1.3267
6.7	1.6579	0.5448	2.1003	1.0201	1.3614
7.9	1.6610	0.5437	2.1014	1.0178	1.3649
9.2	1.6642	0.5421	2.1030	1.0159	1.3684
10.4	1.6680	0.5396	2.0395	0.9820	1.3383
11.6	1.6689	0.5385	2.0406	0.9817	1.3393
12.8	1.6649	0.5381	2.0411	0.9853	1.3350
14.0	1.6608	0.5384	2.1067	1.0206	1.3646
15.3	1.6583	0.5379	2.1072	1.0231	1.3619
16.5	1.6578	0.5368	2.0424	0.9920	1.3274
17.7	1.6556	0.5366	2.0425	0.9940	1.3250
18.9	1.6477	0.5371	2.0421	1.0005	1.3164
.....					

k = 0.999; J = 1.780 m/s; eps(r) = 35.338 %; C0 = 1.058; <Ugl> = 0.275 m/s; <UD> = 0.378 m/s
 eps(Matrix) = 33.881 %; eps(Integral) = 35.353 %

Two lines at the end of this table list some additional values. The symbols have the following meaning:

- k - Factor of adjustment for the calculation of the velocity of the liquid phase,
- J - Middle total superficial velocity,
- eps(r) - Gas fraction integrated over the radius (directly calculated from the files *.epsrad_80),
- C0 - Profile parameter,
- Ugl - Local drift velocity,
- UD - weighted drift velocity calculated,

- eps(Matrix) - Gas fraction calculated from the superficial velocities for water and gas of the test matrix (Tab. 2) and the weighted drift velocity,
- eps(Integral) - Gas fraction calculated from the superficial velocities integrated over the radius for water and gas and the weighted drift velocity.

The gas fractions calculated with the help of the weighted drift velocities are shown in the appendix I.

VI.12 Calibration values for all mesh points of the wire-mesh sensor as matrix

In this files (*.uw), the data used for calibration for each mesh point are given in a matrix presentation similar to the gas fractions in the *.epsxy files. The calibration values are determined by the conductivity of the measurement volumes around the respective wire-mesh sensor points for pure water. Fig. VI.2 shows approx. a quarter of the measurement cross-section:

0	0	0	0	0	0	0	0	0	0	0	0	0	0	0	0	0	0	0
0	0	0	0	0	0	0	0	0	0	0	0	0	0	0	0	0	0	0	0
0	0	0	0	0	0	0	0	0	0	0	0	0	0	0	0	0	0	0	480
0	0	0	0	0	0	0	0	0	0	0	0	0	0	0	0	0	496	1232	1584
0	0	0	0	0	0	0	0	0	0	0	0	0	0	272	1056	1696	1680	1808	
0	0	0	0	0	0	0	0	0	0	0	0	0	416	1408	1680	1872	1792	1888	
0	0	0	0	0	0	0	0	0	0	0	0	752	1488	1824	1824	1952	1872	1952	
0	0	0	0	0	0	0	0	0	0	896	1648	1744	1872	1872	1952	1936	1984		
0	0	0	0	0	0	0	0	160	1008	1664	1824	1824	1952	1952	2016	1968	2032		
0	0	0	0	0	0	0	0	928	1664	1776	1872	1856	1952	1968	2016	1984	2032		
0	0	0	0	0	0	0	960	1648	1792	1840	1920	1888	2000	2000	1984	2016	2048		
0	0	0	0	0	0	672	1680	1760	1856	1872	1952	1936	2000	2016	2016	2016	2016	2064	
0	0	0	0	0	432	1552	1808	1824	1888	1920	1984	1952	2016	2016	2000	2048	2048		
0	0	0	0	160	1360	1744	1840	1856	1936	1936	1984	1952	2048	2000	2016	2032	2064		
0	0	0	0	880	1744	1808	1904	1888	1952	1952	1984	1968	2000	2000	2000	2016	2064		
0	0	0	336	1552	1792	1840	1904	1920	1936	1968	2000	1968	2016	2016	1968	2048	2064		
0	0	0	1168	1744	1888	1920	1984	2000	2016	2032	2048	2032	2096	2080	2048	2128	2144		
0	0	400	1648	1776	1904	1936	1984	2000	2048	2032	2048	2016	2128	2112	2080	2144	2112		
0	0	1200	1728	1792	1952	1952	1984	2000	2032	2016	2032	1952	2096	2032	2016	2096	2080		
0	384	1600	1776	1856	1984	1968	2016	2016	2064	2080	2080	1968	2128	2080	2048	2112	2144		
0	1024	1664	1824	1872	2000	2000	2016	2032	2048	2032	2064	2000	2112	2096	2064	2096	2112		
0	1504	1712	1856	1888	2000	2016	2048	2032	2080	2080	2080	2016	2096	2080	2064	2112	2128		
352	1712	1760	1872	1904	2032	2032	2048	2048	2096	2064	2096	2016	2112	2112	2048	2096	2112		
864	1760	1792	1904	1888	2016	2016	2032	2016	2064	2064	2032	1968	2080	2080	2016	2080	2064		
1344	1808	1856	1968	1952	2080	2080	2064	2096	2128	2096	2112	2048	2208	2128	2064	2176	2208		
1488	1792	1792	1904	1904	2016	2000	2016	2032	2048	2032	2048	1984	2112	2080	2016	2112	2096		
1648	1840	1840	1952	1936	2064	2048	2016	2048	2096	2080	2080	1984	2080	2064	2048	2128	2128		
1728	1856	1856	1952	1936	2064	2048	2032	2048	2080	2080	2080	2048	2144	2128	2064	2128	2160		
1776	1888	1888	1952	1952	2080	2080	2048	2064	2128	2112	2112	2080	2144	2128	2080	2176	2160		
1808	1904	1888	1968	1952	2064	2064	2048	2064	2112	2096	2096	2016	2144	2144	2048	2144	2208		
1808	1904	1888	1952	1936	2064	2048	2016	2048	2064	2080	2096	2016	2128	2096	2064	2144	2128		
1840	1904	1888	1968	1936	2048	2064	2016	2064	2080	2080	2080	2016	2112	2096	2016	2112	2144		
.....																			

Fig. VI.2 Example of the calibration values for a part of the measurement cross-section from a *.uw file

The calibration matrix is calculated for 64 x 64 points. Points located outside of the pipe cross-section are set to zero. The calibration values in these files, as well as in the *.uwrad_80 files are normalised to 4096 ADC values.

VI.13 Azimuthally averaged calibration values

Radial (i.e. azimuthally averaged) profiles of the calibration values are used for the quality assessment of the histogram calibration (see chapter 1.5.1). The averaging is carried out in analogy to the averaging of the gas fraction or gas velocity according to chapter 1.5.2 (cf. Fig. 12) with weighted coefficients. The left part of table VI.8 shows the arrangement of the calibration values. The radii of the centre point of the ring domains used for the azimuthally averaging are listed in the left column. The right column includes the appropriate calibration values.

Tab. VI.8 Examples for the files *.uwrad_80, *.v00, *.vel

0.6	2076.00	0.6	2.581
1.8	2076.00	100.6	1.8	2.581
3.1	2081.17	99.6	3.1	2.581
4.3	2090.73	98.7	4.3	2.581
5.5	2088.69	97.9	5.5	2.581
6.7	2083.10	97.1	6.7	2.647
7.9	2087.58	96.5	7.9	2.647
9.2	2095.03	95.9	9.2	2.647
10.4	2107.30	95.5	10.4	2.581
11.6	2113.51	95.1	11.6	2.581
12.8	2111.34	94.8	12.8	2.581
14.0	2108.42	94.6	14.0	2.647
15.3	2107.56	94.5	15.3	2.647
16.5	2106.22	94.5	16.5	2.581
17.7	2099.05	94.6	17.7	2.581
18.9	2071.38	94.8	18.9	2.581
20.1	2055.96	95.1	20.1	2.581
21.4	2065.63	95.5	21.4	2.581
22.6	2082.10	95.9	22.6	2.518
23.8	2087.42	96.5	23.8	2.518
25.0	2084.30	97.1	25.0	2.518
26.2	2084.88	97.9	26.2	2.518
27.5	2085.93	98.7	27.5	2.518
28.7	2084.28	99.6	28.7	2.518
29.9	2082.76	100.6	29.9	2.518
.....		
Azimuthally calibration (*uwrad_80)	averaged values	Local gas velocities of the point-to-point cross- correlation (*.v00)	Azimuthally averaged gas velocities (*.vel)	

VI.14 Local gas velocities

As described in chapter 1.5.3, point to point cross-correlations of the gas fraction values are used to determine local gas velocities from the mesh points that are arranged one below the other. The results of the point-to-point correlation are stored in the *.v00 files. Table VI.8 provides an example of this file type in the centre column. Similar to the gas fraction data in the *.epsr files the velocity information for the 64 x 64 mesh points are presented in two columns.. The 1st column contains the radial distance of the single mesh point (x, y) from the pipe centre in mm while the

2nd column contains the time averaged local gas velocity. Points outside of the pipe cross-section are set to zero.

Please note, that the information in this file can only be used for control reasons, since the statistical dispersion of the gas velocities is too large to enable analyses for single mesh points.

VI.15 Local azimuthally averaged gas velocities

To improve the statistics, the local averaged gas velocities mentioned in the previous chapter were averaged azimuthally for the above-mentioned ring-shaped domains (cf. chapter 1.5.3). After the averaging, the velocities are calculated for every ring and stored in the files *.vel. The right column of table VI.8 shows an extract from such a file. The left column of the table contains the radial position in mm and the right column contains the appropriate time and azimuthally averaged gas velocities in m/s. The data of these files are illustrated as radial velocity profiles in the appendix I of this report.